



Antimalarial Drug Discovery: Exploring the MEP Pathway

Thesis submitted in accordance with the requirements of the

University of Liverpool

For the degree of

Doctor in Philosophy

By

Kathryn E Price

September 2016

Declaration

This thesis is the result of my own work. The material contained in the thesis has not been presented, or is currently being presented, either wholly or in part for any other degree or qualification.

Kathryn E Price

This research was carried out in the Department of Chemistry at
The University of Liverpool and the Paediatric Department at
Washington University School of Medicine in St. Louis.

Acknowledgements

I would like to thank all of the people that I have had the pleasure of working with throughout my PhD, both in the Chemistry Department at Liverpool University and the Biology and Paediatric Departments at Washington University in St Louis.

In particular, I wish to thank my supervisor Dr. Neil Berry for his invaluable support, guidance and kindness throughout the last four years. And also, Audrey Odom whose enthusiasm and dedication to her work is a true inspiration. I would also like to thank Prof. Paul O'Neill for all of his support and advice.

Special thanks goes to Adam Rolt and Paul McGillan for their unwavering support and friendship. Many thanks also goes to everyone in the Odom lab at Washington University for making me so welcome, sharing with me their expertise and making my time in St Louis such an incredible and enjoyable experience. I would also like to thank the wonderful team of analytical staff in the Liverpool Chemistry Department for their invaluable assistance and all that they make possible.

Abstract

The development of effective antimalarial chemotherapeutics remains a major challenge within drug discovery. Despite a significant scientific progress over the last two decades and an upscaling of antimalarial research programs, malaria is still a major threat to global health with almost half the world's population at risk of contracting the disease. It is the adept ability of the *Plasmodium* parasite to develop drug resistance which so significantly hinders the fight against this disease. Indeed, the present acceleration of *Plasmodium* resistance development is seriously threatening the longevity of the existing antimalarial drug pipeline and the prospects of malaria eradication.

As the pursuit of new antimalarial drugs and novel drug targets has intensified, significant interest has arisen in the chemical manipulation of isoprenoid biosynthesis. Isoprenoids are a diverse class of natural products which play vital roles in many cellular functions and are essential for *Plasmodium* parasite survival. In contrast to mammals, *Plasmodium* parasites use the non-mevalonate (MEP) pathway to generate isoprenoid precursors, delivering a key biological selectivity that makes the MEP pathway highly attractive as an antimalarial target. Fosmidomycin, targeting the MEP IspC enzyme, has validated the pathway as a viable target for antimalarial drug discovery, driving our objective to deliver a lead candidate molecule as a selective inhibitor of *P. falciparum* IspD (*PfIspD*). In particular, we ask the question: Can arrest of the MEP pathway through *PfIspD* inhibition cause parasite death *via* disruption of isoprenoid precursor generation?

A targeted HTS has identified the 1,2-benzo[*d*]isothiazol-3(2*H*)-one (BITZ) chemotype as a promising inhibitor of the *PfIspD* enzyme. Extensive SAR investigations have generated a diverse range of BITZ compounds, including three of the most potent BITZ *PfIspD* inhibitors to date; demonstrating IC₅₀ values as potent as 73 nM against the enzyme and efficacious phenotypic activity of 206 nM against *P. falciparum* parasite growth. Molecular modelling studies have illustrated a mechanism of action which relies on the formation of a covalent *PfIspD*-BITZ adduct that renders the enzyme inactive; this model of inhibition is supported by robust evidence from biological and chemical investigations.

The covalent modification of proteins can be a risky strategy within the context of drug design. As a result, a distinct chemical chemotype, also known to inhibit the *PfIspD* enzyme *via* an alternative non-covalent mechanism is also being explored. The 1*R*,3*S*-MMV-008138 diastereoisomer, a tetrahydro- β -carboline derivative, shows potent inhibition against *PfIspD* and *Plasmodium* parasite growth with a high degree of specificity towards the *PfIspD* target. Considering these two chemical chemotypes, developmental SAR and hit-to-lead optimisation aims to progress towards a lead candidate compound that is suitable for clinical development as a novel antimalarial agent, targeting the *PfIspD* enzyme.

Publications

***Plasmodium* IspD (2-C-Methyl-D-erythritol-4-Phosphate Cytidyltransferase), an Essential and Druggable Antimalarial Target**

Leah S. Imlay, Christopher M. Armstrong, Mary Clare Masters, Ting Li, Kathryn E. Price, Rachel L. Edwards, Katherine M. Mant, Lucy X. Li, Christina L. Stallings, Neil G. Berry, Paul M. O'Neill, Audrey Odom. *ACS Infect. Dis.*, **2015**, 1 (4), pp 157-167. DOI: 10.1021/id500047s

Molecular Mechanism of Action of Antimalarial Benzoisothiazolones: Species-Selective Inhibitors of the *Plasmodium* spp. MEP pathway enzyme, IspD

Kathryn E. Price, Christopher M. Armstrong, Leah S. Imlay, Dana M. Hodge, C. Pidathala, Natalie J. Roberts, Jooyoung Park, Marwa Mikati, Raman Sharma, Alexandre S. Lawrenson, Niraj H. Tolia, Neil G. Berry, Paul M. O'Neill, Audrey R. Odom. *Sci Rep.*, **2016**, 6, pp 36777. DOI: 10.1038/srep36777

Molecular interactions between *Plasmodium falciparum* IspD and the Malaria Box inhibitor, 1*R*,3*S*-MMV008138

Leah S. Imlay, Kathryn E. Price, Matthew Pye, C. Pidathala, Raman Sharma, Alexandre S. Lawrenson, Neil G. Berry, Paul M. O'Neill, and Audrey R. Odom John.

Manuscript in preparation

Abbreviations

1°	Primary
2°	Secondary
3°	Tertiary
2D	Two-dimensional
3D	Three-dimensional
Å	Angström
ABPs	Activity-based probes
ACTs	Artemisinin-based combination therapies
ADME	Absorption, distribution, metabolism and excretion
AIDS	Acquired immune deficiency syndrome
Ala	Alanine
ARDS	Acute respiratory distress syndrome
<i>A. thaliana</i>	<i>Arabidopsis thaliana</i>
AtIspD	<i>A. thaliana</i> IspD
AstraZeneca	AZ
BITZ	1,2-benzo[<i>d</i>]isothiazol-3(2 <i>H</i>)-one
Boc	<i>tert</i> -Butyloxycarbonyl
br d	Broad doublet
br s	Broad singlet
Bu	Butyl
Bn	Benzyl
CCDC	Cambridge Crystallographic Data Centre
CDCl₃	Deuterated chloroform
CDP-ME	4-diphosphocytidyl-2C-methyl-D-erythritol

CDP-MEP	4-diphosphocytidyl-2C-methyl-D-erythritol 2-phosphate
CI	Chemical ionisation
CI	Confidence interval
CTP	Cytidine triphosphate
<i>cytB</i>	Cytochrome <i>b</i>
Cys	Cysteine
Cys-202	Cysteine-202
d	Doublet
DCM	Dichloromethane
dd	Doublet of doublets
DDT	1,1'-(2,2,2-trichloroethane-1,1-diyl)-bis(4-chlorobenzene)
ddd	Doublet of doublet of doublets
DHA	Dihydroartemisinin
DHFR	Dihydrofolate reductase
DHOD	Dihydroorotate dehydrogenase
DHPS	Dihydropteroate synthase
DIPEA	<i>N,N</i> -diisopropylethylamine
Dm	Doublet of multiplets
DMAPP	4-Dimethylallyl pyrophosphate
DME	Dimethoxyethane
DMF	<i>N,N</i> -dimethylformamide
DMSO	Dimethylsulfoxide
DNA	Deoxyribonucleic acid
DOXP	1-deoxy-D-xylulose-5-phosphate
Dscore	Druggability score

dsDNA	Double-stranded DNA
dt	Doublet of triplets
DTT	Dithiothreitol
Dxs	1-deoxy-D-xylulose-5-phosphate synthase
<i>E. coli</i>	<i>Escherichia coli</i>
EclspD	<i>E. coli</i> IspD
em	Emission
eq	Equivalents
ES	Electrospray
Et	Ethyl
EtOH	Ethanol
EtOAc	Ethyl acetate
Et₂O	Diethyl ether
ex	Excitation
FGI	Functional group inter-conversion
FPIX	Ferriprotoporphylin IX
FRET	Föster resonance energy transfer
FSM	Fosmidomycin
GA	Genetic Algorithm
GABA	γ-aminobutyric acid
GFP	Green fluorescent protein
GSH	Glutathione
GSK	GlaxoSmithKline
HATU	1-[Bis(dimethylamino)methylene]-1 <i>H</i> -1,2,3-triazolo[4,5- <i>b</i>]pyridinium 3-oxid hexafluorophosphate
Hb	Haemoglobin

HDAC	Histone deacetylases
hERG	Human ether-a-go-go related gene
HIV	Human Immunodeficiency Virus
HMBPP	2-methyl-2-(<i>E</i>)-butenyl diphosphate
HRMS	High resolution mass spectrometry
HTS	High throughput screening
IC₅₀	Half maximal inhibitory concentration
IPA	Isopropanol
IPP	Isopentyl pyrophosphate
<i>i</i>PPTase	Inorganic pyrophosphatase
<i>i</i>Pr	Isopropyl
IPT	Intermittent preventive treatment
IR	Infrared
IRS	Indoor residual spraying
IspC	1-deoxy-d-xylulose-5-phosphate reductoisomerase
IspD	4-diphosphocytidyl-2C-methyl-D-erythritol cytidyltransferase
IspE	4-diphosphocytidyl-2C-methyl-D-erythritol kinase
IspF	2C-methyl-D-erythritol-2,4-cyclodiphosphate synthase
IspE	4-hydroxy-3-methyl-2-(<i>E</i>)-butenyl-4-diphosphate reductase
ITNs	Insecticide-treated nets
kg	Kilogram
K_m	Substrate concentration at half-maximal enzyme velocity
LC-MS	Liquid Chromatography–Mass Spectrometry
LC-MS/MS	Liquid Chromatography Tandem Mass Spectrometry
LLINs	Long-lasting insecticidal nets

m	Multiplet
MDA	Mass drug administration
Me	Methyl
MEcPP	4-diphosphocytidyl-2C-methyl-D-erythritol 2,4-cyclodiphosphate
MeOD	Deuterated methanol
MeOH	Methanol
MEP	Non-mevalonate pathway
MEP	2C-methyl-D-erythritol 4-phosphate
mg	Milligram
MgSO₄	Magnesium sulphate
ml	Millilitre
mM	Millimolar
MS	Mass spectrometry
MVA	Mevalonic acid
MW	Molecular weight
m/z	Mass to charge ratio
NBD	7-nitrobenza-2-oxa-1,3-diazole
NBD-Cl	4-chloro-7-nitrobenza-2-oxa-1,3-diazole
nM	Nanomolar
nm	Nanometres
NMR	Nuclear magnetic resonance
NOE	Nuclear Overhauser Effect
NOESY	NOE spectroscopy
NS	Number of scans
NSAIDs	Non-steroidal anti-inflammatory drugs

o/n	Overnight
<i>P. berghei</i>	<i>Plasmodium berghei</i>
PBD	Phosphate-buffered saline
<i>P. falciparum</i>	<i>Plasmodium falciparum</i>
PfCRT	<i>P. falciparum</i> chloroquine resistance transported gene
PfIspC	<i>P. falciparum</i> IspC
PfIspD	<i>P. falciparum</i> IspD
Ph	Phenyl
P_i	Inorganic phosphate
PK	Pharmacokinetic
<i>P. knowlesi</i>	<i>Plasmodium knowlesi</i>
<i>P. malariae</i>	<i>Plasmodium malariae</i>
PNP	Purine nucleoside phosphorylase
<i>P. ovale</i>	<i>Plasmodium ovale</i>
Pol	Point of inflection
PP_i	Inorganic pyrophosphate
PPIs	Protein-protein interactions
ppm	Parts per million
Propofol	2,6-diisopropylphenol
Pt	Parasitemia
<i>P. vivax</i>	<i>Plasmodium vivax</i>
q	Quartet
R²	R-squared
RBCs	Red blood cells
RMSD	Root-mean-square deviation

rt	Room temperature
RT	Retention time
s	Singlet
SAR	Structure activity relationship
SD	Standard deviation
SDM	Site direct mutagenesis
SDS	Standard default settings
SEM	Standard error of the mean
SNPs	Single nucleotide polymorphisms
Sum FICs	Sum fractional inhibitory concentrations
t	Triplet
t_{1/2}	Half-life
TB	Tuberculosis
TBVs	Transmission blocking vaccines
TCAMS	Tres Cantos Antimalarial Set
td	Triplet of doublets
TFA	Trifluoroacetic acid
THF	Tetrahydrofuran
tlc	Thin-layer chromatography
TRS	Traditional Random Screening
tt	Triplet of triplets
TTP	Thiamine pyrophosphate
μM	Micromolar
UTI's	Urinary tract infections
UV	Ultraviolet

V_{\max}	Maximum enzyme velocity
WHO	World Health Organisation
wt	Weight

Contents

Declaration	ii
Acknowledgements	iii
Abstract	iv
Publications	v
Abbreviations	vi
Contents	xiv

Chapter 1: Introduction

1.1 Malarial: A Neglected Tropical Disease	1
1.2 Life Cycle of the <i>Plasmodium</i> Parasite	4
1.3 Malaria Control and Elimination Strategies	6
- 1.3.1 Vector Control	6
- 1.3.2 Antimalarial Chemotherapies	7
- 1.3.2.1 Chloroquine: Identification, Application and Resistance Development	7
- 1.3.2.2 Artemisinin: Identification, Application and Resistance Development	10
- 1.3.2.3 New Antimalarial Drugs with Novel Mechanisms of Action Are Needed	15
1.4 Approaches to Antimalarial Drug Development	17
1.5 A Novel Antimalarial Target: Isoprenoid Biosynthesis and The MEP Pathway	23
- 1.5.1 Isoprenoids	23
- 1.5.2 The MEP Pathway	25
- 1.5.3 Known Inhibitors of The MEP Pathway	28
- 1.5.4 The IspC Enzyme and Fosmidomycin	30
- 1.5.5 The IspD Enzyme and Known Inhibitors	32
1.6 Conclusions	38
1.7 References	40

Chapter 2:
**Chemotype Identification; Development of Synthetic Methodologies and
Initial SAR Investigations**

2.1 HTS Studies – A Route to New Antimalarial Compounds	45
- 2.1.1 Phenotypic-based Screening: TCAMs	47
- 2.1.1 Target-based Screening	48
2.2 Chemotype Identification	50
- 2.2.1 Chemoinformatics: Chemotype and Compound Selection	51
2.3 <i>Pf</i> lspD HTS	55
- 2.3.1 <i>Pf</i> lspD Enzymatic Assay	55
- 2.3.2 HTS Outputs and Chemotype Selection	57
2.4 Synthetic Strategies to Generate the 1,2-benzo[<i>d</i>]isothiazol-3(2 <i>H</i>)-one Chemical Motif	60
- 2.4.1 Synthetic Strategy: Route 1	60
- 2.4.2 Synthetic Strategy: Route 2	63
- 2.4.3 Synthetic Strategy: Route 3	65
2.5 Assessment of Compound Activity Against the <i>Pf</i> lspD Enzyme and <i>P. falciparum</i> Growth in Culture	66
- 2.5.1 Assessing <i>P. falciparum</i> Growth Inhibition in Culture	67
2.6 Chemotype Validation: The BITZ Motif is Required to Achieve <i>Pf</i> lspD Inhibition	69
2.7 Preliminary SAR Development	72
2.8 Conclusions and Ongoing Work	76
2.9 Experimental	78
- 2.9.1 General Methodologies	78
- 2.9.1.1 General Chemical Methods	78
- 2.9.1.2 General Biological Methods	79
- 2.9.1.3 Predictions of <i>ClogD</i> and <i>CaqSol</i>	81
- 2.9.2 Organic Synthesis	81

2.9 References	87
----------------	----

**Chapter 3:
Developing an Understanding of SAR Around the BITZ Chemotype and Biological
Evaluations of BITZ Compound Activity**

3.1 Medicinal Chemistry Strategy - TCAMS	91
- 3.1.1 Aims	93
- 3.1.2 SAR Map: Summary of Synthetic Explorations and BITZ Compound Series	93
3.2 Biphenyl BITZ Analogue Series	94
- 3.2.1 Design Rationale and Synthesis	94
- 3.2.2 <i>Pfl</i> spD Enzymatic and Whole Cell Biological Assays	96
- 3.2.3 Lipophilicity	97
3.3 Biphenyl Benzyl-linked BITZ Analogue Series	98
- 3.3.1 Design Rationale and Synthesis	98
- 3.3.2 <i>Pfl</i> spD Enzymatic and Whole Cell Biological Assays	102
3.4 Mono-phenyl Benzyl-linked BITZ Analogue Series	103
- 3.4.1 Design Rationale and Synthesis	103
- 3.4.2 <i>Pfl</i> spD Enzymatic and Whole Cell Biological Assays	104
3.5 Biphenyl Pyridinyl BITZ Analogue Series	105
- 3.5.1 Design Rationale and Synthesis	105
- 3.5.2 <i>Pfl</i> spD Enzymatic and Whole Cell Biological Assays	107
3.6 Biphenyl BITZ Compound Mimetics	108
- 3.6.1 Design Rationale and Synthesis	108
- 3.6.2 <i>Pfl</i> spD Enzymatic and Whole Cell Biological Assays	111
3.7 Variations to the Inhibitor C Ring	112
- 3.7.1 Design Rationale and Synthesis	112
- 3.7.2 <i>Pfl</i> spD Enzymatic and Whole Cell Biological Assays	114

3.8 Alkyl-amino Biphenyl BITZ Analogues	116
- 3.8.1 Design Rationale and Synthesis	116
- 3.8.2 <i>Pf</i> IspD Enzymatic and Whole Cell Biological Assays	118
3.9 Aminoquinoline-BITZ Hybrid Compounds	119
- 3.9.1 Design Rationale and Synthesis	119
- 3.9.2 <i>Pf</i> IspD Enzymatic and Whole Cell Biological Assays	123
3.10 Further SAR Explorations	125
3.11 Biological Evaluation of BITZ Compound Activity at the IspD Enzyme and in Malaria Parasites	128
- 3.11.1 BITZ Compound Activity at Alternative <i>Plasmodium</i> spp. Enzymes	128
- 3.11.2 Correlation Between <i>Pf</i> IspD Enzyme Inhibition and Inhibition of <i>Plasmodium</i> Parasite Growth	129
- 3.11.3 BITZ Compounds Inhibit Isoprenoid Metabolism in Malaria Parasites	130
- 3.11.4 BITZ Compound Activity in the Presence and Absence of IPP Supplementation	132
- 3.11.5 BITZ Activity Against Resistant Parasites	133
3.12 Conclusions and Future Work	134
3.13 Experimental	138
- 3.13.1 Organic Synthesis	138
- 3.13.2 Biological Methods	173
3.14 References	175

Chapter 4:
Determining the Mechanism of Action of the BITZ Chemotype:
A Computational and Biological Study

4.1 Computational Modelling	179
4.2 Utilising IspD Enzyme Homologues	180
- 4.2.1 Comparative Three-Dimensional Modelling at <i>E. coli</i> IspD	182
- 4.2.2 Determining a Docking Protocol	183
- 4.2.3 Molecular Modelling of the HTS Hit Compounds at <i>Ec</i> IspD	187

4.3 <i>PflspD</i> Homology Model	189
- 4.3.1 Molecular Modelling of the Focused Ligand Library of 5000 Compounds at <i>PflspD</i>	190
- 4.3.2 Molecular Modelling of BITZ Compounds at <i>PflspD</i>	192
4.3 Mechanism of Action	196
- 4.3.1 Biomimetic Mechanistic Evaluation	198
- 4.3.2 <i>PflspD</i> Enzyme Rescue	200
- 4.3.3 Molecular Modelling of BITZ Compounds at <i>PflspD</i> (2)	203
4.4 Biological Evaluation of BITZ Inhibitor Mechanism of Action	206
- 4.4.1 Site Directed Mutagenesis	206
- 4.4.1.1 <i>E. coli</i> IspD	207
- 4.4.1.2 <i>P. falciparum</i> IspD	208
- 4.4.2 <i>PflspD</i> and <i>PflspD</i> -C202A Enzymatic Assays	210
- 4.4.3 Kinetic Evaluation of the <i>PflspD</i> and <i>PflspD</i> -C202A Enzymes	212
- 4.4.4 Crystallography	214
4.5 Considering BITZ Reactivity at Cysteine Residues	215
4.6 Conclusions and Future Work	217
4.7 Experimental	220
- 4.7.1 Computational Methods	220
- 4.7.2 Biological Methods	220
- 4.7.3 Organic Synthesis	222
4.8 References	223

Chapter 5:
An Alternative Inhibitor of the *PflspD* Enzyme

5.1 MMV-008138: A Stereospecific Chemotype and <i>PflspD</i> Inhibitor	226
- 5.1.1 Identification of MMV-008138	226
- 5.1.2 Biological Target of MMV-008138	230

- 5.1.3 MMV-008138: Mechanism of Action	233
- 5.1.4 MMV-008138: Competitive Behaviour at <i>Pf</i> lspD	234
5.2 Molecular Modelling of 1 <i>R</i> ,3 <i>S</i> -MMV-008138 at <i>Pf</i> lspD	235
5.3 Can a Combined Administration of the BITZ and Tetrahydro- β -carboline Chemotypes Produce Enhanced Antimalarial Activity?	240
- 5.3.1 Rationale and Background	240
- 5.3.2 1 <i>R</i> ,3 <i>S</i> -MMV-008138-BITZ Inhibitor Combinations and Possible Outcomes	243
- 5.3.3 1 <i>R</i> ,3 <i>S</i> -MMV-008138 and BITZ Inhibitors have Antagonistic Anti-Parasitic Activity	245
- 5.3.4 1 <i>R</i> ,3 <i>S</i> -MMV-008138 and FSM have Additive Anti-Parasitic Activity	248
5.4 Development of SAR Around the Tetrahydro- β -carboline Chemotype	249
- 5.4.1 Preliminary SAR Around the Tetrahydro- β -carboline Chemotype	249
- 5.4.1.1 Modifications to the R Group at C-3	250
- 5.4.1.2 Modifications to the D Ring	253
- 5.4.1.3 Modifications to the 2° Amine in the C Ring	253
5.5 Further Modifications to the D Ring	254
- 5.5.1 Design Rationale and Synthesis	254
- 5.5.2 Enzymatic <i>Pf</i> lspD and Whole Cell Activity Data	260
- 5.5.3 Further SAR Explorations	261
5.6 Conclusion and Future Work	263
5.7 Experimental	266
- 5.7.1 Computational Methods	266
- 5.7.2 Biological Methods	266
- 5.7.3 Organic Synthesis	267
5.8 References	274

Chapter 6:
Considering Off-Target Interactions of the BITZ Chemotype
A Chemical Biology Approach

6.1 Potential Off-Target BITZ Chemotype Reactivity	277
6.2 Biological Probes	278
- 6.2.1 Using Biological Probes to Address Research Questions	279
6.3 Identification of Suitable Chemical Motifs to Generate BITZ and Control Probes	281
6.4 Localisation Studies	282
- 6.4.1 Fluorescent Molecular Probes	282
- 6.4.2 Synthesis of the NBD-Tagged BITZ Probe and NBD-Tagged Control Probe	285
- 6.4.3 Inhibitory Activity of the NBD-Tagged BITZ Probe and NBD-Tagged Control Probe Against <i>PflspD</i>	287
- 6.4.4 Inhibitory Activity of the NBD-Tagged BITZ Probe and NBD-Tagged Control Probe Against 3D7 <i>P. falciparum</i> Parasite Growth	288
- 6.4.5 Localisation Studies using Fluorescent Microscopy	291
6.5 Protein Binding Assays	294
- 6.5.1 Streptavidin Affinity Pull-down Assays	294
- 6.5.2 Design of Biotinylated BITZ and Control Probes	297
- 6.5.3 Synthesis of the Biotinylated BITZ Probe and Control Probe	298
- 6.5.4 Inhibitory Activity of the Biotin-Tagged BITZ Probe and Biotin-Tagged Control Probe Against <i>PflspD</i>	299
- 6.5.5 Inhibitory Activity of the Biotin-Tagged BITZ Probe and Biotin-tagged Control Probe Against 3D7 <i>P. falciparum</i> Parasite Growth	300
6.6 Conclusions and Future Work	301
6.7 Experimental	303
- 6.7.1 Biological Methods	303
- 6.7.2 Organic Synthesis	303
6.8 References	311

Chapter 7:
Final Conclusions and Perspectives

7.1 Final Conclusions and Perspectives	314
--	-----

Appendix

Appendix 1. HTS Output: 54 Hit Compounds Identified as Active Inhibitors of the <i>PflspD</i> enzyme	318
Appendix 2. Summary of preliminary SAR studies around close structural analogues of the DT2009-0168020 hit	337
Appendix 3. Overlaid ¹ H NMR spectra for the <i>cis</i> and <i>trans</i> isomers of compound 11	339
Appendix 4. Representative NOE spectra for compound 11	342

Chapter 1

Introduction

1.1 Malaria: A Neglected Tropical Disease

The development of effective antimalarial chemotherapeutics remains a major challenge within drug discovery. Despite a 37% decrease in global malaria incidence between 2000 and 2015, 97 countries registered ongoing malaria transmission in 2014, with 214 million new cases of malaria worldwide in 2015.^[1] This highlights that the development of new antimalarial drugs and the battle to overcome increasing parasite resistance is a crucial and ongoing challenge.

Malaria is a life-threatening, vector-borne disease which causes over 200 million cases per year and is responsible for nearly half a million deaths therefore putting almost half the world's population, about 3.2 billion people at risk of contracting the disease. In 2015, there were 214 million reported cases of malaria worldwide which lead to an estimated 438,000 deaths.^[1] Of these deaths, 90% occurred in Sub-Saharan African which carries a disproportionately high share of the total global malaria burden (**Figure 1.1**).^[1] Malaria is therefore endemic across the majority of tropical and sub-tropical regions since warm, humid climates promote ideal breeding conditions for *Anopheles* mosquitoes, the transport vectors of malaria, which breed in shallow, freshwater pools. Since 2000, it has been observed that declines in malaria incidence in the 15 sub-Saharan African countries where malaria transmission is ongoing, has significantly fallen behind that of other countries in South-East Asian and Mediterranean regions where the disease is less prevalent.^[1]

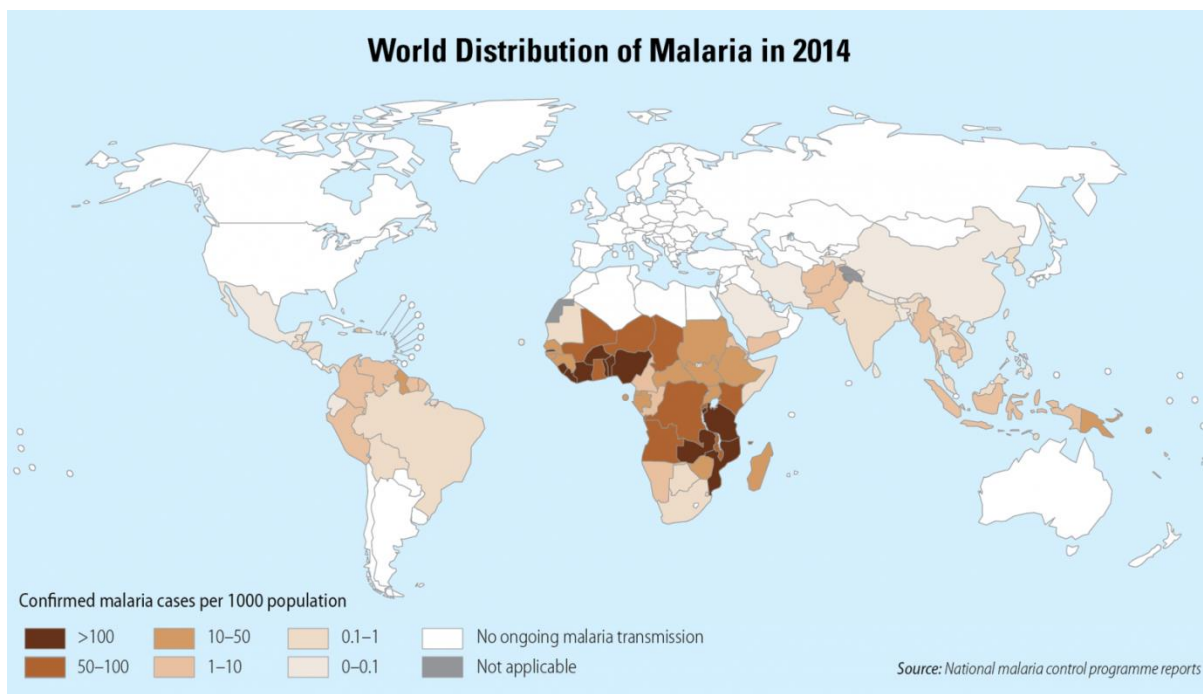


Figure 1.1 Geographical distribution of malaria in 2014; figure reproduced from ^[2].

Malaria is a hematoprotzoan parasitic infection^[3] caused by five parasite species belonging to the *Plasmodium* genus and is transmitted exclusively through the bite of female *Anopheles* mosquitos. *Plasmodium falciparum* (*P. falciparum*), *Plasmodium vivax* (*P. vivax*), *Plasmodium ovale* (*P. ovale*) and *Plasmodium malariae* (*P. malariae*) are the four human malaria species responsible for the spread of malaria from person to person which is facilitated by the *Anopheles* mosquito vector when taking a blood meal. Recently, human cases of malaria caused by *Plasmodium knowlesi* (*P. knowlesi*), the malaria-causing parasite species among monkeys, have also been recorded; however, this is currently thought to only be spread through zoonotic transmission.^[1] Of the protozoan parasite species infective to humans, *P. falciparum* and *P. vivax* present the greatest challenge to public health, contributing to the majority of malarial infections.^[4] *P. falciparum* however, has long been recognised as the deadliest of the parasite species due to its high mortality rates and significant prevalence within sub-Saharan Africa.^[1,5] Conversely, *P. vivax* has much lower incidence levels and very low transmission rates in African countries but has a much broader geographical distribution due to its ability to survive in cooler climates, compared to *P. falciparum*, and develop in the *Anopheles* mosquito at lower temperatures.^[5] *P. vivax* is therefore a substantial cause of morbidity in countries outside of African regions.

As well as the direct cost to health, malaria poses a huge economic burden, particularly in countries where the disease is endemic. Malaria is both a cause and a consequence of poverty,^[6] slowing economic growth and development in already underdeveloped regions which drives the vicious cycle of poverty primarily affecting the poor living in malaria-prone, rural areas where there are often few barriers against mosquitoes and malaria transmission.^[7] In African countries, malaria accounts for 40% of total public health expenditure placing a huge burden on health systems. Since 2001, malaria infection in these countries is estimated to be responsible for an annual cost of almost US\$300 million in case management (diagnosis and treatment of infection) alone.^[1] However, estimates predict that annual investments in malaria control and elimination will need to increase by US\$6.4 billion per year before 2020 if the goal of a 40% reduction in malaria incidence and mortality are to be met, as outlined by the *World Health Organisation* (WHO) within the proposed global technical strategy for malaria 2016–2030.^[1]

The intensity of malaria transmission is dependent on a number of factors including: the *Plasmodium* parasite, the mosquito vector, the human host and the specific environment within which these components are combined. Malaria transmission is often more intense in areas where the mosquito is long-lived due to increased parasite development within the mosquito. Insecticides are often used as methods of malarial vector-control however, increasing selective pressures have led to insecticide

resistance, particularly to the chlorinated hydrocarbon insecticide DDT (**Figure 1.2**),^[8] allowing the development of long-lived mosquitoes.^[9] It is therefore a combination of the long life span and strong human-biting habit of the African *Anopheles* mosquito vector which means 90% of the world's malaria deaths occur in Africa.^[1]

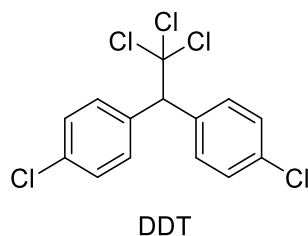


Figure 1.2 Chemical structure of the insecticide 1,1'-(2,2,2-trichloroethane-1,1-diyl)bis(4-chlorobenzene) (DDT).^[8]

Malaria transmission is also dependent on climatic conditions, such as rainfall, temperature and humidity, which affect mosquito population sizes and make transmission seasonal with peaks during and just after the rainy season. The extent of malaria transmission and the risk of epidemics depends on levels of human immunity as well as climatic environment. Partial immunity can be developed over years of exposure to malaria but this doesn't provide full protection against malaria infection or disease development. It is largely for this reason that children under the age of five are particularly at risk to infection since they have little opportunity to develop immunity and also lose maternal immune protection around 18 months of age. Of the estimated 584,000 worldwide malaria deaths in 2013, 78% of these were in children under five years of age.^[1] In addition, 20% of all child deaths in sub-Saharan Africa are due to malaria which remained the leading cause of death amongst this patient group in African regions between 2000 and 2015.^[1] Consequently this highlights the huge paediatric-specific mortality burden of malaria. Pregnancy is also a severe risk factor for contracting malaria and developing a severe form of the disease where pregnant women are three times more likely to contract malaria than non-pregnant woman and have a mortality rate close to 50% from severe malarial infection.^[10] Other groups at high risk of contracting malaria include patients with HIV (human immunodeficiency virus) or AIDS (acquired immune deficiency syndrome), non-immune travellers and mobile populations.^[1]

Malaria is an acute febrile disease from which symptoms are most likely to occur 10-15 days after an infective mosquito bite^[1] since asexual reproduction of *Plasmodium* parasites within human red blood cells (RBCs) (**Section 1.2**) is responsible for the clinical manifestations of the disease and its associated symptoms. Initial malaria symptoms are comparable to those of flu and can therefore be hard to recognise since they include fever, headaches, muscle aches, chills and vomiting and may be

mild.^[1] Such symptoms, with no signs of clinical severity or organ dysfunction, generally suggest a case of uncomplicated malaria which can be caused by all strains of *Plasmodium*. However, *P. falciparum* infection, the most prevalent and more severe of the *Plasmodium* infections, can rapidly progress to a severe form of the disease if not treated quickly.^[11] Severe malaria (or complicated malaria) occurs when untreated *P. falciparum* infection results in organ failure or blood abnormalities as a consequence of parasitic waste expulsion from erythrocytes, cytokine release and RBC sequestration^[12] during the asexual RBC stage of infection. Clinical manifestations of severe malaria include anaemia, hypoglycaemia (more severe amongst children), ketoacidosis, acute respiratory distress syndrome (ARDS) and kidney failure which, without rapid treatment can lead to death.^[13] Headaches, confusion and irritability may also proceed cerebral malarial, a further manifestation of severe malaria caused only by *P. falciparum* infection, which can proceed quickly to more severe cerebral symptoms such as coma, particularly in the cases of non-immune children.^[12]

1.2 Life Cycle of the *Plasmodium* Parasite

The life cycle of the *Plasmodium* parasite is highly complex, requiring specialised mechanisms to invade multiple cell types within the defence systems of both the human host and *Anopheles* mosquito vector.^[14] The life cycle of the malaria parasite (**Figure 1.3**) involves a sexual stage which takes place in the female *Anopheles* mosquito and an asexual stage which occurs in the human host. For this reason, it can be considered that humans are not the “definitive host” of *Plasmodia* since the *Anopheles* mosquito provides the site of sexual reproduction for *Plasmodia* parasites. From a parasite perspective, humans provide the means of accessing *Anopheles* mosquitoes where sexual recombination can occur but from the human perspective: the *Anopheles* mosquito is the vector by which *Plasmodial* malaria transmission occurs.^[15]

The bite of an infected female *Anopheles* mosquito transmits sporozoites, the infectious asexual forms of the parasite, from mosquito salivary glands to the human host during blood extraction when the mosquito takes a blood meal.^[16] Sporozoites swiftly enter human hepatocytes after inoculation into the blood where they begin pre-erythrocytic development in which multiplication occurs over 10-14 days in the human liver stage of the disease (**Figure 1.3**).^[17]

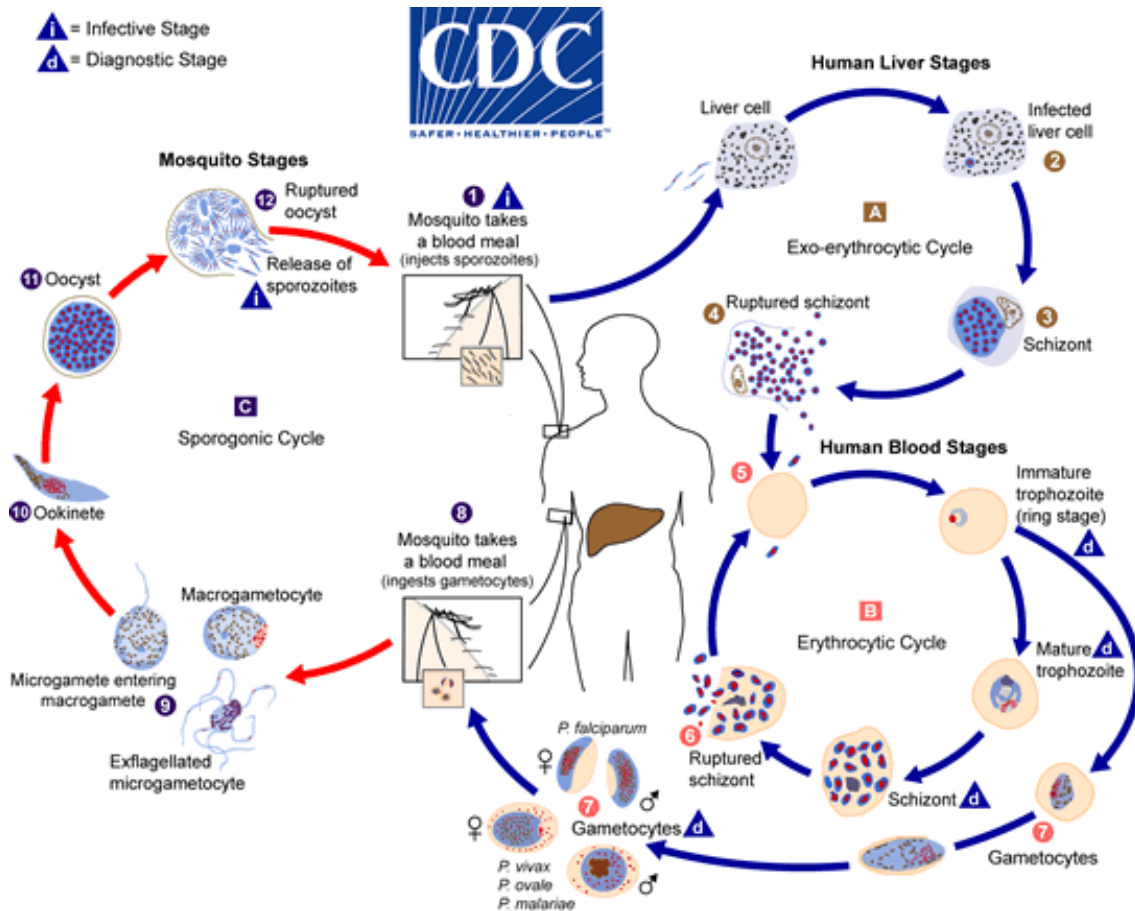


Figure 1.3 The *Plasmodium* life cycle: figure is reproduced from the Centre for Disease Control and Prevention (CDC).^[13]

Sporozoites, known during the liver stage as schizonts, are able to remain concealed from the host's immune system during occupation of hepatocytes. Schizonts, containing thousands of hepatic merozoites, are then liberated from the liver following rupture of parasitized liver cells. This releases the merozoites which initiate erythrocytic infection through invasion of host RBCs in the human blood stage of the life cycle (**Figure 1.3**).^[18] Intracellular development of these merozoites within the erythrocyte, from immature trophozoites (ring stage) into motile parasitic entities (mature trophozoites) allows further evasion of the human host immune system.^[17] To achieve rapid development, the parasite digests large amounts of erythrocyte haemoglobin (Hb) using aspartic proteases which degrade between 25-85% of total Hb from host RBCs. Degraded Hb is transported to the parasite food vacuole where the obtained amino acids are used for parasite growth and maturation.^[19]

A mature trophozoite can undergo mitosis, differentiating to release merozoites and gametocytes upon rupture of the red blood cell. New merozoites can then bind to and enter uninfected red blood cells causing magnification of the parasitic infection. The smaller fraction of gametocytes released on

cell rupture are able to complete the sexual stage of the parasite life cycle once re-ingested by the *Anopheles* mosquito when another blood meal is taken (**Figure 1.3**).^[18] Erythrocyte rupture releases cell debris, parasite waste and infectious parasitic material into the human bloodstream which causes many of the observed clinical symptoms of malaria (**Section 1.1**).^[16] In severe cases, death can occur within 48 hours of symptom presentation, corresponding to one asexual cycle of the *P. falciparum* blood-stage infection. This highlights that preventing maturation of early generation parasites into mature, more pathogenic parasite forms is essential in fighting malaria infection.^[3]

P. vivax has a slightly different life cycle to *P. falciparum* within the human host as some sporozoites in *P. vivax* infections do not develop immediately schizonts within the liver stage. Unlike *P. falciparum* infections, where schizonts exit hepatocytes after one cycle of the human liver stage, schizonts of the *P. vivax* species are able to remain as silent single nuclear hypnozoites within hepatocytes over variable and extended time periods. Reactivation of these dormant parasitic forms, a consequence of unknown factors, produces further hepatic development weeks, months or years after the primary *P. vivax* infection, producing an exoerythrocytic multiplication cycle recognised as the 'liver-form' of the disease.^[18,20] Treatment of *P. vivax* infections can therefore be difficult due to the potential for disease recurrence following initial infection. Consequently, *P. vivax* also poses a significant public health threat across many parts of the world, with estimations suggesting that this *Plasmodium* species was responsible for 13.8 million cases of malaria worldwide in 2015, which amounts to approximately half of the total malaria cases outside of sub-Saharan Africa.^[1] Unlike *P. vivax*, *P. falciparum* parasites have no exoerythrocytic or 'liver-persistent' stage therefore highlighting the requirement for different treatment regimens and chemotherapeutic intervention methods to treat these two parasite species.^[16]

1.3 Malaria Control and Elimination Strategies

1.3.1 Vector Control

Vector control is an essential component of successful malaria control and reducing malaria transmission rates. However economic, administrative and logistical issues often hinder the potential reductions in global malaria burden that could be achieved using these preventative methods.^[21] Of the different strategies available, indoor residual spraying (IRS), insecticide-treated nets (ITNs) and preferentially, long-lasting insecticidal nets (LLINs)^[1] are the most effective forms of vector control that can be used in a wide range of circumstances and are therefore fundamental in protecting individuals at risk of contracting malaria.^[21,22] Early use of the organochloride insecticide, DDT (**Figure 1.2**) highlighted the proficiency of insecticides in dramatically reducing mosquito vector numbers and therefore reducing transmission rates. However, selective pressures led to insecticide

resistance and have consequently enabled the development of long-lived mosquitoes.^[9] In recent decades, pyrethroid insecticides have been the choice chemical for malaria vector control and are currently the only insecticide recommended by the WHO for use on ITNs or LLINs. However, upscaling malaria vector control and increased use of these insecticides within agriculture has seen the development and spread of resistance against pyrethroids.^[22] New insecticides are therefore urgently needed if this method of malaria vector control is to remain effective.

Considering other forms of vector control, upscaling LLIN distribution through mass distribution campaigns have resulted in approximately 49% of households in sub-Saharan Africa owning at least one ITN by the end of 2013, compared to only 3% in 2004.^[22] The public health impact of this form of vector control is substantial: ITNs have been found to reduce the incidence of malaria cases in field trials by more than 50% and reduce malaria mortality rates in sub-Saharan Africa by an estimated 55% in children under five years of age.^[1]

1.3.2 Antimalarial Chemotherapies

Whilst vector control methods can provide effective means of reducing disease transmission and the numbers of individuals contracting malaria, it is drug chemotherapy that has provided the most successful methods for the treatment and prevention of malaria infection.^[23] Over the last century, a broad range of antimalarial treatments have been developed and administered as part of several malaria eradication campaigns which have achieved varying amounts of success.^[24] Whilst a number of antimalarial chemotherapies have been significant in the progress and successes of malaria treatment and eradication efforts, chloroquine and artemisinin can perhaps be considered the most fundamental of these. A brief account of their identification, administration and subsequent impacts are presented below.

1.3.2.1 Chloroquine: Identification, Application and Resistance Development

The natural product quinine (**Figure 1.4**) was first isolated from the bark of the cinchona tree (*Cinchona calisaya*), native to South America, in France in 1820. The use of cinchona bark, a rich source of medicinal alkaloids, was used to treat malaria throughout the 17th century by Jesuit missionaries in Peru. However, it was only after successful extraction of the compound that the superiority of the pure alkaloid as an antimalarial agent was fully realised.^[4,25] It was a fortuitous discovery by the German chemist, William Henry Perkins, in 1856 whilst attempting to synthesise quinine that identified the first aniline dye, mauveine. This discovery launched the development of the synthetic dye industries which swiftly led to the birth of the pharmaceutical industry, in turn facilitating the production of the first synthetic antimalarial agents including chloroquine, mepacrine

(also known as quinacrine) and primaquine (**Figure 1.4**). These synthetic agents, belonging to the 4-aminoquinoline and aryl aminoalcohol chemical classifications, exert their antimalarial effects by interfering with the process of haem polymerisation.^[24] The efficacy demonstrated by these synthetic quinine derivatives meant they were able to replace the use of quinine itself, becoming the foundation of antimalarial chemotherapy over the next two decades.^[4,16]

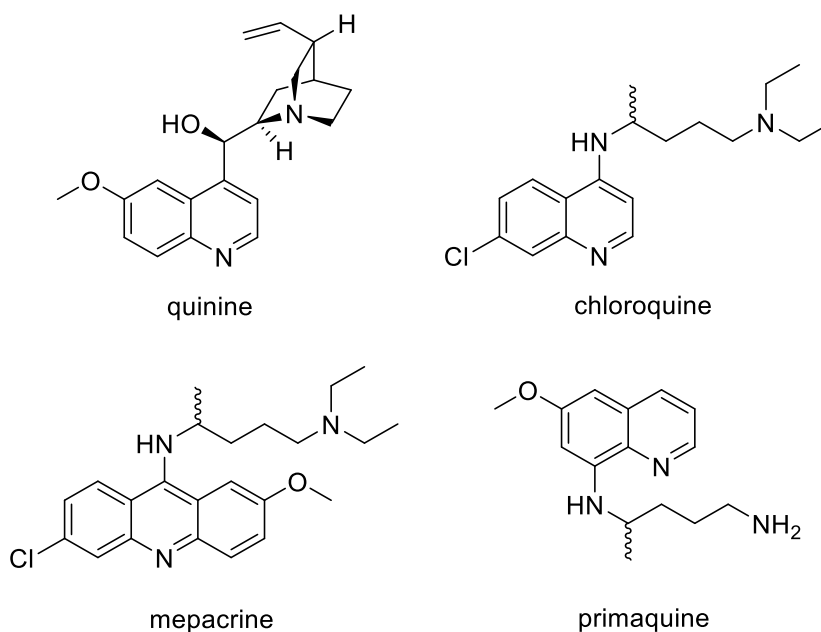


Figure 1.4 Chemical structures of the natural product quinine and early synthetic antimalarials: chloroquine, mepacrine and primaquine.^[16]

The 4-aminoquinoline, chloroquine, is probably one of the most successful and important chemical entities ever developed against an infectious disease.^[26] Chloroquine was discovered in 1934 and became available as an antimalarial treatment in 1946 remaining highly effective as a front-line malaria chemotherapy throughout the mid-1900s. A combination its high clinical efficacy, low toxicity within the human host and affordable synthetic route made chloroquine a significant chemotherapeutic which had a huge impact in malaria therapy, saving thousands of lives and substantially reducing morbidity and mortality from the disease.^[27] It is thought that the efficacy of chloroquine stems from its ability to disrupt haematin detoxification in *Plasmodium* parasites as they mature within host erythrocytes, causing fatal toxic effects towards parasite enzymes.^[26] It is generally accepted that chloroquine binds to ferriprotoporphyrin IX (FPIX), a Hb degradation product that is toxic to the parasite in high concentrations and released as the parasite digests host Hb within its food vacuole.^[28] Under normal conditions, FPIX is detoxified by the parasite through crystallisation into inert, non-toxic crystals of haemozoin to maintain unhindered parasite growth. Treatment with chloroquine leads to parasite death due to the parasites consequent inability to

complete this natural haem detoxification process following chloroquine-FPIX binding and the resulting accumulation of toxic FPIX.^[26,28]

Ultimately, the initial high success rates of chloroquine in reducing global morbidity and mortality from malaria, and its consequent heavy use across the decades, has led to the development of chloroquine resistance in *P. falciparum* and *P. vivax* parasite species.^[26] Therefore, despite the early success of chloroquine and its significant contribution to the 1955 WHO malaria eradication programme, its potent antimalarial efficacy is now significantly reduced following the emergence of resistant parasite strains in 1957, first documented at the Cambodia-Thailand border. Continued resistance development from then onwards means that today, more than 80% of wild-type *Plasmodium* isolates are resistance to chloroquine.^[16]

A single genetic mutation can be all that is required to impart resistance to antimalarial chemotherapies, or indeed any anti-infective agent, if mutation occurs within the molecular target of a specific chemical agent.^[3,29] Such is the case with the antimalarial agents: pyrimethamine and atovaquone (**Figure 1.5**). Pyrimethamine, introduced in the early 1950s for the therapy and prophylactic treatment of malaria, is a competitive dihydrofolate reductase inhibitor which impedes the synthesis of parasite DNA and proteins.^[3] Atovaquone belongs to the chemical family of naphthoquinones and operates its antimalarial effects through inhibition of cytochrome *b* (*cytB*) which is essential for maintaining a functional electron transport chain.^[24] *Plasmodium* resistance to pyrimethamine can be induced by a single point mutation in the gene encoding dihydrofolate reductase (*dhfr*) which has been found to emerge relatively frequently in the human malaria *P. falciparum* parasite.^[3,26,30] Similarly, a single point mutation in the gene encoding cytochrome *b* (*cytB*) is able to confer resistance to atovaquone.^[16]

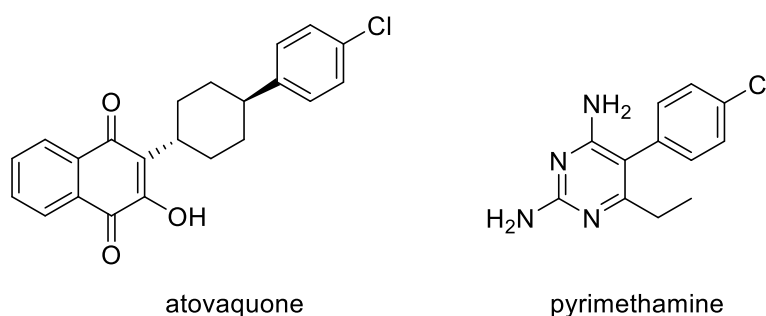


Figure 1.5 Chemical structures of antimalarials atovaquone and pyrimethamine.^[24]

In contrast, chloroquine resistance appears to involve higher genetic complexity than pyrimethamine resistance since resistance to chloroquine took a number of years to develop within initially limited foci and requires multiple mutations in the *Plasmodium* chloroquine resistance

transporter gene (*PfCRT*) to arise.^[26] The Lys276Thr mutation in the parasite genome encoding the gene product *PfCRT* is principally responsible for chloroquine resistance. *PfCRT* is a transmembrane transport protein present in the digestive food vacuole of *Plasmodium* parasites. However, a genetic background where the parasite carries additional mutations within the same gene is also required to infer resistance development against chloroquine.^[31,32] The mutated form of the *PfCRT* transporter protein is able to reduce chloroquine accumulation in the parasite food vacuole where haem polymerisation occurs therefore reducing inhibition of parasite detoxification since chloroquine is unable to accumulate.^[24] In Malawi, following a halt in chloroquine use over the last 15 years, a recovery in chloroquine sensitivity has been observed. This suggests that the identified Lys276Thr mutation also confers a fitness disadvantage to *Plasmodium* parasites when this *PfCRT* gene mutation is present with the absence of drug pressure.^[33,34] However, as Malawi is surrounded by countries where high levels of chloroquine resistance remain, re-introduction of chloroquine treatment is not an option.^[32] This highlights the continued risk of resistance resurgence if these early antimalarial chemotherapeutics remain as front-line antimalarial agents within a number of limited treatment options due to failures to replace expended drugs with new malaria therapies that act against novel molecular targets.

1.3.2.2 Artemisinin: Identification, Application and Resistance Development

Comparable to the botanical origins of quinine, sweet wormwood *Artemisia annua* has been used in Chinese medicine, dating back over two millennia for the treatment of febrile illness.^[4] It wasn't until the late 1960s when the Chinese government supported a research programme to identify antimalarial agents from known Chinese herbal medicines that the synthetic development of artemisinin began.^[4,35] Following the extraction of artemisinin (**Figure 1.6**) from the leaves of *Artemisia annua*, it was in the 1970s that the structure of this 15-carbon (sesquiterpene) peroxide, with its powerful, if unstable, antimalarial properties was identified and characterised. The development of semi-synthetic analogues soon followed demonstrating both increased potency and improved bioavailability than artemisinin, helping to remove initial scepticisms regarding the unusual structure of this new chemical entity.^[4,32]

Chemical exploration of semi-synthetic artemisinins was ongoing throughout the mid-1970s leading the development of artemether, a more stable methyl-ether derivative; artesunate, demonstrating improved water-solubility; and dihydroartemisinin (DHA), the active component of both artesunate and artemether, highlighting their identities as pro-drugs (**Figure 1.6**).^[4,36] Ultimately, these chemical derivatives replaced artemisinin as the parent drug due to superior antimalarial activity profiles and improved compound stability. Despite initial use as monotherapies, it was gradually realised that

these treatments should be administered in combination with additional drug entities, analogous to anti-tuberculosis and anti-retroviral chemotherapies. This aimed to minimise the development of drug resistance in areas where malaria is endemic and chemotherapies must therefore be used in elevated frequencies that create high levels of drug pressure.^[36] Such artemisinin-based combination therapies (ACTs) yield enhanced parasite killing through careful chemical combination: the artemisinin component of ACTs rapidly kills the majority of parasitic organisms quickly reducing initial parasitemia; the combined partner drug, commonly characterised by a longer half-life, is then able to slowly eliminate remaining parasites.^[32] There is therefore a dual benefit to ACTs, not only in optimising the therapeutic effect, but also in protecting both treatment components of the combined therapy, minimising the risk of resistance development against either chemical component.^[32] Today, ACTs are the mainstay of chemotherapeutic intervention for the treatment of *P. falciparum* malaria across the globe.

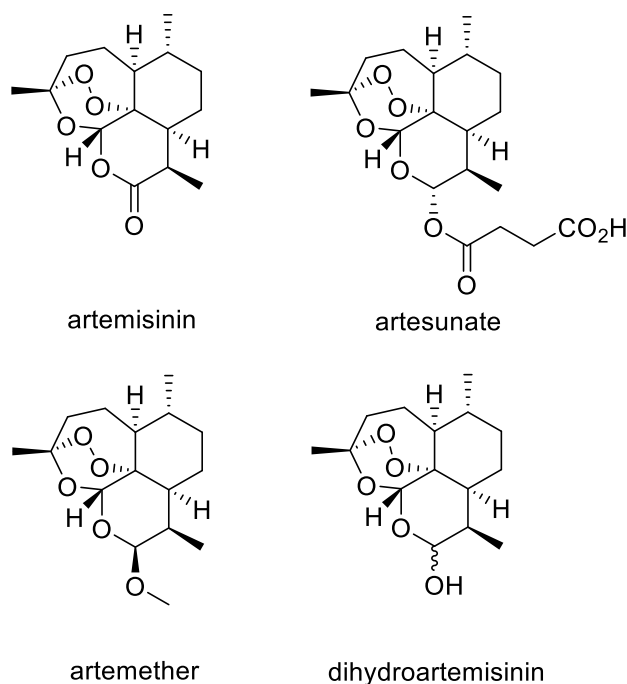


Figure 1.6 Chemical structures of artemisinins and related compounds. Artemisinin is the natural compound produced by the plant *Artemisia annua*; artesunate, artemether and DHA are semi-synthetic derivatives of the natural product.^[32,37]

ACTs were first introduced in the mid-1990s for the treatment of uncomplicated malaria infection.^[38] Since 2005, in nearly all countries where the disease is endemic, ACTs have been the recommended frontline therapies against malaria after a change in treatment policy endorsed by the WHO. This follows a decade of increased malaria treatment failure rates with the use of chloroquine (**Figure 1.4**) and sulfadoxine-pyrimethamine combinations (**Figure 1.5** and **Figure 1.8**) against *P. falciparum* infections.^[32] Sulfadoxine prevents folate biosynthesis through the inhibition of dihydropteroate

synthase (DHPS). Sulfadoxine is typically used in combination with pyrimethamine where this combination has been one of the widest used antimalarial chemotherapies, proven to deliver high efficacy as a prophylaxis and curative treatment. Today, clinical resistance to antifolate treatment is widespread but, remarkably, the administration of sulfadoxine-pyrimethamine is still seen to improve the outcomes of treatments in pregnant women when used as an intermittent preventative therapy.^[24]

Not only do artemisinin derivatives have an excellent safety profile, demonstrate high potency and display a rapid onset of action, but they are also show broad-stage specificity of action compared with other antimalarial agents, demonstrating activity across several stages of the *Plasmodium* spp. life cycle.^[32,36,38] In addition, artemisinins are capable of killing immature and developing gametocytes therefore signifying activity against the sexual stages of the *Plasmodium* spp. life cycle which gives these chemotherapies added value in their ability to reduce malaria transmission and infectivity.^[32] Current recommendations for treating malaria are consequently a three-day course of ACTs with varying drug partner combinations. Indeed, over the last half-decade, five different combinations of fixed-dose ACTs have been approved for use and administration. These include: artemether-lumefantrine, artesunate-amodiaquine, DHA-piperaquine, pyronaridine- artesunate and artesunate-mefloquine.^[39] Further discussion concerning the rationale, design and potential advantages of drug combination therapy is contained within **Chapter 5** (see **Section 5.3**).

There has been much debate regarding the mechanism of action by which artemisinins exert their robust parasite killing effects. Interestingly, like quinolones, artemisinins appear to target the parasite Hb degradation pathway by which parasites obtain amino acids from human host erythrocytes to facilitate growth and maturation during blood-stage infection.^[4] More specifically, it is the endoperoxide bridge, an unusual feature of the 1,2,4-trioxane structure, that distinguishes artemisinin and its derivatives and is responsible for the high potency of these antimalarial agents.^[36]

The endoperoxide bridge is a known source of oxygen free radicals and it has been observed that artemisinin derivatives lacking this structural feature are devoid of antimalarial activity. Unbound ferrous haem, Fe²⁺, released during haemoglobin degradation is thought to be the catalyst responsible for activating artemisinins *via* reduction of the endoperoxide bond. As a result of reduction by ferrous haem, the activated artemisinin structure undergoes rearrangement forming a carbon-centred radical species, which is capable of eliciting parasite-killing effects.^[4,36] Artemisinins therefore behave quite differently from other oxidant drugs, such as pirfenidone (an antifibrotic drug)^[40] and flavonoid antioxidants^[41], which often produce large quantities of oxygen free radicals.^[36] Whilst the importance of this initial endoperoxide bond reduction is widely accepted, the

subsequent downstream processes and specific mechanisms of parasite-killing have long been debated.^[4]

It is most likely that artemisinin derivatives exert their antimalarial effect at more than a single biological target and it is therefore reasonable that a generalised, two-step mechanism of action can be assumed.^[42] In the initial step, haem-mediated activation of artemisinin-based compounds produces carbon-centred free radicals and electrophilic alkylating species which are able to target specific proteins in the parasite. However, it is worthy to note that these electrophilic artemisinin species, unlike other alkylating agents, do not react with DNA.^[37] Instead, these reactive components operate in a number of ways: causing membrane damage in the vicinity of vital parasite enzymes, inducing lipid peroxidation, inhibiting parasites enzymes and linked biological processes and disrupting haem detoxification.^[37,42] Further to this, it has been outlined by *Krishna et al.* that the *P. falciparum* orthologue PfATPase6, the sarcoplasmic/endoplasmic reticulum calcium adenosine triphosphatase (SERCA), represents a key alkylation target of reactive artemisinin species.^[36,42,43] Collectively, these mechanisms compromise parasite viability which ultimately leads to parasite death.^[44]

Despite the high success rates of ACTs, which remain the recommended treatment for uncomplicated *P. falciparum* malaria infection and have substantially reduced global morbidity and mortality from malaria,^[1] continued progression of malaria elimination is again significantly threatened by resistance emergence against these therapies.^[38] Artemisinin resistance became established in western Cambodia more than a decade ago and is now prevalent across an ever expanding area of southeast Asia.^[45] These increasing levels of parasite resistance are characterised by slow parasite clearance rates following artemisinin-based treatment^[46] which is the consequence of a reduction in the susceptibility of ring-stage parasites to drug treatment.^[47] This is ultimately reflected in the increased ACTs failure rates, seen in both Cambodia^[48] and Thailand.^[49] Artemisinin resistance is developing in the same loci, the Thai-Cambodia border, that reared resistance development to the early mainstays of antimalarial treatments including: chloroquine, sulfadoxine-pyrimethamine and mefloquine (**Figures 1.4 and 1.5**).^[50] A combination of prevalent artemisinin monotherapies and poor-quality ACTs, sub-therapeutic dosing and the unregulated use of such agents in poorly developed economic regions of the world, in addition to logistical administration difficulties, are all factors contributing to the development and spread of artemisinin resistance.^[38]

Numerous studies have been conducted to determine molecular markers of resistance and the key determinants of parasite resistance to artemisinin therapy which is now prevalent across Southeast Asia.^[3,15,16,32,37-39,45-50] Most recently, studies have shown that *P. falciparum* resistance to artemisinin

is closely associated with mutations altering the propeller region of a kelch protein, encoded by *kelch13*. A single nucleotide polymorphism (SNP) within *kelch13*, referred to as K13, which causes up-regulation of unfolded protein response pathways, has been found as a determinant of artemisinin resistance and is consistently identified with a delayed and slow-clearance phenotype: a key indication of artemisinin resistance.^[38,45] In further research conducted by Dogovski *et al.* K13 has been linked with enhancing a stress response with the cell which leads to a delayed onset of cell death in resistant parasites that exhibit low levels of ubiquitinated proteins as a consequence of the K13 resistance mutation.^[51] However, it is worth considering that whilst artemisinin resistance is now prevalent across many areas of Southeast Asia and has the undeniable capacity to spread further, eroding treatment successes to date, *Plasmodium* resistance to artemisinin-based therapy does not yet amount to clinical failure.^[52]

In addition to increasing artemisinin treatment failure due to rapidly developing *Plasmodium* resistance, artemisinin and its derivatives also suffer from short *in vivo* half-lives, the requirement for combination treatment regimens and difficulties with synthesis and plant-derived extraction. As a result, much research has focused on the development of novel and completely synthetic endoperoxides, based around the 1,2,4-trioxane pharmacophore, with the aim of retaining potent antimalarial activity against *P. falciparum* and *P. vivax*, whilst exhibiting a good safety profile and improved synthetic tractability.^[24,53]

Development of these synthetic peroxides (or ozonides) perhaps represents one of the best examples of a directed chemistry-based approach that took the chemical structure of a known antimalarial drug, developing SAR around the specified chemotype, to yield new chemical agents with superior antimalarial activity and pharmacology which function as new clinical compounds.^[54] Subsequent ozonide derivatives retained the endoperoxide bridge, known to give artemisinin its potent blood-stage activity, but also included a bulky amantadine ring, to increase compound stability in plasma. The first-generation synthetic peroxide OZ277 (**Figure 1.7**), was the first ozonide to be evaluated in the clinic but did not demonstrate full efficacy in patients after seven days of treatment.^[54]

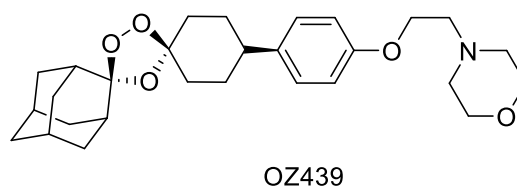
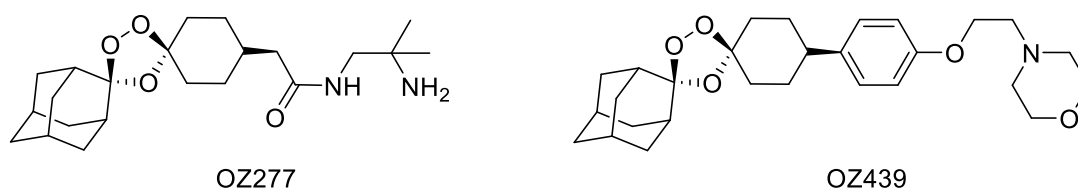


Figure 1.7 Chemical structures of synthetic endoperoxides: OZ277 and OZ439.^[53]

OZ439 (**Figure 1.7**) is a second generation ozonide that demonstrates potent antimalarial activity with both a superior pharmacokinetic and efficacy profile than its predecessor OZ277. OZ439 is fast-acting against all *P. falciparum* blood stages *in vitro* and exhibits prolonged blood concentrations due to designed stabilisation of the pharmacophoric endoperoxide bond.^[53] Since OZ439 has been shown to completely cure *Plasmodium berghei* (*P. berghei*) infected mice with a single 20 mg per kg dose, it is feasible that compounds in the OZ439 chemical series have the potential to provide single-dose antimalarial therapy in humans.^[24,53] However, because ozonides are close structural variants of artemisinins where activity results from the endoperoxide bridge; these synthetic derivatives are also only active against blood-stages of malaria, causing concerns that reduced efficacy may be seen against artemisinin resistant parasites.^[54]

1.3.2.3 New Antimalarial Drugs with Novel Mechanisms of Action Are Needed

A range of chemotherapeutics, spanning a number of pharmacophores, have been identified and optimised over the years: the 4-aminoquinolines, such as amodiaquine and chloroquine; the structurally related 8-aminoquinolines: primaquine and tafenoquine; quinine derivatives including mefloquine and lumefantrine; antifolate drug combinations such as sulfadoxine-pyrimethamine; naphthoquinone compounds such as atovaquone and antibiotics including ciprofloxacin and rifampicin, are to name a few (for representative examples, see **Figure 1.8**).^[16,24] These agents work by diverse mechanisms of action and have been administered in varying treatment regimens, as part of a number of malaria eradications campaigns, all with varying success rates.^[24] However, many of these chemotherapies have now been withdrawn or their administration greatly reduced due to the rise of *Plasmodium* resistance against each drug. Considering all of the examples of malaria treatment loss witnessed, resistance development to specific drugs has occurred at varying rates and across different loci where ultimately resistance has continued to spread and is currently tracked by increasing rates of morbidity and mortality from malaria infection.

This well-known cycle of drug identification, global administration and clinical success, swiftly followed by *Plasmodium* resistance development, increased recrudescence rates and treatment failure, continues to plight and compromise successful malarial treatment and the possibility of disease eradication. The vast history of antimalarial chemotherapies has been well reviewed and documented by many researchers and public health organisations which are summarised in the following publications.^[1,3,4,6,15,16,24,28,29,35,37,39,42,50,54–58] Current antimalarial therapies are based on a handful of established antimalarial drugs, spanning only a few chemical chemotypes, with limited novel drugs and drug combinations in advanced or early stages of clinical studies. Representative

examples of the most common antimalarials (**Figure 1.8**) highlights that the number of chemical chemotypes within current chemotherapy options is somewhat limited, consequently limiting diversity of the associated mechanisms of action by which antimalarial drugs are able to elicit their effects.^[16,24]

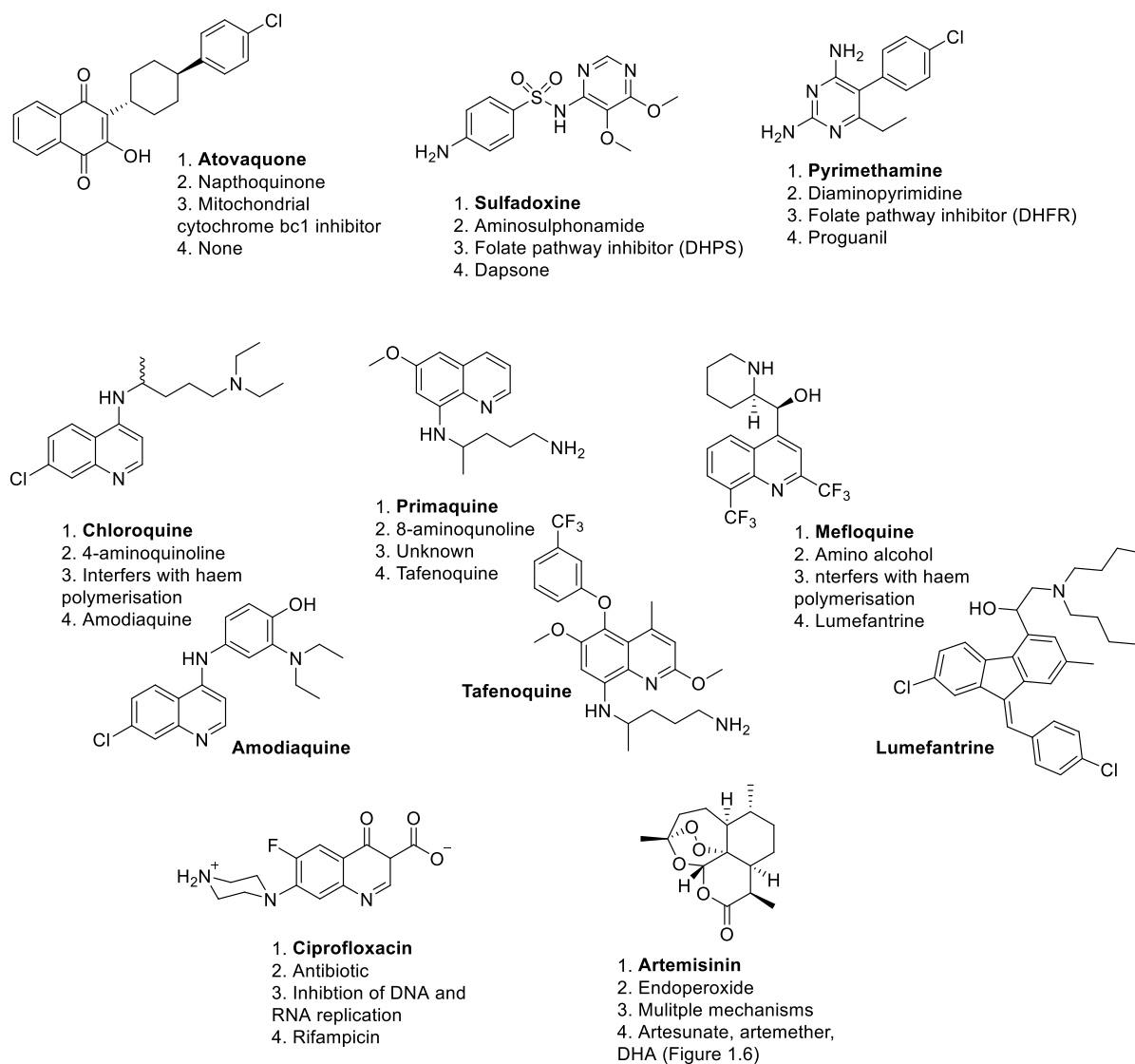


Figure 1.8 Representative compounds of antimalarial chemotypes and derivatives that are approved for clinical use; 1: Name; 2: Chemical family; 3: Mode of action; 4: Other drugs in the chemical family. Figure is adapted from ^[24].

1.4 Approaches to Antimalarial Drug Development

As highlighted by the current state of antimalarial chemotherapy and the known and challenging history of antimalarial drug discovery, it is clear that *Plasmodium* parasites are capable of developing drug resistance at unpredictable and varying rates against a wide range of structurally divergent chemotherapeutic motifs, which work by diverse mechanisms of action. There are global concerns that the efficacy of all current, and potentially pipeline, antimalarial agents will gradually erode. Consequently, there is urgent need to develop novel and inexpensive therapies that are effective in the treatment and prevention of malaria, enabling the replacement of current antimalarial agents against which resistance is growing.^[59] For this to be successful, replacement agents will need to display potent activity against new molecular targets and demonstrate chemical construct around novel chemotypes against which *Plasmodium* parasites have not yet developed resistance.

It can therefore be argued that researchers now face a single option: to adopt a united and two-pronged approach to continue and fortify antimalarial drug discovery efforts. In a collective effort to combat the growing levels of resistance against antimalarial agents, two research strategies should be conducted to drive progress towards improved antimalarial therapies and heighten clinical successes. Firstly, optimisation of ACTs and other currently available antimalarials (**Figure 1.8**) must be continued to prolong and maximise their efficacious lifespan. This approach requires the rational design of new antimalarial drug combinations using existing and available drugs, optimising ACTs regimens and minimising the use of monotherapies. The second arm of the attack needs to pursue research identifying new drugs that act against novel targets and can therefore gradually replace the current antimalarial therapies that are available.^[6,54,60]

Specific research priorities have been outlined which highlight: the development of front-line therapies for non-complicated *P. falciparum* and *P. vivax* malarial infections, drugs to treat severe malaria, drugs for intermittent preventive treatment (IPT) of highly at risk groups, chemoprophylaxis drugs for travel applications and anti-relapse drugs for the treatment of dormant liver-stage *P. vivax* infections, as those which should be most activity sought after.^[56]

A number of medicinal chemistry approaches can be utilised in the identification and development of novel antimalarial agents and new drug combinations. Optimisation of chemical scaffolds of known antimalarial drugs and chemotypes is one such approach and, as previously stated, should be used alongside complementary research to identify novel chemotherapeutic agents. However, continued remodelling and optimisation of known chemical motifs carries associated risks. Currently, no model antimalarial compound or pharmacophore possesses activity across all stages of the *Plasmodium* parasite life cycle so repurposing and compound ‘tweaking’ is perhaps unlikely to

generate a new compound series that could combat issues already faced. However, development of the synthetic ozonides, based on the 1,2,4-trioxane pharmacophore of artemisinin (**Figure 1.6** and **1.8**), provides an apt example of a compound class where a directed chemistry-based approach, modifying a known antimalarial structure, has proven highly successful (**Section 1.3.2.1**).^[54]

Another rational chemistry-based approach involves the design of hybrid molecules where two or more known chemical scaffolds are combined and incorporated within a single therapeutic agent. Such an approach aims to combine chemical functionalities and pharmacophores to create a more ideal molecule with optimised features, such as stability, solubility and potency, which are contributed from the combined entities.^[55] This strategy enables two distinct molecules, each with antimalarial activity, to be covalently linked producing a single hybrid molecule that displays dual activity.^[54] Although such an approach may be an interesting exploration of chemical biology and synthesis, the antimalarial effect of hybrid molecules may also be achieved using an appropriately designed combination therapy. There is also no guarantee that a resulting hybrid molecule won't display any of the chemical or pharmacological liabilities also possessed by component motifs.^[54]

The identification of natural products which harness potent medicinal properties and their subsequent development into powerful pharmaceuticals is another approach to new medicines and drug design that has been used through history. As previously discussed (**Section 1.3.2**), two of the most effective antimalarial drugs, artemisinin and quinine, were derived from natural herbal remedies originally used to treat fever in China and South America.^[4] Another example is atovaquone (**Figure 1.5** and **1.8**), a synthetic naphthoquinone, derived from the natural product lapachol, present in the bark of the pink Lapacho tree and therefore highlights another example of nature providing a chemical agent that is efficacious in the treatment of human disease.^[54] However, many of these herbal remedies have been used for centuries, predating both the chemical and pharmaceutical industries, often without extraction into their pure form and before their full chemotherapeutic potential was realised. It therefore seems unlikely that a similar development scenario will now emerge and progress from a known natural product to a new, currently unimagined antimalarial agent.

More likely, in this modern era of research, is that new therapeutic agents and methods of intervention will be sought, using the ever improving technologies that are at our disposal. A key example of this is the current and on-going research into malaria vaccine development. To date, vaccination remains the most effective method of preventing infectious diseases and represents a huge contribution to immunology. Therefore, much optimism for moving towards the goal of malaria eradication has recently focused on the development of a malaria vaccine.^[61] However,

vaccine development against the *Plasmodium* parasite is a huge challenge made no smaller by the fact that, even after multiple infections, adults in malaria-endemic regions only acquire partial resistance to malaria-causing parasites which is then gradually lost on lessening exposure.^[62] In total, three types of vaccine candidate, targeting different stages of the *Plasmodium* parasite life cycle have been investigated including: transmission-blocking vaccines (TBVs), pre-erythrocytic vaccines and blood-stage vaccines. The liver stage of *P. falciparum* is an attractive therapeutic target for the development of both oral antimalarial drugs and vaccines since it provides the opportunity to interrupt the parasite life cycle at an early stage, targeting the sporozoites which initiate hepatocyte infection.

Consequently, pre-erythrocytic vaccine development has progressed rapidly over the last decade with many vaccine candidates now targeting this stage of the parasite life-cycle. However, for a liver-stage vaccine to be efficient, it must be 100% effective in humans who possess no natural immunity.^[61] Malaria vaccines are species-specific; almost all of the 24 vaccines in the clinical pipeline target *P. falciparum*, with a single exception targeting *P. vivax*. The most advanced vaccine, Mosquirix, is the only vaccine in late-stage Phase III clinical trials and provides efficacy against malaria with 55% protection in children, but only 33% in infants.^[39] It is therefore clear that further improvement is required in malaria vaccine development; particularly as the mass scale administration of any malaria vaccine will face the added challenges of affordability, feasible dosage and implementation strategies, along with issue of global administration and distribution. However, these research efforts contribute to the vital discovery approach which pursues development of novel therapeutics using innovative and under-explored chemical intervention methods with the ultimate aim of replacing the sub-optimal antimalarial agents currently available.

Target-based drug discovery is a popular medicinal chemistry approach that has been used extensively and with great success throughout a huge number drug development programmes; this approach has identified many chemical agents with applications in a broad range of indications. Over the last 10 years and in terms of antimalarial therapies alone, target-bases screens have identified several therapeutic agents capable of effectively inhibiting malaria growth.^[59] Some of the most promising compounds identified by these methods include small molecule inhibitors of *P. falciparum* histone deacetylases (HDAC)^[63,64]; potent and selective biphenylamide and urea-based inhibitors of *P. falciparum* dihydroorotate dehydrogenase (DHODH), the rate-limiting enzyme within pyrimidine biosynthesis;^[65,66] and antifolate antimalarial compounds targeting *P. falciparum* dihydrofolate reductase (DHFR).^[67]

Molecular targets are typically cellular proteins with essential functions where their inhibition disrupts cellular processes and often leads to cell death. In the development of antimalarial chemotherapeutics, such molecular targets are selectively inhibited on the basis that they are essential for *Plasmodium* parasite viability. This is usually indicated when a molecular target is highly conserved across a species and is therefore likely to serve a specific cellular or metabolic function.^[54] Genetic knockout experiments can be used to genetically validate a molecular target and confirm that it is essential for an organism's viability. Chemical validation, confirming a molecular target is susceptible to modulation by a chemical, can also support the selection of a target for chemical inhibition studies. Some examples of chemically validated antimalarial targets include *P. falciparum* dihydrofolate reductase (DHFR), inhibited by antifolates such as pyrimethamine and proguanil (**Figure 1.5** and **1.8**) and *P. falciparum* cytochrome *bc1*, inhibited by atovaquone (**Figure 1.5** and **1.8**) which belongs to the chemical class of naphthoquinones.^[54] **Table 1.1** summarises the presumed molecular targets (or mechanism of action) of antimalarial compounds that were in preclinical and clinical development by the end of 2013.

Presumed molecular target or mechanism of action	Chemical or Product name	Chemical Class
Cytochrome <i>bc1</i>	ELQ-300 (Preclinical)	Quinolone-3-diarylether
PNP (purine nucleoside phosphorylase)	BCX4945 (Preclinical)	Immucillin G
Haemoglobin digestion	OZ277 (Preclinical)	1,2,4-trioxolane
	OZ439 (Phase IIa)	1,2,4-trioxolane
	RKA182 (Preclinical)	1,2,4,5-tetraoxane
DHFR (dihydrofolate reductase)	P218 (Preclinical)	Diaminopyridine
DHOD (dihydroorotate dehydrogenase)	DSM265 (Preclinical and Phase I)	Triazolopyrimidine
<i>PfCarI</i> (cyclic amine resistance locus protein)	KAF156 (Phase IIa)	Imidazolopiperazine
<i>PfATP4</i> (P-type ATPase 4)	KAE609 (Phase IIa)	Spiroindolone
Haemozoin formation	Ferroquine (Phase IIa)	4-aminoquinoline

Table 1.1 Summary of antimalarial compounds in preclinical and clinic development in 2013; table reproduced from ^[54].

As previously acknowledged, the high complexity of the *Plasmodium* parasite life cycle (**Section 1.2**) and its numerous interactions with both the human host and mosquito vector means there is an abundance of potential drug targets which have the capacity to be targeted and exploited in the treatment of malaria infection and transmission.^[4] However, as highlighted in **Table 1.1** and **Figure 1.8**, many of these potential targets remain un-explored, where only a handful of molecular targets

were utilised within preclinical and clinical trials that were ongoing in 2013. In addition, the therapeutic agents under investigation, as inhibitors of this limited range of targets, span only a small number of chemical classes. Several other drugs, including some 8-aminoquinolines and natural product extracts, were also in preclinical and Phase I clinical trials in 2013 however, the molecular targets of these agents remain unknown.^[54] Whilst greatly concerning, perhaps it is unsurprising that so few molecular targets have been identified when current antimalarial agents and those under development span limited chemical space. It is therefore essential that validated, novel parasite targets are identified against which, new and novel chemical drug classes can be found showing potent, and ideally broad-spectrum antimalarial activity.^[54]

The current global portfolio of antimalarial medicines (**Figure 1.9**), as provided by MMV, exemplifies the current state of play within antimalarial drug development and clinical evaluation. It is immediately clear that the majority of chemical agents and drug combinations in the later stages of development and approval are those that have been known to the research community for a number of years. Of the six available treatments which have reached post-development approval, all are familiar antimalarial drugs that have long been recognised as standard malaria treatments and which continuing research efforts are urgently attempting to replace. Whilst there are several ongoing research projects in the stage of lead optimisation, only a limited number of new therapies are in translational research; where a particularly limited number of therapeutic agents are currently in human clinical trials. This further highlights that few novel antimalarial drug targets have been identified, or are currently being utilised within drug discovery programs; representing a significant issue in antimalarial drug discovery that must be overcome in the fight to gain control over malaria.

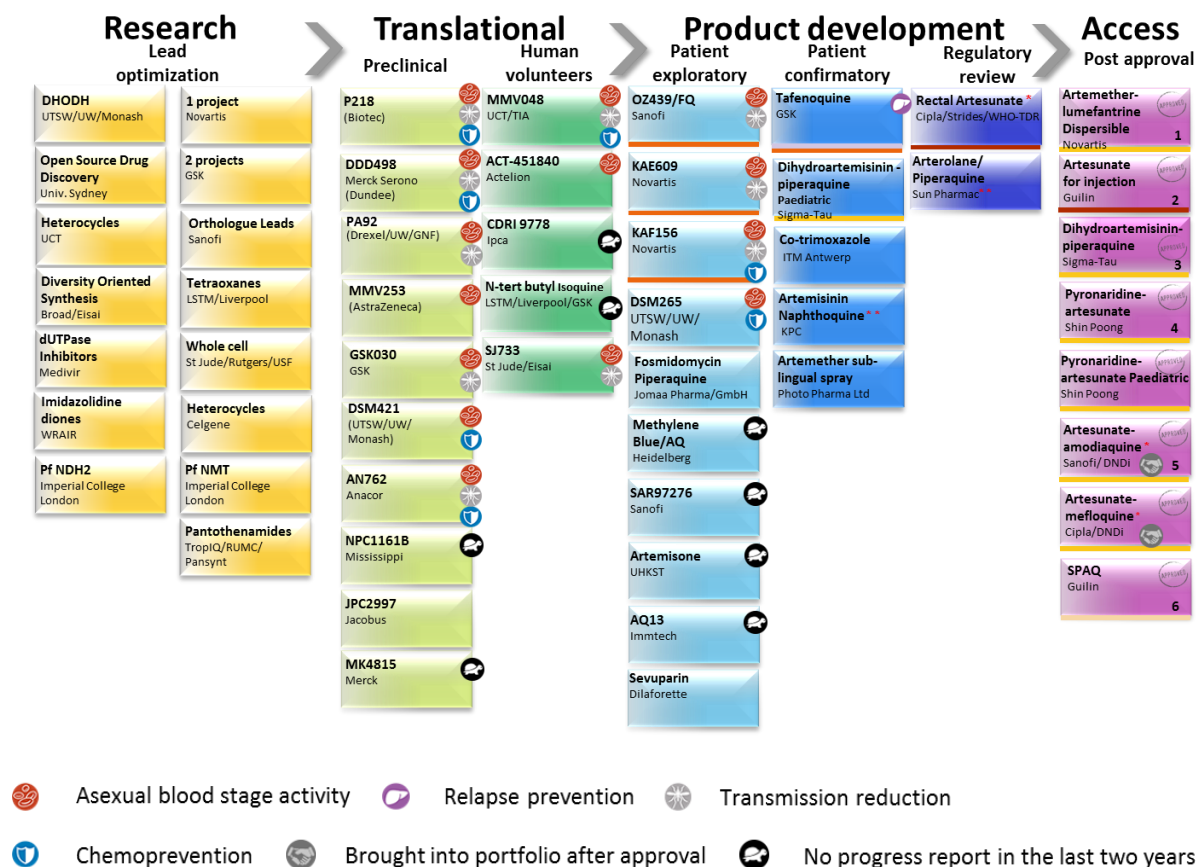


Figure 1.9 Global portfolio of antimalarial medicines, current as of 31 March 2016. Figure reproduced from [11].

In broader terms, the number of known molecular targets which are targeted, not only by antimalarials, but more generally by anti-infective agents is relatively small and remains in the 2-digit range.^[68] Consequently, the majority of potential therapeutic gene products that exist throughout infective organisms are not addressed by antibiotic agents currently available. This suggests that either a large number of molecular targets are still available for discovery in anti-infective therapy, or there is only a small sub-set of gene products that can actually be targeted within gene therapy. If the latter is the case, it is likely that the majority of viable gene products have already been discovered and are now utilised, explaining many of the anti-infective success stories over the last decade.^[68,69] Considering the anti-infective subgroup of *Enterobacteriaceae*, a large family of Gram-negative bacteria, including harmless symbionts and familiar pathogens such as *Escherichia coli* (*E. coli*); genome virulence studies have indicated that the set of potential gene products against which targeted therapies might be feasible is somewhat limited.^[68] However, an encouraging and optimistic outcome of these studies is that enzymes of the non-mevalonate (MEP) pathway, present within this Gram-negative bacteria family as well as in organisms outside this class and phylum,

appear prominent as gene products which have the potential to be successfully targeted in the development of new anti-infective agents.^[68]

1.5 A Novel Antimalarial Target: Isoprenoid Biosynthesis and The MEP Pathway

The identification, development and administration of new drugs will ensure there is a sustained pressure on the *Plasmodium* parasite, enabling us to get closer to achieving malaria eradication.^[60]

With such aims at the forefront of research, the pursuit of novel antimalarial compounds and new antimalarial drug targets has again intensified. As a result, the biosynthesis of isoprenoid precursors has emerged as a metabolic, chemical process that is sensitive to chemical manipulation and represents a promising candidate for the use of drug intervention against the malaria parasite.^[70–74]

The MEP pathway, responsible for the biosynthesis of essential isoprenoid precursors in *Plasmodium* parasites, therefore provides a rich source of potential targets which may prove crucial in the fight against malaria.^[75]

1.5.1 Isoprenoids

Isoprenoids represent the oldest and largest class of natural products and biomolecules, with over 35,000 distinct members identified in nature which span a highly diverse range of structures and functions.^[9,72,76,77] Isoprenoids are essential to all organism classes, including Apicomplexan protozoans and therefore *Plasmodium* parasites, since they play vital roles in many cellular and biochemical functions. Some key examples include: the synthesis of ubiquinone (an isoprene-containing quinone), in the mitochondria of *Plasmodium* parasites to facilitate energy generation in the electron transport chain; protein prenylation, an essential post-translational protein modification to enable subcellular protein regulation; the production of sterols to ensure cellular membrane stability; and the generation of photosynthetic pigments, hormones and plant defence compounds.^[76] Despite the divergent biochemical functions facilitated by isoprenoids, the biosynthesis of this highly diverse class of biological molecules requires only two universal five-carbon isoprene building blocks: isopentenyl pyrophosphate (IPP) and its isomer, dimethylallyl pyrophosphate (DMAPP), (**Figure 1.10**). Subsequent metabolic reactions and assembly of these basic units, generates the vast compound class of naturally occurring isoprenoids which show enormous diversity and complexity.^[71]

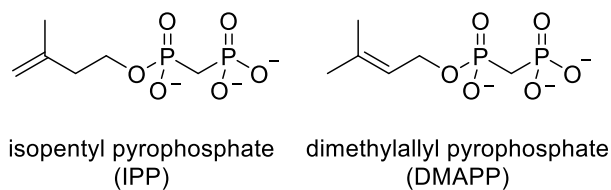


Figure 1.10 Chemical structure of isopentenyl pyrophosphate and dimethylallyl pyrophosphate.^[71,72]

The isoprenoid precursors, IPP and DMAPP, are novel compounds biochemically synthesised by all organisms which comprise the fundamental units for many downstream biochemical processes which may be specific to individual organisms. Isoprenoids are therefore essential for the survival and biological function of many cellular processes across species. In addition, isoprenoids also form the largest group of diverse secondary metabolites, such as plant defensive terpenoids, which have significant commercial importance in the pharmaceutical, food and fragrance industries.^[71]

It was initially thought that the synthesis of isoprenoid precursors was ubiquitous across all organisms and living systems however, it is now recognised that two distinct and independent routes to IPP and DMAPP biosynthesis exist.^[76] Mammals and fungi synthesise IPP and DMAPP through the well-studied mevalonic acid (MVA) pathway which proceeds through a Co-enzyme A (CoA) dependent route, *via* a key mevalonate intermediate.^[72,74,78] The MVA pathway has long been established as an important drug target since the development of statins^[68] for the treatment and prevention of cardiovascular disease; statins inhibit cholesterol biosynthesis, a highly abundant isoprenoid, with key functions in hormone production and regulating membrane fluidity.^[75] Statins as cholesterol-lowering drugs, target HMG-CoA reductase which is the rate-limiting enzyme of the MVA pathway.^[71]

In contrast eubacteria, archaebacteria, chloroplasts, plastid-containing eukaryotes, including *Plasmodium* parasites and other protozoa, synthesise IPP and DMAPP ubiquitously *via* the non-mevalonate pathway (also referred to as the 1-deoxy-D-xylulose-5-phosphate (DOXP) or the 2C-Methyl-D-erythritol 4-Phosphate (MEP) pathway), which is independent of mevalonic acid.^[75] Some notable exceptions include Gram-positive bacteria, such as staphylococci and streptococci, which have retained the MVA pathway for the biosynthesis of isoprenoid precursors.^[71] In contrast to mammals and organisms utilising the MVA pathway, *Plasmodium* parasites are incapable of synthesising sterols, relying instead on scavenging these compounds, such as cholesterol, from host systems.^[75] Because sterol synthesis is not a *de novo* biochemical process carried out by *Plasmodium* parasites, sterol production does not contribute to the biological importance of isoprenoid biosynthesis in parasites, where it is essential for eukaryotic membrane stability.

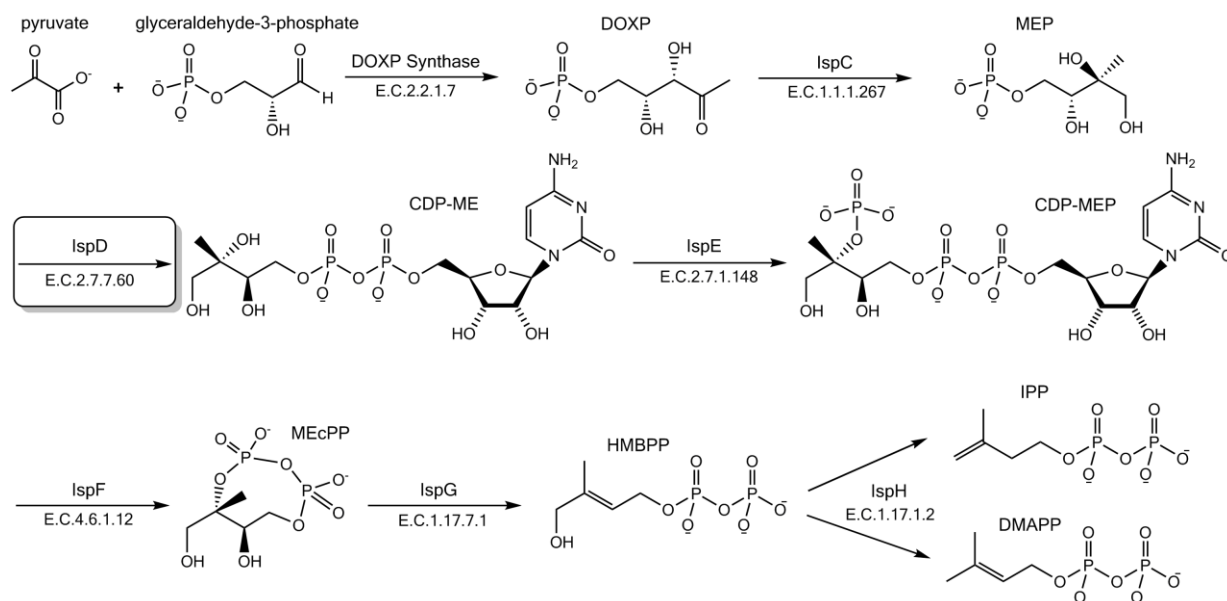
However, many other isoprenoids have functions which are essential for parasite survival and cannot be obtained through other means; this makes their generation dependent on the synthesis of IPP and DMAPP *via* the MEP pathway.^[75] Examples include: protein prenylation, ubiquinone biosynthesis, the production of vitamin E and carotenoids; and the generation of dolichol for N-linked glycosylation, a post-translational protein modification required during intraerythrocytic parasite development.^[75] These diverse isoprenoid-dependent processes are essential for parasite development meaning that, inhibition of *Plasmodium* isoprenoid precursor biosynthesis would disrupt these essential processes, severely compromising parasite growth and survival.^[75] This therefore highlights the biological importance of the MEP pathway and its promise as a novel antimalarial target.

1.5.2 The MEP Pathway

Despite slow identification of this independent biosynthetic route to IPP and DMAPP, the MEP pathway has now been extensively studied using combined efforts from enzymology, crystallography and biophysics meaning that the biochemistry of the pathway is now well documented following extensive genomic evaluation.^[79–81]

The MEP pathway produces IPP and DMAPP through a series of seven enzymatic steps (**Scheme 1.1**)^[71,72,82] and is localised to the apicoplast of *Plasmodium* parasites which is often found proximal to the parasite food vacuole. The enzymes of the MEP pathway are present across all stages of intraerythrocytic *P. falciparum* infection where they are nuclear encoded but transported to the apicoplast.^[83] The apicoplast is a plastid organelle which lacks photosynthetic function and is a unique biological feature of Apicomplexan species (members of the phylum, Apicomplexa), which includes *Plasmodium* parasites.^[75] Unlike plastids present within plant species, the apicoplast is a secondary plastid derived from photosynthetic eukaryotes, which became incorporated into an ancestral apicomplexan that engulfed red alga. Despite its photosynthetic origins, the evolutionary divergence of the apicoplast makes it distinct from the plastids of green plants and Archaeplastida algae, making modulation of this organelle an exciting opportunity for targeted antimalarial drug development.^[84]

The apicoplast has an unusual non-mammalian metabolism and is known to support three specific metabolic functions including: Type II fatty acid biosynthesis, *de novo* haem biosynthesis and isoprenoid biosynthesis. In contrast to fatty acid and haem biosynthesis, which are essential for liver and mosquito stages of parasite development, it has been shown that biosynthesis of isoprenoid precursors is the essential metabolic function of the apicoplast in the asexual intraerythrocytic stage of parasite development, which is also responsible for the clinical manifestations of malaria.^[85,86]



Scheme 1.1 The MEP Pathway.^[71,72]

The seven-step MEP pathway is initiated with the condensation of pyruvate and glyceraldehyde-3-phosphate, catalysed by the enzyme 1-deoxy-D-xylulose-5-phosphate synthase (Dxs) with thiamine pyrophosphate (TPP) acting as co-factor, to afford 1-deoxy-D-xylulose-5-phosphate (DOXP) in the rate-limiting step of the pathway.^[75] The second enzyme, 1-deoxy-D-xylulose-5-phosphate reductoisomerase (IspC) then catalyses an intramolecular isomerisation and reduction of DOXP, producing 2C-methyl-D-erythritol 4-phosphate (MEP). MEP is the first dedicated metabolite of the MEP pathway, from which the biosynthetic route derives its name.^[71] The third step of the pathway involves a coupling reaction whereby 4-diphosphocytidyl-2C-methyl-D-erythritol cytidyltransferase (IspD), a cytidyl transferase enzyme, catalyses the transfer of a diphosphocytidyl group from cytidine triphosphate (CTP) to MEP to generate 4-diphosphocytidyl-2C-methyl-D-erythritol (CDP-ME).^[72]

Phosphorylation of CDP-ME, mediated by an ATP-dependent kinase, 4-diphosphocytidyl-2C-methyl-D-erythritol kinase (IspE), produces 4-diphosphocytidyl-2C-methyl-D-erythritol 2-phosphate (CDP-MEP). IspE is the fourth enzyme and only ATP-dependent enzyme of the MEP pathway.^[75] Cyclisation of CDP-MEP is catalysed by the enzyme 2C-methyl-D-erythritol-2,4-cyclodiphosphate synthase (IspF) in the fifth biosynthetic step, generates 4-diphosphocytidyl-2C-methyl-D-erythritol 2,4-cyclodiphosphate (MEcPP). MEcPP is subsequently reduced in a two-electron reductive ring opening step by the enzyme 1-hydroxy-2-methyl-2-(E)-butenyl-4-diphosphate (IspG) to form 2-methyl-2-(E)-butenyl diphosphate (HMBPP). HMBPP is then further reduced by dehydroxylation to generate IPP and DMAPP, catalysed by the enzyme 4-hydroxy-3-methyl-2-(E)-butenyl-4-diphosphate reductase (IspH), the most distal enzyme of the MEP pathway.^[72,75]

These seven enzymes that construct the MEP pathway are particularly valuable in terms of drug development since each enzyme only actively functions when presented with its unique and defined substrate, then generating its specific product. Consequently, the functions and biochemical roles of these enzymes cannot be compensated for by any other enzyme since they are absolutely unique and essential to the pathway.^[83] Further to this, the MEP pathway is highly linear making each enzyme in the pathway a fundamental requirement for *de novo* isoprenoid biosynthesis.^[71] It can therefore be argued that inhibition of early pathway enzymes may produce greater or increasingly irreversible levels of inhibition than could be achieved by targeting a more distal enzyme. In addition, targeting multiple enzymes throughout the pathway may also achieve stronger levels of inhibition, compared with targeting a single enzyme that may be difficult to reverse or rescue.

The absence of the MEP pathway in humans and mammalian systems is a consequence of independent evolution from the MVA pathway. The two biochemical pathways have distinct origins and are phylogenetically separated, where each pathway uses different substrates to generate isoprenoid precursors.^[71] The absence of MEP pathway enzymes in the human host is highly favourable when considering toxicological aspects of chemotherapy since anti-infective drugs targeting enzymes of the MEP pathway shouldn't produce target-related toxicity within the host system.^[68] The MEP pathway is therefore chemically and enzymatically distinct in its own right. This key biological distinction provides essential selectivity and enables specific inhibition of *Plasmodium* parasite enzymes with minimal toxicity risks to human cell lines.

So in summary, why is the MEP pathway a good biochemical target? In short, the MEP pathway displays a number of characteristics which make it highly favourable for antimalarial drug development. The MEP pathway is essential for *Plasmodium* parasite growth and none of the pathways enzymes are present within mammalian cells therefore minimising the risk of toxicity against human cells due to this species selectivity. The pathway has also been validated as amenable to chemical manipulation and inhibition by the small molecules (**Section 1.5**), highlighting that enzymes within the MEP pathway are indeed druggable and should be further explored within forward antimalarial drug design.^[71] Furthermore, the MEP pathway is present in many pathogens that are responsible for serious human pathologies including malaria, as well as tuberculosis and a number of sexually transmitted diseases.^[83] This makes the MEP pathway an obvious biochemical target due to its potential to support the development of a number of broad spectrum anti-microbial agents which target its component enzymes. Development of such therapies may ultimately hold the key to overcome the levels of drug resistance that we now see against many antimalarial and antimicrobial agents.^[71]

1.5.3 Known Inhibitors of The MEP Pathway

Small molecule inhibitors are known and have been described against each enzyme of the MEP pathway through numerous programs aiming to harness the commercial, agricultural and clinical potential of MEP pathway inhibition.^[74,87–89] The first enzyme of the pathway, Dxs, is known to be inhibited by the pyruvate derivatives and the chemical class of diphenylisoxazoles (**Figure 1.11**); acylated aminobenzothiazoles (**5**, **Figure 1.16**) and azolopyrimidine inhibitors (**6a** and **6b**, **Figure 1.16**) are known to act against the IspD enzyme; and cytidine derived analogues (**Figure 1.11**) have been found to inhibit IspE.^[72,89]

Research by *Crane et al.*^[87] utilised molecular modelling techniques to develop the first designed inhibitors of the IspF enzyme in a structure-based lead generation study. In the absence of any known inhibitors of the IspF enzyme at the time of the study, known crystal structures of *E.coli* IspF (*EclspF*) (PDB ID: 1GX1^[90] and 1JY8^[91]) were used to facilitate identification of CDP-substrate mimics with alkyl-linked aromatic side chains; fluorescent probes were used to determine the affinity of these designed compounds at *EclspF*.^[87] Such results are very encouraging for the development of new inhibitors against MEP pathway enzymes using structure-based design which shows promise for the generation of new compound classes within antimalarial and antimicrobial therapies. This small selection of chemical inhibitors (**Figure 1.11**), demonstrating high structural diversity, highlight the breadth of chemical space that MEP pathway inhibitors have the potential to cover and therefore underlines the vast potential for antimalarial drug development targeting enzymes of this biochemical pathway.

The chemical structures shown (**Figure 1.11**) depict the state of play in 2012 and current knowledge within the field surrounding chemical agents known to act as inhibitors of enzymes within the MEP pathway.^[72]

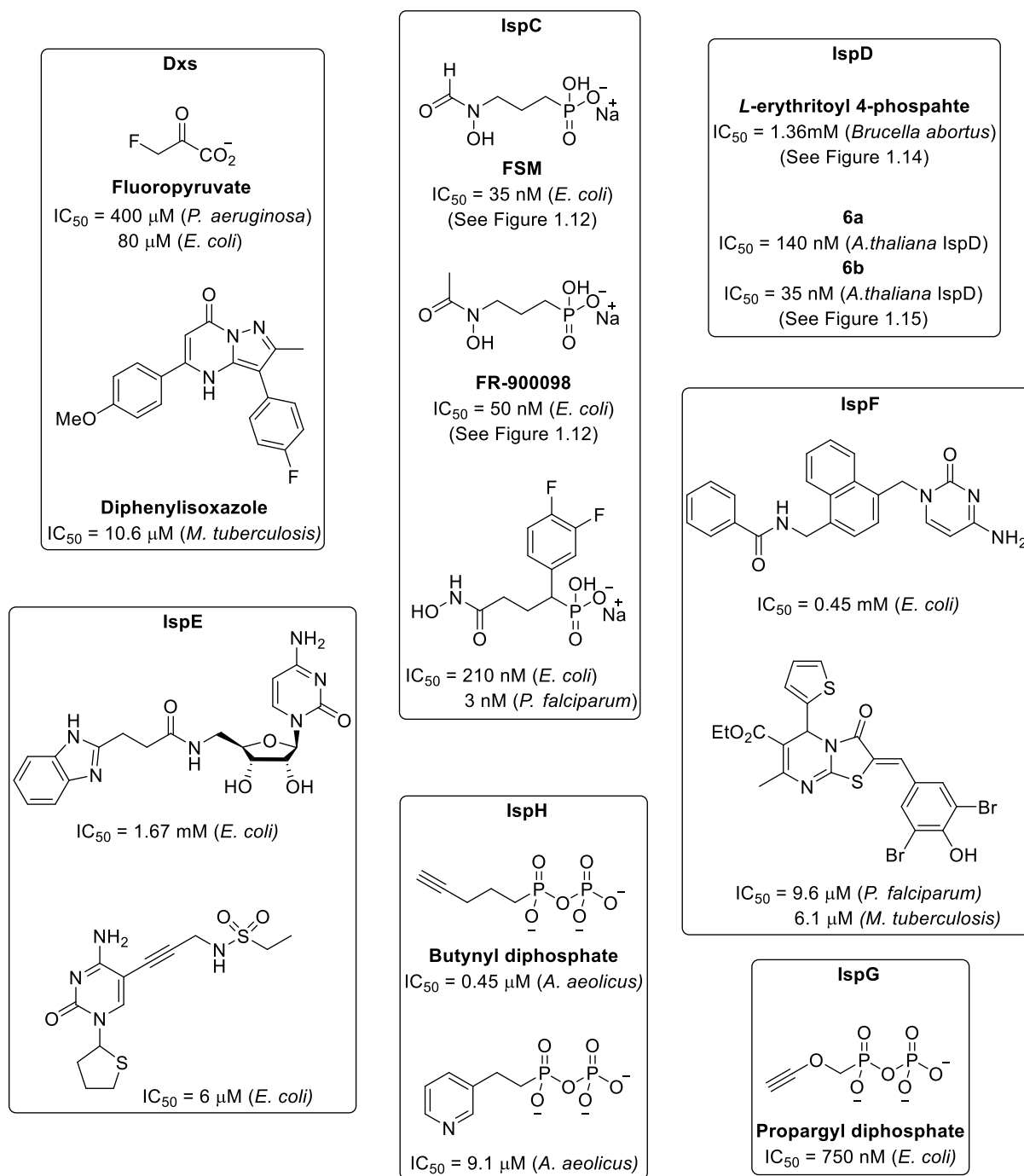


Figure 1.11 Known inhibitors of the MEP pathway.^[72]

Many of the highlighted chemical agents and structural motifs (**Figure 1.11**) are weak inhibitors of MEP pathway enzymes with IC_{50} values generally in the millimolar and upper-micromolar range, and with most compounds showing poor drug-like characteristics. However, these molecular templates are both tractable and structurally diverse again highlighting that a wide range of chemical agents may be developed as inhibitors of the MEP pathway and its component enzymes. This therefore

reiterates that the MEP pathway offers a wide range of molecular targets for modern drug discovery efforts against which diverse chemical agents may be developed and employed.^[72]

1.5.4 The IspC Enzyme and Fosmidomycin

The biological importance of the MEP pathway to *Plasmodium* parasites has been demonstrated by the identification and exploration of the clinical candidate fosmidomycin, a potent antimalarial agent that inhibits isoprenoid precursor biosynthesis. Fosmidomycin (FSM) is probably the most known and best characterised inhibitor of the MEP pathway to date; and as a result, the molecular target of FSM, IspC, is likely the most extensively cited enzyme within the MEP pathway.

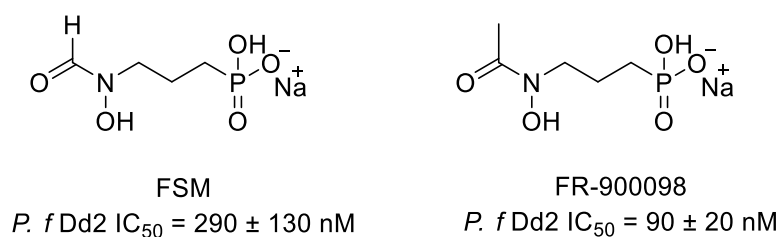


Figure 1.12 Chemical structures and activities of FSM and FR-900098 against *P. falciparum* strain Dd2.^[92,93]

FSM is a phosphonic acid antibiotic (**Figure 1.12**) which was first isolated as a natural antibiotic from *Streptomyces lavendulae* in the 1980's; it was initially involved in clinical development for the treatment of urinary tract infections (UTI's) as an anti-bacterial agent.^[94] More recently, FSM been identified as a substrate mimic and a competitive *in vitro* inhibitor of IspC, the first dedicated enzyme of the MEP pathway.^[82,95]

The structure of IspC proteins in a wide number of microorganisms have been determined using X-ray crystallography, more than thirty crystal structures of the enzyme now known, including structures for *E. coli*, *M. tuberculosis* and *P. falciparum* IspC. These studies have revealed that IspC proteins are C₂-symmetric homodimers with a bivalent metal ion, magnesium (Mg²⁺), cobalt (Co²⁺) or manganese (Mn²⁺), bound in the enzyme active site and which are essential for activity.^[68,72] IspC knockout experiments, disrupting the gene locus of IspC to assess the specific role of the enzyme, have validated it as essential for parasite survival.^[96] In addition, FSM-treated *Plasmodium* parasites can be rescued by subsequent treatment with isoprenoid precursor supplemented growth medium, therefore providing evidence that FSM prevents *Plasmodium* growth specifically through the inhibition of isoprenoid precursors biosynthesis.^[95]

The binding mode of FSM has been analysed within a number of crystallographic studies, all of which have found FSM to bind to IspC in a similar fashion to the natural enzyme substrate, DOXP.^[72,82] It

has been shown that the phosphonate group of FSM interacts with IspC in an analogous manner to DOXP. The flexible loop region of IspC, which shields the active site to bulk solvent molecules, interacts with the FSM carbon backbone whilst the hydroxamate entity of FSM interacts with several protein residues at the IspC active site as well as binding to the active site Mg^{2+} ion in a bidentate fashion.^[72] The structure activity relationship (SAR) between FSM and *E. coli* IspC can therefore be assessed with respect to these three FSM moieties, as a measure of *in vitro* *P. falciparum* growth inhibition.^[92]

FSM has shown strong clinical promise as an antimalarial agent, inhibiting recombinant *P. falciparum* IspC (*Pf*IspC) and killing the malaria parasite. FSM has been used successfully in small clinical studies for the treatment of malaria where early studies demonstrated the high efficacy of FSM and its close derivative FR-900098 (**Figure 1.12**). Both compounds are able to achieve inhibition of *P. falciparum* growth *in vitro* at nanomolar concentrations, with FR-900098 showing almost twice the activity of FSM in both animal models and against cultured parasites.^[93] However, FSM is not an ideal drug as it is a highly polar and water soluble molecule, therefore displaying poor pharmacokinetic (PK) properties. This suboptimal PK profile is characterised by: a short *in vivo* half-life, poor oral bioavailability,^[97] cellular exclusion from erythrocytes and other pathogens, high recrudescence rates and indirect action at other MEP pathway enzymes. Indeed, FSM has shown inhibition of the downstream MEP enzyme IspD; however direct inhibition of IspD homologues has not been observed within *in vitro* studies.^[82,95]

Refinement of the antimalarial performance of FSM alone, or in combination with another chemical agent, is therefore needed to produce a more effective antimalarial therapy.^[92] FSM entered Phase II clinical trials in combination with clindamycin, an antibiotic and semi-synthetic derivative of lincomycin,^[98] for malaria therapy in 2004.^[99] Unfortunately, high recrudescence rates were problematic with this drug combination, alongside poor efficacy, which was observed in the treatment of children under three years of age. Subsequent FSM combination studies have used the 4-aminoquinoline, piperazine, as a partner drug; these studies are currently ongoing and at the stage of Phase II clinical trials treating patients over the age of five.^[39] Several derivatives of FSM, as well as prodrugs which mask the polar phosphonate group of the molecule, have been developed in an attempt to improve PK properties, optimise half-life and improve drug uptake levels. A number of aryl and alkyl FSM analogues have shown improved activity against IspC with IC_{50} values in the single digit nanomolar range.^[68] However, further optimisations are still required and only a few IspC inhibitors have been identified that are structurally distinct from FSM and FR-900098; lipophilic phosphonate inhibitors containing pyridine or quinolone groups represent some of the most

promising examples **1-3** (**Figure 1.13**) which present IC_{50} values in the low micromolar range against *E. coli* IspC.^[97]

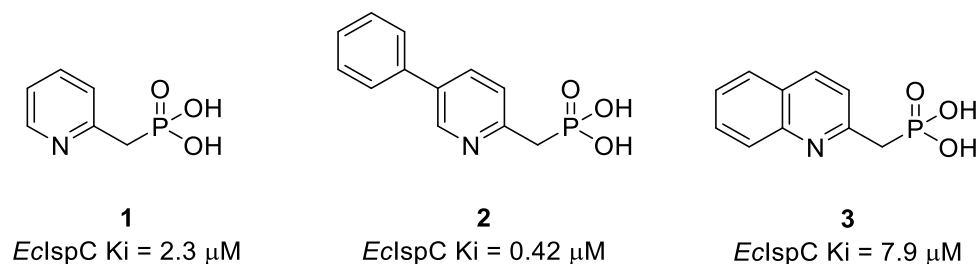


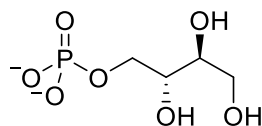
Figure 1.13 Chemical structures and activities of lipophilic phosphonate inhibitors **1-3** of *E. coli* IspC.^[97]

FSM itself demonstrates an impressive safety profile; it has a mouse LD_{50} of $> 11,000 \text{ mg kg}^{-1}$ showing that it is non-toxic to mammalian cells and, to date, no adverse effects have been identified in Phase I or Phase II clinical trials.^[82,94,100] However, the pharmacokinetics of FSM remain suboptimal^[100] meaning further chemical improvements to the antibiotic, its structural derivatives and combination formulations are needed. Nonetheless, FSM demonstrates the safety of targeting the MEP pathway and highlights that the component enzymes of the pathway are not only essential for parasite development, but also sensitive and amenable to small molecule chemical inhibition and manipulation.

1.5.5 The IspD Enzyme and Known Inhibitors

Despite the early success of FSM, no other MEP pathway inhibitors have progressed to clinical trials. Clearly, there are many unexplored opportunities to employ small molecule inhibitors against other MEP pathway enzymes as the pathway continues to be of considerable interest as a biological target for antibiotic, herbicidal and antimalarial therapies and applications. This has led to our objective to develop a lead candidate molecule suitable for clinical development as an antimalarial agent, targeting the third enzyme of the *Plasmodium* MEP pathway, *P. falciparum* IspD (*PfIspD*), which catalyses second dedicated step of the pathway.

In contrast to IspC, IspD has been studied much less extensively. The first known inhibitor of IspD, *L*-erythritoyl 4-phosphate (**Figure 1.14**), showed weak millimolar activity against the bacterial enzyme homologue, for the pathogen *Brucella abortus*.^[72,101]



L-erythritoyl 4-phosphate
Brucella abortus IC₅₀ = 1.36 mM

Figure 1.14 Chemical structure and activity of L-erythritoyl 4-phosphate, the first known bacterial IspD inhibitor.^[72]

To date, at least two crystal structures of IspD enzyme homologues have been solved and reported, with the majority of known structures encompassing *M. tuberculosis* IspD (PDB ID: 3OKR) and several *E. coli* IspD (*EclspD*) enzyme strains. These structures show that the IspD enzyme is a C₂-symmetric homodimer of which, each monomer is comprised of a single domain that adopts an α/β fold; from this fold a long β -arm extends and forms the majority of the dimer interface (**Figure 1.15**). The active site of the enzyme is located at this interface and is therefore solvent-exposed. Homologues of the IspD enzyme have largely been found to display substantial flexibility.^[72,102]

Examination of substrate and product co-crystal bound structures, including *M. tuberculosis* IspD co-crystallised with CTP (PDB ID: 2XWN^[103]) and *EclspD* co-crystallised with CDP-ME and CTP (PDB ID: 1INI^[104] and 1I52^[104] respectively), have revealed that CTP and CDP-ME bind to a glycine-rich loop of IspD and more specifically, the protein residues Pro13 and Arg20. Subsequent mechanistic studies have shown that an ordered and sequential mechanism takes place between the IspD enzyme and its substrates in the transferase coupling reaction that it mediates. Mechanistic evaluations have shown that the Mg²⁺ divalent cation in the IspD active site first coordinates to *EclspD*, followed by CTP protein binding and nucleophilic attack of the MEP phosphate on the α -phosphate of CTP.^[83] The Mg²⁺ ion, known to be essential for activity, coordinates to the α , β and γ phosphate groups of CTP as well as the α -phosphate of CDP-ME (**Figure 1.15**).^[72,102]

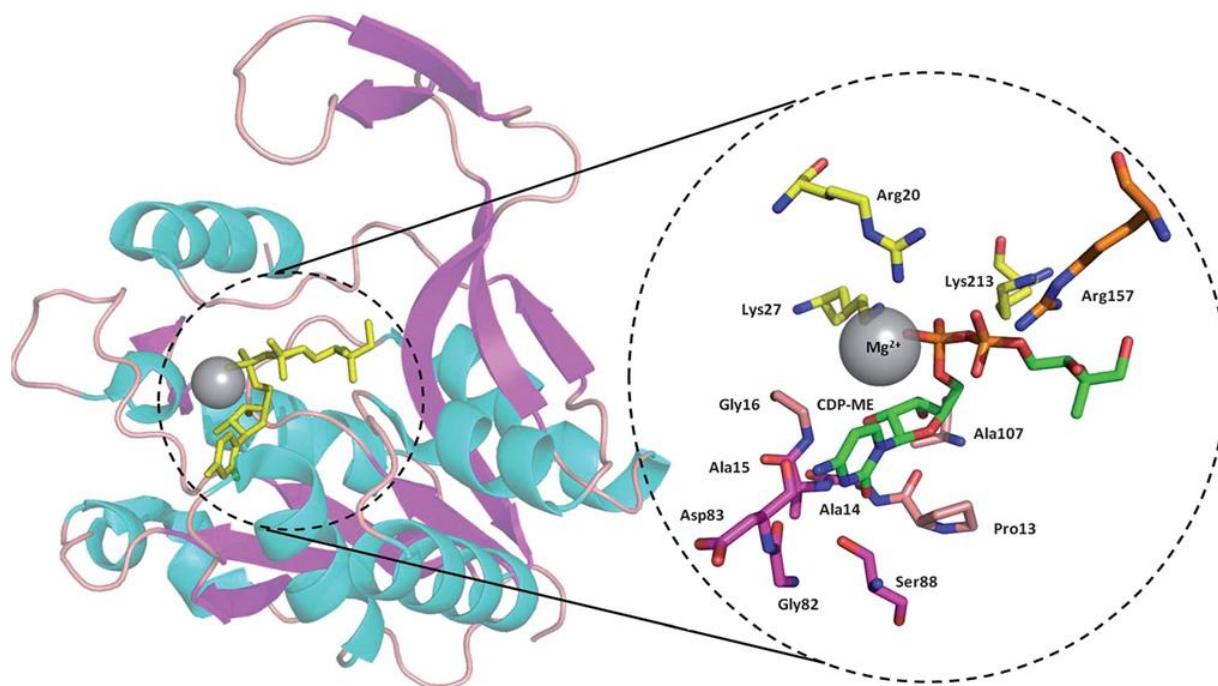


Figure 1.15 Tertiary structure of the *E. coli* IspD monomer with CDP-ME bound (PDB:1INI^[104]); α -helices and β -sheets are shown in cyan and purple cartoon format respectively. In the close-up image of the CTP binding site; the cytosine binding region and residues are rendered pink; the ribose binding region and corresponding residues are rendered tan; and the phosphate and MEP binding residues are rendered yellow and orange respectively. CDP-ME is coloured by element; carbon is green. The Mg^{2+} ion is shown as a grey sphere.^[72,105]

The low lipophilic character and solvent-exposed nature of the IspD binding pocket represents a challenge for competitive-substrate inhibitor design. Indeed, over the last than five years, no potent IspD inhibitors had been reported and few substrate-competitive inhibitors targeting the IspD active site had been developed. Even *L*-erythritoyl 4-phosphate (**Figure 1.14**), a compound of high structural similarity to MEP, shows only very weak inhibition at the IspD enzyme.^[102] This therefore indicates that there are many currently unexplored opportunities to develop novel chemical motifs that are capable of potently inhibiting the IspD enzyme.

Over the last few years, we and others, have reported small molecule inhibitors of IspD (**4** and **5**, **Figure 1.16**) confirming that IspD homologues are amenable to chemical inhibition.^[88,106,107] These IspD inhibitors generally have high-micromolar activity, although some herbaceous *Arabidopsis thaliana* (*A. thaliana*) species-selective chemical motifs have also been identified (**6a** and **6b**, **Figure 1.16**) which display nanomolar activity against the enzyme.^[74]

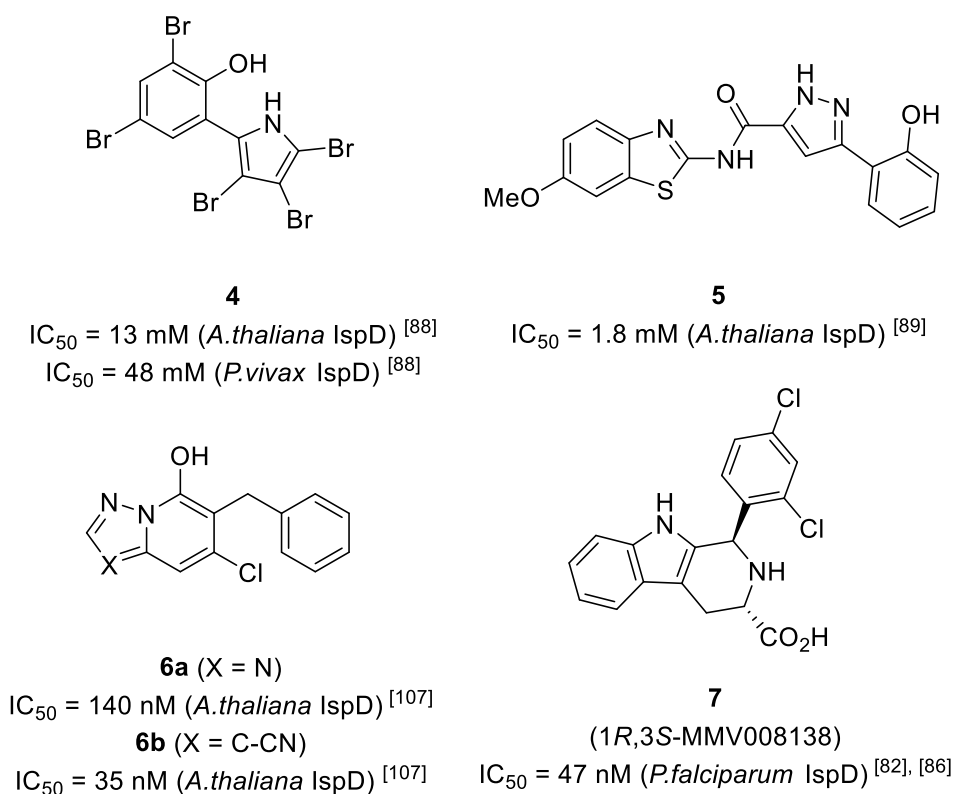


Figure 1.16 Chemical structures and activities of known IspD inhibitors. ^[82,86,88,89,107]

Plants utilise both the MEP and MVA pathways as part of their biochemistry, each is localised in the plant chloroplast and cytosol respectively. MEP pathway function and regulation has been well explored in plant systems following extensive herbicidal research, further iterating the importance of the MEP pathway as a biological target. Such work has been exemplified by Kunfermann *et al.* who identified the pseudilins (**4**, **Figure 1.16**) as chemical inhibitors of plant IspD homologues.^[88] Kunfermann *et al.* conducted a high-throughput screening (HTS) study which identified these highly halogenated marine alkaloids (**4**, **Figure 1.16**), displaying herbicidal activity in plant assays and anti-plasmodial activity in cell-based assays against the MEP pathway IspD enzyme. This attempt to discover new chemical entities acting as herbicidal agents against IspD, required the screening a medium library of 100,000 compounds using a photometrically monitored assay, which identified the pseudilins showing activity against *A. thaliana* IspD (AtIspD) in the nanomolar range. Kunfermann *et al.* used crystallographic studies to elucidate an allosteric mechanism of action whereby these pseudilin-type inhibitors were found to bind at an allosteric pocket of AtIspD, rather than at the IspD active site itself. Cell based assays also highlighted inhibition of *P. vivax* IspD and activity against *P. falciparum* with this class of compounds.^[88]

A study conducted by Masini *et al.*^[102] explored the druggability of enzymes within the MEP pathway. Druggability, as defined by Hopkins and Groom, refers to the capacity of a biological target

to bind a drug-like molecule, with acceptable absorption, permeability and binding affinity, in the nanomolar range.^[102,108] Evaluation of *AtIspD* (PDB ID: 2YC3^[107]) in this druggability study identified the allosteric *IspD* binding site which was attributed a druggability score (Dscore) of 0.79. The study assigned a Dscore of 0 to 1 to any identified enzyme pocket or enzyme sub-pocket following analysis of its geometrical and physicochemical properties relative to its potential binding capabilities.^[102] This is therefore highly encouraging; not only has the *AtIspD* allosteric binding site been identified as having good druggability, but distinct work conducted by separate researchers, has confirmed this with the identification of active inhibitors (**4**, **Figure 1.16**) against this specified binding region.

The druggability study conducted by Masini *et al.* considered all enzymes of the MEP pathway; evaluating all druggable pockets, including active site and allosteric binding regions. Since the natural intermediates of the MEP pathway are all phosphorylated and therefore highly polar, the corresponding active sites of enzymes within the pathway are also of high polarity. Consequently, it must be acknowledged that the structure-based design of drug-like inhibitors against these enzymes may be challenging. However, Masini *et al.* noted that the active site of the *IspD* enzyme is the least lipophilic of all enzymes analysed in the MEP pathway.^[102] Further to this, evaluation of *PfIspC* concluded that it was a druggable enzyme, assigning the *PfIspC* active site a Dscore of 0.80. We can therefore take confidence from the druggability analysis of *PfIspD* since it was given a slightly elevated Dscore of 0.86, compared to that of *PfIspC*. It therefore seems reasonable that mirroring the successes of FSM, as a potent *PfIspC* inhibitor, identifying novel and efficacious pharmacophores that are capable of targeting and inhibiting *PfIspD* are entirely possible. This gives confidence to the identification and selection of *PfIspD* as a specified MEP pathway enzyme target for novel antimalarial development.

A HTS study conducted by Witschel *et al.*^[107] identified the 7-hydroxy-[1,2,4]triazolo[1,5- α]pyrimidine (**6a**, **Figure 1.16**) which demonstrates sub-micromolar activity against *AtIspD* and was also found to bind to the allosteric binding pocket of the enzyme. Despite a number of structural alterations around the heterobicyclic core, only replacement of the N atom with a C-linked cyanide group at the X position, generating **6b** (**Figure 1.16**), was tolerated and gave slightly improved activity compared to the original hit **6a** within this azolopyrimidine series.^[107] In more recent research, conducted and published during the course of our studies, a chemical rescue screen identified **7** (1*R*,3*S*-MMV008138) from the Medicines for Malaria Venture (MMV) “malaria box” as a potent inhibitor of *PfIspD*. **7** displays nanomolar inhibition of recombinant *PfIspD* enzyme activity and sub-micromolar inhibition of parasite growth (**Figure 1.16**);^[82,109] this chemotype therefore

represents a highly promising structural motif which has great potential for SAR development into a potent and novel inhibitor series which is active against the *PflspD* enzyme (**Chapter 5**).

Consequently, it is clear that there is much scope for the development of further inhibitors targeting the *IspD* enzyme. The limited, but conclusive research to date highlights that the *IspD* enzyme is amenable to chemical manipulation by a range of chemical structures and motifs at two potential binding pockets on the enzyme: both the *IspD* active site itself and the *IspD* allosteric binding site. The identification of *PflspD* as a novel cellular target in an under explored, but chemically validated biochemical pathway,^[96] is therefore highly exciting and represents an encouraging development in ongoing research efforts to identify novel antimalarial chemotherapeutics which act against new molecular targets.

1.6 Conclusions

The development of effective antimalarial chemotherapeutics remains a major challenge within drug discovery. Despite significant scientific progress over the last two decades, which saw a 30% decrease in the global incidence of malaria between 2000 and 2013, through up-scaling malarial interventions,^[1] malaria is still a major global health problem with almost half the world's population at risk of contracting the disease. It is the adept ability of the *Plasmodium* parasite to develop drug resistance that so significantly hinders the fight against this entirely preventable disease.^[9] The continuation and acceleration of *Plasmodium* resistance development is seriously threatening the advances made in malaria treatment and prevention, as we are now facing the very real risk of widespread and irreversible *Plasmodium* resistance emerging against all current antimalarial therapies. With 95 countries registering malaria transmission in 2015,^[1] the development of new antimalarial drugs and battle to overcome parasite resistance has never been more crucial.

Very few novel drugs currently exist in the antimalarial drug pipeline and only a very limited number of antimalarial drug targets have been explored within drug development programs to date (**Table 1.1** and **Figure 1.8**). The identification and development of new drugs is needed to ensure there is a sustained pressure on the *Plasmodium* parasite to enable the continuation of effective malaria treatment and progression towards malaria eradication.^[60] Circumventing the increasing problem of resistance against antimalarial agents requires the disease to be fought from several angles; it is not inconceivable that a continuous flow of innovative, novel and effective drugs will be needed to achieve complete eradication of the disease.

The intensified pursuit of new antimalarial drugs and novel molecular targets has caused the spotlight to fall on the chemical manipulation of isoprenoid biosynthesis. Isoprenoids represent the oldest and largest class of natural products which play vital roles in many cellular functions.^[83] In contrast to mammals; malaria-causing *Plasmodium* parasites use the non-mevalonate (MEP) biosynthetic pathway to generate isoprenoid precursors which is essential for parasite survival.^[110] Humans and other mammals use the mevalonate (MVA) pathway for this purpose.^[72,78] This observed biological selectivity makes the MEP pathway highly attractive as an antimalarial chemotherapeutic target, enabling enzymes within the pathway to be selectively inhibited with minimal risk of toxicity to the human host. FSM is currently the most potent and best-characterised MEP pathway inhibitor, targeting the first dedicated enzyme of the pathway, IspC. FSM has therefore validated the pathway as a viable target for antimalarial drug discovery efforts.^[96] As exemplified by the range of chemical motifs found to inhibit various enzymes of the MEP pathway, it

has been highlighted that the pathway is druggable and amenable to chemical manipulation and inhibition by small molecules.

Taken all together, this has led to our objective to deliver a lead candidate molecule suitable for clinical development, targeting the third enzyme of the MEP pathway, *Pf*ispD. This enzyme represents an ideal biological target which is currently underexplored and shows real promise for advancing novel antimalarial drug development. Ultimately, we seek to answer the question: Can arresting the MEP pathway through *Pf*ispD inhibition cause *Plasmodium* parasite death *via* disruption of isoprenoid precursor generation?

1.7 References

- [1] WHO (2015) World Health Organisation, *World Malaria Report*, **2015**.
- [2] WHO (2014) World Health Organisation, *World Malaria Report*, **2014**.
- [3] N. J. White, *J. Clin. Invest.* **2004**, *113*, 1084–1092.
- [4] A. R. Renslo, *ACS Med. Chem. Lett.* **2013**, *4*, 1126–1128.
- [5] K. Mendis, B. J. Sina, P. Marchesini, R. Carter, *Am. J. Trop. Med. Hyg.* **2001**, *64*, 97–106.
- [6] T. N. C. Wells, W. E. Gutteridge, *Malaria : New Medicines for Its Control and Eradication*, **2011**.
- [7] UNICEF, “Malaria,” can be found under http://www.unicef.org/health/index_malaria.html, **2013**.
- [8] J. Bitman, H. C. Cecil, *J. Agric. Food Chem.* **1970**, *18*, 1108–1112.
- [9] W. Van Bortel, H. D. Trung, L. K. Thuan, T. Sochantha, D. Socheat, C. Sumrandee, V. Baimai, K. Keokenchanh, P. Samlane, P. Roelants, et al., *Malar. J.* **2008**, *7*, DOI 10.1186/1475-2875-7-102.
- [10] J. Schantz-Dunn, N. M. Nour, *Rev. Obstet. Gynecol.* **2009**, *2*, 186–92.
- [11] (MMV) Medicines for Malaria Venture, “Malaria and Medicines,” can be found under <http://www.mmv.org>, **2016**.
- [12] W. Stauffer, P. R. Fischer, *Clin. Infect. Dis.* **2003**, *37*, 1340–1348.
- [13] Centre for Disease Control and Prevention (CDC), “Malaria,” can be found under <http://www.cdc.gov/malaria/about/biology/index.html>, **2016**.
- [14] L. Florens, M. P. Washburn, J. D. Raine, R. M. Anthony, M. Grainger, J. D. Haynes, J. K. Moch, N. Muster, J. B. Sacci, D. L. Tabb, et al., *Nature* **2002**, *419*, 520–6.
- [15] J. K. Baird, *N. Engl. J. Med.* **2005**, *352*, 1565–1577.
- [16] M. Schlitzer, *ChemMedChem* **2007**, *2*, 944–986.
- [17] H. Fujioka, M. Aikawa, *Chem. Immunol.* **2002**, *80*, 1–26.
- [18] V. Soulard, H. Bosson-Vanga, A. Lorthiois, C. Roucher, J.-F. Franetich, G. Zanghi, M. Bordessoulles, M. Tefit, M. Thellier, S. Morosan, et al., *Nat. Commun.* **2015**, *6*, 7690.
- [19] J. Liu, E. S. Istvan, I. Y. Gluzman, J. Gross, D. E. Goldberg, *Proc. Natl. Acad. Sci. U. S. A.* **2006**, *103*, 8840–8845.
- [20] M. R. Galinski, E. V. S. Meyer, J. W. Barnwell, *Adv. Parasitol.* **2013**, *81*, 1–26.
- [21] K. Raghavendra, T. K. Barik, B. P. N. Reddy, P. Sharma, A. P. Dash, *Parasitol. Res.* **2011**, *108*, 757–779.
- [22] R. M. Oxborough, R. N’Guessan, J. Kitau, P. K. Tungu, D. Malone, F. W. Mosha, M. W. Rowland, *Malar. J.* **2015**, *14*, 353.

- [23] H. Townson, M. B. Nathan, M. Zaim, P. Gullet, R. Bos, M. Kindhauser, *Bull World Heal. Organ* **2005**, *83*, 942–947.
- [24] F.-J. Gamo, *Drug Discov. Today. Technol.* **2014**, *11*, 81–88.
- [25] D. Greenwood, *J. Antimicrob. Chemother.* **1992**, *30*, 417–427.
- [26] T. E. Wellems, C. V Plowe, *J. Infect. Dis.* **2001**, *184*, 770–776.
- [27] M. Jensen, H. Mehlhorn, *Parasitol. Res.* **2009**, *105*, 609–627.
- [28] P. M. O’Neill, P. G. Bray, S. R. Hawley, S. A. Ward, B. K. Park, *Pharmacol. Ther.* **1998**, *77*, 29–58.
- [29] R. Arav-Boger, T. A. Shapiro, *Annu. Rev. Pharmacol. Toxicol.* **2005**, *45*, 565–585, 1 plate.
- [30] Y. Wu, L. A. Kirkman, T. E. Wellems, *Proc. Natl. Acad. Sci. U. S. A.* **1996**, *93*, 1130–1134.
- [31] D. A. Fidock, T. Nomura, A. K. Talley, R. A. Cooper, S. M. Dzekunov, M. T. Ferdig, L. M. B. Ursos, A. B. S. Sidhu, B. Naude, K. W. Deitsch, et al., *Mol. Cell* **2000**, *6*, 861–871.
- [32] A. M. Dondorp, S. Yeung, L. White, C. Nguon, N. P. J. Day, D. Socheat, L. von Seidlein, *Nat. Rev. Microbiol.* **2010**, *8*, 272–280.
- [33] J. G. Kublin, J. F. Cortese, E. M. Njunju, R. A. G. Mukadam, J. J. Wirima, P. N. Kazembe, A. A. Djimde, B. Kouriba, T. E. Taylor, C. V Plowe, *J. Infect. Dis.* **2003**, *187*, 1870–1875.
- [34] M. K. Laufer, P. C. Thesing, N. D. Eddington, R. Masonga, F. K. Dzinjalama, S. L. Takala, T. E. Taylor, C. V Plowe, *N. Engl. J. Med.* **2006**, *355*, 1959–1966.
- [35] C. Faurant, *Parasite* **2011**, *18*, 215–218.
- [36] N. J. White, *Science* **2008**, *320*, 330–334.
- [37] S. R. Meshnick, T. E. Taylor, S. Kamchonwongpaisan, *Microbiol. Rev.* **1996**, *60*, 301–315.
- [38] E. A. Ashley, M. Dhorda, R. M. Fairhurst, C. Amaratunga, P. Lim, S. Suon, S. Sreng, J. M. Anderson, S. Mao, B. Sam, et al., *N. Engl. J. Med.* **2014**, *371*, 411–423, 13 .
- [39] T. N. C. Wells, R. H. van Huijsduijnen, W. C. Van Voorhis, *Nat. Rev. Drug Discov.* **2015**, *14*, 424–442.
- [40] S. Qi, G. J. M. den Hartog, A. Bast, *Toxicol. Appl. Pharmacol.* **2009**, *237*, 111–118.
- [41] A. Bast, G. R. M. M. Haenen, A. M. E. Bruynzeel, W. J. F. Van der Vijgh, *Cardiovasc. Toxicol.* **2007**, *7*, 154–159.
- [42] P. M. O’Neill, G. H. Posner, *J. Med. Chem.* **2004**, *47*, 2945–2964.
- [43] U. Eckstein-Ludwig, R. J. Webb, I. D. a Van Goethem, J. M. East, a G. Lee, M. Kimura, P. M. O’Neill, P. G. Bray, S. a Ward, S. Krishna, *Nature* **2003**, *424*, 957–961.
- [44] H. M. Ismail, V. Barton, M. Phanchana, S. Charoensutthivarakul, M. H. L. Wong, J. Hemingway, G. A. Biagini, P. M. O’Neill, S. A. Ward, *Proc. Natl. Acad. Sci. U. S. A.* **2016**, *113*, 2080–5.
- [45] M. Dhorda, P. Y. Cheah, S. Pukrittayakamee, E. A. Ashley, T. J. C. Anderson, S. Nair, M. Mcdew-white, N. J. White, C. J. Woodrow, *Lancet Infect. Dis.* **2015**, *15*, 415–421.

- [46] K. Thriemer, N. Van Hong, A. Rosanas-Urgell, B. Q. Phuc, D. M. Ha, E. Pockele, P. Guetens, N. Van Van, T. T. Duong, A. Amambua-Ngwa, et al., *Antimicrob. Agents Chemother.* **2014**, *58*, 7049–7055.
- [47] B. Witkowski, N. Khim, P. Chim, S. Kim, S. Ke, N. Kloeung, S. Chy, S. Duong, R. Leang, P. Ringwald, et al., *Antimicrob. Agents Chemother.* **2013**, *57*, 914–923.
- [48] M. D. Spring, J. T. Lin, J. E. Manning, P. Vanachayangkul, S. Somethy, R. Bun, Y. Se, S. Chann, M. Ittiverakul, P. Sia-ngam, et al., *Lancet Infect. Dis.* **2015**, *15*, 683–691.
- [49] V. I. Carrara, K. M. Lwin, A. P. Phyto, E. Ashley, J. Wiladphaingern, K. Sriprawat, M. Rijken, M. Boel, R. McGready, S. Proux, et al., *PLoS Med.* **2013**, *10*, 1999–2011.
- [50] A. M. Dondorp, F. Nosten, P. Yi, D. Das, A. P. Phyto, J. Tarning, D. Ph, K. M. Lwin, F. Arie, W. Hanpithakpong, et al., *Drug Ther. (NY)*. **2009**, *361*, 455–467.
- [51] C. Dogovski, S. C. Xie, G. Burgio, J. Bridgford, S. Mok, J. M. McCaw, K. Chotivanich, S. Kenny, N. Gnadig, J. Straimer, et al., *PLoS Biol.* **2015**, *13*, 1–26.
- [52] S. Meshnick, *Am. J. Trop. Med. Hyg.* **2012**, *87*, 783–784.
- [53] S. a Charman, S. Arbe-Barnes, I. C. Bathurst, R. Brun, M. Campbell, W. N. Charman, F. C. K. Chiu, J. Chollet, J. C. Craft, D. J. Creek, et al., *Proc. Natl. Acad. Sci. U. S. A.* **2011**, *108*, 4400–4405.
- [54] E. L. Flannery, A. K. Chatterjee, E. A. Winzeler, *Nat. Rev. Microbiol.* **2013**, *11*, 849–862.
- [55] F. W. Muregi, A. Ishih, *Drug Dev. Res.* **2010**, *71*, 20–32.
- [56] The malERA Consultative Group on Drugs, *PLoS Med.* **2011**, *8*, e1000402.
- [57] J. J. Walsh, A. Bell, *Curr. Pharm. Des.* **2009**, *15*, 2970–2985.
- [58] F.-J. Gamo, L. M. Sanz, J. Vidal, C. de Cozar, E. Alvarez, J.-L. Lavandera, D. E. Vanderwall, D. V. S. Green, V. Kumar, S. Hasan, et al., *Nature* **2010**, *465*, 305–310.
- [59] E. R. Derbyshire, M. M. Mota, J. Clardy, *PLoS Pathog.* **2011**, *7*, DOI 10.1371/journal.ppat.1002178.
- [60] T. T. Diagana, *Drug Discov. Today* **2015**, *20*, 1265–1270.
- [61] C. Arama, M. Troye-Blomberg, *J. Intern. Med.* **2014**, *275*, 456–466.
- [62] D. L. Doolan, C. Dobano, J. K. Baird, *Clin. Microbiol. Rev.* **2009**, *22*, 13–36.
- [63] N. Sriwilaijaroen, S. Boonma, P. Attasart, J. Pothikasikorn, S. Panyim, W. Noonpakdee, *Biochem. Biophys. Res. Commun.* **2009**, *381*, 144–147.
- [64] B. K. Chaal, A. P. Gupta, B. D. Wastuwidyaningtyas, Y.-H. Luah, Z. Bozdech, *PLoS Pathog.* **2010**, *6*, e1000737.
- [65] J. Baldwin, C. H. Michnoff, N. A. Malmquist, J. White, M. G. Roth, P. K. Rathod, M. A. Phillips, *J. Biol. Chem.* **2005**, *280*, 21847–21853.
- [66] M. L. Booker, C. M. Bastos, M. L. Kramer, R. H. Barker, R. Skerlj, A. B. Sidhu, X. Deng, C. Celatka, J. F. Cortese, J. E. Guerrero Bravo, et al., *J. Biol. Chem.* **2010**, *285*, 33054–33064.

- [67] R. K. B. Brobey, G. Sano, F. Itoh, K. Aso, M. Kimura, T. Mitamura, T. Horii, *Mol. Biochem. Parasitol.* **1996**, *81*, 225–237.
- [68] T. Graewert, M. Groll, F. Rohdich, A. Bacher, W. Eisenreich, *Cell. Mol. Life Sci.* **2011**, *68*, 3797–3814.
- [69] M. B. Schmid, *Nat. Biotechnol.* **2006**, *24*, 419–420.
- [70] M. Rodriguez-Concepcion, *Curr. Pharm. Des.* **2004**, *10*, 2391–2400.
- [71] A. R. Odom, *PLoS Pathog.* **2011**, *7*, 1–4.
- [72] I. Hale, P. M. O’Neill, N. G. Berry, A. Odom, R. Sharma, *Medchemcomm* **2012**, *3*, 418–433.
- [73] C. A. Testa, M. J. Brown, *Curr. Pharm. Biotechnol.* **2003**, *4*, 248–259.
- [74] K. E. Price, C. M. Armstrong, L. S. Imlay, D. M. Hodge, C. Pidathala, N. J. Roberts, J. Park, M. Mikati, R. Sharma, A. S. Lawrenson, et al., *Sci. Rep.* **2016**, *6*, 36777.
- [75] J.-Y. van der Meer, A. K. H. Hirsch, *Nat. Prod. Rep.* **2012**, *29*, 721.
- [76] B. M. Lange, T. Rujan, W. Martin, R. Croteau, *Proc. Natl. Acad. Sci. U. S. A.* **2000**, *97*, 13172–13177.
- [77] J. Gershenzon, N. Dudareva, *Nat. Chem. Biol.* **2007**, *3*, 408–414.
- [78] A. Endo, *J. Lipid Res.* **1992**, *33*, 1569–1582.
- [79] F. Rohdich, W. Eisenreich, J. Wungsintaweekul, S. Hecht, C. A. Schuhr, A. Bacher, *Eur. J. Biochem.* **2001**, *268*, 3190–3197.
- [80] M. Rohmer, in *Compr. Nat. Prod. Chem.*, Elsevier Science B.V., **1999**, pp. 45–67.
- [81] W. Eisenreich, M. Schwarz, A. Cartayrade, D. Arigoni, M. H. Zenk, A. Bacher, *Chem. Biol.* **1998**, *5*, R221–R233.
- [82] L. S. Imlay, C. M. Armstrong, M. C. Masters, T. Li, K. E. Price, R. L. Edwards, K. M. Mann, L. X. Li, C. L. Stallings, N. G. Berry, et al., *ACS Infect. Dis.* **2015**, *1*, 157–167.
- [83] W. N. Hunter, *J. Biol. Chem.* **2007**, *282*, 21573–21577.
- [84] C. D. Goodman, G. I. McFadden, *Expert Opin. Ther. Targets* **2013**, *17*, 167–177.
- [85] J. D. Wiley, E. F. Merino, P. M. Krai, K. J. McLean, A. K. Tripathi, J. Vega-Rodriguez, M. Jacobs-Lorena, M. Klemba, M. B. Cassera, *Eukaryot. Cell* **2015**, *14*, 128–139.
- [86] E. Yeh, J. L. DeRisi, *PLoS Biol.* **2011**, *9*, DOI 10.1371/journal.pbio.1001138.
- [87] C. M. Crane, J. Kaiser, N. L. Ramsden, S. Lauw, F. Rohdich, W. Eisenreich, W. N. Hunter, A. Bacher, F. Diederich, *Angew. Chemie - Int. Ed.* **2006**, *45*, 1069–1074.
- [88] A. Kunfermann, M. Witschel, B. Illarionov, R. Martin, M. Rottmann, H. W. Hoeffken, M. Seet, W. Eisenreich, H.-J. Knoelker, M. Fischer, et al., *Angew. Chemie, Int. Ed.* **2014**, *53*, 2235–2239.
- [89] M. Witschel, F. Röhl, R. Niggeweg, T. Newton, *Pest Manag. Sci.* **2013**, *69*, 559–563.
- [90] L. E. Kemp, C. S. Bond, W. N. Hunter, *Proc. Natl. Acad. Sci. U. S. A.* **2002**, *99*, 6591–6596.

- [91] S. Steinbacher, J. Kaiser, J. Wungsintaweekul, S. Hecht, W. Eisenreich, S. Gerhardt, A. Bacher, F. Rohdich, *J. Mol. Biol.* **2002**, *316*, 79–88.
- [92] T. Umeda, N. Tanaka, Y. Kusakabe, M. Nakanishi, Y. Kitade, K. T. Nakamura, *Sci. Rep.* **2011**, *1*, 9.
- [93] H. Jomaa, J. Wiesner, S. Sanderbrand, B. Altincicek, C. Weidemeyer, M. Hintz, I. Turbachova, M. Eberl, J. Zeidler, H. K. Lichtenthaler, et al., *Science* **1999**, *285*, 1573–1576.
- [94] J. Wiesner, S. Borrmann, H. Jomaa, *Parasitol. Res.* **2003**, *90*, 71–76.
- [95] B. Zhang, K. M. Watts, D. Hodge, L. M. Kemp, D. A. Hunstad, L. M. Hicks, A. R. Odom, *Biochemistry* **2011**, *50*, 3570–3577.
- [96] A. R. Odom, W. C. Van Voorhis, *Mol. Biochem. Parasitol.* **2010**, *170*, 108–111.
- [97] L. Deng, J. Diao, P. Chen, V. Pujari, Y. Yao, G. Cheng, D. C. Crick, B. V. V. Prasad, Y. Song, *J. Med. Chem.* **2011**, *54*, 4721–4734.
- [98] B. Lell, P. G. Kremsner, *Antimicrob. Agents Chemother.* **2002**, *46*, 2315–2320.
- [99] S. Borrmann, I. Lundgren, S. Oyakhrome, B. Impouma, P. B. Matsiegui, A. A. Adegnika, S. Issifou, J. F. J. Kun, D. Hutchinson, J. Wiesner, et al., *Antimicrob. Agents Chemother.* **2006**, *50*, 2713–2718.
- [100] H. P. Kuemmerle, T. Murakawa, H. Sakamoto, N. Sato, T. Konishi, F. De Santis, *Int. J. Clin. Pharmacol.* **1985**, *23*, 521–528.
- [101] A. M. Lillo, C. N. Tetzlaff, F. J. Sangari, D. E. Cane, *Bioorganic Med. Chem. Lett.* **2003**, *13*, 737–739.
- [102] T. Masini, B. S. Kroezen, A. K. H. Hirsch, *Drug Discov. Today* **2013**, *18*, 1256–1262.
- [103] C. Bjoerkelid, T. Bergfors, L. M. Henriksson, A. L. Stern, T. Unge, S. L. Mowbray, T. A. Jones, *Acta Crystallogr. Sect. D Biol. Crystallogr.* **2011**, *67*, 403–414.
- [104] S. B. Richard, M. E. Bowman, W. Kwiatkowski, I. Kang, C. Chow, A. M. Lillo, D. E. Cane, J. P. Noel, *Nat. Struct. Biol.* **2001**, *8*, 641–648.
- [105] The PyMOL Molecular Graphics System, **2010**, Version 1.3r1.
- [106] P. Gao, Y. Yang, C. Xiao, Y. Liu, M. Gan, Y. Guan, X. Hao, J. Meng, S. Zhou, X. Chen, et al., *Eur. J. Pharmacol.* **2012**, *694*, 45–52.
- [107] M. C. Witschel, H. W. Hoeffken, M. Seet, L. Parra, T. Mietzner, F. Thater, R. Niggeweg, F. Roehl, B. Illarionov, F. Rohdich, et al., *Angew. Chemie, Int. Ed.* **2011**, *50*, 7931–7935, S7931/1–S7931/29.
- [108] A. L. Hopkins, C. R. Groom, *Nat. Rev. Drug Discov.* **2002**, *1*, 727–30.
- [109] W. Wu, Z. Herrera, D. Ebert, K. Baska, S. H. Cho, J. L. DeRisi, E. Yeh, *Antimicrob. Agents Chemother.* **2015**, *59*, 356–364.
- [110] B. M. Lange, T. Rujan, W. Martin, R. Croteau, *Proc. Natl. Acad. Sci. U. S. A.* **2000**, *97*, 13172–13177.

Chapter 2

Chemotype Identification; Development of Synthetic Methodologies and Initial SAR Investigations

2.1 HTS Studies – A Route to New Antimalarial Compounds

High-throughput screening (HTS) is a common strategy within modern drug discovery for identifying hit compounds against new or known molecular targets. With the pharmaceutical industry investing extensively on infrastructure to test ever-expanding compound collections, it now relies heavily on HTS for lead compound identification. The objective of screening large compound libraries is to maximise chances of discovering quality hit compounds for synthetic optimization of potential drug candidates. This uses the simple logic that the examination of a larger compound number can exponentially increase the chances of identifying a compound that acts efficaciously at a molecular target of interest. However, it should also be noted that the screening of large compound libraries, even on the 10 million compound scale, still only provides a small fraction and sample of the vast number of potential compounds that make up drug-like chemical space. It should therefore be realised that optimising the likelihood of identifying a compound which acts efficaciously at a molecular target, required the use of, not only a large, but also a structurally and chemically diverse library. Nonetheless, it is undeniable that many lead compounds have been discovered from HTS campaigns within modern drug discovery programmes.^[1]

Since the 1990's when the genomics era began, the main focus of drug discovery has been based around drug targets, typically proteins which have key roles in a specific disease pathogenesis, where modulation of target activity provides a rational basis for the discovery of new chemotherapeutics. However, before the introduction of target-based design approaches, drug discovery was propelled mainly by phenotypic assays where a limited knowledge of the molecular mechanism of disease pathology was often the case.^[2] Phenotypic screening in discovery programmes measure the effect, or phenotype, that a compound induces in cells, tissues or whole organisms, identifying molecules that produce a desired biological effect or molecular change.^[3] In comparison, target-based screens measure the effects of a compound on a specific, purified target protein using *in vitro* assays.^[3]

Today, these two drug discovery approaches are used throughout a vast number of diverse research programmes, both to varying extents and with varying levels of success. An advantage of a target-based approach is that knowledge of chemical and molecular mechanisms can be applied in order to investigate biological disease states and hypotheses concerning molecular mechanisms of action. However, the identified molecular solution to a suggested treatment strategy may ultimately not turn out to be relevant to the particular pathogenesis or provide an appropriate therapeutic index.^[2]

In contrast, phenotypic drug discovery approaches do not require an understanding of the molecular mechanisms of action and often represent a less biased way of translating cellular assays into

therapeutic impact for a given disease state. Indeed, an arguable advantage to this discovery approach resides in the fact that a biological system can be interrogated without a predisposed bias towards a proposed mechanism of action.^[4] This lends to the identification of compounds that may interact with one or more molecular targets which are not anticipated by a single, mechanism-driven hypothesis. However, the challenge of phenotypic drug discovery lies in the complexity of differentiating compound profiles, gaining complete biological understanding of an observed phenotype and determining a defined mechanism of action.^[4] Incorporating new screening technologies into phenotypic approaches and optimising molecular properties of identified candidate drugs, without knowledge of a molecular mechanism of action, therefore remains highly challenging and possibly explains why phenotypic assays have lower throughput than target-based assays.^[2]

As *P. falciparum* resistant strains continue to emerge against the limited number of available antimalarial drugs, it is clear that new and entirely novel antimalarial chemotherapies must be developed if we are to halt the resurgence in drug-resistant *Plasmodium* parasites and maintain an effective antimalarial drug pipeline. The magnitude of this research problem has led to increased collaboration between industry and academia, placing emphasis on identifying new chemotypes through increased and extensive screening methods.^[5]

In 2010, both St Jude's Children's hospital^[6] and Novartis^[7] published the structures of thousands of compounds that were capable of inhibiting parasite growth, therefore significantly increasing the number of compounds instantly available for antimalarial drug discovery programmes. In the same year, GSK also published the Tres Cantos Antimalarial Set (TCAMS), comprising 13, 533 compounds which resulted from the screening of around two million compounds from within the GSK's corporate collection.^[8] The open and public availability of this large and potent set of drug-like, anti-plasmodial compound structures enables many important research questions to be addressed throughout an increasing number of antimalarial screening programmes and methodologies.^[9] Indeed, a significant amount of work such as this is freely available within the ChEMBL-Neglected Tropical Disease archive^[10] which is an open access repository for primary screening and medicinal chemistry data focusing on neglected and endemic tropical diseases. A number of recent open access publications, involving compound screening and medicinal chemistry optimisation for the purpose of antimalarial drug discovery, can be found here^[11-13].

2.1.1 Phenotypic-based Screening: TCAMs

In 2011, Medicines for Malaria Venture (MMV) in partnership with GSK conducted a HTS programme using the TCAMS library to identify a small subset of compound structures that were made available to the research community as potential starting points for lead optimisation. This bold attempt to initiate novel antimalarial drug discovery, represents an example of a successful phenotypic screen since five separate chemical series were identified displaying potent antimalarial activity against *P. falciparum*.^[8] The aim of the GSK/MMV study was to rapidly identify molecules that have a strong chance of successful antimalarial drug development and a low risk of attrition so as to fast track high quality, but currently unevaluated chemotypes, into lead optimisation. A schematic of this study is depicted below (**Figure 1.2**).^[8]

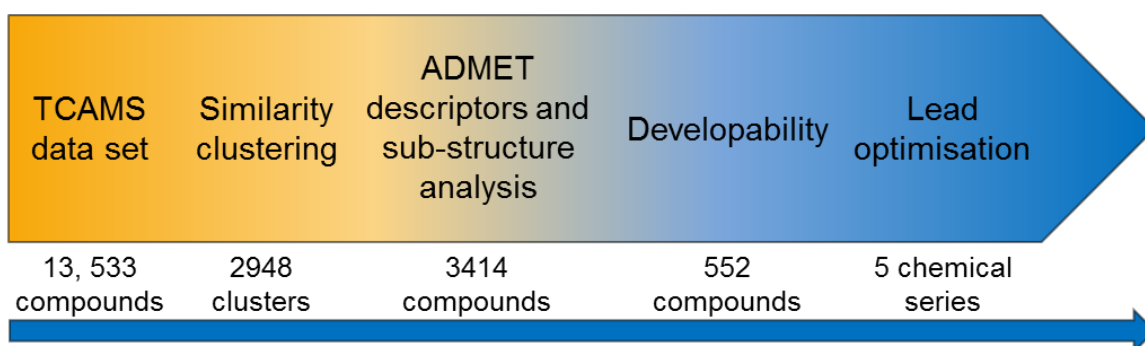


Figure 2.1 Representation of work flow for the identification of chemical starting points from the TCAMS data set for lead optimisation; figure reproduced from ^[8].

The TCAMS library, of over 13, 000 potential starting points, was first clustered using a series of algorithms which produced 2948 sets of data and could be further analysed based on compound similarity. Compounds were prioritised and consequently scored according to their *P. falciparum* (3D7 strain) antimalarial activity and lipophilicity, which was used as a preliminary measure of drug-likeness.^[8] Once all compounds were evaluated, those with a score of less than 15 (out of a possible 30) were discarded. The remaining 3, 414 compounds were filtered to remove less “drug-like” molecules and compounds with chemical structures related to known antimalarials; this aimed to minimise the risk of developing a compound likely to rapidly develop resistance. Ultimately this led to the identification of 522 compounds which were then considered through a non-automated selection process.^[8]

Five distinct chemical series were selected featuring indolines, aryl carboxamides, alkylpyrazoles, thienopyrazoles, and 4-aminopiperidines; all of which complied with the requirements of high potency, druggability, and chemical tractability. An exemplary compound from the aryl carboxamides series was TCMDC-125454 (**Figure 2.2**), a highly potent molecule with a *P.*

falciparum IC₅₀ value of 60 nM, low cytotoxicity and favourable hERG and microsomal stability profiles.

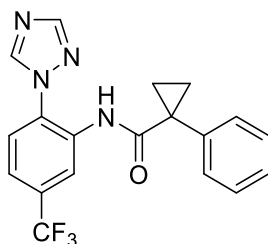


Figure 2.2 Chemical structure of TCMDC-125454.

Other related compounds within the carboxamide analogue set were also attractive from a medicinal chemistry stand point^[8] therefore emphasising the success of the fast-track TCAMS screening programme which identified a number of high quality starting points for antimalarial lead optimisation. However, as is the case with phenotypic screening, the molecular target (or targets) of identified compounds and chemotypes is not determined during this process.

There is therefore a requirement for subsequent target deconvolution to decipher the molecular target of compounds found to elicit desired antimalarial effects. This highlights the required compromise of a phenotypic screen: whilst such an approach has the potential to identify molecules that modify a disease phenotype, by acting on a target which may previously be unknown; the subsequent requirement to determine the relevant target (or targets) of the molecule can be very slow or even impossible.^[3] This often makes the process of drug optimisation following a phenotypic screen highly challenging, due to a lack of knowledge regarding the molecular mechanism of action. An example of a follow-up medicinal chemistry optimisation programme, using outputs from the TCAMS series, is well outlined here ^[14].

2.1.2 Target-based Screening

An alternative method of hit identification, which avoids the drawback of required target deconvolution following phenotypic assessment, is target-based screening. This, traditionally more common approach to drug discovery is generally hypothesis driven, where three hypotheses must be satisfied to enable successful identification of new drug molecules. Firstly, the selected target must be of significant importance in the specified human pathology; secondly, the molecular mechanism of action of the drug candidate at the selected target must elicit the required biological response; and finally, the activity observed in a preclinical screen that is used to select the drug candidate, must translate into clinical efficacy.^[2]

Target-based screens are often considered to be operationally simpler than phenotypic screens since they use pure proteins within biochemical assays. However, this approach requires selection of the target protein prior to screening, which means that the screen conducted can only detect candidate molecules capable of modulating the selected target.^[15]

In contrast to Novartis and GSK, some pharmaceutical companies such as Roche's Genentech have remained focused towards target-based screens due to the argument that a compound with a known molecular target will always be favoured within a drug discovery project due to the added chemical and molecular knowledge that is available and can be utilised and exploited.^[3] Between 1999 and 2008, the use of target-based drug discovery led to the identification of 17 of the 50 first-in-class new molecular entities that were approved by the FDA during this period.^[2] The identification of Eltrombopag, an anti-thrombin agent, was achieved through the screening of small molecule libraries to detect compounds with the ability to activate a reporter molecule of thrombopoietin-dependent cell lines. In research conducted by Kuter *et al.*^[16] hit compounds from this initial screen were optimised to improve pharmaceutical properties and advance biological efficacy, which led to the development of Eltrombopag.^[2,16] This research highlights that cellular assays and biological investigation can be used effectively to discriminate different compound profiles identified in a target-based HTS screen, which can then drive structure-activity relationship (SAR) development and generate efficacious chemotherapeutic treatments.

In a distinct drug discovery programme, aimed at discovering non-peptide endothelin receptor agonists, a class of aryl-sulphonamidopyrimidine compounds were identified from a diverse compound library which led to the identification of Bosentan, a dual endothelin receptor antagonist for the treatment of pulmonary hypertension.^[2] A screen of several thousand compounds, carried out by Hoffmann-La Roche, identified this class of compounds which, after chemical and structural modifications, promoting potency, oral activity and binding affinity, resulted in the most potent analogue of the class, Bosentan.^[17]

The development of six of the new molecular entities, discovered through target-based methodologies between 1999 and 2008, also involved the rationalisation of their molecular mechanism of action at their specified target which was first selected for study and initial screening. Examples include: imatinib (Glivec), a BCR-ABL kinase inhibitor and targeted anti-cancer drug;^[18] the HIV-Integrase inhibitor, raltegravir for the treatment of HIV-AIDS infection;^[19] and maraviroc, a selective allosteric inhibitor of the chemokine receptor CCR5, also used in the treatment of HIV^[20] (**Figure 2.3**).

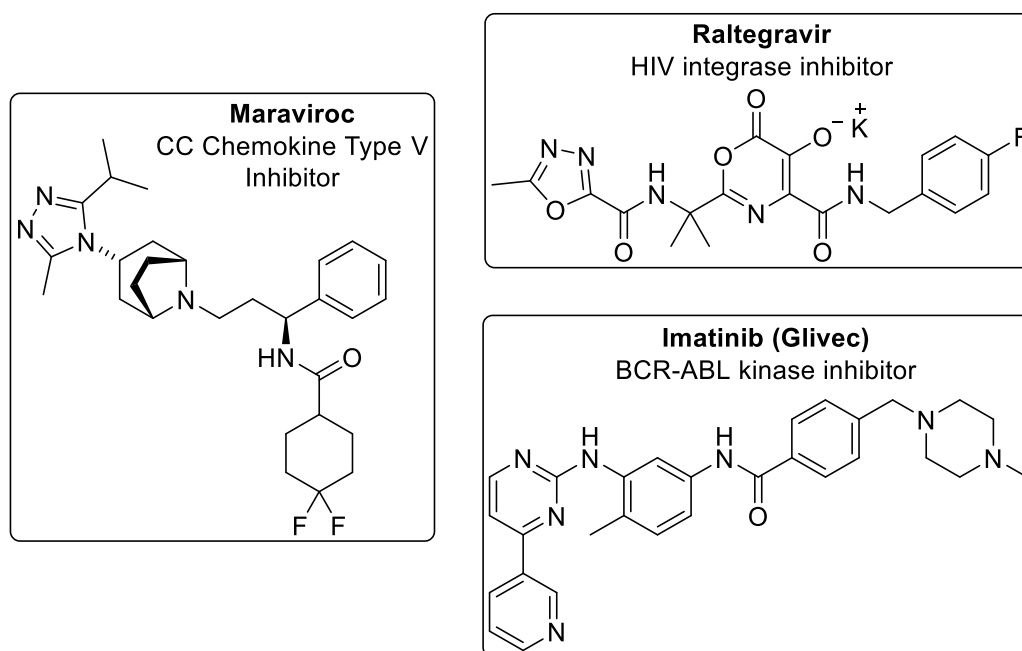


Figure 2.3 Chemical structures of maraviroc, raltegravir and imatinib (Glivec): providing examples of clinically approved chemotherapies that were lead optimised from hit structures identified in HTS studies as part of target-based drug discovery programmes.^[18–20]

These identified inhibitors therefore demonstrate some of the successes of target-based screening, and also highlight the potential that this drug discovery approach facilitates in the determining the molecular mechanism of action at a molecular target, which may not be apparent on initiating the discovery programme.^[2]

To try and replicate some of these drug discovery successes within our own body of research, a target-based screening approach was employed to identify new lead-like inhibitors of the novel *P. falciparum* IspD (*PfIspD*) enzyme. The use of this drug design approach facilitates the screening of a diverse area of chemical space with the aim of identifying novel chemical structures active against the selected *PfIspD* enzyme target which was identified prior to compound screening. Furthermore, the selection of a target-based screening approach also facilitates and recognises future requirements to consider inhibitor mechanism of action studies.

2.2 Chemotype Identification

For this body of research, a novel hit-finding strategy was consequently initiated to explore chemical space using chemoinformatics and virtual screening techniques with the aim of identifying a rational set of diverse chemical compounds, selected from a larger compound library. Cellular assays were subsequently used to profile the inhibitory activity of the identified focused compound library against the *PfIspD* enzyme in a HTS study. This screen identified a number of compounds and chemical distinct chemotypes with which we could initiate hit-optimisation and SAR development.

2.2.1 Chemoinformatics: Chemotype and Compound Selection

Chemoinformatics techniques of virtual screening, diversity selection, activity prediction, compound clustering and filtering can be employed as a rational alternative to more Traditional Random Screening (TRS) approaches. TRS generally produces high hit rates but also tends to identify compounds that may be less optimal for SAR studies.^[21]

In an attempt to combat the issues of low chemotype diversity and poor drug-likeness within known *PflspD* inhibitors, a novel hit finding strategy was developed to explore chemical space using a number of chemoinformatic methodologies. Similarity searching was used to explore and ultimately expand chemical space around compounds known to be active against *PflspD*, alongside the employment of scaffold hopping methods which together aimed to identify new, undiscovered chemotypes. These approaches enabled the selection of a focused ligand library for sequential application in a HTS regimen; a representative scheme depicting the described research strategy is shown below (Figure 2.4).

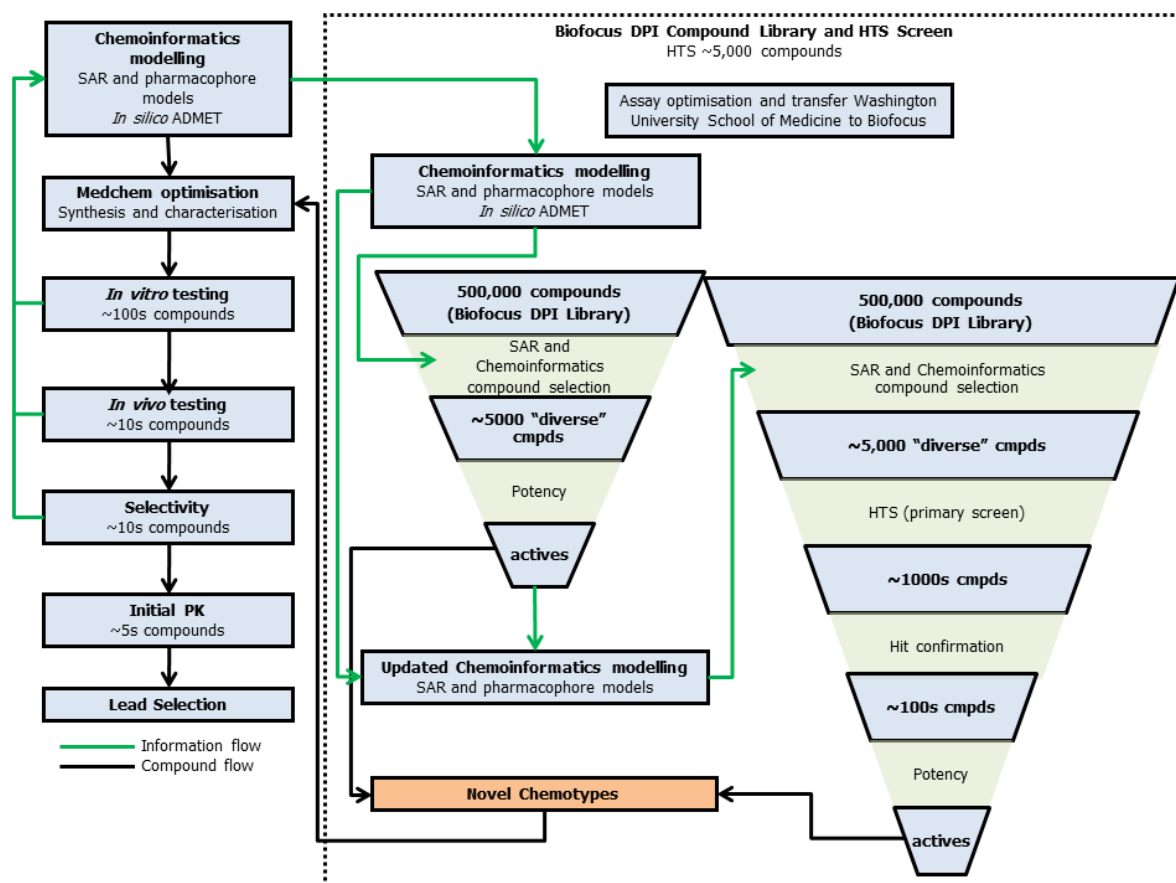


Figure 2.4 Representative flow diagram of sequential chemoinformatics and HTS.^[22]

The initial selection of a focused ligand library was based on the two parallel approaches of ligand-based and structure-based virtual screening. This combined chemoinformatics strategy ultimately led to the selection of 5000 compounds from the divergent “BioFocus Combined Library” of around 500, 000 compounds which was used as the molecular compound library in this virtual screening study. The “Biofocus Combined Library” is a concatenated library of the BioFocus Diverse and BioFocus SoftFocus libraries which together provide close to 540, 000 compounds.^[22]

Focused chemoinformatic compound selection uses a number of methods but is fundamentally based on the similarity principle which specifies that “structurally similar compounds are more likely to exhibit similar properties”^[23]. Chemoinformatic similarity searching was therefore used to try and achieve scaffold hopping across chemical chemotypes.

Scaffold hopping is a strategy for discovering structurally novel compounds, starting from compounds known to be active, and ending with a novel chemotype through modifications to the central core of the original molecule.^[24,25] Scaffold hopping therefore enables the identification of equipotent compounds with novel chemical backbones that display improved molecular properties.^[26] This technique was consequently employed to move away from known chemotypes and chemical structures within current literature, and identify novel *Pfl*spD inhibitors that would expand and develop the limited number of known *Pfl*spD inhibitors at this time, which generally displayed relatively poor mM activity.^[27–31]

Query libraries were constructed around several compound categories (**Table 2.1**) to facilitate similarity searching against which, all compounds in the diverse “Biofocus Combined Library” were assessed. These categories included natural substrates of the IspD enzyme, since substrate mimetics may possess inhibitory enzyme activity; natural substrates of the IspC enzyme using the rationale that additional IspC inhibition may prevent resistance development against an inhibitor capable of dual inhibition; as well as known IspD and IspC inhibitors, active at concentrations of $\leq 1 \mu\text{M}$.

E. coli IspD (*Ecl*spD) is a metalloprotein with a Mg^{2+} ion present in the CTP binding site which is essential for IspD activity.^[27,32] Based on the assumption that the *Pfl*spD homologue is also likely to contain an active site Mg^{2+} ion, similarity searches were performed against metal binding groups and fragment structures, such as sulphonamides and hydroxamic acids, since metal binding groups may prevent *Pfl*spD enzyme turnover. Known biophosphate isosteres, such as CF_2 -linked phosphonic acid, tetrazole and *O*-linked malonyl, were also used as query molecules since phosphate groups are present in the natural substrates, MEP and CTP, of the IspD enzyme (**Chapter 1, Scheme 1.1**^[32,33]).^[22]

Table 2.1 summarises the compound categories of the query molecules used for similarity searching within the 500, 000 compounds of the “Biofocus Combined Library”.

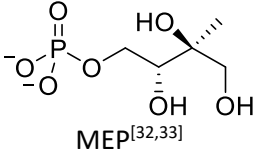
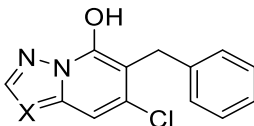
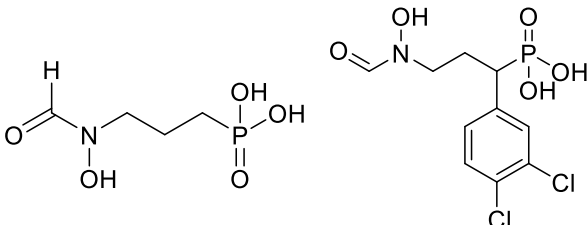
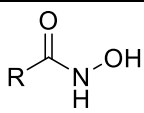
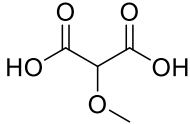
Compound Query Category	Example structure(s)	Number of compounds known in literature
IspD and IspC natural substrates	 MEP ^[32,33]	3
Known IspD inhibitors	 Azolopyrimidine AtIspD inhibitor ^[30]	5
Known IspC inhibitors	 Fosmidomycin and structural analogues ^[34]	41
Metal binding groups	 Hydroxamic acids ^[35]	146
Biophosphate isosteres	 2-methoxymalonic acid ^[22]	7

Table 2.1 Example query structures and associated categories used for similarity searching.

Fingerprint similarity and scaffold-hopping methods were some of the cheminformatics techniques used to select compounds from the “Biofocus Combined Library” that were assessed as being similar to the defined query groups. Compounds with a Tanimoto coefficient > 0.7 compared to any query compound (as defined by ECFP4, FCFP4^[36] or MDL^[37] public key fingerprints) or compounds with an average ECFP4 Tanimoto coefficient between 0.2 to 0.4, used to achieve scaffold hopping,^[38] were selected from the “Biofocus Combined Library”.

Fingerprint similarity methods use molecular fingerprints as a way of encoding the structure of a molecule. The most common type of fingerprint is a series of binary digits (or bits) that represent the presence or absence of particular substructure within a molecule. The comparison of fingerprints between two given structures allows the similarity of the two molecules to be determined and therefore identifies matches to query structures. The similarity between two molecules is most

frequently quantified using the Tanimoto coefficient which gives a measure of the number of fragments in common between two molecules using binary vectors. The Tanimoto coefficient can range from a value of zero to one: a value of one indicates that selected molecules have identical fingerprint representations, but may not necessarily be structurally identical, whereas a value of zero indicates no similarity between compared molecules.^[39,40]

Scaffold-hopping describes the identification compounds which show similar activity to a specified query compounds but which represent different chemotypes of chemical constructs.^[24,26] This chemoinformatics methodology is therefore valuable since it facilitates the identification of alternative compound series which may lack certain chemical motifs which cause suboptimal pharmacokinetics or difficult chemistry within existing development programmes.^[24,39,41] Together, the use of these chemoinformatic selection methods identified 23, 000 unique compounds from the diverse “Biofocus Combined Library” in this chemoinformatic virtual screen.^[22]

To filter these compounds further, this subset of selected molecules were docked against known crystal structures of the IspC and IspD enzymes.^[42] Specifically for the IspD protein docking, known protein structures were used to facilitate compound evaluation at the *E. coli* IspD CDP-ME binding site (PDB: 1IN1^[43]) and also the *A. thaliana* IspD allosteric binding site (PDB: 2YC3^[30]). Binding (or fitness) scores, a measure of a compounds binding affinity at a given protein binding site (**Chapter 4, Section 4.1**),^[44] using the GOLDScore scoring function^[45–47] were assigned to each compound after docking the structures into the IspD and IspC protein complexes. This provided a measure of predicted binding strength of each compound at the given enzymes, allowing compounds to be ranked based on their expected inhibitor activity, as evaluated by their measured binding score.

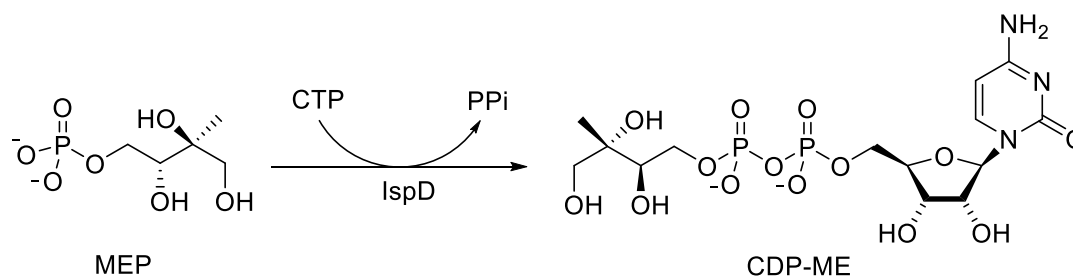
The 23, 000 compounds were then filtered according to calculated compound solubility (see **Section 2.9.1.3**) since acceptable solubility is required for reliable assay readout and inhibitor development. Therefore, compounds with LogS (solubility log) values of > -3.5 were selected to comprise our focused ligand library.^[48] The docking validation studies were therefore used to confirm that no outstanding compounds, as evaluated by the described docking studies, were not taken forwards and considered experimentally as a result of compound filtering by the defined LogS solubility threshold. Ultimately, a focused ligand library of 5000 compounds from the original “Biofocus Combined Library” were selected on the basis of optimal predicted binding affinities and molecular and physicochemical properties from the combined results of these chemoinformatics methodologies.^[22,42] This focused library of 5000 compounds was then entered into our designed HTS study.

2.3 PflspD HTS

In order to profile the inhibitory activity of the selected 5000 compounds against *PflspD*, a HTS was conducted by Biofocus DPI screening the selected compound library. To facilitate this HTS study, a *PflspD* enzymatic assay was developed and transferred from the laboratories of our collaborator Audrey Odom at the Washington University School of Medicine, St Louis, USA (**Section 2.2.3**).^[49] The 5000 compounds identified through the previously described cheminformatics methods, were tested directly against purified *PflspD* to determine their inhibitory activity against the enzyme. Biofocus DPI optimised the *PflspD* enzyme assay for the purpose of HTS, enabling each of the 5000 selected compounds to be screened and evaluated in terms of *PflspD* inhibition; this resulted in the successful screening of 316 plates, comprising the 5000 compounds.

2.3.1 PflspD Enzymatic Assay

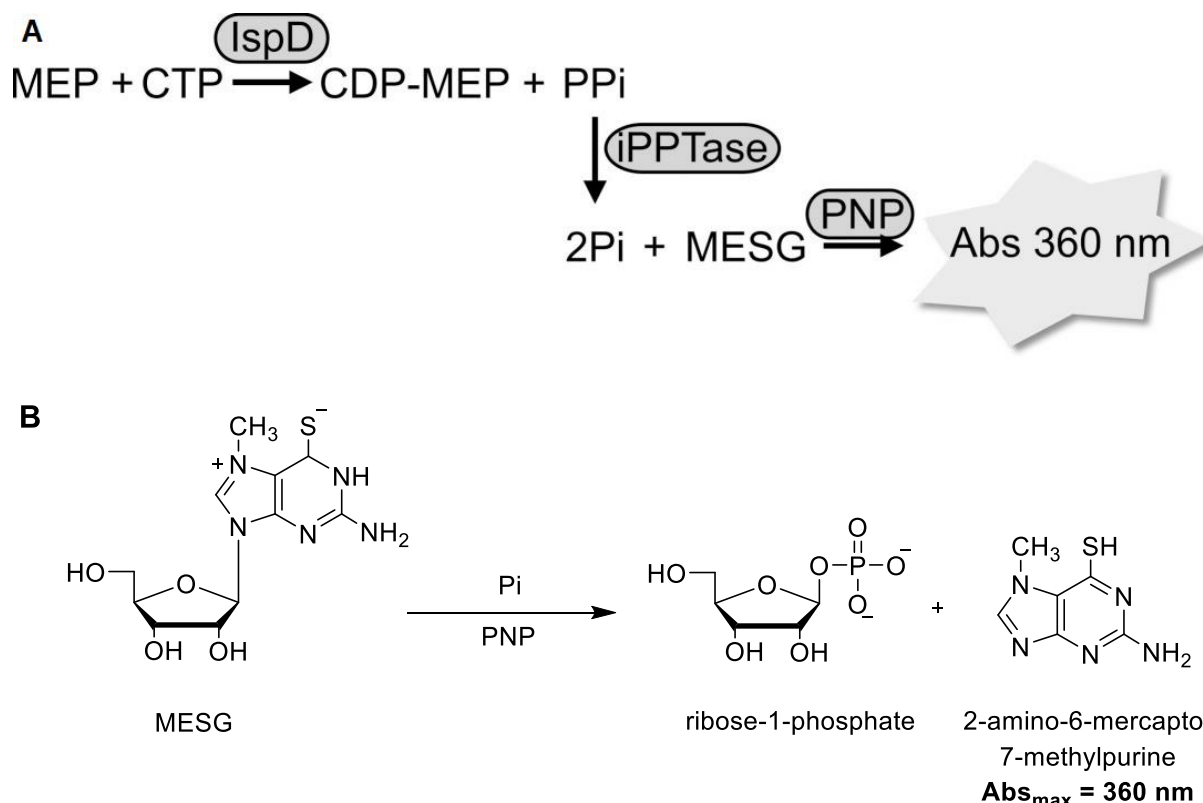
The Odom lab developed a *PflspD* enzyme assay that operates by a linked enzymatic reaction detecting the release of inorganic pyrophosphate by the IspD enzyme (**Scheme 2.1**).^[49] *PflspD* is reacted in the presence of its two substrates, methylerythritol phosphate (MEP) and cytidine triphosphate (CTP) to produce the product, CDP-ME and inorganic pyrophosphate (PPi) as a natural by-product of the reaction.



Scheme 2.1 IspD-catalysed biosynthesis of CDP-ME: the third enzymatic reaction of the MEP pathway.^[29,50]

In order to examine this enzyme-catalysed process, the release of PPi can be monitored, first through reaction with inorganic pyrophosphatase (*i*PPTase), producing inorganic phosphate (Pi) which can then react with the synthetic substrate, 2-amino-6-mercapto-7-methylpurine riboside (MESG). MESG is converted enzymatically by purine nucleoside phosphorylase (PNP), in the presence of Pi, resulting in the release of a ribose-1-phosphate and 2-amino-6-mercapto-7-methyl purine that has a maximal absorption of 360 nm^[51] (**Scheme 2.2**). The measured absorption at 360 nm allows quantification of the Pi consumed in the second enzyme-linked reaction. Since Pi consumption is proportional to the formation of 2-amino-6-mercapto-7-methyl purine; this in turn corresponds to

the quantity of P_i released by *PflspD*, therefore providing a quantifiable measure of *PflspD* enzyme activity.^[49]



Scheme 2.2 A) The *PflspD* enzymatic assay; B) Structural schematic of the enzymatic conversion of MESG to ribose 1-phosphate and 2-amino-6-mercapto-7-methylpurine by PNP.^[49,51]

The *PflspD* enzyme assay is a rapid and quantitative assay which is performed in 96-well plates for standard small-scale laboratory throughput.^[49] It has been verified that the assay is linear with respect to time and enzyme concentration and that assay activity is dependent on the presence *PflspD* and both the CTP and MEP enzyme substrates (**Figure 2.5**).^[49]

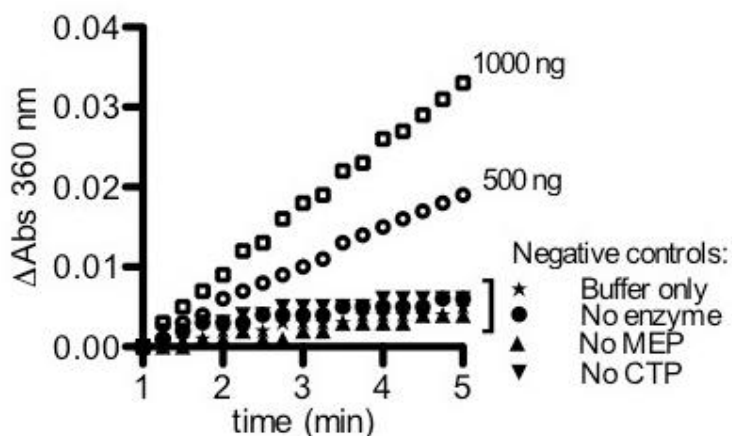


Figure 2.5 *PflspD* enzymatic assay validation: change in 360 nm absorption is linear with respect to time and enzyme concentration; the assay is dependent on the presence of *PflspD*, CTP and MEP.^[49]

The *PflspD* enzyme assay (**Scheme 2.2**) can be modified for the HTS of large compound libraries, as verified by the Biofocus HTS, and is suitable for both steady-state and stopped-flow kinetic analysis of enzymes.^[49]

2.3.2 HTS Outputs and Chemotype Selection

The selected 5000 compounds were profiled for *PflspD* activity using the *PflspD* enzymatic assay in a HTS regimen conducted by Biofocus. Active compounds were defined as those displaying IC_{50} values of $\leq 20 \mu M$ at the *PflspD* enzyme: this led to the initial identification of 76 compounds with *PflspD* inhibitory activity. An expression of the activity of a drug or compound, in terms of the concentration required to produce a defined effect at a specified molecular target, can be given as an IC_{50} measurement when the compound being administered is an antagonist.^[52] The term IC_{50} therefore represents the molar concentration (or dose) of administered compound (antagonist) that is required to cause half-maximal inhibition of the total enzymatic or biological activity.^[53,54]

Activity readouts were considered for two methods of IC_{50} measurement: both point of inflection (PoI) and $y=50$ interpretations.^[55] PoI IC_{50} readings report the IC_{50} value as the data value on the x-axis which corresponds to the point of inflection on the dose-response curve (**Figure 2.6, A**). Alternatively, the $y=50$ method of measurement can be used to report IC_{50} values: here the reported IC_{50} value is the value on the x-axis that corresponds to a 50% response on the y-axis (**Figure 2.6, B**). Using either method of measurement, the resulting IC_{50} value was required to meet a defined threshold of $\leq 20 \mu M$.^[22,42]

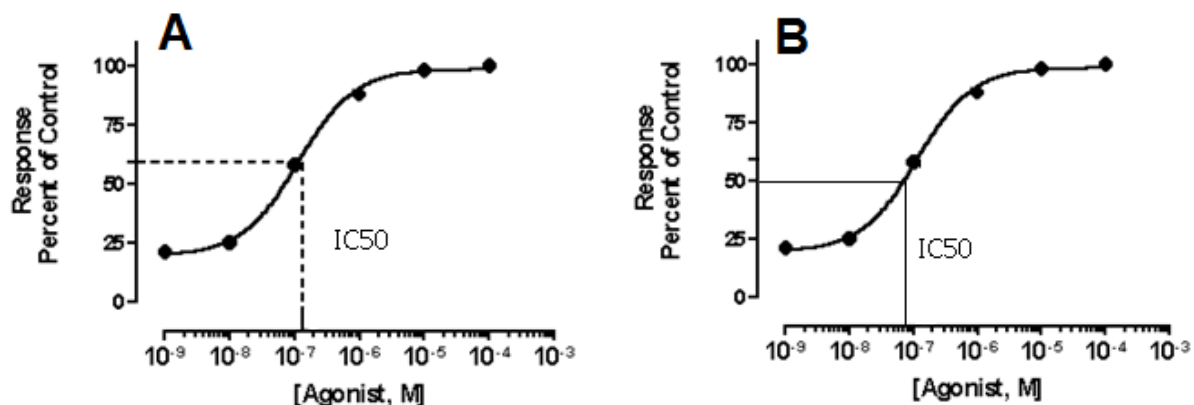


Figure 2.6 Graphical representation of the difference in IC_{50} values using different methods of measurement. **A:** PoI method of IC_{50} measurement; **B:** $y=50$ method of IC_{50} measurement.

Following LC-MS (Liquid Chromatography-Mass Spectrometry) analysis, 54 compounds from the original 76, with acceptable levels of purity ($\geq 75\%$ pure as measured by LC-MS^[22,56]), were selected as HTS hit compounds and classified as active against *PflspD*. These 54 active compounds (**Appendix 1**), comprising more than 10 structural chemotypes, displayed a broad range of activities which varied from the specified 20 μM threshold to sub-micromolar activity levels (**Figure 2.7**).^[22,56]

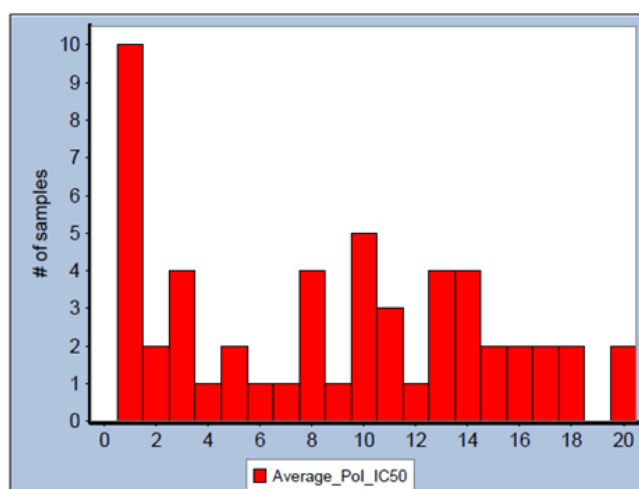


Figure 2.7 Bar graph depicting the range of *PflspD* IC_{50} activities, using PoI IC_{50} values (given in μM), of the 54 hit compounds from the HTS.^[56]

Significantly, the 1,2-benzo[*d*]isothiazol-3(2*H*)-one (BITZ) chemotype was repeatedly identified (three times) within a number of hit structures, including the most active hit from the screen: **DT2009-0168020** which displayed an inhibitory *PflspD* IC_{50} value of 484 ± 149 nM (**Figure 2.8**). In addition, the hit **DT2009-0097223**, based around a thiadiazole phenyl-linked sulphonamide chemotype also displayed encouraging inhibitory *PflspD* activity with an IC_{50} value of 775 nM (**Figure 2.8**). Both hit compounds have a molecular weight (MW) and associated ligand efficiency (LE) appropriate for further exploration.

LE is a method of comparing molecules in terms of their average binding energy per atom. Kuntz *et al.*^[57] described LE as the free binding energy of a molecule divided by its size, as defined by the number of heavy (non-hydrogen) atoms in the molecule.^[58] Therefore, molecules which achieve a given potency with fewer heavy atoms are more efficient.^[1] Lipinski's "Rule of five" indicates that for compounds to have good absorption and permeability, they should meet his specified molecular properties as a good oral drug profile is unlikely when one of these guidelines is not met.^[59] Therefore, in a successful drug discovery setting, and according to Lipinski, compounds should: have no more than five hydrogen bond donors, no more than 10 hydrogen bond acceptors, a MW of less than 500 and a calculated Log P (*ClogP*) of less than five.^[59] However, Lipinski also points out that a drug candidate may still display a good oral drug profile when only one of these parameters is not met by a specified molecule.

Following preliminary investigations around the **DT2009-0097223** hit, subsequent compound analogues were found to be inactive at *PflspD* and did not demonstrate a tractable SAR [based on the synthesis of 14 compounds derived from DT2009-0097223, all of which displayed *PflspD* IC₅₀ values > 50 μM against *PflspD*]. As a result, further inhibitor development based around the thiadiazole phenyl-linked sulphonamide chemotype was terminated.

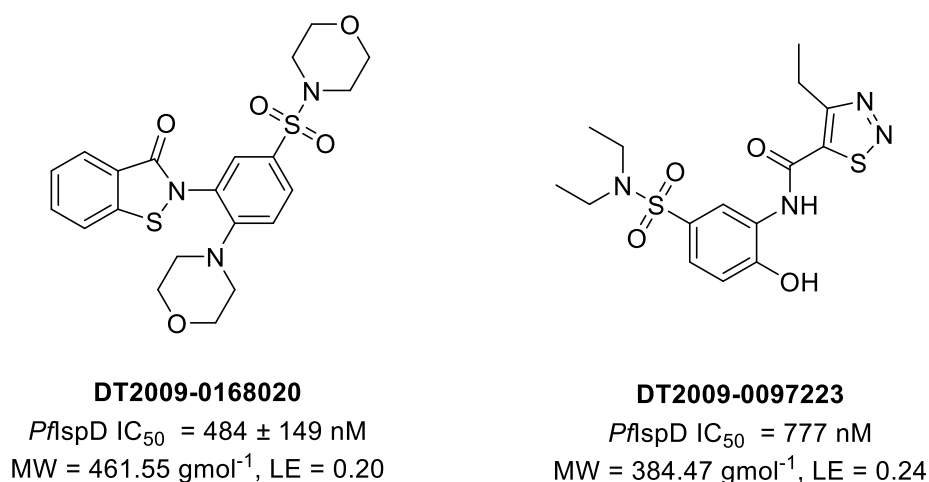


Figure 2.8 Chemical structure, *PflspD* enzyme activity and ligand efficiency of the two most active HTS hit compounds **DT2009-0168020** and **DT2009-0097223**.

The BITZ chemotype was therefore selected as the hit chemotype to take forward for *PflspD* inhibitor design and SAR development. The inhibitory activity of **DT2009-0168020** at *PflspD* was highly encouraging and therefore represented a good starting point for analogue development. A preliminary SAR around the **DT2009-0168020** hit was also evident from outputs of the HTS, thus increasing our confidence in this chemical motif for the development of a tractable series. At the time of hit identification, a series of literature searches found no references relating the BITZ

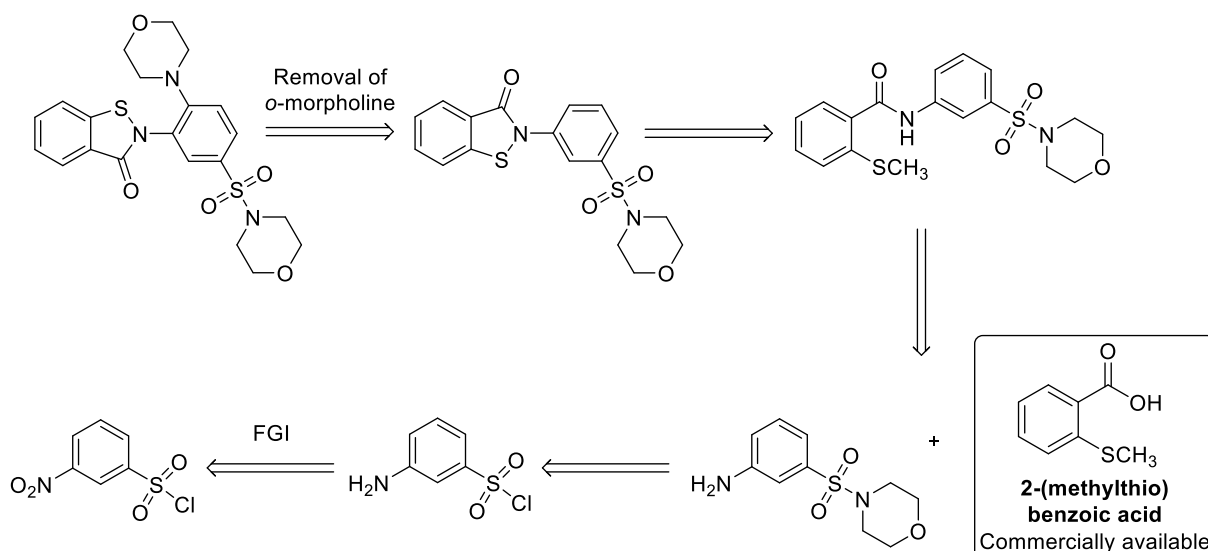
chemotype to *IspD* enzyme inhibition or antimalarial drug development of any kind. With these facts in mind, we proceeded in developing the BITZ chemotype with confidence that this chemical motif represented a distinct starting point for hit-to-lead optimisation.

2.4 Synthetic Strategies to Generate the 1,2-benzo[*d*]isothiazol-3(2*H*)-one Chemical Motif

A number of synthetic pathways have been identified which facilitate generation of the 1,2-benzo[*d*]isothiazol-3(2*H*)-one chemical motif and subsequent analogues of the chemotype. Each synthetic route has been applied with varying success and synthetic efficiency with the reproducibility of each method depending on analogue complexity. The first synthetic requirement was to generate close structural analogues and simplified compound structures of the **DT2009-0168020** HTS hit, facilitating further *PfIspD* enzymatic testing of these structures to enable validation of the selected chemical motif.

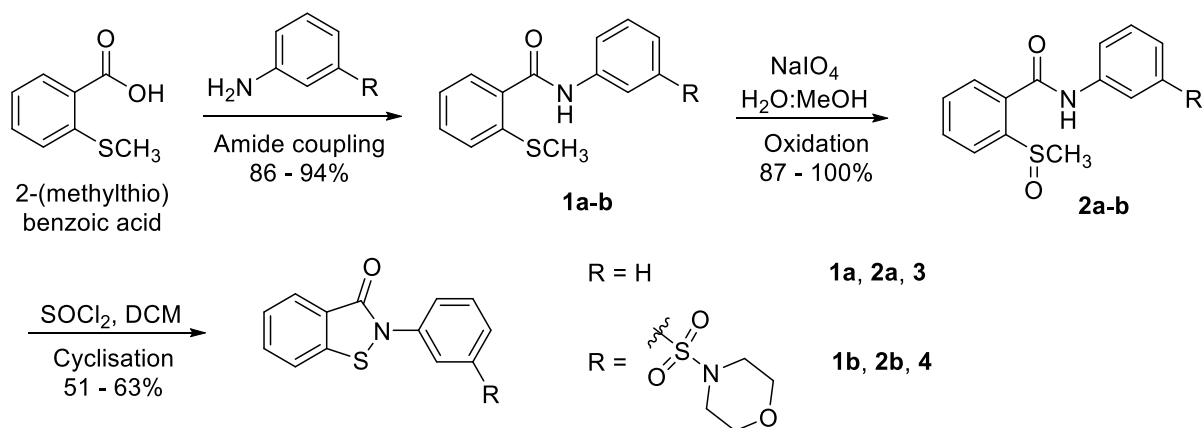
2.4.1 Synthetic Strategy: Route 1

To enable full and extensive SAR development around the BITZ motif there was a requirement for the rapid generation of BITZ analogues in high numbers. Availability of starting materials, ease of chemical synthesis and low cost of component chemicals were therefore key considerations in determining appropriate syntheses. Considering **DT2009-0168020** (Figure 2.8) from the perspective of retrosynthetic analysis, it was quickly apparent that an analogue series, structurally related to this hit compound, was synthetically plausible (Scheme 2.3). A decision was made to remove the *ortho*-morpholine functionality present within the **DT2009-0168020** hit to generate a more simplified starting point from which to determine a plausible synthetic route towards the BITZ chemotype and initiate SAR explorations around the motif. This decision was also supported by observations made in parallel investigative SAR studies on-going at this time (Section 2.5.1). Analysis of the chemical cleavage points within **DT2009-0168020** (having removed the *ortho*-morpholine group) brought us to the commercially available starting material of 2-(methylthio) benzoic acid which, through forward synthesis could quickly be progressed to the required BITZ entities using a thionyl chloride mediated ring closure as the key and final step of BITZ motif generation (Scheme 2.4).



Scheme 2.3 Simplification and retrosynthetic evaluation of the HTS hit, **DT2009-0168020**.

A linear, three-step synthesis of BITZ compounds analogues was devised (**Scheme 2.4**) involving an acid-chloride mediated amide coupling of 2-(methylthio) benzoic acid with appropriately substituted aniline derivatives to generate (methyl-thio)benzamide compounds **1a-b**.^[60,61] This was followed by oxidation of intermediates **1a-b** to the corresponding sulfoxides, methylsulfinyl benzamides **2a-b**,^[60] which were then cyclized using thionyl chloride^[62] to give the required inhibitor structures **3** and **4**. Depending on the structural design of the side chain of specified BITZ compounds, additional synthetic steps can be incorporated into this synthesis (**Scheme 2.4**) in order to generate a wide range of structurally diverse BITZ compounds.



Scheme 2.4 Synthetic **Route 1**: Thionyl chloride mediated generation of BITZ compounds **3** and **4**.

To test the reliability and scope of this synthesis, analogues **3** and **4** (Figure 2.9) were generated by the synthetic route outlined in **Scheme 2.4**. **4** is a simplified analogue of the **DT2009-0168020** hit in which the morpholine functionality *ortho* to the BITZ headgroup has been removed. **3** is a simple BITZ core derivative with an un-substituted *N*-phenyl ring as a basic side chain. **3** is therefore a highly

simplified BITZ derivative of the original **DT2009-0168020** HTS hit and therefore aids rational SAR development by providing a distinct point of reference against which the activity and structural development of all subsequent, more complex, BITZ inhibitors can be evaluated.

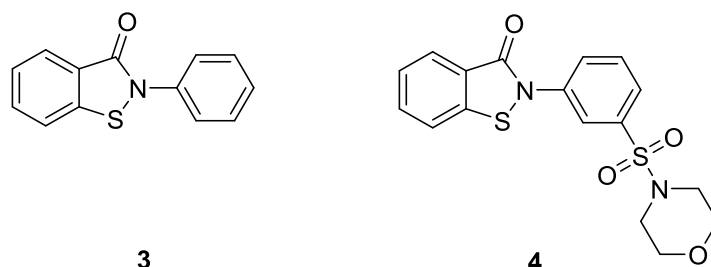
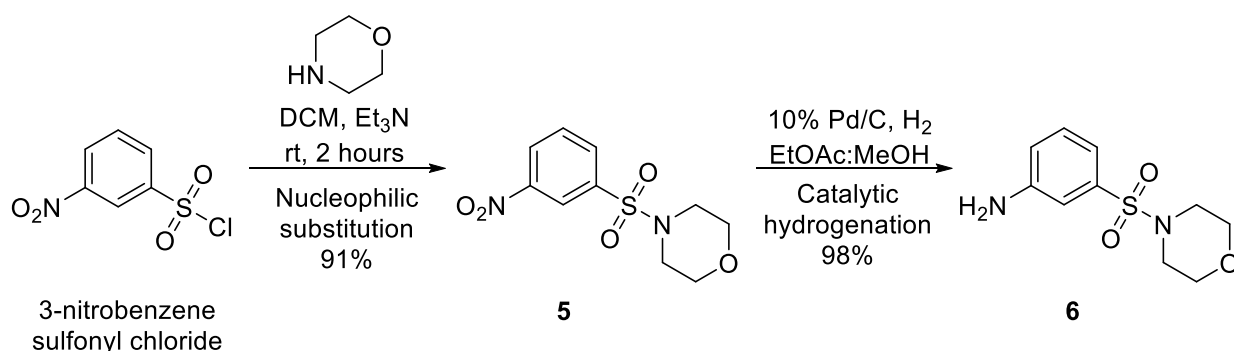


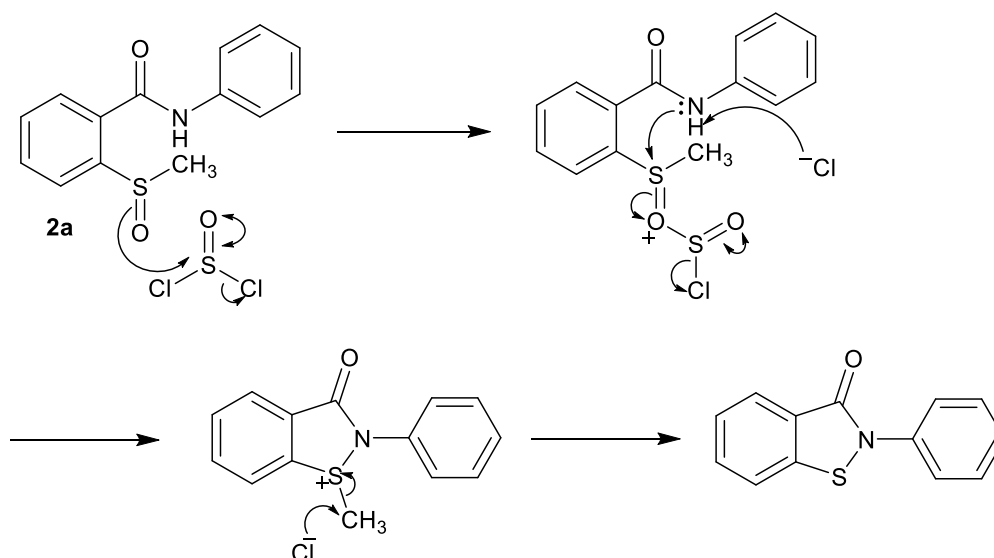
Figure 2.9 Chemical structures of simplified BITZ analogues **3** and **4**.

To generate **4**, the morpholine sulfonyl side chain was first synthesised in a straightforward two-step reaction (**Scheme 2.5**) using established methodology. Accordingly, reaction between morpholine and 3-nitrobenzene sulfonyl chloride gave **5**^[63] followed by Pd-catalysed hydrogenation, converting the nitro functionality into a 1° amine.^[64] This gave the *meta*-substituted aniline derivative **6** for use in the initial amide couple step of **Route 1** (**Scheme 2.4**). For the synthesis of **3**, un-substituted aniline was used directly in the first synthetic step.



Scheme 2.5 Synthesis of **6**.

All steps of the combined syntheses (**Schemes 2.4** and **2.5**) proceeded in moderate to high yields, over short reaction times with straightforward isolation and purification of all target compounds and intermediates. The final step of thionyl chloride mediated ring closure, generating the closed BITZ motif and final analogues **3** and **4**, performed consistently well with moderate yields that were not compromised by the increased structural complexity of **4** compared to **3**. Indeed, the mechanism by which this ring closure proceeds may be considered slightly unusual but can be described in the following manner (**Scheme 2.6**).



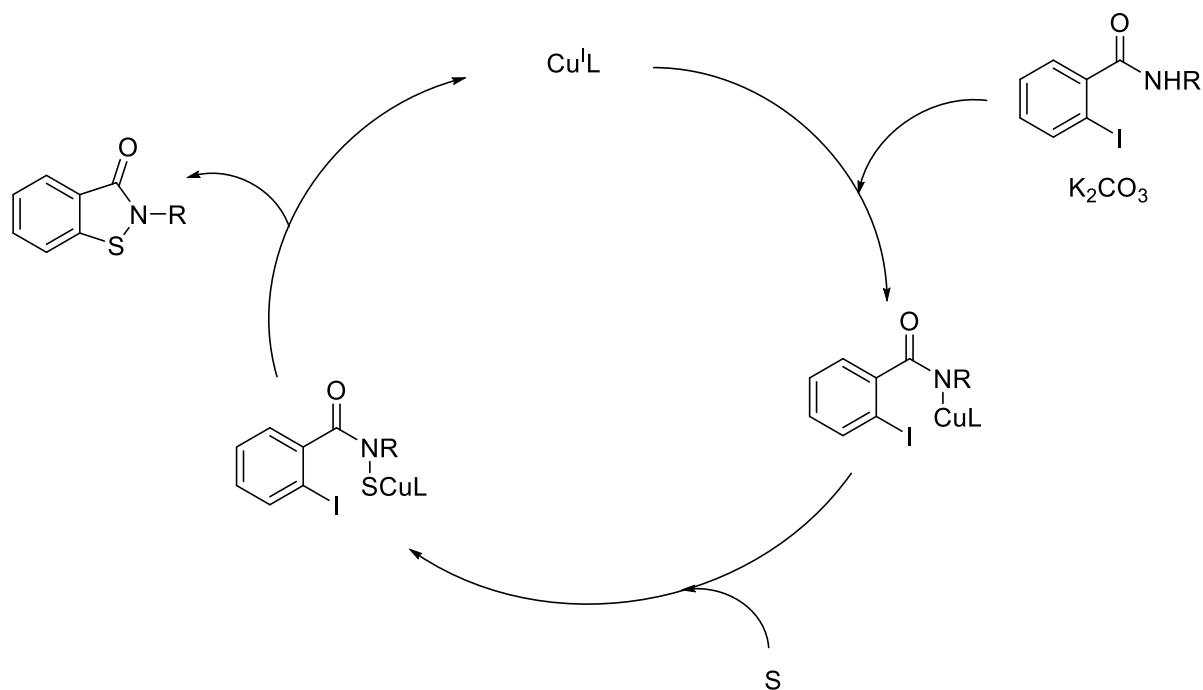
Scheme 2.6 Proposed mechanism for the thionyl chloride mediated ring closure and cyclisation of the BITZ ring.^[62]

Initial attack of the sulfoxide of **2a** on thionyl chloride generates a positively charged intermediate. The N-S bond is formed in a rapid 5-membered ring cyclisation which is accompanied by the entropically favourable loss of gaseous SO_2 . This is followed by sulfur demethylation *via* an $\text{S}_{\text{N}}2$ -mediated reaction with chloride to generate the BITZ motif and analogue, restoring a +2 oxidation state at the sulfur atom.^[62]

This synthetic route was used to generate a number of BITZ inhibitors as, despite a linear pathway, this synthesis is easily modified to incorporate varying chemical constructs to generate a range of BITZ side chain derivatives.

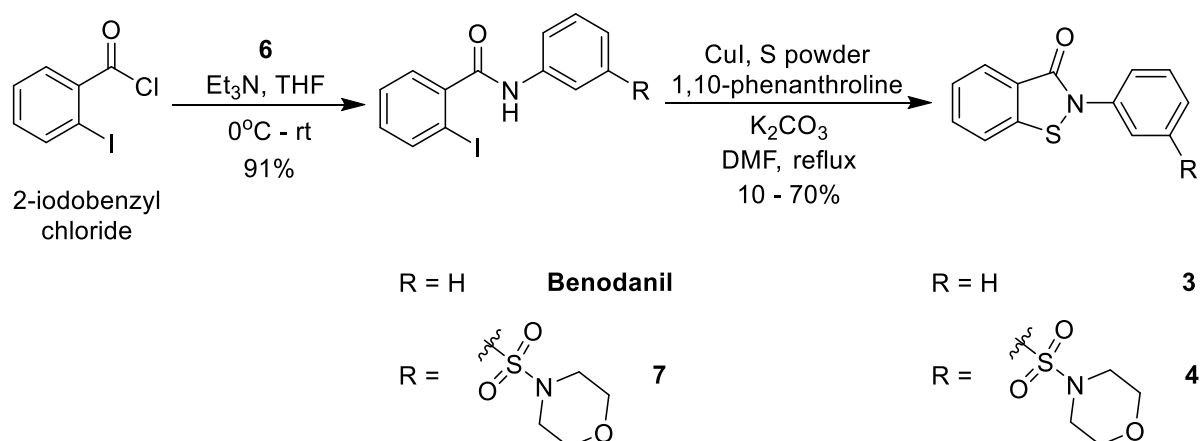
2.4.2 Synthetic Strategy: Route 2

An alternative synthesis, constructing the BITZ motif *via* a copper-mediated heteroatom coupling reaction, using copper(I) iodide and sulfur powder, has also been explored. This copper-mediated sulfur-nitrogen heteroatom coupling, outlined by B. S. Bhakuni *et al.*^[65] has been proposed as ‘an environmentally benign method’ of accessing a diverse library of aryl benzoisothiazolones from readily available substrates including 2-halo-arylamides, as hyper-valent iodine reagents, sulfur powder and the ligand 1,10-phenanthroline. The catalytic cycle has been proposed to proceed *via* a LCu-NR amide complex, where the S atom inserts into the LCu-NR bond which then reacts intramolecularly *via* reductive elimination to give the benzoisothiazolone ring and regenerated copper(I) iodide complex (**Scheme 2.7**).^[65]



Scheme 2.7 Proposed mechanism for the copper-mediated synthesis of S-N heterocycles^[65].

This chemistry was applied to generate **3** and **4** via a significantly shorter synthetic route than Route 1 (**Scheme 2.4**), using readily accessible and low cost starting materials (**Scheme 2.8**). The commercially available starting material, **Benodanil** (2-iodobenzanilide), was used for the straightforward, single-step generation of **3** which proceeded rapidly with a short reaction time of three hours in a clean reaction which gave **3** in a 70% yield. For the synthesis of **4**, and to determine the tolerance of **Route 2** (**Scheme 2.8**) to increased molecular complexity (additional functional groups), a short two-step synthesis was employed. To generate the 2-halo-arylamide reagent **7**, required to yield the side chain of **4**, a simple amide coupling step, preceding the copper-mediated ring closure was used. The synthesis of intermediate **7** required coupling the acid chloride, 2-iodobenzyl chloride, with **6** (**Scheme 2.5**).

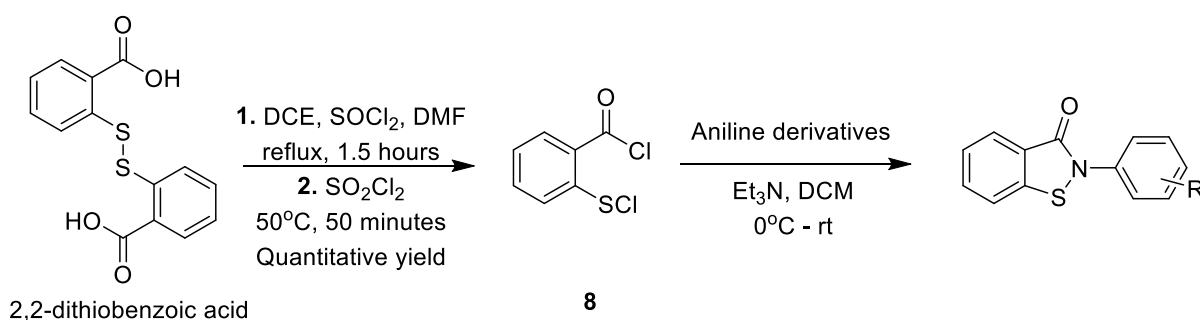


Scheme 2.8 Synthetic **Route 2**: Copper(I) iodide-mediated sulfur-nitrogen heteroatom coupling for the generation of BITZ compounds **3** and **4**.^[65]

Despite the ease of synthesis and high yield achieved in the synthesis of **3**, this was not reproduced with **4** where only a 9.9% yield was observed in the copper-mediated heteroatom coupling step. This indicated that this synthetic route is less tolerant to the increased reagent complexity needed for more structurally complex BITZ analogues, despite the consistent yields reported by B. S. Bhakuni *et al.* with analogues explored in their study.^[65]

2.4.3 Synthetic Strategy: Route 3

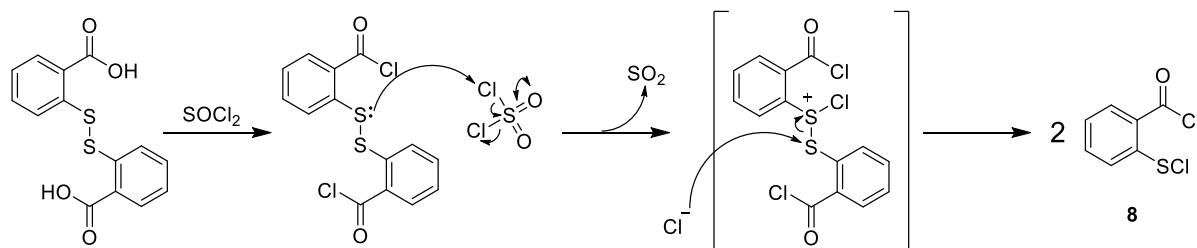
Identification of a third synthetic pathway, using a stable and isolatable acid chloride **8**, enabled the rapid synthesis of many BITZ analogues, supporting the incorporation of a varied and diverse range of side chains. The generation of the 2-chlorothiobenzoyl chloride intermediate **8** occurs in a rapid two-step, one-pot synthesis using the disulphide, 2,2-dithiobenzoic acid.^[66] Condensation of **8** with an appropriately substituted aniline derivative then enables the required BITZ scaffold to be easily and swiftly obtained (**Scheme 2.9**).



Scheme 2.9 Synthetic **Route 3**: Acid chloride-mediated amide coupling and simultaneous heteroatom ring closure for the generation of BITZ derived compounds.^[66]

For the generation of **8**, thionyl chloride initially converts the two carboxylic acid components of 2,2-dithiobenzoic acid to the corresponding acid chlorides. This is then followed by cleavage of the

disulphide bond, mediated by suluryl chloride in the second step, producing two molecules of **8** (Scheme 2.9).^[66]



Scheme 2.10 Proposed mechanism for the disulfide bond cleavage of 2,2-dithiobenzoic acid, mediated by suluryl chloride in the generation of **8**.

This rapid and efficient synthesis of **8** is low in cost, uses readily available starting materials and is capable of producing large quantities of the acid chloride in quantitative yield, without the need for purification before use in subsequent reactions. Since **8** appears to be stable under a N₂ atmosphere over a period of several weeks, this methodology offers a point of divergence within the synthesis of BITZ derived compounds. The outlined synthetic pathway facilitates divergent syntheses since the *N*-linked side chain adjacent to the BITZ core can be synthesised discretely, without requirement for component structure of the BITZ warhead to be present. As a result, this broadens synthetic possibilities, enabling the development of more chemically complex and diverse side chains as any structural component carrying a 1° amine functionality can be incorporated as a BITZ core side chain in a single synthetic step with **8**: a simple amide coupling and simultaneous ring closure (Scheme 2.9). Consequently, the length of synthesis for the generation of target BITZ compounds *via* this synthetic route is dependent only on the side chain complexity of each designed inhibitor.

Synthetic **Routes 1** and **3** have been used frequently throughout this research, generating a diverse range of small molecule inhibitors based around the BITZ chemotype and core motif.

2.5 Assessment of Compound Activity Against the *PflspD* Enzyme and *P. falciparum* Growth in Culture

The *PflspD* enzyme assay^[49,51,67] was utilised throughout this body of research in order to assess and determine the inhibitory activity of designed BITZ compounds against the *PflspD* enzyme. Application of the enzyme assay provided biological data measuring the inhibitory *PflspD* activity of BITZ derived compounds, therefore enabling SAR to be developed around the selected chemotype and motif.

2.5.1 Assessing *P. falciparum* Growth Inhibition in Culture

Following assessment of compounds in the *Pf*lspD enzymatic assay and subject to the inhibitory activity measured, *P. falciparum* whole cell assays were performed to evaluate the activity of designed compounds against *P. falciparum* growth in culture. Prior to measurement of the inhibitory activity of a compound against the parasite, an acceptable measure of activity against the *Pf*lspD enzyme, now specified as a threshold IC₅₀ value of $\leq 5 \mu\text{M}$, should first be observed.

Ideally, we aim to observe potent *Pf*lspD enzyme inhibition in the initial enzyme assay which subsequently translates into comparable inhibition of *P. falciparum* whole cell growth as this would highlight an effective antimalarial agent that targets the *Pf*lspD enzyme. To adhere to target candidate profiles outlined by MMV, we have defined $\leq 1 \mu\text{M}$ as a suitable threshold for phenotypic activity.^[68] Compounds which display phenotypic activity at $\leq 1 \mu\text{M}$ are therefore defined capable of inhibiting *P. falciparum* whole cell growth in the early stages of hit to lead optimisation. Indeed, if BITZ compounds display a strong correlation between inhibitory activity against the *Pf*lspD enzyme and *P. falciparum* growth, this suggests that these compounds are able to prevent *P. falciparum* parasite growth as a result of inhibiting the *Pf*lspD enzyme target.

As stated, all compounds that demonstrate acceptable inhibition of the *Pf*lspD enzyme (IC₅₀ $\leq 5 \mu\text{M}$) were subsequently be evaluated against the intraerythrocytic stage of *P. falciparum* in culture. A standard *in vivo* protocol will be used to quantify *P. falciparum* parasite growth, facilitated by application of the DNA fluorophore PicoGreen®.^[69] This is a method that is regularly used in the microbiology lab of our collaborators at Washington University and is consequently well validated.^[49] Consequently, it was a simple decision to continue utilising this assay to determine the inhibitory activity of novel BITZ compounds against *P. falciparum* parasite growth within this body of work.

This established *in vivo* methodology quantifying *P. falciparum* parasite growth represents an efficient and accurate method to assess antimalarial agents, based on the intercalation of the PicoGreen® fluorophore into *Plasmodium* DNA. This method detects the amount of *Plasmodium* DNA in a short-term culture, using a 96-well plate assay format, following incubation with potential antimalarial agents, therefore facilitating a quantitative measurement of anti-plasmodial activity across a large number of samples.^[69]

PicoGreen® is an ultra-sensitive nucleic acid dye that intercalates with double-stranded DNA (dsDNA) therefore enabling its detection in solution. Using a spectrofluorometer and the appropriate $\lambda_{\text{ex}}/\lambda_{\text{em}}$ wavelengths, as little as 25 pg/ml of dsDNA can be detected when intercalated with PicoGreen®.^[69] Parasites are first incubated with a potential antimalarial agent for 72 hours,^[49,67] followed by the

addition of PicoGreen® and a further incubation period of between five and 30 minutes before measurement of the resulting fluorescence.

The extent of parasite replication is directly proportional to the amount of fluorescence; a linear relationship between the two is observed in assays that maintain a parasitemia (Pt) of between 0.1% and 15%.^[69] The amount of resulting fluorescence, corresponding directly to plasmodial DNA content, can be easily read using a fluorescent Microplate reader. It has been demonstrated that cultures of both synchronised and non-synchronised parasites can be used with no observed differences in fluorescence output.^[69] In addition, it has been shown that it is possible for assay samples to be stored at -20°C before measuring cellular fluorescence without a significant change in the observed signal strength.^[69] This therefore highlights a further practical advantage of this methodology.

The described microfluorimetric assay for detecting anti-plasmodial compounds in an *in vivo Plasmodium* assay holds a number of advantages over previous *in vivo* methodologies which monitored the incorporation of ³H-hypoxanthine by *Plasmodium* parasites.^[69,70] Measurement of intercalation between the PicoGreen® fluorophore and *Plasmodium* DNA is highly appropriate for antimalarial drug discovery programs within developing countries, which is in contrast to previous anti-plasmodial radioactive isotope assays which were often not suitable for initiating drug discovery programs in developing regions due to financial restrictions and limited access to resources.^[69–71]

In terms of data analysis, the inhibitory concentration (IC₅₀) determined by application of this assay is defined as the drug concentration that produces 50% of the net fluorescence observed with non-treated control cultures. In addition to regular and successful use of this methodology by researchers at the microbiology laboratory at Washington University, the assay has also been validated through the assessment of known antimalarial drugs by others.^[69,72] It has been shown that the dose-response for Chloroquine, as determined by the microfluorimetric method (IC₅₀ = 31 ± 0.7 nM, mean ± SD) was comparable and in line with previously reported dose-response values determined by ³H-hypoxanthine incorporation (IC₅₀ = 29 ± 9 nM).^[69,72]

It is worth noting that the final dilution of anti-plasmodial agents in these assays contains less than 0.1 DMSO of the total assay solution since this amount has been found to have no measurable effect on parasite survival within the described system.^[69] This is therefore a parameter that is to be maintained throughout all applications of this assay.

2.6 Chemotype Validation: The BITZ Motif is Required to Achieve *PflspD* Inhibition

Having identified a number of synthetic routes by which to generate the BITZ motif, as well as the enzymatic and whole cell readouts to assess the potency of generated analogues, further validation of the chemotype and its chemical construct was required. To confirm the requirement for the selected BITZ chemotype and that this chemical headgroup is essential for achieving *PflspD* enzyme inhibition, some small molecule manipulations were made around the BITZ core (**Table 2.2**). These included heteroatom replacements within the BITZ headgroup, substituting the sulfur heteroatom for alternative functionalities, and also determining the activity of a ring open analogue of the BITZ motif **1a** at *PflspD*.

Replacement of heteroatoms in the thiazolone ring of the BITZ headgroup with alternative atoms enables the importance of each specific atom to be assessed. The assessment of each atom, as a measure of biological activity, provides a clear illustration of the importance of each heteroatom in maintaining *PflspD* activity due to its specified position within the headgroup. Measuring the inhibitory *PflspD* activity of an open ring BITZ derivative provides an assessment of the requirement for the closed BITZ motif in achieving *PflspD* inhibition. These chemotype validation studies also have the potential to inform mechanism of action studies (**Chapter 4**).

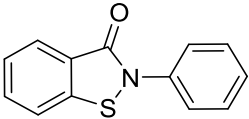
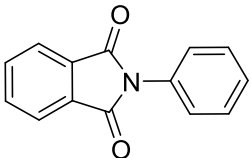
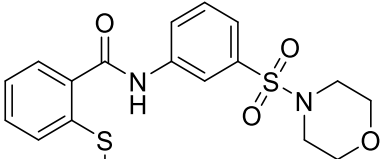
Compound Structure	<i>PflspD</i> Inhibition IC ₅₀ (μM)	Whole Cell Growth (3D7) Inhibition IC ₅₀ (μM)
 3	0.599	5.49
 2-phenylisoindoline-1,3-dione	>100	-
 1b	>350	>80

Table 2.2 Chemical structures and corresponding inhibitory activity against *PflspD* and *P. falciparum* 3D7 growth in culture (IC₅₀ given in μM) of compounds representing small molecular manipulations around the BITZ core.

Testing the simplest derivative of the BITZ core **3** proved to be highly encouraging since it was found to inhibit *PflspD* with comparable level of activity to that of the **DT2009-0168020** hit. This not only

provides an optimum reference point to our hit structure, against which evaluation of all future inhibitors can be made, but it also validates the selection of the BITZ chemotype, highlighting the importance of this chemical structure for *PflspD* inhibition.

Replacement of the sulfur heteroatom in the BITZ core with a carbonyl functionality, exemplified by 2-phenylisoindoline-1,3-dione, was shown to completely abolish inhibitory *PflspD* enzyme activity of the resulting structure (**Table 2.2**). This therefore highlights the requirement for the specific chemical construct of the BITZ headgroup and in particular, the presence of the sulfur atom adjacent and directly bound to the nitrogen atom, within the thiazolone ring system. Further to this, **1b**, the ring-open structure of **4**, confirms the absolute need for a closed and intact BITZ ring to infer inhibitory activity against the *PflspD* enzyme. Since the presence of the unbroken N-S heteroatom bond within the BITZ motif is clearly required for inhibitory *PflspD* activity, it seems reasonable that the sulfur atom and N-S bond contribute to the mechanism of inhibitory activity of this chemotype (**Chapter 4**).

The assessment of alternative heteroatom replacements within the BITZ headgroup, replacing sulfur with other atoms and small functional groups, as well as similar evaluation regarding the nitrogen atom, has also been considered (**Table 2.3**). This question of specific heteroatom replacement around the BITZ headgroup has been addressed by a number of individuals in our research group (*indicated) where the results, thus far, are summarised in **Table 2.3**.

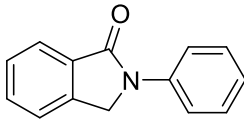
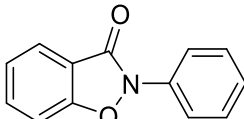
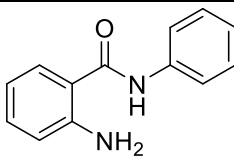
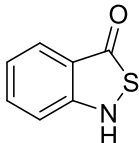
Compound Structure	<i>PflspD</i> Inhibition IC ₅₀ (μM)
 2-phenylisoindolin-1-one	Not synthesised
 2-phenylbenzo[d]isoxazol-3(2H)-one	Not synthesised
 2-amino- <i>N</i> -phenylbenzamide	> 200
 benzo[c]isothiazol-3(1H)-one*	> 200

Table 2.3 Chemical structures of resulting compounds considering the replacement of specified heteroatoms with the thiazolone ring of the BITZ headgroup; *PflspD* inhibitory activity of compounds generated given in μM where synthesis was successful. (*Matthew Pye, unpublished).

The generation of designed structures (**Table 2.3**) has not been possible across all specified compounds within research to date, as a result of synthetic difficulties and a lack of commercial availability of the described compounds. However, further testing of a second ring-open compound (2-Amino-*N*-phenylbenzamide) and a rearrangement of the BITZ headgroup, exchanging the nitrogen and sulfur atom positions and removing the linked *N*-phenyl, to give benzo[c]isothiazol-3(1H)-one, resulted in a complete loss of inhibitory activity against *PflspD*. This again highlights that the BITZ core headgroup of **3** (**Figure 2.9**) is explicitly required to achieve inhibition of the *PflspD* enzyme. Therefore, these structures provide interesting points of comparison to enable distinct SAR studies around the core BITZ headgroup using a range of heteroatom replacements and considering alternative atoms and functional groups. This work represents an area of ongoing research.

2.7 Preliminary SAR development

In order to rapidly determine an early picture of SAR around our selected hit and BITZ chemotype, a number of compounds, structurally similar to our HTS hit **DT2009-0168020** were purchased and tested to determine their activity against the *Pf*lspD enzyme. The aim of this was to initiate preliminary considerations concerning structural modifications that may optimise BITZ derived inhibitors. Compounds **9-11** (Table 2.4) were specifically selected due to their subtle chemical and structural differences to the **DT2009-0168020** hit. Assessment of these structures were able to highlight quickly some specific and essential structural requirements that must be preserved in subsequent BITZ inhibitor series to ensure activity against *Pf*lspD. In addition, the biological testing results of **9-11** (Table 2.4) also revealed some areas of the hit motif that might be more amenable to structural variation and chemical modifications.

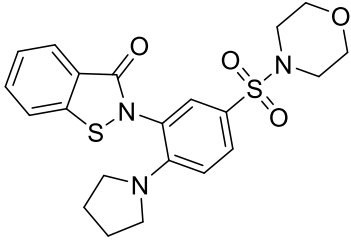
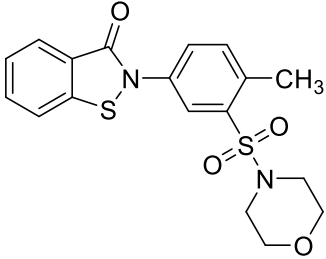
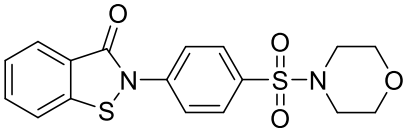
Compound number	Chemical Structure	<i>Pf</i> lspD Inhibition IC ₅₀ (μM)	Whole Cell Growth (3D7) Inhibition IC ₅₀ (μM)
9		1.00	5.193
10		0.401	2.774
11		5.789	16.04

Table 2.4 Chemical structures and corresponding inhibitory activity against *Pf*lspD and *P. falciparum* 3D7 growth in culture (IC₅₀ given in μM) of compounds **9-11** that are structurally similar to the HTS hit **DT2009-0168020**. (Compounds purchased for testing).

As shown by the inhibitory effects of compounds **9** and **10**, variation in the size of substituents around the C ring is tolerated to varying extents, highlighting that there is room for SAR development around this central ring. The loss of enzymatic activity demonstrated by *para*-substituted compound **11** indicates the requirement to maintain a *meta*-substitution pattern across the C ring, compound **4** (Figure 2.9) is the representative comparison. This observation may reflect

key spatial constraints at the *Pf*lspD binding site. The molecular ‘kink’ across the C ring (**Figure 2.9**) that appears to be required within inhibitor structures suggests that linear, rigid molecules might not be tolerated at the *Pf*lspD active site.

In addition to the small selection of purchased compounds **9-11**, other work within the group^[73] examined close structural derivatives of the **DT2009-0168020** hit (**Figure 2.8**). Within this series of compounds, the *meta*-sulphonamide group present in the original **DT2009-0168020** hit was maintained, varying the amine component of this functionality using a range of amine heterocycles. Small structural variations were also made at the *ortho* position of the C ring, replacing the original *ortho*-morpholine group with smaller hydroxy and methoxy functionalities. In addition, both directly attached and methylene-linked side chains were considered within this series. An overall summary of these structural explorations and the resulting compounds that were synthesised and tested for activity against the *Pf*lspD enzyme and parasite growth is given below (**Figure 2.10**).

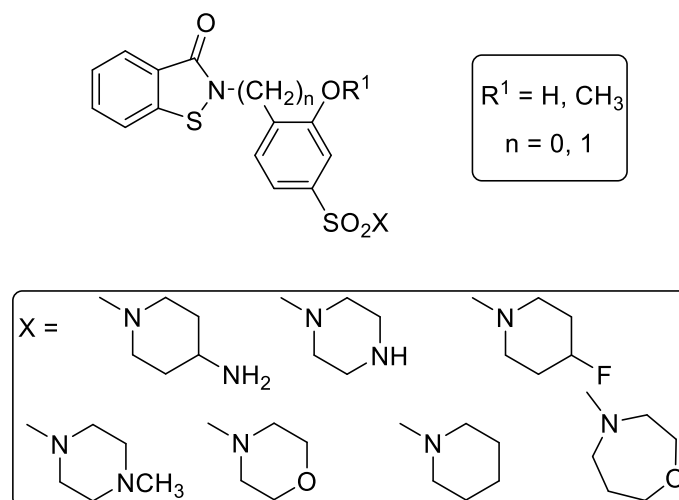


Figure 2.10 Initial analogues synthesised and tested against the *Pf*lspD enzyme and *P. falciparum* parasite growth as close structural derivatives of the **DT2009-0168020** hit.^[73]

Following identification and selection of the BITZ chemotype and chemical motif, subsequent compounds based around the BITZ core will only be considered active inhibitors of the *Pf*lspD enzyme if they display a *Pf*lspD IC_{50} value of $< 5 \mu M$. Whilst some compounds within the described series (**Figure 2.10**) demonstrated enzymatic activity against *Pf*lspD close to that of the original **DT2009-0168020** hit, a number of compounds, close to a quarter of the 21 compounds generated, displayed very weak inhibitory activity against the *Pf*lspD enzyme with IC_{50} values $> 5 \mu M$ and are therefore considered to be inactive (**Appendix 2**).

Further analysis of biological data also revealed that almost half of the compounds generated, displaying activity against *Pf*lspD under the $5 \mu M$ threshold, only displayed weak inhibition with

PflspD IC₅₀ values between 1-5 μM. In addition to the distinct lack of inhibitory *PflspD* activity, sub-optimal whole cell activity was consistent across all 21 analogues with 3D7 whole cell inhibition spanning a broad and weak activity range of ~ 2.5 - 33 μM. Only a single derivative, compound **12** (**Figure 2.11**), displayed sub-micromolar activity against 3D7 whole cell parasite growth with an EC₅₀ value of 0.98 μM; however, this was not supported by enzymatic *PflspD* activity which was > 1 μM. Despite the general lack of activity identified against the *PflspD* enzyme and *P. falciparum* parasite growth with this analogue series (**Figure 2.10**), these results are somewhat encouraging as they demonstrate that SAR exists around the selected chemotype, and that further development of SAR may lead to potent and selective inhibitors of the *PflspD* enzyme and *P. falciparum* parasite growth.

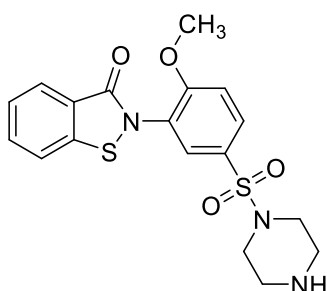


Figure 2.11 Chemical structure of **12**.^[73]

Taken all together, these studies highlight that analogues comprised of this specific chemical construct (**Figure 2.11** and **Appendix 2**) do not have potential as small molecule *PflspD* inhibitors or, more broadly as antimalarial agents. An initial outcome of these results was to remove any substitution at the *ortho* position of the C ring, adjacent to the BITZ headgroup. It was also decided to remove the sulphonamide group from subsequent inhibitor structures since this functionality has not been seen to significantly contribute to the activity of this BITZ inhibitor series (**Appendix 2**), compared to activity of simple BITZ derivative **3**. These results therefore add to our knowledge and SAR understanding gained from the evaluation of **9-11** (**Table 2.4**), facilitating an in-depth SAR exploration initiated from a simplified BITZ compound, such as **3** (**Figure 2.9**), from which more complex analogues can be derived. In addition, **4** provides a measure of the inhibitory effect of the sulphonamide group, relative to **3**, which can be reintroduced if necessary following subsequent SAR development.

The preliminary SAR map below (**Figure 2.12**) provides a summary of the SAR requirements identified in the structural explorations discussed in this chapter (**Section 2.4** and **2.5**). **Figure 2.12** denotes the known SAR requirements of the BITZ chemotype and motif learnt from these initial studies, following chemotype selection and therefore represents our knowledge of this chemical motif at the point of progression into hit-to-lead optimisation studies (see **Chapter 3**).

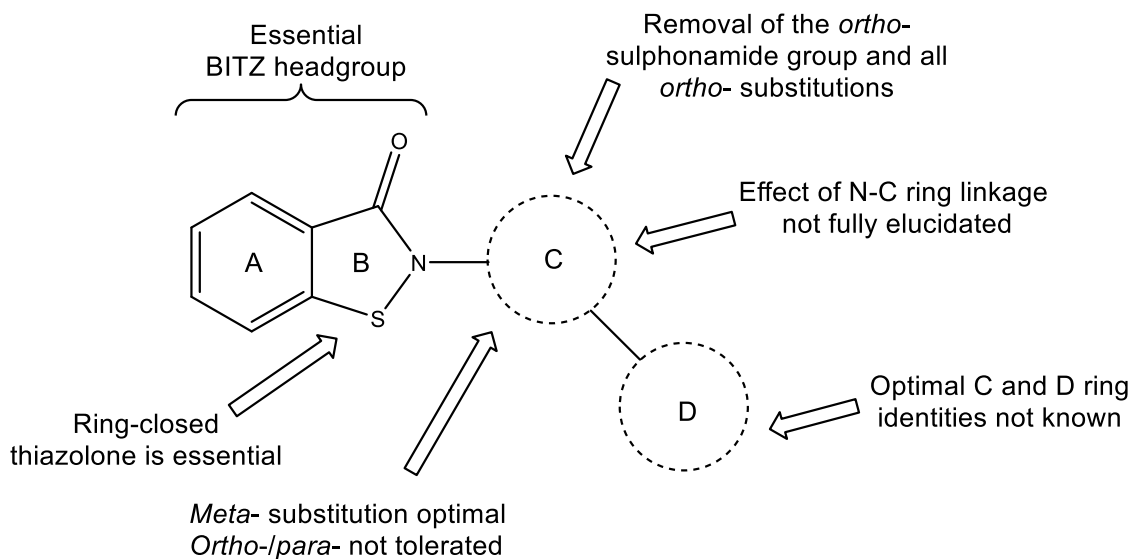


Figure 2.12 Preliminary BITZ SAR Map.

Structural refinement, including precise embellishment and chemical functionalisation, is clearly required around this simplified BITZ framework; however, we were confident that it represents an optimal foundation from which to address subsequent SAR questions and initiate more detailed *PflspD* inhibitor design and development.

2.8 Conclusions and Ongoing Work

Virtual screening and cheminformatics studies generated a focused ligand library of 5000 compounds, selected from the 'Biofocus Combined Library', to facilitate a target-based screen with the aim of identifying novel compounds that inhibit the *PflspD* enzyme. The 5000 compounds were subjected to a HTS study, facilitated by upscaling the *PflspD* enzymatic assay which was designed by collaborators in the Molecular and Cellular Biology Research Group at Washington University in St Louis.^[49] The HTS screen resulted in the identification of 54 novel compound structures which showed activity against the *PflspD* enzyme; each compound met the specified IC₅₀ value of $\leq 20 \mu\text{M}$ which was used to define compounds as active against *PflspD*. This small series of 54 compounds spanned a diverse range of chemical space and was made up of compounds structured around 10 different chemical motifs. Of these chemotypes (or motifs), the 1,2-benzo[d]isothiazol-3(2H)-one (BITZ) chemotype was repeatedly identified within a number of hit structures and therefore selected as our hit chemotype to take forward for *PflspD* inhibitor design and SAR development.

Subsequent SAR investigations, facilitated by organic synthesis, have been able to confirm that the specific chemical construct of the selected BITZ headgroup is essential for achieving inhibition of the *PflspD* enzyme. This has been rationalised through a series of small molecule manipulations around the thiazolone ring (B ring) of the BITZ headgroup, highlighting that alteration of the specific BITZ construct abolishes inhibitory *PflspD* activity in resulting compounds. The question of tolerated chemical and structural variation around the BITZ headgroup has been addressed by several members of our group; research efforts are currently ongoing and aim to further evaluate heteroatom replacement within the BITZ core motif and the extent to which it may be tolerated. Overall, it is hoped that these studies will contribute to deciphering the mechanism of action by which BITZ compounds exert their inhibitory effects at the *PflspD* enzyme. Indeed, the importance of the sulfur heteroatom and N-S bond within the thiazolone ring has already been realised.

A number of synthetic strategies have been identified that enable the successful and efficient generation of the BITZ chemotype and derived inhibitors. In particular, two syntheses seem highly promising as they are shown to be efficient, with tolerance to varying chemical groups, and offer scope for further synthetic modifications, facilitating the generation of chemically diverse BITZ compounds. The two most appealing synthetic methodologies are represented by **Route 1** and **Route 3, (Section 2.3)** which correspond to a thionyl chloride-mediated generation of the BITZ motif and the condensation of a stable and isolatable acid-chloride with various primary amines. Use of these identified syntheses, with appropriate modifications, will facilitate the generation of a large number of BITZ-derived compounds, comprising various analogue series.

Preliminary SAR investigations, conducted by myself and others, have provided an early picture of SAR around the BITZ core motif and selected HTS hit, **DT2009-0168020**. This has delivered a structural foundation on which further, more precise SAR development can be initiated. Following these preliminary studies, exploratory SAR development will probe more specific questions concerning the chemical construct of BITZ inhibitors. The particular influence of selected molecular functionalities will be questioned, assessing the effects that certain chemical groups may have on inhibitory compound activity, against both the *PflspD* enzyme and *P. falciparum* parasite growth. As more in-depth SAR analysis is instigated, facilitating hit-to-lead optimisation, a revised activity threshold is now specified where an IC_{50} value of $\leq 5 \mu\text{M}$ will define a compound as active against the *PflspD* enzyme.

The identified synthetic methodologies, together with a strong preliminary SAR platform, will support and enable an efficient transition into the next stage of compound development which will begin with more detailed SAR investigations. Hit-to-lead optimisation will therefore enable knowledge of the selected BITZ chemotype to develop and expand, promoting chemical and structural properties of BITZ derived compounds, aiming to enhance inhibitory effects against the *PflspD* enzyme and *P. falciparum* parasite growth.

2.9 Experimental

2.9.1 General Methodologies

2.9.1.1 General Chemical Methods

The following general chemical techniques were used for the synthesis and characterisation of all chemical compounds synthesised and described in the experimental sections throughout this thesis.

Reagents

All reagents were purchased from FluoroChem, Alfa Aesar or Sigma-Aldrich and were used without purification unless otherwise indicated. Reactions that were air and moisture sensitive were performed in dry solvent, under a nitrogen atmosphere in oven dried or flame dried glassware.

Solvents

Anhydrous solvents were obtained from commercial sources or dried and distilled prior to use. Distillation was carried out under the flow of dry nitrogen; THF was distilled from sodium; dichloromethane (DCM) was distilled from calcium hydride.

Thin Layer Chromatography (TLC)

Analytical thin layer chromatography was performed with 0.25 mm Merck silica gel 60 F-254 plates. Chromatograph plates were visualised by UV at 254 nm light or treated with potassium permanganate, *p*-anisaldehyde, ninhydrine or iodine, as appropriate and developed using a heat gun.

Flash Column Chromatography

Purification of products was achieved by flash column chromatography unless otherwise stated. Flash column chromatography was performed using the required amount of silica (particle size 40 – 63 μm , supplied by Aldrich) made into a slurry with the appropriate volume of the desired eluent system. The slurry was added to the column over a thin base layer of sand. Crude material was applied to the column, either dissolved in a minimum volume of eluent system or pre-absorbed onto silica. The column was then eluted with the eluent and fractions were collected and analysed by TLC.

Nuclear Magnetic Resonance Spectroscopy (NMR)

^1H and ^{13}C NMR spectra were recorded on a Bruker AMX-400 spectrometer (^1H 400 MHz; ^{13}C 101 MHz) or on a Bruker Avance III HD spectrometer (^1H 500 MHz; ^{13}C 101 MHz) in deuterated solvents as indicated with the experimental data. Chemical shifts are reported in parts per million (δ , ppm)

downfield from an internal standard of tetramethylsilane (TMS); coupling constants (J) are reported in hertz (Hz).

Mass Spectrometry and Elemental Analysis

Mass spectrometry (MS) and High Resolution Mass Spectrometry (HRMS) were recorded using an in house service within the Chemistry Department at the University of Liverpool. MS and HRMS was conducted on a VG analytical 7070E machine, Frisons TRIO mass spectrometers or Agilent QTOF 7200 using electron ionisation (EI), chemical ionisation (CI) or electrospray (ES). Elemental analysis (%C, %H, %N and %S where specified) were determined by the University of Liverpool Microanalysis Laboratory.

2.9.1.2 General Biological Methods

The following biological methodologies were used for the enzymatic and whole cell growth assays of chemical compounds tested in these described assays. Biological testing has been conducted in the Molecular and Cellular Biology lab at Washington University School of Medicine, St Louis, coordinated by our collaborator Audrey Odom.

Purification of IspD proteins

Plasmids derived from pBG1861, containing wildtype or mutant alleles of *Plasmodium* spp. or *E. coli* IspD, were used to transform Artic Express (DE3) RIL *E. coli* cells (Stratagene). Cells were grown in LB broth with 100 µg/mL ampicillin at 37°C and 200 rpm. During mid-logarithmic growth, cultures were cooled to 8°C, and protein expression was induced with 1 mM IPTG for 16 hours.

After induction, cell pellets were lysed by sonication in lysis buffer (25 mM Tris pH 7.5, 250 mM NaCl, 1 mM MgCl₂, 1 mM dithiothreitol (DTT), 20 mM imidazole, 10% glycerol, 0.1% Triton X-100, 200 µM PMSF, 1 mg/mL lysozyme, 0.3 U/mL benzonase nuclease (Novagen), and Roche Complete EDTA-free protease inhibitor). 6His-tagged IspD proteins were purified from soluble lysate over Ni-NTA resin (Goldbio). Beads were washed with 250 mM NaCl, 25 mM Tris pH 7.5, 1 mM MgCl₂, 20 mM imidazole, and protein was eluted with 250 mM NaCl, 25 mM Tris pH 7.5, 1 mM MgCl₂, 300 mM imidazole. Affinity purification of *Pv*IspD proceeded similarly to *Pf*IspD purifications, except that 0.1% Triton X-100 and 10% glycerol were not present in the lysis buffer. 10% glycerol was also absent from the lysis buffer used in purifying wildtype and A14C *E. coli* IspD, and lysis buffer used in purifying wildtype and C202A *Pf*IspD used in mechanistic studies (**Chapter 4, Figures 4.21 to 4.25**).

Affinity-purified proteins were further purified over a HiLoad 16/60 Superdex 200 gel filtration column (GE Health Sciences), using an AKTA Explorer 100 FPLC (GE Health Sciences). FPLC buffer contained 250 mM NaCl, 25 mM Tris pH 7.5, 1 mM MgCl₂. Fractions containing purified protein (> 90% pure as evaluated by SDS-PAGE) were pooled and concentrated by centrifugation using Amicon Ultra-15 Centrifugal Filter Units (EMD Millipore). Concentrated protein was supplemented with 10% glycerol and 1 mM DTT (although DTT was omitted from wildtype and C202A *PflspD* preparations used in mechanism of action studies, (Chapter 4, Figures 4.21 to 4.25), flash-frozen in liquid nitrogen, and stored at -80 °C. Protein concentration was measured using a BCA protein assay kit (Thermo Scientific).

Enzymatic *IspD* assay conditions

Phosphate released by *IspD* was quantified using the EnzChek Phosphate Assay Kit (Invitrogen, Life Technologies), as previously described.^[67] 2-Amino-6-mercapto-7- methylpurine riboside (MESG) and purine nucleoside phosphorylase (PNP) were diluted and stored according to the manufacturer's instructions. Final concentrations of reagents were as follows: 100 mM NaCl, 25 mM Tris pH 7.5, 7.5 mM MgCl₂, 1 U/ml PNP, 0.1 U/mL yeast inorganic pyrophosphatase (New England Biolabs). Unless otherwise specified, IC₅₀ assays contained 50 nM enzyme, 400 μM CTP (Sigma), 200 μM MEP (Echelon Biosciences), 2% DMSO (vehicle), and 200 μM MESG. Reactions were performed in 50 μL final volumes in 96-well clear flat bottom plates. In general, enzymes, buffers, and inhibitors were pre-warmed approximately 15 minutes at 37 °C, and reactions were then initiated by addition of the MEP substrate. Timed inhibitor IC₅₀ assays (5, 20, 35, and 50 minute incubations) and comparisons between behaviour at 100 μM and 400 μM CTP were initiated by the addition of the CTP substrate and contained 100 nM enzyme. Assays using *E. coli* *IspD* used 7.5 nM *EclspD*-wt or 75 nM *EclspD*-A14C. Absorbance at 360 nm was measured over time on a BMG POLARStar plate reader, preheated to 37°C. Nonlinear regression analysis was performed using GraphPad Prism software. Values reflect the mean and standard error from ≥ 3 independent experimental and were compared using the Student's t-test (two-tailed). Slopes of changing absorbance values were converted to (μM MEP) (μM enzyme)⁻¹ s⁻¹ using a phosphate standard curve.

P. falciparum culture

Unless otherwise specified, *P. falciparum* parasites were cultured as previously described,^[74,75] in a 2% suspension of human erythrocytes in RPMI-1640 medium (Sigma Aldrich) supplemented with 27 mM sodium bicarbonate, 11 mM glucose, 5 mM HEPES, 1 mM sodium pyruvate, 0.37 mM hypoxanthine, 0.01 mM thymidine, 10 μg ml⁻¹ gentamicin and 0.5% Albumax (Life Technologies). Cultures were maintained in 5% O₂/5% CO₂/90% N₂ at 37°C. Parasite growth was monitored by

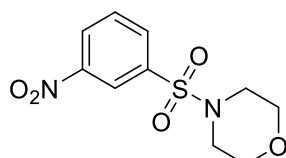
microscopy of Giemsa-stained parasites. 3D7 strain parasites were obtained from the Malaria Research and Reference Reagent Resource Center, ATCC, Manassas, Virginia. D6 and 7G8 strains were obtained through BEI Resources Repository, NIAID, NIH: *Plasmodium falciparum*, Strain D6, MRA-285, contributed by D.E. Kyle; *Plasmodium falciparum*, Strain 7G8, MRA-152, contributed by David Walliker. The IPC 5202 strain was provided by the Malaria Research and Reference Reagent Resource Center (MR4) for distribution by BEI Resources NIAID, NIH: *Plasmodium falciparum*, Strain IPC 5202, also known as CAM3.IR539T; MRA-1240, contributed by Didier Ménard.

2.9.1.3 Predictions of *ClogD* and *CaqSol*

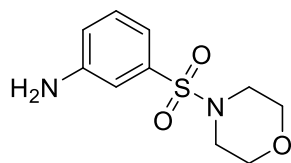
The distribution coefficient (*ClogD*) and aqueous solubility (*CaqSol*) were predicted for all BITZ derived compounds that were synthesised and then tested in the enzymatic IspD assay. AstraZeneca have previously described the design of good models for the accurate prediction of the *logD* and solubility of organic compounds.^[76,77] Collaboration between AZ and The University of Liverpool has provided access to these models which have been used to predict *ClogD* (at pH 7.4) and *CaqSol* (given in μM) for all designed and evaluated BITZ compounds; where all *ClogD* and *CaqSol* predictions were conducted by collaborators at AstraZeneca, Alderley Park.

2.9.2 Organic Synthesis

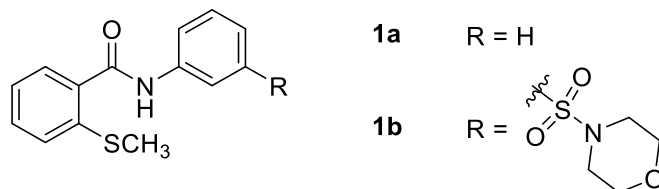
Preparation of 4-((3-Nitrophenyl)sulfonyl)morpholine 5



To a solution of 3-nitrobenzene sulfonyl chloride (2.0 g, 9.02 mmol) in DCM (40 ml) under a N_2 atmosphere, morpholine (1.0 ml, 10.8 mmol, 1.2 eq) and triethylamine (1.5 ml, 10.8 mmol, 1.2 eq) were added. The resulting solution was allowed to stir at room temperature for 2 hours. The crude material was diluted with brine (40 ml), the organic layer extracted into DCM (3 x 30 ml), washed with 2N HCl (30 ml), dried over MgSO_4 and concentrated under reduced pressure to give **5** as white crystalline solid in a 91.1% yield. $R_f = 0.31$ (1:1 EtOAc:hexane). $^1\text{H NMR}$ (400 MHz, CDCl_3) δ 8.60 (t, $J = 1.9$ Hz, 1H), 8.50 (ddd, $J = 8.2, 2.2, 1.0$ Hz, 1H), 8.09 (ddd, $J = 7.8, 1.6, 1.1$ Hz, 1H), 7.81 (t, $J = 8.1$ Hz, 1H), 3.78 (t, $J = 4.6$ Hz, 4H), 3.08 (t, $J = 4.8$ Hz, 4H); $^{13}\text{C NMR}$ (101 MHz, CDCl_3) δ 148.9, 138.2, 133.6, 131.0, 127.9, 123.3, 66.4 (2C), 46.4 (2); **Elemental analysis** (%) found: C, 43.92; H, 4.43; N, 10.18; S, 11.78%. $\text{C}_{10}\text{H}_{12}\text{N}_2\text{O}_5\text{S}$ requires C, 44.11; H, 4.44; N, 10.29; S, 11.77%; **ES+HRMS** m/z 295.0373 $[\text{M}+\text{Na}]^+$ $\text{C}_{10}\text{H}_{12}\text{N}_2\text{O}_5\text{S}$ requires 272.05.

Preparation of **3-(Morpholinofonyl)aniline 6**

10% Pd/C (0.05 g, 10% by mass) was added to a solution of **5** (0.5 g, 1.83 mmol) in 50:50 EtOAc-MeOH. The solution was put under a hydrogen atmosphere at room temperature overnight after which time the reaction was complete. The solution was filtered through Celite under vacuum and resulting material was washed with 50:50 EtOAc-hexane and concentrated under reduced pressure to give **6** as an orange-brown solid in a 98.4% yield. $R_f = 0.14$ (1:1 EtOAc:hexane). $^1\text{H NMR}$ (400 MHz, CDCl_3) δ 7.32 (t, $J = 7.9$ Hz, 1H), 7.12 (ddd, $J = 7.7, 1.3, 0.8$ Hz, 1H), 7.06 (t, $J = 1.9$ Hz, 1H), 6.92 (dd, $J = 8.1, 1.6$ Hz, 1H), 3.74 (t, $J = 4.7$ Hz, 4H), 3.01 (t, $J = 4.8$ Hz, 4H); $^{13}\text{C NMR}$ (101 MHz, CDCl_3) δ 146.9, 136.3, 130.5, 120.0, 118.3, 114.2, 66.5 (2C), 46.5 (2C); **Elemental analysis** (%) found: C, 49.69; H, 5.87; N, 11.48%. $\text{C}_{10}\text{H}_{14}\text{N}_2\text{O}_3\text{S}$ requires C, 49.57; H, 5.82; N, 11.56%; **CI+MS** m/z 243.1 $[\text{M}+\text{H}]^+$ $\text{C}_{10}\text{H}_{14}\text{N}_2\text{O}_3\text{S}$ requires 242.07.

Preparation of **2-(Methylthio)-N-phenylbenzamides 1a and 1b****General Procedure (A)**

To a stirring solution of 2-(methylthio)benzoic acid **1** (1.0 eq) in anhydrous toluene (10 ml/mmol) under a N_2 atmosphere, thionyl chloride (3.0 eq) was added followed by 3 drops of *N,N*-dimethylformamide: the resulting solution was refluxed for 2 hours. Solvent and thionyl chloride were removed under reduced pressure to give the acid chloride intermediate. The appropriate 1° amine (1.2 eq) was dissolved in anhydrous THF (10 ml/mmol), to which triethylamine (2.0 eq) was added. The crude acid chloride was re-dissolved in anhydrous THF (10 ml/mmol) and added dropwise to the amine and base solution over 10 minutes at 0°C . After a further 10 minutes, the solution was warmed to room temperature and allowed to stir for 20 hours. The solvent was removed under reduced pressure; the resulting crude material diluted with water and extracted into EtOAc (3 x 20 ml). The combined organic extracts were washed with 1M HCl (15 ml), saturated aq. NaHCO_3 (15 ml) and brine (20 ml), dried over NaSO_4 and concentrated under reduced pressure to give the pure products.

Preparation of 2-(Methylthio)-*N*-phenylbenzamide **1a**

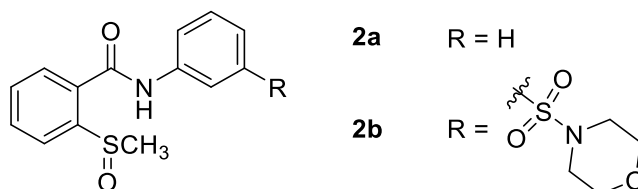
The general procedure (A) was followed using aniline (0.65 ml, 7.13 mmol) to give **1a** as an off-white solid in a 93.8% yield. $R_f = 0.70$ (50:50 EtOAc:hexane). $^1\text{H NMR}$ (400 MHz, CDCl_3) δ 8.31 (s, 1H, NH), 7.73 (d, $J = 7.5$ Hz, 1H), 7.66 (d, $J = 7.8$ Hz, 2H), 7.44 (td, $J = 8.0, 1.5$ Hz, 1H), 7.41 – 7.35 (m, 3H), 7.29 (dd, $J = 7.5, 1.3$ Hz, 1H), 7.16 (t, $J = 7.4$ Hz, 1H), 2.50 (s, 3H).

Preparation of 2-(Methylthio)-*N*-(3-(morpholinofonyl)phenyl)benzamide **1b**

The general procedure (A) was followed using **6** (0.22 g, 0.926 mmol) to give **1b** as an off-white solid in a 85.5% yield. $R_f = 0.27$ (6:4 EtOAc:hexane). $^1\text{H NMR}$ (400 MHz, CDCl_3) δ 8.64 (s, 1H, NH), 8.04 (br s, 1H), 7.98 (dt, $J = 7.4, 1.9$ Hz, 1H), 7.78 (dd, $J = 7.7, 1.4$ Hz, 1H), 7.60 – 7.52 (m, 2H), 7.48 (td, $J = 7.3, 1.5$ Hz, 1H), 7.41 (dd, $J = 7.9, 1.1$ Hz, 1H), 7.31 (td, $J = 7.6, 1.3$ Hz, 1H), 3.76 (t, $J = 4.6$ Hz, 4H), 3.07 (t, $J = 4.8$ Hz, 4H), 2.52 (s, 3H); $^{13}\text{C NMR}$ (101 MHz, CDCl_3) δ 166.5, 139.2, 137.1, 136.5, 134.7, 132.0, 130.4, 129.9, 128.7, 126.4, 124.7, 123.9, 119.4, 66.5 (2C), 46.4 (2C), 17.5; **Elemental analysis** (%) found: C, 54.73; H, 5.31; N, 7.01; S, 16.27%. $\text{C}_{18}\text{H}_{20}\text{N}_2\text{O}_4\text{S}_2$ requires C, 55.08; H, 5.14; N, 7.14; S, 16.34%; **ES+HRMS** m/z 415.0761 $[\text{M}+\text{Na}]^+$ $\text{C}_{18}\text{H}_{20}\text{N}_2\text{O}_4\text{S}_2$ requires 392.09.

Preparation of 2-(Methylsulfinyl)-*N*-phenylbenzamides **2a** and **2b**

General Procedure (B)



A solution of sodium periodate (1.3 eq) in water was added dropwise to the appropriate 2-(methylthio)-*N*-phenylbenzamide in MeOH at room temperature. The biphasic solution (10 ml/mmol; 1:1 water:MeOH) was heated to 50°C for 4-5 hours before the solvent was removed under reduced pressure. The crude precipitate was diluted with water, filtered through a sinter and washed with water before drying for a desiccator to give the pure products.

Preparation of 2-(Methylsulfinyl)-*N*-phenylbenzamide **2a**

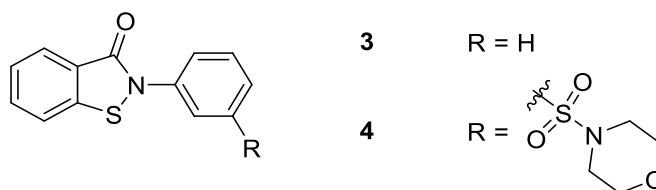
The general procedure (B) was followed using **1a** (0.5 g, 0.215 mmol) to give **2a** as an off-white solid in quantitative yield. $R_f = 0.08$ (50:50 EtOAc:hexane). $^1\text{H NMR}$ (400 MHz, CDCl_3) δ 8.95 (s, 1H, NH), 8.12 (dd, $J = 7.4, 1.6$ Hz, 1H), 7.78 (d, $J = 7.1, 1.3$ Hz, 1H), 7.69 (d, $J = 7.9$ Hz, 2H), 7.64 – 7.54 (m, 2H), 7.41 (t, $J = 7.6$ Hz, 2H), 7.20 (t, $J = 7.4$ Hz, 1H), 2.93 (s, 3H).

Preparation of 2-(Methylsulfinyl)-*N*-(3-(morpholinofonyl)phenyl)benzamide **2b**

The general procedure (**B**) was followed using **1a** (0.1 g, 0.255 mmol) to give **2b** as a cream solid in a 86.6% yield. $R_f = 0.10$ (9:1EtOAc:hexane). $^1\text{H NMR}$ (400 MHz, CDCl_3) δ 9.65 (s, 1H, NH), 8.14 (br s, 1H), 8.11 (dd, $J = 7.8, 1.0$ Hz, 1H), 8.07 (dt, $J = 7.6, 1.6$ Hz, 1H), 7.95 (d, $J = 7.5$ Hz, 1H), 7.65 (td, $J = 7.6, 0.9$ Hz, 1H), 7.62 – 7.54 (m, 3H), 3.76 (t, $J = 4.4$ Hz, 4H), 3.07 (t, $J = 4.7$ Hz, 4H), 2.96 (s, 3H).

Preparation of 2-Phenylbenzo[*d*]isothiazol-3(2*H*)-ones **3** and **4**

General Procedure (C)



Thionyl chloride (1.3 eq) was added dropwise to a stirring solution of the required 2-(methylsulfinyl)-*N*-phenylbenzamide (**2a** or **2b**, 1.0 eq) in DCM (15-20 ml) under a N_2 atmosphere. The solution was heated to reflux at 50°C for 1.5 hours. Solvent and excess thionyl chloride were removed under reduced pressure to give the crude products.

Preparation of 2-Phenylbenzo[*d*]isothiazol-3(2*H*)-one **3**

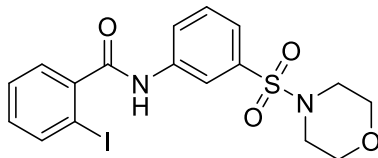
The general procedure (**C**) was followed using **2a** (0.25 g, 0.964 mmol) to give **3**, as a white crystalline solid, following purification by trituration with Et_2O , in a 51.0% yield. $R_f = 0.69$ (6:4 EtOAc:hexane). $^1\text{H NMR}$ (400 MHz, CDCl_3) δ 8.12 (dt, $J = 7.9, 0.8$ Hz, 1H), 7.74 – 7.70 (m, 2H), 7.68 (td, $J = 8.3, 1.2$ Hz, 1H), 7.60 (dt, $J = 8.1, 0.8$ Hz, 1H), 7.51 – 7.43 (m, 3H), 7.33 (tt, $J = 7.5, 1.3$ Hz, 1H); $^{13}\text{C NMR}$ (101 MHz, CDCl_3) δ 164.5, 140.3, 137.6, 132.8, 129.8 (2C), 127.6, 127.5, 126.2, 125.3, 125.0 (2C), 120.5; **Elemental analysis** (%) found: C, 68.53; H, 4.07; N, 6.07; S, 14.21%. $\text{C}_{13}\text{H}_9\text{NOS}$ requires C, 68.70; H, 3.99; N, 6.16; S, 14.11%; **ES+HRMS** m/z 250.0299 $[\text{M}+\text{Na}]^+$ $\text{C}_{13}\text{H}_9\text{NOS}$ requires 227.04.

Preparation of 2-(3-(Morpholinofonyl)phenyl)benzo[*d*]isothiazol-3(2*H*)-one **4**

The general procedure (**C**) was followed using **2b** (0.09 g, 0.233 mmol) to give **4** purified by flash column chromatography, as a pale orange solid in a 63.2 % yield. $R_f = 0.65$ (85:15 EtOAc:hexane). $^1\text{H NMR}$ (400 MHz, CDCl_3) δ 8.12 (t, $J = 1.0$ Hz, 1H), 8.05 (d, $J = 7.9$ Hz, 1H), 7.94 (dt, $J = 6.7, 2.3$ Hz, 1H), 7.68 – 7.59 (m, 3H), 7.56 (t, $J = 7.2$ Hz, 1H), 7.42 (td, $J = 7.9, 0.8$ Hz, 1H), 3.70 (t, $J = 4.6$ Hz, 4H), 3.03 (t, $J = 4.7$ Hz, 4H); $^{13}\text{C NMR}$ (101 MHz, CDCl_3) δ 164.7, 139.9, 138.8, 137.0, 133.4, 130.6, 128.5, 127.8, 126.7, 124.0, 124.8, 123.6, 120.7, 66.5 (2C), 46.4

(2C); **Elemental analysis** (%) found: C, 54.28; H, 4.49; N, 7.22; S, 17.05%. $C_{17}H_{16}N_2O_4S_2$ requires C, 54.24; H, 4.28; N, 7.44; S, 17.03%; **ES+MS** m/z 399.0447 $[M+Na]^+$ $C_{17}H_{16}N_2O_4S_2$ requires 376.06.

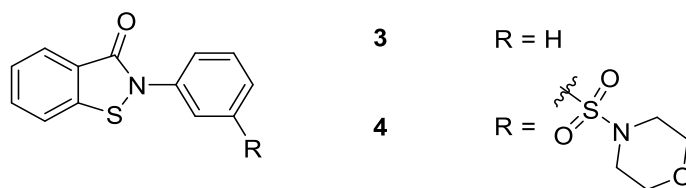
Preparation of 2-Iodo-*N*-(3-(morpholinosulfonyl)phenyl)benzamide **7**



To a solution of **6** (0.49 g, 2.03 mmol, 1.2 eq) in THF (8 ml) under a N_2 atmosphere, triethylamine (0.45 ml, 3.38 mmol, 2.0 eq) was added. The solution was cooled to $0^\circ C$ before the dropwise addition of 2-iodobenzoylchloride (0.45 g, 1.69 mmol, 1.0 eq) dissolved in THF (8 ml). The resulting solution was allowed to warm to room temperature and stir overnight. Solvent was removed under reduced pressure and the crude material re-suspended in 50:50 EtOAc:water and extracted into EtOAc. The combined organic extracts were washed with 2N HCl (30 ml), $NaHCO_3$ (25 ml) and brine (25 ml), dried over $MgSO_4$ and concentrated under reduced pressure to give **7** as a white-yellow crystalline solid in a 91.1% yield. $R_f = 0.24$ (4:6 EtOAc:hexane). 1H NMR (400 MHz, $CDCl_3$) δ 8.04 – 7.98 (m, 2H), 7.92 (d, $J = 7.7$ Hz, 1H), 7.88 (br s, 1H), 7.58 (t, $J = 7.9$ Hz, 1H), 7.54 (dd, $J = 6.1, 1.3$ Hz, 2H), 7.46 (td, $J = 7.5, 0.8$ Hz, 1H), 7.18 (td, $J = 7.7, 1.7$ Hz, 1H), 3.74 (t, $J = 4.6$ Hz, 4H), 3.04 (t, $J = 4.6$ Hz, 4H); ^{13}C NMR (101 MHz, $CDCl_3$) δ 167.8, 141.7, 140.6, 138.9, 136.5, 132.3, 130.5, 129.1, 128.9, 124.7, 124.2, 119.5, 92.6, 66.5 (2C), 46.4 (2C); **ES+HRMS** m/z 494.9839 $[M+Na]^+$ $C_{17}H_{17}N_2O_4S$ requires 472.00.

Preparation of 2-Phenylbenzo[*d*]isothiazol-3(2*H*)-ones **3** and **4**

General Procedure (D)



To a solution of 1,10-phenanthroline (0.25 eq) in DMF (10 ml) under a N_2 atmosphere, copper(I) iodide (0.25 eq) was added at room temperature and the resulting solution allowed to stir for 15 minutes. The appropriate 2-iodo-*N*-phenylbenzamide was then added, followed by sulfur powder (1.25 eq) and K_2CO_3 (1.25 eq). The N_2 atmosphere was restored and the solution stirred at room temperature for a further 15 minutes before heating to reflux at $110^\circ C$ for 3 hours. The crude solution was allowed to cool to room temperature before pouring into brine (50 ml) and stirring for 1.5 hours. The organic layer was then extracted into EtOAc (3 x 25 ml), dried over Na_2SO_4 and

concentrated under reduced pressure. The crude products were purified by flash column chromatography.

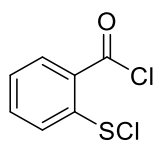
Preparation of **2-Phenylbenzo[*d*]isothiazol-3(2*H*)-one 3**

The general procedure (**D**) was followed using 2-iodo-*N*-phenylbenzamide (0.2 g, 0.619 mmol) to give **3** as a white crystalline solid in a 70.0% yield. $R_f = 0.49$ (4:6 EtOAc:hexane). $^1\text{H NMR}$ (400 MHz, CDCl_3) δ 8.11 (ddd, $J = 7.9, 0.8, 0.3$ Hz, 1H), 7.74 - 7.68 (m, 2H), 7.68 - 7.64 (m, 1H), 7.59 (dt, $J = 8.1, 0.8$ Hz, 1H), 7.52 - 7.42 (m, 3H), 7.33 (tt, $J = 7.4, 1.1$ Hz, 1H); $^{13}\text{C NMR}$ (101 MHz, CDCl_3) δ 164.6, 140.3, 137.6, 132.8, 129.8 (2C), 127.6, 127.5, 126.2, 125.3, 125.0 (2C), 120.5; **Elemental analysis** (%) found: C, 68.49; H, 4.06; N, 6.07; S, 14.26%. $\text{C}_{13}\text{H}_9\text{NOS}$ requires C, 68.70; H, 3.99; N, 6.16; S, 14.11%; **ES+HRMS** m/z 250.0295 $[\text{M}+\text{Na}]^+$ $\text{C}_{13}\text{H}_9\text{NOS}$ requires 227.04.

Preparation of **2-(3-(Morpholin sulfonyl)phenyl)benzo[*d*]isothiazol-3(2*H*)-one 4**

The general procedure (**D**) was followed using **7** (0.4 g, 0.847 mmol) to give **4** as a pale-orange solid in a 9.97% yield. $R_f = 0.32$ (6:4 EtOAc:hexane). $^1\text{H NMR}$ (400 MHz, CDCl_3) δ 8.20 (t, $J = 1.6$ Hz, 1H), 8.12 (dd, $J = 7.9, 0.7$ Hz, 1H), 8.03 - 7.99 (m, 1H), 7.72 (td, $J = 8.2, 1.2$ Hz, 1H), 7.70 - 7.67 (m, 2H), 7.64 (t, $J = 7.5$ Hz, 1H), 7.49 (td, $J = 8.0, 0.9$ Hz, 1H), 3.78 (t, $J = 4.7$ Hz, 4H), 3.10 (t, $J = 4.8$ Hz, 4H); $^{13}\text{C NMR}$ (101 MHz, CDCl_3) δ 164.7, 139.9, 138.8, 137.0, 133.4, 130.6, 128.5, 127.8, 126.7, 124.0, 124.8, 123.6, 120.7, 66.5 (2C), 46.4 (2C); **Elemental analysis** (%) found: C, 53.69; H, 4.44; N, 7.35; S, 15.79%. $\text{C}_{17}\text{H}_{16}\text{N}_2\text{O}_4\text{S}_2$ requires C, 54.24; H, 4.28; N, 7.44; S, 17.03%; **ES+HRMS** m/z 399.0459 $[\text{M}+\text{Na}]^+$ $\text{C}_{17}\text{H}_{16}\text{N}_2\text{O}_4\text{S}_2$ requires 376.06.

Preparation of **2-(Chlorothio)-benzoyl chloride 8**



Thionyl chloride (22.8 mmol, 7.0 eq) and *N,N*-dimethylformamide (3 drops) were added to a solution of 2,2'-dithiobenzoic acid (3.26 mmol) in anhydrous dichloroethane (25 ml) under a N_2 atmosphere at room temperature. The stirring solution was heated to reflux at 80°C for 1.5 hours. Sulfuryl chloride (4.24 mmol, 1.3 eq) was added to the cooled solution at 25°C before heating the solution to 50°C for 45 minutes. Solvent, excess thionyl chloride and excess sulfuryl chloride were removed under reduced pressure to generate **9**, a yellow-green solid as pure product in quantitative yield. $R_f = 0.79$ (50:50 EtOAc:hexane). $^1\text{H NMR}$ (400 MHz, CDCl_3) δ 8.34 (dd, $J = 8.0, 1.2$ Hz, 1H), 7.93 (dd, $J = 8.2, 0.4$ Hz, 1H), 7.77 (dt, $J = 8.5, 1.3$ Hz, 1H), 7.42 (dt, $J = 8.0, 0.8$ Hz, 1H); $^{13}\text{C NMR}$ (101 MHz, CDCl_3) δ 169.5, 146.1, 135.8, 134.7, 127.4, 125.8, 124.4.

2.10 References

- [1] S. D. Bembenek, B. A. Tounge, C. H. Reynolds, *Drug Discov. Today* **2009**, *14*, 278–283.
- [2] D. C. Swinney, J. Anthony, *Nat. Rev. Drug Discov.* **2011**, *10*, 507–19.
- [3] B. J. Kotz, S. Editor, S. Frye, M. Varney, J. Wells, *Nat. Publ. Gr.* **2012**, 1–3.
- [4] Lilly, *Open Innov. Drug Discov.* **2013**, 1–5.
- [5] T. N. C. Wells, R. H. van Huijsduijnen, W. C. Van Voorhis, *Nat. Rev. Drug Discov.* **2015**, *14*, 424–442.
- [6] W. A. Guiguemde, A. A. Shelat, D. Bouck, S. Duffy, G. J. Crowther, P. H. Davis, D. C. Smithson, M. Connelly, J. Clark, F. Zhu, et al., *Nature* **2010**, *465*, 311–315.
- [7] D. Plouffe, A. Brinker, C. McNamara, K. Henson, N. Kato, K. Kuhen, A. Nagle, F. Adrián, J. T. Matzen, P. Anderson, et al., *Proc. Natl. Acad. Sci. U. S. A.* **2008**, *105*, 9059–64.
- [8] F. Calderon, D. Barros, J. M. Bueno, J. M. Coteron, E. Fernandez, F. J. Gamo, J. L. Lavandera, M. L. Leon, S. J. F. MacDonald, A. Mallo, et al., *ACS Med. Chem. Lett.* **2011**, *2*, 741–746.
- [9] F.-J. Gamo, L. M. Sanz, J. Vidal, C. de Cozar, E. Alvarez, J.-L. Lavandera, D. E. Vanderwall, D. V. S. Green, V. Kumar, S. Hasan, et al., *Nature* **2010**, *465*, 305–310.
- [10] A. P. Bento, A. Gaulton, A. Hersey, L. J. Bellis, J. Chambers, M. Davies, F. A. Krüger, Y. Light, L. Mak, S. McGlinchey, et al., *Nucleic Acids Res.* **2014**, *42*, 1083–1090.
- [11] G. J. Crowther, H. K. Hillesland, K. R. Keyloun, M. C. Reid, M. J. Lafuente-Monasterio, S. Ghidelli-Disse, S. E. Leonard, P. He, J. C. Jones, M. M. Krahn, et al., *PLoS One* **2016**, *11*, 1–16.
- [12] J. Swann, V. Corey, C. A. Scherer, N. Kato, E. Comer, M. Maetani, Y. Antonova-Koch, C. Reimer, K. Gagaring, M. Ibanez, et al., *ACS Infect. Dis.* **2016**, acsinfecdis.5b00143.
- [13] M. Kaiser, P. M??ser, L. P. Tadoori, J. R. Ioset, R. Brun, D. J. Sullivan, *PLoS One* **2015**, *10*, 1–16.
- [14] M. McConville, J. Fernandez, I. Angulo-Barturen, N. Bahamontes-Rosa, L. Ballell-Pages, P. Castaneda, C. De Cozar, B. Crespo, L. Guijarro, M. B. Jimenez-Diaz, et al., *J. Med. Chem.* **2015**, *58*, 6448–6455.
- [15] E. R. Derbyshire, M. M. Mota, J. Clardy, *PLoS Pathog.* **2011**, *7*, DOI 10.1371/journal.ppat.1002178.
- [16] D. J. Kuter, **2016**, *109*, 4607–4617.
- [17] G. Remuzzi, N. Perico, A. Benigni, *Nat. Rev. Drug Discov.* **2002**, *1*, 986–1001.
- [18] R. Capdeville, E. Buchdunger, J. Zimmermann, A. Matter, *Nat. Rev. Drug Discov.* **2002**, *1*, 493–502.
- [19] V. Summa, A. Petrocchi, F. Bonelli, B. Crescenzi, M. Donghi, F. Fiore, C. Gardelli, O. G. Paz, D. J. Hazuda, P. Jones, et al., **2008**, 5843–5855.
- [20] P. Dorr, M. Westby, S. Dobbs, P. Griffin, B. Irvine, M. Macartney, J. Mori, G. Rickett, C. Smith-Burchnell, C. Napier, et al., *Antimicrob. Agents Chemother.* **2005**, *49*, 4721–4732.

- [21] E. Lionta, G. Spyrou, D. K. Vassilatis, Z. Cournia, *Curr. Top. Med. Chem.* **2014**, *14*, 1923–38.
- [22] N. G. Berry, *Personal Communication*, **2012**.
- [23] G. M. Maggiora, M. A. Johnson, in *Concepts Appl. Mol. Similarity*, Wiley, **1990**, pp. 1–13.
- [24] H. J. Böhm, A. Flohr, M. Stahl, *Drug Discov. Today Technol.* **2004**, *1*, 217–224.
- [25] G. Schneider, P. Schneider, S. Renner, *QSAR Comb. Sci.* **2006**, *25*, 1162–1171.
- [26] H. Sun, G. Tawa, A. Wallqvist, *Drug Discov. Today* **2012**, *17*, 310–324.
- [27] T. Masini, B. S. Kroezen, A. K. H. Hirsch, *Drug Discov. Today* **2013**, *18*, 1256–1262.
- [28] P. Gao, Y. Yang, C. Xiao, Y. Liu, M. Gan, Y. Guan, X. Hao, J. Meng, S. Zhou, X. Chen, et al., *Eur. J. Pharmacol.* **2012**, *694*, 45–52.
- [29] A. Kunfermann, M. Witschel, B. Illarionov, R. Martin, M. Rottmann, H. W. Hoeffken, M. Seet, W. Eisenreich, H.-J. Knoelker, M. Fischer, et al., *Angew. Chemie, Int. Ed.* **2014**, *53*, 2235–2239.
- [30] M. C. Witschel, H. W. Hoeffken, M. Seet, L. Parra, T. Mietzner, F. Thater, R. Niggeweg, F. Roehl, B. Illarionov, F. Rohdich, et al., *Angew. Chemie, Int. Ed.* **2011**, *50*, 7931–7935, S7931/1–S7931/29.
- [31] M. Witschel, F. Röhl, R. Niggeweg, T. Newton, *Pest Manag. Sci.* **2013**, *69*, 559–563.
- [32] I. Hale, P. M. O’Neill, N. G. Berry, A. Odom, R. Sharma, *Medchemcomm* **2012**, *3*, 418–433.
- [33] A. R. Odom, *PLoS Pathog.* **2011**, *7*, 1–4.
- [34] V. Devreux, J. Wiesner, H. Jomaa, J. Van der Eycken, S. Van Calenbergh, *Bioorganic Med. Chem. Lett.* **2007**, *17*, 4920–4923.
- [35] F. E. Jacobsen, J. A. Lewis, S. M. Cohen, *ChemMedChem* **2007**, *2*, 152–171.
- [36] D. Rogers, M. Hahn, *J. Chem. Inf. Model.* **2010**, *50*, 742–754.
- [37] K. H. Baringhaus, G. Hessler, *Drug Discov. Today Technol.* **2004**, *1*, 197–202.
- [38] M. Vogt, D. Stumpfe, H. Geppert, J. Bajorath, *J. Med. Chem.* **2010**, *53*, 5707–5715.
- [39] A. R. Leach, V. J. Gillet, *An Introduction to Chemoinformatics.*, Kluwer Academic Publishers, **2003**.
- [40] P. Willett, V. Winterman, D. Bawden, *J. Chem. Inf. Model.* **1986**, *26*, 36–41.
- [41] Y.-J. Xu, M. Johnson, *J. Chem. Inf. Comput. Sci.* **2002**, *42*, 912–926.
- [42] A. S. Lawrenson, Antimalarial Drug Design: Targeting the Plasmodium Falciparum Cytochrome bc1 Complex through Computational Modelling, Chemical Synthesis and Biological Testing, **2012**.
- [43] S. B. Richard, M. E. Bowman, W. Kwiatkowski, I. Kang, C. Chow, A. M. Lillo, D. E. Cane, J. P. Noel, *Nat. Struct. Biol.* **2001**, *8*, 641–648.
- [44] A. Dhanik, L. E. Kaviraki, *Protein-Ligand Interactions: Computational Docking*, **2012**.
- [45] D. B. Kitchen, H. Decornez, J. R. Furr, J. Bajorath, *Nat Rev Drug Discov* **2004**, *3*, 935–949.

- [46] J. W. Liebeschuetz, J. C. Cole, O. Korb, *J. Comput. Aided. Mol. Des.* **2012**, *26*, 737–748.
- [47] M. L. Verdonk, J. C. Cole, M. J. Hartshorn, C. W. Murray, R. D. Taylor, *Proteins Struct. Funct. Genet.* **2003**, *52*, 609–623.
- [48] I. V. Tetko, V. Y. Tanchuk, T. N. Kasheva, A. E. P. Villa, *J. Chem. Inf. Comput. Sci.* **2001**, *41*, 1488–1493.
- [49] A. R. Odom, *Personal Communication*, **2012**.
- [50] W. N. Hunter, *J. Biol. Chem.* **2007**, *282*, 21573–21577.
- [51] M. R. Webb, *Proc. Natl. Acad. Sci. U. S. A.* **1992**, *89*, 4884–7.
- [52] R. R. Neubig, M. Spedding, T. Kenakin, A. Christopoulos, *Pharmacol. Rev.* **2003**, *55*, 597–606.
- [53] R. M. Campbell, J. Dymshitz, B. J. Eastwood, R. Emkey, D. P. Greenen, J. M. Heerding, D. Johnson, T. H. Large, T. Littlejohn, C. Montrose, et al., *Assay Guid. Man.* **2004**, 1–20.
- [54] B. Beck, Y. Chen, W. Dere, V. Dev, B. J. Eastwood, W. Mark, S. J. Iturria, P. W. Iv, S. D. Kahl, R. a Moore, et al., **2004**, 1–7.
- [55] BioFocus, *Identification of Compounds Which Inhibit Plasmodium Falciparum Methylerythritol Cytidyltransferase (IspD) For*, **2012**.
- [56] A. S. Lawrenson, *Personal Communication*, **2012**.
- [57] I. D. Kuntz, K. Chen, K. a Sharp, P. a Kollman, *Proc. Natl. Acad. Sci. U. S. A.* **1999**, *96*, 9997–10002.
- [58] A. L. Hopkins, G. M. Keserü, P. D. Leeson, D. C. Rees, C. H. Reynolds, *Nat. Rev. Drug Discov.* **2014**, *13*, 105–21.
- [59] C. A. Lipinski, F. Lombardo, B. W. Dominy, P. J. Feeney, *Adv. Drug Deliv. Rev.* **1997**, *23*, 3–25.
- [60] H. Kagano, H. Goda, K. Yoshida, M. Yamamoto, S. Sakaue, *Method for Producing 1,2-Benzisothiazole-3-Ones Useful as Antibacterial and Antifungal Agents.*, **1996**.
- [61] I. Mohammed, M. K. Parai, X. Jiang, N. Sharova, G. Singh, M. Stevenson, T. M. Rana, *ACS Med. Chem. Lett.* **2012**, *3*, 465–469.
- [62] Y. Uchida, S. Kozuka, *Bull. Chem. Soc. Jpn.* **1982**, *55*, 1183–1187.
- [63] A. M. Qandil, M. A. Hassan, N. A. Al-Shar'i, *Arch. Pharm. (Weinheim).* **2008**, *341*, 99–112.
- [64] S.-K. Anandan, R. D. Gless, *Bioorg. Med. Chem. Lett.* **2010**, *20*, 2740–2744.
- [65] B. S. Bhakuni, S. J. Balkrishna, A. Kumar, S. Kumar, *Tetrahedron Lett.* **2012**, *53*, 1354–1357.
- [66] S. Aprile, E. Del Grosso, G. Grosa, *Xenobiotica* **2011**, *41*, 212–225.
- [67] B. Zhang, K. M. Watts, D. Hodge, L. M. Kemp, D. A. Hunstad, L. M. Hicks, A. R. Odom, *Biochemistry* **2011**, *50*, 3570–3577.
- [68] (MMV) Medicines for Malaria Venture, “Malaria and Medicines,” can be found under <http://www.mmv.org>, **2016**.

- [69] Y. Corbett, L. Herrera, J. Gonzalez, L. Cubilla, T. L. Capson, P. D. Coley, T. A. Kursar, L. I. Romero, E. Ortega-Barria, *Am. J. Trop. Med. Hyg.* **2004**, *70*, 119–124.
- [70] R. E. Desjardins, C. J. Canfield, J. D. Haynes, J. D. Chulay, *Antimicrob. Agents Chemother.* **1979**, *16*, 710–718.
- [71] T. A. Kursar, C. C. Caballero-George, T. L. Capson, L. Cubilla-Rios, W. H. Gerwick, M. V. Heller, A. Ibañez, R. G. Linington, K. L. McPhail, E. Ortega-Barría, et al., *Biodivers. Conserv.* **2007**, *16*, 2789–2800.
- [72] M. T. Makler, J. M. Ries, J. A. Williams, J. E. Bancroft, R. C. Piper, B. L. Gibbins, D. J. Hinrichs, *Am. J. Trop. Med. Hyg.* **1993**, *48*, 739–741.
- [73] Maria Mondini, Novel Antimalarial Compounds Targeting the Non-Mevalonate Pathway: Design and Synthesis Optimization, **2014**.
- [74] A. M. Guggisberg, J. Park, R. L. Edwards, M. L. Kelly, D. M. Hodge, N. H. Tolia, A. R. Odom, *Nat. Commun.* **2014**, *5*, 4467.
- [75] W. Trager, J. B. Jensen, *Science* **1976**, *193*, 673–675.
- [76] J. C. Stålring, L. A. Carlsson, P. Almeida, S. Boyer, *J. Cheminform.* **2011**, *3*, 28.
- [77] D. J. Wood, D. Buttar, J. G. Cumming, A. M. Davis, U. Norinder, S. L. Rodgers, *Mol. Inform.* **2011**, *30*, 960–972.

Chapter 3

Developing an Understanding of SAR Around the BITZ

Chemotype and Biological Evaluations of BITZ

Compound Activity

3.1 Medicinal Chemistry Strategy - TCAMS

This chapter will present the research that has been conducted, taking the **DT2009-0168020** HTS hit (**Chapter 2, Section 2.2.4, Figure 2.8**) towards an optimised lead structure *via* SAR exploration and through the optimisation of physicochemical properties. As an introduction to this work, first presented is an example of a medicinal chemistry program carrying out a similar approach of hit to lead optimisation within drug design, from which we have taken inspiration.

As discussed in Chapter 2 (**Section 2.1**), a phenotypic screen of the 13, 533 chemical structures published by GSK in 2010 comprising the Tres Cantos Antimalarial Set (TCAMS) compound library was performed. It identified 47 high quality starting points of then unevaluated chemotypes to fast track into lead optimisation studies with the purpose of initiating open and innovative antimalarial drug discovery.^[1] Five compound series were ultimately selected, each complying with the chief requirements of antiplasmodial potency, druggability and synthetic tractability.

A series of indoline compounds was one of the five selected compound series, in which; the primary hit was TCMDC-139046 (**Figure 3.1**), a highly potent compound with good *in vitro* antimalarial activity (IC₅₀ value of 80 nM against *P. falciparum* 3D7A in a 48-hour assay).^[2] Whilst the TCMDC-139046 hit is metabolically stable with little cytotoxicity, the molecular weight (MW) and lipophilicity of the compound were high and, as part of the indoline series, also known to have activity against the 5-HT_{2c} receptor.^[1,3]

Inhibition of the 5-HT_{2c} receptor is associated with the treatment of depression and anxiety and therefore may complicate clinical development of an antimalarial compound series; consequently, minimising activity at this receptor type was a priority for subsequent SAR development around the TCMDC-139046 hit.^[2] Work by Calderon *et al.* addressed this challenge in a double SAR study that aimed to drive antimalarial potency at both *P. falciparum* 3D7 and *P. falciparum* Dd2, whilst avoiding interaction with 5-HT_{2c} receptors.^[2] Optimisation of TCMDC-139046 also aimed to improve the physicochemical profile of the compound, already known to have a poor pharmacokinetic (PK) profile of high lipophilicity and low solubility in aqueous media.^[2]

A diverse range of functional group substitutions and chemical modifications were made to the TCMDC-139046 hit, summarised in **Figure 3.1**, in a full SAR analysis conducted by Calderon *et al.* Functional group substitutions were explored at R¹ to determine if the lipophilic trifluoromethoxy group could be replaced with more desirable polar groups such as F, H and CF₃.

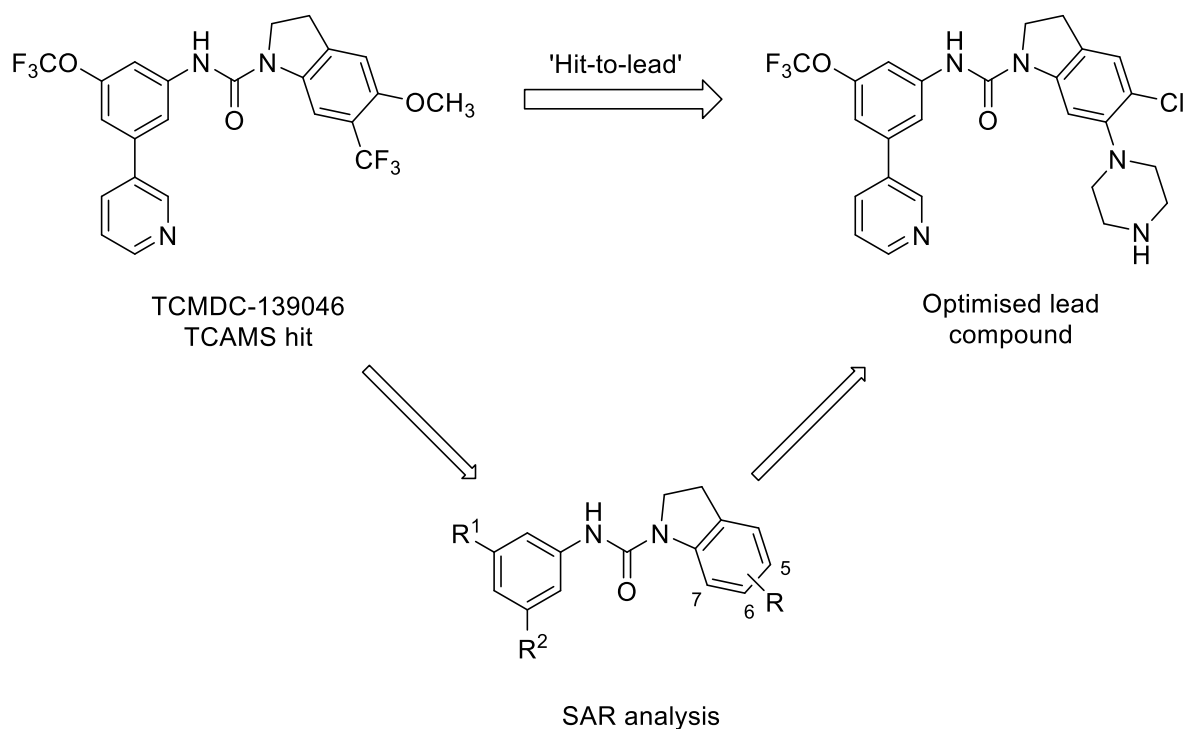


Figure 3.1 SAR development and optimisation of the TCAMS TCMDC-139046 hit to a lead antimalarial compound: figure reproduced from [1] and [2].^[1,2]

In addition, varying the pyridyl ring structure at R² was also examined. However, replacement of the pyridyl ring with various functionalities, including H, Br and Me, showed a loss in antiplasmodial activity; substitution with a pyrimidyl ring gave a slightly improved physicochemical profile, due to a small reduction in lipophilicity, but showed no great improvement in terms of potency. Overall, SAR analysis around the left hand side of the molecule, as drawn, revealed that the trifluoromethoxy group at R¹ represented the best substitution for maintaining antimalarial activity and that the 3-pyridyl ring at R² represents the optimal functionality for minimising activity at the 5-HT_{2c} receptor.^[2]

Calderon *et al.* acknowledged that a wide variety of substituents would be tolerated in the indole ring, as highlighted by the diversity seen in the TCAMS. Subsequently, a wide range of substitutions were made at a number of positions in the indoline core (**Figure 3.1**), comparing antimalarial activity results to an unsubstituted indoline structure to determine clearly the effect of each structural modification. SAR development around the right hand side of the TCMDC-139046 structure was therefore extensive^[2] and ultimately led to the development and rationalisation of the optimised lead compound (**Figure 3.1**) where R⁵ = Cl, R⁶ = piperidine and R⁷ = H. The resulting structure, depicted above, therefore represented the most promising compound since it was able to demonstrate a divergent SAR between *in vitro* antimalarial activity and affinity for the 5-HT_{2c} receptor. It also had an acceptable physicochemical profile in terms of oral absorption, lipophilicity and *in vitro* clearance; the next stage of research from this point aimed to improve *in vivo* efficacy.^[2]

The work conducted by Calderon *et al.*^[2] therefore represents a good example of a successful medicinal chemistry optimisation program with full SAR analysis, moving from a hit starting point to an optimised lead compound. Medicinal chemistry optimisation was performed identifying progressively optimised compounds, designed to display specific and divergent activity at different molecular targets, as required by the specifications of this research problem. Altogether, a clear progression was made moving from a HTS hit to an optimised lead compound; advancing into an area of improved chemical space and optimal biological performance.

Relating this to our own antimalarial research question, we took inspiration from the work of Calderon *et al.*^[2] and aimed to mirror this successful medicinal chemistry approach in the application of hit to lead optimisation around the identified of 1,2-benzo[d]isothiazol-3(2*H*)-one (BITZ) chemotype.

3.1.1 Aims

Having identified the BITZ chemotype and derivatives as novel, small-molecule inhibitors of the *P. falciparum* IspD (*Pf*IspD) enzyme, the aims of research were to undertake a medicinal chemistry optimisation program. The long term aims were to deliver a lead candidate molecule targeting *P. falciparum* methylerythritol cytidyltransferase (*Pf*IspD) that is suitable for clinical development as an antimalarial drug. With organic synthesis facilitating structural modifications to the BITZ side chain, the resulting inhibitors aim to develop SAR around the BITZ chemical chemotype and *Pf*IspD enzyme active site which are informed and guided by *Pf*IspD enzymatic activity assays and 3D7 whole cell activity assays of resulting BITZ compounds.

The primary objectives of research were to enhance the efficacy and pharmacokinetic properties of the HTS hit, **DT2009-0168020**. Therefore, optimisation of drug-like properties, removal of metabolic and pharmacokinetic vulnerabilities, probing chemical space, determining the nature of the *Pf*IspD enzyme target and the role of BITZ inhibitor in achieving enzyme inhibition were key developmental priorities.

3.1.2 SAR Map: Summary of Synthetic Explorations and BITZ Compound Series

Several series of BITZ compounds, with defined structural variations and specific chemical modifications, have been designed and synthesised around a simple BITZ compound framework (**Figure 3.2**). SAR development and hit to lead optimisation was initiated from this simplified BITZ structure since it was close to a “leadlike” starting point therefore allowing growth in molecular weight whilst being able to optimise drug-like properties.^[4] Each BITZ compound series has a specific and well-defined design rationale with the aim of informing SAR and developing an understanding of optimal

functionality, promoting inhibitory activity against *Pf*lspD. These structural explorations and design rationales, along with their outcomes, are outlined and discussed throughout this chapter.

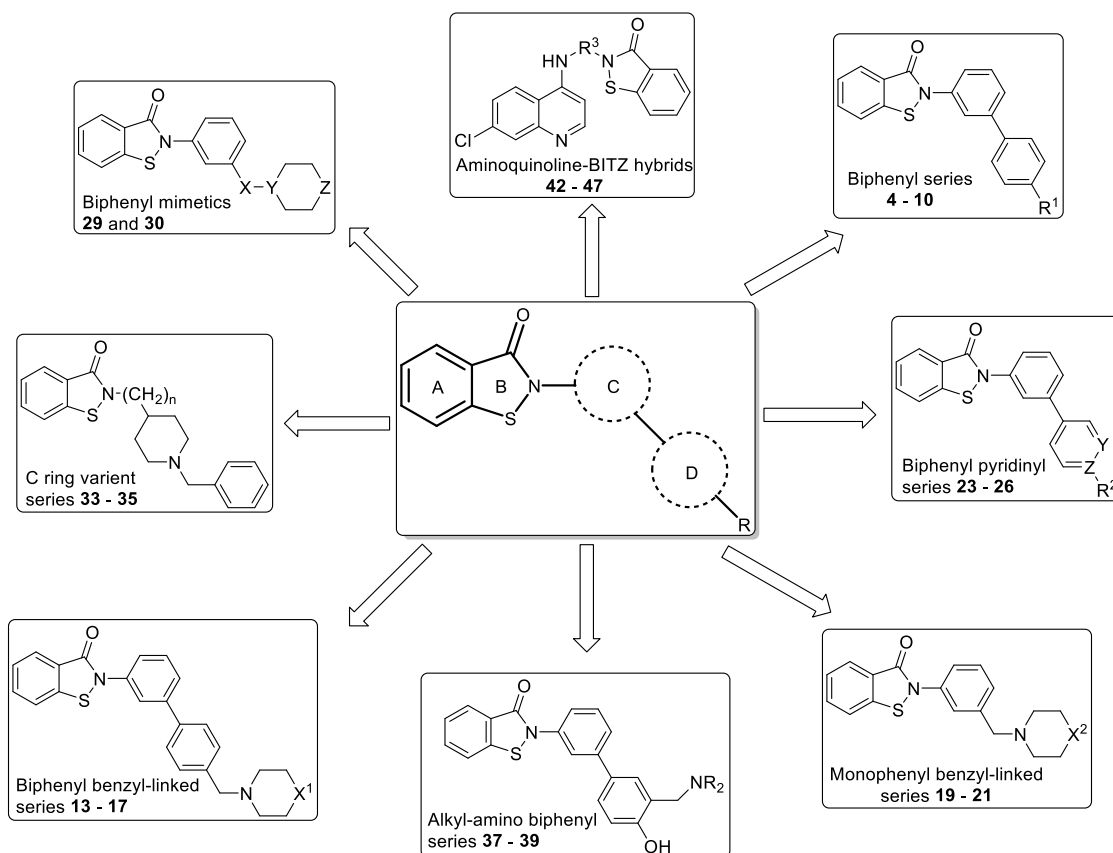


Figure 3.2 Summary of BITZ compound series developed around the selected chemotype.

Based around the synthetic explorations discussed in Chapter 2 (**Section 2.3**), distinct synthetic strategies have been used to generate more than 30 BITZ compound analogues which make up the eight discrete compound series, shown in **Figure 3.2**. A series of structural modifications have been made to the C and D rings in the side chain of the hit scaffold with the aims of varying lipophilicity, improving solubility and introducing functionality to promote potency against *Pf*lspD. Each BITZ analogue generated has been tested in both the *Pf*lspD enzymatic assay (**Chapter 2, Section 2.2.3**) and the 3D7 whole cell parasite growth assay (**Chapter 2, Section 2.3.5**) to determine the extent of inhibitory compound activity against *Pf*lspD and *Plasmodium* parasite growth.

3.2 Biphenyl BITZ Analogue Series

3.2.1 Design Rationale and Synthesis

The first of BITZ compound series was established on the basis of knowledge gained from preliminary SAR investigations around the HTS hit, **DT2009-0168020** (**Chapter 2, Section 2.5**). The sulphonamide group of the **DT2009-0168020** hit was therefore removed and the required *meta*-substitution pattern

across the C ring was maintained, but with all C ring *ortho*-functionalities removed. The purpose of the biphenyl analogue series was to determine the optimal D ring for BITZ derived *Pfl*spD inhibitors and which functional group substituents were best tolerated. Consequently, in this series of BITZ analogues, comprised of seven derivatives, the D ring is specified as a *para*-substituted phenyl ring with the inclusion of various electron-donating and accepting groups to explore the effects of various *para*-substitutions in the aromatic D ring. A single exception to this structural motif exists in the case of compound **10** where the phenyl D ring was replaced with a thiophene ring (**Figure 3.3**).

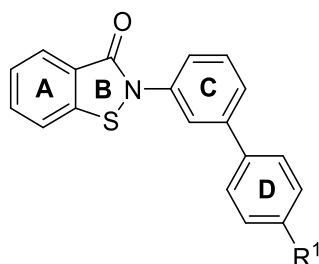
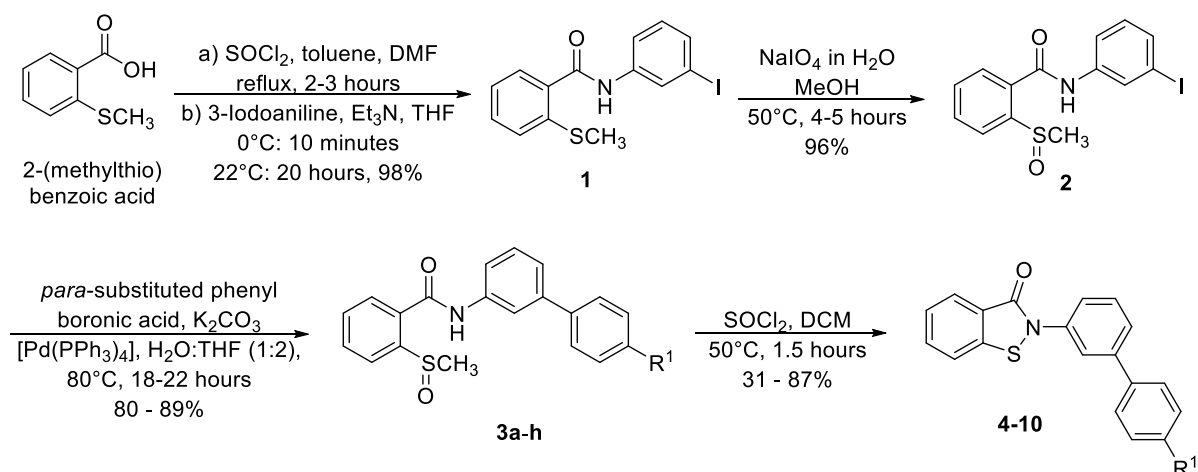


Figure 3.3 Chemical structure and substitution pattern of BITZ compounds **4-10**.

All compounds in this series were synthesised using a synthetic scheme which was derived from **Route 1** (**Chapter 2, Section 2.3.1, Scheme 2.4**), facilitating generation of the BITZ motif and related analogues from the commercially available starting material, 2-(methylthio) benzoic acid (**Scheme 3.1**).

The BITZ headgroup itself was generated in the final synthetic step of the synthesis, *via* the previously discussed thionyl chloride-mediated ring closure of methylsulfinyl benzamide intermediates (**Chapter 2, Section 2.3.1, Scheme 2.6**). In order to incorporate the *para*-substituted D ring of desired inhibitor structures (**4-10**), Suzuki-Miyaura cross-coupling reactions^[5] were incorporated into the synthetic procedure, producing a representative four-step synthesis of compounds **4-10**, as depicted below.



Scheme 3.1 General synthetic strategy for BITZ compounds **4-10**.

Acid-chloride mediated amide coupling of 2-(methylthio) benzoic acid and 3-iodoaniline, generated the (methylthio)benzamide **1**.^[6] Oxidation of **1** to the corresponding sulfoxide, **2**,^[6] followed by Suzuki-Miyaura cross-coupling reactions,^[5] using a range of *para*-substituted phenyl boronic acids, was employed to generate intermediates **3a-h**. The methylsulfinyl benzamides intermediates **3a-h** were finally cyclized using thionyl chloride-mediated ring closure^[7] to give the required BITZ derivatives **4-10**. All synthetic steps proceeded in moderate to good yields with the straightforward purification of all intermediates and target compounds by trituration or flash column chromatography.

3.2.2 *PflspD* Enzymatic and Whole Cell Biological Assays

All of the compounds in this series demonstrated low micromolar to nanomolar inhibitory activity against *PflspD* as well as low micromolar activity against *Plasmodium* parasite growth; highlighting the efficacy of these compounds and their developmental potential. These initial results show that *para*-substitution in the phenyl D-ring, using electron releasing or withdrawing groups (**4-10**) was well tolerated, with *PflspD* IC₅₀ values as low as 73 ± 20 nM and a parasite EC₅₀ of 1.04 ± 0.164 μM for the *para*-chloro analogue **5**.

Compound number	R ¹ /D ring	<i>PflspD</i> IC ₅₀ (μM)	Whole cell 3D7 EC ₅₀ (μM)	MW (g mol ⁻¹)	<i>ClogD</i>	<i>CaqSol</i> (μM)
4	OCH ₃	0.206 ± 0.089	0.920 ± 0.066	333.08	4.72	1.40
5	Cl	0.073 ± 0.020	1.080 ± 0.164	337.03	4.98	0.56
6	CF ₃	0.273 ± 0.015	0.646 ± 0.021	371.06	5.26	0.38
7	OCF ₃	0.290 ± 0.195	0.411	387.05	5.55	0.26
8	CO ₂ CH ₃	0.393 ± 0.096	1.00 ± 0.237	361.08	4.82	0.53
9	OH	0.660	2.450	319.07	4.33	3.61
10	Thiophene	0.265 ± 0.021	2.877	309.03	4.49	3.71

Table 3.1 Inhibitory activity of compounds **4-10** against *PflspD* and *P. falciparum* growth in culture (strain 3D7); predicted *ClogD* and *CaqSol* values calculated using algorithms from AstraZeneca (as predicted for all BITZ compounds).^[8,9]

Whilst *para*-chloro analogue **5** was seen to be the most potent inhibitor in series against *PflspD*, the *para*-methoxy analogue **4** and *para*-trifluoromethyl analogue **6** were found to possess comparable enzymatic *PflspD* activity of 206 ± 89 nM and 273 ± 15 nM respectively. This encouraging enzymatic activity was also translated into whole cell growth inhibition, with 3D7 EC₅₀ values of 920 ± 66 nM and 646 ± 21 nM displayed by **4** and **6** respectively. Importantly, it should be pointed out that the most potent inhibitor of the biphenyl series against *PflspD*, *para*-chloro analogue **5**, demonstrates inhibition of the enzyme at a potency six-fold higher than that of the original HTS hit, **DT2009-0168020** (Figure

3.15), highlighting that a substantial amount of structural optimisation has been achieved. These results are therefore encouraging as they not only show that BITZ compounds are capable of potentially inhibiting the *Pf*lspD enzyme target but that this also translates into whole cell antimalarial activity.

In slight contrast to inhibitors **4-7**, a reduction in activity against both the *Pf*lspD enzyme and *Plasmodium* parasite growth was observed with the thiophene derivative **10**. This result suggests that a substituted aromatic phenyl ring, as the D-ring of the inhibitor side chain, may be preferable to the slightly smaller, aromatic thiophene heterocycle. This may also reflect spatial requirements and inhibitor shape-fit at the *Pf*lspD active site however, further SAR investigation is needed to support this inference.

A consistent issue across the biphenyl BITZ series is high compound lipophilicity, tracking with poor predicted aqueous solubility, which was particularly apparent with some of the most potent inhibitors in the series, **4-8** (**Table 3.1**). The ability of a drug to penetrate biological membranes and tissues is a key factor which mediates the extent of drug interactions with a biological system and therefore the ability of chemical agents to achieve their desired effect.^[10] Consequently, optimisation of aqueous solubility has remained a key priority throughout BITZ compound development with acceptable aqueous solubility defined as $> 50 \mu\text{M}$; which is consistent with accepted pharmacokinetic (PK) parameters as defined in literature.^[11] In order to gain an awareness of the probable lipophilicity and solubility of the designed BITZ compounds, we requested predicted distribution coefficient and solubility measurements from AstraZeneca (AZ) for all BITZ compounds synthesised within this research. In these papers^[8,9] AZ highlight the design of good predictive models for the *logD* and aqueous solubility of organic compounds. The strategic collaboration between The University of Liverpool and AZ for research into tropical diseases enabled our access to these *in silico* models, allowing us to obtain pharmacokinetic (PK) predictions for our BITZ derived compounds.^[12]

3.2.3 Lipophilicity

Compound polarity, electronic and steric parameters, as well as molecular weight and geometry are important physicochemical factors which are strongly correlated with biological activity.^[10] However, lipophilicity is possibly one of the most important physicochemical properties to be considered in the development of potential drugs due to its major role and influence in compound solubility, absorption and membrane penetration, plasma protein binding and distribution within biological systems.

Lipophilicity represents the affinity of a molecule for a lipophilic environment and is measured by its distribution behaviour within a biphasic system.^[13] Lipophilicity, most commonly measured as *LogP*, is a component of Lipinski's Rule of Five^[14] for predicting the drug-likeness of molecules. *LogP* values

provide the partition coefficient of a neutral (or unionised) molecule between aqueous and water phases, usually octanol and water (**Figure 3.4**). A partition (or distribution) coefficient signifies the tendency of a molecule to differentially compartmentalise between two immiscible phases.^[15]

$$\text{LogP}_{\text{oct/wat}} = \log \left(\frac{[\text{compound}]_{\text{octanol}}}{[\text{compound}]_{\text{water}}} \right)$$

Figure 3.4 The octanol/water partition coefficient (*logP*) defining the intrinsic lipophilicity of a drug molecule.^[16]

Since many known drug molecules are ionisable species, and the lipophilicity of a compound changes as a function of pH, *LogD* (distribution coefficient) is often used as a measure of lipophilicity in drug discovery and development programs. The distribution constant *LogD* is pH dependent and therefore provides an appropriate description of molecule lipophilicity at any specified pH. Since ionisable groups within drug molecules are likely to be charged at physiological pH (pH 7.4), *LogD* provides a more accurate representation of a compounds lipophilicity when present within a biological system.^[16] In order to adhere with literature guidelines and optimise the prospect of developing compounds that display optimal PK profiles, we aim to generate compounds that observe our target parameters for *ClogP* and *ClogD*. More specifically, designed compounds should ideally demonstrate *ClogP* values of < 5 in order to conform to Lipinski's guidelines and enhance the likelihood of achieving optimised drug-likeness and compound bioavailability.^[14,17,18] Considering parameters for *ClogD* (pH 7.4), values between 1.1 and 3.1 represent a suitable target range for compound design since our compounds are likely to span the MW category of 300 – 450 g mol⁻¹; and it is now well documented in literature that compounds with distribution coefficients inside these parameters tend to have good solubility and permeability (i.e. favourable oral absorption and cell membrane permeability).^[19]

3.3 Biphenyl Benzyl-linked BITZ Analogue Series

3.3.1 Design Rationale and Synthesis

Compound lipophilicity has long been recognised as important for aqueous solubility of compounds, where a lack of sufficient solubility is a significant and often challenging obstacle in medicinal chemistry optimisation.^[19–21] Therefore, to reduce the highly lipophilic nature of the biphenyl BITZ analogues **4-10**, as well as improve aqueous solubility, a new compound series (**13-17**) was designed. This biphenyl benzyl-linked series, comprised of five compounds, incorporates a methylene link between the phenyl D ring and various polar heterocyclic groups, maintaining *para*-substitution in the terminal D ring (**Figure 3.5**).

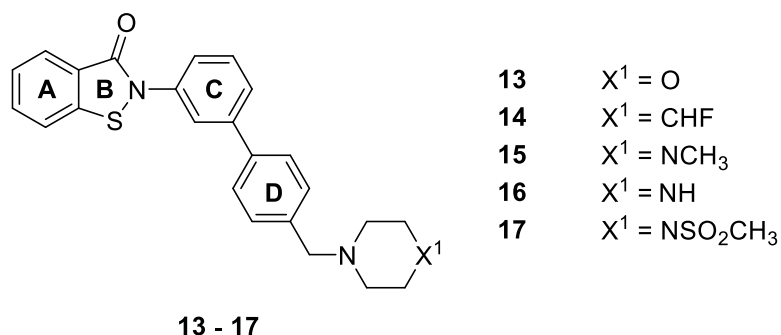
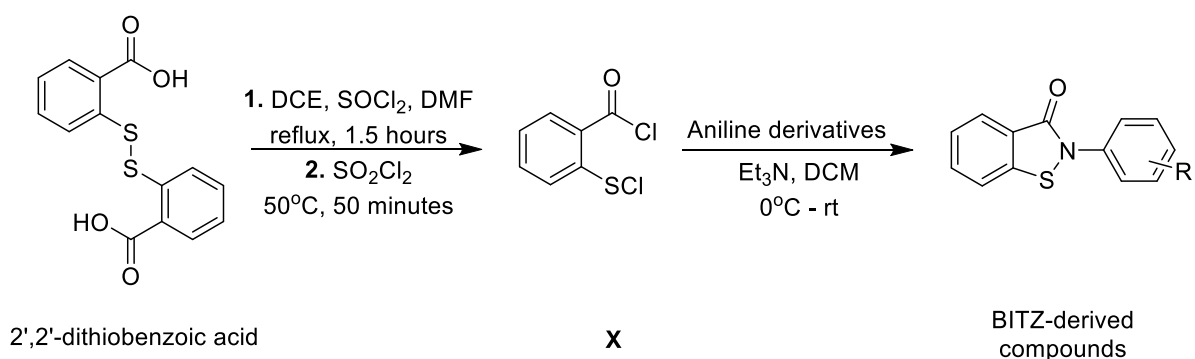


Figure 3.5 Chemical structures and substitution pattern of BITZ compounds **13-17**.

The main aim of this molecular addition was to promote aqueous solubility and reduce compound lipophilicity through introduction of a basic protonation site. In addition, the introduction of this basic protonation site from the attachment of heterocycles offers the possibility of administering the resulting compounds as salts, to facilitating solubility for drug administration.^[22] Furthermore, extension of the BITZ inhibitor side chain potentially enables additional protein-ligand contacts to be made, at the *PflspD* active site, therefore potentiating increased strength of BITZ compound binding. The benzyl linker adds a degree of ligand flexibility to **13-17** which may enable an increased number of ligand binding poses and inhibitor orientations to be adopted within the *PflspD* binding site. This may therefore support new protein-inhibitor contacts and promote the strength of inhibitor binding and therefore the magnitude of enzyme inhibition.

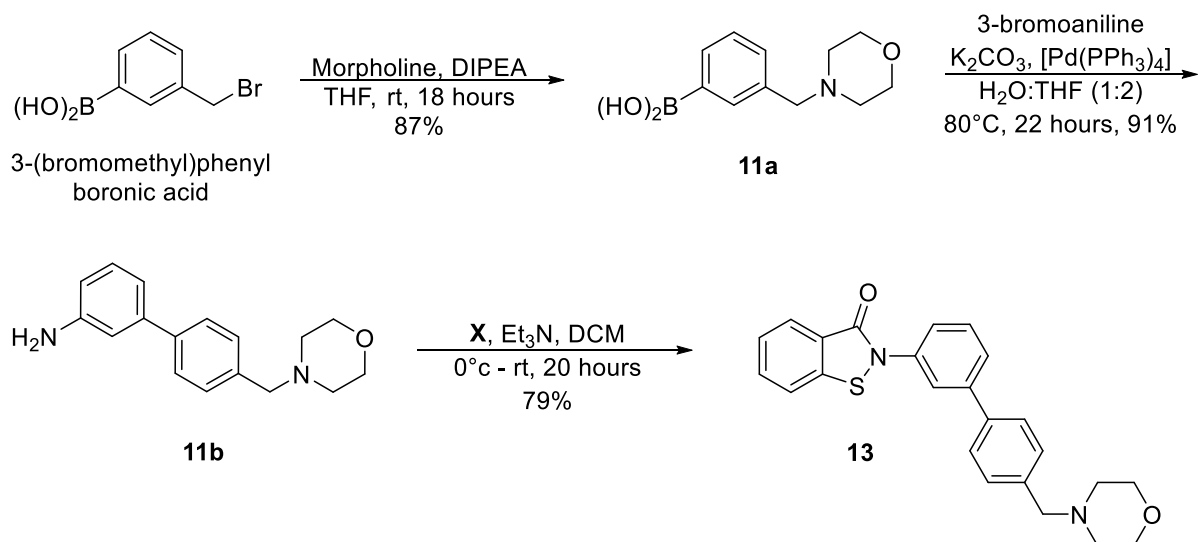
The synthesis of this inhibitor series was approached using two distinct synthetic routes. Initially, inhibitors **14** and **15** were generated using the previously described synthetic route (**Section 3.2.1, Scheme 3.1**) where yields were found to be consistent with those previously observed. However, larger and more complex boronic acid species were required to incorporate the benzyl-linked side chains of **16** and **17** within the Suzuki-Miyaura cross-coupling synthetic step. To maintain this synthetic approach using more complex boronic acid species, the chemical reagents required became notably higher in cost, increasing the total expense of analogue production. Since high developmental costs are not in line with the affordability ethos of antimalarial drug development programs and aims for economic viability,^[23,24] a revised synthesis was sought.

As a result, an alternative three-step route, using the previously discussed acid chloride-mediated synthesis (**Chapter 2, Section 2.3.3**), was used to generate the morpholine-linked analogue **13** (**Scheme 3.3**). The synthesis of 2-(chlorothio)-benzoyl chloride **X** occurs *via* a rapid and quantitative two-step, one-pot reaction using the disulphide; 2',2'-dithiobenzoic acid (**Scheme 3.2**).^[25] In addition, **X** is air stable at room temperature making it a versatile chemical intermediate to incorporate since it can be isolated and stored over short periods of time.



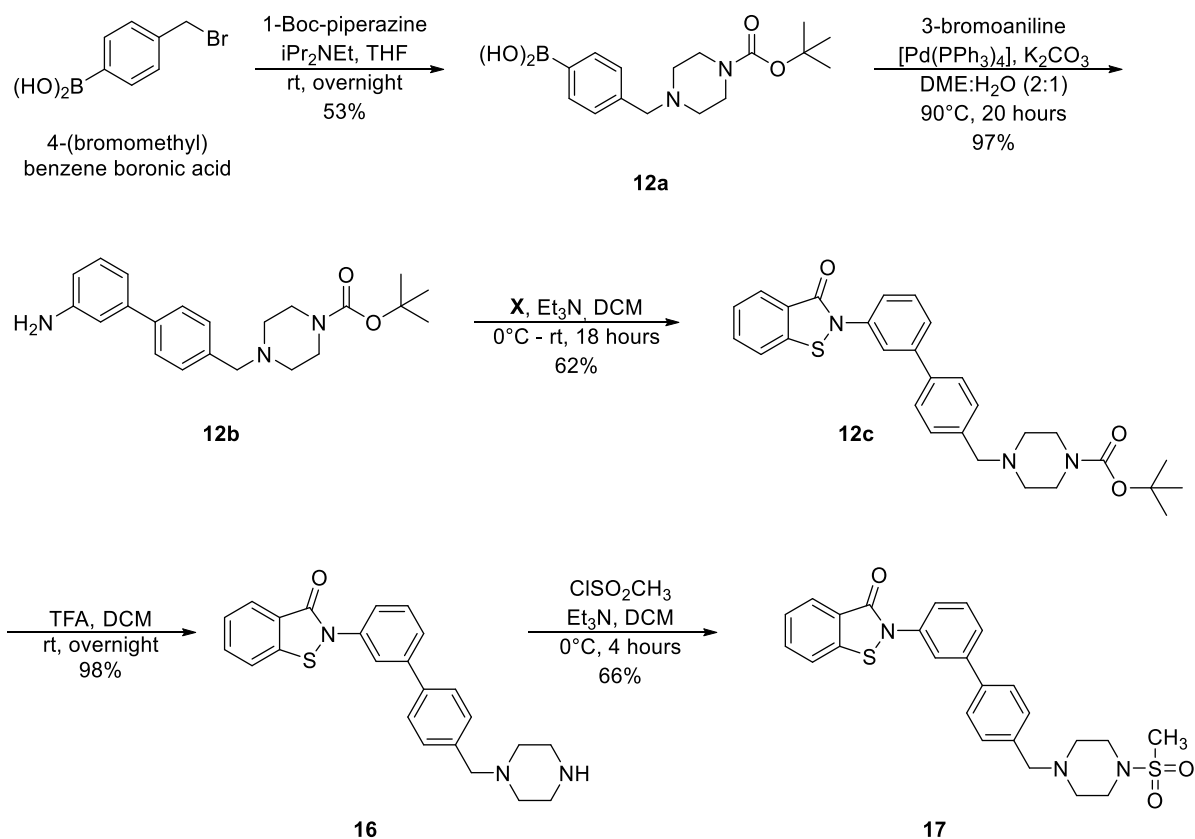
Scheme 3.2 Synthesis of **X** and the subsequent synthetic strategy for the generation of BITZ derived compounds by acid chloride-mediated amide coupling and ring closure between **X** and appropriate aniline derivatives.^[25]

Towards the synthesis of BITZ compound **13**, **11a** was generated *via* nucleophilic displacement using morpholine and the corresponding benzylbromine.^[26] This was then subject to a Suzuki-Miyaura cross-coupling reaction with 3-bromoaniline to generate the intermediate **11b**. Cyclization of **11b** with acid chloride **X** (**Scheme 3.2**),^[25] in a simultaneous amide coupling and ring closure mechanism, produced **13**^[27,28] with all reactions proceeding in high yields.



Scheme 3.3 Synthetic strategy for compound **13**.

In order to generate BITZ analogues **16** and **17**, a separate synthesis was devised due to the requirement for Boc-protection of the piperazine heterocycle and the subsequent sulfonylation of compound **16** to give **17**. As a result, generation of **16** and **17** required a linear, five-step synthesis which is shown in **Scheme 3.4**.



Scheme 3.4 Synthetic strategy for compounds **16** and **17**.

Nucleophilic displacement of a 4-(bromomethyl)benzene boronic acid by 1-Boc-piperazine gave **12a**^[26] which, analogous to the conversion of **11a** to **11b**, underwent a Suzuki-Miyaura cross-coupling reaction with 3-bromoaniline to generate the intermediate **12b**. **12b** was then cyclized with **X** via the described simultaneous amide coupling and ring closure mechanism to produce **12c**.^[27,28] Removal of the Boc-protecting group was achieved under acidic conditions, using TFA, in high yield to reveal the free piperazine heterocycle and generate **16**. Compound **16** was subsequently converted to **17** in moderate yield by simple nucleophilic substitution with methanesulfonyl chloride,^[29] generating the methylsulfonyl-substituted piperazine heterocycle and the final target of this series (**17**). Despite the linear nature of this synthesis (**Scheme 3.4**), all synthetic steps proceeded in reasonable to good yield with the straightforward isolation and purification of all intermediate compounds.

In accordance with the aim of this BITZ compound series, incorporation of the piperidine heterocycle intended to promote the aqueous solubility of **16** and lower the predicted distribution coefficient of the compound. Specifically, the piperidine functionality adds an additional hydrogen bonding capacity to **16** since it is hydrogen donating and therefore provides a subtle contrast to the hydrogen bond acceptor capabilities of the morpholine and *N*-methyl piperazine functionalities of **13** and **15**. This BITZ compound series has therefore utilised a range of saturated heterocyclic rings, providing both hydrogen bond donating and accepting capabilities, intended to facilitate hydrogen bonding

interactions at the *Pf*lspD active site and promote compound solubility. In addition, compound **17** facilitates further extension of the BITZ side chain, together with increased structural flexibility. This side chain extension could enable increased protein-ligand interactions at *Pf*lspD through increased inhibitor bulk and therefore greater occupation of the *Pf*lspD active site.

3.3.2 *Pf*lspD Enzymatic and Whole Cell Biological Assays

All compounds in this series **13-17** demonstrated low micromolar activity against *Pf*lspD which also translated into comparable low micromolar activity against parasite growth in the case of compounds **13-15**. Compound **14** showed the most potent parasite killing effects with a 3D7 EC₅₀ value of 0.323 ± 0.092 μM (**Table 3.2**). Biological analysis and physicochemical property predictions highlight that incorporation of benzyl-linked heterocycles into the BITZ side chain improves the solubility and lowers the lipophilicity of resulting inhibitors. This is particularly notable with compounds **16** and **17** which also demonstrate inhibitory against the *Pf*lspD enzyme and Plasmodium parasite growth.

Compound number	X ¹	<i>Pf</i> lspD IC ₅₀ (μM)	Whole cell 3D7 EC ₅₀ (μM)	MW (g mol ⁻¹)	<i>ClogD</i>	<i>CaqSol</i> (μM)
13	O	0.400 ± 0.082	0.413 ± 0.082	402.14	4.13	2.51
14	CHF	0.862 ± 0.107	0.323 ± 0.092	418.15	4.64	1.86
15	NCH ₃	0.446 ± 0.075	0.416 ± 0.006	415.17	3.80	56.23
16	NH	0.160 ± 0.007	3.25	401.16	2.56	52.86
17	NSO ₂ CH ₃	0.523 ± 0.09	1.47	479.13	3.99	1.08

Table 3.2 Inhibitory activity of compounds **13-17** against *Pf*lspD and *P. falciparum* growth in culture (strain 3D7); calculated *ClogD* and *CaqSol* values given.

Particularly encouraging from this series is the significantly enhanced aqueous solubility of **15**; likely a consequence of the *N*-methyl piperazine heterocycle which introduces two basic protonation sites into the molecule. Indeed, compound **15** showed a 100-fold increase in predicted aqueous solubility compared to our most active *Pf*lspD inhibitor **5** (**Table 3.1**), a reduction in *ClogD* from 4.98 to 3.80 and ~ 3-fold enhanced activity against cultured *P. falciparum*. In addition, compound **16**, incorporating the unsubstituted piperazine heterocycle, also displayed significantly enhanced aqueous solubility compared to other analogues, as well as potent *Pf*lspD enzymatic activity with a corresponding IC₅₀ value of 0.160 μM. Disappointingly, the enzymatic activity of **16** was not translated into whole cell 3D7 growth inhibition, as achieved with compounds **13-15**. This may be a consequence of the reduced lipophilicity of **16** since a reduction in lipophilicity can be mirrored by reduced compound permeability

within a biological system.^[30,31] Taken together, these results demonstrate that the inhibitory activity of BITZ compounds can be maintained whilst enhancing the drug-like properties of analogues through structural modification and chemical manipulations.

Following much debate and research, it is now commonly recognised that the optimal *logD* parameters for any compound are dependent on molecular weight.^[19] However a general assumption can be made that the optimal *logD* for a potential drug molecule lies in the narrow range of ~ 1-3.^[32] Considering this compound series, the calculated distribution coefficient of each analogue currently lies outside of this range. Further inhibitor modifications were therefore required to try and reduce *ClogD* values further, whilst maintaining *PfIspD* enzymatic and whole cell activity, alongside compound solubility.

3.4 Mono-phenyl Benzyl-linked BITZ Analogue Series

3.4.1 Design Rationale and Synthesis

Guided by previous results, a series of mono-phenyl inhibitors **19-21** were designed and synthesised, maintaining *meta*-benzylic heterocycle substitution at the C ring (**Figure 3.6**). The aromatic phenyl D ring of previous analogues was removed to reduce lipophilicity in this resulting mono-phenyl series; while the heterocycle functionalities were conserved to retain compound solubility. The overall aim was to retain inhibitor activity and optimise aqueous solubility whilst lowering inhibitor lipophilicity. Therefore, this analogues series may provide a means of exploring the extent or lack of lipophilicity is tolerated in the SAR of BITZ analogues. Given that a phenyl ring has an associated *ClogP* value of 2.14,^[33] removal of the phenyl D ring moves the mono-phenyl series into our target zone for *ClogP* and *ClogD*. In other words, the compound series (**19-21**) was used to assess if inhibitory whole cell growth activity correlates with increased lipophilicity, which would likely be as a result of enhanced membrane penetration.

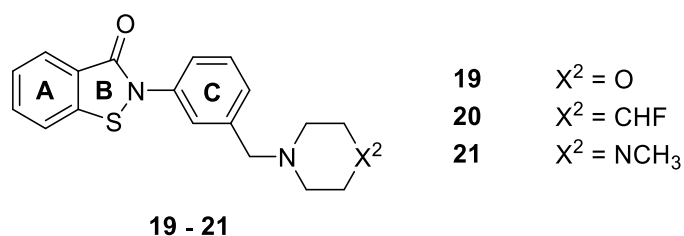
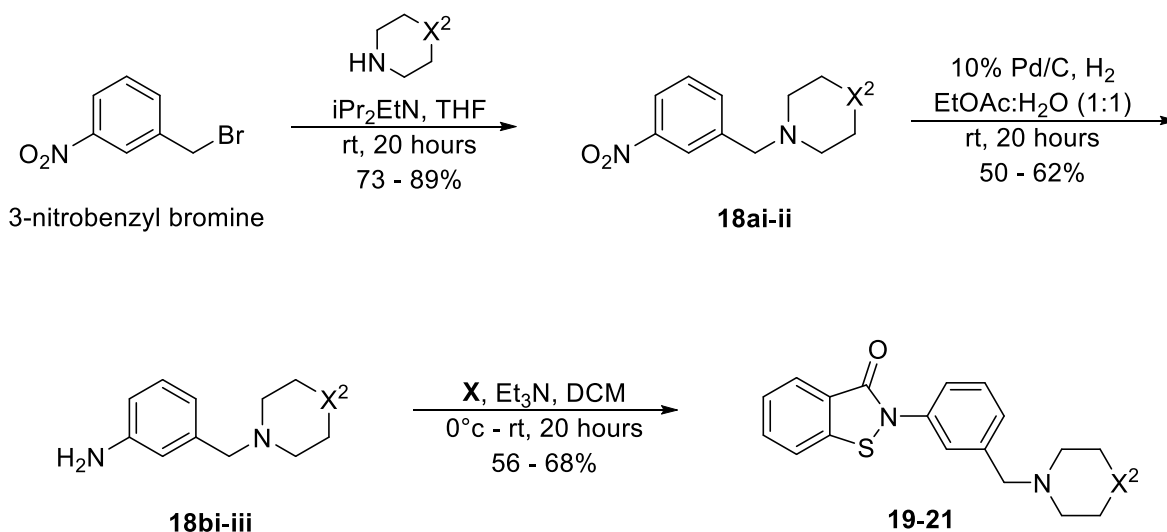


Figure 3.6 Chemical structures and substitution pattern of BITZ compounds **19-21**.

The mono-phenyl inhibitor series was generated using a straightforward three-step synthesis. The required inhibitor side chain was first constructed in the initial two steps of the synthesis which was

completed by acid chloride-mediated amide coupling and ring closure to generate the BITZ motif (Scheme 3.5).



Scheme 3.5 Synthetic strategy for mono-phenyl BITZ compounds **19-21**; **18bi** (3-morpholine-4-yl methyl-phenylamine) was purchased from Sigma Aldrich.

The first synthetic step involved nucleophilic displacement of 3-nitrobenzyl bromide by treatment with the appropriate heterocycle, in the presence of diisopropylethyl amine (iPr_2EtN), to yield the 3-nitrobenzyl heterocycle intermediates **18ai-ii**. A subsequent hydrogenation reaction converted the nitro functionality of intermediates **18ai-ii** into the corresponding 1° amines, giving 3-aminobenzyl heterocycles **18bi-iii**. In the final synthetic step, the acid chloride $\text{X}^{[25]}$ facilitated simultaneous amide coupling and ring closure^[27,28] introducing the BITZ headgroup into the final inhibitor structures **19-21**.

3.4.2 *Pfl*spD Enzymatic and Whole Cell Biological Assays

The mono-phenyl BITZ derivatives demonstrated a reduction in lipophilicity, the immediate consequence of removing an aromatic ring, and improved solubility, which overall is likely due to reduced molecular size and retention of the saturated heterocyclic ring. Considering these favourable physicochemical parameters it seemed likely that this compound series would be able demonstrate good permeability in biological systems due to average molecular weights < 400 and predicted AZlogD parameters of > 1.3.^[19]

Compound number	X ²	<i>Pf</i> lspD IC ₅₀ (μM)	Whole cell 3D7 EC ₅₀ (μM)	MW (g mol ⁻¹)	<i>ClogD</i>	<i>CaqSol</i> (μM)
19	O	0.540	5.71	326.11	2.60	119.9
20	CHF	0.530 ± 0.027	2.18 ± 0.340	342.12	3.16	71.89
21	NCH ₃	0.524	1.88	339.14	2.18	1343

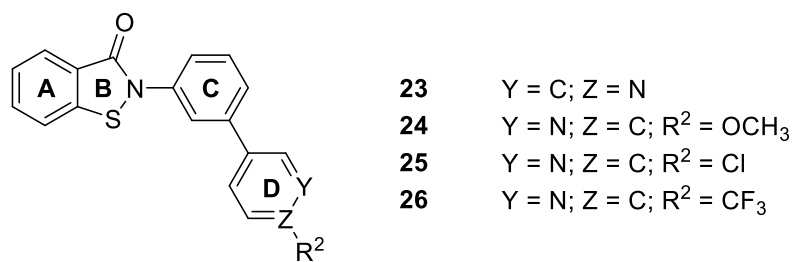
Table 3.3 Inhibitory activity of compounds **19-21** against *Pf*lspD and *P. falciparum* growth in culture (strain 3D7); calculated *ClogD* and *CaqSol* values given.

Enzymatic *Pf*lspD activity of mono-phenyl compounds **19-21** was highly comparable across the series and also close to that of the equivalent biphenyl compounds **13-15**. The mono-phenyl compound **20**, the 4-fluoropiperidine analogue, demonstrated an inhibitory *Pf*lspD IC₅₀ value of 0.530 μM which demonstrates a 1.6-fold increase in potency compared to the equivalent biphenyl compound **14** (**Table 3.2** and **Table 3.3**). Despite increased and comparable potency against *Pf*lspD; this was not translated into efficacious activity against whole cell parasite growth with the observation of only mild 3D7 growth inhibition. Indeed, all mono-phenyl inhibitors displayed whole cell EC₅₀ values > 1 μM (**Table 3.3**) which is in the range of six to 18 times less potent than the whole cell inhibitory activity of **14** (**Table 3.2**). This result therefore contradicts predictions of high cellular permeability that was thought to be achievable with this compound series since the predicted *logD* values are notably lower than earlier biphenyl benzyl-linked BITZ inhibitors (**Section 3.3**).

3.5 Biphenyl Pyridinyl BITZ analogue series

3.5.1 Design Rationale and Synthesis

In order to try and restore the 3D7 growth inhibition lost with inhibitors in the mono-phenyl compound series, the biphenyl BITZ side chain was revisited. Having evaluated the effects of solubilising saturated heterocycles on inhibitor structures; this functionality was again removed in order to determine the effects of alternative structural motifs. Again considering the D ring, the phenyl ring was converted to a pyridine ring with functionality *ortho* to the ring nitrogen; this therefore maintained aromaticity throughout the side chain but varied the electronics within the terminal D ring (**Figure 3.7**). Conversion of an aromatic phenyl ring to an aromatic pyridine ring is a classic isosteric substitution that aids compound solubility and helps to reduce hydroxylation of resulting rings through the reduction of metabolic bioactivation.^[34] Bioisosteres are structurally distinct compounds that provide alternative and often subtle variations in physicochemical properties, but which are recognised similarly by biological systems. Typically bioisosteres are less exact than structural compound mimetics but are generally more alike in biological and physical properties.^[34]

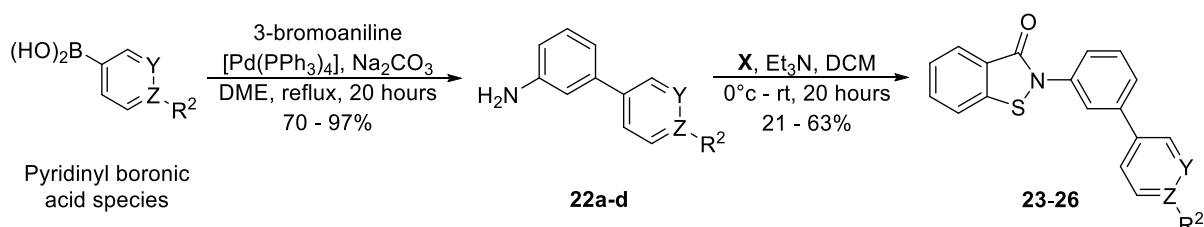


23 - 26

Figure 3.7 Chemical structures and substitution pattern of BITZ compounds **23-26**.

The incorporation of a pyridine ring into inhibitor structures served a number of purposes, the most important of which is lowering lipophilicity and enhancing compound solubility; a key requirement having removed the saturated heterocycle functionality. The pyridine nitrogen atom provides an additional protonation site and hydrogen bond acceptor group which has the potential to facilitate protein-ligand interactions at the *Pf*ispD active site, promoting the strength of ligand binding.^[34,35] Where additional functional group substitution in the pyridine ring was included (**24-26**), the incorporated functionalities were selected to enable a head to head comparison with compounds **4-6** since these three compounds were the most potent BITZ-derived inhibitors generated thus far.

All analogues in the pyridine series were synthesised in a rapid two-step synthesis which involved Suzuki-Miyaura cross-coupling reactions between 3-bromoaniline and various pyridinyl boronic acids^[36] to generate the required analogue side chain. This was followed by incorporation of the BITZ core by reaction of the pyridinyl aniline intermediates **22a-d** with **X**^[25,27] generating target compounds **23-26** (**Scheme 3.6**). The specific conditions of the Suzuki cross-coupling reaction were altered slightly for the synthesis of **23-26** compared to previous conditions (**Scheme 3.1** and **Scheme 3.3**). Dimethoxyethane (DME), rather than a system of H₂O/ THF, was used as the solvent, enabling the reaction to be refluxed at a slightly elevated temperature of 90°C. The base was also exchanged (previously K₂CO₃, now Na₂CO₃) according to methods outlined in literature.^[36]

**Scheme 3.6** Synthetic strategy for biphenyl pyridinyl BITZ compounds **23-26**.

Generation of the pyridinyl aniline intermediates (**22a-d**) *via* the described Suzuki cross-coupling reactions^[36] proceeded without issue and in high yield in the case of each pyridinyl boronic acid

derivative used. In contrast, a significant reduction in yield was observed in the final acid-chloride mediated cyclisation step^[27] compared to previous analogue syntheses. This outcome may be the result of the pyridine ring reducing the reactivity the 1° amine, although no unreacted starting material was detected in these reactions, or alternatively, a consequence of the age of the acid chloride used in these specific reactions. Whilst the acid chloride **X** can be isolated and is therefore highly stable in comparison to many acid chlorides, it shows a gradual loss of reactivity over time which may be a result of slow decomposition. This consequently suggests that **X** should be prepared at regular intervals when using over extended time periods and syntheses to ensure consistent reaction yields and reaction efficiency.

3.5.2 *PflspD* Enzymatic and Whole Cell Biological Assays

The predicted distribution coefficients of this biphenyl pyridinyl compound series (**Table 3.4**) was comparable to the BITZ analogues containing heterocyclic functionalities **13-15** (**Table 3.2**). This therefore highlights that, in this case, inclusion of a pyridine ring is able to circumvent a significant increase in compound lipophilicity which would generally accompany the removal of six-membered ring saturated heterocycles. In other words, the pyridine system is able to sustain comparable physiochemical properties to those achieved with saturated heterocycles in a comparable systems and compounds.

Compound number	Y	Z	R ²	<i>PflspD</i> IC ₅₀ (μM)	Whole cell 3D7 EC ₅₀ (μM)	MW (g mol ⁻¹)	<i>ClogD</i>	<i>CaqSol</i> (μM)
23	C	N	-	5.94	3.65	304.07	3.57	14.14
24	N	C	OCH ₃	58.5	1.67	334.08	4.30	4.088
25	N	C	Cl	> 100	2.34	338.03	4.24	3.431
26	N	C	CF ₃	> 100	1.91	372.05	4.33	2.576

Table 3.4 Inhibitory activity of compounds **23-26** against *PflspD* and *P. falciparum* growth in culture (strain 3D7); calculated *ClogD* and *CaqSol* values given.

Biological testing results for this compound series were somewhat unexpected since the pyridinyl analogues **23-26** showed a significant loss of activity at the *PflspD* enzyme, but maintained inhibition of 3D7 whole cell parasite growth at levels close to that seen with the previous mono-phenyl analogue series **19-21** (**Table 3.3**). The fact that a complete loss of *PflspD* enzyme activity was witnessed with some analogues in this series (**24-26**), alongside a reduction in compound lipophilicity, perhaps suggests that the SAR around the BITZ chemotype may be assisted by increased compound lipophilicity. In addition, these could also results suggest that BITZ compounds **23-26** may be involved

in off-target contributions that lead to an expression of antimalarial potency, since inhibitory activity against parasite growth is retained when *Pf*lspD activity is lost.

Increased lipophilicity in a molecule can sometimes increase the observed potency at the target; however, this is at the risk of increasing off-target interactions and altering observed phenotypic activity.^[32] Since loss of *Pf*lspD enzymatic activity was observed across **23-26** but a level of antimalarial potency sustained, a scenario of increased off-target interactions due to altered lipophilicity may here be the case. A direct comparison can therefore be made with the mono-phenyl compounds **19-21** which have lower predicted lipophilicities than pyridinyl analogues **23-26** and display similar potencies against both *Pf*lspD and *Plasmodium* parasite growth (Table 3.3).

3.6 Biphenyl BITZ Compound Mimetics

3.6.1 Design Rationale and Synthesis

In order to determine if levels of *Pf*lspD enzyme activity correlate with increased compound lipophilicity; a small inhibitor series was designed comprised of two BITZ analogues which display significantly lower *ClogD* values than any BITZ compounds considered to this point. In attempt to generate compounds with reduced molecular weight and lipophilicity, notably distinct side chains were incorporated to explore a contrasting BITZ inhibitor structure with complete replacement of the aromatic D ring, **28** and **30** (Figure 3.8).

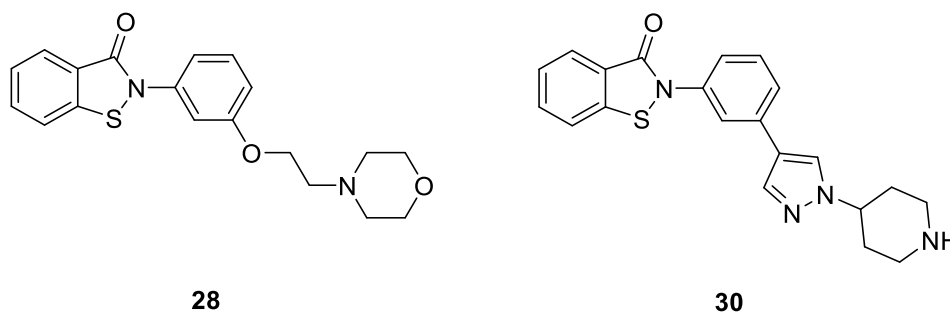


Figure 3.8 Chemical structures of BITZ compounds **28** and **30**.

Increasing compound potency, at any specified molecular target, is often achieved by increasing the molecular weight and lipophilicity of compounds; since increasing compound lipophilicity, and therefore molecular permeability, eases the access of a compound to a defined molecular target.^[20] However, potency often has an unhealthy correlation with molecular obesity (defined as high molecular weight and lipophilicity)^[20] and may also be consistent with increasing non-specific protein-ligand interactions, which is an undesirable consequence^[37] of amplifying these two parameters.

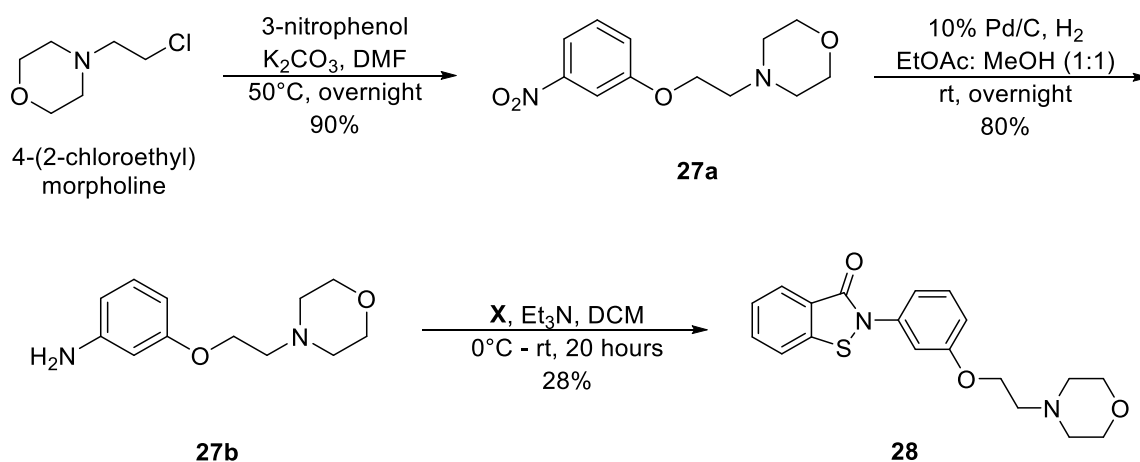
As a result, this small compound series aimed to reduce BITZ compound lipophilicity, consequently promoting analogue solubility, whilst preserving an appropriate molecular size of < 400 Da, which is highlighted in the GSK '4/400' rule as a likely promoter of favourable ADMET compound properties.^[38] More specifically, the GSK '4/400' rule suggests that compounds which have a *ClogP* of > 4, alongside a molecular mass of > 400 Da, are likely to demonstrate a less favourable ADMET profile.^[38,39]

The biphenyl side chain of previous analogues **13-17** is likely to show limited rotation (considering the side chain component itself) and therefore may adopt a relatively linear projection or trajectory in the *PflspD* binding site. A further aim of this analogue series is therefore to increase the extent of flexibility in the BITZ side chain by introducing a structural motif which displays an increase in degrees of freedom. Such a motif would consequently be capable of increased rotation and flexibility, potentially promoting new and improved protein-inhibitor interactions at *PflspD* due to reduced ligand rigidity.

In the case of **28** and **30**, the phenyl D ring was replaced with distinct functionalities, both of which mimic the previous biphenyl side chain by occupying a comparable area of space but which have the potential to adopt varying and more diverse conformations and structural orientations. Considering compound **28**, an ether-containing hydrocarbon chain links the phenyl C ring to a terminal morpholine heterocycle, notably increasing rotatable bond number within the compound. Indeed, the side chain of **28** contains four rotatable bonds compared to the side chain of **4** (**Figure 3.3** and **Table 3.1**), which has only two. In compound **30**, the phenyl D ring is replaced with the aromatic and polar pyrazole ring, a generally well tolerated and metabolically stable group,^[34] which is linked directly to piperidine. The respective morpholine and piperidine heterocycles were incorporated as terminal heterocyclic rings to aid compound solubility.

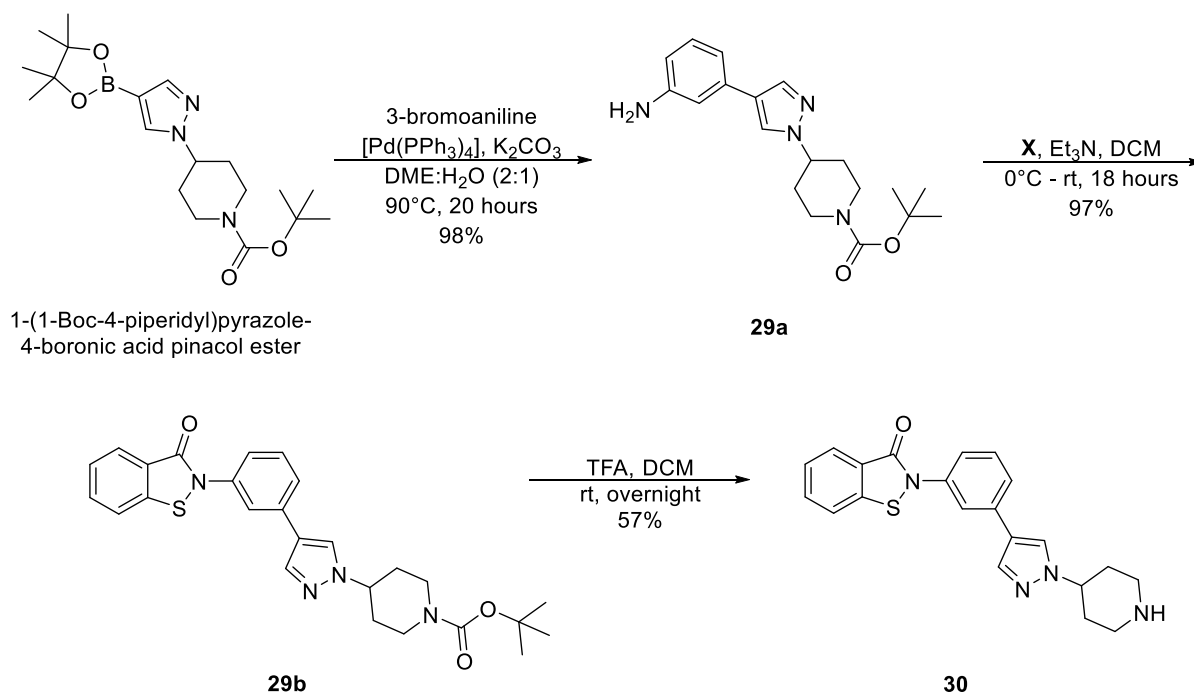
For the synthesis of compounds **28** and **30**, two separate synthetic routes were developed, outlined in **Scheme 3.7** and **Scheme 3.8** respectively. As has been the case for many BITZ compounds, synthesis was initiated with the generation of the specified side chains of **28** and **30**, before attachment of the BITZ motif in a final synthetic step using the acid chloride **X** (**Scheme 3.2**).^[25,27]

To generate **28**, a three-step synthesis was required, initiated by a S_N2 -substitution between commercially available 4-(2-chloroethyl)morpholine and 3-nitrophenol to give the 4-(2-(3-nitrophenoxy)ethyl)morpholine intermediate **27a** (**Scheme 3.7**).^[40] **27a** was subject to hydrogenation, converting the *meta*-nitro group of **27a** into the corresponding 1° amine **27b**; the final acid-chloride mediated amide coupling and cyclisation with **X** produced the target biphenyl BITZ mimetic **28** (**Scheme 3.7**).



Scheme 3.7 Synthetic strategy for BITZ biphenyl mimetic compound **28**.

The synthesis of **28** was relatively straightforward with high yielding reactions for the first two synthetic steps. However, the final acid-chloride coupling and cyclisation was particularly low yielding, which is generally inconsistent with the synthesis of other analogues. In contrast, the synthesis of **30** proceeded with moderate to high yields across all steps. Compound **30** also required three synthetic steps, initiated by a Suzuki-Miyaura cross-coupling reaction between 3-bromoaniline and a pinacol ester boronic acid derivative (**Scheme 3.8**) to generate the Boc-protected side chain **29a**. **29a** was coupled to the BITZ core *via* reaction with the acid chloride **X**^[25,27] which proceeded in high yield to give the Boc-protected structure **29b**. The final synthetic step involved the acid-mediated Boc-deprotection of **29b** to generate BITZ compound **30** (**Scheme 3.8**).



Scheme 3.8 Synthetic strategy for BITZ biphenyl mimetic compound **30**.

3.6.2 *Pf*lspD Enzymatic and Whole Cell Activity Data

As was the aim with these biphenyl side-chain mimetics, the distribution coefficients of compounds **28** and **30** were significantly reduced compared to previous biphenyl BITZ derivatives **4-10**, **13-15** and **17** (Table 3.1 and Table 3.2). The significant decrease in distribution coefficients was also represented by a large increase in the predicted aqueous solubility of compounds **28** and **30** (Table 3.5). In particular, incorporation of the pyrazole ring and polar piperidine moiety into **30** resulted in a compound that displays a significantly lower predicted distribution coefficient than one of the most potent BITZ inhibitors to date, the biphenyl analogue **6**, with greater than a 3-fold reduction in predicted *ClogD* and more than a 400-fold increase in aqueous solubility.

Compound number	<i>Pf</i> lspD IC ₅₀ (μM)	Whole cell 3D7 EC ₅₀ (μM)	MW (g mol ⁻¹)	<i>ClogD</i>	<i>CaqSol</i> (μM)
28	0.340 ± 0.018	5.15	356.12	2.52	119.1
30	0.232 ± 0.002	8.17	376.14	1.64	159.9

Table 3.5 Inhibitory activity of compounds **28** and **30** against *Pf*lspD and *P. falciparum* growth in culture (strain 3D7); calculated *ClogD* and *CaqSol* values given.

The resulting biological activities of compounds **28** and **30**, show that both analogues have nanomolar activity against the *Pf*lspD enzyme (Table 3.5). These results were highly encouraging, particularly in the case of **30**, since the level of measured enzymatic activity is equivalent to that displayed by the methoxy and trifluoromethyl biphenyl BITZ analogues **4** and **6** (Table 3.1), which are two of the most potent *Pf*lspD BITZ inhibitors generated to date. This therefore demonstrates that compounds with reduced lipophilicity are also capable producing potent inhibition of the *Pf*lspD target. This is highly encouraging for forward inhibitor design and the improvement of physicochemical compound properties for lead optimisation. Compounds **28** and **30** both conform to Lipinski's Rule of Five, defining parameters for likely compound bioavailability,^[18] and the GSK '4/400' guideline, relating compounds with a *ClogP* of < 4 and a molecular weight of less than 400 with more favourable ADMET profile.^[38]

However, neither **28** nor **30** were able to translate observed activity against *Pf*lspD into whole cell parasite growth inhibition (Table 3.5). This is potentially an effect of reduced compound lipophilicity and a consequent decrease in cellular permeability within biological systems; despite a significant increase in aqueous solubility that may have been thought to aid compound absorption.

3.7 Variations to the Inhibitor C Ring

3.7.1 Design Rationale and Synthesis

Having considered a number of structural modifications involving functional changes around the D ring of the BITZ side chain, a discrete compound series was developed to assess the effects of structural variations at the C ring of the BITZ inhibitor construct. Alterations were made to the C ring system itself, as well as revisions to the linker functionality between the BITZ core and the adjacent C ring (**Figure 3.9**) within a strategy that aimed to mirror a design approach outlined by *Luo et al.*^[41]

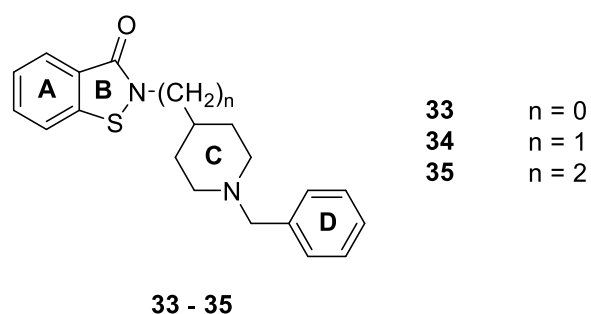


Figure 3.9 Chemical structures of BITZ compounds **33-35**.

Work by *Luo et al.* describes the synthesis and evaluation of multi-target-directed ligands, generated by fusing the cholinesterase inhibitor donepezil and the antioxidant Ebselen (**Figure 3.10**), for the treatment of Alzheimer's disease.^[41] Ebselen (or 2-phenyl-1,2-benzisoselenazol-3(2*H*)-one) is an organoselenium compound, categorised chemically as an electrophile, and also a lipid-soluble molecule which can readily enter the cells of biological systems.^[41,42] Ebselen is a definitive example of a glutathione peroxidase mimic, catalysing the reduction of reactive oxygen species through reactions with specific cysteine thiol groups in proteins, and is therefore a promising synthetic antioxidant.^[42,43] Ebselen is a clinically safe compound with a well-known pharmacology profile. It is currently part of a number of clinical trials for the prevention and treatment of various disorders including cardiovascular disease, arthritis and cancer.^[44]

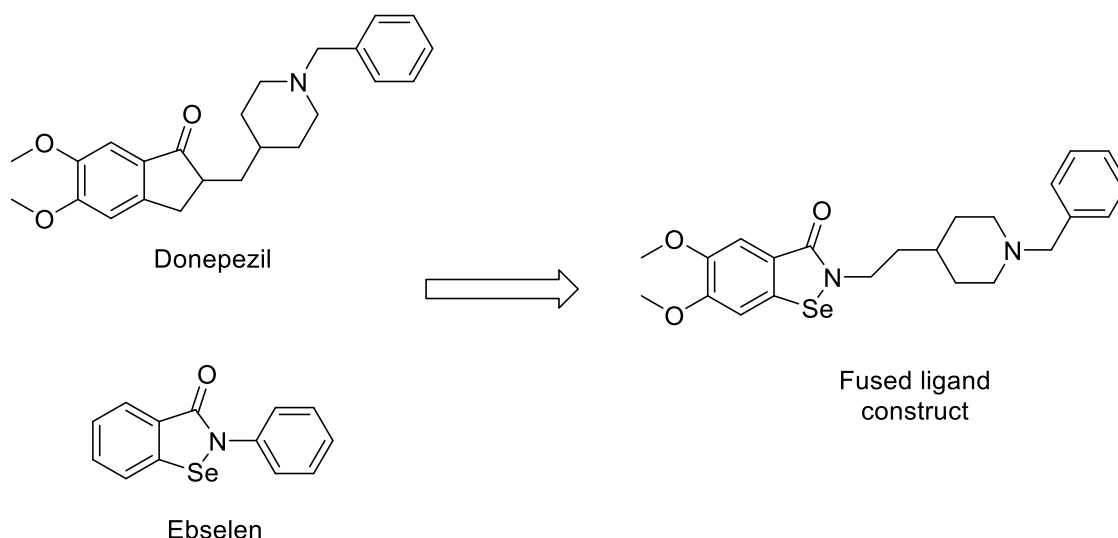
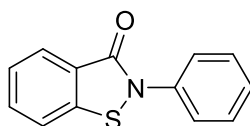


Figure 3.10 Design strategy and chemotype fusion conducted by *Luo et al.* towards the generation of novel compounds for the treatment Alzheimer's disease; figure reproduced from ^[41].

Luo et al. adopted a design principle that involved the fusion of the two pharmacophores, Donepezil and Ebselen, generating new hybrid molecules and a fused ligand construct, without major structural modifications to the selected pharmacophores (**Figure 3.10**). The resulting hybrid molecules possessed the strong acetylcholinesterase inhibitory activity of Donepezil as well as many of the pharmacological benefits of Ebselen: notably its antioxidant and anti-inflammatory properties which are closely related to the aetiology of Alzheimer's disease and is therefore highly appropriate to this indication.^[41]

Combination of the core Ebselen motif with the Donepezil side chain produced a fused ligand structure with a saturated heterocyclic ring as a surrogate structure to the adjacent phenyl ring system of Ebselen, with an alkyl linker connecting the two entities (**Figure 3.10**). *Luo et al.* subsequently demonstrated that combination of these structural components produced optimal pharmacology, including appropriate parameters of lipophilicity and solubility, whilst retaining potent acetylcholinesterase inhibitor activity.^[41] As a result of this research, structural modifications were introduced to BITZ inhibitors to mirror the scaffold of the fused inhibitors designed by *Luo et al.*

The close structural similarity between Ebselen (**Figure 3.10**) and our simplified BITZ chemotype core inhibitor structure **31** (**Figure 3.11**), was an additional driving force behind the rationale of this approach. The phenyl C ring of BITZ inhibitors was replaced with a saturated, non-aromatic piperidine group with a methylene linker to a conserved aromatic D ring where no further substitution was present (**Figure 3.9**).

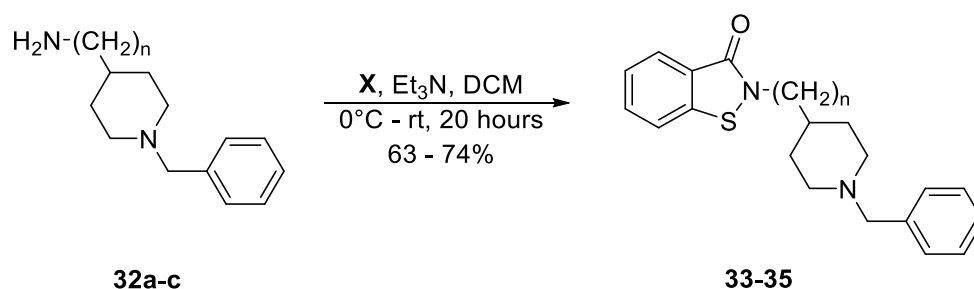


31

Figure 3.11 Chemical structures of simplified BITZ compound **31**.

Further to replacement of the C ring system, variations to the length of the alkyl linker between the BITZ core and heterocyclic C ring were also made: *n* was varied between 0 and 2 generating the corresponding BITZ compounds **33-35** (**Figure 3.9** and **Table 3.6**). The overall aim of this compound series was to mirror the successes outlined by Luo *et al.*^[41] through introduction of a non-aromatic, surrogate C ring to determine the direct effects on *Pf*spD enzyme activity. This inhibitor series also aimed to introduce increased ligand flexibility by extension of the alkyl linker and optimise the physicochemical properties of resulting analogues with reduced lipophilicity and enhanced solubility.

Due to the commercial availability of the required benzyl-piperidine 1° amine compounds **32a-c** (**Scheme 3.9**), the synthesis of each target compound within this series required only a single synthetic step. The purchased amino benzyl-piperidine starting materials **32a-c** were reacted with the stable acid-chloride **X** in the previously discussed simultaneous amine coupling and BITZ ring closure^[25,27] (**Chapter 2, Section 2.3.3**) to generate the designed BITZ analogues **33-35** (**Scheme 3.9**) in moderate to good yields.



Scheme 3.9 Synthetic strategy for BITZ analogues **33-35**.

3.7.2 *Pf*spD Enzymatic and Whole Cell Activity Data

Whilst the distribution coefficients of analogues **33-35** are low, with predicted *ClogD* values of consistently less than three; extension of the alkyl linker between the BITZ headgroup and inhibitor side chain was accompanied by a notable decrease in the aqueous solubility of resulting compounds (**Table 3.6**). Most significantly, **34** is ~ 2.5 times less soluble than analogue **33**, which is the consequence of introducing a methylene linker between the BITZ core and side chain, rather than

direct attachment as with **33**. In comparison, introducing an ethylene linker group (**35**) between the BITZ core and C ring produces ~ a 3.25-fold loss of aqueous solubility, comparing **33** with **35**, but which only corresponds to a further decrease in aqueous solubility of about a third when considering replacement of the methylene linker, **34**, with the ethylene group, **35**. Generally, the molecular weight of compounds in this series is slightly below that of previous biphenyl mimetic BITZ analogues.

Compound number	n	<i>Pf</i> lspD IC ₅₀ (μM)	Whole cell 3D7 EC ₅₀ (μM)	MW (g mol ⁻¹)	<i>ClogD</i>	<i>CaqSol</i> (μM)
33	0	8.22	13.28	324.13	2.94	225
34	1	40.1	7.45	338.15	2.84	88.59
35	2	> 100	2.00	352.16	2.90	69.21

Table 3.6 Inhibitory activity of compounds **33-35** against *Pf*lspD and *P. falciparum* growth in culture (strain 3D7); calculated *ClogD* and *CaqSol* values given.

Disappointingly, biological testing highlighted that none of the analogues **33-35** can be considered active inhibitors of either the *Pf*lspD enzyme or whole cell 3D7 growth since all *Pf*lspD IC₅₀ values were > 5 μM and whole cell 3D7 growth inhibition was measured in the mid to low micromolar region.

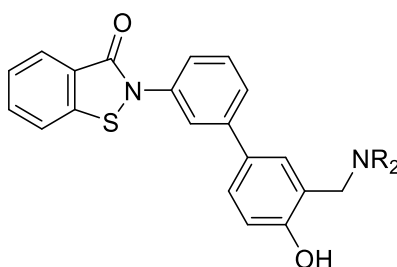
Whilst it is therefore clear that **33-35** are inactive at both the *Pf*lspD enzyme and the level of the whole cell, directly opposing activity trends can clearly be seen when comparing enzymatic and whole cell biological activity (**Table 3.6**). Lengthening the alkyl chain between the BITZ core and piperidine C ring resulted in a rapid loss of *Pf*lspD enzyme activity, as highlighted by **34** and **35** which are increasingly inactive against *Pf*lspD. In contrast, a slight improvement in parasite growth inhibition is observed as the alkyl chain linker is extended through n = 0 to n = 2. This possibly reflects a slight increase in lipophilicity caused by extending the alkyl linker region which will aid the permeation of resulting compounds on exposure to a biological system, likely facilitating enhanced whole cell inhibition due to improved compound access to the cell and improved permeation of biological membranes.

These results therefore suggest that maintaining aromaticity in the C ring of BITZ inhibitors is required to conserve both inhibition of the *Pf*lspD enzyme and *Plasmodium* parasite growth. Furthermore, resulting data highlights that direct *N*-aryl attachment between the BITZ core and side chain represents an optimal structural arrangement.

3.8 Alkyl-amino Biphenyl BITZ Analogues

3.8.1 Design Rationale and Synthesis

As a result of the micromolar *Pf*lspD inhibitory activity of **9** (Table 3.1), the biphenyl *para*-hydroxy BITZ compound, a series of alkyl amino derivatives of this analogue have been synthesised and evaluated. In addition to encouraging inhibitory enzyme activity, **9** displays slightly enhanced physiochemical properties compared to other analogues in the biphenyl series (Table 3.1). Inhibitor **9** has the lowest predicted *ClogD* value of all the biphenyl analogues and slightly improved aqueous solubility, almost 10-fold of that displayed by the potent CF₃ analogue **6**. Therefore, the generally poor aqueous solubility of biphenyl BITZ analogues (**15** and **16** are exceptions) supported the decision to synthesise a further BITZ compound series, comprising three analogues **37-39** (Figure 3.12) which incorporate an alkyl-amino substituent *ortho*- to the *para*-hydroxy group in the D ring. The rationale of this design motif was to improve the aqueous solubility of resulting structures and promote parasite growth inhibition through improved cellular accumulation due to increased BITZ compound concentration at the *Pf*lspD enzyme target.



37 - 39

Figure 3.12 Chemical structures of BITZ compounds **37-39**.

Further support of this design rationale was provided by work conducted by Cooke *et al.*^[45] which demonstrated the successful use of similar alkyl-amino groups in generating water-soluble compounds that retained the inhibitory activity of their more lipophilic counterparts, in a drug discovery program based around the anaesthetic activity of propofol analogues.^[45] Propofol (2,6-diisopropylphenol) is used extensively as an intravenous anaesthetic which acts on GABA_A receptors as a positive allosteric modulator of γ -aminobutyric acid (GABA).^[46] However, the administration of propofol is complicated by the fact that it must be formulated as an emulsion since it lacks water solubility.^[47] Consequently, research by Cooke *et al.* aimed to produce a number of water-soluble propofol analogues, containing *para*-alkylamino substituents which were found to successfully maintain good intravenous anaesthetic activity in rodents.^[45]

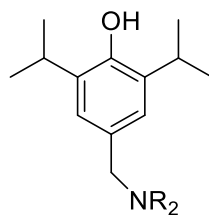
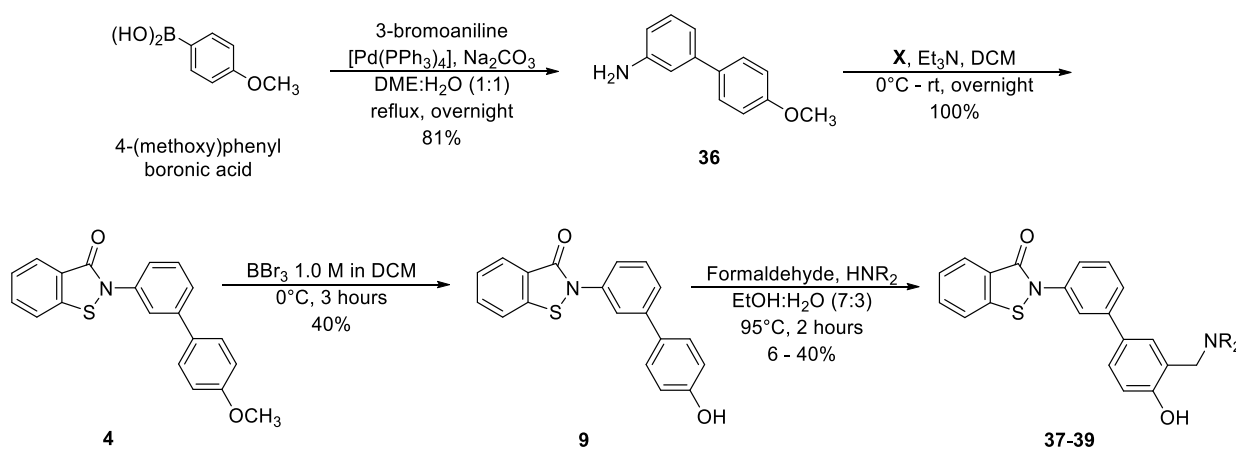


Figure 3.13 Chemical structure of water-soluble Propofol analogues designed and synthesised by Cooke *et al.* R_2 is representative of a variety of tertiary amines. Figure reproduced from [45].

Within this research, synthesis of **37-39** was achieved using the biphenyl methoxy BITZ inhibitor **4** as a starting point. De-methylation of **4** generated the corresponding biphenyl hydroxy inhibitor **9** which was able to undergo Mannich base reactions with various 2° amines to generate the required alkyl-amino biphenyl BITZ derivatives **37-39** (**Scheme 3.10**). In contrast to initial syntheses of **4** (**Scheme 3.1**), the alternative acid-chloride **X** mediated synthesis of BITZ derivatives^[25,27] was employed to generate the required quantities of **4** for the described synthesis towards **37-39** (**Scheme 3.10**). The generation of **4** by this alternative route was highly successful: both the Suzuki-Miyaura cross-coupling reaction between 3-bromoaniline and 4-(methoxy)phenyl boronic acid, generating the side chain **36**, and the subsequent amide coupling and ring closure with acid chloride **X**, to generate compound **4**, proceeded without complication and in high yield.



Scheme 3.10 Synthetic strategy for alkyl-amino BITZ analogues **37-39**.

De-methylation of **4** to **9** using boron tribromide^[48] proceeded rapidly but in low yield. Conversion of **9** to BITZ alkyl-amino derivatives **37-39** was achieved using a Mannich base synthesis. This involved reaction of **9** with aqueous formaldehyde solution (37 wt. % in H_2O) and the appropriate 2° amine in a 7:3 ethanol:water mixture under reflux conditions.^[45] The Mannich reaction is a classic method of preparing β -amino ketones and aldehydes and is widely used as a chemical transformation which facilitates C-C bond formation and the construction of nitrogen-containing compounds.^[49,50] Whilst the synthesis and isolation of **37-39** was achieved using the outlined synthetic strategy (**Scheme 3.10**),

the yields of the Mannich base reactions were consistently poor ranging from 6-40% over the synthesis of the three analogues **37-39**. The isolation and purification of these compounds was also very challenging; it is therefore likely a combination of poor reaction yields, the generation of side products and high compound polarity made purification difficult. In addition, all three Mannich base syntheses had to be performed on a small reaction scales due to the poor yield of the previous de-methylation step, further hindering the ease of synthesis and successful product isolation.

3.8.2 *PflspD* Enzymatic and Whole Cell Activity Data

The design rationale of the alkyl-amino biphenyl BITZ motif was to promote the aqueous solubility of compounds within the series. Whilst compounds **37-39** demonstrated acceptable distribution coefficients, only the pyrrolidine analogue **39** was predicted to have good aqueous solubility, almost equivalent to that of the heterocycle-linked biphenyl BITZ analogues **15** and **16** (Table 3.2).

Compound number	NR ₂	<i>PflspD</i> IC ₅₀ (μM)	Whole cell 3D7 EC ₅₀ (μM)	MW (g mol ⁻¹)	<i>ClogD</i>	<i>CaqSol</i> (μM)
37	Morpholine	0.501	0.736	418.14	3.96	7.245
38	Diethylamine	2.33	0.438	404.16	3.61	33.53
39	Pyrrolidine	0.507	0.133 ± 0.016	402.14	3.42	52.59

Table 3.7 Inhibitory activity of compounds **37-39** against *PflspD* and *P. falciparum* growth in culture (strain 3D7); calculated *ClogD* and *CaqSol* values given.

Interestingly, a slight loss in *PflspD* enzymatic activity was observed with this compound series, particularly in the case of the dialkylamino analogue **38**, which showed more than a five-fold reduction in activity against *PflspD* compared to **15** (Table 3.2). This is somewhat surprising given that the predicted physicochemical properties of analogues **37-39** are largely comparable to those predicted for the heterocycle-linked biphenyl series (Section 3.3, Table 3.2), which generally show improved activity at the enzyme.

In contrast to this observation, the measured whole cell 3D7 activity of the alkyl-amino compound series (Table 3.7) is more potent than that of the heterocycle-linked biphenyl series (Section 3.3, Table 3.2), with the most potent pyrrolidine analogue **39** demonstrating a 3D7 EC₅₀ value of 133 nM. Indeed, alkyl-amino analogues **37-39** demonstrate increased activity against the parasite, producing noticeably improved inhibitory activity against 3D7 parasite growth than the *PflspD* enzyme. This observation may be an effect of improved compound solubility, although this is not uniform across the series, but is best supported in the case of the pyrrolidine analogue **39** which displays enhanced predicted aqueous solubility and the most potent whole cell growth inhibition within the series.

Alternatively, heightened inhibitory activity against the whole cell compared to that seen at the *Pf*lspD enzyme may lead to the suggestion that these compounds are capable of exerting inhibitory effects at additional biological targets within *P. falciparum* (i.e. off target effects that are not specific to the *Pf*lspD enzyme). Further exploration of this suggestion is needed since off-target activity can complicate and confuse observed phenotypic effects, making the interpretation of biological activity difficult, as well as increasing the risk of unwanted associated toxicities.^[51]

3.9 Aminoquinoline-BITZ Hybrid Compounds

3.9.1 Design Rationale and Synthesis

The exploration of an alternative design rationale led to the design and synthesis of a series of BITZ-aminoquinoline hybrid analogues. This structurally distinct BITZ compound series incorporates the BITZ chemotype, using various hydrocarbon linkers (R^3), into the familiar antimalarial chemotype of 7-chloro-4-aminoquinoline (**Figure 3.14**).

Molecular hybridisation is a useful strategy in drug design and provides an attractive and alternative approach to the design of antimalarial chemotherapies as requirements shift to focus on the development of novel and affordable drugs which can prevent resistance development.^[52] There are now many examples of this design approach within antimalarial drug discovery programs which have been well reviewed and discussed extensively throughout literature; some key applications of this design approach are summarised in the following publications.^[52–55]

Molecular hybridisation aims to combine different pharmacophores of biologically active and distinct materials to produce new hybrid compounds that show affinity at the molecular targets of the component pharmacophores and therefore increase phenotypic efficacy compared to the individual pharmacophores of the hybrid structure.^[56,57] This methodology identifies covalent linkage points between two or more pharmacophoric motifs, enabling the stable assembly of specific functionalities to generate a single unit and new drug entity which is designed to perform as a dual-acting compound. Resulting hybrid molecules are typically larger than the component drugs and, as a result, are often more lipophilic. It is therefore important that the incorporated linker region or functional group between component pharmacophores is as simple as possible.^[52]

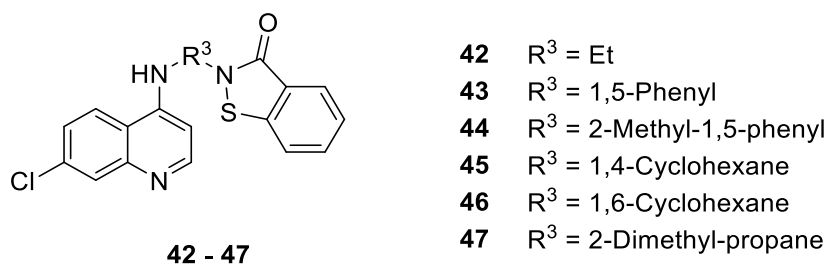


Figure 3.14 Chemical structures of aminoquinoline-BITZ hybrid compounds **42-47**.

Such an approach to compound design is particularly appropriate for the development of new antimalarial agents which aim to combat the onset of drug-resistant *Plasmodium* parasites by generating multi-targeted and pharmacologically enhanced antimalarial compounds.^[58] In this context, the hybridisation strategy aims to incorporate key pharmacophoric features (and the associated biological behaviours) from existing antimalarial drugs, and design novel molecules of new chemical structure which display efficacy and an improved resistance profile. This approach has been successful within a number of drug design efforts, generating novel and effective chemical agents against protozoan parasites.^[54]

Combination therapies which employ the simultaneous use of two or more antimalarial drugs, administering two or more chemical agents with differing modes of action, have frequently been used as a therapeutic approach to reduce the effects of *Plasmodium* parasite drug resistance. New generations of hybrid antimalarial compounds provide an alternative to combined administration therapies of two or more individual drugs, and have the associated advantage of lower drug-drug interaction risks since two pharmacophores are combined in the same molecular entity rather than co-administered. In addition, this approach can also promote improved treatment adherence.^[54,59,60]

Applying the concept of hybrid agents to antimalarial drug design can be challenging for a number of reasons. Firstly, the complexity of the *Plasmodium* parasite life cycle means only a small number of validated targets are known across the life cycle. Added to this, an incomplete understanding of *Plasmodium* parasite biology may compromise and add difficulty to hybrid drug design in antimalarial therapy.^[52] However, if these obstacles are overcome, the molecular outcomes and resulting therapeutic effects can be highly rewarding as outlined in reviews by Walsh^[55] and Muregi^[54] as well as in the work carried out by Pinheiro *et al.*^[60] Pinheiro *et al.* demonstrated the success of the hybrid design approach in aiming to enhance to the anti *P. falciparum* activity of quinolone derivatives by designing of a series of hybrid quinolones containing the pharmacophoric groups of 7-chloroquinoline and arylsulfonamide. Pinheiro *et al.* connected these two structural entities with a linker group that

was distinct from the pharmacophore framework of either parent drug: chloroquine (CQ) and sulfadoxine.^[60]

To mirror this approach, a series of synthetic hybrid BITZ-aminoquinoline compounds (**42-47**, **Figure 3.14**) have been designed with the aim of generating dual-targeted antimalarial agents with enhanced activity against *P. falciparum* parasite growth and which show good PK and resistance profiles. Inclusion of the 7-chloroquinoline pharmacophore was desirable due to its presence in CQ, representing one of the most successful antimalarial compounds within the history of antimalarial drug design.^[24,61,62] The BITZ headgroup remained the selected chemotype of choice following our HTS screen and identification of the **DT2009-0168020** hit (**Figure 3.15**).

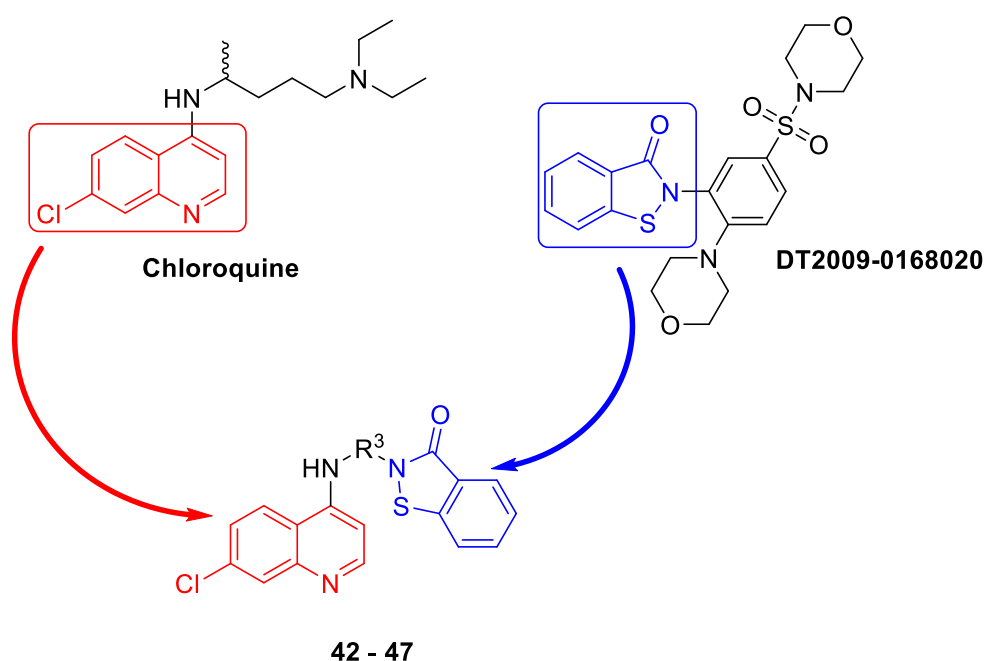
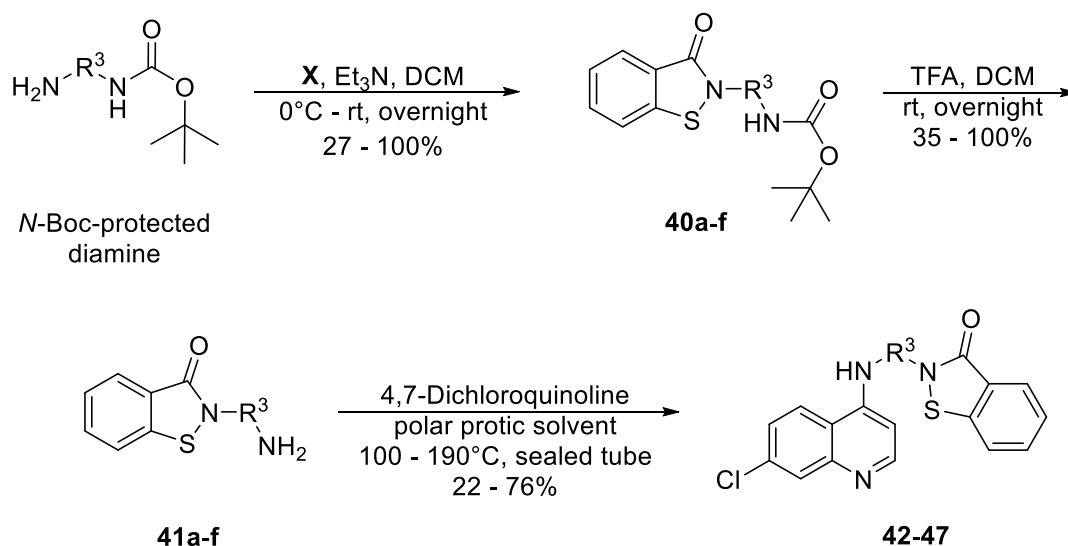


Figure 3.15 Rational approach to drug design of hybrid compounds **42-47**.

Extensive research over the last few decades has highlighted that the 7-chloro-4-aminoquinoline nucleus (**Figure 3.14**) is essential for the antimalarial activity of 4-aminoquinoline compounds, enabling the inhibition of β -haematin formation and accumulation of this antimalarial chemotype at the target site of the parasite food vacuole.^[63] In contrast, the BITZ chemotype is proposed to target and inhibit the *Pf*lspD enzyme within the MEP pathway, thereby disrupting isoprenoid precursor biosynthesis and preventing parasite growth, which ultimately causes parasite death. The combination of these two pharmacophores therefore aims to produce a series of compounds which are capable of behaving by a dual-mechanism of action. To adhere to suggestions from literature, a range of simple linker groups have been incorporated to covalently join the two pharmacophoric

systems.^[52] These include simple alkyl chains, aromatic rings, branched alkyl chains and saturated ring systems (**Figure 3.14** and **Table 3.8**).

The synthetic route to generate **42-47** is shown in **Scheme 3.11** and is comprised of three synthetic steps. The commercial availability of a number mono-Boc-protected diamines enabled the synthesis of **42-47** to be initiated from mono Boc-protected hydrocarbon linker groups (R^3) that were incorporated into each analogue. The presence of a second free amine within these *N*-Boc-protected diamines (**Scheme 3.11**) facilitated amide coupling with acid-chloride **X** (**Scheme 3.2**) to generate the BITZ pharmacophore and Boc-protected intermediates **40a-f**. TFA-mediated deprotection of intermediates **40a-f** revealed a free 1° amine functionality in the resulting structures **41a-f**, facilitating the final substitution step of the synthesis.



Scheme 3.11 Synthetic strategy for the aminoquinoline-BITZ hybrids **42-47**.

To afford the target BITZ-aminoquinoline hybrid structures, an aromatic nucleophilic substitution was employed as the final synthetic step of the synthesis. A similar synthetic approach was previously outlined by Apelt *et al.* in their preparation of non-imidazole histamine H_3 receptor ligands.^[64] To generate the histamine H_3 receptor antagonists, Apelt *et al.* combined the required amino molecular component with a range of chloroquinolines, including 4,7-dichloroquinoline, using phenol as the solvent and heating to 140°C for 12 hours. A comparable synthesis, using phenol and heating to 140°C in a sealed tube, was successfully employed for the generation of **42** and **43**. However, a significant drop in reaction yield following the synthesis of **43** highlighted that alternative reaction conditions should be considered for the more sterically bulky R^3 linkers. Indeed, notable alterations were needed regarding the solvent and reaction temperature to generate BITZ-hybrid analogues when R^3 was saturated or bulky.

Apelt *et al.* suggested that the use of phenol as a solvent increases the reactivity of the quinolone component by enhancing stability of the leaving group. It was also found that when using 4,7-dichloroquinoline, aromatic substitution only took place at the 4-position due to the low electrophilic activity at the 7-position.^[64] Whilst phenol achieved aromatic nucleophilic substitution between 4,7-dichloroquinoline and **41b** and **41a**, with poor to moderate yields respectively, extensive refinement of synthetic conditions was needed in order to generate **44-47**.

For the synthesis of **44**, using **41c** and 4,7-dichloroquinoline, anhydrous ethanol was used in replacement of phenol due to its lower boiling point, easing solvent removal and purification of the crude material. In the synthesis of **45** and **46**, no reaction was observed between 4,7-dichloroquinoline and the required amines **41d** and **41e** after 12 hours. Therefore, two equivalents of DIPEA were added to each reaction and the resulting solutions heated to a temperature of 110°C in a sealed tube for two days. DIPEA was introduced with the aim of promoting the nucleophilic substitution between the non-aromatic, saturated amine intermediates **41d** and **41e** and 4,7-dichloroquinoline: however, this was not achieved.

Replacement of ethanol with isopropanol (IPA), with the addition of triethylamine (4.0 eq) and extension of the reaction time to four days at 140°C, was trialled in the synthesis of **45** and **46**. IPA was proposed to improve reagent solubility and achieve better material dissolution under reflux; however, no reaction was observed with either analogue.

Since the use of high temperatures over extended reactions times and the use of various solvents was unsuccessful in the generation of **45-47**, harsher reaction conditions were evidently required. To circumvent the issue of slow and sluggish nucleophilic substitution, microwave reactor-mediated syntheses were attempted using the appropriate BITZ-amine intermediate **41d-f** and 4,7-dichloroquinoline in IPA, in the absence of base which proved to be a successful method for the generation of **45-47**. Two short heating intervals at 190-200°C was used in the microwave-mediated generation of **45**; whereas a single temperature elevation to 190°C, over 45 minutes to 1 hour, was optimal for the generation of **46** and **47**.

3.9.2 *PflspD* Enzymatic and Whole Cell Activity Data

It was anticipated that designed aminoquinoline-BITZ hybrid compounds **42-47** (Figure 3.13) would retain activity against the *PflspD* enzyme due to the presence of the BITZ pharmacophore which remained accessible as a chemical entity in the hybrid structures. However, it was also considered probable that increased activity against *Plasmodium* parasite growth, compared to *PflspD*, could be seen with these compounds. Furthermore, it was plausible that **42-47** may display greater efficacy

against *Plasmodium* parasite growth than the *Pf*lspD target itself due to the hybrid nature of the compounds, designed for the purpose of dual-activity.

As expected with the approach of compound hybridisation, **42-47** are larger in molecular size than earlier BITZ analogues, which are based around the inhibitory BITZ motif alone (see **Table 3.1** for representative examples **4-10**). The average MW of hybrid compounds **42-47** is 407.41 gmol⁻¹, which contrasts with the lower average MW of BITZ inhibitors **4-10** which is 345.34 gmol⁻¹. Comparing predicted PK parameters of these two inhibitor classes, aminoquinoline-BITZ hybrid compounds **42-47** and biphenyl BITZ derivatives **4-10** display similar distribution coefficients (*ClogD*) and solubility (*CaqSol*) values, as predicted by AZ^[8,9] (**Table 3.1** and **3.8**). It should also be noted that the aminoquinoline-BITZ hybrids consistently display poor predicted aqueous solubility (**Table 3.8**). *CaqSol* values of < 10 µM were predicted across **42-47** which does not meet our defined aqueous solubility threshold of > 50 µM (**Section 3.2.2**).

Compound number	R ³	<i>Pf</i> lspD IC ₅₀ (µM)	Whole cell 3D7 EC ₅₀ (µM)	MW (gmol ⁻¹)	<i>ClogD</i>	<i>CaqSol</i> (µM)
42	Ethyl	19.0	-	355.05	3.73	6.47
43	1,5-Phenyl	5.84	-	403.05	4.28	0.67
44	2-Methyl-1,5-phenyl	> 10	-	471.07	4.50	0.71
45	1,4-Cyclohexyl	3.757 ± 0.881	0.091 ± 0.048	409.10	3.93	3.22
46	1,6-Cyclohexyl	> 15	> 100	409.10	4.25	3.17
47	2-Dimethyl-propane	3.673 ± 0.564	0.015 ± 0.006	397.10	4.40	3.41

Table 3.8 Inhibitory activity of compounds **42-47** against *Pf*lspD and *P. falciparum* growth in culture (strain 3D7); compound MW and calculated *ClogD* and *CaqSol* values are given.

As anticipated, the aminoquinoline-BITZ hybrid series displayed enhanced activity against *P. falciparum* growth compared to activity against *Pf*lspD; where compounds **45** and **46** explicitly demonstrate this effect. Compound **45** displays activity against *Plasmodium* parasite growth (EC₅₀ = 0.091 ± 0.048 µM) which is 41 times more potent than that measured against the *Pf*lspD enzyme (EC₅₀ = 0.091 ± 0.048 µM). Even more striking are the effects of **47** which most strongly demonstrates this activity distinction. **47** has an IC₅₀ value of 3.673 ± 0.564 µM against *Pf*lspD, compared to an EC₅₀ =

0.015 ± 0.006 μM against *Plasmodium* parasite growth, representing a 245-fold increase in potency against the parasite compared to the *Pf*lspD enzyme target.

Considering the strong activity distinction shown by **45** and **47**, the measured activity of **46** could be considered an anomalous result as **46** shown to be inactive against both *Pf*lspD and *Plasmodium* parasite growth. Since **46** is a regioisomer of **45**, it could reasonably be expected to demonstrate comparable biological activity. However, the lack of inhibitory activity demonstrated by **46** may be a consequence of significant steric clashes and the bulky construct of the compound, a consequence of the 1,6-disubstitution pattern within the cyclohexane R³ linker (**Figure 3.15** and **Table 3.8**). The 1,6-disubstitution pattern holds the aminoquinoline and BITZ pharmacophores in very close proximity, generating a large amount of steric bulk and potential molecular clashes within the analogue; this could potentially hinder the performance of **46** in both the *Pf*lspD enzymatic and *Plasmodium* parasite whole cell growth assays.

Hybrid compounds **42-44** all performed poorly against *Pf*lspD with activity data outside the required threshold of < 5 μM as a definition of activity against the *Pf*lspD enzyme. Furthermore, the very poor solubility of these analogues, particularly **43** and **44**, meant whole cell activity data couldn't be obtained for **42-44**, which was a disappointing outcome within this analogue series.

3.10 Further SAR Explorations

This thesis describes a distinct body of work that was conducted as part of a collaborative research project between the Medicinal Chemistry research group at The University of Liverpool, coordinated by Dr Neil Berry and Professor Paul O'Neill, and the Molecular and Cellular Microbiology group, coordinated by Audrey Odom, at the School of Medicine at Washington University in St Louis. Additional SAR studies have therefore been conducted around the BITZ chemotype by other researchers in the medicinal chemistry group at the University of Liverpool which have focused on structural modifications to the A and B rings of the BITZ core (**Figure 3.2**).

A series of BITZ compounds have been synthesised, incorporating functional group substitutions to the A ring of the BITZ core (**Figure 3.16**). The aim of these analogues was to assess if the metabolism profile of BITZ compounds could be altered by the introduction of fluorine or nitrogen into the aromatic A ring, whilst maintaining *Pf*lspD enzymatic and phenotypic activity. Fluorine is known to modulate the metabolism profile of compounds by reducing the extent Phase I metabolism, through reduced hydroxylation and therefore increased compound stability; whilst the presence of nitrogen within a ring can be used to block a site of metabolism on related analogues.^[35,65]

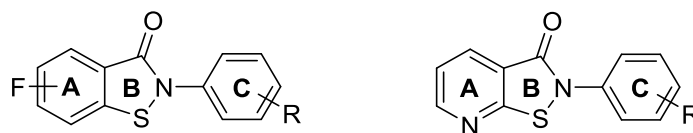
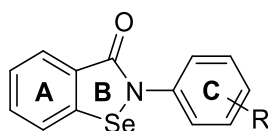


Figure 3.16 Chemical structure of BITZ analogues with modifications to the A ring.

Work within the Liverpool University medicinal chemistry group has therefore generated a number of BITZ compounds, incorporating the described A-ring modifications alongside variations to the BITZ side chain, as depicted by the R group in the C ring (**Figure 3.16**). Whilst it is not possible to discuss the full scope of this work and range of syntheses here, it can be broadly summarised that A ring substitutions were not well tolerated, producing only moderate to poor levels of activity against the *Pf*lspD enzyme and showing significant losses of whole cell activity against parasite growth.

In other work carried out within the group, the structure of the Ebselen motif was revisited. The close structural similarity between Ebselen (**Figure 3.10, Section 3.7.1**) and our simplified BITZ chemotype core **31** (**Figure 3.11**) promoted a series of compounds to be generated, based around the BITZ motif but replacing the sulfur heteroatom with selenium (Se) (**Figure 3.17**), therefore mirroring the core Ebselen construct. Not only are **31** (**Figure 3.11**) and **48** (**Figure 3.17**) highly similar in structure, but Ebselen (2-phenyl-1,2-benziselenazol-3(2*H*)-one), an electrophilic antioxidant possessing glutathione peroxidase-like activity, has been shown to mediate this activity due through its ability to induce cysteine-targeted oxidation of cellular proteins.^[43] The demonstration of cysteine reactivity is therefore relevant to our own research, since our proposed mechanism of BITZ activity at *Pf*lspD involves formation of a covalent adduct to a cysteine protein residue in the *Pf*lspD active site (see **Chapter 4**). These comparable methods of protein binding and enzyme inhibition therefore strengthened our interest in the Ebselen chemotype and led to an SAR study generating a series of complimentary BITZ analogues, incorporating selenium as a replacement atom to sulfur in the B ring of the BITZ headgroup (**Figure 3.17**).



48 (R = H)

Figure 3.17 Chemical structure of Selenium (Se) BITZ analogues.

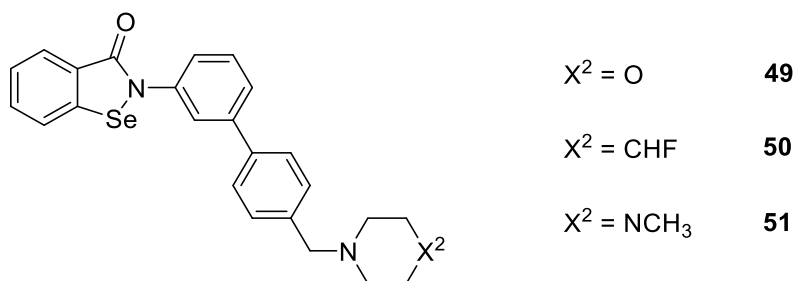
Direct comparison of the biological activities of **31** and **48** highlights that replacement of sulfur with selenium in the BITZ motif does not improve phenotypic or *Pf*lspD enzymatic activity (**Table 3.9**). Whilst both enzymatic and phenotypic activity levels are comparable for **48**, a significant, 15-fold loss

of *PflspD* inhibitory activity was observed comparing **48** to the simple BITZ scaffold **31**. From this direct comparison, and as an initial assumption, this result provides further evidence that the BITZ core is specifically required to achieve consistent inhibition of the *IspD* enzyme.

Compound number	<i>PflspD</i> IC ₅₀ (μM)	Whole cell 3D7 EC ₅₀ (μM)	MW (g mol ⁻¹)	<i>ClogD</i>	<i>CaqSol</i> (μM)
31	0.5995	5.49	227.04	2.97	112.4
48	9.374	9.65	274.98	2.48	84.9

Table 3.9 Inhibitory activity of **31** and **48** against *PflspD* and *P. falciparum* growth in culture (strain 3D7); MW and calculated *ClogD* and *CaqSol* values are given.

Further analogues of the selenium compound series were made with the aim of mimicking the construct of previous BITZ compounds to provide direct measures of activity. Generally, all of the resulting selenium analogues displayed very poor phenotypic activity with consistently weak activity against the *PflspD* enzyme itself. Displaying an exception to this trend are compounds **49-51** (Figure 3.18) which were designed as parallel analogues to the biphenyl benzyl-linked BITZ compounds **13-15** (Figure 3.5 and Table 3.2).



49 - 51

Figure 3.18 Chemical structures of selenium compounds **49-51**.

Compounds **49-51** displayed inhibitory *PflspD* activity close to the 100 nM region; however, this was not translated into phenotypic activity, measured at > 2 μM for all three compounds. Considering the biological activities of other selenium analogues generated, it was concluded that SAR around these BITZ mimetics was not tractable since consistently poor phenotypic activity was demonstrated. Further development of this compound series therefore wasn't continued.

3.11 Biological Evaluation of BITZ Compound Activity at the IspD Enzyme and in Malaria Parasites

3.11.1 BITZ Compound Activity at Alternative *Plasmodium* spp. Enzymes

Having synthesised and tested a wide range of BITZ derived compounds as targeted inhibitors of the *PfIspD* enzyme, the potential for broad-spectrum antimalarial activity of this compound class was also considered.

The known and observed capabilities of *Plasmodium* parasites to develop drug resistance against a wide variety of structurally diverse chemotherapeutic motifs has led to the current state of play with global concerns questioning the longevity and continued efficacy of the current antimalarial pipeline. As previously discussed (see **Chapter 1**), there is urgent need to develop inexpensive and novel chemotherapies that are effective in the treatment and prevention of malaria, enabling the replacement of current antimalarial agents.^[66] It is also essential that new and novel chemical drug classes are identified which show both potent and broad-spectrum antimalarial activity.^[67]

Of the protozoan parasite species infective to humans, *P. falciparum* and *P. vivax* present the greatest challenges to public health, contributing to the majority of malarial infections.^[62] *P. vivax* infections have lower incidence levels and very low transmission rates compared to *P. falciparum* infections within African countries.^[68] However, the geographical distribution of *P. vivax* infections is very broad due to the parasites ability to survive in cooler climates. Consequently, *P. vivax* poses a significant public health threat across many parts of the world with estimations suggesting that this *Plasmodium* species was responsible for 13.8 million cases of malaria in 2015, accounting for approximately half the total malaria cases outside sub-Saharan Africa in that year.^[69] Many current antimalarial drug development campaigns focus on the well-studied blood stage of the *Plasmodium* parasite life cycle; however, the *Anopheles* mosquito vector and liver stages of the parasite life cycle also represent good options for eradication campaigns, more specifically targeting *P. vivax* and *P. ovale* species parasites.^[66]

In light of this, some of our most potent *PfIspD* BITZ inhibitors were selected and tested against the purified and recombinant *P. vivax* IspD (*PvIspD*) enzyme. The selected BITZ compounds (**4-6** and **13-15**, **Table 3.9**) demonstrated low micromolar to nanomolar activity against both the *P. falciparum* and *P. vivax* IspD enzymes, successfully inhibiting the two enzyme species. This consequently highlights, not only the efficacy of these compounds, but also their potential to act as broad spectrum antimalarial agents.

Compound number	<i>PflspD</i> IC ₅₀ (μM)	Whole cell 3D7 EC ₅₀ (μM)	<i>PvlspD</i> IC ₅₀ (μM)
4	0.206 ± 0.089	0.920 ± 0.066	0.054 ± 0.003
5	0.073 ± 0.020	1.080 ± 0.164	0.057 ± 0.013
6	0.273 ± 0.015	0.646 ± 0.021	0.041 ± 0.018
13	0.400 ± 0.082	0.413 ± 0.082	0.050 ± 0.016
14	0.862 ± 0.107	0.323 ± 0.092	0.240 ± 0.100
15	0.446 ± 0.075	0.416 ± 0.006	0.062 ± 0.026

Table 3.9 Inhibitory activity of **4-6** and **13-15** (mean and SEM; n ≥ 3) against *PflspD* and *PvlspD* enzyme homologues and corresponding inhibitory activity against *P. falciparum* parasite growth in culture (strain 3D7).

All the selected BITZ compounds displayed encouraging inhibitory activity against *PvlspD*, with a number of compounds (**4** and **6-13**) showing enhanced potency at the *PvlspD* enzyme compared to *PflspD*. Interestingly all BITZ compounds examined, apart from **14**, displayed potent activity against *PvlspD* with IC₅₀ values consistently < 100 nM (**Table 3.9**). Also of note, all BITZ compounds evaluated in **Table 3.9**, with the exception of **5**, demonstrate sub-micromolar to nanomolar activity against both the *PflspD* and *PvlspD* enzymes, as well as *P. falciparum* parasite growth. **5** is in fact the most potent BITZ inhibitor identified against the *PflspD* enzyme with an IC₅₀ value of 73 ± 20 nM, but which demonstrates a slight loss of activity against parasite growth (**Table 3.9**). In particular, this study highlights that overall BITZ compounds **4** and **6** demonstrate the most potent and consistent inhibition against both the *PflspD* and *PvlspD* enzymes as well as against whole cell 3D7 parasite growth. **4** and **6** can therefore be considered as two of the most potent *IspD* enzyme inhibitors identified to date, demonstrating strong potential as broad-spectrum antimalarial agents.

3.11.2 Correlation Between *PflspD* Enzyme Inhibition and Inhibition of *Plasmodium* Parasite Growth

To further evaluate **4** and **6**, and reiterate that the observed potency against *PflspD* and *PvlspD* translates directly into antimalarial activity, the relationship between *PflspD* enzymatic and whole cell parasite growth inhibition was directly evaluated (**Figure 3.19**).

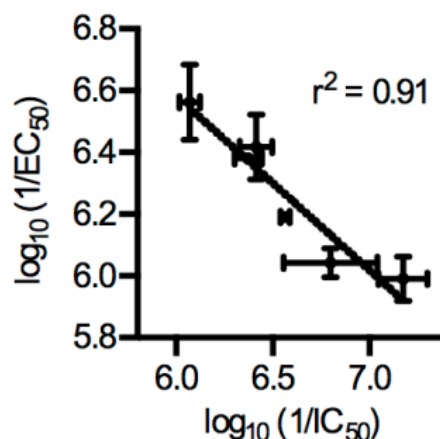
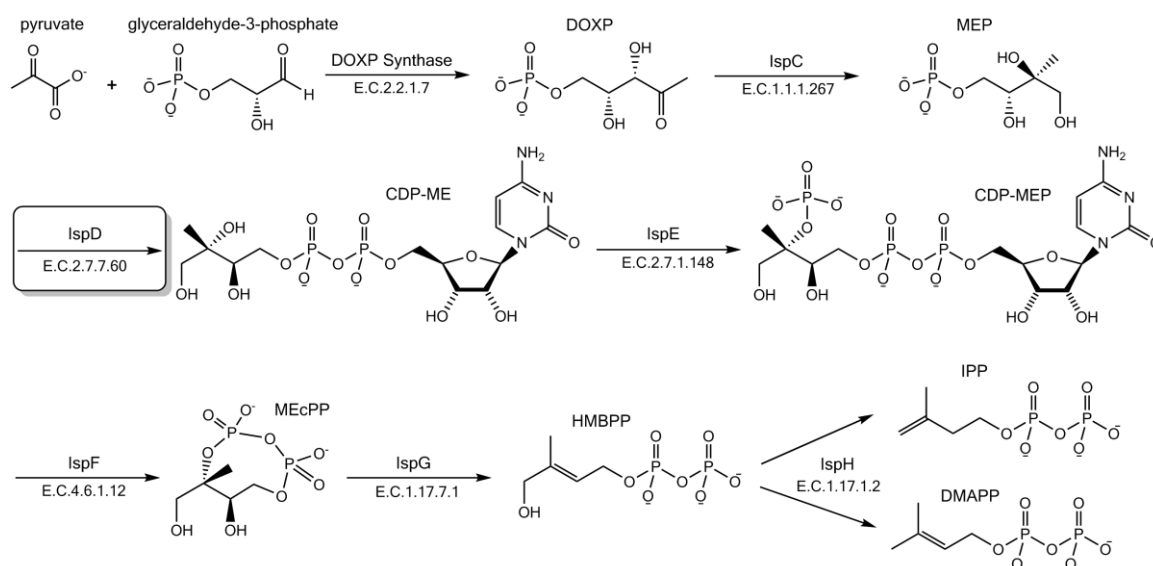


Figure 3.19 Correlation of *Pf*lspD enzymatic inhibition and anti-parasitic activity for BITZ inhibitors **4-6** and **13-15**.

Dose-dependent inhibition of *Pf*lspD enzyme activity and *P. falciparum* parasite growth was measured for **4-6** and **13-15** (Table 3.9) and half-maximal inhibitory concentrations determined prior to least-squares linear regression analysis (coefficient of determination, $r^2 = 0.91$; GraphPad Prism: mean activity values given with SEM; $n \geq 3$). Overall, BITZ compounds **4-6** and **13-15** demonstrated good correlation between *Pf*lspD enzyme inhibition and inhibition of *Plasmodium* parasite growth ($r^2 = 0.91$, Figure 3.19) which indicates that arrest of *Pf*lspD activity corresponds to an impediment of parasite growth. It can therefore be suggested that inhibiting the MEP pathway, through inhibition of the *Pf*lspD enzyme, is able to cause parasite death.

3.11.3 BITZ Compounds Inhibit Isoprenoid Metabolism in Malaria Parasites

To test this indication and establish that observed antiparasitic activity is the result of MEP pathway inhibition: targeted metabolic profiling of MEP pathway intermediates was performed in *P. falciparum* parasites that were treated with our BITZ *Pf*lspD inhibitors. Early-stage cultures of *P. falciparum* were treated with BITZ compound concentrations at ~ five times the IC_{50} of inhibitor **4** for 10 hours. To enable a comparative study, separate *P. falciparum* cultures were also treated with fosmidomycin (FSM) for 10 hours. The MEP pathway intermediates DOXP and MEcPP (Figure 3.12) present within the treated cultures, were quantified by LC-MS/MS (Liquid Chromatography Tandem Mass Spectrometry) analysis and compared to the metabolic levels observed in untreated *P. falciparum* cultures, as described in previous work by Odom *et al.*^[70]



Scheme 3.12 The MEP Pathway.^[71,72]

Similar to the MEP inhibitor, FSM (**Chapter 1, Section 1.5.1**), BITZ inhibitor **4** produced a significant decrease in MEcPP levels ($p = 0.0042$ **Figure 3.20**) which are comparable to those observed under treatment with FSM ($p = 0.0038$ **Figure 3.20**). However, treatment with **4** did not affect the levels of the upstream metabolite, DOXP ($p = 0.94$: **Figure 3.20**). These results again mirror those seen under comparable treatment of *P. falciparum* cultures with the established IspC inhibitor, FSM,^[73] and therefore confirm that BITZ compounds are capable of inhibiting the *Plasmodium* MEP pathway at levels that affect asexual parasite growth.

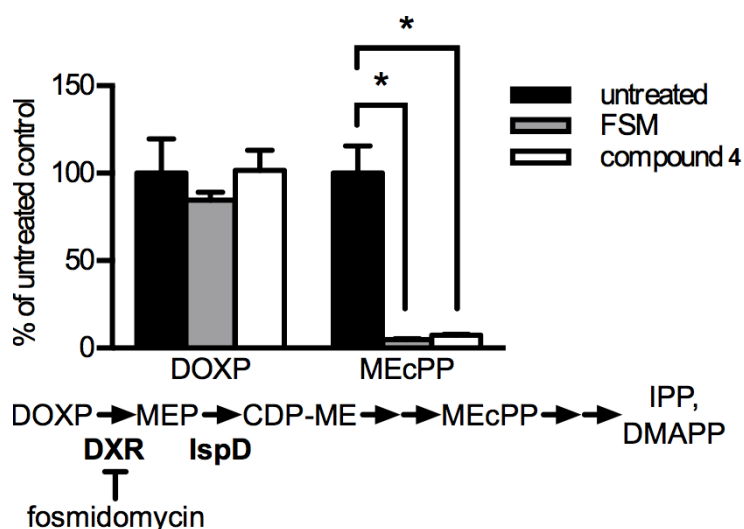


Figure 3.20 Bar graph demonstrating that, comparable to FSM, BITZ compound **4** inhibits the MEP pathway in *P. falciparum* shown with the targeted metabolic profiling of MEP pathway intermediates. Mean and standard error values from three separate experiments displayed. Asterisks (*) indicate significance threshold (α) = 0.05.

This study and observed data therefore highlights that the treatment of *P. falciparum* with growth-inhibitory concentrations of BITZ compounds is sufficient to disrupt *de novo* production of isoprenoid precursors through MEP pathway inhibition. Consequently, these findings strongly indicate that BITZ compounds inhibit parasite growth through cellular inhibition of the MEP pathway, by targeting the *Pf*lspD enzyme.

3.11.4 BITZ Compound Activity in the Presence and Absence of IPP Supplementation

In malaria parasite cultures, supplementation with the isoprenoid precursor, isopentyl pyrophosphate (IPP) (**Scheme 3.12**) has been demonstrated to rescue MEP pathway dysfunction. Indeed, IPP supplementation has been shown to allow the continuation of *Plasmodium* parasite growth during treatment of parasite cultures with the *lspC* inhibitor, FSM, and the *lspD* inhibitor, 1*R*,3*S*-MMV008138.^[74–76] In order to determine whether BITZ compound inhibition is specific to activity against the MEP pathway, we tested for observed IPP rescue during treatment of *P. falciparum* cultures with BITZ compound **8**.

Parasite growth inhibition assays were performed in both the presence and absence of supplementation with the MEP pathway product and isoprenoid precursor, IPP. Over the course of this study, *Plasmodium* parasite growth rescue was not observed following the supplementation of *P. falciparum* cultures with IPP that had initially been treated with **8** ($p = 0.75$, **Table 3.10**). The previously observed and acknowledged correlation between *Pf*lspD enzymatic inhibition and parasite growth inhibition (**Figure 3.19**), as well as metabolic analysis of MEP pathway intermediates (**Figure 3.20**), suggest that parasite growth inhibition by treatment with BITZ compounds involves inhibition of the *lspD* enzyme. However, the observed lack of rescue by IPP supplementation suggests that off-target activity may also contribute to parasite growth inhibition.^[77]

<i>Plasmodium</i> parasite growth conditions	Whole Cell 3D7 Growth Inhibition EC ₅₀ (μM)
No supplementation	0.92 ± 0.066
200 μM IPP	0.98 ± 0.24

Table 3.10 Activity of **8** against *Plasmodium* parasite growth in both the presence and absence of IPP supplementation; mean EC₅₀ data and SEM given for $n \geq 3$).^[77]

Although side-by-side experiments conducted with the *lspC* inhibitor, FSM, demonstrated IPP rescue of FSM-treated parasite cultures, we did not observe rescue of *Plasmodium* parasites that were first treated with BITZ compound **8** (**Table 3.10**). Since IPP rescue is not observed, it must therefore be rationalised that the apparent inhibition of *P. falciparum* parasite growth by BITZ derived compounds does not only result from the established activity against the *lspD* enzyme. However, further studies

can be conducted that may shed light on additional targets which BITZ compounds may be capable of inhibiting, potentially contributing towards the observed inhibition of *Plasmodium* parasite growth (see Chapter 6).

3.11.5 BITZ Activity Against Resistant Parasites

Given the ongoing and widespread issues of multiple drug resistance to *P. falciparum* infections,^[69] it is critical that existing drug-resistant parasites are not cross-resistant to novel antimalarial therapies currently in development. Taking account of this, the antimalarial potency of BITZ compounds was evaluated against a series of lab-adapted field isolates of *P. falciparum*, which included parasite strains resistant to chloroquine, mefloquine and artemisinin: the archetypes of antimalarial chemotherapy.^[78] Following growth inhibition studies, it was identified that **4**, one of the most potent BITZ inhibitors against both the *Pf*lspD enzyme and parasite growth, also effectively inhibits the growth of three lines of drug-resistant *P. falciparum* parasites (Table 3.11).

<i>P. falciparum</i> strain	Whole Cell Growth Inhibition EC ₅₀ (μM)
3D7	0.92 ± 0.066
D6	0.80 ± 0.12
7G8	1.02 ± 0.25
IPC 5202	1.38 ± 0.19

Table 3.11 Inhibitory activity of **4** against drug-resistant *P. falciparum* parasites grown in culture; mean EC₅₀ data and SEM given for ≥ 3 .

The inhibitory activity of BITZ compound **4** was found to be in the low micromolar region against three drug-resistant *P. falciparum* parasite strains and consistent with observed inhibitory activity against 3D7, the pan-sensitive *P. falciparum* strain (Table 3.10). Of the drug-resistant *P. falciparum* parasite strains examined, including: the mefloquine-resistant D6 strain,^[79] the multidrug (chloroquine)-resistant 7G8 strain^[80] and the artemisinin-resistant IPC 5202 strain,^[81] **4** showed the greatest inhibition against drug-resistant *P. falciparum* strain D6, with a parasite EC₅₀ of 800 ± 120 nM. This level of whole cell growth inhibition was actually slightly more pronounced than that observed against the 3D7 *P. falciparum* strain with a measured parasite EC₅₀ value of 950 ± 72 nM. These results demonstrate that BITZ compounds are able to inhibit parasite growth in *P. falciparum* parasite strains with acquired resistance against current antimalarial drugs. This therefore highlights the promise of BITZ derived compounds as novel antimalarial therapies which have the potential to show broad spectrum antimalarial activity across both drug-resistant and non-drug-resistant *Plasmodium* parasites.

3.12 Conclusions and Future Work

This chapter has provided an account of the SAR explorations that have been conducted around the of 1,2-benzo[*d*]isothiazol-3(2*H*)-one (BITZ) chemotype for the development and optimisation of novel *Pf*lspD inhibitors, as inspired by previous medicinal chemistry programs demonstrating successful hit-to-lead optimisation. This chapter provides the details of SAR developments and corresponding syntheses that I, myself, have designed and performed, as well as some of the key SAR studies and findings that have been carried out by others in the Liverpool medicinal chemistry group.

A diverse range of BITZ derived compounds have been synthesised, comprising a wide variety of chemical constructs which have been generated using a number of distinct synthetic routes. Ultimately, this work has identified, to the best of our knowledge, three of the most potent BITZ derived inhibitors against the *IspD* enzyme to date, all of which belong to the biphenyl BITZ inhibitor compound series. Compound **5** (Figure 3.3 and Table 3.1) has been identified as the most potent BITZ inhibitor against the *Pf*lspD enzyme itself, demonstrating an impressive IC₅₀ value of 73 ± 20 nM which is six-times more potent than our original HTS hit, DT2009-0168020 (Figure 3.15). BITZ compounds **4** and **6** can be described, not only as potent *Pf*lspD inhibitors, but also as the most effective antimalarial compounds identified within this research. Compounds **4** and **6** display potent inhibition against the *Pf*lspD enzyme with IC₅₀ values of 206 nM and 273 nM respectively; we also observe that this translates into improved inhibition of *P. falciparum* parasite growth for these two compounds, compared to that achieved with the most potent *Pf*lspD enzyme inhibitor **5** [EC₅₀ values for **4** and **6** are 920 nM and 646 nM respectively].

Since our most potent BITZ inhibitors belong to the same structural family of biphenyl derived compounds, this suggests that this inhibitor series fits well within the active site of the *Pf*lspD enzyme, enabling efficient protein-ligand contacts to be formed which translates to potent enzyme inhibition. To further address the alignment and behaviour of BITZ compounds at *Pf*lspD, molecular modelling studies will be undertaken to evaluate these BITZ inhibitors at the enzyme target, as well as explore the nature of the *Pf*lspD active site itself. Molecular modelling studies have the potential to inform further compound design and shed light onto the possible mechanism of action by which BITZ compounds are capable of achieving *Pf*lspD enzyme inhibition.

Also of note, BITZ inhibitor **15** shows potent activity of the *Pf*lspD enzyme which translates favourably into inhibition of *P. falciparum* parasite growth at a similar, and slightly enhanced order of magnitude: *Pf*lspD IC₅₀ value = 446 nM alongside a parasite growth EC₅₀ value of 416 nM (Figure 3.5 and Table 3.2). This result gives confidence in that the biphenyl BITZ analogue series doesn't represent the only

BITZ series which is capable of displaying potent inhibition of both the *Pf*lspD enzyme and *P. falciparum* parasite growth.

Using some of our most promising BITZ inhibitors, it has been possible to conduct a number of biological studies evaluating BITZ compound activity at the lspD enzyme and in malaria-causing *Plasmodium* parasites. We have shown that BITZ compounds offer potential as a broad spectrum antimalarial agents as they are able to inhibit the activity of the *P. vivax* lspD enzyme homologue. Several BITZ compounds demonstrate low micromolar to nanomolar activity against *Pv*lspD (**Table 3.9**), highlighting the efficacy of these compounds across *Plasmodium* enzyme species and therefore their potential to act as broad spectrum antimalarial agents. Importantly, this meets a key developmental requirement in antimalarial drug design since there is an increasing necessity for new therapies to show both potent and broad-spectrum antimalarial activity.^[67]

In addition, it has been demonstrated that BITZ derived compounds express inhibitory activity against *P. falciparum* parasite strains which show drug resistance to existing antimalarial therapies (**Table 3.11**). This finding is of significant importance given the current malaria climate and the wide spread drug resistance shown by the *P. falciparum* parasite species. It is crucial that existing drug-resistant parasites show sensitivity to new and novel antimalarial therapies and do not risk pre-determined resistance against them. Encouragingly, our data is in line with this requirement as BITZ compounds display inhibitory activity against existing drug-resistant parasite strains.

Considering more specifically the effects of BITZ inhibitors at the *Pf*lspD enzyme target and consequent effects on *P. falciparum* parasite growth; selected BITZ inhibitors **4-6** and **13-15** have demonstrated good correlation between *Pf*lspD enzyme inhibition and inhibition of parasite growth (**Figure 3.9**), which indicates that inhibition of the MEP pathway, through targeted inhibition of *Pf*lspD, is able to cause parasite death. In addition, metabolic profiling of MEP pathway intermediates, following treatment of *P. falciparum* cultures with growth-inhibitory concentrations of BITZ compounds, have established that observed anti-parasitic activity is the result of MEP pathway inhibition which is sufficient to disrupt *de novo* production of isoprenoid precursors. Taken together, these findings strongly indicate that BITZ compounds are able to inhibit *Plasmodium* parasite growth and do so, at least in part, through the inhibition of cellular lspD.

In contrast to these lines of evidence, highlighting effective inhibition of *Pf*lspD by the BITZ chemotype which translates into the disruption of *Plasmodium* parasite growth, several series of BITZ compounds indicate slightly differing behaviour towards the *Pf*lspD enzyme and parasite growth. In particular, the biphenyl-pyridinyl BITZ series, alkyl-amino biphenyl BITZ series and aminoquinoline-BITZ hybrid

compounds (**Sections 3.5, 3.8 and 3.9** respectively) suggest that BITZ derived compounds may also be capable of eliciting off-target inhibitory effects that may contribute to the observed inhibition of *Plasmodium* parasite growth.

A loss of *Pf*lspD enzymatic activity is observed across the biphenyl-pyridinyl BITZ compound series, with enzymatic IC₅₀ values consistently outside the required threshold of 5 µM; however, a notable level of anti-parasitic activity is maintained, where low micromolar efficacy is displayed against parasite growth with all derivatives in the series (**Section 3.5**). This consistent activity trend is indicative of off-target interactions which are capable of inhibiting *Plasmodium* parasite growth, despite a lack of activity against the selected enzyme target. Similarly, this effect is also observed in the alkyl-amino biphenyl BITZ compound series (**Section 3.8**). Whilst BITZ derivatives in this series are classified as active against the *Pf*lspD enzyme, an increase in efficacy against parasite growth is also observed, with a 3.5-5-fold potency increase against parasite growth, compared to activity against *Pf*lspD.

A less distinct pattern of activity was observed with the aminoquinoline-BITZ hybrid compounds (**Section 3.9**). Inhibitory activity against the *Pf*lspD enzyme was abolished with over half the compounds in the series and consequently, the extent of inhibitory activity against parasite growth was not tested for these compounds. However, two hybrid compounds within the series displayed moderate activity against *Pf*lspD but highly potent activity (in the low nanomolar region) against *Plasmodium* parasite growth. Indeed, it is worth noting that the aminoquinoline-BITZ hybrid compounds were designed with the purpose of achieving dual-target activity. However, the heightened activity observed against *Plasmodium* parasite growth, with up to a 245-fold potency increase compared to *Pf*lspD inhibition for one analogue (**41**), far outweighs that expected from the previous distinctions between enzymatic and phenotypic activity which has been observed with other BITZ analogues. Consequently, this result may alternatively suggest that the BITZ chemotype is capable of off-target activity which may contribute to overall inhibition of parasite growth.

In addition to the highlighted potential for off-target BITZ reactivity, exemplified by enzymatic and phenotypic activity data, IPP rescue experiments also suggest that parasite growth inhibition by BITZ derived compounds does not solely result from activity against the *lspD* enzyme. As a consequence, further studies will be conducted with the aim of identifying any additional molecular targets that the BITZ chemotype and derived compounds may be capable of inhibiting.

Despite the suggestion of off-target BITZ reactivity, it has also been clearly demonstrated that the BITZ chemotype potently inhibits the *Pf*lspD enzyme, which translates into disruption of isoprenoid

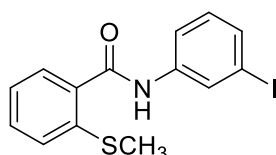
precursor synthesis and, as a result, causes *Plasmodium* parasite death. Indeed, the structurally divergent BITZ analogues generated demonstrate a wide range of inhibitory activity against the *PflspD* enzyme. Considering requirements for future work, a necessary task is to determine the mechanism of action by which this chemical construct achieves inhibition of the *PflspD* enzyme. In addition, the question of BITZ compound metabolism should also be addressed to provide a measure of BITZ compound stability, half-life ($t_{1/2}$) and clearance when introduced to a biological system. This will involve assessing the metabolism profiles of existing BITZ compounds, followed by further SAR studies to facilitate any appropriate chemical modifications to enable movement towards an optimised lead structure.

3.13 Experimental

For general chemical and biological methodologies see **Chapter 2, Section 2.7.1**.

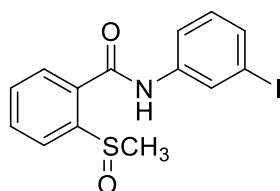
3.13.1 Organic Synthesis

Preparation of *N*-(3-iodophenyl)-2-(methylthio)benzamide **1**



To a stirring solution of 2-(methylthio)benzoic acid (13.8 mmol) in anhydrous toluene (25 ml) under a N_2 atmosphere, thionyl chloride (41 mmol, 3.0 eq) was added followed by 3 drops of *N,N*-dimethylformamide: the resulting solution was refluxed for 2-3 hours. Solvent and thionyl chloride were removed under reduced pressure to give the acid chloride intermediate as a white solid. 3-iodoaniline (16.4 mmol, 1.2 eq) was dissolved in anhydrous THF (10 ml/mmol) to which triethylamine (Et_3N) (27.4 mmol, 2.0 eq) was added. The crude acid chloride was re-dissolved in anhydrous THF (10 ml/mmol) and added drop-wise to the amine and base solution over 10 minutes at $0^\circ C$. After a further 10 minutes, the solution was warmed to room temperature and allowed to stir for 20 hours. The solvent was removed under reduced pressure; the resulting crude material diluted with water and extracted into EtOAc (3 x 30 ml). The combined organic extracts were washed with 5% HCl (50 ml), saturated aq. $NaHCO_3$ (50 ml) and brine (50 ml), dried over $MgSO_4$ and concentrated under reduced pressure to give **1** in 97.7% yield. $R_f = 0.62$ (40:60 EtOAc:hexane). $R_f = 0.62$ (4:6 EtOAc:hexane). 1H NMR (400 MHz, $CDCl_3$) δ 8.69 (s, 1H), 8.08 (s, 1H), 7.70 – 7.61 (m, 2H), 7.51 – 7.46 (m, 1H), 7.46 – 7.41 (m, 1H), 7.40 – 7.35 (m, 1H), 7.29 – 7.24 (m, 1H), 7.09 (t, $J = 8.1$ Hz, 1H) and 2.50 (s, 3H); ^{13}C NMR (101 MHz, $CDCl_3$) δ 139.4, 137.3, 135.2, 133.9, 131.6, 130.9, 129.3, 120.0, 128.2, 126.0, 119.6, 115.5, 94.6 and 17.3; **ES+HRMS** m/z 391.9570 [$M+Na$] $^+$ $C_{14}H_{12}INOS$ requires 368.97.

Preparation of *N*-(3-iodophenyl)-2-(methylsulfinyl)benzamide **2**

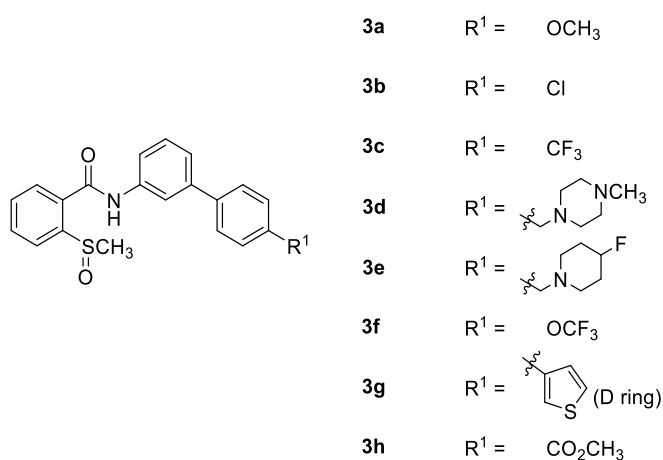


A solution of sodium periodate (11.68 mmol, 1.6 eq) in water (30 ml) was added dropwise to **1** (13.4mmol, 1.0 eq) in MeOH (10 ml/mmol) at room temperature. The biphasic solution was heated to $50^\circ C$ for 4-5 hours before the solvent was removed under reduced pressure. The crude precipitate

was diluted with water, filtered through a sinter and washed with water before drying for 12 hours in a desiccator to give **2** as a fine brown powder in 96.3% yield. **Rf** = 0.14 (100% EtOAc). ¹H NMR (500 MHz, DMSO) δ 10.67 (s, 1H, NH), 8.21 (t, *J* = 1.8 Hz, 1H), 8.16 (dd, *J* = 7.8, 1.3 Hz 1H), 7.99 (dd, *J* = 7.8, 1.0 Hz, 1H), 7.88 (td, *J* = 7.4, 1.3 Hz, 1H), 7.72 (ddd, *J* = 4.5, 2.8, 1.1 Hz, 2H), 7.51 (ddd, *J* = 7.8, 1.7, 1.0 Hz, 1H), 7.19 (t, *J* = 8.1 Hz, 1H), 2.83 (s, 3H, CH₃); ¹³C NMR (101 MHz, DMSO) δ 165.1, 148.9, 140.5, 133.2, 132.9, 132.3, 131.3, 130.9, 128.9, 128.5, 124.2, 120.0, 94.9, 45.1; **ES+HRMS** *m/z* 407.9529 [M+Na]⁺ C₁₄H₁₂INO₂S requires 384.96.

Preparation of biphenyl methylsulfonyl benzamides **3a-h**

General procedure (1)



To a solution of K₂CO₃ (3.3 eq), **2** (1.0 eq), and Pd(PPh₃)₄ (0.025 eq) in water (5 ml), the required phenyl boronic acid (1.2 eq) was added. The stirring solution was evacuated and purged with N₂ before adding anhydrous THF (10 ml) and heating to 80°C for 18-22 hours. The solution was quenched with 2N HCl (15 ml) and extracted into EtOAc (3 x 30 ml). The combined organic extracts were washed with brine (30 ml), dried over MgSO₄ and concentrated under reduced pressure. The crude products were purified by flash column chromatography.

Preparation of *N*-(4'-methoxy-[1,1'-biphenyl]-3-yl)-2-(methylsulfinyl)benzamide **3a**

The general procedure (1) was followed using 4-(methoxy) phenyl boronic acid to give **3a** as a cream-brown crystalline solid in 85.9% yield. **Rf** = 0.59 (5:95 MeOH:EtOAc). ¹H NMR (500 MHz, DMSO) δ 10.66 (s, 1H, NH), 8.17 (d, *J* = 7.8 Hz, 1H), 8.02 (d, *J* = 7.6 Hz, 1H), 7.98 (s, 1H), 7.89 (t, *J* = 7.6 Hz, 1H), 7.77 – 7.68 (m, 2H), 7.59 (d, *J* = 8.6 Hz, 2H), 7.44 (t, *J* = 7.8 Hz, 1H), 7.39 (d, *J* = 7.7 Hz, 1H), 7.06 (d, *J* = 8.6 Hz, 2H), 3.81 (s, 3H, CH₃), 2.84 (s, 3H, CH₃); ¹³C NMR (101 MHz, DMSO) δ 165.2, 159.5, 148.8, 140.9, 139.6, 132.8, 132.8, 132.7, 130.9, 129.7, 128.5, 128.2 (2C), 124.12, 122.6, 119.2, 118.7, 114.9 (2C), 55.7, 45.1; **ES+HRMS** *m/z* 388.0974 [M+Na]⁺ C₂₁H₁₉NO₃S requires 365.11.

Preparation of **N-(4'-chloro-[1,1'-biphenyl]-3-yl)-2-(methylsulfinyl)benzamide 3b**

The general procedure (1) was followed using 4-(chloro) phenyl boronic acid to give **3b** as a white solid in 83.4% yield. **Rf** = 0.15 (8:2 EtOAc:hexane). ¹H NMR (400 MHz, MeOD) δ 8.23 (dd, *J* = 8.0, 1.0 Hz, 1H), 8.05 – 8.00 (m, 1H), 7.98 (d, *J* = 1.7 Hz, 1H), 7.88 (td, *J* = 7.7, 1.2 Hz, 1H), 7.73 (td, *J* = 7.6, 1.2 Hz, 1H), 7.69 – 7.65 (m, 1H), 7.65 – 7.61 (m, 2H), 7.49 – 7.41 (m, 4H) and 2.98 (s, 3H); ¹³C NMR (101 MHz, DMSO) δ 165.1, 148.7, 139.8, 139.6, 139.2, 132.9, 132.7, 132.5, 130.8, 129.9, 129.4, 128.8, 128.4, 124.0, 122.9, 120.1, 118.9 and 45.0; **ES+HRMS** *m/z* 392.0474 [M+Na]⁺ C₂₀H₁₆ClNO₂S requires 369.06.

Preparation of **2-(methylsulfinyl)-N-(4'-(trifluoromethyl)-[1,1'-biphenyl]-3-yl) benzamide 3c**

The general procedure (1) was followed using 4-(trifluoromethyl) phenyl boronic acid to give **3c** as a cream solid in 86.8% yield. **Rf** = 0.23 (8:2 EtOAc:hexane). ¹H NMR (500 MHz, DMSO) δ 10.75 (s, 1H, NH), 8.18 (dd, *J* = 7.7, 1.0 Hz 1H), 8.12 – 8.10 (m, 1H), 8.03 (dd, *J* = 7.7, 1.0 Hz, 1H), 7.89 (ddd, *J* = 7.9, 7.4, 1.3 Hz, 1H), 7.87 (s, 4H), 7.84 – 7.79 (m, 1H), 7.74 (td, *J* = 7.5, 1.3 Hz, 1H), 7.54 – 7.52 (m, 2H), 2.84 (s, 3H, CH₃); ¹³C NMR (101 MHz, DMSO) δ 165.3, 148.9, 144.5, 139.8, 139.7, 132.8, 132.6, 130.9, 130.1, 128.5 (d, ²*J*_{CF} = 31.8 Hz, 1C), 128.5, 127.9 (2C), 126.4 (d, ³*J*_{CF} = 3.9 Hz, 2C), 124.8 (d, ¹*J*_{CF} = 271.9 Hz, 1C), 124.2, 123.4, 120.8, 119.4, 45.1; **ES+HRMS** *m/z* 426.0750 [M+Na]⁺ C₂₁H₁₆F₃NO₂S requires 403.09.

Preparation of **N-(4'-((4-methylpiperazin-1-yl)methyl)-[1,1'-biphenyl]-3-yl)-2-(methylsulfinyl) benzamide 3d**

The general procedure (1) was followed using 1-methyl-4-[4-(4,4,5,5-tetramethyl-1,3,2-dioxaborolan-2-yl)benzyl]piperazine to give **3d** as a clear pale yellow viscous oil in 85.9% yield. **Rf** = 0.14 (5:95 MeOH:EtOAc). ¹H NMR (400 MHz, MeOD) δ 8.25 (d, *J* = 7.6 Hz, 1H), 8.05 (d, *J* = 7.6 Hz, 1H), 8.01 (s, 1H), 7.90 (t, *J* = 7.4 Hz, 1H), 7.75 (t, *J* = 7.4 Hz, 1H), 7.68-7.63 (m, 3H), 7.47-7.44(m, 4H), 3.62 (s, 2H, CH₂), 2.99 (s, 3H, CH₃), 2.69 (br s, 8H), 2.82-2.48 (s, 3H, CH₃); ¹³C NMR (101 MHz, MeOD) δ 165.3, 147.0, 141.5, 139.7, 138.6, 136.3, 132.4, 132.4, 130.7, 129.8 (2C), 129.0, 127.9, 126.6 (2C), 123.6, 123.1, 119.5, 119.1, 61.9, 54.2 (2C), 51.9 (2C), 44.4, 43.8. **Elemental analysis** (%) found: C, 68.19; H, 6.57; N, 9.21; S, 6.26%. C₂₆H₂₉N₃O₂S requires C, 69.77; H, 6.53; N, 9.39; S, 7.16%; **ES+HRMS** *m/z* 448.2063 [M+H]⁺ C₂₆H₂₉N₃O₂S requires 447.20.

Preparation of **N-(4'-((4-fluoropiperidin-1-yl)methyl)-[1,1'-biphenyl]-3-yl)-2-(methylsulfinyl) benzamide 3e**

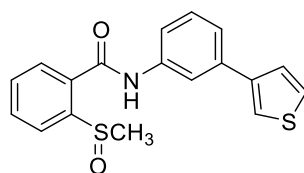
The general procedure (1) was followed using 4-((4-fluoropiperidine-1-yl)methyl)phenyl boronic acid to give **3e** as a white solid in 79.7% yield. **Rf** = 0.16 (5:95 MeOH:EtOAc). ¹H NMR (400 MHz, MeOD) δ 8.25 (dd, *J* = 7.9, 1.0 Hz, 1H), 8.05 (d, *J* = 7.1 Hz, 1H), 8.00 (s, 1H), 7.90 (dt, *J* = 7.6, 1.1 Hz, 1H), 7.75 (dt,

$J = 7.6, 1.0$ Hz, 1H), 7.67 (m, 3H), 7.46 (m, 4H), 4.68 (m, 1H), 3.60 (s, 2H), 2.99 (s, 3H), 2.56 (m, 4H), 1.90 (m, 4H). $^{13}\text{C NMR}$ (101 MHz, MeOD) δ 165.3, 147.0, 141.6, 139.8, 138.6, 136.6, 132.4, 132.4, 130.7, 129.9 (2C), 129.0, 127.5(2C), 126.6, 123.6, 123.1, 119.5, 119.2, 88.8. (d, $^1J_{\text{CF}} = 179.8$ Hz, 1C), 62.1, 49.0 (d, $^3J_{\text{CF}} = 5.4$ Hz, 2C), 43.8, 30.8 (d, $^2J_{\text{CF}} = 19.8$ Hz, 2C). **Elemental analysis** (%) found: C, 68.12; H, 5.99; N, 5.98%. $\text{C}_{26}\text{H}_{27}\text{FN}_2\text{O}_2\text{S}$ requires C, 69.31; H, 6.03; N, 6.22%; **ES+HRMS** m/z 451.1844 $[\text{M}+\text{H}]^+$ $\text{C}_{26}\text{H}_{27}\text{FN}_2\text{O}_2\text{S}$ requires 450.18.

Preparation of 2-(methylsulfinyl)-*N*-(4'-(trifluoromethoxy)-[1,1'-biphenyl]-3-yl)benzamide **3f**

The general procedure (**1**) was followed using 4-(trifluoromethoxy)-benzene boronic acid to give **3f** as a cream-brown crystalline solid in 83.6% yield. **Rf** = 0.26 (8:2 EtOAc:hexane). $^1\text{H NMR}$ (400 MHz, MeOD) δ 8.13 (dd, $J = 8.0, 0.9$ Hz, 1H), 7.93 (dd, $J = 7.7, 0.7$ Hz, 1H), 7.90 (s, 1H), 7.78 (td, $J = 7.8, 1.2$ Hz, 1H), 7.64 (br d, $J = 11.5$, Hz, 3H), 7.59 (dt, $J = 7.5, 1.8$ Hz, 1H), 7.41 – 7.32 (m, 2H), 7.27 (d, $J = 8.0$ Hz, 2H), 2.87 (s, 3H); $^{13}\text{C NMR}$ (101 MHz, MeOD) δ 165.3, 148.7, 147.0, 140.4, 139.8, 138.7, 132.4, 132.4, 130.7, 129.2, 128.33 (2C), 127.6, 123.6, 123.2, 121.0 (2C), 120.6 (q, $^1J_{\text{CF}} = 255.4$ Hz, 1C), 112.0, 119.2, 43.8; **Elemental analysis** (%) found: C, 59.58; H, 3.81; N, 3.13%. $\text{C}_{21}\text{H}_{16}\text{F}_3\text{NO}_3\text{S}$ requires C, 60.14; H, 3.85; N, 3.34%; **ES+HRMS** m/z 442.0710 $[\text{M}+\text{Na}]^+$ $\text{C}_{21}\text{H}_{16}\text{F}_3\text{NO}_3\text{S}$ requires 419.08.

Preparation of 2-(methylsulfinyl)-*N*-(3-(thiophen-3-yl)phenyl)benzamide **3g**



The general procedure (**1**) was followed using 3-thienylboronic acid to give **3g** as a fine orange-brown solid in 88.7% yield. **Rf** = 0.17 (8:2 EtOAc:hexane). $^1\text{H NMR}$ (400 MHz, MeOD) δ 8.26 (dd, $J = 8.0, 0.9$ Hz, 1H), 8.05 (dd, $J = 7.7, 0.8$ Hz, 1H), 8.02 (t, $J = 1.7$ Hz, 1H), 7.91 (td, $J = 7.5, 1.2$ Hz, 1H), 7.76 (td, $J = 7.6, 1.2$ Hz, 1H), 7.69 – 7.67 (m, 1H), 7.64 (dd, $J = 7.9, 1.3$ Hz, 1H), 7.55 – 7.48 (m, 3H), 7.44 (t, $J = 7.9$ Hz, 1H), 3.01 (s, 3H); $^{13}\text{C NMR}$ (101 MHz, MeOD) δ 165.3, 147.0, 141.7, 138.6, 136.6, 132.4, 132.4, 130.7, 129.0, 127.6, 126.0, 125.8, 123.6, 122.5, 120.3, 119.3, 118.5, 43.7; **ES+HRMS** m/z 364.0435 $[\text{M}+\text{Na}]^+$ $\text{C}_{18}\text{H}_{15}\text{NO}_2\text{S}_2$ requires 341.05.

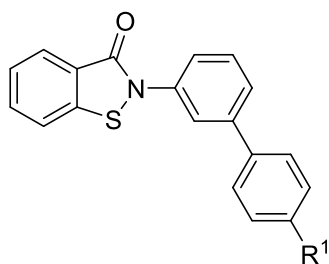
Preparation of methyl 3'-(2-(methylsulfinyl)benzamido)-[1,1'-biphenyl]-4-carboxylate **3h**

The general procedure (**1**) was followed using 4-(methoxycarbonyl)phenyl boronic acid and an extended reaction time of 2 days to give **3h** as a cream solid in 80.7% yield. **Rf** = 0.31 (8:2

EtOAc:hexane). $^1\text{H NMR}$ (400 MHz, DMSO) δ 10.69 (br s, 1H, NH), 8.21 (t, $J = 1.7$ Hz, 1H), 8.19 – 8.13 (m, 1H), 8.09 (d, $J = 8.5$ Hz, 1H), 7.98 (dd, $J = 7.6, 0.7$ Hz, 1H), 7.92 – 7.85 (m, 1H), 7.72 (d, $J = 8.5$ Hz, 1H), 7.72 (t, $J = 7.5$ Hz, 3H), 7.54 – 7.47 (m, 2H), 7.18 (t, $J = 8.0$ Hz, 1H), 3.89 (s, 3H), 2.84 (s, 3H); **ES+MS** m/z 416.1 $[\text{M}+\text{Na}]^+$ $\text{C}_{221}\text{H}_{19}\text{NO}_4\text{S}$ requires 393.10.

Preparation of benzo[*d*]isothiazol-3(2*H*)-ones 8-12

General procedure (2)



4	$\text{R}^1 = \text{OCH}_3$
5	$\text{R}^1 = \text{Cl}$
6	$\text{R}^1 = \text{CF}_3$
15	$\text{R}^1 = $
14	$\text{R}^1 = $
7	$\text{R}^1 = \text{OCF}_3$
10	$\text{R}^1 = $ (D ring)
8	$\text{R}^1 = \text{CO}_2\text{CH}_3$

Thionyl chloride (1.3 eq) was added dropwise to a stirring solution of the required biphenyl benzamide (**3a-h**, 1.0 eq) in dichloromethane (DCM) (15-20 ml) under a N_2 atmosphere. The solution was heated to reflux at 50°C for 1.5 hours. Solvent and excess thionyl chloride were removed under reduced pressure and the crude products purified by flash column chromatography.

Preparation of 2-(4'-methoxy-[1,1'-biphenyl]-3-yl)benzo[*d*]isothiazol-3(2*H*)-one 4

The general procedure (2) was followed using **3a** (0.56 mmol) to give **4** as a white-yellow crystalline solid in 58.4% yield. $\text{Rf} = 0.64$ (55:45 EtOAc:hexane). $^1\text{H NMR}$ (400 MHz, DMSO) δ 8.08 (d, $J = 8.1$ Hz, 1H), 7.98 (d, $J = 7.7$ Hz, 1H), 7.95 (d, $J = 1.7$ Hz, 1H), 7.78 (dt, $J = 8.2, 1.1$ Hz, 1H), 7.67 (d, $J = 8.8$ Hz, 2H), 7.65 – 7.56 (m, 3H), 7.53 (t, $J = 7.8$ Hz, 1H), 7.07 (d, $J = 8.8$ Hz, 2H) and 3.82 (s, 3H); $^{13}\text{C NMR}$ (101 MHz, DMSO) δ 163.9, 159.8, 141.6, 140.6, 138.2, 133.1, 132.0, 130.5, 128.4 (2C), 126.6, 126.5, 125.3, 124.8, 123.1, 122.7, 122.4, 115.0 (2C) and 55.7; **Elemental analysis** (%) found: C, 71.95; H, 4.47; N, 4.41; S, 9.77%. $\text{C}_{20}\text{H}_{15}\text{NO}_2\text{S}$ requires C, 72.05; H, 4.54; N, 4.20; S, 9.62%; **ES+HRMS** m/z 356.0712 $[\text{M}+\text{Na}]^+$ $\text{C}_{20}\text{H}_{15}\text{NO}_2\text{S}$ requires 333.08.

Preparation of 2-(4'-chloro-[1,1'-biphenyl]-3-yl)benzo[d]isothiazol-3(2H)-one **5**

The general procedure (**2**) was followed using **3b** (0.46 mmol) to give **5** as a white crystalline solid in 52.2% yield. **Rf** = 0.06 (8:2 EtOAc:hexane). **¹H NMR** (500 MHz, DMSO) δ 8.08 (dt, J = 8.1, 0.8 Hz, 1H), 8.02 (t, J = 2.1, 1H), 7.98 (ddd, J = 7.8, 1.3, 0.7 Hz, 1H), 7.79 (dt, J = 8.4, 1.3 Hz, 1H), 7.75 (dt, J = 8.7, 2.1 Hz, 2H), 7.71 – 7.67 (m, 2H), 7.64 (t, J = 7.9 Hz, 1H), 7.57 (dt, J = 8.7, 2.4 Hz 2H), 7.53 (dt, J = 8.0, 1.0 Hz, 1H); **¹³C NMR** (101 MHz, DMSO) δ 163.9, 140.6, 140.6, 138.5, 138.3, 133.4, 133.2, 130.7, 129.5 (2C), 129.1 (2C), 126.7, 126.6, 125.8, 124.7, 124.2, 123.2, 122.4. **Elemental analysis** (%) found: C, 67.03; H, 3.62; N, 4.13; S, 8.91%. C₁₉H₁₂ClNOS requires C, 67.55; H, 3.58; N, 4.15; S, 9.49%; **ES+HRMS** m/z 360.0215 [M+Na]⁺ C₁₉H₁₂ClNOS requires 337.03.

Preparation of 2-(4'-(trifluoromethyl)-[1,1'-biphenyl]-3-yl)benzo[d]isothiazol-3(2H)-one **6**

The general procedure (**2**) was followed using **3c** (0.43 mmol) to give **6** as a white crystalline solid in 73.6% yield. **Rf** = 0.06 (8:2 EtOAc:hexane). **¹H NMR** (500 MHz, DMSO) δ 8.11 – 8.07 (m, 2H), 7.99 (ddd, J = 7.8, 1.3, 0.7 Hz, 1H), 7.97 (d, J = 8.2 Hz, 2H), 7.87 (d, J = 8.2 Hz, 2H), 7.79 (dt, J = 8.3, 1.3 Hz, 1H), 7.78 – 7.74 (m, 2H), 7.69 (t, J = 8.0 Hz, 1H), 7.54 (ddd, J = 8.0, 1.0 Hz, 1H); **¹³C NMR** (101 MHz, DMSO) δ 163.5, 143.7, 140.6, 140.3, 138.4, 133.2, 130.8, 128.8 (d, $^2J_{CF}$ = 31.7 Hz, 1C), 128.2 (2C), 126.7, 126.6, 126.4 (d, $^3J_{CF}$ = 3.7 Hz, 2C), 126.1, 124.8 (d, $^1J_{CF}$ = 272.0 Hz, 1C), 124.8, 124.7, 123.6, 122.5; **Elemental analysis** (%) found: C, 62.68; H, 3.22; N, 3.19%. C₂₀H₁₂F₃NOS requires C, 64.68; H, 3.26; N, 3.77; **ES+HRMS** m/z 394.0492 [M+Na]⁺ C₂₀H₁₂F₃NOS requires 371.06.

Preparation of 2-(4'-((4-methylpiperazin-1-yl)methyl)-[1,1'-biphenyl]-3-yl)benzo[d]isothiazol-3(2H)-one **15**

The general procedure (**2**) was followed using **3d** (0.549 mmol) to give **15** as an off-white solid in 58.0% yield. **Rf** = 0.12 (10:90 MeOH:EtOAc). **¹H NMR** (400 MHz, MeOD) δ 8.07 (d, J = 7.9 Hz, 1H), 7.96 (s, 1H), 7.89 (d, J = 8.1 Hz, 1H), 7.79 (t, J = 7.5 Hz, 1H), 7.69-7.62 (m, 5H), 7.55 (t, J = 7.6 Hz, 1H), 7.47 (d, J = 7.6 Hz, 2H), 3.61 (s, 2H, CH₂), 2.90-2.22 (br s, 8H), 2.33 (s, 3H, CH₃). **¹³C NMR** (101 MHz, MeOD) δ 164.8, 142.3, 140.8, 139.0, 137.4, 136.9, 132.6, 129.9 (2C), 129.7, 126.7 (2C), 126.1, 125.9, 125.9, 124.2, 123.6, 123.3, 120.8, 61.9, 54.2 (2C), 52.0 (2C), 44.5; **ES+HRMS** m/z 416.1810 [M+H]⁺ C₂₅H₂₅N₃OS requires 415.17.

Preparation of 2-(4'-((4-fluoropiperidin-1-yl)methyl)-[1,1'-biphenyl]-3-yl)benzo[d]isothiazol-3(2H)-one **14**

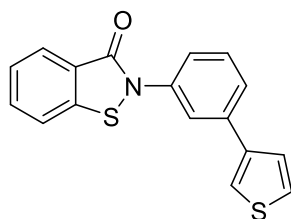
The general procedure (**2**) was followed using **3e** (0.44 mmol) to give **14** as an off-white fine crystalline solid in 70.0% yield. **Rf** = 0.49 (5:95 MeOH:EtOAc). **¹H NMR** (400 MHz, DMSO) δ 8.08 (d, J = 8.1 Hz, 1H),

8.02-7.95 (m, 2H), 7.78 (t, $J = 7.7$ Hz, 1H), 7.71-7.59 (m, 5H), 7.53 (t, $J = 7.6$ Hz, 1H), 7.43 (d, $J = 7.8$ Hz), 4.69 (d, $J = 50.9$ Hz, 1H), 3.52 (s, 2H), 2.60-2.25 (m, 4H), 1.95-1.85 (m, 4H); $^{13}\text{C NMR}$ (101 MHz, DMSO) δ 163.9, 141.7, 140.6, 138.8, 138.3, 138.2, 133.2, 130.6, 130.0 (2C), 127.1 (2C), 126.7, 126.5, 125.7, 124.8, 123.7, 123.1, 122.4, 89.0 (d, $^1J_{\text{CF}} = 169.8$ Hz, 1C), 61.91, 49.53 (d, $^3J_{\text{CF}} = 6.0$ Hz, 2C), 31.63 (d, $^2J_{\text{CF}} = 19.0$ Hz, 2C); **Elemental analysis** (%) found: C, 71.47; H, 5.56; N, 6.62%. $\text{C}_{25}\text{H}_{23}\text{FN}_2\text{OS}$ requires C, 71.75; H, 5.54; N, 6.69; S, 7.66%; **ES+HRMS** m/z 419.1603 $[\text{M}+\text{H}]^+$ $\text{C}_{25}\text{H}_{23}\text{FN}_2\text{OS}$ requires 418.15.

Preparation of **2-(4'-(trifluoromethoxy)-[1,1'-biphenyl]-3-yl)benzo[d]isothiazol-3(2H)-one 7**

The general procedure (**2**) was followed using **3f** (0.43 mmol) to give **7** as an off-white crystalline solid in 87.2% yield. **Rf** = 0.05 (8:2 EtOAc:hexane). $^1\text{H NMR}$ (400 MHz, MeOD) δ 8.06 (d, $J = 7.9$ Hz, 1H), 7.98 (t, $J = 1.7$ Hz, 1H), 7.88 (d, $J = 8.2$ Hz, 1H), 7.83 – 7.74 (m, 3H), 7.71 – 7.67 (m, 2H), 7.63 (t, $J = 7.73$ Hz, 1H), 7.55 (td, $J = 8.0, 0.9$ Hz, 1H), 7.40 (d, $J = 8.0$ Hz, 2H); $^{13}\text{C NMR}$ (101 MHz, MeOD) δ 164.8, 149.0, 141.1, 140.7, 138.9, 137.5, 132.6, 129.8, 128.5 (2C), 126.1, 126.0, 125.9, 124.2, 124.0, 123.5, 121.1 (2C), 120.74, 120.6 (q, $^1J_{\text{CF}} = 255.7$ Hz, 1C); **Elemental analysis** (%) found: C, 60.75; H, 3.37; N, 3.33%. $\text{C}_{20}\text{H}_{12}\text{F}_3\text{NO}_2\text{S}$ requires C, 62.01; H, 3.12; N, 3.62%; **CI+HRMS** m/z 388.0606 $[\text{M}+\text{H}]^+$ $\text{C}_{20}\text{H}_{12}\text{F}_3\text{NO}_2\text{S}$ requires 387.05.

Preparation of **2-(3-(thiophen-3-yl)phenyl)benzo[d]isothiazol-3(2H)-one 10**

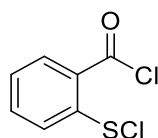


The general procedure (**2**) was followed using **3g** (0.49 mmol) to give **10** as a yellow-cream solid in 85.7% yield. **Rf** = 0.63 (55:45 EtOAc:hexane). $^1\text{H NMR}$ (400 MHz, DMSO) δ 8.07 (d, $J = 8.1$ Hz, 1H), 8.04 – 8.00 (m Hz, 1H), 8.00 – 7.96 (m, 2H), 7.79 (ddd, $J = 8.0, 7.2, 1.2$ Hz, 1H), 7.76 – 7.72 (m, 1H), 7.69 (dd, $J = 5.0, 2.9$ Hz, 1H), 7.61 (dd, $J = 5.1, 1.3$ Hz, 1H), 7.60 – 7.57 (m, 2H), 7.56 – 7.50 (td, $J = 8.0, 0.9$ Hz, 1H); $^{13}\text{C NMR}$ (101 MHz, DMSO) δ 163.8, 140.8, 140.6, 138.0, 136.7, 133.0, 130.4, 127.8, 126.6, 126.5, 126.4, 125.2, 124.6, 123.8, 122.8, 122.4, 122.3; **ES+HRMS** m/z 332.0170 $[\text{M}+\text{Na}]^+$ $\text{C}_{17}\text{H}_{11}\text{NOS}_2$ requires 309.03; **HPLC** (purity analysis %) found: 96.73%; RT: 7.90 min/ 40 min (25/75, 0.5 ml/min IPA:HEXANE, Signal = 230 nm, SYNCHROSILICA).

Preparation of methyl 3'-(3-oxobenzo[*d*]isothiazol-2(3*H*)-yl)-[1,1'-biphenyl]-4-carboxylate **8**

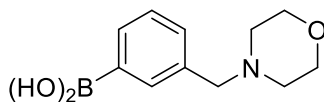
The general procedure (**2**) was followed using **3h** (0.49 mmol) to give **8** as a yellow-cream solid in 31.0% yield. $R_f = 0.32$ (30:70 EtOAc:hexane). $^1\text{H NMR}$ (400 MHz, DMSO) δ 8.08 (br d, $J = 8.5$ Hz, 4H), 7.98 (d, $J = 7.8$ Hz, 1H), 7.89 (d, $J = 7.8$ Hz, 2H), 7.82 – 7.71 (m, 3H), 7.67 (t, $J = 7.7$ Hz, 1H), 7.53 (t, $J = 7.5$ Hz, 1H), 3.89 (s, 3H); $^{13}\text{C NMR}$ (101 MHz, DMSO) δ 166.5, 163.9, 144.1, 140.6, 140.5, 138.4, 133.2, 130.8, 130.4 (2C), 129.4, 127.7 (2C), 126.7, 126.6, 126.0, 124.7 (2C), 123.5, 122.5, 52.7; **Elemental analysis** (%) found: C, 69.44; H, 4.21; N, 3.87; S, 8.90%. $\text{C}_{21}\text{H}_{15}\text{NO}_3\text{S}$ requires C, 69.79; H, 4.18; N, 3.88; S, 8.87%; **CI+HRMS** m/z 362.0838 $[\text{M}+\text{H}]^+$ $\text{C}_{21}\text{H}_{15}\text{NO}_3\text{S}$ requires 361.08.

Preparation of 2-(chlorothio)-benzoyl chloride **X**



Thionyl chloride (22.8 mmol, 7 eq) and *N,N*-dimethylformamide (3 drops) were added to a solution of 2,2'-dithiobenzoic acid (3.26 mmol) in anhydrous dichloroethane (25 ml) under a N_2 atmosphere at room temperature. The stirring solution was heated to reflux at 80°C for 1.5 hours. Sulfuryl chloride (4.24 mmol, 1.3 eq) was added to the cooled solution at 25°C before heating the solution to 50°C for 45 minutes. Solvent, excess thionyl chloride and excess sulfuryl chloride were removed under reduced pressure to generate **X**, a yellow-green solid as pure product in quantitative yield. $R_f = 0.79$ (50:50 EtOAc:hexane). $^1\text{H NMR}$ (400 MHz, CDCl_3) δ 8.34 (dd, $J = 8.0, 1.2$ Hz, 1H), 7.93 (dd, $J = 8.2, 0.4$ Hz, 1H), 7.77 (dt, $J = 8.5, 1.3$ Hz, 1H), 7.42 (dt, $J = 8.0, 0.8$ Hz, 1H); $^{13}\text{C NMR}$ (101 MHz, CDCl_3) δ 169.5, 146.1, 135.8, 134.7, 127.4, 125.8, 124.4.

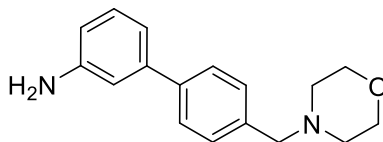
Preparation of (4-(morpholinomethyl)phenyl)boronic acid **11a**



Morpholine (5.56 mmol, 2.0 eq) and *N,N*-diisopropylethylamine (6.98 mmol, 2.5 eq) were added to a stirring solution of 4-methylbromophenyl boronic acid (2.79 mmol) in anhydrous THF (25 ml) under a N_2 atmosphere. The solution was stirred at room temperature for 18 hours before being quenched with brine (30 ml) and extracted into EtOAc (3 x 30 ml). The combined organic extracts were dried over MgSO_4 , filtered and concentrated under reduced pressure to give **11a** as a pale orange solid in 87.0% yield which was used as crude in the following step. $R_f = 0.08$ (100% EtOAc and 1%

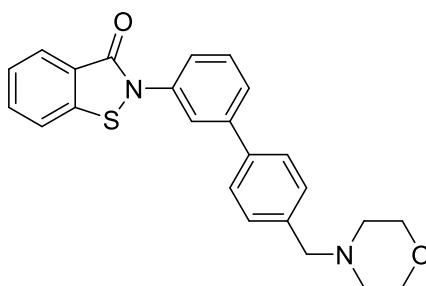
triethylamine). $^1\text{H NMR}$ (400 MHz, MeOD) δ 7.50 (s, 2H), 7.21 (d, $J = 7.9$ Hz, 2H), 3.58 (t, $J = 4.6$ Hz, 4H), 3.43 (s, 2H, CH_2), 2.37 (br s, 4H).

Preparation of 4'-(morpholinomethyl)-[1,1'-biphenyl]-3-amine **11b**



To a solution of K_2CO_3 (6.20 mmol, 3.3 eq), **11a** (2.25 mmol, 1.2 eq) and $\text{Pd}(\text{PPh}_3)_4$ (0.0047 mmol, 0.025 eq) in water (5 ml), 3-bromoaniline (1.88 mmol, 1.0 eq) was added. The stirring reaction was evacuated and purged with N_2 before the addition of anhydrous THF (10 ml) and heating to 80°C for 22 hours. The solution was quenched with brine (50 ml), extracted into EtOAc (3 x 35 ml) and the combined organic extracts dried over MgSO_4 before concentrating under reduced pressure. The crude product was purified by flash column chromatography to give **11b** as a pale yellow-brown oil in 91.0% yield. $\text{Rf} = 0.22$ (100% EtOAc and 1% triethylamine). $^1\text{H NMR}$ (400 MHz, CDCl_3) δ 7.52 (d, $J = 8.2$ Hz, 2H), 7.37 (d, $J = 8.2$ Hz, 2H), 7.22 (t, $J = 7.8$ Hz, 1H), 6.99 (d, $J = 8.0$ Hz, 1H), 6.90 (t, $J = 2.0$ Hz, 1H), 6.68 (ddd, $J = 7.9, 2.3, 0.8$ Hz, 1H), 3.73 (t, $J = 4.6$ Hz, 4H), 3.53 (s, 2H), 2.48 (m, $J = 4.2$ Hz, 4H). $^{13}\text{C NMR}$ (101 MHz, MeOD) δ 147.7, 141.6, 140.7, 135.7, 129.6 (2C), 129.1, 126.4 (2C), 116.6, 114.3, 113.6, 66.3 (2C), 62.6, 53.2 (2C); **CI+HRMS** m/z 269.1650 $[\text{M}+\text{H}]^+$ $\text{C}_{17}\text{H}_{20}\text{N}_2\text{O}$ requires 268.16.

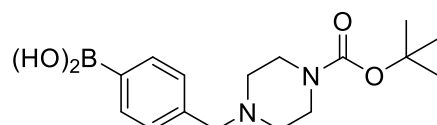
Preparation of 2-(4'-(morpholinomethyl)-[1,1'-biphenyl]-3-yl)benzo[d]isothiazol-3(2H)-one **13**



To a solution of **11b** (1.59 mmol, 1.0 eq) in DCM, 2-(chlorothio)-benzoyl chloride (1.9 mmol, 1.2 eq) was added at 0°C under a N_2 atmosphere. Et_3N (5.24 mmol, 3.3 eq) was added to the solution which was allowed to warm to room temperature and stirred for 20 hours. The solution was quenched with brine (40 ml), extracted into EtOAc (3 x 50 ml) and the combined organic extracts dried over MgSO_4 before concentrating under reduced pressure. The crude product was purified by flash column chromatography to give **13** as a yellow crystalline solid in 79.0% yield. $\text{Rf} = 0.15$ (80:20 EtOAc:hexane and 1% triethylamine). $^1\text{H NMR}$ (400 MHz, MeOD) δ 8.05 (d, $J = 7.9$ Hz, 1H), 7.94 (t, $J = 1.7$ Hz, 1H), 7.87 (d, $J = 8.2$ Hz, 1H), 7.77 (dt, $J = 7.2, 1.1$ Hz, 1H), 7.68-7.62 (m, 4H), 7.59 (d, $J = 7.6$ Hz, 1H), 7.54 (dt,

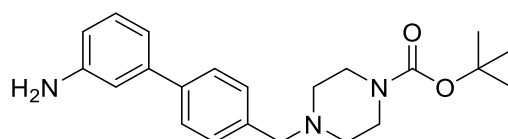
$J = 7.9, 0.8$ Hz, 1H), 7.46 (d, $J = 8.2$ Hz, 2H), 3.71 (t, $J = 4.7$ Hz, 4H), 3.57 (s, 2H), 2.49 (br s, 4H); $^{13}\text{C NMR}$ (101 MHz, MeOD) δ 164.8, 142.2, 140.7, 138.9, 137.4, 136.8, 132.6, 129.9 (2C), 129.7, 126.7 (2C), 126.1, 125.8, 125.8, 124.2, 123.5, 123.3, 120.7, 66.3 (2C), 62.5, 53.2 (2C). **Elemental analysis** (%) found: C, 71.34; H, 5.57; N, 6.78; S, 7.64%. $\text{C}_{24}\text{H}_{22}\text{N}_2\text{O}_2\text{S}$ requires C, 71.62; H, 5.51; N, 6.96; S, 7.97%; **ES+HRMS** m/z 403.1491 $[\text{M}+\text{H}]^+$ $\text{C}_{24}\text{H}_{22}\text{N}_2\text{O}_2\text{S}$ requires 402.14.

Preparation of **4-((4-(tert-butoxycarbonyl)piperazin-1-yl)methyl)phenyl)boronic acid 12a**



To a solution of 4-bromomethyl benzene boronic acid (1.0 g, 4.65 mmol) in a solution of anhydrous THF (20 ml) under a N_2 atmosphere, 1-Boc-piperazine (2.0 eq, 9.31 mmol) was added, followed by $i\text{Pr}_2\text{EtN}$ (2.5 eq, 2.1 ml). The N_2 atmosphere was restored and the resulting solution allowed to stir overnight at room temperature. The solution was quenched with brine (50 ml) and the organic layer extracted into EtOAc (3 x 40 ml). The combined organic extracts were then dried with MgSO_4 and concentrated *in vacuo*. The crude product was purified by flash column chromatography to give **12a** as a clear viscous oil in a 53.0% yield. $R_f = 0.68$ (5:95 MeOH:EtOAc and 1% triethylamine with permanganate stain). **$^1\text{H NMR}$** (400 MHz, MeOD) δ 7.68 (br s, 2H), 7.30 (d, $J = 7.8$ Hz, 2H), 3.54 (s, 2H), 3.43 (t, $J = 4.4$ Hz, 4H), 2.42 (t, $J = 5.0$ Hz, 4H), 1.46 (s, 9H); **$^{13}\text{C NMR}$** (101 MHz, MeOD) δ 155.0, 133.4 (2C), 128.3 (4C), 79.9, 62.6, 46.2 (2C), 43.5, 42.6, 27.2 (3C).

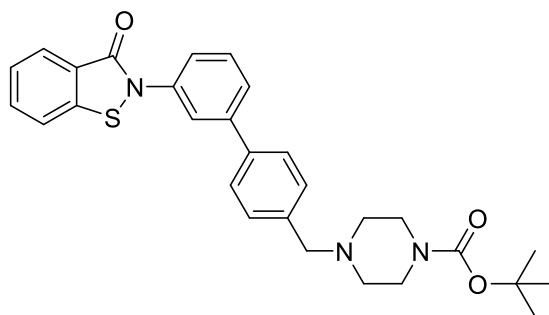
Preparation of **tert-butyl 4-((3'-amino-[1,1'-biphenyl]-4-yl)methyl)piperazine-1-carboxylate 12b**



To a solution of Na_2CO_3 (0.53 g, 5.02 mmol, 2.1 eq), **12a** (0.77g, 2.39 mmol) and $\text{Pd}(\text{PPh}_3)_4$ (0.069 g, 0.060 mmol, 0.025 eq) in DME:water (15:7.5 ml), 3-bromoaniline (0.27 ml, 2.63 mmol, 1.1 eq) was added. The stirring solution was evacuated and purged with N_2 before heating to 90°C for 18 hours. The solution was concentrated under reduced pressure to remove DME. The crude material was then quenched with brine (20 ml) and organic layer extracted into EtOAc (2 x 30 ml), dried over MgSO_4 and concentrated under reduced pressure. The crude product was purified by flash column chromatography to give **12b** as a yellow-brown visocus oil in a 96.7% yield. $R_f = 0.51$ (100% EtOAc and 1% triethylamine). **$^1\text{H NMR}$** (400 MHz, CDCl_3) δ 7.52 (d, $J = 8.1$ Hz, 2H), 7.36 (d, $J = 8.1$ Hz, 2H), 7.22 (t,

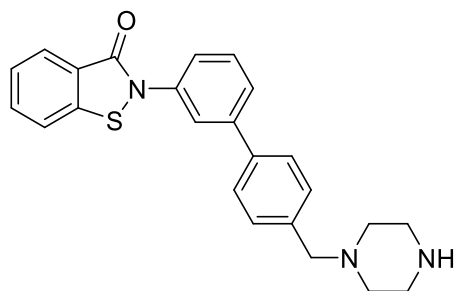
$J = 7.8$ Hz, 1H), 6.99 (d, $J = 7.7$ Hz, 1H), 6.90 (s, 1H), 6.68 (dd, $J = 7.9, 1.7$ Hz, 1H), 3.54 (s, 2H), 3.44 (t, $J = 4.6$ Hz, 4H), 2.42 (s, 4H), 1.46 (s, 9H); **13C NMR** (101 MHz, CDCl₃) δ 154.8, 146.7, 142.1, 140.3, 136.8, 129.7, 129.5 (2C), 127.0 (2C), 117.6, 114.1, 113.8, 79.6, 62.8, 52.9 (2C), 44.1 (2C), 28.4 (3C); **ES+HRMS** m/z 368.2327 [M+H]⁺ C₂₂H₂₉N₃O₂ requires 367.23.

Preparation of **tert-butyl 4-((3'-(3-oxobenzo[d]isothiazol-2(3H)-yl)-[1,1'-biphenyl]-4-yl)methyl)piperazine-1-carboxylate 12c**



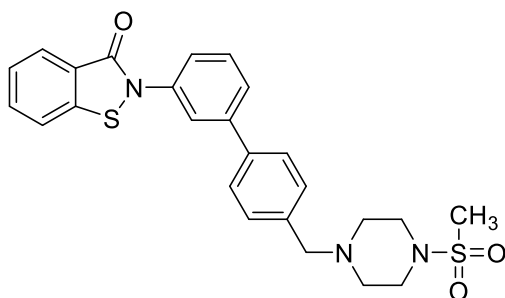
To a solution of **12b** (0.85 g, 2.31 mmol) in DCM, **X** (1.2 eq, 2.77 mmol) was added at 0°C under a N₂ atmosphere. Et₃N (4.5 eq, 9.24 mmol) was added to the solution which was allowed to gradually warm to room temperature and stir for 20 hours. The solution was quenched with NaHCO₃ (30 ml) and the organic layer extracted into DCM (3 x 30 ml). The combined organic extracts were then washed with brine (30 ml), dried over MgSO₄ and concentrated under reduced pressure. The crude product was purified by flash column chromatography to give **12c** as a yellow-orange foam in a 61.7% yield. **R_f** = 0.68 (100% EtOAc and 1% triethylamine). **1H NMR** (400 MHz, DMSO) δ 8.09 (d, $J = 8.1$ Hz, 1H), 8.00 (t, $J = 1.8$ Hz, 1H), 7.98 (d, $J = 7.7$ Hz, 1H), 7.79 (td, $J = 8.3, 1.2$ Hz, 1H), 7.71 – 7.65 (m, 4H), 7.62 (t, $J = 7.5$ Hz, 1H), 7.53 (td, $J = 7.9, 0.7$ Hz, 1H), 7.43 (d, $J = 8.2$ Hz, 2H), 3.53 (s, 2H), 3.33 (br s, 4H), 2.34 (d, $J = 4.8$ Hz, 4H), 1.39 (s, 9H); **13C NMR** (101 MHz, DMSO) δ 163.9, 154.3, 141.7, 140.6, 138.4, 138.3, 138.2, 133.1, 130.6, 130.1 (2C), 127.2 (2C), 126.7, 126.5, 125.7, 124.8, 123.7, 123.1, 122.5, 79.2, 65.4, 52.9 (2C), 44.1 (2C), 28.5 (3C); **ES+HRMS** m/z 524.1982 [M+Na]⁺ C₂₉H₃₁N₃O₃S requires 501.21.

Preparation of **2-(4'-(piperazin-1-ylmethyl)-[1,1'-biphenyl]-3-yl)benzo[d]isothiazol-3(2H)-one 16**



To a solution of **12c** (0.69 g, 1.38 mmol) in DCM (8 ml) under a N₂ atmosphere, trifluoroacetic acid (TFA) (1.6 ml, 20.7 mmol, 15.0 eq) was added and allowed to stir at room temperature overnight. After this time, DCM and excess TFA were removed under reduced pressure. The crude material was quenched with NaHCO₃ and the organic layer extracted into DCM (3 x 40 ml), washed with brine (40 ml), dried with MgSO₄ and concentrated *in vacuo* to give **16** as a yellow solid in a 89.4% yield. **Rf** = 0.03 (5:95 MeOH:EtOAc and 1% triethylamine). **¹H NMR** (400 MHz, MeOD) δ 8.07 (d, J = 7.9 Hz, 1H), 7.97 (t, J = 1.8 Hz, 1H), 7.89 (d, J = 8.2 Hz, 1H), 7.79 (td, J = 7.2, 1.2 Hz, 1H), 7.68 (d, J = 8.2 Hz, 3H), 7.64 (t, J = 7.6 Hz, 2H), 7.56 (td, J = 8.0, 0.9 Hz, 1H), 7.47 (d, J = 8.2 Hz, 2H), 3.62 (s, 2H), 2.96 (t, J = 5.0 Hz, 4H), 2.56 (br s, 4H); **¹³C NMR** (101 MHz, CDCl₃) δ 164.2, 142.3, 139.9, 139.1, 137.7, 137.5, 132.5, 129.8, 129.7 (2C), 127.2, 127.2 (2C), 125.9, 125.7, 124.8, 123.3, 123.3, 120.1, 63.0, 53.1 (2C), 45.3 (2C); **ES+HRMS** m/z 402.1629 [M+H]⁺ C₂₄H₂₃N₃OS requires 401.16.

Preparation of **2-(4'-((4-(methylsulfonyl)piperazin-1-yl)methyl)-[1,1'-biphenyl]-3-yl)benzo[d]isothiazol-3(2H)-one 17**

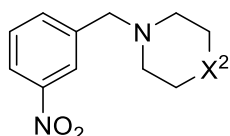


To a solution of **16** (0.10 g, 0.249 mmol) in DCM (8 ml) under a N₂ atmosphere at 0°C, methanesulfonyl chloride (0.03 ml, 0.299 mmol, 1.2 eq) and Et₃N (0.07 ml, 0.498 mmol, 2.0 eq) were added. The resulting solution was allowed to stir at 0°C for 4.5 hours. After this time, the crude material was diluted with brine and the organic layer extracted into DCM (2 x 40 ml), dried with MgSO₄ and concentrated *in vacuo*. The crude product was purified by flash column chromatography to give **17** as an off-white solid in a 65.7% yield. **Rf** = 0.73 (15:85 MeOH:EtOAc and 1% triethylamine). **¹H NMR** (400 MHz, MeOD) δ 8.07 (d, J = 7.8 Hz, 1H), 7.97 (t, J = 1.8 Hz, 1H), 7.89 (d, J = 8.2 Hz, 1H), 7.79 (td, J = 7.2,

1.1 Hz, 1H), 7.72 – 7.60 (m, 5H), 7.57 (td, $J = 7.9, 0.8$ Hz, 1H), 7.48 (d, $J = 8.2$ Hz, 2H), 3.65 (s, 2H), 3.26 (t, $J = 4.7$ Hz, 4H), 2.86 (s, 3H), 2.61 (t, $J = 4.8$ Hz, 4H); **¹³C NMR** (101 MHz, DMSO) δ 163.9, 141.7, 140.6, 138.5, 138.3, 138.2, 133.1, 130.6, 130.0 (2C), 127.2 (2C), 126.7, 126.5, 125.7, 124.8, 123.8, 123.1, 122.5, 61.6, 52.3 (2C), 46.0 (2C), 34.0; **Elemental analysis** (%) found: C, 61.05; H, 5.27; N, 8.51; S, 13.01%. $C_{25}H_{25}N_3O_3S_2$ requires C, 62.61; H, 5.25; N, 8.76; S, 13.37%; **ES+MS** m/z 502.1246 $[M+Na]^+$ $C_{25}H_{25}N_3O_3S_2$ requires 479.13.

Preparation of (3-nitrobenzyl) heterocycles **18a-i**, **18a-ii**

General procedure (3)



18a-i $X^2 = CHF$

18a-ii $X^2 = NCH_3$

To a solution of 3-nitrobenzyl bromide (0.8 g, 3.70 mmol) in a solution of anhydrous THF (15 ml) under a N_2 atmosphere, the appropriate heterocycle (2.0 eq, 7.41 mmol) was added, followed by iPr_2EtN (2.2 - 3.2 eq). The N_2 atmosphere was restored and the resulting solution allowed to stir overnight at room temperature. The solution was quenched with brine (50 ml) and the organic layer extracted into EtOAc (2 x 40 ml). The combined organic extracts were then dried with $MgSO_4$ and concentrated *in vacuo* to afford the crude product.

Preparation of 4-fluoro-1-(3-nitrobenzyl)piperidine **18a-i**

The general procedure (3) was followed using 4-fluoropiperidine hydrochloride. The resulting crude product was purified by flash column chromatography to give **18a-i** as a clear yellow oil in 72.7% yield. **Rf** = 0.66 (2:98 MeOH:EtOAc and 1% triethylamine). **¹H NMR** (400 MHz, $CDCl_3$) δ 8.21 (s, 1H), 8.11 (dd, $J = 8.2, 1.3$ Hz, 1H), 7.67 (d, $J = 7.6$ Hz, 1H), 7.49 (t, $J = 8.3$ Hz, 1H), 4.84 – 4.59 (dm, $^2J_{HF} = 48.6$ Hz, 1H), 2.67 – 2.50 (m, 2H), 2.50 – 2.31 (m, 2H), 2.01 – 1.80 (dm, $^3J_{HF} = 24.4$ Hz, 4H); **¹³C NMR** (101 MHz, $CDCl_3$) δ 148.4, 141.1, 134.8, 129.2, 123.6, 122.2, 88.2 (d, $J = 170.8$ Hz, 1C), 62.0, 49.5 (d, $J = 5.5$ Hz, 2C), 31.4 (d, $J = 19.6$ Hz, 2C); **CI+HRMS** m/z 239.1192 $[M+H]^+$ $C_{12}H_{15}FN_2O_2$ requires 238.11.

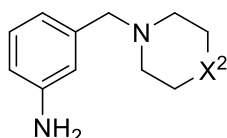
Preparation of 1-methyl-4-(3-nitrobenzyl)piperazine **18a-ii**

The general procedure (3) was followed using *N*-methylpiperazine. The resulting crude product was purified by trituration with Et_2O to give **18a-ii** as an off-white solid in 88.7% yield. **Rf** = 0.10 (5:95 MeOH:EtOAc and 1% triethylamine). **¹H NMR** (400 MHz, $CDCl_3$) δ 8.21 (s, 1H), 8.11 (dd, $J = 8.2, 1.5$ Hz, 1H), 7.67 (d, $J = 7.6$ Hz, 1H), 7.48 (t, $J = 7.9$ Hz, 1H), 3.60 (s, 2H), 2.49 (br s, 8H), 2.30 (s, 3H); **¹³C NMR**

(101 MHz, CDCl₃) δ 148.4, 140.8, 135.0, 129.1, 123.7, 122.2, 62.0, 55.1 (2C), 53.1 (2C), 46.0; **CI+HRMS** m/z 236.1393 [M+H]⁺ C₁₂H₁₇N₃O₂ requires 235.13.

Preparation of (3-aminobenzyl) heterocycles **18b-i**, **18b-ii**, **18b-iii**

General procedure (4)



18b-i (Purchased from Sigma Aldrich)	X ² = O
18b-ii	X ² = CHF
18b-iii	X ² = NCH ₃

To a solution of the appropriate (3-nitrobenzyl) heterocycle (**4i-5i**) in 50:50 EtOAc-MeOH (10 ml/mmol) 10% Pd/C (10% by mass) was added. The solution was placed under a H₂ atmosphere and allowed to stir overnight at room temperature. After this time, the solution was filtered through Celite under vacuum, the resulting material washed with 50:50 EtOAc-hexane and concentrated under reduced pressure. The crude products were purified by flash column chromatography.

Preparation of 3-((4-fluoropiperidin-1-yl)methyl)aniline **18b-ii**

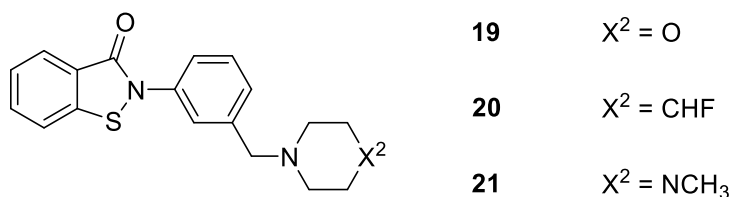
The general procedure (**4**) was followed using **18a-i** (0.6 g, 2.52 mmol) to give **18b-ii** as a white solid in 49.8% yield. **Rf** = 0.15 (EtOAc and 1% triethylamine). ¹H NMR (400 MHz, MeOD) δ 7.07 (t, J = 7.7 Hz, 1H), 6.72 (t, J = 1.7 Hz, 1H), 6.69 – 6.63 (m, 2H), 4.75 – 4.54 (dm, ²J_{HF} = 48.9 Hz, 1H), 3.43 (s, 2H), 2.68 – 2.50 (m, 2H), 2.52 – 2.32 (m, 2H), 2.00 – 1.73 (dm, ³J_{HF} = 25.1 Hz, 4H); ¹³C NMR (101 MHz, MeOD) δ 148.7, 139.3, 130.0, 120.6, 117.8, 115.7, 89.2 (d, J = 170.8 Hz, 1C), 64.1, 50.5 (d, J = 5.8 Hz, 2C), 32.17 (d, J = 19.8 Hz, 2C); **CI+HRMS** m/z 209.1450 [M+H]⁺ C₁₂H₁₇FN₂ requires 208.14.

Preparation of 3-((4-methylpiperazin-1-yl)methyl)aniline **18b-iii**

The general procedure (**4**) was followed using **18a-ii** (0.77 g, 3.29 mmol) to give **18b-iii** as a whitish-yellow solid in 62.1% yield. **Rf** = 0.14 (1:5 MeOH:EtOAc and 1% triethylamine). ¹H NMR (400 MHz, MeOD) δ 7.06 (t, J = 7.7 Hz, 1H), 6.72 (t, J = 1.6 Hz, 1H), 6.69 – 6.62 (m, 2H), 3.44 (s, 2H), 2.52 (br s, 8H), 2.30 (s, 3H); ¹³C NMR (101 MHz, MeOD) δ 148.8, 139.0, 130.0, 120.6, 117.8, 115.7, 64.0, 55.6 (2C), 53.5 (2C), 45.9; **CI+HRMS** m/z 206.1649 [M+H]⁺ C₁₂H₁₉N₃ requires 205.16.

Preparation of Mono-phenyl, methylene-linked saturated heterocyclic benzo[d]isothiazol-3(2H)-ones 19-21

General procedure (5)



To a solution of the appropriate (3-aminobenzyl) heterocycle (**18b-i** - **18b-iii**) (1.2 eq, 1.2 mmol) in DCM, 2-(chlorothio)-benzoyl chloride (**X**) (1.0 eq, 1.00 mmol) was added at 0°C under a N₂ atmosphere. Et₃N (3.3 eq, 3.3 mmol) was added to the solution which was allowed to gradually warm to room temperature and stir for 20 hours. The solution was quenched with NaHCO₃ (30 ml) and the organic layer extracted into DCM (3 x 30 ml). The combined organic extracts were then washed with brine (30 ml), dried over MgSO₄ and concentrated under reduced pressure. The crude products were purified by flash column chromatography.

Preparation of 2-(3-(morpholinomethyl)phenyl)benzo[d]isothiazol-3(2H)-one 19

The general procedure (5) was followed using **3-morpholine-4-yl methyl-phenylamine (18b-i)** (purchased from Sigma Aldrich) to give **19** as a bright yellow solid in 56.0% yield. *R_f* = 0.35 (2:98 MeOH:EtOAc and 1% triethylamine). ¹H NMR (400 MHz, CDCl₃) δ 8.11 (dd, *J* = 7.9, 0.8 Hz, 1H), 7.71 (s, 1H), 7.67 (td, *J* = 8.2, 1.2 Hz, 1H), 7.63 – 7.57 (m, 2H), 7.45 (td, *J* = 8.0, 1.0 Hz, 1H), 7.42 (t, *J* = 7.9 Hz, 1H), 7.29 (d, *J* = 7.7 Hz, 1H), 3.72 (t, *J* = 4.6 Hz, 4H), 3.56 (s, 2H), 2.48 (t, *J* = 4.5 Hz, 4H); ¹³C NMR (101 MHz, CDCl₃) δ 164.1, 139.9, 139.6, 137.3, 132.4, 129.2, 127.7, 127.2, 125.8, 125.1, 124.9, 123.3, 120.1, 67.0 (2C), 63.0, 53.6 (2C); **Elemental analysis** (%) found: C, 65.89; H, 5.63; N, 8.47; S, 9.65%; C₁₈H₁₈N₂O₂S requires C, 66.23; H, 5.66; N, 8.58; S, 9.82%; **CI+HRMS** *m/z* 327.1165 [M+H]⁺ C₁₈H₁₈N₂O₂S requires 326.11.

Preparation of 2-(3-((4-fluoropiperidin-1-yl)methyl)phenyl)benzo[d]isothiazol-3(2H)-one 20

The general procedure (5) was followed using **18b-ii** to give **20** as a yellow crystalline solid in 68.2% yield. *R_f* = 0.28 (100% EtOAc). ¹H NMR (400 MHz, MeOD) δ 8.04 (d, *J* = 7.9 Hz, 1H), 7.87 (d, *J* = 8.2 Hz, 1H), 7.77 (td, *J* = 7.2, 1.1 Hz, 1H), 7.70 (s, 1H), 7.62 (d, *J* = 8.0 Hz, 1H), 7.54 (td, *J* = 7.9, 0.7 Hz, 1H), 7.51 (t, *J* = 7.9 Hz, 1H), 7.39 (d, *J* = 7.6 Hz, 1H), 4.77 – 4.58 (dm, ²*J*_{HF} = 48.8 Hz, 1H), 3.62 (s, 2H), 2.79 – 2.56 (m, 2H), 2.57 – 2.33 (m, 2H), 2.02 – 1.78 (dm, ³*J*_{HF} = 25.5 Hz, 4H); ¹³C NMR (101 MHz, MeOD) δ 164.7, 140.7, 139.4, 136.9, 132.5, 129.1, 128.4, 126.1, 125.8, 125.7, 124.2, 123.8, 120.7, 87.7 (d, *J* = 171.3 Hz,

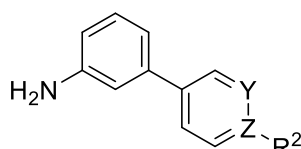
1C), 61.9, 49.1 (d, $J = 5.9$ Hz, 2C), 30.9 (d, $J = 19.7$ Hz, 2C). **Elemental analysis** (%) found: C, 66.39; H, 5.63; N, 8.13; S, 9.52%; $C_{19}H_{19}FN_2OS$ requires C, 66.64; H, 5.59; N, 8.18; S, 9.36%; **ES+HRMS** m/z 343.1283 $[M+H]^+$ $C_{19}H_{19}FN_2OS$ requires 342.12.

Preparation of **2-(3-((4-methylpiperazin-1-yl)methyl)phenyl)benzo[d]isothiazol-3(2H)-one 21**

The general procedure (5) was followed using **18b-iii** to give **21** as a yellow-brown solid in 64.5% yield. **Rf** = 0.10 (1:5 MeOH:EtOAc and 1% triethylamine). **1H NMR** (400 MHz, MeOD) δ 8.05 (d, $J = 7.9$ Hz, 1H), 7.88 (d, $J = 8.2$ Hz, 1H), 7.78 (td, $J = 7.2, 1.2$ Hz, 1H), 7.71 (s, 1H), 7.62 (d, $J = 8.0$ Hz, 1H), 7.58 – 7.48 (m, 2H), 7.40 (d, $J = 7.6$ Hz, 1H), 3.64 (s, 2H), 2.56 (br s, 8H), 2.31 (s, 3H); **^{13}C NMR** (101 MHz, MeOD) δ 164.7, 140.7, 139.2, 136.9, 132.5, 129.1, 128.3, 126.1, 125.8, 125.6, 124.2, 123.8, 120.8, 61.7, 54.3 (2C), 52.0 (2C), 44.5; **Elemental analysis** (%) found: C, 66.60; H, 6.27; N, 12.27; S, 9.12%; $C_{19}H_{21}N_3OS$ requires C, 67.23; H, 6.24; N, 12.38; S, 9.45%; **CI+HRMS** m/z 340.1480 $[M+H]^+$ $C_{19}H_{21}N_3OS$ requires 339.14.

Preparation of 3-pyridinyl anilines **22a-d**

General procedure (6)



- 22a** Y = C, X = N
22b Y = N, X = C, $R^2 = OCH_3$
22c Y = N, X = C, $R^2 = Cl$
22d Y = N, X = C, $R^2 = CF_3$

The appropriate pyridinyl boronic acid (1.5 eq) was combined with 3-bromo aniline in a solution of DME (15 ml) at room temperature. Na_2CO_3 (2.1 eq) and $Pd(PPh_3)_4$ (0.03 eq) in water (3 ml) (giving a 1:5 H_2O :DME ratio) were added to the stirring solution which was evacuated and purged with N_2 before refluxing at $90^\circ C$ for 18 hours. Solvent was removed under reduced pressure and the crude material re-suspended in DCM (40 ml), dried over $MgSO_4$ and concentrated under reduced pressure. The crude products were purified by flash column chromatography.

Preparation of **3-(pyridin-4-yl)aniline 22a**

The general procedure (6) was followed using 4-pyridinyl phenyl boronic acid (0.4 g, 3.25 mmol) to give **22a** as a white solid in 97.3% yield. **Rf** = 0.14 (7:3 EtOAc:hexane). **1H NMR** (400 MHz, MeOD) δ 8.55 (d, $J = 4.6$ Hz, 1H), 8.55 (d, $J = 4.6$ Hz, 1H), 7.68 (d, $J = 4.6$ Hz, 1H), 7.67 (d, $J = 4.6$ Hz, 1H), 7.25 (t, $J = 7.8$ Hz, 1H), 7.09 (t, $J = 1.9$ Hz, 1H), 7.05 (ddd, $J = 7.6, 1.5, 0.9$ Hz, 1H), 6.83 (ddd, $J = 8.0, 2.2, 0.9$ Hz,

1H); ^{13}C NMR (101 MHz, MeOD) δ 150.0, 148.9 (2C), 148.5, 138.2, 129.6, 121.7 (2C), 116.0, 116.0, 113.1; **CI+HRMS** m/z 171.0920 $[\text{M}+\text{H}]^+$ $\text{C}_{11}\text{H}_{10}\text{N}_2$ requires 170.08.

Preparation of **3-(6-methoxypyridin-3-yl)aniline 22b**

The general procedure (**6**) was followed using 6-methoxy-3-pyridinyl phenyl boronic acid (0.5 g, 3.27 mmol) to give **22b** as a yellow-brown oil solid in 70.5% yield. **Rf** = 0.54 (7:3 EtOAc:hexane). ^1H NMR (400 MHz, CDCl_3) δ 8.36 (d, J = 2.5 Hz, 1H), 7.76 (dd, J = 8.6, 2.5 Hz, 1H), 7.23 (t, J = 7.8 Hz, 1H), 6.92 (d, J = 7.7 Hz, 1H), 6.83 (t, J = 2.0 Hz, 1H), 6.80 (d, J = 8.6 Hz, 1H), 6.68 (ddd, J = 8.0, 2.3, 0.7 Hz, 1H), 3.98 (s, 3H); ^{13}C NMR (101 MHz, CDCl_3) δ 163.6, 146.9, 144.9, 139.1, 137.5, 130.3, 129.9, 117.2, 114.1, 113.3, 110.7, 53.6; **CI+HRMS** m/z 201.1027 $[\text{M}+\text{H}]^+$ $\text{C}_{12}\text{H}_{12}\text{N}_2\text{O}$ requires 200.09.

Preparation of **3-(6-chloropyridin-3-yl)aniline 22c**

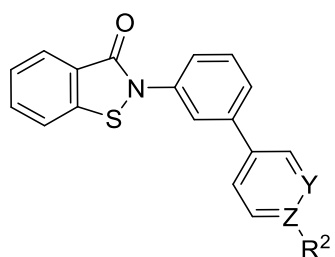
The general procedure (**6**) was followed using (6-chloro-pyridin-3-yl)boronic acid (0.2 g, 1.27 mmol) to give **22c** as an orange oil in 89.5% yield. **Rf** = 0.68 (8:2 EtOAc:hexane and 1% triethylamine). ^1H NMR (400 MHz, CDCl_3) δ 8.57 (dd, J = 2.5, 0.4 Hz, 1H), 7.81 (dd, J = 8.3, 2.6 Hz, 1H), 7.38 (dd, J = 8.3, 0.6 Hz, 1H), 7.26 (t, J = 7.7 Hz, 1H), 6.92 (ddd, J = 7.6, 1.6, 0.9 Hz, 1H), 6.84 (t, J = 2.0 Hz, 1H), 6.74 (ddd, J = 8.0, 2.3, 0.8 Hz, 1H), 3.82 (s, 2H, NH_2); ^{13}C NMR (101 MHz, CDCl_3) δ 150.2, 147.9, 147.1, 137.6, 137.2, 135.9, 130.2, 124.2, 117.4, 115.1, 113.4; **CI+HRMS** m/z 205.0635 $[\text{M}+\text{H}]^+$ $\text{C}_{11}\text{H}_9\text{ClN}_2$ requires 204.05.

Preparation of **3-(6-(trifluoromethyl)pyridin-3-yl)aniline 22d**

The general procedure (**6**) was followed using 2-(trifluoromethyl)pyridine-5-boronic acid (0.4 g, 2.10 mmol) to give **22d** as an off-white crystalline solid in quantitative yield. **Rf** = 0.72 (7:3 EtOAc:hexane and 1% triethylamine). ^1H NMR (400 MHz, CDCl_3) δ 8.91 (d, J = 1.9 Hz, 1H), 8.00 (dd, J = 8.1, 1.7 Hz, 1H), 7.73 (d, J = 8.1 Hz, 1H), 7.29 (t, J = 7.8 Hz, 1H), 6.97 (ddd, J = 7.6, 1.5, 0.8 Hz, 1H), 6.89 (t, J = 2.0 Hz, 1H), 6.78 (ddd, J = 8.0, 2.3, 0.7 Hz, 1H), 3.85 (s, 2H, NH_2); ^{13}C NMR (101 MHz, CDCl_3) δ 148.5, 147.2, 146.69 (q, $^2J_{\text{CF}}$ = 34.8 Hz, 1C), 139.7, 137.5, 135.5, 130.3, 121.73 (q, $^1J_{\text{CF}}$ = 273.8 Hz, 1C), 120.37 (q, $^3J_{\text{CF}}$ = 2.6 Hz, 1C), 117.64, 115.6, 113.6; **CI+HRMS** m/z 239.0790 $[\text{M}+\text{H}]^+$ $\text{C}_{12}\text{H}_9\text{F}_3\text{N}_2$ requires 238.07.

Preparation of biphenyl-pyridinyl benzo[d]isothiazol-3(2H)-ones **23-26**

General procedure (7)



23	Y = C, X = N
24	Y = N, X = C, R ² = OCH ₃
25	Y = N, X = C, R ² = Cl
26	Y = N, X = C, R ² = CF ₃

To a solution of the appropriate 3-pyridinyl aniline **22a-d** in DCM (10 ml/mmol), **X** (1.2 eq) was added at 0°C under a N₂ atmosphere. Et₃N (3.3 eq) was added to the solution which was allowed to gradually warm to room temperature and stir for 20 hours. The solution was quenched with NaHCO₃ (30 ml) and the organic layer extracted into DCM (3 x 30 ml). The combined organic extracts were then washed with brine (30 ml), dried over MgSO₄ and concentrated under reduced pressure. The crude products were purified by trituration using Et₂O and EtOAc.

Preparation of **2-(3-(pyridin-4-yl)phenyl)benzo[d]isothiazol-3(2H)-one 23**

The general procedure (7) was followed using **22a** (0.2 g, 1.18 mmol) to give **23** as an off-white solid in 21.1% yield. *R_f* = 0.25 (8:2 EtOAc:hexane). ¹H NMR (400 MHz, MeOD) δ 8.64 (br s, 2H), 8.12 (t, J = 1.8 Hz, 1H), 8.05 (d, J = 7.9 Hz, 1H), 7.87 (d, J = 8.2 Hz, 1H), 7.82 – 7.72 (m, 5H), 7.68 (t, J = 7.9 Hz, 1H), 7.54 (td, J = 7.1, 0.8 Hz, 1H); ¹³C NMR (101 MHz, MeOD) δ 164.8, 149.3 (2C), 148.1, 140.7, 139.0, 137.9, 132.7 (2C), 130.1, 126.2, 125.9, 125.8, 125.4, 124.1, 123.4, 120.8; **Elemental analysis** (%) found: C, 70.42; H, 4.07; N, 9.27; S, 10.54%; C₁₈H₁₂N₂OS requires C, 71.03; H, 3.97; N, 9.20; S, 10.54%; **CI+HRMS** m/z 305.0749 [M+H]⁺ C₁₈H₁₂N₂OS requires 304.07.

Preparation of **2-(3-(6-methoxypyridin-3-yl)phenyl)benzo[d]isothiazol-3(2H)-one 24**

The general procedure (7) was followed using **22b** (0.13 g, 0.67 mmol) to give **24** as an off-white solid in 33.9% yield. *R_f* = 0.65 (6:4 EtOAc:hexane). ¹H NMR (400 MHz, DMSO) δ 8.54 (d, J = 2.5 Hz, 1H), 8.12 – 8.04 (m, 2H), 8.01 - 7.94 (m, 2H), 7.79 (td, J = 8.3, 1.2 Hz, 1H), 7.72 – 7.58 (m, 3H), 7.53 (td, J = 7.9, 0.7 Hz, 1H), 6.96 (d, J = 8.6 Hz, 1H), 3.92 (s, 3H); ¹³C NMR (101 MHz, DMSO) δ 163.9, 163.9, 145.4, 140.6, 138.8, 138.3, 138.2, 133.1, 130.7, 128.9, 126.7, 126.5, 125.5, 124.7, 123.9, 122.9, 122.4, 111.2, 53.8; **Elemental analysis** (%) found: C, 65.50; H, 4.44; N, 8.18; S, 9.38%; C₁₉H₁₄N₂O₂S requires C, 68.24; H, 4.22; N, 8.38; S, 9.59%; **CI+HRMS** m/z 335.0581 [M+H]⁺ C₁₉H₁₄N₂O₂S requires 334.08.

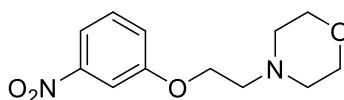
Preparation of 2-(3-(6-chloropyridin-3-yl)phenyl)benzo[d]isothiazol-3(2H)-one **25**

The general procedure (**7**) was followed using **22c** (0.05 g, 0.26 mmol) to give **25** as an off-white solid in 49.3% yield. **Rf** = 0.65 (6:4 EtOAc:hexane). ¹H NMR (400 MHz, DMSO) δ 8.80 (d, *J* = 2.6 Hz, 1H), 8.23 (dd, *J* = 8.4, 2.7 Hz, 1H), 8.82 – 8.76 (m, 2H), 7.98 (d, *J* = 7.8 Hz, 1H), 7.82 – 7.72 (m, 3H), 7.71 – 7.62 (m, 2H), 7.53 (td, *J* = 7.9, 0.7 Hz, 1H); ¹³C NMR (101 MHz, DMSO) δ 163.9, 150.2, 148.5, 140.7, 138.5, 138.4, 137.4, 134.6, 133.2, 130.8, 126.7, 126.6, 126.1, 125.1, 125.0, 124.6, 123.6, 122.5; **CI+HRMS** *m/z* 339.0363 [M+H]⁺ C₁₈H₁₁ClN₂OS requires 338.03; **HPLC** (purity analysis %) found: 99.10%; RT: 9.11 min/40 min (25/75, 0.5 ml/min IPA:HEXANE, Signal = 230 nm, SYNCHROSILICA).

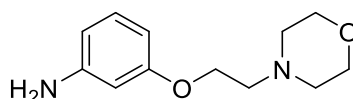
Preparation of 2-(3-(6-(trifluoromethyl)pyridin-3-yl)phenyl)benzo[d]isothiazol-3(2H)-one **26**

The general procedure (**7**) was followed using **22d** (0.19 g, 0.81 mmol) to give **26** as an off-white solid in 62.5% yield. **Rf** = 0.71 (6:4 EtOAc:hexane). ¹H NMR (400 MHz, DMSO) δ 9.15 (d, *J* = 1.9 Hz, 1H), 8.43 (dd, *J* = 8.1, 1.9 Hz, 1H), 8.17 (t, *J* = 1.8 Hz, 1H), 8.09 (d, *J* = 8.1 Hz, 1H), 8.04 (d, *J* = 8.2 Hz, 1H), 7.99 (d, *J* = 7.7 Hz, 1H), 7.87 – 7.76 (m, 3H), 7.72 (t, *J* = 7.9 Hz, 1H), 7.54 (td, *J* = 7.9, 0.8 Hz, 1H); ¹³C NMR (101 MHz, DMSO) δ 164.0, 148.9, 146.1 (q, ²J_{CF} = 34.0 Hz, 1C), 140.7, 138.5, 137.3, 136.9, 133.2, 130.9, 126.7, 126.6, 126.5, 126.3, 125.6, 124.6, 124.0, 122.5, 122.2 (q, ¹J_{CF} = 274.2 Hz, 1C), 121.4 (q, ³J_{CF} = 2.8 Hz, 1C); **CI+HRMS** *m/z* 373.0617 [M+H]⁺ C₁₉H₁₁F₃N₂OS requires 372.05; **HPLC** (purity analysis %) found: 99.47%; RT: 8.71 min/40 min (25/75, 0.5 ml/min IPA:HEXANE, Signal = 230 nm, SYNCHROSILICA).

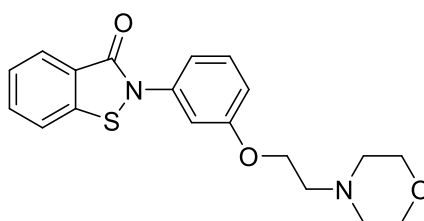
Preparation of 4-(2-(3-nitrophenoxy)ethyl)morpholine **27a**



3-nitrophenol (1.0 g, 7.19 mmol), K₂CO₃ (2.09 g, 15.1 mmol, 2.1 eq) and 4-(2-chloroethyl)morpholine hydrochloride (1.47 g, 7.91 mmol, 1.1 eq) were dissolved in DMF (10 ml) and placed under a N₂ atmosphere and the solution heated to 50°C overnight. After 16 hours the reaction was complete and DMF was removed under reduced pressure to produce an orange/red crude solid which was partitioned between EtOAc (50 ml) and H₂O (50 ml). The organic layer was extracted into EtOAc (2x40 ml), dried with Na₂CO₃ and concentrated under reduced pressure. The crude product was purified by column chromatography to give **27a** as clear brown oil in a 90.0% yield. **Rf** = 0.10 (8:2 EtOAc:hexane). ¹H NMR (400 MHz, CDCl₃) δ 7.83 (ddd, *J* = 8.1, 1.3, 0.6 Hz, 1H), 7.75 (t, *J* = 2.3 Hz, 1H), 7.43 (t, *J* = 8.2 Hz, 1H), 7.24 (ddd, *J* = 7.7, 1.9, 0.6 Hz, 1H), 4.19 (t, *J* = 5.6 Hz, 2H), 3.74 (apparent t, *J* = 4.7 Hz, 4H), 2.84 (t, *J* = 5.6 Hz, 2H), 2.59 (*J* = 4.6 Hz, 4H); ¹³C NMR (101 MHz, CDCl₃) δ 159.9, 149.2, 130.0, 121.8, 115.9, 108.9, 66.9 (2C), 66.8, 57.4, 54.1 (2C); **CI+HRMS** *m/z* 253.1181 [M+H]⁺ C₁₂H₁₆N₂O₄ requires 252.1

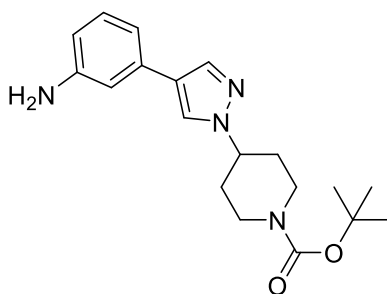
Preparation of **3-(2-morpholinoethoxy)aniline 27b**

10% Pd/C (0.05g, 10% by mass) was added to a solution of **27a** (0.5 g, 1.98 mmol) in 50:50 EtOAc-MeOH (30 ml). The solution was put under a hydrogen atmosphere at room temperature overnight after which time the reaction was complete. The solution was filtered through Celite under vacuum and resulting material was washed with 50:50 EtOAc-hexane and concentrated under reduced pressure to give **27b** as the pure product, a red/orange viscous oil in a 80.0% yield. **Rf** = 0.10 (EtOAc and 1% triethylamine). ¹H NMR (400 MHz, CDCl₃) δ 7.05 (t, *J* = 7.7 Hz, 1H), 6.31 (apparent t, *J* = 8.9 Hz, 2H), 6.25 (s, 1H), 4.07 (br s, 2H), 3.73 (s, 4H), 3.64 (s, 2H, NH), 2.78 (s, 2H), 2.57 (s, 4H); ¹³C NMR (101 MHz, CDCl₃) δ 159.9, 147.8, 130.1, 108.1, 104.6, 101.8, 70.0 (2C), 65.6, 57.7, 54.1 (2C); **CI+HRMS** *m/z* 223.1449 [M+H]⁺ C₁₂H₁₈N₂O₂ requires 222.1.

Preparation of **2-(3-(2-morpholinoethoxy)phenyl)benzo[d]isothiazol-3(2H)-one 28**

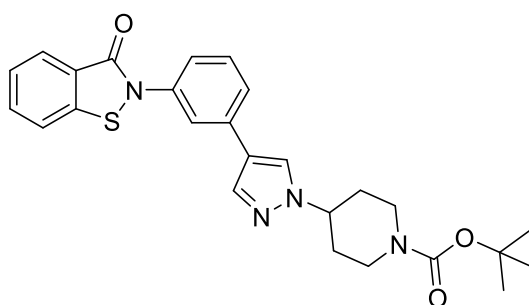
A solution of **27b** (0.388 g, 1.75 mmol) in DCM (12 ml) was added to a solution of **X** (0.434 g, 2.09 mmol, 1.2 eq) in DCM (12 ml) at 0°C under a N₂ atmosphere. Et₃N (0.80 ml, 5.76 mmol, 3.3 eq) was added to the solution, the flask evacuated and purged with N₂ before gradually warming to room temperature and allowed to stir overnight. The solution was quenched with brine (30 ml) and the organic layer extracted into DCM (2 x 30 ml), washed with NaHCO₃ (30 ml), dried with MgSO₄ and concentrated *in vacuo*. The crude product was purified by column chromatography to give **28** as a yellow solid in a 28.4% yield. **Rf** = 0.30 (5:95 MeOH:EtOAc and 1% triethylamine). ¹H NMR (250 MHz, MeOD) δ 8.02 (dt, *J* = 7.6, 1.1 Hz, 1H), 7.84 (dt, *J* = 8.1, 0.9 Hz, 1H), 7.75 (td, *J* = 8.3, 1.2 Hz, 1H), 7.52 (td, *J* = 8.0, 1.1 Hz, 1H), 7.43 (t, *J* = 8.1 Hz, 1H), 7.35 (t, *J* = 2.2 Hz, 1H), 7.23 (ddd, *J* = 8.0, 2.0, 0.9 Hz, 1H), 6.99 (ddd, *J* = 8.3, 2.5, 0.9 Hz, 1H), 4.21 (t, *J* = 5.5 Hz, 2H), 3.72 (t, *J* = 4.7 Hz, 4H), 2.84 (t, *J* = 5.5 Hz, 2H), 2.61 (t, *J* = 4.7 Hz, 4H); ¹³C NMR (63MHz, MeOD) δ 164.7, 159.5, 140.7, 137.9, 132.6, 130.0, 126.1, 125.8, 124.3, 120.7, 116.9, 113.6, 111.2, 66.2 (2C), 65.3, 57.2, 53.7 (2C); **Elemental analysis** (%) found: C, 63.92; H, 5.56; N, 7.95; S, 8.48%. C₁₉H₂₀N₂O₃S requires C, 64.02; H, 5.66; N, 7.86; S, 9.00%; **ES+HRMS** *m/z* 357.1270 [M+H]⁺ C₁₉H₂₀N₂O₃S requires 356.12.

Preparation of **tert-butyl 4-(4-(3-aminophenyl)-1H-pyrazol-1-yl)piperidine-1-carboxylate 29a**



To a solution of Na_2CO_3 (0.295 g, 2.78 mmol, 2.1 eq), 1-(1-Boc-4-piperidyl)pyrazole-4-boronic acid pinacol ester (0.26 g, 0.82 mmol) and $\text{Pd}(\text{PPh}_3)_4$ (0.038 g, 0.033 mmol, 0.025 eq) in DME:water (10:5 ml), 3-bromoaniline (1.6 ml, 1.46 mmol, 1.1 eq) was added. The stirring solution was evacuated and purged with N_2 before heating to 91°C for 18 hours. The solution was then concentrated under reduced pressure to remove DME and the crude material quenched with brine (20 ml) and organic layer extracted into EtOAc (2 x 30 ml), dried over MgSO_4 and concentrated under reduced pressure. The crude product was purified by column chromatography to give **29a** as a yellow-brown oil in a 97.5% yield. $R_f = 0.60$ (EtOAc and 1% triethylamine). $^1\text{H NMR}$ (400 MHz, CDCl_3) δ 7.74 (s, 1H), 7.62 (s, 1H), 7.14 (t, $J = 7.8$ Hz, 1H), 6.87 (d, $J = 7.7$ Hz, 1H), 6.80 (t, $J = 1.9$ Hz, 1H), 6.56 (dd, $J = 7.9, 1.6$ Hz, 1H), 4.33 – 4.21 (m, 3H), 3.69 (br s, NH_2), 2.90 (t, $J = 11.7$ Hz, 2H), 2.15 (dd, $J = 12.6, 1.8$ Hz, 2H), 1.94 (ddd, $J = 24.4, 12.2, 4.2$ Hz, 2H), 1.48 (s, 9H); $^{13}\text{C NMR}$ (101 MHz, CDCl_3) δ 154.6, 146.8, 136.5, 133.6, 129.8, 123.6, 122.9, 116.0, 113.4, 112.1, 79.9, 59.4, 42.7 (2C), 32.4 (2C), 28.4 (3C); **ES+HRMS** m/z 365.1952 $[\text{M}+\text{Na}]^+$ $\text{C}_{19}\text{H}_{26}\text{N}_4\text{O}_2$ requires 342.21.

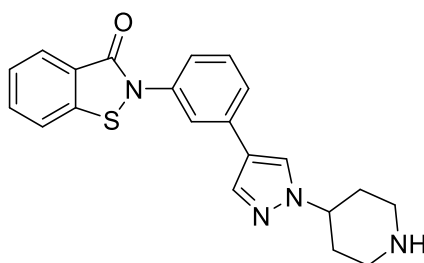
Preparation of **tert-butyl 4-(4-(3-(3-oxobenzo[d]isothiazol-2(3H)-yl)phenyl)-1H-pyrazol-1-yl)piperidine-1-carboxylate 29b**



A solution of **29a** (0.422 g, 1.23 mmol) in DCM (12 ml) was added to a solution of **X** (0.31 g, 1.48 mmol, 1.2 eq) in DCM (12 ml) at 0°C under a N_2 atmosphere. Et_3N (0.60 ml, 4.07 mmol, 3.3 eq) was added to the solution, the flask evacuated and purged with N_2 before gradually warming to room temperature and allowed to stir overnight. The solution was diluted further with DCM (15 ml) and washed with

brine (30 ml). The organic layer was then extracted into DCM (2 x 30 ml), washed with NaHCO₃ (30 ml), dried with MgSO₄ and concentrated *in vacuo*. The crude product was purified by trituration with Et₂O to give **29b** as a yellow viscous liquid in a 96.5% yield. **Rf** = 0.31 (7:3 EtOAc:hexane and 1% triethylamine). ¹H NMR (400 MHz, CDCl₃) δ 8.12 (d, J = 7.9 Hz, 1H), 7.89 (t, J = 1.5 Hz, 1H), 7.82 (s, 1H), 7.73 (s, 1H), 7.68 (dt, J = 8.2, 1.2 Hz, 1H), 7.60 (d, J = 8.1 Hz, 1H), 7.53 – 7.40 (m, 4H), 4.37 – 4.21 (m, 3H), 3.08 – 2.85 (m, 2H), 2.17 (d, J = 10.4 Hz, 2H), 1.95 (ddd, J = 24.5, 12.3, 4.4 Hz, 3H), 1.49 (s, 9H); ¹³C NMR (101 MHz, CDCl₃) δ 164.2, 154.6, 139.9, 137.8, 136.6, 134.1, 132.5, 129.86, 127.2, 125.9, 124.8, 124.1, 124.0, 122.2, 122.0, 121.7, 120.172, 80.0, 59.6, 43.2 (2C), 32.5 (2C), 28.4 (3C); **ES+HRMS** m/z 499.1790 [M+Na]⁺ C₂₆H₂₈N₄O₃S requires 476.19.

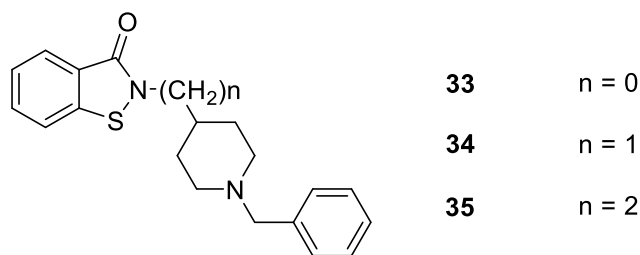
Preparation of **2-(3-(1-(piperidin-4-yl)-1H-pyrazol-4-yl)phenyl)benzo[d]isothiazol-3(2H)-one 30**



To a solution of **29b** (0.588 g, 1.23 mmol) in DCM (7 ml) under a N₂ atmosphere, trifluoroacetic acid (TFA) (1.5 ml, 18.5 mmol, 15.0 eq) was added and allowed to stir at room temperature overnight. After this time, DCM and excess TFA were removed under reduced pressure. The crude material was quenched with NaHCO₃ and the organic layer extracted into DCM (additional drops of MeOH to add solubility) (3 x 40 ml), washed with brine (40 ml), dried with MgSO₄ and concentrated *in vacuo*. The crude product was purified by trituration with Et₂O to give **30** as an off-white solid in a 58.7% yield. **Rf** = 0.02 (8:2 EtOAc:hexane and 1% triethylamine). ¹H NMR (400 MHz, MeOD) δ 8.19 (s, 1H), 8.06 (d, J = 7.9 Hz, 1H), 7.94 (s, 1H), 7.91 (t, J = 1.7 Hz, 1H), 7.89 (d, J = 8.2 Hz, 1H), 7.79 (td, J = 8.2, 1.1 Hz, 1H), 7.64 (dt, J = 7.3, 1.5 Hz, 1H), 7.58 – 7.48 (m, 3H), 4.37 (tt, J = 11.5, 3.9 Hz, 1H), 3.25 (d, J = 13.0 Hz, 2H), 2.83 (td, J = 12.8, 2.4 Hz, 2H), 2.18 (d, J = 12.3 Hz, 2H), 1.95 (ddd, J = 24.9, 12.6, 4.1 Hz, 2H); ¹³C NMR (101 MHz, MeOD) δ 164.8, 140.8, 137.4, 136.4, 134.1, 132.6, 129.7, 126.1, 125.9, 125.7, 124.4, 124.1, 122.7, 121.9, 121.7, 120.7, 57.2, 43.5 (2C), 30.5 (2C); **ES+HRMS** m/z 377.1430 [M+H]⁺ C₂₁H₂₀N₄OS requires 376.14.

Preparation of 2-(1-benzylpiperidin-4-yl)-linked benzo[d]isothiazol-3(2H)-ones 33-35

General Procedure (8)



To a solution of **X** (1.00 mmol) in DCM (15 ml), the appropriate amino benzyl piperidine (1.2 mmol, 1.2 eq) was added at 0°C under a N₂ atmosphere. Et₃N (3.3 mmol, 3.3 eq) was then added to the solution which was allowed to warm gradually to room temperature and stir overnight. The solution was diluted with DCM (30 ml), washed with brine (30 ml) and NaHCO₃ (30 ml), extracted into DCM (3 x 30 ml) and the combined organic extracts dried over MgSO₄ before concentrating under reduced pressure. The crude products were purified by flash column chromatography.

Preparation of 2-(1-benzylpiperidin-4-yl)benzo[d]isothiazol-3(2H)-one **33**

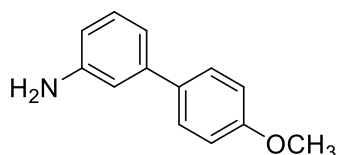
The general procedure (8) was followed using 4-amino-1-benzylpiperidine (1.2 mmol) to give **33** as a off-white solid in 71.0% yield. **Rf** = 0.36 (8:2 EtOAc:hexane). **¹H NMR** (400 MHz, CDCl₃) δ 8.03 (d, *J* = 7.9 Hz, 1H), 7.62 – 7.53 (m, 2H), 7.39 (dt, *J* = 8.0, 1.4 Hz, 1H), 7.33 (apparent d, *J* = 4.4 Hz 4H), 7.31 – 7.26 (m, 1H), 4.64 (tt, *J* = 11.5, 4.7 Hz, 1H), 3.55 (s, 2H), 3.01 (d, *J* = 11.9 Hz, 2H), 2.19 (td, *J* = 11.7, 2.6 Hz, 2H), 2.05 – 1.85 (m, 4H); **¹³C NMR** (101 MHz, CDCl₃) δ 165.0, 140.3, 138.2, 131.5, 129.2 (2C), 128.3 (2C), 127.2, 126.5, 125.4, 125.3, 120.4, 62.9, 52.8 (2C), 51.6, 32.0 (2C); **Elemental analysis** (%) found: C, 70.13; H, 6.22; N, 8.52; S, 9.86%. C₁₉H₂₀N₂OS requires C, 70.34; H, 6.21; N, 8.63; S, 9.88%; **ES+HRMS** *m/z* 325.1375 [M+H]⁺ C₁₉H₂₀N₂OS requires 324.13.

Preparation of 2-((1-benzylpiperidin-4-yl)methyl)benzo[d]isothiazol-3(2H)-one **34**

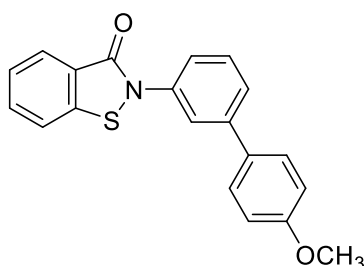
The general procedure (8) was followed using C-(1-benzyl)-piperidin-4-yl methylamine (1.2 mmol) to give **34** as a yellow viscous oil in 63.0% yield. **Rf** = 0.07 (100% EtOAc). **¹H NMR** (400 MHz, CDCl₃) δ 8.03 (d, *J* = 7.9 Hz, 1H), 7.60 (td, *J* = 8.1, 1.1 Hz, 1H), 7.53 (d, *J* = 8.1 Hz, 1H), 7.39 (td, *J* = 7.9, 0.9 Hz, 1H), 7.30 (apparent d, *J* = 4.4 Hz, 4H), 7.24 (m, 1H), 3.78 (d, *J* = 7.2 Hz, 2H), 3.49 (s, 2H), 2.88 (d, *J* = 11.8 Hz, 2H), 1.96 (td, *J* = 11.7, 2.3 Hz, 2H), 1.91 – 1.79 (m, 1H), 1.69 (apparent d, *J* = 15.9 Hz, 2H), 1.42 (qd, *J* = 11.9, 3.7 Hz, 2H); **¹³C NMR** (101 MHz, CDCl₃) δ 165.5, 140.2, 138.5, 131.7, 129.1 (2C), 128.2 (2C), 126.9, 126.7, 125.4, 124.6, 120.2, 63.2, 53.1 (2C), 49.5, 36.3, 29.8 (2C); **Elemental analysis** (%) found: C, 70.53; H, 6.46; N, 8.19; S, 9.36%. C₂₀H₂₂N₂OS requires C, 70.97; H, 6.55; N, 8.28; S, 9.47%; **ES+HRMS** *m/z* 339.1530 [M+H]⁺ C₂₀H₂₂N₂OS requires 338.15.

Preparation of 2-(2-(1-benzylpiperidin-4-yl)ethyl)benzo[d]isothiazol-3(2H)-one 35

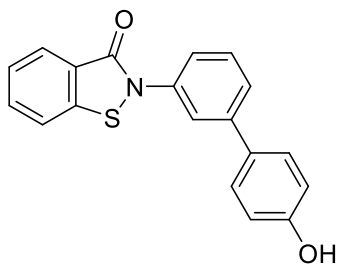
The general procedure (**8**) was followed using 2-(1-benzyl)-4-piperidinyl ethanamine (1.2 mmol) to give **35** as a clear yellow-brown oil in 73.6% yield. $R_f = 0.15$ (5:95 MeOH: EtOAc). $^1\text{H NMR}$ (400 MHz, CDCl_3) δ 8.03 (d, $J = 7.9$ Hz, 1H), 7.60 (d, $J = 8.1, 1.2$ Hz, 1H), 7.54 (d, $J = 8.0$ Hz, 1H), 7.40 (td, $J = 8.0, 1.0$ Hz, 1H), 7.30 (apparent d, $J = 4.3$ Hz, 4H), 7.26 – 7.22 (m, 1H), 3.93 (t, $J = 7.1$ Hz, 2H), 3.48 (s, 2H), 2.87 (d, $J = 11.7$ Hz, 2H), 1.94 (t, $J = 11.1$ Hz, 2H), 1.80 – 1.61 (m, 5H), 1.40 – 1.31 (m, 2H); $^{13}\text{C NMR}$ (101 MHz, CDCl_3) δ 165.3, 140.1, 138.4, 131.7, 129.2 (2C), 128.1 (2C), 127.0, 126.7, 125.5, 124.8, 120.3, 63.4, 53.6 (2C), 41.7, 36.1, 33.1, 32.1 (2C); **Elemental analysis** (%) found: C, 71.46; H, 6.85; N, 7.94; S, 9.18%. $\text{C}_{21}\text{H}_{24}\text{N}_2\text{OS}$ requires C, 71.55; H, 6.86; N, 7.95; S, 9.10%; **ES+HRMS** m/z 353.1689 $[\text{M}+\text{H}]^+$ $\text{C}_{21}\text{H}_{24}\text{N}_2\text{OS}$ requires 352.16.

Preparation of 4'-methoxy-[1,1'-biphenyl]-3-amine 36

To a solution of Na_2CO_3 (1.22 g, 11.52 mmol, 2.1 eq), 4-(methoxy)phenyl boronic acid (1.0 g, 6.58 mmol, 1.2 eq) and $\text{Pd}(\text{PPh}_3)_4$ (0.16 g, 0.137 mmol, 0.025 eq) in DME:water (20:10 ml), 3-bromoaniline (0.60 ml, 5.48 mmol) was added. The stirring solution was evacuated and purged with N_2 before heating to 90°C for 18 hours. The solution was concentrated under reduced pressure to remove DME. The crude material was then quenched with brine (40 ml) and organic layer extracted into EtOAc (2 x 40 ml), dried over MgSO_4 and concentrated under reduced pressure. The crude product was purified by flash column chromatography to give **36** as an off-white solid in a 80.9% yield. $R_f = 0.54$ (45:55 EtOAc:hexane). $^1\text{H NMR}$ (400 MHz, CDCl_3) δ 7.50 (dt, $J = 8.8, 2.1$ Hz, 2H), 7.21 (t, $J = 7.8$ Hz, 1H), 7.01 – 6.92 (m, 3H), 6.87 (t, $J = 2.0$ Hz, 1H), 6.64 (ddd, $J = 7.9, 2.3, 0.9$ Hz, 1H), 3.85 (s, 3H), 3.72 (s, 2H, NH_2); $^{13}\text{C NMR}$ (101 MHz, CDCl_3) δ 159.1, 146.7, 142.1, 134.0, 129.7, 128.1 (2C), 117.3, 114.1 (2C), 113.6, 113.5, 55.3; **CI+HRMS** m/z 200.1069 $[\text{M}+\text{H}]^+$ $\text{C}_{13}\text{H}_{13}\text{NO}$ requires 119.10.

Preparation of 2-(4'-methoxy-[1,1'-biphenyl]-3-yl)benzo[d]isothiazol-3(2H)-one **4**

To a solution of **36** (0.87 g, 4.35 mmol) in DCM (20 ml), **X** (1.08 g, 5.22 mmol, 1.2 eq) was added at 0°C under a N₂ atmosphere. Et₃N (2.0 ml, 14.3 mmol, 3.3 eq) was added to the solution which was allowed to gradually warm to room temperature and stir for 20 hours. The solution was quenched with NaHCO₃ (30 ml) and the organic layer extracted into DCM (3 x 30 ml). The combined organic extracts were then washed with brine (30 ml), dried over MgSO₄ and concentrated under reduced pressure to give the pure product **4** as a cream solid in quantitative yield. **Rf** = 0.65 (50:50 EtOAc:hexane). **¹H NMR** (400 MHz, DMSO) δ 8.07 (d, J = 8.1 Hz, 1H), 7.97 (d, J = 7.8 Hz, 1H), 7.95 (t, J = 1.8 Hz, 1H), 7.77 (td, J = 7.1, 1.2 Hz, 1H), 7.66 (dt, J = 8.8, 2.0 Hz, 2H), 7.64 – 7.55 (m, 3H), 7.52 (td, J = 7.9, 0.7 Hz, 1H), 7.06 (d, J = 8.8, 2.0 Hz, 2H), 3.81 (s, 3H); **¹³C NMR** (101 MHz, DMSO) δ 163.7, 159.8, 141.6, 140.6, 138.2, 133.1, 132.0, 130.5, 128.4(2C), 126.7, 126.5, 125.36, 124.8, 123.1, 122.7, 122.4, 115.0 (2C), 55.7; **ES+HRMS** m/z 356.0720 [M+Na]⁺ C₂₀H₁₅NO₂S requires 333.08.

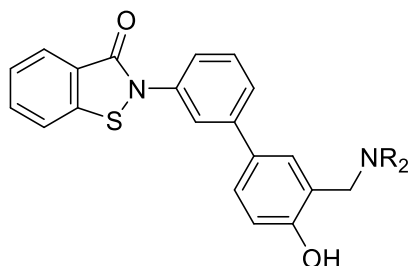
Preparation of 2-(4'-hydroxy-[1,1'-biphenyl]-3-yl)benzo[d]isothiazol-3(2H)-one **9**

To a solution of **4** (1.49 g, 4.47 mmol) in DCM (20 ml), BBr₃ (1.0 M in DCM, 9.0 ml, 8.95 mmol, 2.0 eq) was added under a N₂ atmosphere at 0°C. The resulting solution was maintained at 0°C for 2 hours, after which time the reaction was complete. The solution was quenched with MeOH (6 ml), extracted into DCM (3 x 50 ml), washed with NaHCO₃ (30 ml) and brine (40 ml), dried with MgSO₄ and concentrated *in vacuo* to give **9** as the pure product, an off-white solid in a 36.9% yield. **Rf** = 0.46 (50:50 EtOAc:hexane). **¹H NMR** (400 MHz, DMSO) δ 9.65 (s, 1H, OH), 8.07 (d, J = 8.1 Hz, 1H), 7.97 (d, J = 7.5 Hz, 1H), 7.90 (t, J = 1.5 Hz, 1H), 7.77 (td, J = 7.1, 1.2 Hz, 1H), 7.62 – 7.48 (m, 6H), 6.88 (dt, J = 8.7, 2.0 Hz, 2H); **¹³C NMR** (101 MHz, DMSO) δ 163.8, 158.1, 142.0, 140.6, 138.2, 133.1, 130.4, 130.4, 128.4 (2C), 126.6, 126.5, 125.0, 124.8, 122.8, 122.5, 122.4, 116.3 (2C); **Elemental analysis** (%) found: C,

70.32; H, 4.44; N, 4.11; S, 9.66%. $C_{19}H_{13}NO_2S$ requires C, 71.45; H, 4.10; N, 4.39; S, 10.04%; **CI+HRMS** m/z 320.0745 $[M+H]^+$ $C_{19}H_{13}NO_2S$ requires 319.07

Preparation of **2-methylene-amino-(4-hydroxy)-[1,1'-biphenyl]-3-yl)benzo[d]isothiazol-3(2H)-ones 37-39**

General Procedure (9)



- 37** $NR_2 =$ Morpholine
38 $NR_2 =$ Diethylamine
39 $NR_2 =$ Pyrrolidine

To a solution of **9** (0.15 g, 0.469 mmol) in 7:3 EtOH:H₂O (15ml), the appropriate 2° amine (3.0 – 5.0 eq) and formaldehyde 37% wt in H₂O (3.0 – 5.0 eq) were added at room temperature. The resulting solution was heated to reflux at 95°C overnight under normal atmospheric conditions. After this time, the crude solution was diluted in EtOAc (20 ml), washed with H₂O (25 ml) and extracted into EtOAc (3 x 30 ml). The combined organic extracts were then washed with brine (30 ml), dried with MgSO₄ and concentrated under reduced pressure. The crude products were purified by flash column chromatography.

Preparation of **2-(4'-hydroxy-3'-(morpholinomethyl)-[1,1'-biphenyl]-3-yl)benzo[d]isothiazol-3(2H)-one 37**

The general procedure (**9**) was followed using the 2° amine morpholine (1.41 mmol, 3.0 eq) and 3.0 eq of formaldehyde 37% wt in H₂O to give **37** as an off-white crystalline solid in 39.7% yield. **Rf** = 0.24 (50:50 EtOAc:hexane). ¹H NMR (400 MHz, MeOD) δ 8.07 (d, J = 7.9 Hz, 1H), 7.93 – 7.86 (m, 2H), 7.79 (td, J = 8.2, 1.0 Hz, 1H), 7.65 – 7.53 (m, 4H), 7.51 (dd, J = 8.4, 2.3 Hz, 1H), 7.46 (d, J = 2.2 Hz, 1H), 6.89 (d, J = 8.4 Hz, 1H), 3.81 (s, 2H), 3.76 (t, J = 4.6 Hz, 4H), 2.61 (br s, 4H); ¹³C NMR (101 MHz, CDCl₃) δ 164.2, 157.6, 142.3, 139.9, 137.6, 132.4, 131.4, 129.7, 127.8, 127.7, 127.2, 125.9, 125.3, 124.9, 122.9, 122.6, 121.1, 120.1, 116.6, 66.8 (2C), 61.9, 53.0 (2C); **Elemental analysis** (%) found: C, 67.40; H, 5.32; N, 6.39; S, 7.28%. $C_{24}H_{22}N_2O_3S$ requires C, 68.88; H, 5.30; N, 6.69; S, 7.66%; **ES+HRMS** m/z 419.1422 $[M+H]^+$ $C_{24}H_{22}N_2O_3S$ requires 418.14.

Preparation of **2-(3'-((diethylamino)methyl)-4'-hydroxy-[1,1'-biphenyl]-3-yl)benzo[d]-isothiazol-3(2H)-one 38**

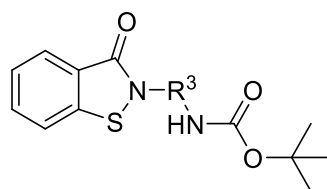
The general procedure (9) was followed using the 2° amine diethylamine (2.41 mmol, 5.0 eq) and 5.0 eq of formaldehyde 37% wt in H₂O to give **38** as a yellow/cream crystalline solid in in 22.8% yield. **Rf** = 0.22 (50:50 EtOAc:hexane and 1% triethylamine). **¹H NMR** (400 MHz, CDCl₃) δ 8.13 (d, J = 7.9 Hz, 1H), 7.89 (s, 1H), 7.68 (td, J = 8.0, 0.9 Hz, 1H), 7.63 – 7.56 (m, 2H), 7.52 – 7.38 (m, 4H), 7.29 – 7.23 (m, 1H, under solvent peak), 6.88 (d, J = 8.4 Hz, 1H), 3.84 (s, 2H), 2.66 (q, J = 7.2 Hz, 4H), 1.13 (t, J = 7.2 Hz, 6H); **¹³C NMR** (101 MHz, CDCl₃) δ 164.2, 158.5, 142.5, 140.0, 137.6, 132.4, 130.8, 129.6, 127.3, 127.2, 127.2, 125.8, 125.3, 124.9, 122.9, 122.4, 120.1, 116.6, 57.0, 46.3 (2C), 11.2 (2C); **ES+HRMS** m/z 405.1631 [M+H]⁺ C₂₄H₂₄N₂O₂S requires 404.16

Preparation of **2-(4'-hydroxy-3'-(pyrrolidin-1-ylmethyl)-[1,1'-biphenyl]-3-yl)benzo[d]-isothiazol-3(2H)-one 39**

The general procedure (9) was followed using the 2° amine pyrrolidine (1.34 mmol, 3.0 eq) and 3.0 eq of formaldehyde 37% wt in H₂O to give **39** as a translucent yellow-cream film in in 5.9% yield. **Rf** = 0.18 (50:50 EtOAc:hexane and 1% triethylamine). **¹H NMR** (400 MHz, CDCl₃) δ 8.13 (d, J = 7.9 Hz, 1H), 7.89 (s, 1H), 7.68 (td, J = 7.2, 0.8 Hz, 1H), 7.64 – 7.55 (m, 2H), 7.49 (d, J = 5.1 Hz, 2H), 7.47 – 7.38 (m, 2H), 7.28 – 7.26 (m, 1H, under solvent peak), 6.91 (d, J = 8.4 Hz, 1H), 3.95 (s, 2H), 2.82 – 2.61 (m, 4H), 1.92 – 1.84 (m, 4H); **¹³C NMR** (101 MHz, CDCl₃) δ 164.3, 158.2, 142.5, 134.0, 137.5, 132.4, 130.8, 129.7, 127.5, 127.2, 126.9, 125.9, 125.3, 124.9, 122.9, 122.6, 122.5, 120.1, 116.6, 58.7, 53.6 (2C), 23.6 (2C); **ES+HRMS** m/z 403.1477 [M+H]⁺ C₂₄H₂₂N₂O₂S requires 402.14.

Preparation of **tert-butyl-(benzo[d]isothiazol-2(3H)-yl) carbamates 40a-f**

General Procedure (10)



40a	R ³ = Ethyl
40b	R ³ = 1,5-Phenyl
40c	R ³ = 2-Methyl-1,5-phenyl
40d	R ³ = 1,4-Cyclohexane
40e	R ³ = 1,6-Cyclohexane
40f	R ³ = 2-Dimethyl-propane

To a solution of **X** (1.2 eq) in DCM (20 ml), the appropriate *N*-Boc-(Y)-amine (1.0 eq) was added at 0°C under a N₂ atmosphere. Et₃N (3.3 eq) was then added to the solution which was allowed to warm

gradually to room temperature and stir overnight. The solution was diluted with DCM, washed with NaHCO₃ (30 ml) and brine (30 ml), extracted into DCM (3 x 40 ml) and the combined organic extracts dried over MgSO₄ before concentrating under reduced pressure to give the crude products.

Preparation of **tert-butyl (2-(3-oxobenzo[d]isothiazol-2(3H)-yl)ethyl)carbamate 40a**

The general procedure (10) was followed using *N*-Boc-ethylenediamine (0.5 g, 3.12 mmol) to give **40a** as the pure product, a yellow-brown solid, in quantitative yield. **Rf** = 0.42 (60:40 EtOAc:hexane and 1% triethylamine). ¹H NMR (400 MHz, MeOD) δ 7.98 (d, J = 7.9 Hz, 1H), 7.80 (d, J = 8.1 Hz, 1H), 7.70 (t, J = 7.4 Hz, 1H), 7.47 (t, J = 7.5 Hz, 1H), 3.99 (t, J = 5.7 Hz, 2H), 3.43 (t, J = 5.7 Hz, 2H), 1.40 (s, 9H); ¹³C NMR (101 MHz, MeOD) δ 166.1, 157.0, 141.3, 131.8, 125.6, 125.3, 123.9, 120.7, 78.9, 43.6, 39.2, 27.3 (3C); **ES+HRMS** *m/z* 317.0931 [M+Na]⁺ C₁₄H₁₈N₂O₃S requires 294.10.

Preparation of **tert-butyl(3-(3-oxobenzo[d]isothiazol-2(3H)-yl)phenyl)carbamate 40b**

The general procedure (10) was followed using *N*-Boc-*m*-phenyl-enediamine (1.1 g, 5.26 mmol). The crude product was purified by flash column chromatography to give **40b** as a yellow oil in a 27.2% yield. **Rf** = 0.37 (30:70 EtOAc:hexane and 1% triethylamine). ¹H NMR (400 MHz, CDCl₃) δ 8.10 (d, J = 7.9 Hz, 1H), 7.87 (s, 1H), 7.66 (td, J = 8.2, 1.2 Hz, 1H), 7.57 (d, J = 8.1 Hz, 1H), 7.44 (td, J = 8.0, 0.9 Hz, 1H), 7.41 – 7.27 (m, 3H), 6.66 (s, 1H, NH), 1.52 (s, 9H); ¹³C NMR (101 MHz, CDCl₃) δ 164.1, 152.5, 139.9, 139.5, 137.9, 132.4, 129.8, 127.2, 125.8, 124.9, 120.0, 118.7, 116.8, 114.4, 80.9, 28.3 (3C); **ES+HRMS** *m/z* 365.0934 [M+Na]⁺ C₁₈H₁₈N₂O₃S requires 342.10.

Preparation of **tert-butyl(4-methyl-3-(3-oxobenzo[d]isothiazol-2(3H)-yl)phenyl)carbamate 40c**

The general procedure (10) was followed using 5-(Boc-amino)-2-methylaniline (0.40 g, 1.79 mmol). The crude product was purified by flash column chromatography to give **40c** as a cream solid in a 49.8% yield. **Rf** = 0.62 (60:40 EtOAc:hexane and 1% triethylamine). ¹H NMR (400 MHz, MeOD) δ 8.03 (d, J = 7.9 Hz, 1H), 7.87 (d, J = 8.2 Hz, 1H), 7.77 (td, J = 8.2, 1.0 Hz, 1H), 7.54 (m, 2H), 7.40 (dd, J = 8.4, 2.0 Hz, 1H), 7.29 (d, J = 8.4 Hz, 1H), 2.13 (s, 3H), 1.51 (s, 9H); ¹³C NMR (101 MHz, MeOD) δ 165.0, 153.6, 141.9, 138.5, 134.5, 132.4, 131.0, 130.8, 126.1, 125.8, 123.4, 120.9, 119.5, 118.3, 79.7, 27.2 (3C), 15.8; **ES+HRMS** *m/z* 379.1081 [M+Na]⁺ C₁₉H₂₀N₂O₃S requires 356.12.

Preparation of **tert-butyl((1R,4R)-4-(3-oxobenzo[d]isothiazol-2(3H)-yl)cyclohexyl)carbamate 40d**

The general procedure (10) was followed using *N*-Boc-trans-1,4-cyclohexane-diamine (0.40 g, 1.87 mmol). The crude product was purified by flash column chromatography to give **40d** as a yellow/off-white fine crystalline solid in a 58.9% yield. **Rf** = 0.40 (60:40 EtOAc:hexane and 1% triethylamine). ¹H

NMR (400 MHz, MeOD) δ 7.96 (d, J = 7.9 Hz, 1H), 7.81 (d, J = 8.2 Hz, 1H), 7.68 (td, J = 8.2, 1.0 Hz, 1H), 7.47 (td, J = 7.8, 0.5 Hz, 1H), 4.53 (tt, J = 12.0, 3.5 Hz, 1H), 3.41 (tt, J = 15.1, 4.8 Hz, 1H), 2.06 (bd, J = 10.6 Hz, 4H), 1.81 (qd, J = 12.2, 3.1 Hz, 2H), 1.55 – 1.39 (m, 11H); **^{13}C NMR** (101 MHz, MeOD) δ 165.4, 156.4, 140.9, 131.8, 125.4, 125.4, 124.6, 120.8, 78.6, 52.8, 48.4, 31.5 (2C), 30.9 (2C), 27.4 (3C); **ES+HRMS** m/z 371.1412 $[\text{M}+\text{Na}]^+$ $\text{C}_{18}\text{H}_{24}\text{N}_2\text{O}_3\text{S}$ requires 348.15.

Preparation of ***tert*-butyl((1*R*,2*R*)-2-(3-oxobenzo[*d*]isothiazol-2(3*H*)-yl)cyclohexyl) carbamate 40e**

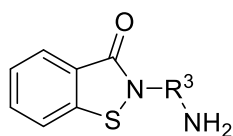
The general procedure (**10**) was followed using *tert*-butyl(*trans*-2-aminocyclohexyl) carbamate (0.45 g, 2.10 mmol). The crude product was purified by flash column chromatography to give **40e** as off-white solid crystals in a 53.5% yield. **R_f** = 0.51 (60:40 EtOAc:hexane and 1% triethylamine). **^1H NMR** (400 MHz, MeOD) δ 7.96 (d, J = 8.0 Hz, 1H), 7.78 (d, J = 8.2 Hz, 1H), 7.67 (t, J = 7.67 Hz, 1H), 7.45 (t, J = 7.6 Hz, 1H), 4.45 (td, J = 11.5, 4.0 Hz, 1H), 3.71 (td, J = 10.5, 4.2 Hz, 1H), 2.12 – 2.00 (m, 2H), 1.93 – 1.75 (m, 3H), 1.52 – 1.40 (m, 3H), 1.15 (s, 9H); **^{13}C NMR** (101 MHz, MeOD) δ 166.4, 156.0, 141.2, 131.8, 125.5, 125.2, 124.4, 120.7, 78.6, 57.4, 53.3, 32.7, 32.0, 27.0 (3C), 24.9, 24.6; **ES+MS** m/z 371.1398 $[\text{M}+\text{Na}]^+$ $\text{C}_{18}\text{H}_{24}\text{N}_2\text{O}_3\text{S}$ requires 348.15.

Preparation of ***tert*-butyl(2,2-dimethyl-3-(3-oxobenzo[*d*]isothiazol-2(3*H*)-yl)propyl) carbamate 40f**

The general procedure (**10**) was followed using *tert*-butyl-3-amino-2,2-dimethylpropyl carbamate (0.25 g, 1.24 mmol). The crude product was filtered through a pad of silica and washed with 50:50 EtOAc:hexane to give **40f** as a brown solid in a 92.6% yield. **R_f** = 0.21 (20:80 EtOAc:hexane and 1% triethylamine). **^1H NMR** (400 MHz, MeOD) δ 7.97 (d, J = 7.9 Hz, 1H), 7.79 (d, J = 8.2 Hz, 1H), 7.71 (td, J = 7.1, 1.2 Hz, 1H), 7.48 (td, J = 8.0, 0.9 Hz, 1H), 3.75 (s, 2H), 2.95 (s, 2H), 1.46 (s, 9H), 1.02 (s, 6H); **^{13}C NMR** (101 MHz, MeOD) δ 167.0, 157.2, 141.3, 132.1, 125.7, 125.5, 123.4, 120.5, 78.7, 51.9, 47.3, 37.3, 27.4 (3C), 22.7 (2C); **ES+HRMS** m/z 359.1401 $[\text{M}+\text{Na}]^+$ $\text{C}_{17}\text{H}_{24}\text{N}_2\text{O}_3\text{S}$ requires 336.15.

Preparation of 2-(R³)-(benzo[d]isothiazol-2(3H)-yl) amines **41a-f**

General Procedure (11)



- 41a** R³ = Ethyl
- 41b** R³ = 1,5-Phenyl
- 41c** R³ = 2-Methyl-1,5-phenyl
- 41d** R³ = 1,4-Cyclohexane
- 41e** R³ = 1,6-Cyclohexane
- 41f** R³ = 2-Dimethyl-propane

To a solution of the appropriate *tert*-butyl-(benzo[d]isothiazol-2(3H)-yl) carbamate **40a-f** in DCM (15-25 ml) under a N₂ atmosphere, trifluoroacetic acid (TFA) (15.0 eq) was added and allowed to stir at room temperature overnight. After this time, DCM and excess TFA were removed under reduced pressure. The crude material was re-dissolved in DCM (30 ml), quenched with NaHCO₃ (30 ml) and the organic layer extracted into DCM (3 x 40 ml). The combined organic layers were then washed with brine (40 ml), dried with MgSO₄ and concentrated *in vacuo* to isolate the pure product.

Preparation of 2-(2-aminoethyl)benzo[d]isothiazol-3(2H)-one **41a**

The general procedure (11) was followed using **40a** (0.92 g, 3.13 mmol) to give **41a** as a yellow-brown viscous oil in a 35.3% yield. *R_f* = 0.14 (10:90 MeOH:EtOAc and 1% triethylamine). ¹H NMR (400 MHz, CDCl₃) δ 8.04 (d, J = 7.9 Hz, 1H), 7.61 (t, J = 7.4 Hz, 1H), 7.55 (d, J = 8.0 Hz, 1H), 7.40 (t, J = 7.4 Hz, 1H), 3.97 (t, J = 5.9 Hz, 2H), 3.10 (t, J = 5.5 Hz, 2H); ¹³C NMR (101 MHz, CDCl₃) δ 165.9, 140.4, 131.9, 126.7, 125.6, 124.5, 120.3, 47.0, 41.5; **CI+HRMS** *m/z* 195.0590 [M+H]⁺ C₉H₁₀N₂OS requires 194.05.

Preparation of 2-(3-aminophenyl)benzo[d]isothiazol-3(2H)-one **41b**

The general procedure (11) was followed using **40a** (0.14 g, 0.414 mmol) to give **41b** as a yellow-orange solid in a 97.2% yield. *R_f* = 0.31 (65:35 EtOAc:hexane and 1% triethylamine). ¹H NMR (400 MHz, CDCl₃) δ 8.09 (d, J = 7.9 Hz, 1H), 7.65 (Td, J = 8.1, 1.1 Hz, 1H), 7.57 (d, J = 8.0 Hz, 1H), 7.44 (t, J = 7.5 Hz, 1H), 7.22 (t, J = 8.0 Hz, 1H), 7.15 (t, J = 2.1 Hz, 1H), 7.01 (dd, J = 8.0, 1.4 Hz, 1H), 6.62 (dd, J = 8.0, 1.8 Hz, 1H), 3.82 (s, 2H, NH₂); ¹³C NMR (101 MHz, CDCl₃) δ 164.1, 147.4, 139.9, 138.2, 132.3, 130.1, 127.1, 125.7, 125.1, 120.0, 114.2, 113.8, 111.1; **CI+HRMS** *m/z* 243.0590 [M+H]⁺ C₁₃H₁₀N₂OS requires 242.05.

Preparation of 2-(5-amino-2-methylphenyl)benzo[d]isothiazol-3(2H)-one 41c

The general procedure (11) was followed using 40c (0.31 g, 0.868 mmol) to give 41c as a yellow solid in a 98.2% yield. *R_f* = 0.33 (60:40 EtOAc:hexane and 1% triethylamine). ¹H NMR (400 MHz, CDCl₃) δ 8.11 (d, *J* = 7.9 Hz, 1H), 7.67 (td, *J* = 8.2, 1.1 Hz, 1H), 7.59 (d, *J* = 8.1 Hz, 1H), 7.45 (td, *J* = 7.9, 0.8 Hz, 1H), 7.10 (d, *J* = 7.8 Hz, 1H), 6.74 – 6.65 (m, 2H), 3.43 (s, 2H, NH₂), 2.12 (s, 3H); ¹³C NMR (101 MHz, CDCl₃) δ 164.5, 145.3, 141.2, 135.2, 132.1, 131.9, 127.2, 127.1, 125.6, 124.0, 120.2, 116.8, 115.5, 17.0; **CI+HRMS** *m/z* 257.0753 [M+H]⁺ C₁₄H₁₂N₂OS requires 256.07.

Preparation of 2-((1R,4R)-4-aminocyclohexyl)benzo[d]isothiazol-3(2H)-one 41d

The general procedure (11) was followed using 40d (0.37 g, 1.07 mmol) to give 41d as a yellow solid in a 75.7% yield. *R_f* = 0.00 (60:40 EtOAc:hexane and 1% triethylamine). ¹H NMR (400 MHz, CDCl₃) δ 8.04 (d, *J* = 7.9 Hz, 1H), 7.60 (td, *J* = 8.0, 1.1 Hz, 1H), 7.56 (d, *J* = 7.6 Hz, 1H), 7.40 (td, *J* = 8.0, 1.3 Hz, 1H), 4.60 (tt, *J* = 11.9, 3.9 Hz, 1H), 2.79 (t, *J* = 11.0 Hz, 1H), 2.13 – 1.95 (m, 4H), 1.83 – 1.60 (m, 4H), 1.46 – 1.30 (m, 2H, NH₂); ¹³C NMR (101 MHz, CDCl₃) δ 165.0, 140.2, 131.6, 126.5, 125.4, 125.4, 120.4, 52.4, 49.7, 35.4 (2C), 31.3 (2C); **ES+HRMS** *m/z* 249.1056 [M+H]⁺ C₁₃H₁₆N₂OS requires 248.10.

Preparation of 2-((1R,2R)-2-aminocyclohexyl)benzo[d]isothiazol-3(2H)-one 41e

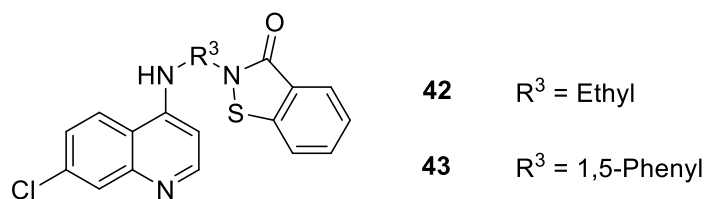
The general procedure (11) was followed using 40e (0.37 g, 1.07 mmol) to give 41e as an opaque, off-white oil in quantitative yield. *R_f* = 0.04 (EtOAc and 1% triethylamine). ¹H NMR (400 MHz, CDCl₃) δ 8.06 (d, *J* = 7.9 Hz, 1H), 7.62 (td, *J* = 8.0, 0.9 Hz, 1H), 7.58 (d, *J* = 7.4 Hz, 1H), 7.42 (td, *J* = 7.9, 1.3 Hz, 1H), 4.37 (ddd, *J* = 10.3, 4.0, 1.3 Hz, 1H), 2.85 (t, *J* = 4.0 Hz, 1H), 2.19 – 1.96 (m, 2H), 1.85 (m, 2H), 1.62 (qd, *J* = 12.3, 3.3 Hz, 1H, NH), 1.54 – 1.23 (m, 4H and NH); ¹³C NMR (101 MHz, CDCl₃) δ 166.0, 140.2, 131.8, 126.8, 125.5, 125.2, 120.5, 60.8, 54.8, 35.4, 32.2, 25.4, 25.1; **CI+HRMS** *m/z* 249.1065 [M+H]⁺ C₁₃H₁₆N₂OS requires 248.10.

Preparation of 2-(3-amino-2,2-dimethylpropyl)benzo[d]isothiazol-3(2H)-one 41f

The general procedure (11) was followed using 40f (0.38 g, 1.12 mmol) to give 41f as a pale-yellow, cloudy viscous oil in a 80.0% yield. *R_f* = 0.00 (50:50 EtOAc:hexane and 1% triethylamine). ¹H NMR (400 MHz, CDCl₃) δ 8.04 (d, *J* = 7.9 Hz, 1H), 7.62 (td, *J* = 8.1, 1.2 Hz, 1H), 7.53 (d, *J* = 8.1 Hz, 1H), 7.41 (td, *J* = 7.9, 0.9 Hz, 1H), 3.76 (s, 2H), 2.55 (s, 2H), 1.84 (br s, 2H, NH₂), 1.04 (s, 6H); ¹³C NMR (101 MHz, CDCl₃) δ 166.5, 140.7, 131.9, 126.8, 125.4, 124.0, 120.0, 51.7, 49.7, 29.7, 24.0 (2C); **ES+HRMS** *m/z* 237.1058 [M+H]⁺ C₁₂H₁₆N₂OS requires 236.10.

Preparation of 7-chloroquinolin-4-yl-amine-linked benzo[d]isothiazol-3(2H)-ones **42-43**

General Procedure (12)



To a solution of the appropriate **2-(R³)-(benzo[d]isothiazol-2(3H)-yl) amine (41a-b)** in phenol (5-10 ml) under atmospheric conditions, 4,7-dichloroquinoline (1.1 eq) was added. The resulting solution was heated to 140°C in a sealed tube for 12 hours. Excess phenol was removed under reduced pressure (as an azeotrope with toluene) and the crude products were purified by flash column chromatography.

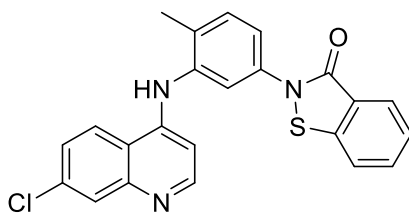
Preparation of **2-(2-((7-chloroquinolin-4-yl)amino)ethyl)benzo[d]isothiazol-3(2H)-one 42**

The general procedure (12) was followed using **41a** (0.195 g, 1.00 mmol) to give **42** as an off-white solid in a 61.9% yield. **R_f** = 0.54 (5:95 MeOH:EtOAc and 1% triethylamine). **¹H NMR** (400 MHz, DMSO) δ 8.41 (d, J = 5.4 Hz, 1H), 8.19 (d, J = 9.1 Hz, 1H), 7.94 (d, J = 8.1 Hz, 1H), 7.89 (d, J = 7.8 Hz, 1H), 7.81 (d, J = 2.2 Hz, 1H), 7.67 (td, J = 8.2, 1.0 Hz, 1H), 7.56 (t, J = 5.6 Hz, 1H), 7.50 – 7.41 (m, 2H), 6.64 (d, J = 5.5 Hz, 1H), 4.11 (m, 2H), 3.66 (q, J = 5.8 Hz, 2H), 3.18 (d, J = 5.2 Hz, 2H); **¹³C NMR** (101 MHz, DMSO) δ 165.2, 152.4, 150.2, 149.6, 141.5, 134.0, 132.3, 128.0, 126.0, 125.9, 124.8, 124.4, 124.3, 122.3, 118.1, 99.2, 49.1, 42.2; **Elemental analysis** (%) found: C, 60.14; H, 4.07; N, 11.63%; C₁₈H₁₄ClN₃OS requires C, 60.76; H, 3.97; N, 11.81%; **ES+MS** *m/z* 356.0622 [M+H]⁺ C₁₈H₁₄ClN₃OS requires 355.05.

Preparation of **2-(3-((7-chloroquinolin-4-yl)amino)phenyl)benzo[d]isothiazol-3(2H)-one 43**

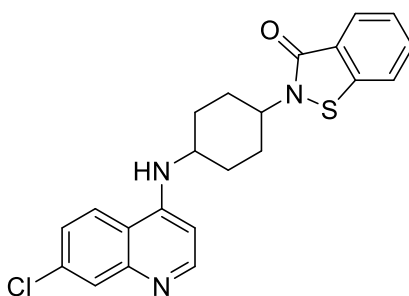
The general procedure (12) was followed using **41b** (0.089 g, 0.367 mmol) to give **43** as an off-white/yellow solid in a 21.8% yield. **R_f** = 0.46 (65:35 EtOAc:hexane and 1% triethylamine). **¹H NMR** (400 MHz, DMSO) δ 9.31 (s, 1H), 8.55 (d, J = 5.3 Hz, 1H), 8.45 (d, J = 9.1 Hz, 1H), 8.08 (d, J = 8.2 Hz, 1H), 7.98 (d, J = 7.8 Hz, 1H), 7.94 (d, J = 2.1 Hz, 1H), 7.82 (s, 1H), 7.78 (t, J = 7.3 Hz, 1H), 7.62 (dd, J = 9.0, 2.0 Hz, 1H), 7.60 – 7.49 (m, 2H), 7.45 (dd, J = 7.9, 1.1 Hz, 1H), 7.38 (dd, J = 7.9, 0.9 Hz, 1H), 7.17 (d, J = 5.3 Hz, 1H), 4.05 (br s, NH); **Elemental analysis** (%) found: C, 64.35; H, 3.81; N, 9.81; S, 7.17%. C₂₂H₁₄ClN₃OS requires C, 65.42; H, 3.49; N, 10.40; S, 7.94%; **ES+HRMS** *m/z* 404.0612 [M+H]⁺ C₂₂H₁₄ClN₃OS requires 403.05.

Preparation of **2-(5-((7-chloroquinolin-4-yl)amino)-2-methylphenyl)benzo[d]isothiazol-3(2H)-one 44**



To a solution of **41c** (0.196 g, 0.766 mmol) in anhydrous ethanol (5.5 ml), 4,7-dichloroquinoline (1.1 eq) was added. The solution was placed under a N₂ atmosphere and heated to 100°C for 12 hours in a sealed tube. Excess ethanol was removed under reduced pressure to give a crude product which was insoluble in EtOAc. The crude product was purified by trituration with EtOAc and recrystallization with DCM-EtOAc at room temperature to give **44** as a pale yellow solid in a 75.8% yield. **Rf** = 0.13 (60:40 EtOAc:hexane and 1% triethylamine). **¹H NMR** (400 MHz, MeOD) δ 8.57 (d, J = 9.1 Hz, 1H), 8.43 (d, J = 7.1 Hz, 1H), 8.06 (d, J = 7.9 Hz, 1H), 7.97 (d, J = 1.9 Hz, 1H), 7.90 (d, J = 8.2 Hz, 1H), 7.83 – 7.76 (m, 2H), 7.67 – 7.62 (m, 1H), 7.60 – 7.53 (m, 3H), 7.04 (d, J = 7.1 Hz, 1H), 2.31 (s, 3H); **¹³C NMR** (101 MHz, MeOD) δ 165.3, 156.0, 143.1, 141.9, 140.2, 139.2, 137.7, 136.0, 135.7, 132.7, 132.7, 128.0, 126.7, 126.2, 126.1, 126.0, 124.9, 123.1, 121.1, 119.1, 116.1, 100.4, 16.4; **Elemental analysis** (%) found: C, 64.35; H, 3.81; N, 9.81; S, 7.17%. C₂₃H₁₆ClN₃OS requires C, 66.10; H, 3.86; N, 10.05; S, 7.67%; **ES+HRMS** m/z 418.0771 [M+H]⁺ C₂₃H₁₆ClN₃OS requires 471.07.

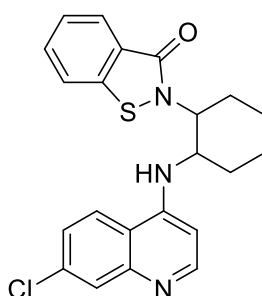
Preparation of **2-((1R,4R)-4-((7-chloroquinolin-4-yl)amino)cyclohexyl)benzo[d]isothiazol-3(2H)-one 45**



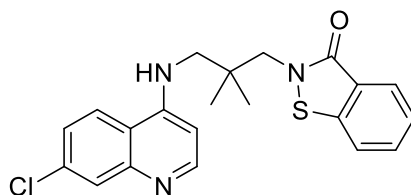
To a solution of **41d** (0.168 g, 0.677 mmol) in isopropanol (IPA) (3 ml), 4,7-dichloroquinoline (1.2 eq) was added. The solution was heated to 190°C in a microwave reactor where it was maintained for 30 minutes before cooling slowly to 50°C and then to room temperature. To improve reaction progression, the solution was heated again to 200°C in a microwave reactor where it was maintained for 30 minutes before cooling. IPA was removed under reduced pressure to provide the crude product which was purified by flash column chromatography to give **45** as a fine, yellow solid in a 38.8% yield. **Rf** = 0.23 (80:20 EtOAc:hexane and 1% triethylamine). **¹H NMR** (400 MHz, DMSO) δ 8.41 (d, J = 5.4 Hz,

1H), 8.36 (d, J = 9.1 Hz, 1H), 8.02 (d, J = 8.1 Hz, 1H), 7.89 (d, J = 7.7 Hz, 1H), 7.79 (d, J = 2.2 Hz, 1H), 7.70 (td, J = 8.1, 1.0 Hz, 1H), 7.50 – 7.41 (m, 2H), 7.02 (d, J = 7.7 Hz, 1H, NH), 6.66 (d, J = 5.6 Hz, 1H), 4.51 (tt, J = 14.8, 3.9 Hz, 1H), 3.75 – 3.63 (m, 1H), 2.22 – 2.11 (m, 2H), 2.01 – 1.99 (m, 2H), 1.95 – 1.81 (m, 2H), 1.71 – 1.56 (m, 2H); ¹³C NMR (101 MHz, DMSO) δ 164.4, 152.4, 149.8, 149.7, 140.8, 133.8, 132.2, 127.9, 126.0, 126.0, 125.2, 124.9, 124.4, 122.4, 118.0, 99.7, 52.4, 50.2, 31.1 (2C), 31.0 (2C); **Elemental analysis** (%) found: C, 64.21; H, 4.96; N, 10.15; S, 7.56%; C₂₂H₂₀ClN₃OS requires C, 64.46; H, 4.92; N, 10.25; S, 7.82%; **ES+MS** m/z 410.1084 [M+H]⁺ C₂₂H₂₀ClN₃OS requires 409.10.

Preparation of **2-((1R,2R)-2-((7-chloroquinolin-4-yl)amino)cyclohexyl)benzo[d]isothiazol-3(2H)-one 46**



To a solution of **41e** (0.250 g, 1.01 mmol) in isopropanol (IPA) (3 ml), 4,7-dichloroquinoline (1.2 eq) was added. The solution was heated to 190°C in a microwave reactor where it was maintained for 60 minutes before cooling slowly to 55°C and then to room temperature at which point the reaction was complete. IPA was removed under reduced pressure to provide the crude product which was purified by flash column chromatography to give **46** as a pale yellow, powdery solid in a 53.9% yield. **Rf** = 0.16 (80:20 EtOAc:hexane and 1% triethylamine). ¹H NMR (400 MHz, DMSO) δ 8.27 (d, J = 5.5 Hz, 1H), 8.10 (d, J = 9.1 Hz, 1H), 7.85 (d, J = 8.1 Hz, 1H), 7.74 (d, J = 7.8 Hz, 1H), 7.68 (d, J = 2.2 Hz, 1H), 7.57 (dt, J = 8.2, 1.1 Hz, 1H), 7.39 (dd, J = 9.0, 2.2 Hz, 1H), 7.33 (t, J = 7.4 Hz, 1H), 7.05 (d, J = 9.0 Hz, 1H, NH), 6.65 (d, J = 5.6 Hz, 1H), 4.70 (app td, J = 11.3, 3.7 Hz, 1H), 4.11 – 4.05 (m, 1H), 2.20 – 2.02 (m, 2H), 1.92 – 1.70 (m, 3H), 1.64 – 1.38 (m, 3H); ¹³C NMR (101 MHz, DMSO) δ 165.3, 152.2, 149.7, 149.6, 140.8, 133.8, 132.1, 127.8, 125.8, 125.8, 125.0, 124.4 (2C), 122.2, 117.8, 99.0, 60.2, 57.1, 32.0, 25.3, 24.4, 21.2; **ES+HRMS** m/z 410.1078 [M+H]⁺ C₂₂H₂₀ClN₃OS requires 409.10; **HPLC** (purity analysis %) found: 99.41%; RT: 10.81 min/ 40 min (25/75, 1.0 ml/min IPA:HEXANE, Signal = 230 nm, SYNCHROSILICA).

Preparation of 2-(3-((7-chloroquinolin-4-yl)amino)-2,2-dimethylpropyl)benzo[d]-isothiazol-3(2H)-one **47**

To a solution of **41f** (0.291 g, 0.93 mmol) in isopropanol (IPA) (3 ml), 4,7-dichloroquinoline (1.2 eq) was added. The solution was heated to 190°C in a microwave reactor where it was maintained for 45 minutes before cooling slowly to 55°C and then to room temperature. IPA was removed under reduced pressure to provide the crude product which was purified by flash column chromatography and trituration with Et₂O to give **47** as a cream, powdery solid in a 64.1% yield. **R_f** = 0.19 (70:30 EtOAc:hexane and 1% triethylamine). **¹H NMR** (400 MHz, MeOD) δ 8.32 (d, J = 5.7 Hz, 1H), 8.26 (d, J = 9.0 Hz, 1H), 8.05 (d, J = 7.9 Hz, 1H), 7.81 (d, J = 8.2 Hz, 1H), 7.78 (d, J = 2.1 Hz, 1H), 7.72 (td, J = 8.0, 0.8 Hz, 1H), 7.49 (t, J = 7.8 Hz, 1H), 7.46 (dd, J = 8.9, 2.1 Hz, 1H), 6.64 (d, J = 5.8 Hz, 1H), 3.88 (s, 2H), 3.25 (s, 2H), 1.13 (s, 6H); **¹³C NMR** (101 MHz, MeOD) δ 167.4, 151.9, 151.0, 148.5, 141.5, 135.1, 132.3, 126.3, 125.8, 125.6, 124.8, 123.4, 122.9, 120.6, 117.3, 98.3, 52.1, 48.4, 38.3, 23.1 (2C); **Elemental analysis** (%) found: C, 63.51; H, 5.18; N, 10.59; S, 7.75%; C₂₁H₂₀ClN₃OS requires C, 63.39; H, 5.07; N, 10.56; S, 8.06%; **ES+MS** m/z 398.1083 [M+H]⁺ C₂₁H₂₀ClN₃OS requires 397.10.

3.13.2 Biological Methods

MEP Metabolite Profiling

Prior to treatment, parasites were synchronized by 1-2 treatments with 5% sorbitol until > 8% parasitemia and > 75% ring-stage cultures were achieved. At this point, cultures were treated 10 hours with 5 μ M compound 4, 5 μ M fosmidomycin, or left untreated. Following treatment, parasite-infected erythrocytes were lysed with 0.1% saponin, washed in phosphate-buffered saline, and stored at -80°C until extraction and quantitative LC-MS/MS measurement of DOXP and MEcPP, as previously described. Values reflect the mean and standard error from \geq 3 independent experiments and were compared using the Student's t-test (two-tailed).

Cloning of *Pf*lspD and Orthologues

P. falciparum: The construct used for expression of the codon-optimized *Pf*lspD protein has been described previously.^[73] To generate the *Pf*lspD variants containing the C202A mutation, N- and C-terminal fragments of the optimized *Pf*lSPD gene were amplified from the above vector using the following primers. C202A N-terminal fragment: T7 Fwd primer, 5'-TAATACGACTCACTATAGGG-3', with C202A Rev primer, 5'-GTTTGCCAATACCGCCGGCTAGCAGGATACTATGAATG-3'; C202 C-terminal fragment, C202A Fwd primer, 5'-CATTCATAGTATCCTGCTAGCCGGCGGTATTGGCAAAC-3', with T7 Rev primer, 5'-GCTAGTTATTGCTCAGCGG-3'. Amplicons containing the entire *Pf*lSPD gene were generated using *Pf*lspD Fwd and Rev primers, which introduce a 6-His tag, with N- and C-terminal fragments as template (*Pf*lspD Fwd primer: 5'-CTCACCACCACCACCACCATATGATGCACATCTACGATAATAATAA-3'; *Pf*lspD Rev: 5'-ATCCTATCTTACTCACTTATTTTGAGGAGTAGTAGAAT-3'). Following amplification, *Pf*lSPD variants were cloned into pBG1861 by ligation-independent cloning as previously described,^[73,82] and verified by Sanger sequencing.

P. vivax: The construct used for expression of codon-optimized *Pv*lspD (*P. vivax* Sal-1; PVX_081425) has been previously described.^[73]

E. coli: The construct used for expression of *Ecl*spD-wt has been previously described.^[70] The A14C mutation was introduced by first generating N- and C-terminal gene fragments containing the mutation. These fragments were generated using the following primers: A14C N-terminal fragment: T7 Fwd primer, 5'-TAATACGACTCACTATAGGG-3', with A14C Rev primer, 5'-CATTCGACGGCCAAATCCGGCACACGGAACCACGGCGCAAACATC-3'; A14C C-terminal fragment, A14C Fwd primer, 5'-GATGTTTGCGCCGTGGTTCCGTGTGCCGGATTTGGCCGTCTGAATG-3', with T7 Rev

primer, 5'-GCTAGTTATTGCTCAGCGG-3'. Amplicons containing the entire *E. coli IspD* gene were generated using *EclspD* Fwd and Rev primers, which introduce a 6-His tag, with N- and C-terminal fragments as template (*EclspD* Fwd primer: 5'-CTCACCACCACCACCACCATATGATGGCAACCACTCATTTGG-3'; *EclspD* Rev primer: 5'-ATCCTATCTTACTCACTTATTTGTATTCTCCTGATGG-3'). Following amplification, *E. coli A14C-IspD* was cloned into pBG1861 by ligation-independent cloning as previously described,^[82] and verified by Sanger sequencing.

Parasite Sensitivity Assays

Asynchronous cultures of *P. falciparum* strain 3D7 were diluted to 1% parasitemia and cultured at indicated concentrations of inhibitor compounds in 100 μ L culture volumes. During rescue experiments, parasite growth medium was supplemented with 200 μ M isopentenyl pyrophosphate (IPP; Echelon Biosciences). After 72 hours, parasite growth was quantified using PicoGreen dye (Invitrogen) to measure DNA content as previously described.^[70] PicoGreen fluorescence was measured (485 nm excitation/ 528 nm emission) in a POLARStar Omega microplate reader (BMG Labtech). IC₅₀ values were calculated by nonlinear regression analysis using GraphPad Prism software, and reflect the mean and standard error from ≥ 3 independent experiments. Values were compared using the Student's t-test (two-tailed).

3.14 References

- [1] F. Calderon, D. Barros, J. M. Bueno, J. M. Coteron, E. Fernandez, F. J. Gamo, J. L. Lavandera, M. L. Leon, S. J. F. MacDonald, A. Mallo, et al., *ACS Med. Chem. Lett.* **2011**, *2*, 741–746.
- [2] F. Calderon, J. Vidal-Mas, J. Burrows, J. C. de la Rosa, M. B. Jimenez-Diaz, T. Mulet, S. Prats, J. Solana, M. Witty, F. J. Gamo, et al., *ACS Med. Chem. Lett.* **2012**, *3*, 373–377.
- [3] S. M. Bromidge, S. Dabbs, D. T. Davies, D. M. Duckworth, I. T. Forbes, P. Ham, G. E. Jones, F. D. King, D. V. Saunders, S. Starr, et al., *J. Med. Chem.* **1998**, *41*, 1598–1612.
- [4] P. D. Leeson, R. J. Young, *ACS Med. Chem. Lett.* **2015**, *6*, 722–725.
- [5] N. Miyaura, K. Yamada, A. Suzuki, *Tetrahedron Lett.* **1979**, 3437–3440.
- [6] H. Kagano, H. Goda, K. Yoshida, M. Yamamoto, S. Sakaue, *Method for Producing 1,2-Benzisothiazole-3-Ones Useful as Antibacterial and Antifungal Agents.*, **1996**.
- [7] Y. Uchida, S. Kozuka, *Bull. Chem. Soc. Jpn.* **1982**, *55*, 1183–1187.
- [8] J. C. Stålring, L. A. Carlsson, P. Almeida, S. Boyer, *J. Cheminform.* **2011**, *3*, 28.
- [9] D. J. Wood, D. Buttar, J. G. Cumming, A. M. Davis, U. Norinder, S. L. Rodgers, *Mol. Inform.* **2011**, *30*, 960–972.
- [10] E. Pop, D. C. Oniciu, M. E. Pape, C. T. Cramer, **2004**, *77*, 301–306.
- [11] H. D. Williams, N. L. Trevaskis, S. A. Charman, R. M. Shanker, W. N. Charman, **2013**, 315–499.
- [12] N. G. Berry, *Personal Communication*, **2012**.
- [13] C. G. Wermuth, C. R. Ganellin, P. Lindberg, L. a. Mitscher, *Pure Appl. Chem.* **1998**, *70*, 1129–1143.
- [14] P. J. Lipinski, C.A.; Lombardo, F.; Dominy, B.W.; Feeney, *Adv. Drug Deliv. Rev.* **2012**, *64*, 4–17.
- [15] G. L. Patrick, *An Introduction to Medicinal Chemistry, 2nd Edition.*, Oxford University Press, **2001**.
- [16] D. Smith, C. Allerton, A. S. Kalgutkar, H. van de Waterbeemd, D. K. Walker, *Pharmacokinetics and Metabolism in Drug Design, Third Edition.*, Wiley-VCH, **2012**.
- [17] C. A. Lipinski, *J. Pharmacol. Toxicol. Methods* **2000**, *44*, 235–249.
- [18] C. A. Lipinski, F. Lombardo, B. W. Dominy, P. J. Feeney, *Adv. Drug Deliv. Rev.* **1997**, *23*, 3–25.
- [19] M. J. Waring, *Bioorganic Med. Chem. Lett.* **2009**, *19*, 2844–2851.
- [20] M. M. Hann, *Medchemcomm* **2011**, *2*, 349–355.
- [21] A. P. Hill, R. J. Young, *Drug Discov. Today* **2010**, *15*, 648–655.
- [22] S. Kalepu, V. Nekkanti, *Acta Pharm. Sin. B* **2015**, *5*, 442–453.
- [23] A. Agarwal, S. Paliwal, R. Mishra, S. Sharma, A. Kumar Dwivedi, R. Tripathi, S. Gunjan, *Sci Rep* **2015**, *5*, 13838.

- [24] T. N. C. Wells, W. E. Gutteridge, *Malaria : New Medicines for Its Control and Eradication*, **2011**.
- [25] S. Aprile, E. Del Grosso, G. Grosa, *Xenobiotica* **2011**, *41*, 212–225.
- [26] J. L. Moore, S. M. Taylor, V. A. Soloshonok, *Ark. (Gainesville, FL, United States)* **2005**, 287–292.
- [27] M. Pietka-Ottlik, P. Potaczek, E. Piasecki, J. Mlochowski, *Molecules* **2010**, *15*, 8214–8228.
- [28] K. H. Baggaley, P. D. English, L. J. Jennings, B. Morgan, B. Nunn, A. W. Tyrrell, *J. Med. Chem.* **1985**, *28*, 1661–1667.
- [29] W. K. C. Park, R. M. Kennedy, S. D. Larsen, S. Miller, B. D. Roth, Y. Song, B. A. Steinbaugh, K. Sun, B. D. Tait, M. C. Kowala, et al., *Bioorganic Med. Chem. Lett.* **2008**, *18*, 1151–1156.
- [30] V. A. Voicu, A. V. Medvedovici, K. Sakurada, H. Ohta, F. S. Radulescu, D. S. Miron, *Expert Opin. Drug Metab. Toxicol.* **2016**, *12*, 743–752.
- [31] A. Dahan, J. M. Miller, *AAPS J.* **2012**, *14*, 244–251.
- [32] M. J. Waring, *Expert Opin. Drug Discov.* **2010**, *5*, 235–248.
- [33] T. J. Ritchie, S. J. F. Macdonald, *Drug Discov. Today* **2009**, *14*, 1011–1020.
- [34] N. A. Meanwell, *J. Med. Chem.* **2011**, *54*, 2529–2591.
- [35] D. J. S. Jean, C. Fotsch, **2012**, DOI 10.1021/jm300343m.
- [36] J. Wells, A. R. Renslo, D. Wolan, J. Zorn, *Preparation of Chromonecarboxamides and Related Compounds as Activators of Executioner Procaspases 3, 6 and 7.*, **2009**.
- [37] P. Selzer, H. J. Roth, P. Ertl, A. Schuffenhauer, *Curr Opin Chem Biol* **2005**, *9*, 310–316.
- [38] M. P. Gleeson, *J. Med. Chem.* **2008**, *51*, 817–834.
- [39] M. M. Hann, G. M. Keserü, *Nat. Rev. Drug Discov.* **2012**, *11*, 355–365.
- [40] R. Singh, C. Sylvain, S. Holland, J. Zhang, J. J. Partridge, J. Clough, *Preparation of Triazole Derivatives as Axl Inhibitors.*, **2007**.
- [41] Z. Luo, J. Sheng, Y. Sun, C. Lu, J. Yan, A. Liu, H. Bin Luo, L. Huang, X. Li, *J. Med. Chem.* **2013**, *56*, 9089–9099.
- [42] G. K. Azad, R. S. Tomar, *Mol. Biol. Rep.* **2014**, *41*, 4865–4879.
- [43] T. Sakurai, M. Kanayama, T. Shibata, K. Itoh, A. Kobayashi, M. Yamamoto, K. Uchida, *Chem. Res. Toxicol.* **2006**, *19*, 1196–1204.
- [44] S. Thangamani, W. Younis, M. N. Seleem, *Sci. Rep.* **2015**, *5*, 11596.
- [45] A. Cooke, A. Anderson, K. Buchanan, A. Byford, D. Gemmell, N. Hamilton, P. McPhail, S. Miller, H. Sundaram, P. Vijn, *Bioorg. Med. Chem. Lett.* **2001**, *11*, 927–930.
- [46] A. Concas, G. Santoro, M. P. Mascia, M. Serra, E. Sanna, G. Biggio, *J. Neurochem.* **1990**, *55*, 2135–2138.
- [47] H. M. Bryson, B. R. Fulton, D. Faulds, *Drugs* **1995**, *50*, 513–559.

- [48] J. F. W. McOmie, M. L. Watts, D. E. West, *Tetrahedron* **1968**, *24*, 2289–2292.
- [49] M. Arend, B. Westermann, N. Risch, *Angew. Chem. Int. Ed.* **1998**, *37*, 1044–1070.
- [50] B. M. Trost, L. R. Terrell, *J. Am. Chem. Soc.* **2003**, *125*, 338–339.
- [51] A. L. Jackson, P. S. Linsley, *Nat. Rev. Drug Discov.* **2010**, *9*, 57–67.
- [52] R. Oliveira, D. Miranda, J. Magalhães, R. Capela, M. J. Perry, P. M. O’Neill, R. Moreira, F. Lopes, *Bioorganic Med. Chem.* **2015**, *23*, 5120–5130.
- [53] A. Boudhar, X. W. Ng, C. Y. Loh, W. N. Chia, Z. M. Tan, F. Nosten, B. W. Dymock, K. S. W. Tan, *Antimicrob. Agents Chemother.* **2016**, *60*, 3076–3089.
- [54] F. W. Muregi, A. Ishih, *Drug Dev. Res.* **2010**, *71*, 20–32.
- [55] J. J. Walsh, A. Bell, *Curr. Pharm. Des.* **2009**, *15*, 2970–2985.
- [56] C. Viegas-Junior, A. Danuello, V. da Silva Bolzani, E. J. Barreiro, C. A. M. Fraga, *Curr. Med. Chem.* **2007**, *14*, 1829–1852.
- [57] C. A. M. Fraga, *Expert Opin. Drug Discov.* **2009**, *4*, 605–609.
- [58] M. Kannan, A. V. Raichurkar, F. R. N. Khan, P. S. Iyer, *Bioorganic Med. Chem. Lett.* **2015**, *25*, 1100–1103.
- [59] R. Morphy, Z. Rankovic, *J. Med. Chem.* **2005**, *48*, 6523–6543.
- [60] L. C. S. Pinheiro, N. Boechat, M. D. L. G. Ferreira, C. C. S. Júnior, A. M. L. Jesus, M. M. M. Leite, N. B. Souza, A. U. Krettli, *Bioorganic Med. Chem.* **2015**, *23*, 5979–5984.
- [61] J. K. Baird, *N. Engl. J. Med.* **2005**, *352*, 1565–1577.
- [62] A. R. Renslo, *ACS Med. Chem. Lett.* **2013**, *4*, 1126–1128.
- [63] V. R. Solomon, W. Haq, K. Srivastava, S. K. Puri, S. B. Katti, *J. Med. Chem.* **2007**, *50*, 394–398.
- [64] J. Apelt, X. Ligneau, H. H. Pertz, J.-M. Arrang, C. R. Ganellin, J.-C. Schwartz, W. Schunack, H. Stark, *J. Med. Chem.* **2002**, *45*, 1128–1141.
- [65] H. Ishida, S. Isami, T. Matsumura, H. Umehara, Y. Yamashita, J. Kajita, E. Fuse, H. Kiyoi, T. Naoe, S. Akinaga, et al., *Bioorganic Med. Chem. Lett.* **2008**, *18*, 5472–5477.
- [66] E. R. Derbyshire, M. M. Mota, J. Clardy, *PLoS Pathog.* **2011**, *7*, DOI 10.1371/journal.ppat.1002178.
- [67] E. L. Flannery, A. K. Chatterjee, E. A. Winzeler, *Nat. Rev. Microbiol.* **2013**, *11*, 849–862.
- [68] K. Mendis, B. J. Sina, P. Marchesini, R. Carter, *Am. J. Trop. Med. Hyg.* **2001**, *64*, 97–106.
- [69] WHO (2015) World Health Organisation, *World Malaria Report*, **2015**.
- [70] B. Zhang, K. M. Watts, D. Hodge, L. M. Kemp, D. A. Hunstad, L. M. Hicks, A. R. Odom, *Biochemistry* **2011**, *50*, 3570–3577.
- [71] A. R. Odom, *PLoS Pathog.* **2011**, *7*, 1–4.
- [72] I. Hale, P. M. O’Neill, N. G. Berry, A. Odom, R. Sharma, *Medchemcomm* **2012**, *3*, 418–433.

- [73] L. S. Imlay, C. M. Armstrong, M. C. Masters, T. Li, K. E. Price, R. L. Edwards, K. M. Mann, L. X. Li, C. L. Stallings, N. G. Berry, et al., *ACS Infect. Dis.* **2015**, *1*, 157–167.
- [74] W. Wu, Z. Herrera, D. Ebert, K. Baska, S. H. Cho, J. L. DeRisi, E. Yeh, *Antimicrob. Agents Chemother.* **2015**, *59*, 356–364.
- [75] E. Yeh, J. L. DeRisi, *PLoS Biol.* **2011**, *9*, DOI 10.1371/journal.pbio.1001138.
- [76] J. D. Bowman, E. F. Merino, C. F. Brooks, B. Striepen, P. R. Carlier, M. B. Cassera, *Antimicrob. Agents Chemother.* **2014**, *58*, 811–819.
- [77] K. E. Price, C. M. Armstrong, L. S. Imlay, D. M. Hodge, C. Pidathala, N. J. Roberts, J. Park, M. Mikati, R. Sharma, A. S. Lawrenson, et al., *Sci. Rep.* **2016**, *6*, 36777.
- [78] F.-J. Gamo, *Drug Discov. Today. Technol.* **2014**, *11*, 81–88.
- [79] A. M. J. Oduola, N. F. Weatherly, J. H. Bowdre, R. E. Desjardins, *Exp. Parasitol.* **1988**, *66*, 86–95.
- [80] S. J. Foote, D. E. Kyle, R. K. Martin, A. M. Oduola, K. Forsyth, D. J. Kemp, A. F. Cowman, *Nature* **1990**, *345*, 255–8.
- [81] J. Straimer, N. F. Gnädig, B. Witkowski, C. Amaratunga, V. Duru, A. P. Ramadani, M. Dacheux, N. Khim, L. Zhang, S. Lam, et al., *Science (80-.)*. **2014**, *2624*, 428–431.
- [82] A. Alexandrov, M. Vignali, D. J. LaCount, E. Quartley, C. de Vries, D. de Rosa, J. Babulski, S. F. Mitchell, L. W. Schoenfeld, S. Fields, et al., *Mol. Cell. Proteomics* **2004**, *3*, 934–938.

Chapter 4

**Determining the Mechanism of Action
of the BITZ Chemotype:
A Computational and Biological Study**

4.1 Computational Modelling

In addition to *in vitro* enzymatic and cellular analysis of 1,2-benzo[*d*]isothiazol-3(2*H*)-one (BITZ) compound inhibition, molecular modelling studies were undertaken to provide insight as to how BITZ compounds may bind to the *PflspD* enzymatic target. Three-dimensional modelling of the *IspD* active site, using natural substrates and products of the enzyme, as well as potential inhibitor structures has been used to refine compound selection, guide rational inhibitor design and inform mechanism of action studies.

Ligand-protein docking is a computational approach that attempts to predict how small molecules bind to the structure of macromolecular targets and 'scores' their complementarity to the binding site. This computational technique, when used for virtual screening, can be used as a tool of enrichment increasing the potential of identifying compounds likely to show activity, potency and selectivity at an enzyme, making it widely used in both hit identification and lead optimisation stages of drug discovery.^[1]

The prediction of a compounds inhibitory activity can be made through the assessment of a molecule's binding affinity at a given binding site; this assessment determines how strongly a ligand interacts with enzyme protein which can be quantified by a measure known as a fitness score.^[2] Molecular docking involves an exploration of "docking space" where molecules are computationally placed in different conformations, orientations and locations within an enzyme active site to identify the most favourable binding "pose". The predicted binding energies of compounds and these identified binding "poses" are evaluated using scoring functions.^[1] Broadly, two docking methods can be adopted to explore "docking space": rigid-docking which treats both the ligand and protein as rigid molecules, or flexible-docking where the ligand, receptor or indeed both are treated as flexible entities. However, the two consistent features of all docking strategies are a search algorithm and a scoring function.^[2]

Docking algorithms generate "poses" of molecules at a docking site, sampling the "docking space" of a molecule to determine whether a given conformer or ligand orientation fits into a specified enzyme site.^[1] These docking algorithms consequently identify a molecular conformation that best complements the receptor structure. Genetic algorithms (GA) represent a stochastic search method, based on various computational models of evolution, which aim to mimic the natural process of evolution in determining an optimal combination of binding features.^[3,4] GAs represent a way of searching conformational space for an optimal docking solution that considers the number of degrees of freedom of the docked ligand and how each proposed ligand conformation may fit into the defined binding site of a macromolecule. GAs do not just search for a single solution but combine the best

aspects of good solutions, considering both ligand orientation and receptor alignment, therefore increasing the fitness of identified solutions to determine optimal binding poses.

Scoring functions predict the biological activity of compounds through the evaluation of interactions between the docked compound and biological target in an identified “pose”; this allows a fitness score to be assigned to the “pose” and the docking algorithm to be completed.^[1] The evaluation and ranking of predicted ligand conformations is a therefore crucial aspect of molecular modelling and computational screening approaches. The scoring functions used within docking programs often make various assumptions and simplifications in the evaluation of modelled protein-ligand complexes where three main types of scoring function are commonly used: force-field-based, empirical and knowledge-based scoring functions.^[1] Each of these categories classifies a number of distinct scoring functions, where each has unique subtleties that may be more suited to a specific modelling scenario. It is therefore unsurprising that much time and research has been invested in the optimisation and refinement of scoring functions, as well as determining specific scoring functions that may be most suited to a particular research question. Detailed analysis and evaluations of docking programs and scoring functions are well reviewed elsewhere.^[5–9]

Force-field-based scoring functions use molecular mechanic force fields to quantify the sum of two energies: the receptor–ligand interaction energy and internal ligand energy. With examples including GOLD and AutoDock, most force-field scoring functions consider only a single protein conformation, making it possible to eliminate the calculation of internal protein energy which greatly simplifies scoring. Empirical scoring functions, such as ChemScore or F-Score, are able to reproduce experimental data and are based on the idea that binding energies can be approximated by a summation of individual uncorrelated terms. Finally, knowledge-based scoring functions, such as DrugScore, are designed to reproduce experimental structures rather than binding energies.^[1,5,7,9–11]

This chapter will discuss the use of such molecular modelling techniques and described docking methods for the purpose of assessing BITZ compound alignment at the *PflspD* enzyme active site and subsequent deduction of protein-ligand interactions and a proposed mechanism of BITZ compound inhibition.

4.2 Utilising IspD Enzyme Homologues

Due to difficulties crystallising the *P. falciparum* IspD (*PflspD*) enzyme, we have not had access to the crystal structure of *PflspD* within our studies to date. Therefore, to facilitate docking studies of small molecules at the IspD enzyme, it was necessary to identify a IspD protein homologue with sequence

similarity to *PflspD* that could be used as a protein model to predict how small molecules are likely to bind to *PflspD*.

Comparison of *E. coli* and *P. falciparum* IspD enzyme homologues (enzyme active site defined as residues within 5 Å of the proposed binding site) indicates that 13 out of the 21 active site protein residues are identical between the two species, giving a 62% identity between *E. coli* and *P. falciparum* IspD at the active site. Considering the entire proteins of the two IspD homologues, 14% of protein residues show similarity, as opposed to exact identity, which puts the overall structure similarity of *E. coli* IspD (*EclspD*) and *PflspD* close to 23%, but with notably increased sequence and homologue identity at the active site. This heightened degree of active site similarity gives reassurance that *EclspD* (**Figure 4.1**) can be used as a suitable surrogate protein for *PflspD*.

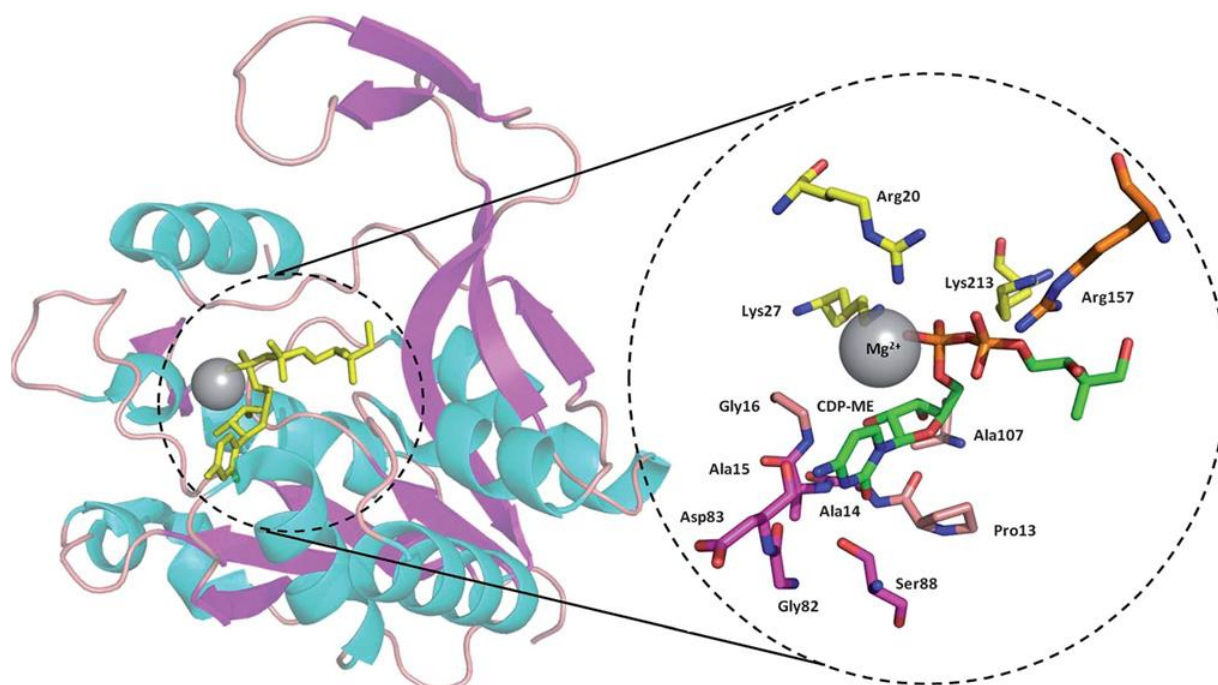


Figure 4.1 Tertiary structure of the *E. coli* IspD monomer with CDP-ME bound (PDB:1INI^[12]); α -helices and β -sheets are shown as cyan and purple cartoons respectively. In the close-up image of the CTP binding site; the cytosine binding region and residues are rendered pink; the ribose binding region and corresponding residues are rendered tan; the phosphate and MEP binding residues are rendered yellow and orange respectively. CDP-ME is coloured by element; carbon is green. The active site Mg^{2+} ion is shown as a grey sphere.^[13,14]

Working on the understanding that *EclspD* has an acceptable active site similarity to *PflspD*; it was selected as a surrogate protein for comparative three-dimensional docking studies and will continue to be used within molecular modelling studies until a crystal structure of *PflspD* is available. *EclspD* was therefore selected as a protein homologue of *PflspD* to identify a suitable modelling protocol with which to dock small molecules at the IspD active site. The rationale being that the identified docking protocol could then be transferred and applied to a homology model of the *PflspD* protein to facilitate

the assessment of small molecule BITZ inhibitors at the *P. falciparum* homologue of the IspD antimalarial enzyme target.

Evaluation of the binding poses of inhibitor structures at the *PfIspD* enzyme not only provides insight into aspects of the mechanism of action of BITZ compounds, but also facilitates application of the molecular design loop (**Figure 4.2**). The molecular design loop is comprised of three phases, molecular modelling, organic synthesis and biological testing, where knowledge gained from each phase can be fed directly into the next, therefore informing all stages of molecular design and continuing iterations of the cycle.^[15] With this depiction of a design and feedback strategy (**Figure 4.2**), it is easy to see that determining the predicted activities of small molecules at *PfIspD* will facilitate a more informed and predictive approach to inhibitor design, therefore enabling a refined compound selection process and optimised drug design.

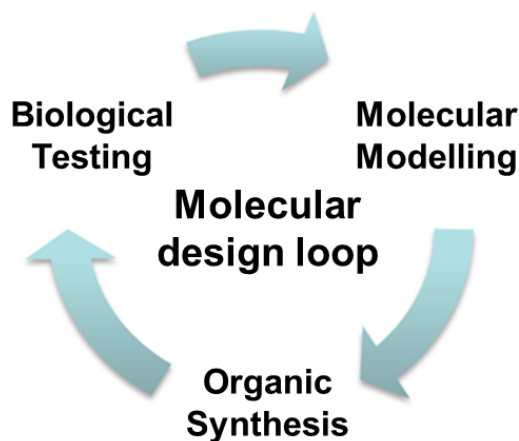


Figure 4.2 The molecular design loop.

4.2.1 Comparative Three-Dimensional Modelling at *E. coli* IspD

Due to the aforementioned sequence similarity between *EclspD* and *PfIspD* (**Section 4.1.1**), the known crystal structure of *EclspD* with the natural product, CDP-ME, co-crystallised in the enzyme active site (PDB: 1INI^[12]) was selected as the *EclspD* surrogate protein for comparative three-dimensional modelling studies. The first stage of these studies was to extract co-crystallised CDP-ME from the 1INI structure and re-dock the extracted ligand back into the *E. coli* enzyme. Molecular docking was initially carried out using the docking program GOLD 5.0.1^[5,6,16,17] and the ChemPLP scoring function,^[18] aiming to reproduce the crystallographic binding pose of CDP-ME at the *EclspD* active site of the 1INI structure. The overall aim of this process was to determine a well-defined docking protocol capable of reproducing the crystallographic binding pose of the 1INI protein-ligand complex,^[12] as obtained from the Protein Data Bank (PDB) archive.^[19] Identification of an accurate docking protocol then

facilitates the docking of unknown (or previously unstudied) small molecules at *EclspD* to determine a measure of binding affinity and an initial outlook as to the feasibility of proposed molecular docking studies.

4.2.2 Determining a Docking Protocol

The ligand docking program GOLD 5.0.1 (Genetic Optimisation for Ligand Docking), a component of the GOLD suite and work of The Cambridge Crystallographic Data Centre (CCDC),^[16,19] has been used as the docking program for molecular modelling studies throughout this body of research. GOLD software searches for the best ligand-protein interaction (“poses”) using GAs as previously described (Section 4.1).

A number of docking protocols were examined in order to identify an optimal protocol capable of accurately reproducing the crystallographic binding pose of CDP-ME in the *EclspD* 1INI active site. A suitable and accurate docking protocol is capable of consistently reproducing the experimental binding mode of a ligand (i.e. the binding mode defined by a crystallographic structure) which can be quantified by root-mean-square deviation (RMSD). RMSD provides a measure of the difference in values predicted by a model or estimator, compared to known values, and is therefore a measure of accuracy since it provides a means of comparing and measuring the 3D similarity of molecular poses. The prediction of a binding mode is considered successful, and therefore the docking protocol accurate, if the calculated RMSD value is below a threshold of 2 Å.^[16]

For each protocol generated, all standard default settings (SDS) in the GOLD Docking Setup remained unaltered, with the exception of the specified changes outlined in the tables below (Tables 4.1, 4.3 and 4.5). The natural enzyme product, CDP-ME, was used to define the ligand binding site as residues within 10 Å of the known crystallographic CDP-ME pose within *EclspD* (PDB ID: 1INI^[12]). Early docking termination was not allowed across all protocols. Varying numbers of GA runs were specified (Table 4.2, 4.4, 4.6 and 4.8) and performed for each protocol; this enabled a range of poses to be collected and an assessment made as to the effects of altering the number of GAs requested on the accuracy of resulting docking poses. Tables 4.2, 4.4, 4.6 and 4.8 illustrate the average fitness scores across the poses generated for each specification of GAs (10, 50, 100 and 500 respectively), as well as the associated RMSD values as compared to the native ligand, CDP-ME. ChemPLP was initially used as the scoring function in Protocols 1-3 since it had recently been identified as one of the best performing scoring functions for applications both in pose prediction and virtual screening studies.^[18]

Previous molecular modelling studies have indicated that a specified water molecule (HOH1091) in the active site of *EclspD* PDB ID: 1INI^[12]) may be involved in mediating protein-ligand interactions

between the *EclspD* protein and native ligands, facilitating a water-mediated hydrogen bonding interaction between *EclspD* protein residues and bound ligands. Further consideration and assessment of this water molecule was therefore considered appropriate in determining our docking protocol for application with this protein. It was important to be aware that HOH1091 may retain a role or exert influence in ligand docking and molecular pose alignment in ongoing docking studies.

Protocol 1	
Mg ²⁺ (Atom 1717)	Tetrahedral coordination geometry
Protonation	Hydrogens added
Waters	Water molecule HOH1091 extracted All other waters deleted
Ligands	'A' (CDP-ME) extracted
Binding site	Defined as 10 Å
Number of GA Runs	10, 50, 100, 500 (4 docking runs)
Scoring function	ChemPLP

Table 4.1 Specified parameters of docking **Protocol 1**.

GA Runs	10	50	100	500	Average
Average Fitness Score	107.58	104.77	105.52	100.99	103.97
Fitness Score SD	12.67	12.82	15.13	14.13	13.69
Average RMSD	5.11	4.29	5.23	5.29	4.98

Table 4.2 Outputs of CDP-ME docking into *EclspD* using **Protocol 1**.

The average RMSD of docking solutions generated using **Protocol 1** (**Table 4.1**) were significantly above the specified threshold of 2 Å (**Table 4.2**), highlighting that protein-ligand poses with low 3D similarity were being predicted and were not representative of the known crystallographic binding pose. It was therefore clear that **Protocol 1** (**Table 4.1**) could not accurately reproduce the CDP-ME binding pose of 1INI.

In order to improve the accuracy and reproducibility of docking predictions (reducing the RMSD of calculated poses) the specified ligand binding site was reduced from considering residues within 10 Å to those within 6 Å of the crystallographic CDP-ME binding orientation. This enabled the docking algorithm to search a more defined area of space within the *EclspD* binding pocket, slightly reducing the range and diversity of possible poses that could be identified, through a reduced number of degrees of freedom, therefore aiming to increase the accuracy of the protein-ligand poses identified.^[18]

Protocol 2	
Mg ²⁺ (Atom 1717)	Tetrahedral coordination geometry
Protonation	Hydrogens added
Waters	Water molecule HOH1091 extracted All other waters deleted
Ligands	'A' (CDP-ME) extracted
Binding site	Defined as 6 Å
Number of GA Runs	10, 50, 100, 500 (4 docking runs)
Scoring function	ChemPLP

Table 4.3 Specified parameters of docking **Protocol 2**.

GA Runs	10	50	100	500	Average
Average Fitness Score	109.03	96.42	99.89	97.37	100.68
Fitness Score SD	9.81	14.59	15.45	14.95	13.70
Average RMSD	3.79	5.08	4.86	5.13	4.72

Table 4.4 Outputs of CDP-ME docking into EclspD using **Protocol 2**.

The decrease in measured RMSD on reducing the specified binding site around the CDP-ME ligand from 10 Å to 6 Å, denoted an improvement in the accuracy of **Protocol 2** (**Table 4.3**) compared to **Protocol 1** (**Table 4.1**). However, the reduction in RMSD was not deemed sufficient (**Table 4.4**) and therefore additional changes to the docking protocol were made.

Protocol 3	
Mg ²⁺ (Atom 1717)	Metal ion extracted
Protonation	Hydrogens added
Waters	Water molecule HOH1091 extracted All other waters deleted
Ligands	'A' (CDP-ME) extracted
Binding site	Defined as 6 Å
Number of GA Runs	10, 50, 100, 500 (4 docking runs)
Scoring function	ChemPLP

Table 4.5 Specified parameters of docking **Protocol 3**.

GA Runs	10	50	100	500	Average
Average Fitness Score	94.84	90.60	84.24	85.45	88.78
Fitness Score SD	6.44	16.35	16.35	14.95	13.52
Average RMSD	2.72	3.97	4.31	4.30	3.83

Table 4.6 Outputs of CDP-ME docking into EclspD using **Protocol 3**.

Extraction of the Mg^{2+} ion in the application of **Protocol 3** (**Table 4.5**) was seen to slightly reduce the RMSD of generated poses; however, the reduction in RMSD still did not meet the required 2 Å value and, in addition, an undesirable reduction in the average fitness scores of poses was now also seen. This is perhaps unsurprising as the Mg^{2+} divalent cation is a known feature of the EclspD binding site and should therefore be retained during the development of a docking protocol. Comparison of the outputs from **Protocols 1-3** highlight that the measured fitness scores were generally higher when the Mg^{2+} ion was specified as part of the docking procedure.

Overall, **Protocols 1-3**, (**Tables 4.1, 4.3** and **4.5**) were unable to accurately reproduce the crystallographic binding pose of CDP-ME as defined by the 1INI crystal structure, as highlighted by consistent RMSD values of > 2 Å, indicating inaccuracy in the protocol. It was therefore decided that the scoring function specified in the docking protocol should be replaced in an attempt to correct this problem. GoldScore was selected as the scoring function to replace ChemPLP in **Protocol 4** (**Table 4.7**) due to previous successes with this scoring function in other molecular modelling studies conducted within the group.^[20]

Protocol 4	
Mg ²⁺ (Atom 1717)	Mg²⁺ ion present Coordination geometry not specified
Protonation	Hydrogens added
Waters	Water molecule HOH1091 extracted All other waters deleted
Ligands	'A' (CDP-ME) extracted
Binding site	Defined as 6 Å
Number of GA Runs	10, 50, 100, 500 (4 docking runs)
Scoring function	GoldScore

Table 4.7 Specified parameters of docking **Protocol 4**.

GA Runs	10	50	100	500	Average
Average Fitness Score	95.63	89.36	93.26	92.91	92.79
Fitness Score SD	12.97	11.78	12.90	12.59	12.56
Average RMSD	2.56	2.09	1.79	1.96	2.10

Table 4.8 Outputs of CDP-ME docking into *EclspD* using **Protocol 4**.

The docking outputs from **Protocol 4** (**Table 4.7**) showed improved levels of accuracy, with RMSD values now $< 2 \text{ \AA}$ (**Table 4.8**) when ≥ 100 GA docking poses were requested. The improvement in protocol accuracy, in terms of increased average fitness scores and lower RMSD values, may be due to a combination of both reducing the specified binding site around the CDP-ME ligand and altering the scoring function used to predict the strength of binding of identified poses. Docking **Protocol 4** (**Table 4.7**) was consequently selected and applied within our *EclspD* molecular modelling studies from this point.

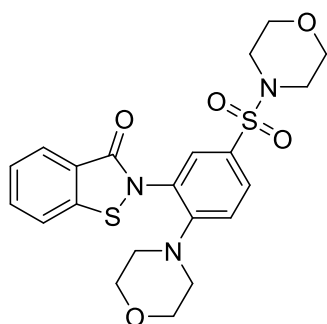
4.2.3 Molecular Modelling of the HTS Hit Compounds at *EclspD*

Docking **Protocol 4** (**Table 4.7**) was used to model the 76 hit compounds identified from the initial chemoinformatic HTS and virtual screening study conducted using the “Biofocus Combined Library” (**Section 2.2.1** and **Appendix 1**). 50 GA docking poses were modelled for each ligand in order to achieve an acceptable compromise between docking accuracy and computational calculation time. The selected 76 ligands were built manually using ChemDraw^[21] and energy minimised using Spartan '08.^[22] Spartan '08 was used to perform equilibrium geometry calculations using the molecular mechanics MMFF level of theory,^[23] prior to docking the built ligands at the *EclspD* active site. The GoldScore scoring function was used to evaluate the docking poses of these 76 ligands at *EclspD*; where the identified poses were then rescored (a method of pose re-evaluation)^[11] using the ChemPLP and ChemScore scoring functions. The process of rescored identified poses in a separate step, distinct from the initial docking procedure, using alternative scoring functions is a way of certifying that consistent and optimal docking poses are identified by a defined docking protocol and the original scoring function used.^[11]

The 76 docked compounds were ranked according to their associated fitness scores for complementarity to the binding site which gave a prediction of inhibitory compound activity at the *EclspD* enzyme. A higher assigned fitness score (or higher average fitness score from across the 50 GA poses calculated for each molecule) gave a higher compound ranking, therefore indicating likely enhanced inhibitory activity at *EclspD*. Of the 76 HTS hit compounds docked at the *EclspD* active site,

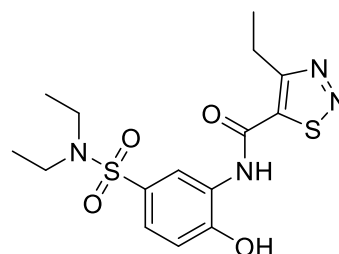
GA docking poses were identified for 12 compounds that had measured GoldScore fitness scores of > 70.

Of these 12 compounds, 10 showed consistent levels of complementarity to the *EclspD* binding site with average GoldScore fitness scores of > 61 (averaged across the 50 docking poses). Although these values not as high as the average GoldScore score calculated for the native CDP-ME ligand; [CDP-ME GoldScore = 89.36; Fitness Score SD = 11.78; averaged across 50 GA poses using **Protocol 4** at *EclspD* (**Table 4.7**)]; comparison of these predicted protein-ligand binding energies provides a general measure of our HTS compound complementarity to *EclspD*, compared to the native enzyme product. Significantly, the two most active HTS hit compounds **DT2009-0097223** and **DT2009-0168020** (**Figure 4.3**, see also **Chapter 2, Section 2.2.4**) were present in this small group of 10 compounds that were highlighted as showing satisfactory and consistent complementarity to *EclspD*.



DT2009-0168020

PflspD IC₅₀ = 484 ± 149 nM
 MW = 461.55 gmol⁻¹, LE = 0.20
 Average GoldScore Fitness score: 61.48
 GoldScore Fitness score of the highest scored
 predicted binding pose: 71.23



DT2009-0097223

PflspD IC₅₀ = 777 nM
 MW = 384.47 gmol⁻¹, LE = 0.24
 Average GoldScore Fitness score: 63.05
 GoldScore Fitness score of the highest scored
 predicted binding pose: 73.94

Figure 4.3 Chemical structure; *PflspD* enzyme activity; molecular weight; ligand efficiency, average GoldScore fitness score and the GoldScore fitness score of the highest scored binding pose predicted in *EclspD* molecular docking studies of **DT2009-0097223** and **DT2009-0168020**.

An appropriate and functioning docking protocol (**Protocol 4, Table 4.7**) was therefore identified that is capable of accurately reproducing the known crystallographic binding pose of CDP-ME (PDB ID: 1INI^[12]) and generating rational protein-ligand binding poses (since no negative or anomalous binding scores were identified) with a diverse range of small molecules. The latter was highlighted by the successful assessment of the 76 HTS hit compounds (**Appendix 1**) at *EclspD*. These ligands cover a broad range of chemical space that is very much unrelated to the native CDP-ME ligand and therefore confirms that docking **Protocol 4** is capable of assessing a broad range of molecules at a defined binding site. Having acquired confidence in **Protocol 4**, the outlined docking protocol (**Table 4.7**) was

transferred and applied to the study of the *Pf*lspD enzyme, enabling the evaluation of small molecules at this selected antimalarial target.

4.3 *Pf*lspD Homology Model

A homology model of the *Pf*lspD enzyme (**Figure 4.4**), based on the primary sequence Q8I273 and the 1INI *E. coli* structure template^[12] was created with the PHYRE online homology modelling tool^[24] and, after validation using the WHATIF interface, was assessed to have a confidence of 98.2%.^[25] The *Pf*lspD homology model and determined protocol (**Protocol 4, Table 4.7**) were used to dock BITZ compounds into the CTP binding site of *Pf*lspD using GOLD 5.0.1 software.^[16]

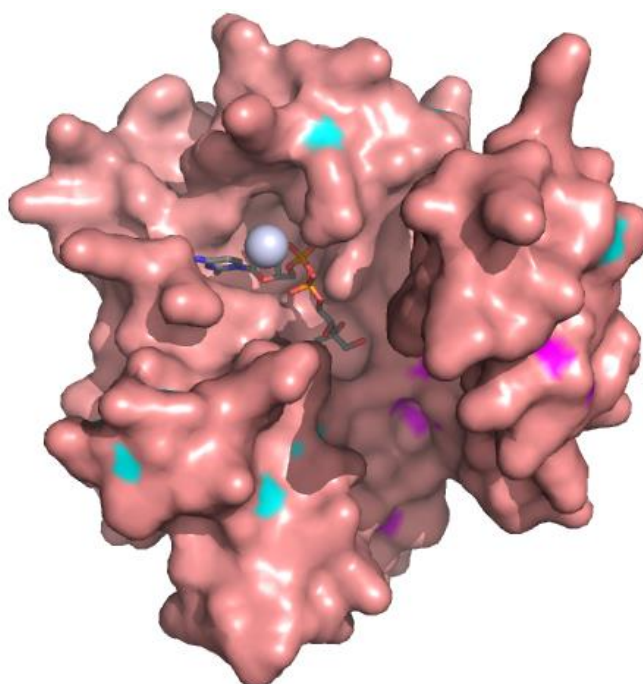


Figure 4.4 Tertiary structure of the *P. falciparum* IspD homology model with the natural ligand, CDP-ME, occupying the enzyme binding pocket. The surface of *Pf*lspD homology model is rendered pink; CDP-ME is shown as a stick representation and coloured by element: carbon atoms are grey; the Mg²⁺ divalent cation is shown as a grey sphere.^[20] Image created using PyMOL.^[26]

As an initial docking study, the CTP enzyme substrate was docked into the *Pf*lspD homology model and found itself to have an average GoldScore of 72.0 ± 4 . This enabled a more precise and informed assessment of the predicted binding energies of BITZ derived compounds in subsequent molecular modelling, giving a truer picture and more exact measure of the relative binding affinity of specified BITZ compounds at the *Pf*lspD CTP binding site. The aims of modelling studies from this point were to determine the likely binding mode and alignment of BITZ derived compounds as inhibitors of *Pf*lspD; visualize contacts made between these inhibitors and the defined protein binding site; assess the

strength of inhibitor-protein interactions and therefore estimate the binding affinity and behaviour of BITZ compounds at the *Pf*lspD active site (**Figure 4.5**).

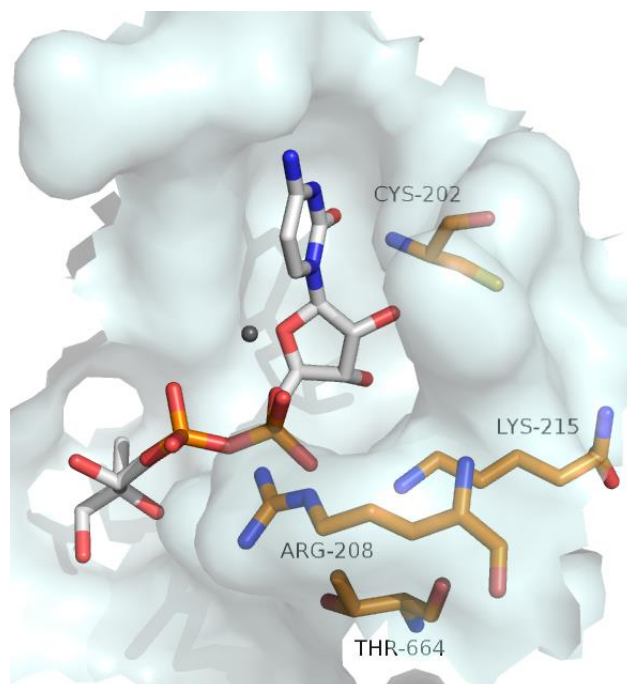


Figure 4.5 Image of the *P. falciparum* IspD homology model active site with the natural product, CDP-ME, occupying the binding pocket. The surface of *Pf*lspD active site is rendered white; CDP-ME is shown as a stick representation and coloured by element: carbon atoms are light-grey, nitrogen atoms are blue, oxygen atoms are red and phosphorus atoms are orange. Selected *Pf*lspD active site protein residues, Cys-202, Lys-215, Thr-664 and Arg-208, are highlighted and depicted as sticks with their carbon protein backbone coloured orange. The Mg^{2+} divalent cation is shown as a small sphere and rendered dark grey.^[20] Image created using PyMOL.^[26]

4.3.1 Molecular Modelling of the Focused Ligand Library of 5000 Compounds at *Pf*lspD

To ensure that comparable docking outputs to those achieved with *Ecl*spD (PDB ID: 1INI^[12]), in terms of rational docking poses and similar docking scores (in the 40 – 70 range), could be achieved using the *Pf*lspD homology model: the original focused ligand library of 5000 compounds, selected from the “Biofocus Combined Library” (**Chapter 2, Section 2.2.1**), was docked into the *Pf*lspD homology model using **Protocol 4 (Table 4.7)**. 10 GA searches were specified per ligand and GoldScore was used as the scoring function. Compared with earlier *Ecl*spD molecular docking (**Section 4.2.2**), the number of GA searches requested per ligand, now using the *Pf*lspD homology model, was reduced from 50 GA to 10 GA to minimise the computational time expenditure required to dock and assess the large number of compounds within the focused ligand library.

Following docking of these 5000 compounds into the active site of the *Pf*lspD homology model, all assessed ligands were attributed a GoldScore docking score within the range of 20-70. Consequently,

it can be argued that the initial molecular docking outputs using *PflspD* are broadly representative of the varying *PflspD* activity of the compounds identified within the focused ligand library (**Chapter 2, Section 2.2.4**). The majority of compounds from the focused ligand library were predicted to adopt docking poses that were assessed to have mid-range fitness scores (between 30 and 50). This suggests a lack of complementarity to the *PflspD* active site for the majority of the 5000 compounds and therefore a likely lack of *PflspD* inhibitory activity. This assessment is supported by the findings of the HTS output in which > 4900 of the compounds screened were found to possess suboptimal *PflspD* activity of less than the required activity threshold of 20 μM against the enzyme.

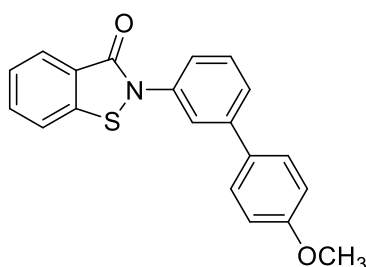
A small number of the 5000 docked compounds were predicted to adopt binding poses of acceptable complementarity to *PflspD* which was reflected in higher attributed binding scores (values ≥ 50) of these predicted poses. The docking outputs therefore suggest that a small proportion of the 5000 compounds are likely to display inhibitory activity against *PflspD*. This general observation is reflected in and supported by the identification of 76 hit compounds (a small compound subset) from the initial HTS study of the “Biofocus Combined Library” (**Chapter 2, Section 2.2.4**) as being active against *PflspD*.

Further computational analysis has shown that these docking studies, and the resulting binding scores for predicted compound poses, did not provide a good indication of whether a compound would be active or inactive against the *PflspD* enzyme. Average docking scores of compounds categorised as active were highly similar to the average scores of those classified as inactive, showing that the distribution of compound binding scores did not correlate to classifications of enzymatic activity.^[20] Despite this, we were able to take confidence from these molecular modelling studies using the ‘Focused Ligand Library’ as attentions were now focused towards docking designed BITZ inhibitors into the *PflspD* homology model.

4.3.2 Molecular Modelling of BITZ Compounds at *PflspD*

To gain insight into the behaviour, alignment and spatial fit of BITZ inhibitors within the *PflspD* active site, one of the most promising BITZ compounds **1** (**Figure 4.6**) (see also **Chapter 3, Section 3.2, Figure 3.3, Table 3.1: Compound 4**) was modelled in the *PflspD* homology model using docking **Protocol 4** (**Section 4.2.1, Table 4.7**).

BITZ inhibitor **1** (**Figure 4.6**) was docked into the active site of the *PflspD* homology model using **Protocol 4** (**Table 4.7**) with a search criteria of 50 GA predictions to assess the alignment and predicted docking pose of **1** at *PflspD*. The highest scored binding pose and average fitness scores from the 50 calculated binding poses are given below (**Figure 4.6**), along with the chemical structure of **1**.



1

PflspD IC₅₀ = 0.21 ± 0.089 μM
 Whole Cell 3D7 EC₅₀ = 0.95 ± 0.089 μM
 MW = 333.08 gmol⁻¹
 Average GoldScore Fitness score: 53.27
 Standard deviation: 3.74
 GoldScore Fitness score of the highest scored
 predicted binding pose: 59.36

Figure 4.6 Chemical structure; *PflspD* enzyme activity; whole cell 3D7 activity; molecular weight; average GoldScore fitness score and the GoldScore fitness of the highest scored binding pose predicted in *PflspD* molecular docking studies of **1** in the *PflspD* homology model.

Molecular docking of **1** and the subsequent evaluation of resulting conformational poses has revealed that BITZ compounds target the CTP binding pocket of *PflspD* and adopt a broadly similar binding alignment to the natural product, CDP-ME (**Figure 4.7**). BITZ compounds therefore demonstrate good complementarity and shape-fit to the *PflspD* active site where a number of hydrogen bonding and hydrophobic interactions can be made between BITZ inhibitors and the protein residues in the active site which aid initial non-covalent recognition and protein-ligand interactions.

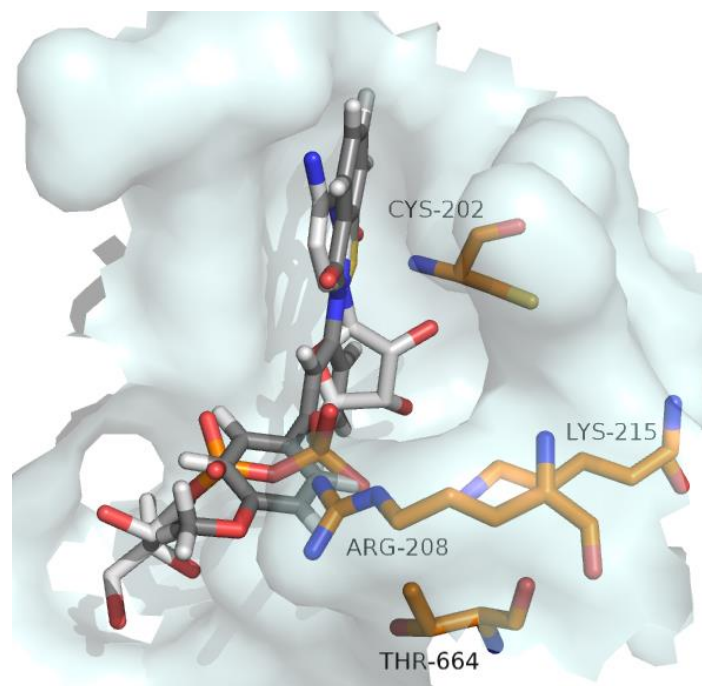


Figure 4.7 Inhibitor **1** and CDP-ME modelled in the active site of the *PflspD* homology model. *PflspD* active site rendered as a white surface. Key active site protein residues are depicted as sticks: carbon atoms coloured orange; inhibitor **1** is shown as a stick representation: carbon atoms are dark grey; CDP-ME shown as a stick representation: carbon atoms are light-grey. Image created using PyMOL.^[26]

Overlaying the two modelled structures of **1** and CDP-ME highlights that they occupy the same area of space within the *PflspD* active site and that the BITZ analogue is aligned to make a number of hydrogen bond contacts and hydrophobic interactions with protein residues in the binding site (**Figure 4.8**).

A hydrogen bonding interaction of 2.9 Å is predicted (highlighted in **Figure 4.8**) between the oxygen atom of the methoxy functionality in **1** and the Arg-208 *PflspD* active site protein residue. A second binding interaction was also identified between a hydrogen atom on the aromatic phenyl D ring of **1** and the Thr-664 *PflspD* active site protein residue: the measured distance between these two entities is 3.4 Å and therefore likely represents a second hydrogen bonding interaction, or potentially a hydrophobic interaction. These two identified molecular interactions represent non-covalent protein-ligand contacts which aid initial compound recognition in the *PflspD* active site therefore promoting the alignment and binding of **1**.

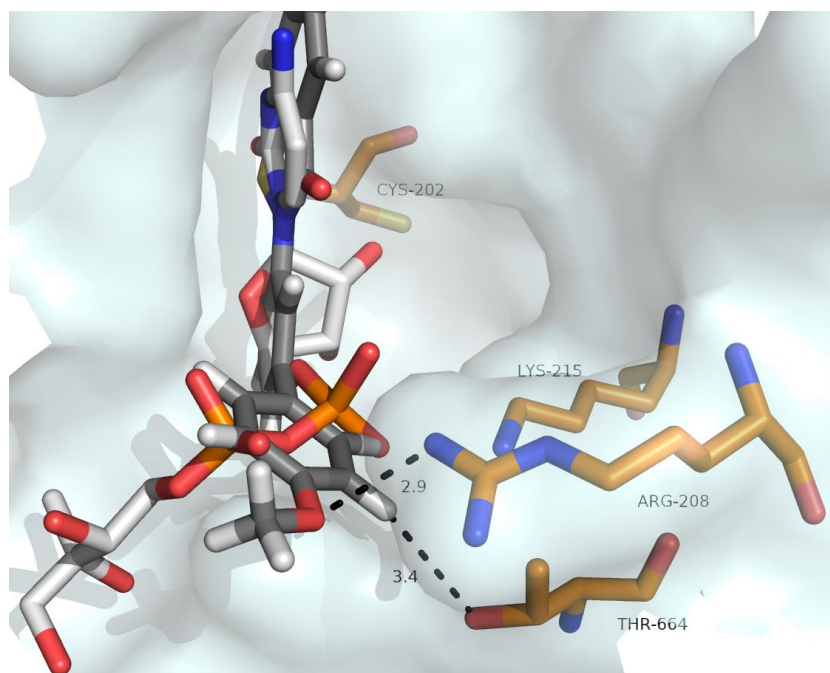


Figure 4.8 Inhibitor **1** and CDP-ME modelled in the active site of the *PflspD* homology model. Key protein residues are depicted as sticks: carbon atoms coloured orange; inhibitor **1** is shown as a stick representation: carbon atoms are dark grey; CDP-ME is shown as a stick representation: carbon atoms are light-grey; hydrogen bonds between **1** and specified protein residues are depicted as black, dotted lines with predicted hydrogen bond distance in Ångstroms. Image created using PyMOL.^[26]

Indeed, a number of potential docking poses were predicted for compound **1** which were assigned a range of binding scores (representative example, **Figure 4.9**) However, since these predicted poses predominately mirror the binding alignment of CDP-ME (**Figure 4.5**), this supports the assessment that the identified BITZ poses are representative of the true binding orientation and alignment of BITZ inhibitors at the *PflspD* active site.

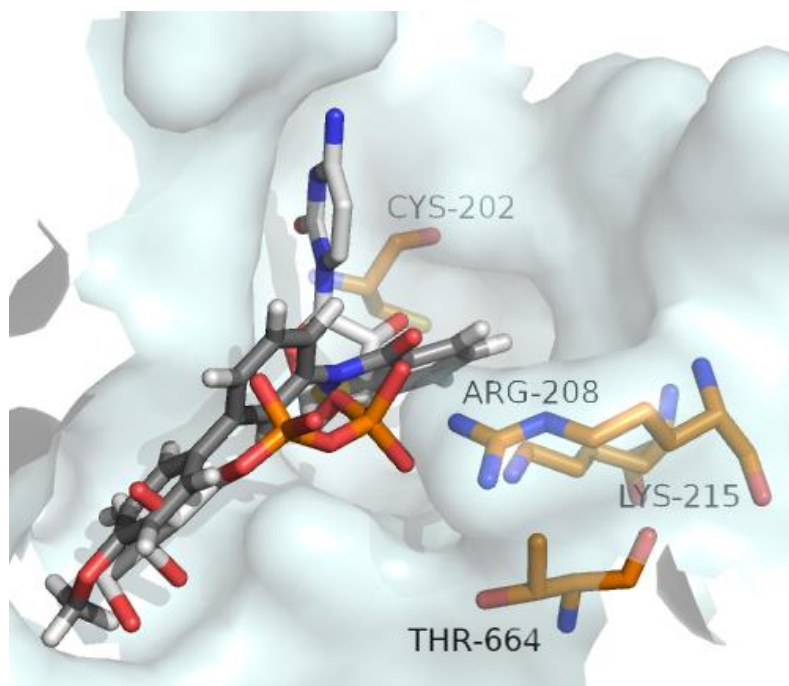


Figure 4.9 Image shows an alternative binding pose predicted for **1** modelled with CDP-ME in the active site of the *PflspD* homology model. The depiction of this alternative predicted binding pose highlights that **1** remains aligned to CDP-ME in the *PflspD* active site. Image created using PyMOL.^[26]

Visualisation of **1** within the *PflspD* binding pocket also provides an assessment of inhibitor shape fit at the active site. Docking images clearly show that the C-ring *meta*-substitution pattern within BITZ compounds enhances complementarity to the binding site through the presence of this molecular 'kink' that mirrors the shape of the active site. Molecular modelling therefore highlights that the *PflspD* active site is neither linear nor tube-like in shape which perhaps explains the loss of *PflspD* inhibitory activity observed with linear BITZ analogues.

It can therefore be rationalised that the chemical construct of linear BITZ analogues, with *para*-substitution across the C-ring are likely to have poor complementarity to the *PflspD* active site, with poor shape-fit and little alignment to active site amino acids (as observed (**Chapter 2, Section 2.7**)). However, it is also clear from the construct of the *PflspD* active site there is room for expansion of the BITZ construct both in the inhibitor side chain and around the BITZ head group itself. Structural expansion of BITZ analogues could enable more complete occupation of the *PflspD* active site and therefore increase the likelihood of achieving protein-ligand contacts which may in turn promote stronger compound binding. This, in theory, should produce more active *PflspD* BITZ inhibitors.

4.3 Mechanism of Action

In addition to inhibitor alignment and spatial fit with the *PflspD* active site, molecular modelling studies also enabled insights to be gained into the proposed mechanism of *PflspD* enzyme inhibition. Molecular docking of **1** clearly indicates that the inhibitor binds within the CTP substrate-binding pocket, aligned with the natural product CDP-ME. This identified alignment and orientation places the BITZ warhead proximal to the *PflspD* active site cysteine-202 (Cys-202) residue (**Figure 4.10**).^[27]

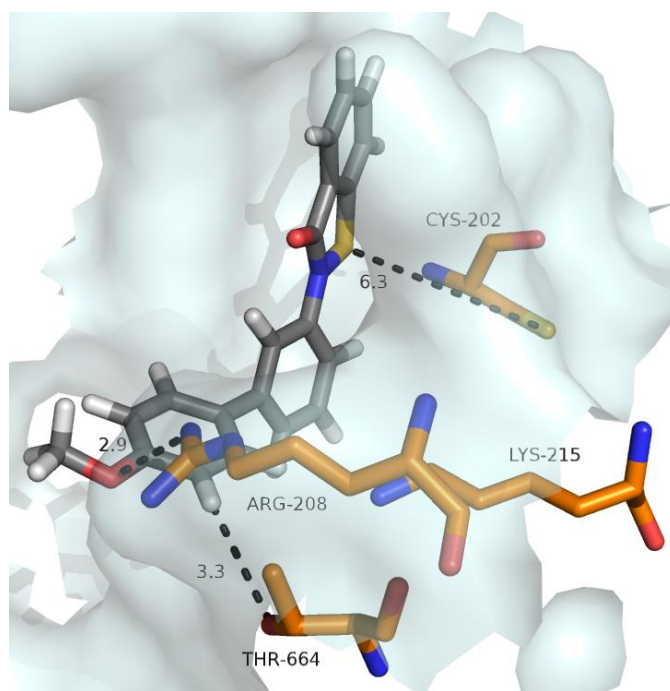


Figure 4.10 Inhibitor **1** modelled in the active site of *PflspD* homology model with potential interactions between the compound and active site protein residues highlighted. Points of interaction are depicted by black, dotted lines with predicted distances given in Ångstroms. Image created using PyMOL.^[26]

It is predicted that the thiol moiety of Cys-202 could react with the sulfur heteroatom of the BITZ warhead, forming a covalent disulfide adduct, while the carbonyl oxygen of the head group would be within hydrogen bonding distance of the backbone nitrogen atoms of the Gly-203 and Gly-204 residues (**Figure 4.11**). Formation of this covalent adduct would result in the occlusion of the *PflspD* active site, preventing natural substrate binding and therefore render the enzyme inactive.^[27] Taken all together, a distinctive mechanism of action can be proposed for these novel *PflspD*-inhibiting BITZ compounds, which proceeds with initial non-covalent active site recognition, promoted by complimentary shape fit and non-covalent protein-inhibitor interactions; but that ultimately relies on the formation of a covalent enzyme-inhibitor adduct which renders the enzyme inactive.

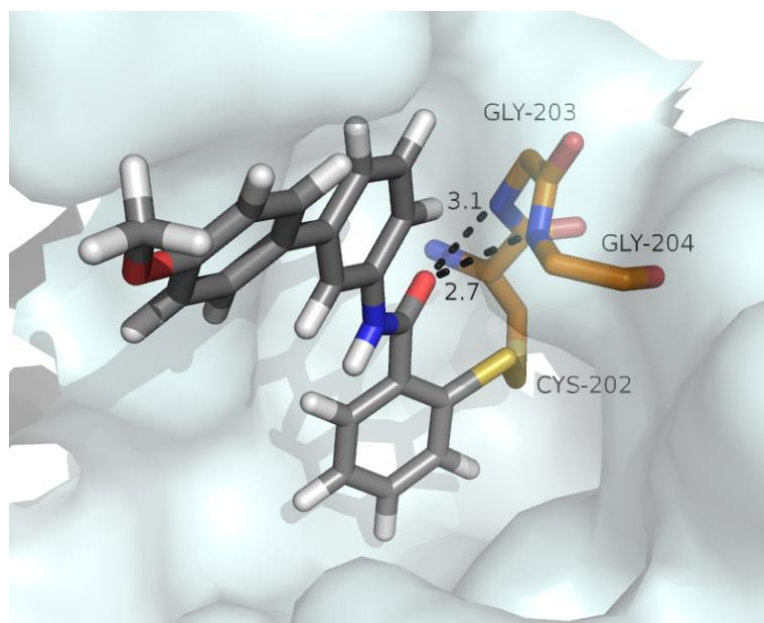
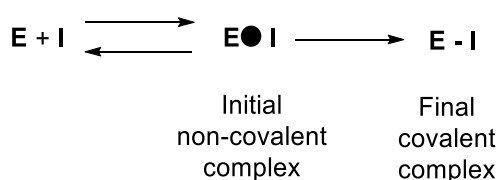


Figure 4.11 Inhibitor **1** modelled in the active site of *PflspD* homology model, covalently bound to the Cys-202 residue. The *PflspD* active site is rendered as a white surface. Active site protein residues predicted to interact with BITZ inhibitors (Gly-203 and Gly-204, hydrogen bonds; Cys-202, disulfide adduct) are depicted as sticks with carbon atoms coloured orange; inhibitor **1** is displayed as sticks: carbon atoms are dark grey; hydrogen bonds are depicted as black, dotted lines with predicted hydrogen bond distance in Ångstroms. Image created using PyMOL.^[26]

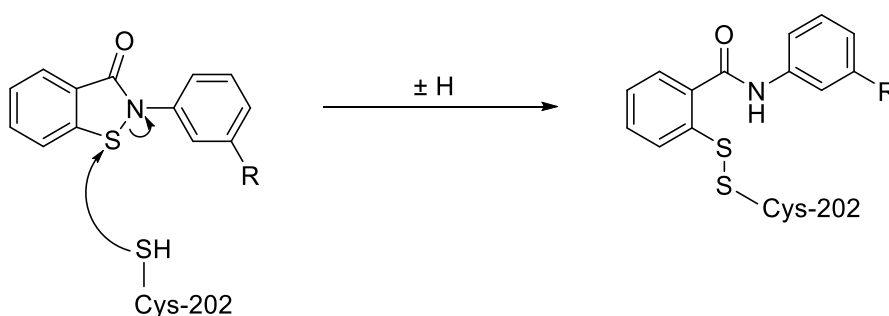
The model of proposed covalent *PflspD* enzyme inhibition is in line with known mechanistic features of this mode of protein inhibition and a general description of target-specific covalent inhibition (**Scheme 4.1**) which occurs over at least two steps.^[28] For covalent inhibition to occur, a compound must first bind non-covalently to its target protein, placing a reactive electrophile in the inhibitor close to a specific nucleophile within the target protein. The resulting non-covalent complex can then undergo targeted and specific bond formation between these two entities, giving rise to the final inhibited complex (**Scheme 4.1**).



Scheme 4.1 The generic mechanism of action of target-specific covalent inhibition. Scheme adapted from ^[28].

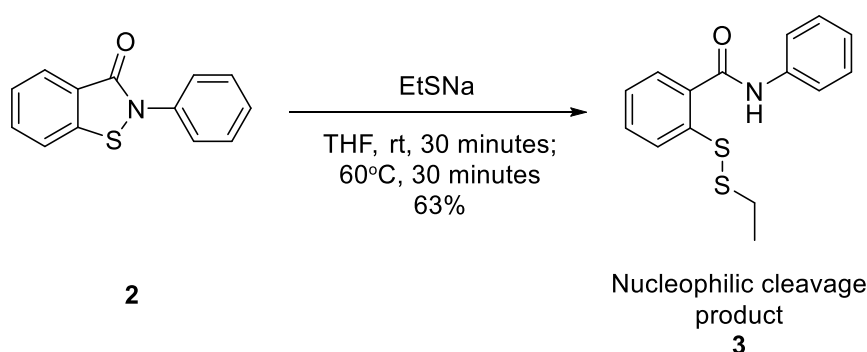
4.3.1 Biomimetic Mechanistic Evaluation

The proposed mechanism of action of BITZ derived inhibitors involves a combination of N-S bond cleavage in the BITZ warhead and cysteine-trapping of the Cys-202 residue in the *PflspD* active site. Disulfide bond formation between the BITZ motif and Cys-202 is mediated by nucleophilic attack of the Cys-202 thiol onto the sulfur atom of the N-S bond within the BITZ core (**Scheme 4.2**). Cleavage of the N-S heteroatom bond results in disulfide bond formation which ultimately blocks the *PflspD* active site to entry and binding of natural enzyme substrates: CTP and MEP.



Scheme 4.2 Proposed mechanism of BITZ ring opening mediated by the Cys-202 residue in the *PflspD* active site.

To explore the validity of this proposal, ring opening of the benzo[*d*]isothiazol-3(2*H*)-one core was assessed by reaction of **2** with the nucleophilic species, sodium ethanethiolate to chemically cleave the N-S bond of the BITZ head group.^[29] Detection of BITZ ring opening was assessed by ¹H NMR and mass spectrometry.



Scheme 4.3 Synthetic strategy for compound **3**; cleavage and ring opening of **2** mediated by the nucleophilic species sodium ethanethiolate.^[29]

Despite the rapid synthetic route used to generate **3**, which proceeded in moderate yield; analysis of the resulting material by ¹H NMR was unable to confirm generation of required chemical construct of **3**. The obtained ¹H NMR spectra identified a broad singlet, with an integration of one, at 10.57 ppm, which likely corresponds to the NH of the amide functionality in **3** and therefore suggests that sodium

ethanethiolate causes ring opening of **2**. However, the characteristic ethyl splitting pattern (a quartet, with an integration of two, and a triplet, with an integration of three) was not present. Analysis of the synthesised material by mass spectrometry identified a mass ion (the base peak of the spectrum) with an associated ES+HRMS m/z of 479.0868 $[M+Na]^+$. It is likely that this mass ion corresponds to the proposed dimer structure **4** (Figure 4.12), that would be generated through the self-dimerization of **3** following ring opening and cleavage of **2** by sodium ethanethiolate.

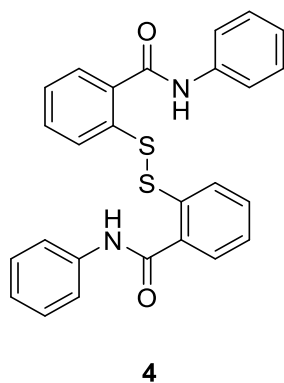


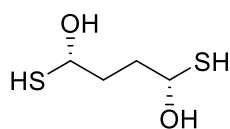
Figure 4.12 Chemical structure of the proposed dimer **4**.

Further analysis of the product material (**Scheme 4.3**) by infrared (IR) spectroscopy was unable to detect the proposed disulfide bond of **3** due to its weak absorption and low wavenumber at ~ 500 cm^{-1} which is difficult to detect in the fingerprint region of IR spectra.^[30] In addition, no thiol peak, usually detectable as a narrow and weak absorption between $2600 - 2400$ cm^{-1} , or a S-CH₂ stretch at ~ 2860 cm^{-1} could be identified.^[30] Together, these results strongly suggest that **4** is the isolatable and detectable product following the nucleophilic ring opening of **2**, outlined in **Scheme 4.3**, due to the self-dimerization of **3** following the initial reaction of **2** with sodium ethanethiolate. This result therefore remains consistent with the nucleophilic ring opening of the BITZ motif, supporting the proposed mechanism of inhibition *via* disulfide bond formation through attack of the active site cysteine-202 residue on the BITZ core, occluding the *Pfl*spD active site and causing inhibition of the enzyme.

4.3.2 *PflspD* Enzyme Rescue

In order to provide further evidence that inhibition of *PflspD* by BITZ compounds is the result of disulfide bond formation, some *PflspD* enzyme rescue experiments were conducted. The aim of these experiments was to determine if *PflspD* enzyme activity could be restored (or 'rescued') by application of a disulfide reducing agent following inhibition of the *PflspD* enzyme by treatment with BITZ compounds.

Dithiothritol (DTT) (**Figure 4.13**), also known as Cleland's reagent, is a small, highly potent redox reagent that is widely used in the analysis of protein structure and function.^[31] This synthetic reagent is able to completely reduce disulfide bonds as well as protect thiol groups (-SH) from oxidation, therefore making it an ideal protecting agent for this chemical functionality.^[32] In relation to our study, DTT is able to reduce disulfide bonds between cysteine residues and can therefore be used to specifically implicate these residues in the biological activity of molecules at protein targets.^[31]



Dithiothreitol

Figure 4.13 Chemical structure of 1,4-dithiothreitol (DTT).

PflspD enzyme rescue experiments using DTT were performed in a proof-of-concept study to confirm that BITZ compounds induce *PflspD* enzyme inhibition through formation of a covalent disulfide bond to cysteine residues in the enzyme active site. Since a reducing agent, such as DTT, is capable of reducing and therefore breaking the inhibitory sulfur-Cys-202 bond, relief of *PflspD* enzyme inhibition should be observed following addition of the reducing agent into the *PflspD* enzyme assay. Observation of this phenomenon would consequently provide further support for the proposed mechanism of *PflspD* inhibition through formation of a disulfide bond between the sulfur heteroatom of the BITZ warhead and the Cys-202 residue.

Consequently, a modified *PflspD* enzyme assay (**Chapter 2, Section 2.2.3**) was carried out in which the assay was spiked with DTT seven minutes into the usual protocol. Standard *PflspD* enzyme assays were conducted, with and without 5 μ M of **1**; after seven minutes of standard conditions, the assay was spiked with DTT to give a final concentration of 5 mM. DTT spiking of the *PflspD* enzyme assay, first treated with 5 μ M of **1**, was shown to relieve inhibition of the enzyme (**Figure 4.14**). The bar graph depicts the level of *PflspD* enzyme activity, measured by 2-amino-6-mercapto-7-methyl purine release

at an absorption of 360 nm^[33] (Chapter 2, Section 2.2.3), both pre- and post-DDT treatment in separate experiments, that were conducted with and without the presence of **1**.

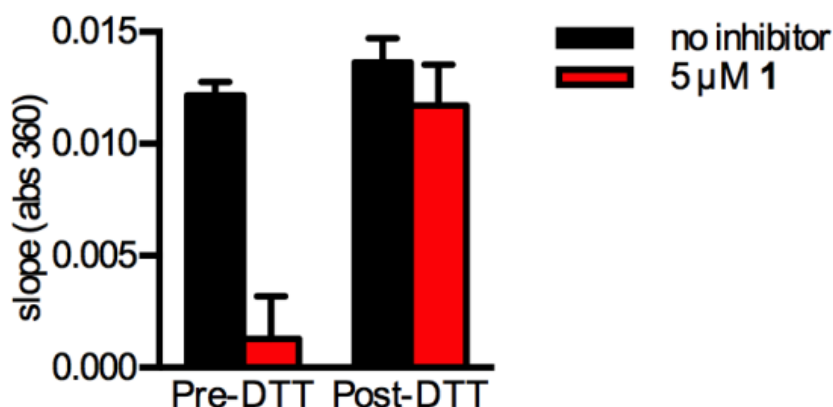


Figure 4.14 Bar graph representing the reaction rate of purified recombinant *PflspD*, in the presence and absence of 5 μM **1**, before and after treatment with 5 mM DTT. All data points are representative of four independent replicates.

The average measured absorption at 360 nm in the *PflspD* enzyme assay, without treatment with **1** (represented by black bars, **Figure 4.14**; and the black line, **Figure 4.15**), is highly comparable both before and after treatment with DTT: (without **1**, pre-DDT: 0.012 ± 0.001 ; without **1**, post-DDT: 0.014 ± 0.0001). Whereas, measured absorption in the *PflspD* enzyme assay, when treated with 5 μM **1** (represented by red bars, **Figure 4.14**; and the red line, **Figure 4.15**), changes considerably after treatment with DTT: (with **1**, pre-DDT: 0.001 ± 0.002 ; with **1**, post-DDT: 0.012 ± 0.002).

Statistical analysis by means of a student t-test showed that, when comparing pre-DDT (abs360) slopes, there is a statistically significant difference in *PflspD* enzyme activity comparing the untreated enzyme and following treatment with 5 μM of **1** ($p = 0.002$). (A student t-test represents a significance test for the mean value of a normal distribution of data^[34]). Considering the same data from the perspective of a line graph (**Figure 4.15**), it is clear that when *PflspD* activity is inhibited by the presence of **1**, addition of DTT to the *PflspD* enzyme assay at a time point of seven minutes, restores *PflspD* activity (shown by an increase in absorbance at 360 nm), indicating restored enzyme turnover.^[33,35]

In contrast, in the *PflspD* enzyme assay that is not treated with **1**, an arrest of enzyme activity is not observed at any point, prior to or following treatment with DTT. This highlights that DTT does not affect the *PflspD* enzyme assay when BITZ inhibitors are not present.

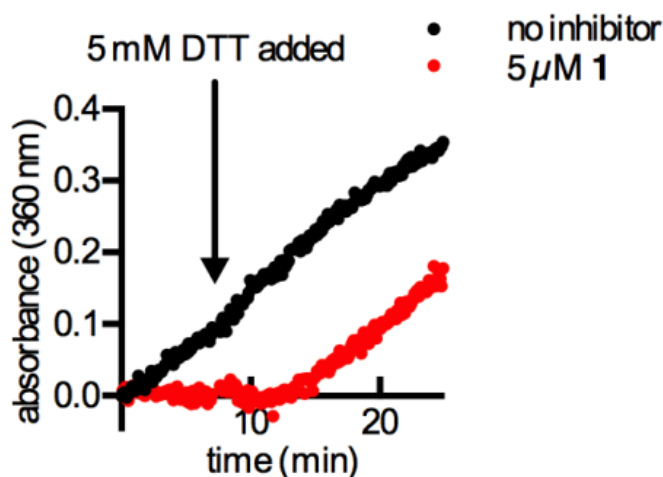


Figure 4.15 Line graph representing *PflspD* enzyme activity in the presence and absence of 5 μM **1**, treating with DTT at a seven-minute time point.

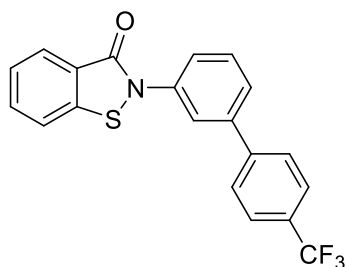
Comparing the absorbance slopes at 360 nm following addition of DTT to the *PflspD* enzyme assay, there is no statistically significant difference between the activity of the untreated *PflspD* enzyme and that treated with 5 μM of **1** ($p = 0.402$); highlighting that DTT successfully relieves *PflspD* inhibition following treatment with BITZ inhibitors.

Alternative analysis of the data shows that the addition of DTT did not cause a statistically significant difference in the slope of the reactions (*PflspD* enzyme activity) in assays that were not treated with **1** ($p = 0.283$). And furthermore, the addition of DTT caused a statistically significant increase in the slope of the reaction (rate of *PflspD* enzyme activity) in the assay that was treated with **1**, prior to DTT ($p = 0.008$).

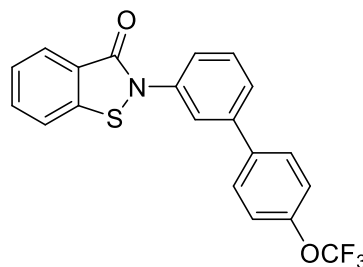
This *PflspD* enzyme rescue experiment therefore demonstrates that the addition of DTT following initial incubation of the *PflspD* enzyme with **1** produces rapid enzyme rescue, relieving the effects of BITZ compound inhibition and restoring *PflspD* enzyme activity. This observation strongly indicates that DTT reduces the sulfur-Cys-202 bond of the proposed enzyme-inhibitor complex, releasing the active site Cys-202 residue and enabling *PflspD* enzymatic activity to be restored. This result therefore provides further evidence that BITZ compounds specifically target the *PflspD* enzyme and supports our proposed model of *PflspD* enzyme inhibition.

4.3.3 Molecular Modelling of BITZ Compounds at *PflspD* (2)

To further support our proposed model of BITZ compound activity, comparable molecular modelling studies were carried out with BITZ inhibitors, **5** and **6**, which also demonstrate good inhibitory *PflspD* activity (**Figure 4.16**). Compounds **5** and **6** were docked into the active site of the *PflspD* homology model using **Protocol 4** (**Table 4.7**) and a search criteria requesting 50 GA pose predictions for each compound. The docking procedure was analogous to that previously conducted with **1** (**Figure 4.6**).

**5**

PflspD IC₅₀ = 0.0273 ± 0.015 μM
 Whole Cell 3D7 EC₅₀ = 0.646 ± 0.021 μM
 MW = 371.06 gmol⁻¹
 Average GoldScore Fitness score: 52.72
 Standard Deviation: 1.88
 GoldScore Fitness score of highest scored predicted binding pose: 54.27

**6**

PflspD IC₅₀ = 0.290 ± 0.195 μM
 Whole Cell 3D7 EC₅₀ = 0.411 μM
 MW = 387.05 gmol⁻¹
 Average GoldScore Fitness score: 51.34
 Standard Deviation: 4.20
 GoldScore Fitness score of highest scored predicted binding pose: 59.52

Figure 4.16 Chemical structure; *PflspD* enzyme activity; whole cell 3D7 activity; molecular weight; average GoldScore fitness score and GoldScore fitness of the highest scored binding pose predicted in *PflspD* molecular docking studies of **5** and **6** using the *PflspD* homology model.

Molecular modelling of **5** and **6** produced comparable docking poses and binding scores to those initially identified with **1** (**Figure 4.6**); three-dimensional evaluation of additional BITZ analogues therefore supports a similar mode of binding to that observed with **1**. In these studies, inhibitor binding was again characterised by initial non-covalent recognition within the enzyme active site (**Figures 4.17** and **4.18**); followed by covalent disulfide bond formation between the BITZ warhead and active site Cys-202 residue, facilitated by their relative alignment and proximity.

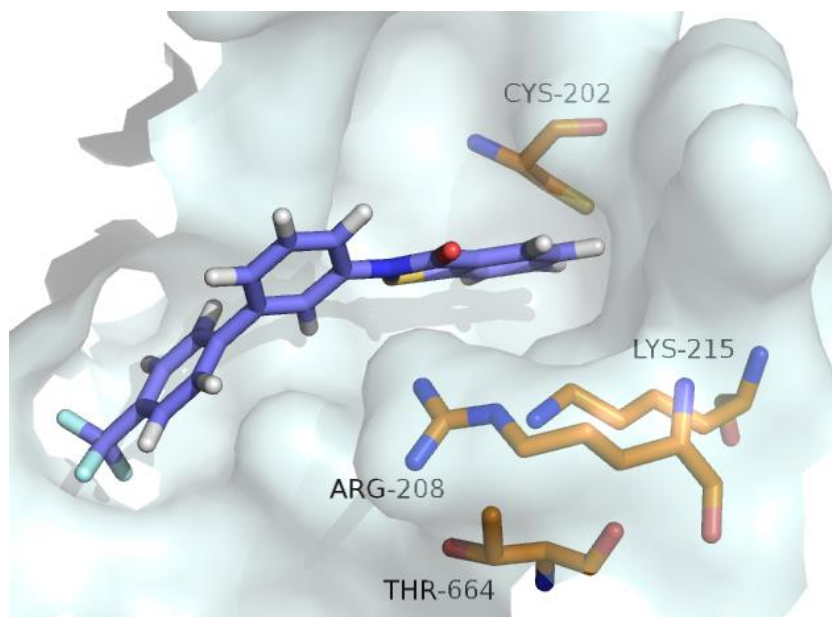


Figure 4.17 inhibitor **5** modelled in the active site of *PflspD* homology model. The *PflspD* active site is rendered as a white surface; inhibitor **5** is displayed as sticks and coloured by element: carbon atoms are purple; the selected *PflspD* active site protein residues (Cys-202, Lys-215, Thr-664 and Arg-208) are highlighted and depicted as sticks with carbon atoms coloured orange. Image created using PyMOL.^[26]

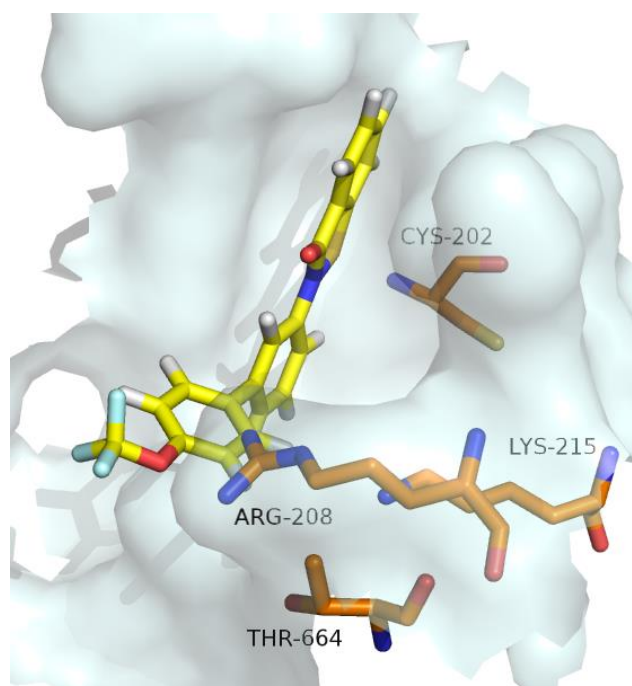


Figure 4.18 Inhibitor **6** modelled in the active site of *PflspD* homology model. The *PflspD* active site is rendered as a white surface; inhibitor **6** is displayed as sticks and coloured by element: carbon atoms are yellow; the selected *PflspD* active site protein residues (Cys-202, Lys-215, Thr-664 and Arg-208) are highlighted and depicted as sticks with carbon atoms coloured orange. Image created using PyMOL.^[26]

As again illustrated from the molecular docking of **5** and **6**, initial non-covalent alignment of BITZ inhibitors at *PflspD* facilitates disulfide bond formation in the active site through attack of Cys-202 on the sulfur heteroatom of the BITZ warhead, resulting in covalent modification of the *PflspD* binding site (**Figures 4.19** and **4.20**). These additional docking studies therefore support the proposed mechanism of covalent modification and inhibition of *PflspD* by BITZ derived compounds, as initially proposed following the molecular docking of **1**.

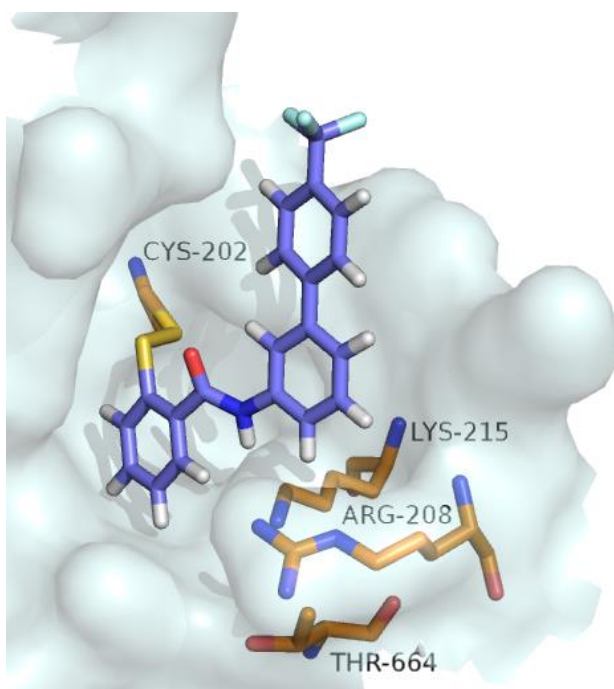


Figure 4.19 Inhibitor **5** modelled in the *PflspD* homology model, covalently bound to the active site Cys-202 residue and occupying the *PflspD* binding pocket. The *PflspD* active site is rendered as a white surface; inhibitor **5** is displayed as sticks and coloured by element: carbon atoms are purple; the selected *PflspD* active site protein residues (Cys-202, Lys-215, Thr-664 and Arg-208) are highlighted and depicted as sticks with carbon atoms coloured orange. Image created using PyMOL.^[26]

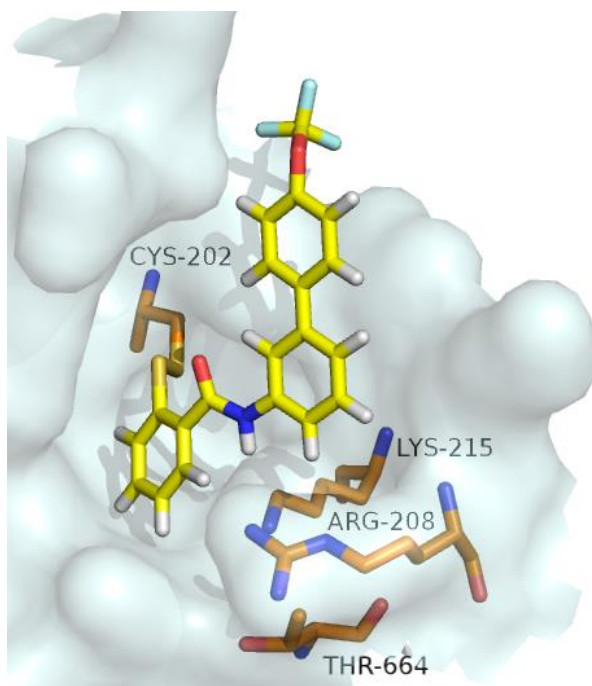


Figure 4.20 Inhibitor **6** modelled in the *PflspD* homology model, covalently bound to the active site Cys-202 residue and occupying the *PflspD* binding pocket. The *PflspD* active site is rendered as a white surface; inhibitor **6** is displayed as sticks and coloured by element: carbon atoms are yellow; the selected *PflspD* active site protein residues (Cys-202, Lys-215, Thr-664 and Arg-208) are highlighted and depicted as sticks with carbon atoms coloured orange. Image created using PyMOL.^[26]

4.4 Biological Evaluation of BITZ Inhibitor Mechanism of Action

Mechanistic evaluations and development of SAR has specifically highlighted that the N-S bond of the BITZ warhead and Cys-202 residue in the *PflspD* active site are crucial to achieve *PflspD* enzyme inhibition *via* disulfide bond formation. Small structural manipulations around the core BITZ motif (**Chapter 2, Section 2.4**) have confirmed the requirement for the specified BITZ chemotype in achieving *PflspD* enzyme inhibition. Having demonstrated modelling and chemical evidence for the importance of the N-S bond for this proposed mechanism of action, biological investigations were also undertaken to further support this hypothesis.

4.4.1 Site Directed Mutagenesis

Site directed mutagenesis (SDM) is a technique used to characterise genes and proteins, determining the functions that enable their biology and the interactions which may occur between proteins and compounds that may become associated.^[36] SDM involves altering a nucleotide sequence of interest using synthetic oligonucleotides in order to study the effect on the resulting gene function. SDM introduces a mutation at a defined site within a DNA sequence to make specific changes in a portion of the gene which encodes the protein product of interest: this is usually with the purpose of assessing

a specific gene and its functional role in biology.^[36] The methods by which the micromanipulation (or SDM) of genes can be approached are now highly advanced and the subsequent applications are immensely broad. As a result, it is possible to modify a gene so that any amino acid within the product protein can be replaced by any other specified amino acid therefore varying the construct, shape, function and activity of the resulting modified protein.^[37]

4.4.1.1 *E. coli* IspD

The IspD active site Cys-202 residue is conserved in *Plasmodium* spp. IspD enzymes but not in bacterial enzyme homologues (**Figure 4.21**) which have been found to be insensitive to BITZ derived inhibitors. BITZ compounds are ineffective against the *EclspD* enzyme (**Figure 4.22**) which therefore supports the proposed involvement of and specific requirement for the active site Cys-202 residue which is present in *PflspD* but not in the *E. coli* enzyme homologue.^[27]

<i>P. falciparum</i>	192–	KKKNIHSILL	CGGIGKRTE	LIGPKQFLKLN	DIPLFIYSFN	LFIKCNLIKSL	TL	–244
<i>P. vivax</i>	187–	HKKNIHAILL	CGGIGQRTE	LASRKQFLKLN	DVPLFVYSFN	LKVKNLIKAITL		–239
<i>P. berghei</i>	159–	NKKNIHSIFL	CGGVGKRTE	LASRKQFLHLD	NIPIFIYSFN	LFIKCNLIKSL		–211
<i>E. coli</i>	4–	THLDVCAVVP	AAGFGRRMQ	TECPKQYLSI	GNQTILEHS	VYALLAHPRV	KRVVI	–56
<i>M. tuberculosis</i>	4–	EAGEVVAIVP	AAGSGERL	AVGVPKAFYQ	LDGQTLIER	AVDGLLD	SGVVDTVVV	–56

Figure 4.21 Alignment of IspD enzyme homologues highlighting interspecies variation.^[27]

The alignment of IspD enzyme homologues across five different MEP-pathway containing pathogens highlights that the active site Cys residue is conserved in *Plasmodium* spp. but is absent in *E. coli* and *M. tuberculosis* bacterial orthologues; where the corresponding residue in bacteria is alanine (Ala) (**Figure 4.21**). Both *P. falciparum* and *P. vivax* IspD, possessing the active site Cys-202 residue, have been shown to be sensitive to inhibition by BITZ compounds (**Chapter 3, Section 3.11**). However, exposure of recombinant *EclspD* (*EclspD*-wt) to BITZ compound **1** found the enzyme to be highly resistant to inhibition by the compound (**Figure 4.22** and **Table 4.9**) providing a distinct contrast to the inhibitory IspD activity shown by the same compound at *P. falciparum* and *P. vivax* IspD homologues (**Chapter 3, Section 3.11, Table 3.9**).

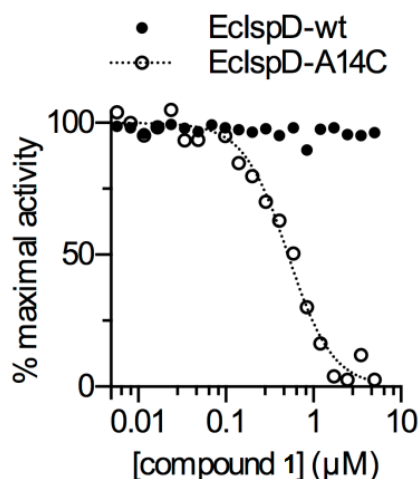


Figure 4.22 Dose-dependent inhibition of recombinant *EclspD* and *EclspD-A14C* following treatment with **1**; representative data shown; $n \geq 3$.

To confirm the critical role of active site Cys residues in *PflspD* inhibition, a mutant *EclspD* protein was generated, using SDM, in which the corresponding Ala residue was substituted with a Cys residue by introduction of the A14C mutation. Encouragingly, *EclspD-A14C* was rendered sensitive to **1** (Table 4.9 and Figure 4.22) highlighting that the *E. coli* enzyme can be rendered sensitive to BITZ derived compounds through replacement of the specified alanine residue with cysteine.

<i>E. coli</i> IspD enzyme variant	Enzyme inhibition IC ₅₀ (nM)
<i>EclspD-wt</i>	> 10, 000
<i>EclspD-A14C</i>	440 ± 48

Table 4.9 Inhibitory enzyme activity of **1** against wildtype *EclspD* and the mutant *EclspD-A14C* enzyme. Mean IC₅₀ and SEM displayed; representative data shown: $n \geq 3$.^[27]

This result further validates the requirement for active site Cys residues to achieve *PflspD* inhibition and therefore supports the proposed mechanism of enzyme inhibition. In addition, this data also provides an explanation for the marked species-selectivity of BITZ compounds and their selective inhibitory activity amongst IspD homologues, despite the overall sequence homology across this group of enzymes.

4.4.1.2 *P. falciparum* IspD

Together, *PflspD* molecular modelling studies and SDM in *EclspD* clearly implicate the specific Cys-202 residue as the likely site of enzyme modification by BITZ compounds. Consequently, it was predicted that mutation of Cys-202 to an Ala residue would decrease the sensitivity of *PflspD* to the BITZ compound class since formation of the covalent disulfide bond would no longer be able to occur.

Indeed, introducing this *Pf*lspD mutation resulted in a six-fold decrease in sensitivity of the *Pf*lspD enzyme to inhibition by BITZ compounds (Table 4.10 and Figure 4.23). This was highlighted following treatment of both wildtype (*Pf*lspD-wt) and mutant (*Pf*lspD-C202A) *Pf*lspD enzymes over prolonged 50 minute incubations with **1**.

<i>P. falciparum</i> lspD enzyme variant	Enzyme inhibition IC ₅₀ (nM)
<i>Pf</i> lspD-wt	81 ± 13
<i>Pf</i> lspD-C202A	470 ± 39

Table 4.10 Inhibitory activity of **1** against wildtype *Pf*lspD and the mutant *Pf*lspD-C202A enzyme. Mean IC₅₀ and SEM displayed; representative data shown: n ≥ 3.^[27]

This clear change in enzyme sensitivity (Figure 4.23) reiterates the importance of Cys-202 for BITZ inhibitor activity since we find that mutation of active site Cys-202 to an alanine residue significantly reduces the sensitivity of recombinant *Pf*lspD to the effect of BITZ derived inhibitors. However, it should be acknowledged that this sensitivity change may reflect both a loss of covalent bond formation as well as a change in compound fit and complementarity within the active site, following introduction of the C202A mutation to the *Pf*lspD inhibitor binding region.^[27] Furthermore, introduction of the *Pf*lspD-C202A mutation is only observed as causing reduced sensitivity of the *Pf*lspD enzyme to the BITZ chemotype rather than complete resistance against it (Figure 4.23).

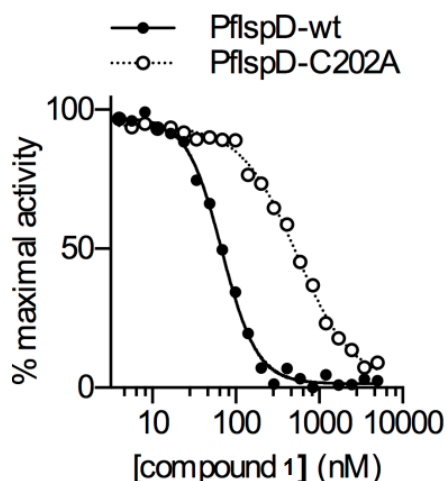


Figure 4.23 Dose-dependent inhibition of recombinant *Pf*lspD and *Pf*lspD-C202A following treatment with **1**; representative data shown; n ≥ 3.

The observation of weakened BITZ inhibition against the *Pf*lspD-C202A mutant enzyme reinforces the indication of an initial non-covalent inhibitory effect of BITZ compounds which **1** is still able to produce against the mutant *Pf*lspD-C202A, likely due to complementary shape-fit, despite reduced protein-ligand recognition and the absence of covalent mechanistic interactions. Alternatively, the

observation of weak, but detectable, BITZ compound inhibition of *PflspD*-C202A may suggest an independent mode of weak inhibitory activity at the mutant *PflspD* enzyme.

4.4.2 *PflspD* and *PflspD*-C202A Enzymatic Assays

To further assess and compare the behaviour of BITZ compounds at both the wildtype and mutant *PflspD* enzymes, a series of *PflspD* and *PflspD*-C202A enzymatic assays were conducted with inhibitor **1**. These assays involved pre-incubating the respective enzymes with **1** and varying the time points at which IC_{50} measurements were taken.

During reversible inhibition, an equilibrium is typically established between component enzymes, inhibitors, and enzyme-inhibitor complexes.^[10] In contrast, covalent inhibition is often marked by an increase in the apparent potency of an inhibitor over time, as irreversible associations are gradually made between the inhibitor and the enzyme.^[28] To evaluate this premise with respect to the proposed mechanism of enzyme inhibition, *PflspD* enzyme variants were evaluated in time-dependent *IspD* enzyme assays using BITZ inhibitor **1**. Various concentrations of **1** were pre-incubated in the presence of *PflspD* prior to measurement of enzyme activity. As expected for covalent inhibition, the potency of **1** was seen to increase over time when pre-incubated with the wildtype *PflspD* enzyme ($p = 0.001$, corresponding to *PflspD*-wt data **Figure 4.24** and **Table 4.11**).

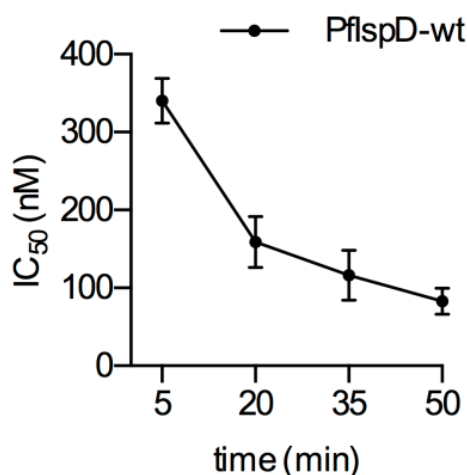


Figure 4.24 Time-dependent changes in inhibition of recombinant *PflspD*-wt enzyme activity following treatment with **1**. Mean IC_{50} and SEM displayed; $n \geq 4$ for each data point.

In contrast, no such substantial or significant change in *PflspD*-C202A inhibition was observed over the same time period with exposure to and pre-incubation with **1** ($p = 0.32$, corresponding to *PflspD*-C202A data **Table 4.11**) which suggests that covalent enzyme inhibition was no longer occurring. These results highlight the importance and validity of the proposed covalent interactions with Cys-202 during inhibition of *PflspD* by BITZ compounds.

<i>P. falciparum</i> IspD enzyme variant	Pre-incubation time (minutes)	Enzyme inhibition IC ₅₀ (nM)
<i>Pf</i> IspD-wt	5	330 ± 57
<i>Pf</i> IspD-wt	50	81 ± 13
<i>Pf</i> IspD-C202A	5	860 ± 220
<i>Pf</i> IspD-C202A	50	470 ± 39

Table 4.11 Inhibitory activity of **1** against wildtype *Pf*IspD and mutant *Pf*IspD-C202A following pre-incubation of the enzyme and inhibitor prior to measurement of enzyme activity.

Considering the mechanism of covalent enzyme inhibition, once an inhibitor-enzyme adduct has formed, increasing concentrations of the natural enzyme substrate should not relieve covalent inhibition of the protein.^[38] Consistent with this model, the susceptibility of *Pf*IspD-wt to inhibition by **1**, following prolonged incubation, was not substantially affected by varying concentrations of the natural enzyme substrate, CTP (**Figure 4.25, b**). In contrast, inhibition of *Pf*IspD-wt by **1** was somewhat relieved under higher CTP concentrations over shorter incubation periods (**Figure 4.25, a**), as is typically observed for reversible competitive inhibitors.^[38]

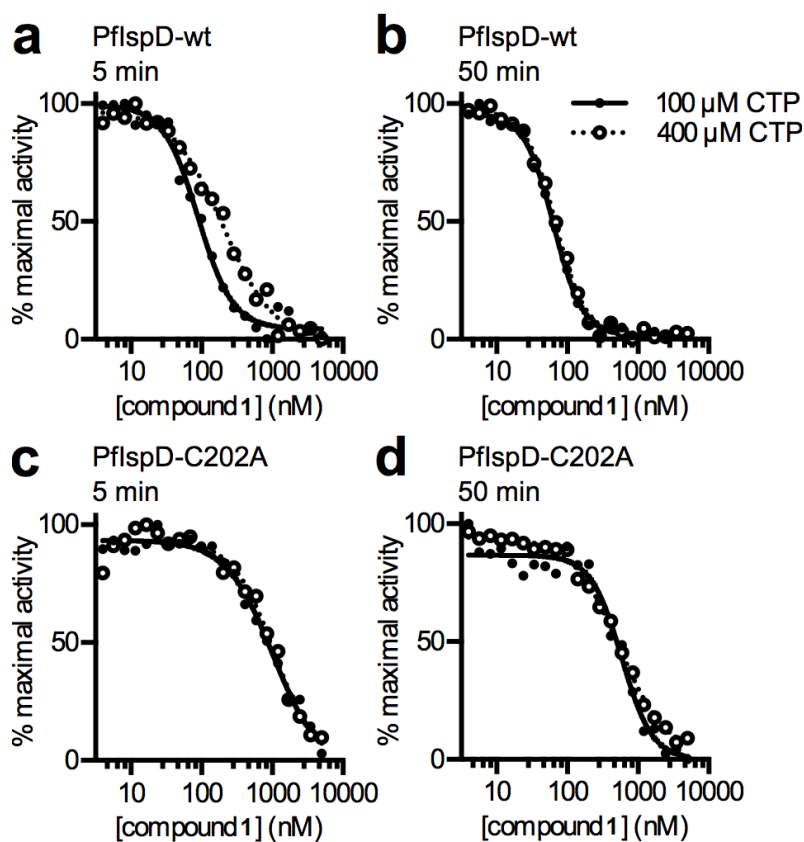


Figure 4.25 Inhibition of recombinant *Pf*IspD enzymes by BITZ inhibitor **1**.^[27]

Together, these observations are consistent with relatively slow inhibitor-enzyme adduct formation within the CTP binding site, as predicted by our molecular docking model. In contrast, inhibition of *PflspD*-C202A activity was not significantly affected by CTP concentrations over short or long incubation periods with **1** (Figure 4.25, c and d). This demonstrates that the CTP-site binding does not substantially contribute to inhibition of the mutant *PflspD*-C202A enzyme; and therefore suggests an independent mode of inhibition.

4.4.3 Kinetic Evaluation of the *PflspD* and *PflspD*-C202A Enzymes

In order to evaluate the function of the *PflspD*-C202A mutant enzyme, kinetic parameters (K_{cat} , and the Michaelis constant, K_m)^[38] were characterised for the enzyme. Kinetic analysis demonstrated that introduction of the C202A mutation, replacing the active site Cys-202 residue with Ala, results in decreased K_{cat} and increased K_m [CTP] values (Figure 4.26, A and B). This result is consistent with changes to the CTP binding site, as expected in the *PflspD*-C202A mutant.

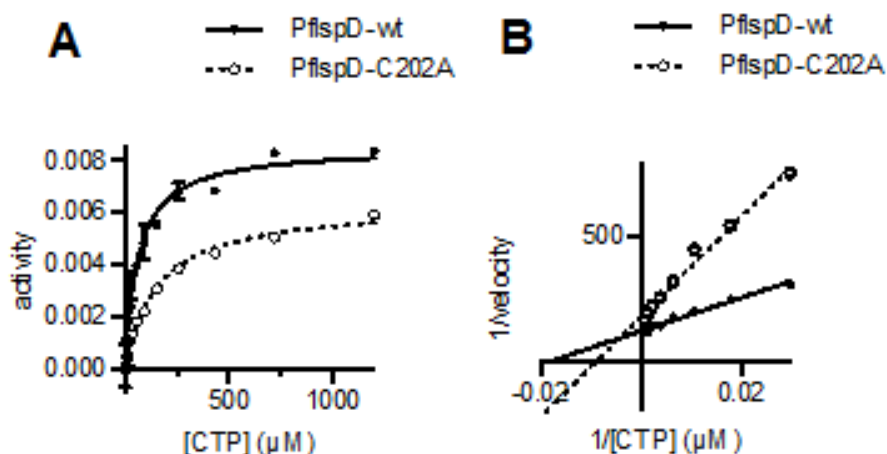


Figure 4.26 Michaelis-Menten kinetics of the *PflspD*-wt and *PflspD*-C202A enzymes; **A:** direct activity plot of enzyme activity vs. [CTP]; **B:** Lineweaver-Burke plot: $1/V_{max}$ vs. $-1/K_m$ where changes in the y-intercept indicate changes in V_{max} and changes in the x-axis indicate changes in K_m .

K_{cat} is a measure of maximum enzyme velocity (V_{max}) expressed in activity per amount of enzyme (i.e. μmol of substrate converted per μmol of enzyme per second) and therefore provides a measure of enzyme turnover. K_m provides a measurement of substrate concentration at half-maximal enzyme velocity and is therefore a measure of the affinity of a particular enzyme for its substrate; as a result, K_m is often used as an indicator of the change in the enzyme's ability to use (or process) a particular substrate.^[38]

Kinetic evaluation of the *PflspD*-C202A enzyme highlights that introduction of the C202A mutation confers changes to both the K_{cat} (or V_{max}) and the K_m [CTP] (**Figure 4.26, A and B** and preliminary data, **Table 4.12**). The notable increase in K_m [CTP] values for *PflspD*-C202A indicates that the mutant enzyme has a reduced ability to use CTP as a substrate. This therefore supports our prediction, based on the *PflspD* homology model, that the Cys-202 residue is located within the CTP binding site.

Enzyme	K_{cat} [CTP] (s^{-1})	K_m [CTP] (μM)
<i>PflspD</i> -wt	0.42	64
<i>PflspD</i> -C202A	0.31	160

Table 4.12 Preliminary K_{cat} and K_m kinetic data with respect to [CTP] for the *PflspD*-wt and *PflspD*-C202A enzymes.

The finding that a change to the *PflspD* inhibitor binding site, by introduction of the C202A mutation, has an effect on the utilisation of CTP in the *PflspD*-C202A enzyme is also consistent with our hypothesis that BITZ inhibitor binding and CTP binding occur within the same site.

4.4.4 Crystallography

SDM rendered the *EclspD*-wt enzyme sensitive to the effect of BITZ inhibitors following introduction of the A14C mutation at the *EclspD* active site. This single point mutation replaced the Ala residue of the *E. coli* IspD homologue with a Cys residue, facilitating BITZ compound activity at the mutant enzyme. To support these studies, *EclspD*-A14C was co-crystallized in the presence of 5 mM of **1** (Table 4.13) which revealed the formation of a new intramolecular disulfide bond between Cys-14 and Cys-25, providing supportive structural evidence for our mutant enzyme activity data.

	<i>EclspD</i>-A14C
Data collection	
Space group	C2
Cell dimensions	
<i>a</i> , <i>b</i> , <i>c</i> , (Å)	94.68, 47.67, 53.95
α , β , γ (°)	90.00, 99.515, 90.00
Resolution (Å)*	20-1.60 (1.70-1.60)*
<i>R</i> _{meas}	7.3% (46.4%)
<i>I</i> / σ <i>I</i>	11.29 (2.56)
Completeness (%)	96.3% (98.2%)
Redundancy	3.52 (3.43)
Refinement	
Resolution (Å)	20-1.60
No. of reflections	30,303
<i>R</i> _{work} / <i>R</i> _{free}	17.46/19.98
No. of atoms	
Protein	1,775
Ca	1
Water	165
<i>B</i> -factors	
Protein	26.43
Ligands	18.16
Water	32.95
R.m.s. deviations	
Bond lengths (Å)	0.008
Bond angles (°)	1.246

Table 4.13 Data collection and refinement statistics for co-crystallization of *EclspD*-A14C with inhibitor **1** at 5 mM.^[27]

Previous crystal structures of the enzyme show that in the absence of CTP, loop spanning residues 14-25 are disordered and flexible in the *EclspD* protein (PDB ID: 1VGT^[39], 1H3M^[40], 3N9W^[41]). Whereas, in the presence of CTP (PDB ID: 1I52^[12]), this loop region becomes ordered and makes several important contacts with CTP. In the mutant *EclspD*-A14C structure, while electron density corresponding to **1** was not observed, the resulting crystal structure revealed formation of a now-accessible disulfide bridge in a closed conformation of the loop which caused occlusion of the *EclspD*-A14C CTP binding site (Figure 4.27).

Introduction of the cysteine residue into *EclspD*-A14C therefore enables formation of a disulfide bridge which can occlude and inhibit the mutant *E. coli* IspD enzyme in an analogous manner to the proposed inhibition of the *PflspD* enzyme. This provides a direct contrast to *EclspD*-wt which is insensitive to inhibition by BITZ compounds since disulfide bond formation, required to occlude the active site and inhibit the enzyme, is not viable in the absence of the active site Cys-202 residue.

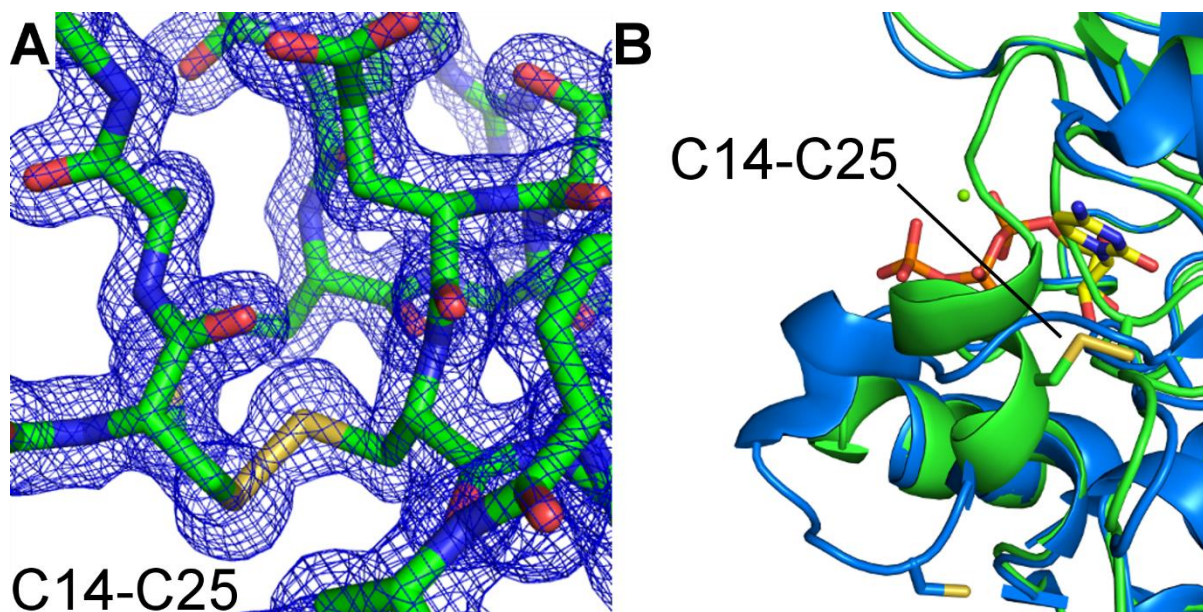


Figure 4.27 Crystallographic image of induced disulfide-bridge formation at the *EclspD*-A14C active site on treatment of the *EclspD*-A14C enzyme with BITZ inhibitor **1**.^[27]

This crystallographic data therefore provides modest additional evidence for a temporary covalent interaction between BITZ inhibitor **1** and the Cys-14 residue in the mutant *EclspD*-A14C enzyme. Together with SDM work and molecular modelling evaluations, these studies provide evidence that the *PflspD* enzyme is inhibited by BITZ compounds *via* covalent bond formation between the active site Cys-202 residue and the BITZ core and that this same effect can be induced and observed in IspD enzyme homologues which do not naturally possess the required active site protein sequence to facilitate this mode of enzyme inhibition.

4.5 Considering BITZ Reactivity at Cysteine Residues

The demonstrated cysteine reactivity of BITZ compounds suggests that development of a BITZ inhibitor series may be hampered or compromised by possible polypharmacology. However, several recent literature reviews have noted that covalent mechanisms of action are prevalent amongst successful drugs and that the covalent modification of proteins and drug targets is becoming increasingly popular, representing an expanding approach to drug discovery and development.^[28,42] Indeed, aspirin which is also a covalent modifier, is one of the most widely used drug in the world.^[10,28]

The polypharmacology of bioactive molecules^[43,44] and approved drugs^[45] has similarly been studied and is consistent with the concept that safe and effective drugs are invariably active at many targets. One such study has calculated that, on average, approved therapeutic drug entities are active against approximately seven different molecular targets and still produce the desired pharmacology and phenotypic effect.^[46] It is clear that continued vigilance will be required as BITZ compounds and their derivatives are progressed further into antimalarial drug development with continued monitoring for potential inhibitor promiscuity and off-target reactivity, which could lead to toxicity in the human host.

However, it should be also noted that other compounds based around the BITZ chemotype have demonstrated successful medicinal chemistry optimisation within a number of drug development programs.^[47–53] Recently, a molecule containing a BITZ construct began Phase II clinical trials as an antiviral agent, thus providing further supportive evidence that the potential reactivity of the BITZ moiety alone is not incompatible with a safe therapeutic profile.^[54]

Separate research by Dahl *et al.*^[55] provides further support for use of this chemical chemotype within drug design and medicinal chemistry optimisation. As part of their studies into benzoisothiazolone phosphomannose isomerase inhibitors, Dahl and co-workers conducted a glutathione (GSH) binding assay with BITZ-derived compound **7** (**Figure 4.28**) which is highly analogous to compound **8** (**Figure 4.28**), a simplified BITZ derivative from our own studies.

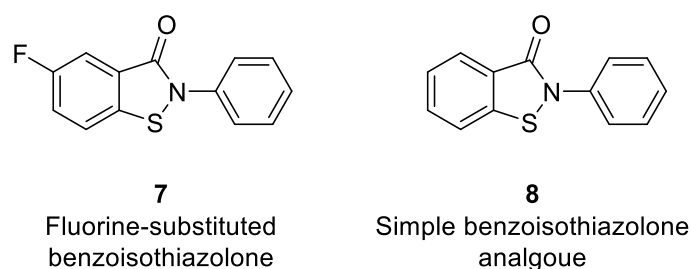


Figure 4.28 Chemical structures of BITZ derived compounds **7**^[55] and **8**.

The S9-based GSH transferase assay provides a means of identifying compounds which have a tendency to react with GSH *in vivo* and therefore may present a risk of generating GSH-trapped reactive metabolites.^[55] This is therefore an efficient means of determining the extent of promiscuous binding and non-specific binding events associated with a given chemical chemotype. When tested in the S9-based GSH transferase assay, Dahl *et al.* identified no GSH adducts of **7** using liquid chromatography–mass spectrometry (LCMS).^[55] This result gives further support for the inclusion of the BITZ warhead and chemical chemotype within drug design since these studies show that indiscriminate chemical or enzymatic turnover is limited with GSH and goes some way to suggest that the BITZ chemotype does not behave promiscuously at non-specific GSH residues *in vivo*.

4.6 Conclusions and Future Work

A docking protocol suitable for the molecular modelling of small molecules binding to *PflspD* was determined using the *EclspD* enzyme homologue as a surrogate protein. A lack of availability of the *PflspD* crystal structure required that the *EclspD* enzyme to be selected as a substitute homologue, enabled by the active site similarity between the two enzymes.

EclspD was consequently used to identify a suitable modelling protocol with which to dock small molecules at the *IspD* active site; the aim of which was to apply the identified protocol to a homology model of the *PflspD* protein to examine the binding of small molecules at the active site. Extracting and re-docking the natural *IspD* enzyme product, CDP-ME, co-crystallised in the known 1INI *E. coli* crystal structure,^[12] enabled the docking protocol parameters to be identified which were capable of accurately reproducing the known CDP-ME binding pose, thus verifying the protocol both accurate and reproducible.

Following generation of the *PflspD* homology model, further molecular modelling studies were conducted to investigate the alignment and orientation of BITZ derived molecules at the *PflspD* active site; where examination of the resulting docking poses revealed a consistent molecular alignment of BITZ compound at *PflspD*. As a result, a mechanism of enzyme inhibition has been proposed which is initiated by non-covalent active site recognition, promoted by complementary shape-fit and non-covalent protein-inhibitor interactions, but ultimately relies on the formation of a covalent enzyme-inhibitor adduct which renders the enzyme inactive.

A combination of further molecular modelling studies, SDM, enzyme activity assays and crystallographic evaluation has enabled us to substantiate this proposed mechanism of enzyme inhibition as the mechanism by which the BITZ chemotype and its analogues are able to inhibit the *PflspD* enzyme. More specifically, a mechanism of enzyme inhibition has been deciphered whereby a disulfide protein-inhibitor adduct is formed between the *PflspD* active site Cys-202 residue and the electrophilic sulfur atom of the BITZ inhibitor core, which is facilitated by the proximal alignment of these entities in the *PflspD* binding site. The nucleophilic thiol group of Cys-202 is responsible for attacking the sulfur atom of the N-S heteroatom bond within the BITZ core, this causes N-S bond cleavage and subsequent formation of a sulfur-Cys-202 disulfide bond which results in inhibition of the *PflspD* enzyme. In line with this proposed mechanism, the demonstrated species-selectivity of BITZ compounds for *PflspD* over other enzyme homologues relies on the presence of the active site Cys-202 residue.

Several biological methods have been effectively used to confirm the proposed inhibitory mechanism of the BITZ chemotype at *PflspD*. DTT enzyme rescue experiments have shown that the addition of this reducing agent to the *PflspD* enzymatic assay, following treatment with BITZ compounds, produces rapid enzyme rescue and relieves the effects of BITZ inhibition, restoring *PflspD* enzyme activity. This result therefore indicates that DTT is able to reduce the inhibitory sulfur-Cys-202 bond, proposed as the key interaction within the enzyme-inhibitor complex, releasing the *PflspD* active site Cys-202 residue and re-establishing *PflspD* enzyme activity. DTT rescue experiments therefore provide evidence that the BITZ chemotype specifically targets the *PflspD* enzyme through formation of a disulfide bond, strongly supporting our proposed model of enzyme inhibition.

Since the *IspD* active site Cys-202 residue is not conserved in bacterial homologues of the enzyme, site directed mutagenesis (SDM) has been used to confirm the specific requirement for this key cysteine residue in facilitating *PflspD* enzyme inhibition by our proposed model of covalent inhibition with the BITZ chemotype. BITZ compounds have been found to be ineffective against wildtype *EclspD*. However, generation of the *EclspD*-A14C enzyme (possessing the specified active site Cys residue) and subsequent treatment with BITZ compounds, has shown this mutant enzyme is sensitive to inhibition by BITZ compounds. This result therefore demonstrates that *EclspD* can be rendered sensitive to BITZ-derived compounds through specific mutation and introduction of the active site Cys-202 residue, providing further evidence role of this protein residue in *PflspD* active site inhibition. In addition, crystallography work has provided supportive structural evidence for our demonstrated mutant A14C-*EclspD* enzyme activity data.

SDM also generated the *PflspD*-C202A mutant enzyme, replacing the active site Cys-202 residue with an alanine residue in the *PflspD* homologue. Subsequent treatment of the resulting mutant enzyme with BITZ compounds showed this mutation caused around a six-fold decrease in enzyme sensitivity, compared to inhibition of wildtype *PflspD* by BITZ compounds. This observation indicates that covalent enzyme inhibition was no longer able to occur in the *PflspD*-C202A enzyme, further highlighting the essential involvement of the Cys-202 residue in achieving covalent inhibition of *PflspD*. However, the weakened inhibitory activity shown against *PflspD*-C202A is likely to signify that the non-covalent recognition element of BITZ compound inhibition at the enzyme is still able to produce a diminished level of activity against *PflspD*-C202A. This weak, non-covalent inhibitory contribution is most likely a consequence of some complementary shape-fit between the mutant protein and BITZ inhibitor, despite reduced recognition and the absence of covalent mechanistic interactions. In addition, the lack of effect varying CTP concentration during inhibition of *PflspD*-C202A with BITZ compound **1**,

suggests that blocking the CTP binding site does not substantially contribute to inhibition of the mutant enzyme, therefore indicating an alternative mode of *PflspD*-C202A inhibition.

Altogether, these studies provide a robust explanation for the marked species-selectivity of BITZ compounds and their inhibitory activity amongst *IspD* homologues. In addition, kinetic evaluation of wildtype *PflspD* and *PflspD*-C202A has demonstrated that the *PflspD*-C202A mutant enzyme has a reduced ability to utilise CTP as an enzyme substrate, supporting our prediction, based on the *PflspD* homology model, that the Cys-202 residue is located within the CTP binding site.

In addition to the described molecular docking studies, computational techniques could be used to further rationalise the behaviour and alignment of BITZ derived inhibitors within the *PflspD* active site. As a result, more extensive docking studies and molecular evaluation may facilitate a predictive approach to compound design, providing informed indications of 'drug-like' compounds which should be prioritised for lead optimisation. Such an approach would enhance computational contributions to the molecular design loop. Indeed, refined evaluation of identified docking poses, prediction of ligand-protein binding energies and calculating molecular properties could be used in a data mining approach that is able to accurately determine if a given compound or chemical structure will show activity against the *PflspD* enzyme, more significantly informing compound design.

It has been acknowledged that the cysteine reactivity of BITZ compounds at *PflspD* must be carefully monitored to ensure that there is no significant off-target reactivity or risk of toxicity towards the human host. Indeed, the potential promiscuity of the BITZ warhead means that non-specific binding events at additional protein contacts may be possible and must continue to be evaluated and monitored throughout continuing further compound development. However, the inclusion of the BITZ chemical motif in a number of successful medicinal chemistry optimisation programs, has demonstrated that the promiscuity and potential reactivity of the BITZ chemotype itself, is not incompatible with a safe therapeutic profile and the development of effective chemotherapeutic agents. Therefore, as interest in the covalent modification of drug targets increases, similar techniques and experiments to those outlined here may be used to probe other identified cysteine modifiers which may be capable of mirroring this mode of covalent modification.

4.7 Experimental

For general chemical and biological methodologies see **Chapter 2, Section 2.7.1**.

4.7.1 Computational Methods

Molecular Modelling

A homology model of *Pf*lspD was constructed using the PHYRE online homology modelling program.^[24] *Pf*lspD primary sequence Q8I273 was obtained from UNIPROT (<http://www.uniprot.org/>, accessed 10/12/14). A number of protein alignments and homology models were constructed by PHYRE, and the model with 98.82% confidence was selected, which was based on an *E. coli* lspD structure (PDB accession code 1I52).^[12] 1I52 is a 1.50-Å resolution crystal structure of *E. coli* lspD, complexed with CDP-ME in the active site. The structure of the model was validated using the WHATIF web interface.^[25] BITZ inhibitors **1**, **5** and **6** were modelled *in silico* using the homology model described above in order to visualize the interactions between each analogue and the active site. Using GOLD, protons were added and docking was performed with default parameters, except that GoldScore was used and 50 docking poses were obtained for comparison and analysis. Covalent docking was performed using GOLD with the C-alpha atom of Cys-202 as the link atom to BITZ inhibitors **1**, **5** and **6**.^[16]

4.7.2 Biological Methods

Cloning of lspD Orthologues

P. falciparum: The construct used for expression of the codon-optimized *Pf*lspD protein has been described previously.^[56] To generate the *Pf*lspD variants containing the C202A mutation, N- and C-terminal fragments of the optimized *Pf*lspD gene were amplified from the above vector using the following primers. C202A N-terminal fragment: T7 Fwd primer, 5'-TAATACGACTCACTATAGGG-3', with C202A Rev primer, 5'-GTTTGCCAATACCGCCGGCTAGCAGGATACTATGAATG-3'; C202 C-terminal fragment, C202A Fwd primer, 5'-CATT CATAGTATCCTGCTAGCCGGCGGTATTGGCAAAC-3', with T7 Rev primer, 5'-GCTAGTTATTGCTCAGCGG-3'. Amplicons containing the entire *Pf*lspD gene were generated using *Pf*lspD Fwd and Rev primers, which introduce a 6-His tag, with N- and C-terminal fragments as template (*Pf*lspD Fwd primer: 5'-CTCACCACCACCACCACCATATGATGCACATCTACGATAATAATAA-3'; *Pf*lspD Rev: 5'-ATCCTATCTTACTCACTTATTTTGAGGAGTAGTAGAAT-3'). Following amplification, *Pf*lspD variants were cloned into pBG1861 by ligation-independent cloning as previously described,^[56,57] and verified by Sanger sequencing.

P. vivax: The construct used for expression of codon-optimized *PvlspD* (*P. vivax* Sal-1; PVX_081425) has been previously described.^[56]

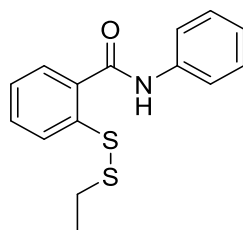
E. coli: The construct used for expression of *EclspD*-wt has been previously described.^[58] The A14C mutation was introduced by first generating N- and C-terminal gene fragments containing the mutation. These fragments were generated using the following primers: A14C N-terminal fragment: T7 Fwd primer, 5'-TAATACGACTCACTATAGGG-3', with A14C Rev primer, 5'-CATTCGACGGCCAAATCCGGCACACGGAACCACGGCGCAAACATC-3'; A14C C-terminal fragment, A14C Fwd primer, 5'-GATGTTTGCGCCGTGGTTCCGTGTGCCGATTGGCCGTCGAATG-3', with T7 Rev primer, 5'-GCTAGTTATTGCTCAGCGG-3'. Amplicons containing the entire *E. coli lspD* gene were generated using *EclspD* Fwd and Rev primers, which introduce a 6-His tag, with N- and C-terminal fragments as template (*EclspD* Fwd primer: 5'-CTCACCACCACCACCACCATATGATGGCAACCACTCATTTGG-3'; *EclspD* Rev primer: 5'-ATCCTATCTTACTCACTTATTTGTATTCTCTGATGG-3'). Following amplification, *E. coli A14C-lspD* was cloned into pBG1861 by ligation-independent cloning as previously described,^[57] and verified by Sanger sequencing.

Crystallisation

Following nickel affinity purification, *EclspD*-A14C was further purified by gel chromatography using a HiLoad 16/60 Superdex 200pg column (GE Healthcare) equilibrated with 10 mM Tris (pH 8.0) and 150 mM NaCl. The fractions containing *EclspD*-A14C were pooled and concentrated to 15 mg/mL using an Amicon centrifugal filter. The protein sample was pre-incubated on ice with 5 mM final concentration of compound **1**. The protein crystallized in 0.2 M calcium acetate, 0.1 M HEPES (pH 7.5), 10% PEG 8000. Crystals were flash-frozen under liquid nitrogen for data collection. X-ray data were collected from a single crystal using a wavelength of 1 Å at synchrotron beamline 4.2.2 of the Advanced Light Source in Berkeley, CA. Data were processed with XDS and the coordinates from PDB ID: 1VGT^[39] were used as a search model for phase determination by molecular replacement using PHENIX. Automatic model rebuilding was performed in PHENIX. Subsequent iterated manual building/rebuilding and refinement of models were performed using Coot and PHENIX, respectively. The structure validation server MolProbity was used to monitor refinement. A complete summary of final crystallographic refinement statistics is given in **Table 4.13**. Figures were generated and rendered in PyMOL.^[13]

4.7.3 Organic Synthesis

Preparation of 2-(ethyldisulfanyl)-*N*-phenylbenzamide **3**



To a solution of 2-phenylbenzo[*d*]isothiazol-3(2*H*)-one **2** (0.05 g, 2.19 mmol, 1.0 eq) in anhydrous THF (5 ml), sodium ethanethiolate (0.02 g, 0.264 mmol, 1.2 eq) was added and the N₂ atmosphere restored. The resulting solution was stirred at room temperature for 30 minutes before heating to 60°C under reflux conditions for a further 40 minutes. THF was removed under reduced pressure and the crude material was quenched with water (25 ml). The organic material was extracted into DCM (3 x 25 ml) and the combined organic layers dried with Na₂SO₄, filtered and concentrated under reduced pressure to give the pure product as a white solid in a 63.1% yield. *R_f* = 0.51 (50:50 EtOAc:hexane). **¹H NMR** (400 MHz, DMSO) δ 10.57 (s, 1H, NH), 7.80 – 7.71 (m, 4H), 7.52 (dt, *J* = 7.5, 1.4 Hz, 1H), 7.43 – 7.34 (m, 3H), 7.14 (tt, *J* = 7.4, 1.1 Hz, 1H); **ES+HRMS** *m/z* 479.0868 [M+Na]⁺ C₁₅H₁₅NOS₂ requires 289.06; C₂₆H₂₀N₂O₂S₂ (corresponding to **4** from the self-dimerization of **3**) requires 456.10.

4.8 References

- [1] D. B. Kitchen, H. Decornez, J. R. Furr, J. Bajorath, *Nat Rev Drug Discov* **2004**, *3*, 935–949.
- [2] A. Dhanik, L. E. Kaviraki, *Protein-Ligand Interactions: Computational Docking*, **2012**.
- [3] B. H. Sumida, A. I. Houston, J. M. McNamara, W. D. Hamilton, *J. Theor. Biol.* **1990**, *147*, 59–84.
- [4] D. E. Goldberg, *No Title Genetic Algorithms in Search, Optimization and Machine Learning*, **1989**.
- [5] C. Bissantz, G. Folkers, D. Rognan, *Nature* **2000**, 4759–4767.
- [6] M. Kontoyianni, L. M. McClellan, G. S. Sokol, *J. Med. Chem.* **2004**, *47*, 558–565.
- [7] M. Stahl, M. Rarey, *J. Med. Chem.* **2001**, *44*, 1035–1042.
- [8] G. L. Warren, C. W. Andrews, A. M. Capelli, B. Clarke, J. LaLonde, M. H. Lambert, M. Lindvall, N. Nevins, S. F. Semus, S. Senger, et al., *J. Med. Chem.* **2006**, *49*, 5912–5931.
- [9] M. H. J. Seifert, *Drug Discov. Today* **2009**, *14*, 562–569.
- [10] R. A. Copeland, *Evaluation of Enzyme Inhibitors in Drug Discovery*, **2013**.
- [11] R. T. Kroemer, *Curr. Protein Pept. Sci.* **2007**, *8*, 312–328.
- [12] S. B. Richard, M. E. Bowman, W. Kwiatkowski, I. Kang, C. Chow, A. M. Lillo, D. E. Cane, J. P. Noel, *Nat. Struct. Biol.* **2001**, *8*, 641–648.
- [13] The PyMOL Molecular Graphics System, **2010**, Version 1.3r1.
- [14] I. Hale, P. M. O’Neill, N. G. Berry, A. Odom, R. Sharma, *Medchemcomm* **2012**, *3*, 418–433.
- [15] A. R. Leach, V. J. Gillet, *An Introduction to Chemoinformatics.*, Kluwer Academic Publishers, **2003**.
- [16] M. L. Verdonk, J. C. Cole, M. J. Hartshorn, C. W. Murray, R. D. Taylor, *Proteins Struct. Funct. Genet.* **2003**, *52*, 609–623.
- [17] J. C. Cole, J. W. M. Nissink, R. Taylor, *Drug Discov. Ser.* **2005**, *1*, 379–415.
- [18] J. W. Liebeschuetz, J. C. Cole, O. Korb, *J. Comput. Aided. Mol. Des.* **2012**, *26*, 737–748.
- [19] H. M. Berman, J. Westbrook, Z. Feng, G. Gilliland, T. N. Bhat, H. Weissig, I. N. Shindyalov, P. E. Bourne, *Nucleic Acids Res.* **2000**, *28*, 235–242.
- [20] N. G. Berry, *Personal Communication*, **2012**.
- [21] D. A. Evans, *Angew. Chemie - Int. Ed.* **2014**, *53*, 11140–11145.
- [22] Spartan, Wavefunction INC, **2008**.
- [23] T. a Halgren, *J. Comput. Chem.* **1996**, *17*, 490–519.
- [24] L. A. Kelley, M. J. E. Sternberg, *Nat. Protoc.* **2009**, *4*, 363–371.
- [25] G. Vriend, *J. Mol. Graph.* **1990**, *8*, 29,52-56.

- [26] L. Schrödinger, *The {PyMOL} Molecular Graphics System, Version 1.3*, **2010**.
- [27] K. E. Price, C. M. Armstrong, L. S. Imlay, D. M. Hodge, C. Pidathala, N. J. Roberts, J. Park, M. Mikati, R. Sharma, A. S. Lawrenson, et al., *Sci. Rep.* **2016**, *6*, 36777.
- [28] J. Singh, R. C. Petter, T. a Baillie, A. Whitty, *Nat. Rev. Drug Discov.* **2011**, *10*, 307–317.
- [29] J. P. Sanchez, *J. Heterocycl. Chem.* **1997**, *34*, 1463–1467.
- [30] E. Pretsch, P. Buehlmann, C. Affolter, *Structure Determination of Organic Compounds: Tables of Spectral Data.*, Springer, **2003**.
- [31] M. C. Alliegro, *Anal. Biochem.* **2000**, *282*, 102–106.
- [32] J. P. Lopes De Almeida, C. Saldanha, *Clin. Hemorheol. Microcirc.* **2010**, *46*, 51–56.
- [33] M. R. Webb, *Proc. Natl. Acad. Sci. U. S. A.* **1992**, *89*, 4884–7.
- [34] M. S. Nikulin, in *Encycl. Math.*, Springer, **2001**.
- [35] A. R. Odom, *Personal Communication*, **2012**.
- [36] P. E. Carrigan, P. Bailar, S. Tuzmen, *Methods Mol. Biol. (New York, NY, United States)* **2011**, *700*, 107–124.
- [37] M. Smith, *Philos. Trans. R. Soc. London, Ser. A Math. Phys. Eng. Sci.* **1986**, *317*, 295–304.
- [38] J. Berg, J. Tymoczko, L. Stryer, *The Michaelis-Menten Model Accounts for the Kinetic Properties of Many Enzymes, Biochemistry. 5th Edition*, **2002**.
- [39] J. Badger, J. M. Sauder, J. M. Adams, S. Antonysamy, K. Bain, M. G. Bergseid, S. G. Buchanan, M. D. Buchanan, Y. Batiyenko, J. A. Christopher, et al., *Proteins Struct. Funct. Bioinforma.* **2005**, *60*, 787–796.
- [40] L. E. Kemp, C. S. Bond, W. N. Hunter, *Acta Crystallogr. Sect. D Biol. Crystallogr.* **2003**, *D59*, 607–610.
- [41] J. Behnen, H. Koester, G. Neudert, T. Craan, A. Heine, G. Klebe, *ChemMedChem* **2012**, *7*, 248–261.
- [42] A. J. Wilson, J. K. Kerns, J. F. Callahan, C. J. Moody, *J. Med. Chem.* **2013**, *56*, 7463–7476.
- [43] Y. Hu, J. Bajorath, *Drug Discov. Today* **2013**, *18*, 644–650.
- [44] Y. Hu, J. Bajorath, *Medchemcomm* **2013**, *4*, 1196.
- [45] Y. Hu, E. Lounkine, J. Bajorath, *AAPS J.* **2014**, *16*, 847–59.
- [46] Y. Hu, D. Gupta-Ostermann, J. Bajorath, *Comput Struct Biotechnol J* **2014**, *9*, e201401003.
- [47] M. T. Harris, D. M. Walker, M. E. Drew, W. G. Mitchell, K. Dao, C. E. Schroeder, D. P. Flaherty, W. S. Weiner, J. E. Golden, J. C. Morris, *Antimicrob. Agents Chemother.* **2013**, *57*, 3731–3737.
- [48] D. Liu, Z. Tian, Z. Yan, L. Wu, Y. Ma, Q. Wang, W. Liu, H. Zhou, C. Yang, *Bioorganic Med. Chem.* **2013**, *21*, 2960–2967.
- [49] S. Sidique, R.-P. Dhanya, D. J. Sheffler, H. H. Nickols, L. Yang, R. Dahl, A. Mangravita-Novo, L.

- H. Smith, M. S. D'Souza, S. Semenova, et al., *J. Med. Chem.* **2012**, *55*, 9434–9445.
- [50] P. J. Tummino, P. J. Harvey, T. McQuade, J. Domagala, R. Gogliotti, J. Sanchez, Y. Song, D. Hupe, *Antimicrob. Agents Chemother.* **1997**, *41*, 394–400.
- [51] S. W. Wright, J. J. Petraitis, M. M. Abelman, D. G. Batt, L. L. Bostrom, R. L. Corbett, C. P. Decicco, M. S. V Di, B. Freimark, J. V Giannaras, *J. Med. Chem.* **1994**, *37*, 3071–3078.
- [52] S. D. Furdas, I. Hoffmann, D. Robaa, B. Herquel, W. Malinka, P. Swia, A. Akhtar, W. Sippl, M. Jung, **2014**, 1856–1862.
- [53] Y. Bravo, P. Teriete, R.-P. Dhanya, R. Dahl, P. S. Lee, T. Kiffer-Moreira, S. R. Ganji, E. Sergienko, L. H. Smith, C. Farquharson, et al., *Bioorg. Med. Chem. Lett.* **2014**, *24*, 4308–4311.
- [54] J. B. Baell, *Future Med. Chem.* **2010**, *2*, 1529–1546.
- [55] R. Dahl, Y. Bravo, V. Sharma, M. Ichikawa, R.-P. Dhanya, M. Hedrick, B. Brown, J. Rascon, M. Vicchiarelli, A. Mangravita-Novo, et al., *J. Med. Chem.* **2011**, *54*, 3661–3668.
- [56] L. S. Imlay, C. M. Armstrong, M. C. Masters, T. Li, K. E. Price, R. L. Edwards, K. M. Mann, L. X. Li, C. L. Stallings, N. G. Berry, et al., *ACS Infect. Dis.* **2015**, *1*, 157–167.
- [57] A. Alexandrov, M. Vignali, D. J. LaCount, E. Quartley, C. de Vries, D. de Rosa, J. Babulski, S. F. Mitchell, L. W. Schoenfeld, S. Fields, et al., *Mol. Cell. Proteomics* **2004**, *3*, 934–938.
- [58] B. Zhang, K. M. Watts, D. Hodge, L. M. Kemp, D. A. Hunstad, L. M. Hicks, A. R. Odom, *Biochemistry* **2011**, *50*, 3570–3577.

Chapter 5
An Alternative Inhibitor of the
***PflspD* Enzyme**

5.1 MMV-008138: A Stereospecific Chemotype and *Pf*lspD Inhibitor

It has been previously acknowledged that covalent modification and the use of covalent modifiers can be a risky strategy within drug design programmes and the development of chemotherapeutic agents.^[1,2] The cysteine reactivity demonstrated by 1,2-benzo[*d*]isothiazol-3(2*H*)-one (BITZ) compounds (**Chapter 4**) poses a possible issue that corresponding BITZ inhibitors may be compromised by polypharmacology. Indeed, vigilance will be required should BITZ compounds progress further in antimalarial drug development. The noted potential for BITZ compounds to interact with off-target proteins in promiscuous binding events highlights a risk of unpredictable reactivity and presents a need for monitoring the extent of inhibitor promiscuity to minimise toxicity risks in the human host.^[3-5] It was therefore decided reasonable, and within the scope of this research, to consider alternative means of achieving *Pf*lspD inhibition.

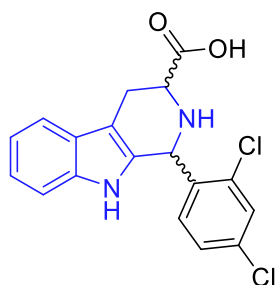
Research efforts remain focused on achieving inhibition of the *Pf*lspD enzyme target as a method of disrupting MEP pathway biosynthesis in *Plasmodium* spp. parasites, consequently preventing essential isoprenoid precursor synthesis as a means of inhibiting *Plasmodium* parasite growth. However, synthetic, biological, computational and mechanistic evaluations are now focused on a complementary strategy towards an alternative inhibitor scaffold that is constructed around a discrete chemical chemotype. Since research thus far has focused on optimising inhibition of the *Pf*lspD enzyme through covalent means, with the identification and development of the BITZ chemotype, attentions are now directed towards a non-covalent method of achieving *Pf*lspD enzyme inhibition.

This chapter will discuss and evaluate the potential of a tetrahydro- β -carboline chemotype (**Figure 5.1**) as a potent inhibitor of the *Pf*lspD enzyme operating *via* an alternative non-covalent mechanism of action. We will consider the similarities and differences of β -carboline-derived compounds with respect to the BITZ chemotype, since both are inhibitors of *Pf*lspD enzyme. In addition, development of the structure-activity-relationship (SAR) around the tetrahydro- β -carboline chemotype will also be explored.

5.1.1 Identification of MMV-008138

Recently the Malaria Box compound, MMV-008138 [(2,4-dichloro-phenyl)-2,3,4,9-tetrahydro-1*H*-pyrido[3,4-*b*]indol-2-ium-3-carboxylate)], was identified through a phenotypic screen of the large GlaxoSmithKline (GSK) screening library.^[6] MMV-008138, based around the tetrahydro- β -carboline chemical construct (**Figure 5.1**), was identified in an isopentenyl pyrophosphate (IPP) chemical rescue screen. MMV-008138 was found to be a potent antimalarial compound, inhibiting *P. falciparum* growth as a result of activity against the *Plasmodium* parasite apicoplast.^[7,8] Since MMV-008138 was

identified in a phenotypic screen (**Chapter 2, Section 2.1 and 2.1.1**), the specific antimalarial target of the compound was initially unknown and as such, the mechanism by which MMV-008138 was capable of apicoplast dysfunction was unclear.^[9]



MMV-008138

Figure 5.1 Chemical structure of MMV-008138 with the tetrahydro- β -carboline chemotype and chemical core highlighted in blue.

An interesting structural feature of MMV-008138 is that the compound contains two stereogenic centres, meaning that four distinct stereoisomers of the compound are possible (**Figure 5.2**).^[9] The presence of chirality within a potential drug molecule represents a point of consideration for forward drug design and SAR development since chemical chirality can dictate precise 3D structural requirements that must be adhered to or preserved within chiral analogues in order to maintain activity. Chirality within chemical analogues and synthetic species also presents hurdles of additional synthetic complexity, stereo-specificity and the performance of required reactions, as well as the ease by which particular diastereoisomers may be isolated.

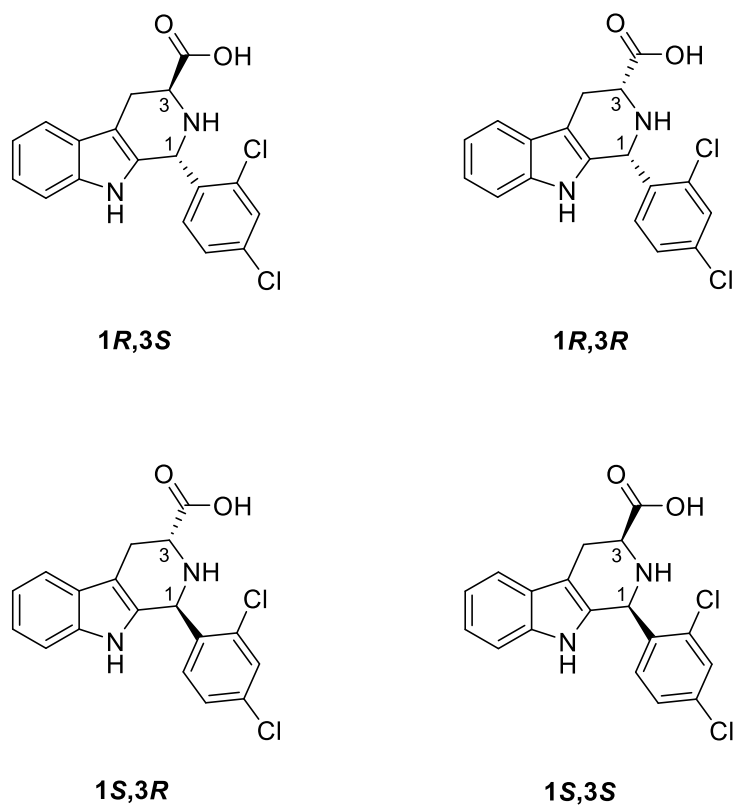


Figure 5.2 Chemical structures of the four diastereoisomers of MMV-008138 where the stereochemistry of each is depicted.

There are also some benefits to molecular chirality and the presence of stereo-centres in potential chemotherapeutic agents, in terms of the longevity and success of compounds moving through the drug design process. A number of diverse research programs have shown that the survival rate of compounds in the drug design process can be improved by increasing the number of chiral centres within a molecule. Indeed, it has been demonstrated that both the complexity and presence of chiral centres within drug molecules correlates, in some cases, with the successful transition of compounds from drug discovery to clinical candidates.^[10]

It is argued that chemical chirality constructively increases molecular complexity and can therefore enhance compound potency through more appropriate complementarity of a particular isomer to a specified target which is achieved without increasing the molecular weight (MW) of a compound.^[11] The appropriate use of chiral motifs can therefore be used to enhance compound specificity, and potentially potency, at an enzyme or protein without needing to alter other structural aspects of a compound, which may otherwise compromise other physicochemical properties such as MW, lipophilicity and therefore compound solubility, permeability and distribution.

In relation to our research, use of molecular chirality may prove to be a useful tool in enriching compound specificity towards the *PflspD* enzyme target. This may help to circumvent current concerns

regarding the promiscuity and potential off-target cysteine reactivity of BITZ inhibitors by considering the development of alternative *Pf*ispD inhibitors that show enhanced selectivity for *Pf*ispD. Indeed, the increased molecular complexity associated with a chiral motif, may provide an additional degree of molecular recognition and therefore specificity in resulting compounds which may in turn enhance potency at the *Pf*ispD molecular target.^[12]

Initial evaluation of MMV-008138, including its identification as an IPP rescue phenotype in the Malaria Box screen, was carried out using racemic mixtures of the compound which contained unspecified ratios of diastereoisomers.^[9] The initial screen identifying MMV-008138 as a compound that acts against the *Plasmodium* apicoplast, demonstrated that MMV-008138 could produce > 95% growth inhibition at 5 μ M of the compound alone with an IC_{50} value of 350 ± 50 nM against the *P. falciparum* Dd2 strain, in the absence of IPP.^[8]

Further investigations by Wu *et al.* confirmed the IPP rescue phenotype of MMV-008138, with an EC_{50} of 772 nM (664 to 741 nM) against the *P. falciparum* W2 strain in the absence of IPP.^[9] Whilst such evaluations clearly highlighted the activity of MMV-008138 against *Plasmodium* spp. growth, these initial studies only indicated that MMV-008138 targets an apicoplast pathway, but provided no further insight into how stereochemistry affects activity or the specific molecular target at which the compound acts.

In a study to determine the activity of the four MMV-008138 stereoisomers, Wu *et al.* identified that the 1*R*,3*S* isomer is the most active stereoisomer of the MMV-008138 compound; demonstrating an EC_{50} of 110 nM and IPP rescue up to 25 μ M (Table 5.1).^[9]

MMV-008138 diastereoisomer	Parasite growth EC_{50} (μ M)	Parasite growth EC_{50} (μ M) + IPP
1 <i>R</i> ,3 <i>S</i>	0.11 (0.10 – 0.12)	> 25
1 <i>R</i> ,3 <i>R</i>	3.8 (2.7 – 5.3)	> 25
1 <i>S</i> ,3 <i>R</i>	18.6 (12.4 – 28.0)	> 25
1 <i>S</i> ,3 <i>S</i>	> 50	> 50

Table 5.1 Inhibitory activities of the four MMV-008138 stereoisomers against *Plasmodium* parasite growth, both with and without the presence of IPP; data represents means values with 95% confidence intervals.^[9]

Both the 1*R*,3*R* and 1*S*,3*R* isomers showed notably reduced activity against parasite growth compared to the 1*R*,3*S* isomer; where measured activity of these two isomers showed more than a 30-fold and 160-fold decrease in activity compared to the 1*R*,3*S* isomer. However, all three of the aforementioned MMV-008138 isomers demonstrated IPP-rescuable activity of up to 25 μ M.^[9] In contrast, the 1*S*,3*S*

isomer was found to be completely inactive against parasite growth, both with and without the presence of IPP. Taken all together, the stereospecificity of parasite growth inhibition by MMV-008138 stereoisomers is clearly evident and strongly indicates that a specific MMV-008138 stereoisomer is likely to bind to and inhibit a specific cellular target.^[9]

5.1.2 Biological Target of MMV-008138

Following its identification, there is now substantial evidence that MMV-008138 is capable of inhibiting *P. falciparum* growth through potent and selective activity against the *Pf*lspD enzyme, which is already established as a key enzyme of the MEP pathway, involved in mediating isoprenoid precursor biosynthesis within the apicoplast of *Plasmodium* parasites.^[9,13-17]

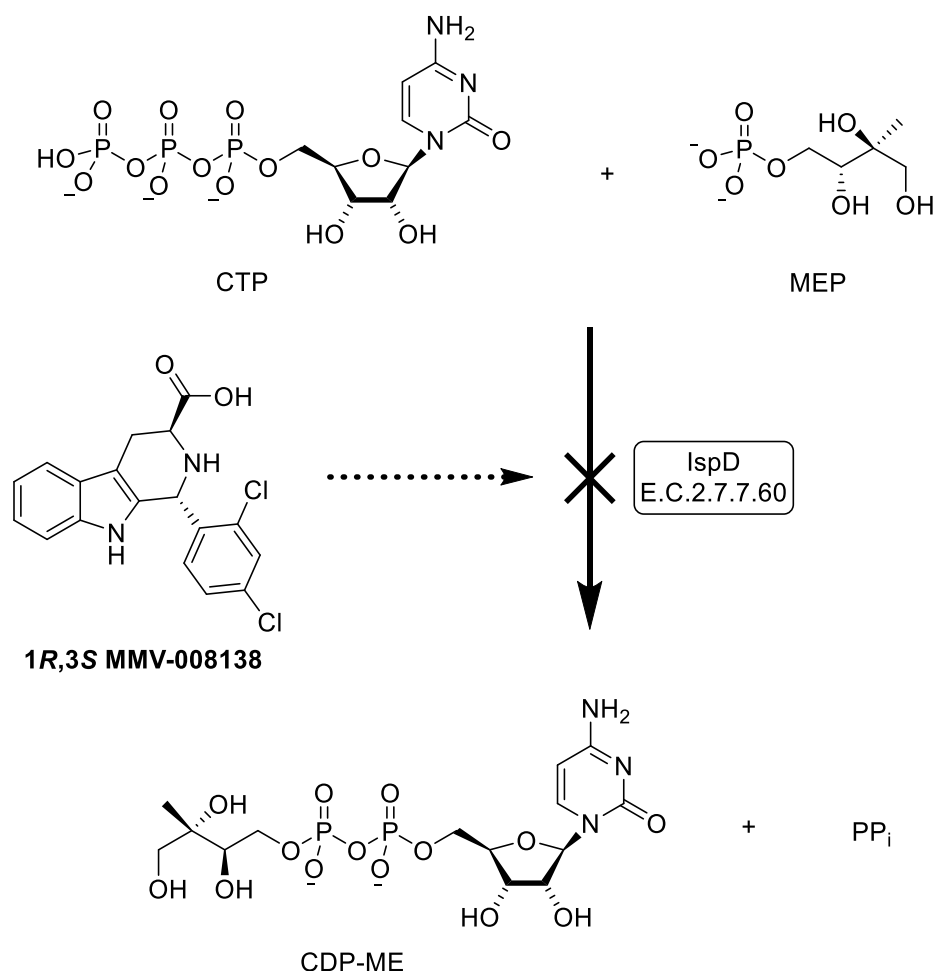
To determine the biological target of MMV-008138, and thus consider a possible mechanism of action, *Plasmodium* parasites resistant to MMV-008138 were generated in work conducted by others.^[9] Whole-genome sequencing of three drug-resistant populations revealed three non-synonymous mutations that conferred resistance to MMV-008138. Within all three resistant populations, the mutated gene was of common identity and encoded the 4-diphosphocytidyl-2C-methyl-D-erythritol cytidyltransferase (lspD) enzyme of the MEP isoprenoid precursor pathway, highlighting this enzyme as the likely molecular target of MMV-008138.^[9]

In order to determine if MMV-008138 was indeed capable of directly inhibiting *Pf*lspD, and therefore if this was the molecular target of the compound, Wu *et al.* expressed and purified the *Pf*lspD enzyme to enable measurement of its enzymatic activity following treatment with MMV-008138 and the use of a pyrophosphate release assay.^[9] Comparable to the pattern of inhibitory activity against *Plasmodium* parasite growth observed with the four MMV-008138 stereoisomers, inhibition of the *Pf*lspD enzyme by the different MMV-008138 stereoisomers was also stereospecific and analogous to that demonstrated in parasite growth inhibition (**Table 5.2**).^[9]

MMV-008138 diastereoisomer	Parasite growth EC ₅₀ (μM)	<i>Pf</i> lspD activity IC ₅₀ (nM)
1 <i>R</i> ,3 <i>S</i>	0.11 (0.10-0.12)	7.1 (6.1-8.3)
1 <i>R</i> ,3 <i>R</i>	3.8 (2.7-5.3)	170 (140-200)
1 <i>S</i> ,3 <i>R</i>	18.6 (12.4-28.0)	2500 (1900-3100)
1 <i>S</i> ,3 <i>S</i>	> 50	> 2500

Table 5.2 Inhibitory activities of the four MMV-008138 stereoisomers against purified *Pf*lspD; mean data values given with 95% confidence intervals.^[9]

The most active diastereoisomer of MMV-008138 was again the 1*R*,3*S* isomer which displayed potent inhibition of the *Pf*lspD enzyme with activity in the low nanomolar region: *Pf*lspD IC₅₀ value = 7.1 nM. All other diastereoisomers of MMV-008138 were considerably less potent and the 1*S*,3*S* isomer completely inactive (**Table 5.2**).^[9] A combination of genetic and biochemical data has therefore identified the *Pf*lspD enzyme of the MEP apicoplast pathway as the specific cellular target of the MMV-008138 compound (**Scheme 5.1**). MMV-008138 inhibition of blood-stage *P. falciparum* growth is both potent and stereospecific, with the most active 1*R*,3*S* stereoisomer demonstrating an EC₅₀ value of 110 nM against parasite growth and directly inhibiting *Pf*lspD *in vitro* at an IC₅₀ value of 7.1 nM (**Table 5.2**).^[9] These findings are strongly supported by the work of others^[15] who also suggest that *in vivo* 1*R*,3*S*-MMV-008138 inhibition of *Pf*lspD is likely to result in decreased cellular levels of MEP pathway metabolites that are enzymatically downstream of the IspD enzyme.^[15]



Scheme 5.1 Proposed inhibition of IspD enzymatic activity by 1*R*,3*S*-MMV-008138.^[15]

Further studies conducted by Imlay *et al.* have addressed the question of species-selectivity and the potential antimicrobial activity spectrum of the 1*R*,3*S*-MMV-008138 isomer. Consistent with previous reports,^[9] 1*R*,3*S*-MMV-008138 was found to be inactive against bacterial orthologues of the IspD

enzyme. *E. coli* IspD (EclspD) is not inhibited with treatment of 1*R*,3*S*-MMV-008138 up to 30 μ M and *Mycobacterium tuberculosis* IspD (MtlspD) is insensitive to 1*R*,3*S*-MMV-008138 (Figure 5.3).^[15] These results are well aligned with previous studies which also found MMV-008138 to lack activity against the *A. thaliana* IspD (AtlspD) enzyme homologue.^[9]

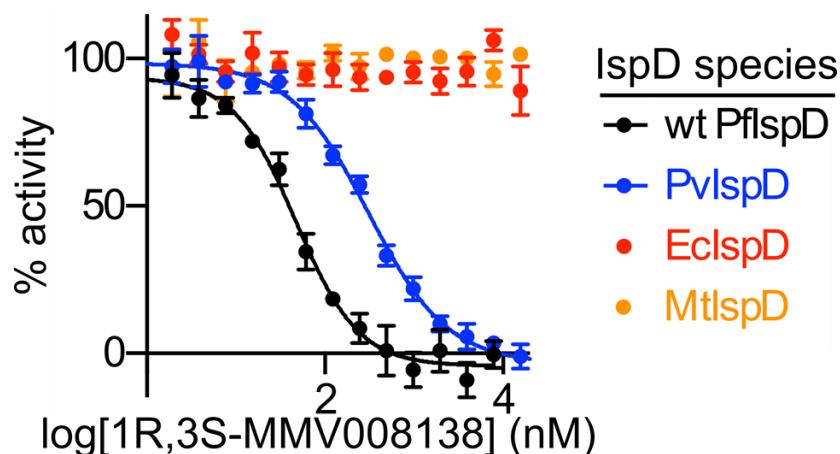


Figure 5.3 Species selectivity of 1*R*,3*S*-MMV-008138 against various IspD homologues.^[15]

In contrast to the lack of activity against bacterial IspD orthologues, 1*R*,3*S*-MMV-008138 was shown to potently inhibit *P. vivax* IspD (PvIspD) with an IC₅₀ value of 310 nM (95% CI 240-400 nM); however, the PflspD enzyme was shown to remain the most sensitive IspD orthologue evaluated with a measured IC₅₀ value of 47 nM (95% CI 37-60 nM).^[15] The 1*R*,3*S* MMV-008138 isomer therefore shows promise as broad spectrum antimalarial agent with the potential to treat *P. vivax* malaria infections.

This result is highly comparable to the activity spectrum and species selectivity that we have observed with the BITZ inhibitor chemotype which successfully inhibits *P. falciparum* and *P. vivax* IspD enzymes but shows no activity against bacterial IspD enzyme orthologues.^[17] We have shown that BITZ compounds are species-selective IspD inhibitors and do not possess activity against the EclspD enzyme (Chapter 4, Section 4.4.1.1, Figure 4.21 and Table 4.9),^[17] but in contrast show activity against the PvIspD enzyme, which is comparable to that demonstrated against PflspD. Enzymatic assays using both purified *P. vivax* and *P. falciparum* IspD enzymes have shown that a range of BITZ analogues (Chapter 3, Section 3.11, BITZ compounds 4-6 and 13-15, Table 3.9) demonstrate low micromolar to nanomolar activity against these two *Plasmodium* IspD enzyme species. Considered together, these recent studies suggest that, like the BITZ chemotype, further modifications to the MMV-008138 scaffold may widen the therapeutic scope of this chemotype, facilitating broad-spectrum activity against multiple malaria species.

5.1.3 MMV-008138: Mechanism of Action

Targeted metabolic profiling of MEP pathway metabolites in *P. falciparum* cells has been performed by Imlay *et al.* in order to establish the anti-parasitic mechanism of action of the 1*R*,3*S*-MMV008138 isomer. Already knowing *Pf*ispD to be the cellular target of 1*R*,3*S*-MMV008138, Imlay *et al.* suggested that *in vivo* inhibition of *Pf*ispD is therefore likely to result in decreased cellular levels of MEP pathway metabolites that are enzymatically downstream of IspD.^[15] Targeted metabolic profiling studies therefore aimed to confirm that 1*R*,3*S*-MMV008138 is capable of arresting the MEP pathway through specific and targeted inhibition of the *Pf*ispD enzyme.

It was found that treatment of *P. falciparum* with 1*R*,3*S*-MMV-008138 dramatically reduced cellular levels of the most distal MEP metabolite, methylerythritol cyclic diphosphate (MEcPP) (**Figure 5.4**). 1*R*,3*S*-MMV008138 was shown to reduce levels of MEcPP to $12 \pm 4\%$ of control levels which is consistent with cellular inhibition of MEP pathway metabolism upstream from MEcPP. Of note, this observed effect was not replicated with the 1*S*,3*R*-MMV008138 isomer, previously shown to be inactive against *Pf*ispD.^[15]

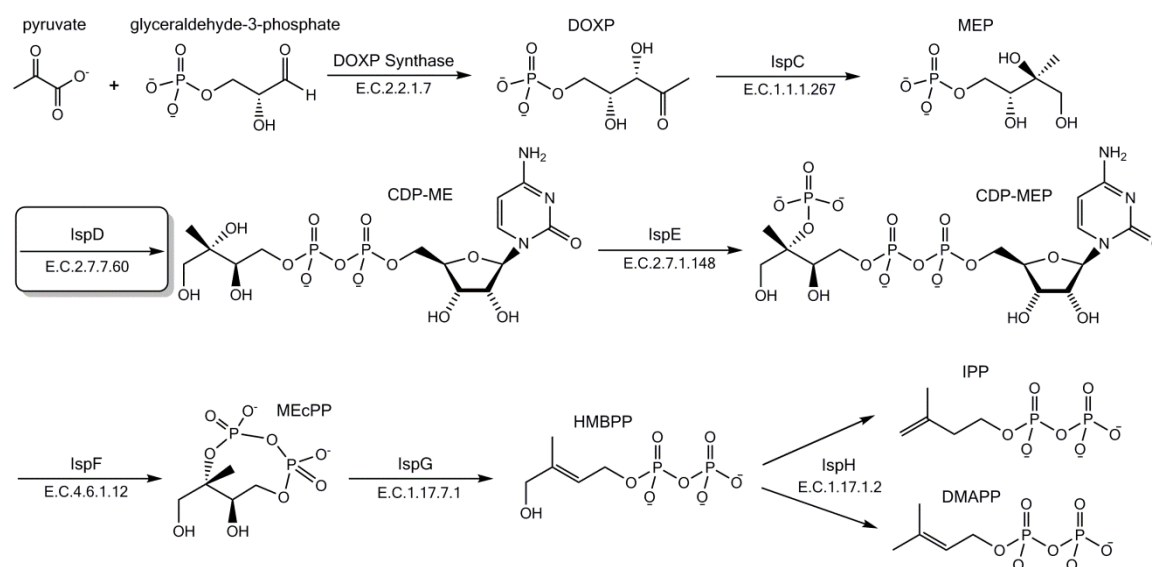


Figure 5.4 The MEP Pathway.^[13,16]

This result is consistent with work previously described^[18] determining the downstream effects of fosmidomycin (FSM), the established phosphonic acid IspC inhibitor, on distal metabolite levels within the MEP pathway. Comparably, treatment of *P. falciparum* with FSM causes a $95 \pm 2\%$ decrease in cellular levels of MEcPP compared to control levels. A further consistency, observed through targeted metabolic profiling, is the comparable effect of the BITZ chemotype on MEP pathway metabolite levels which had also been shown to produce a significant decrease in MEcPP levels (**Chapter 3, Section 3.12, Figure 3.19**).

Treatment of *P. falciparum* with selected BITZ compounds and 1*R*,3*S*-MMV-008138 does not affect the levels of the DOXP metabolite which is metabolically upstream from the IspC and IspD MEP pathway enzymes. Together, these studies confirm that both the BITZ chemotype and 1*R*,3*S*-MMV-008138 are capable of inhibiting the *Plasmodium* MEP pathway at levels which affect asexual parasite growth. In addition, 1*R*,3*S*-MMV-008138-treated parasites which are then supplemented with 200 μ M IPP, one of the key isoprenoid precursors (**Figure 5.4**), are found to be viable. This further establishes that the metabolic effects and inhibition of parasite growth by 1*R*,3*S*-MMV-008138 are specific to MEP pathway inhibition since it has been demonstrated that the antimalarial potency of this compound is relieved by media supplementation with IPP.^[8,15]

5.1.4 MMV-008138: Competitive Behaviour at *Pf*IspD

It is well established,^[13,16,19,20] and has been previously discussed (**Chapter 1, Section 1.4.2 and 1.5.2**) that the third enzyme of the MEP pathway (IspD) catalyses the transfer of a cytidyl group from CTP to MEP, therefore utilising the two substrates of the enzyme and generating the enzyme product CDP-ME. In order to determine the molecular mechanism of action by which 1*R*,3*S*-MMV-008138 is capable of inhibiting the *Pf*IspD enzyme, kinetic characterisation of *Pf*IspD was carried out by Imlay *et al.*^[15]

Kinetic analysis supports a model of inhibition whereby 1*R*,3*S*-MMV-008138 behaves in a competitive manner with respect to the CTP substrate at the *Pf*IspD enzyme (**Figure 5.5; a and b**). In contrast, parallel studies demonstrate a non-competitive model of inhibition of 1*R*,3*S*-MMV-008138 with respect to the MEP substrate at *Pf*IspD (**Figure 5.5; c and d**). **Figure 5.5** depicts the Michaelis-Menten kinetics of *Pf*IspD following treatment with various concentrations of 1*R*,3*S*-MMV-008138, showing that inhibition of *Pf*IspD with 1*R*,3*S*-MMV-008138 is competitive with respect to CTP but not MEP.^[15]

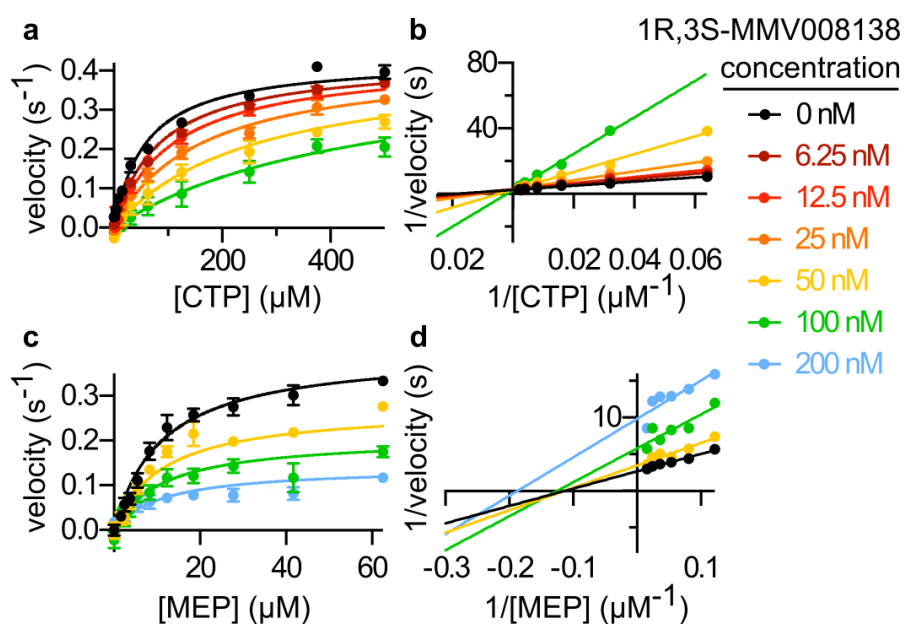


Figure 5.5 Michaelis-Menten kinetics of *PflspD* following treatment with 1*R*,3*S*-MMV-008138; **a**: direct plot of *PflspD* activity vs. [CTP]; **b**: Lineweaver-Burke plot of *PflspD* activity at a range of CTP concentrations; **c**: direct plot of *PflspD* activity vs. [MEP]; **d**: Lineweaver-Burke plot of *PflspD* activity at a range of MEP concentrations.^[15]

Since 1*R*,3*S*-MMV-008138 has been shown to be capable of inhibiting the *PvlspD* enzyme homologue (**Figure 5.3**), subsequent kinetic enzyme studies were also conducted to determine the mode of 1*R*,3*S*-MMV-008138 inhibition at *PvlspD*. Kinetic evaluations indicate that, as seen for *PflspD*, inhibition of *PvlspD* also occurs *via* competition with the CTP substrate.^[15] Therefore, this work not only establishes that *PflspD* represents the enzymatic target of 1*R*,3*S*-MMV-008138, but also demonstrates that 1*R*,3*S*-MMV-008138 inhibits *PflspD* competitively with the CTP enzyme substrate.^[15]

5.2 Molecular Modelling of 1*R*,3*S*-MMV-008138 at *PflspD*

In addition to enzymatic and cellular analysis of 1*R*,3*S*-MMV-008138, molecular modelling studies were carried out to provide insight into the spatial alignment and binding mode of 1*R*,3*S*-MMV-008138 at the *PflspD* enzyme. This body of work denotes the beginning of our involvement in the evaluation and development of the MMV-008138 compound (and more broadly the tetrahydro- β -carboline chemical chemotype) as a *PflspD* inhibitor and potential antimalarial chemotherapeutic agent.

Equivalent to our previous molecular modelling studies with the BITZ chemotype and derived compounds, the *PflspD* homology model (**Chapter 4, Section 4.3**)^[21] was used to dock 1*R*,3*S*-MMV-008138 into the CTP binding site of the enzyme using the previously defined docking protocol (**Protocol 4; Chapter 4, Section 4.2.1, Table 4.7**). The docking program GOLD 5.0.1^[22,23] was used to assess the strength of interactions between 1*R*,3*S*-MMV-008138 and the *PflspD* homology model as well as visualise non-covalent interactions between the inhibitor and the enzyme binding site.^[23]

Previous studies have demonstrated that IspD enzyme homologues in other organisms are amenable to inhibition by small molecules (**Chapter 1, Section 1.5.2**); most notable perhaps is inhibition of the herbaceous *Arabidopsis thaliana* IspD (*AtIspD*) orthologue which occurs by a number of structurally diverse small molecules.^[24,25] However, it is significant that these previously described molecules all demonstrate allosteric inhibition of the *AtIspD* orthologue. In contrast, initial docking of 1*R*,3*S*-MMV-008138 highlighted that the tetrahydro- β -carboline inhibitor appears to target the CTP binding site of *PfIspD* (**Figure 5.6**). Indeed, visualisation of 1*R*,3*S*-MMV-008138 in the *PfIspD* CTP binding site shows the identified pose of 1*R*,3*S*-MMV-008138 to be comparable to the alignment of the natural enzyme product, CDP-ME, closely mimicking the binding mode of the cytidine phosphate moiety, as defined by the *E. coli* crystal structure (PDB: 1I52).^[26]

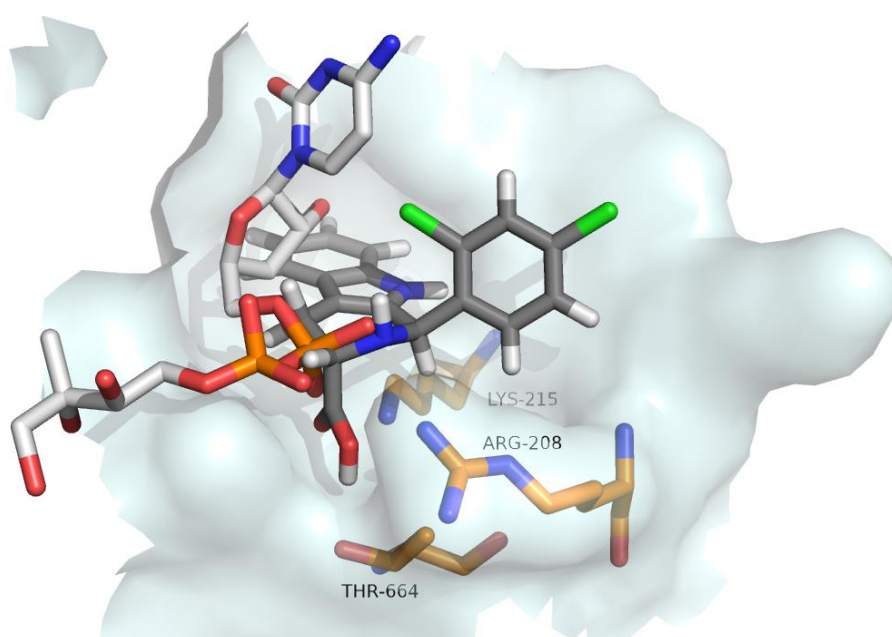


Figure 5.6 1*R*,3*S*-MMV-008138 and CDP-ME modelled in the CTP binding site of the *PfIspD* homology model. The active site is rendered as a white surface; selected residues are depicted as sticks: carbon atoms are orange; oxygen atoms are red; nitrogen atoms are blue. 1*R*,3*S*-MMV-008138 is displayed as sticks: carbon atoms are dark grey. CDP-ME is displayed as sticks: carbon atoms are light-grey. Image created using PyMOL.^[27]

This observation draws strong parallels to the assessment of the BITZ chemotype at *PfIspD* since our previous modelling studies have also shown BITZ derived inhibitors to target and occupy the CTP binding site of the *PfIspD* enzyme (**Chapter 4, Section 4.3.2**). Indeed, overlaying identified binding poses of the two inhibitor chemotypes, using representative BITZ compound **1** (**Table 5.3**) and 1*R*,3*S*-MMV-008138, clearly highlights the similar alignment of the two compounds which both broadly mirror the known pose and orientation of the CDP-ME enzyme product^[26] (**Figure 5.7**).

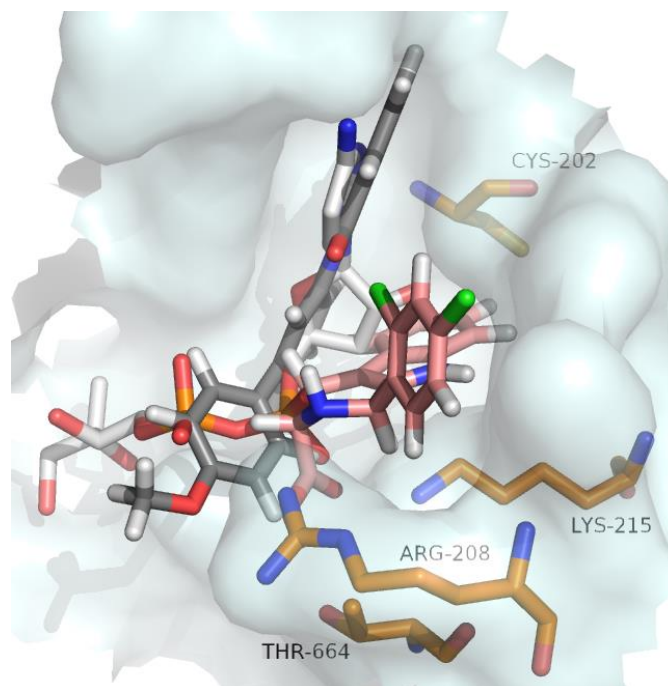


Figure 5.7 1*R*,3*S*-MMV-008138, **1** and CDP-ME modelled in the CTP binding site of the *PflspD* homology model. The active site is rendered as a white surface; selected residues are depicted as sticks: carbon atoms are orange; oxygen atoms are red; nitrogen atoms are blue. 1*R*,3*S*-MMV-008138 is displayed as sticks: carbon atoms are pink; **1** is displayed as sticks: carbon atoms are dark grey; CDP-ME is displayed as sticks: carbon atoms are light-grey. Image created using PyMOL.^[27]

Using the previously specified Protocol 4 (**Chapter 4, Section 4.2.1, Table 4.7**), 50 GA docking poses were calculated for 1*R*,3*S*-MMV-008138 at *PflspD* to further assess the predicted alignment and orientation of the compound. 1*R*,3*S*-MMV-008138 demonstrated excellent spatial fit in the CTP binding pocket and was predicted to bind to the *PflspD* active site with an average GoldScore^[23,28] of 49.6 ± 3 ; where the CTP enzyme substrate itself has a GoldScore of 72.0 ± 4 . The higher GoldScore of CTP, compared to that predicted for 1*R*,3*S*-MMV-008138, is likely due to the negative charge on the triphosphate group of CTP, forming enhanced hydrogen bonds to Arg208, compared to that of the neutral 1*R*,3*S*-MMV-008138 compound.^[15]

1*R*,3*S*-MMV008138 is predicted to form an array of four hydrogen bonds between the carboxylic acid functionality of the compound and the three active site protein residues: Thr-664, Arg-208, and Lys-215 (**Figure 5.8**). These predicted enzyme-inhibitor contacts mirror those formed by the phosphate group of CTP in the 1I52 crystal structure^[26] and therefore support the competitive nature of 1*R*,3*S*-MMV-008138 with CTP, as previously observed in enzymology studies.^[15] It can therefore be deduced that 1*R*,3*S*-MMV-008138 has a non-covalent mechanism of action at *PflspD*, targeting the CTP binding site of the enzyme, as a competitive inhibitor of CTP.

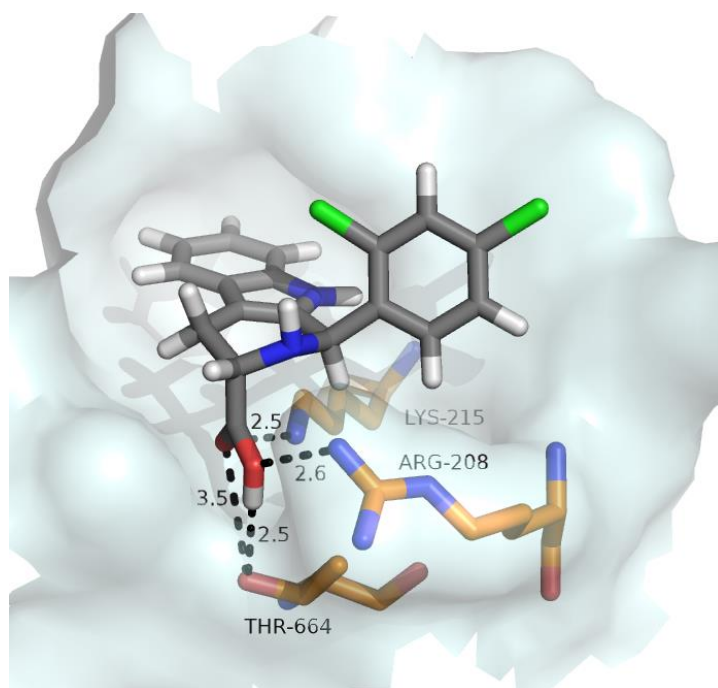


Figure 5.8 Docking pose of 1*R*,3*S*-MMV-008138 in the CTP binding site of the *PflspD* homology model. The active site is rendered as a white surface and residues forming hydrogen bonds with 1*R*,3*S*-MMV-008138 are depicted as sticks: carbon atoms are orange; oxygen atoms are red; nitrogen atoms are blue. 1*R*,3*S*-MMV-008138 is displayed as sticks: carbon atoms are dark grey. Hydrogen bonds are shown as dotted black lines with distance given in angstroms. Image created using PyMOL.^[15,27]

The requirement for the 1*R*,3*S* diastereoisomer of MMV-008138 to achieve potent *PflspD* enzyme inhibition (**Table 5.2**) can now be rationalised through the spatial demands of the *PflspD* CTP binding site, as shown by the enzyme surface depicted in **Figures 5.6** and **5.8**. It is evident from docking predictions (**Figure 5.8**) that 1*R*,3*S*-MMV-008138 adopts a binding pose that spatially, is very tight-fitting within the CTP binding pocket and therefore may be strongly influenced by *PflspD* active site protein residues with which the compound closely aligns and associates. Consequently, it is plausible that there may be little room for significant structural variation around certain regions of the 1*R*,3*S*-MMV-008138 compound which must be taken into consideration for future inhibitor design; most notably, restrictions seem likely around the carboxylic acid functionality.

As already established, both the 1*R*,3*S*-MMV-008138 compound and BITZ inhibitors (represented here by **1**) bind to the CTP binding pocket of *PflspD* where some pose overlap is observed between the two chemotypes, as well as close to alignment of both compounds to the natural product CDP-ME (**Figure 5.7**). However, the tetrahydro- β -carboline and BITZ chemotypes both occupy slightly different spatial alignments with respect to each other in the CTP binding pocket and as such, display subtle differences in proximity to various protein residues in the *PflspD* active site (**Figure 5.9**).

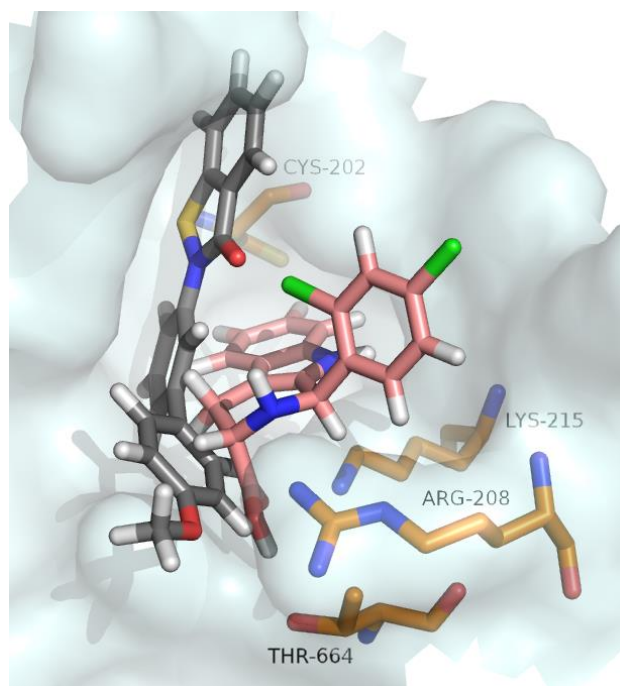


Figure 5.9 1R,3S-MMV-008138 and **1** modelled in the CTP binding site of the *PflspD* homology model. The active site is rendered as a white surface; selected residues are depicted as sticks: carbon atoms are orange; oxygen atoms are red; nitrogen atoms are blue. 1R,3S-MMV-008138 is displayed as sticks: carbon atoms are pink; **1** is displayed as sticks: carbon atoms are dark grey. Image created using PyMOL.^[27]

The depiction of the two *PflspD* inhibitors in the CTP binding pocket (**Figure 5.9**) highlights comparable proximities of the two compounds to the Thr-664 and Arg-208 active site residues. Noticeably, BITZ inhibitor **1** appears to extend further into the binding site, facilitating alignment with and therefore covalent attachment to the Cys-202 residue. In contrast, the identified protein-ligand interactions between 1R,3S-MMV-008138 and *PflspD* consist mainly of hydrogen bonding interactions between the carboxylic acid functionality and the active site protein residues: Thr-664, Arg-208, and Lys-215 (**Figure 5.8**). This strongly suggests a non-covalent mechanism of enzyme inhibition regarding 1R,3S-MMV-008138 which outcompetes CTP for occupancy of *PflspD* the binding site.

Two distinct mechanisms of action can therefore be rationalised for the BITZ and tetrahydro- β -carboline chemotypes, despite the extent of similarities displayed by these chemical motifs in targeting and inhibiting the *PflspD* enzyme. As already established and providing further evidence that these two chemical motifs are capable of producing the same cellular effects against *Plasmodium* parasites, metabolic profiling of MEP pathway intermediates when treated with these two chemotypes also yields highly comparable results (**Section 5.1.3**).

The comparable features identified between the tetrahydro- β -carboline and BITZ chemotypes led us to ask the question: how would these two chemical motifs behave if administered in combination and

what would be the resulting effects on inhibition of parasite growth and overall antimalarial efficacy? Put simply, are these two chemotypes capable of behaving with synergy at the *Pf*spD enzyme target, producing an enhanced level of potency against the enzyme and subsequently parasite growth as a result of co-administration? In order to answer these questions, a series of competition experiments were undertaken to determine the antimalarial effects of the combination of the two compounds, selecting a derivative of both the BITZ and tetrahydro- β -carboline chemotypes to be representative.

5.3 Can a Combined Administration of the BITZ and Tetrahydro- β -carboline Chemotypes Produce Enhanced Antimalarial Activity?

5.3.1 Rationale and Background

It is widely accepted that there is a dual benefit to the use of combination therapies within drug design. The combination of chemical agents, known to produce the desired biological effect, can not only optimise the resulting therapeutic outcome, but may also protect the components of the combined therapy, minimising the risk of resistance development against either chemical entity.^[29]

Therefore, a desirable advantage in the use of combination chemotherapies within antimalarial drug design is the potential that the resulting therapy may be capable of delaying the onset of *Plasmodium* resistance to new chemical agents, as well as reduce the effects of resistance to therapies that may already have diminished antimalarial efficacy when administered alone.^[30,31] However, for a combination therapy to be successful, the component drugs must be capable of working synergistically, producing a heightened therapeutic effect than could be achieved by administering either component drug alone. Consequently, a combined therapy approach can enable effective and efficacious antimalarial therapies to be administered that contain smaller doses of the component drugs; therefore producing effective, lower-dose therapies that may be beneficial for the development of alternative dosing regimens in poor and disadvantaged regions which are often hard to access and are where malaria is endemic.^[32]

The use of combination therapies is by no means a new phenomenon; over the last century, advances in genetics and cell biology have facilitated the increasing use of drug combinations to tackle therapeutic challenges in modern medicine.^[33] It is now well understood that biological disease states, often interconnected by multiple molecular pathways, are likely to be more susceptible to the simultaneous action of multiple drugs due to the chances of improved efficacy, decreased toxicity and a reduced risk of resistance development.^[34,35] For exactly these reasons, combination therapies have become treatment standards in several areas of disease therapy including cancer,^[36] hypertension^[37] and AIDS,^[38] as well as antimalarial therapy.^[34] Indeed, artemisinin-based combination therapies

(ACTs) were introduced in the mid-1990's and became recommended at the first-line treatment for all cases of *P. falciparum* malaria infection by the WHO in 2005.^[31]

Whilst ACTs have remained the gold standard of care for over a decade for the treatment of non-complicated malaria infection, some highly effective non-artemisinin based combination therapies have also been developed and successfully administered.^[29,39] The combination of atovaquone-proguanil, brand name: Malarone (**Chapter 1, Section 1.3.2.3**, refer to **Figure 1.8**), is a good example of a successful combination therapy that has been used primarily for the treatment and prevention of malaria infection in non-immune travellers; wider administration of this combination has been limited due to the high cost of the treatment regimen and the requirement for daily dosage.^[29,39]

Until recently, a combination of sulfadoxine-pyrimethamine (**Chapter 1, Section 1.3.2.3, Figure 1.8**) was also used as a chemoprotectant against malaria. This combination was used to prevent infection in some of the most vulnerable groups, predominantly expectant mothers and young children, in areas with an absence of intense malaria transmission which often means that partial immunity against the disease doesn't develop within a population.^[39] It is therefore evident that combination therapies have already played a vital role in malarial treatment and prevention strategies and should continue to be used and developed as the fight against *Plasmodium* parasite resistance intensifies.

Interactions between known chemotherapeutics or potential chemical agents, investigated using isobologram competition experiments, can provide essential insight and knowledge into the combined effects of two chemical agents on a disease phenotype.^[30] When two or more drugs are given in combination, there are three potential outcomes of the resulting drug-drug interactions: these are the effect of synergy, antagonism or simply an additive effect.^[30,40]

If two or more drugs behave with synergy when given in combination, they may demonstrate activity or produce a phenotypic effect that is greater than expected from the individual potencies and efficacies of the component drugs when administered alone. In contrast, some drug combinations show simple additivity where the combined effect of the drugs is simply consistent with the individual drug potencies. The term additivity does not mean an addition of magnitudes but rather provides a basis for assessing the extent of synergy or antagonism observed and is derived from a more basic concept of dose equivalence.^[41]

At the other end of the spectrum, an effect of antagonism represents a lesser or reduced effect produced by drugs given in combination than the simple additive effect expected from the knowledge of each component drug, and its associated potency when administered alone.^[34] An ideal scenario in this method of drug design and administration is one where a drug combination synergies the desired

therapeutic effect but exhibits a simple additive effect for any associated and undesirable side effects either of the combined treatments; this can be rationalised since all chemotherapies are likely to be associated with some adverse effects.^[41]

The most common method for the quantitative assessment of interactions between drugs is the method of isoboles.^[41] The isobologram provides a graphical method of assessing the extent of synergism or antagonism between drug combinations. The isobole approach is therefore applicable to pairs of drugs that produce overtly similar and measurable effects, i.e. two drugs of the same classification, such as two antimalarials, which are each known to induce the desired biological effect or phenotype.^[40]

An isobole is the set of doses (or concentrations) of the two distinct compounds from within the same drug classification that, when administered together produce a specific and measurable effect in the system under study. Importantly the two component drugs should be capable of producing the required biological effect when administered alone. When this is the case, the resulting isobole is displayed as a curve in a Cartesian coordinate system (**Figure 5.10**) in which the doses (or concentrations) of the two component drugs are represented on the x- and y-axes.^[42] The straight-line joining these intercepts (between the top left of the y-axis to the bottom right of the x-axis) represents the dose pairs of component drugs and is called an isobole. The isobole represents where there is no interactions between the co-administered drugs and conveys the reduction required in the dose of one drug that accompanies the presence of a specified dose of the second drug. In other words, the negative slope of the line shows that the increase in quantity of Drug A means a reduced quantity of Drug B is needed to achieved to a specified level of therapeutic effect.^[41]

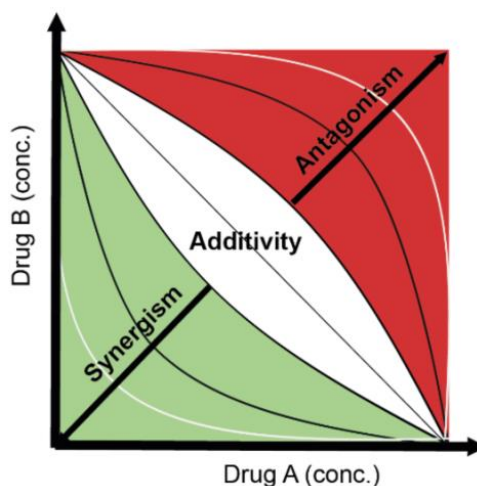
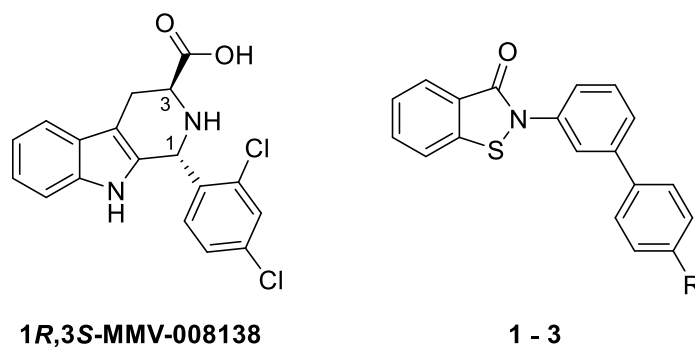


Figure 5.10 Schematic isobologram showing the Cartesian plane for a generic combination of Drug A and Drug B at a specified levels; figure reproduced from ^[43].

When the doses of Drug A and Drug B required to achieve the desired biological or phenotypic effect are less than expected, the combined effect of Drug A and Drug B is synergistic and the coordinate location within the isobologram plane is below the line of additivity, as represented by the green region of the isobologram graph (**Figure 5.10**). Conversely, when greater than expected doses of Drug A and Drug B are required to achieve the desired therapeutic effect, the combined effect of the two drugs is antagonistic. Such a result demonstrates that the administration of this particular drug combination has the effect of reducing and impeding the efficacy of the component drugs within the combination. The graphical representation of an antagonistic effect is a coordinate location above the additivity line of the isobologram plane, as represented by the red region of the graph (**Figure 5.10**).^[43]

5.3.2 1*R*,3*S*-MMV-008138-BITZ Inhibitor Combinations and Possible Outcomes

We have explored the possibility of antagonism or synergy between 1*R*,3*S*-MMV-008138 and three of the most active BITZ derived compounds (**1-3**), using a modified fixed-ratio isobole method.^[30] Structures and activities of each selected component inhibitor, when administered as a single agent are given in **Table 5.3**.



Compound	R	<i>Pf</i> lspD IC ₅₀ (μM)	Whole cell 3D7 EC ₅₀ (μM)
1R,3S-MMV-008138	-	0.017 ± 0.004	0.00035 ± 3.0 × 10 ⁻⁵
1	OCH ₃	0.21 ± 0.089	0.95 ± 0.089
2	Cl	0.073 ± 0.020	1.1 ± 0.160
3	CF ₃	0.27 ± 0.015	0.65 ± 0.021

Table 5.3 Chemical structures; *Pf*lspD enzymatic activity and whole cell 3D7 activity of 1R,3S-MMV-008138 and BITZ inhibitors **1-3**.

Two arguments were made for the possible outcomes of these studies as we sought to evaluate whether the combined use of these inhibitors, from covalent and non-covalent inhibitor classes, would be capable of producing a more enhanced antimalarial effect. Considering the two selected chemotypes and an argument for likely antagonism, it could be rationalised that one motif is likely to outcompete the other, since both the tetrahydro-β-carboline and BITZ chemotype target the same MEP pathway enzyme and are predicted to occupy the CTP binding site of *Pf*lspD. It is therefore plausible that the presence of both components may simply prevent full and effective binding with respect to each other at the *Pf*lspD active site and consequently render the presence of one compound ineffective.

Equally, an argument for synergy was also considered. Research to date^[15,17] has outlined that BITZ derived compounds and 1R,3S-MMV-008138 behave *via* different mechanisms of action to achieve inhibition of the *Pf*lspD enzyme. We have established that the BITZ chemotype operates *via* a distinctive mechanism of action that relies on formation of a covalent enzyme-inhibitor adduct between the sulfur atom of the BITZ core and the *Pf*lspD Cys-202 residue. Formation of this disulfide bridge subsequently occludes the active site and prevents substrate binding rendering *Pf*lspD inactive.^[17]

In contrast, 1*R*,3*S*-MMV-008138 (and structural analogues) work *via* a mechanism of non-covalent inhibition, behaving competitively with the CTP enzyme substrate at *PflspD*.^[15] Since both chemical motifs induce inhibition of the *PflspD* enzyme by distinct mechanisms, it is reasonable that these two chemotypes may work simultaneously, and synergistically, *via* these contrasting mechanisms of action to produce enhanced inhibition of *PflspD*. Furthermore, it is known that the *PflspD* enzyme exists as a c_2 -symmetric homodimer in the whole cell;^[13] it is therefore plausible that the binding of one inhibitor chemotype may facilitate enhanced binding of the second to its own unique binding region as a result of induced conformational changes in the *PflspD* enzyme, a consequence of protein-ligand interactions with one component inhibitor motif.

Such an effect would be consistent with a model of allosteric modulation where one chemotype is able to affect the potency and binding of the other component drug. However, such an effect may be considered unlikely within this research scenario since neither the tetrahydro- β -carboline or BITZ chemotypes are allosteric modulators of *PflspD*; with both known to bind at the CTP binding site of the *PflspD* enzyme.^[15,17]

5.3.3 1*R*,3*S*-MMV-008138 and BITZ Inhibitors have Antagonistic Anti-Parasitic Activity

Parasite growth was assayed after co-treatment with a variety of 1*R*,3*S*-MMV008138 and BITZ inhibitor concentrations. Pairs of concentrations (e.g. [1*R*,3*S*-MMV008138] vs. [**1**] **Figure 5.11**) at which 50% growth inhibition (EC_{50}) was observed were plotted to indicate the resulting antiparasitic activity of the specified chemotype combinations. The isoboles generated from these competition experiments, using a modified fixed-ratio isobole method as demonstrated previously by others,^[15,30] indicate that the anti-parasitic action of 1*R*,3*S*-MMV-008138 in combination with various BITZ inhibitors (**1-3**) is antagonistic.

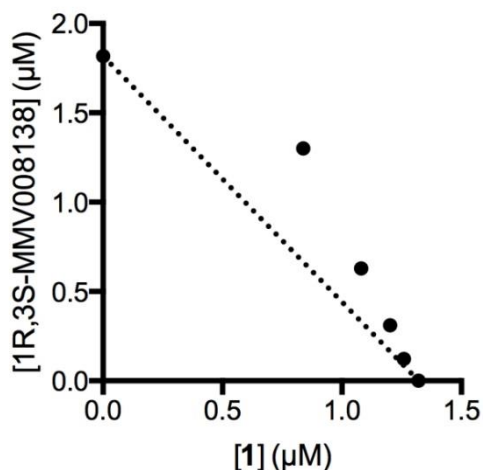


Figure 5.11 Combined antiparasitic effects of 1*R*,3*S*-MMV008138 and **1**. The linear dotted line is representative of additive antiparasitic activity; the black data points are representative of measured antiparasitic effects between 1*R*,3*S*-MMV008138 and **1**; data averaged from three independent experiments and indicates antagonistic antiparasitic activity.

A result of antagonism is quickly rationalised from the three isobologram experiments (**Figures 5.11-5.13**), since the Cartesian plane for the combination of the tetrahydro- β -carboline and BITZ chemotypes lies above the line of additivity (**Figure 5.10**) and is consistent across all three 1*R*,3*S*-MMV-008138-BITZ inhibitor combinations (**Table 5.3**). The data obtained from these studies was further quantified through the calculation of sum fractional inhibitory concentrations (sum FICs) where a sum FIC value of < 0.5 reflects a measurement of synergy and a sum FIC value of > 2.0 signifies a measurement of antagonism.^[44]

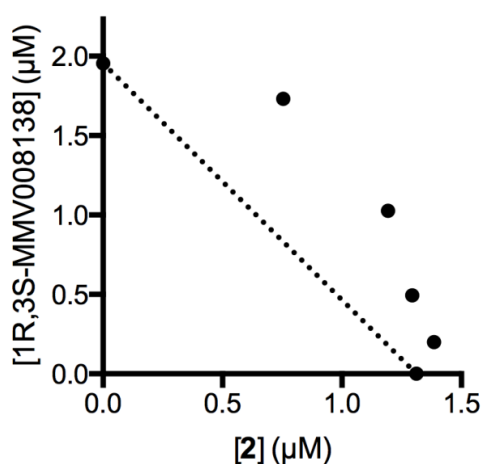


Figure 5.12 Combined antiparasitic effects of 1*R*,3*S*-MMV008138 and **2**. The linear dotted line is representative of additive antiparasitic activity; the black data points are representative of measured antiparasitic effects between 1*R*,3*S*-MMV008138 and **2**; data averaged from three independent experiments and indicates antagonistic antiparasitic activity.

We found that the sum FIC value of 1*R*,3*S*-MMV-008138 and **1** (Figure 5.11) was 1.15 ± 0.14 ; the sum FIC value of 1*R*,3*S*-MMV-008138 and **2** (Figure 5.12) was 1.32 ± 0.15 ; and the sum FIC value of 1*R*,3*S*-MMV-008138 and **3** (Figure 5.13) was 1.40 ± 0.26 . Where the data corresponding to each isobologram (Figures 5.11-5.13) is representative of $n = 3$ replicates.

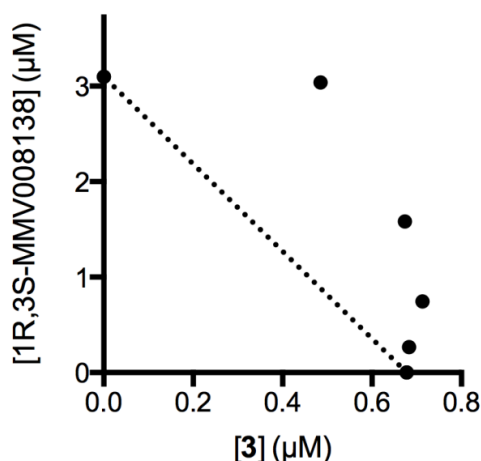


Figure 5.13 Combined antiparasitic effects of 1*R*,3*S*-MMV008138 and **3**. The linear dotted line is representative of additive antiparasitic activity; the black data points are representative of the measured antiparasitic effects between 1*R*,3*S*-MMV008138 and **3**; data averaged from three independent experiments and indicates antagonistic antiparasitic activity.

The isobolograms generated illustrate a consistent pattern of antagonism across all combinations of 1*R*,3*S*-MMV008138 with **1**, **2**, and **3** respectively (Figures 5.11-5.13); however, the calculated sum FIC values across the three combinations do not meet the specified value of > 2.0 to be categorised as significantly antagonistic.^[44] Considering the sum FIC values alone, we can therefore conclude that the interactions between the tetrahydro- β -carboline and BITZ chemotypes are at least mildly antagonistic.

Yet, it is clear graphically that the measured data points lie consistently above the line of additivity (Figures 5.11-5.13) and in no way indicate any synergy within the combinations explored. It is therefore evident that drug combinations of these chemical chemotypes is not feasible and would not produce the desired biological effect of a potent anti-parasitic activity and inhibition of *P. falciparum* growth. A drug combination with tetrahydro- β -carboline and BITZ derivatives as component drugs can be concluded as incompatible and need not be pursued further.

However, as previously discussed, a drug combination such as this may never have been feasible since neither the tetrahydro- β -carboline nor BITZ chemotype are allosteric modulators of *Pf*IspD, and both are known to act at the same binding site. Indeed, few drug combination strategies have been employed where the component drugs are known to act at a single molecular target. A rare example of such a combination was between Ritonavir and Lopinavir, generating a fixed-dose combination for

the treatment of HIV, where both component drugs are of the protease inhibitor class. Administered alone, lopinavir shows insufficient bioavailability however, a strategy of co-administration with sub-therapeutic doses of ritonavir (an inhibitor of cytochrome P450 3A4) was enough to boost the pharmacokinetic parameters of the resulting combination providing an effective therapy.^[45] However, this unique example aside, the isobologram experiments conducted and the resulting data obtained, provides further evidence that both the tetrahydro- β -carboline and BITZ chemical chemotypes target the *Pf*lspD MEP pathway enzyme.

5.3.4 1*R*,3*S*-MMV-008138 and FSM have Additive Anti-Parasitic Activity

In contrast to the effects of antagonism demonstrated between 1*R*,3*S*-MMV-008138 and BITZ inhibitors **1-3** (Table 5.3), similar studies evaluating the combination of 1*R*,3*S*-MMV-008138 and FSM demonstrate a different result. In work carried out by Imlay *et al.*, a modified fixed-ratio isobole^[30] was used to measure the extent of synergy or antagonism between 1*R*,3*S*-MMV-008138 and the potent IspC inhibitor, FSM.^[15] The isobole generated from these studies (Figure 5.14) indicates that the anti-parasitic action of 1*R*,3*S*-MMV-008138 and FSM is additive, not synergistic, since the resulting isobole is linear. In other words, no substantial interaction occurs between 1*R*,3*S*-MMV-008138 and FSM and as such, no enhancement of anti-parasitic activity is observed when these chemical entities are combined, compared to the potency of 1*R*,3*S*-MMV-008138 and FSM when administered alone.^[15]

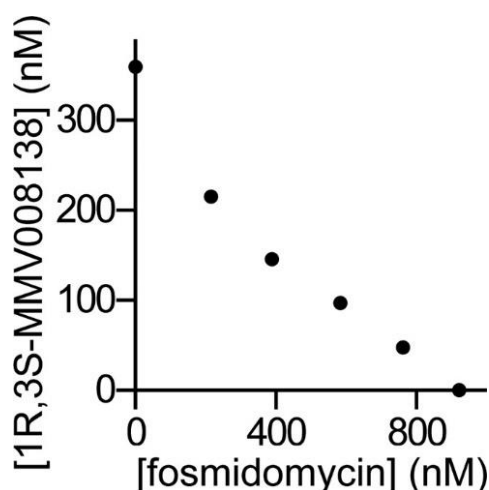


Figure 5.14 A linear isobole indicating that the anti-parasitic effects of 1*R*,3*S*-MMV-008138 and FSM are additive; data points represent averages from at least three independent experiments.^[15]

Comparing the effects of combining 1*R*,3*S*-MMV-008138 with both BITZ derived compounds and FSM, a noteworthy observation is that an antagonistic effect is seen when two components are combined which act against the same molecular target (here the *Pf*lspD enzyme). In contrast, combining two components which act against different molecular targets within the same biological pathway (i.e.

PflspC and *PflspD* with the combination of FSM and 1*R*,3*S*-MMV-008138 respectively) produces an additive anti-parasitic effect. The possible inference is therefore that combining two chemical components which display an antimalarial phenotype but which act against distinct targets in discrete biological pathway, may produce a synergistic antiparasitic effect.

5.4 Development of SAR Around the Tetrahydro- β -carboline Chemotype

5.4.1 Preliminary SAR Around the Tetrahydro- β -carboline Chemotype

Having concluded that the BITZ and tetrahydro- β -carboline chemotypes need to be considered as distinct chemical entities for their continued development as inhibitors of the *PflspD* enzyme, SAR development around the tetrahydro- β -carboline chemotype was next considered. Organic synthesis was used to facilitate structural modifications to the tetrahydro- β -carboline chemotype in order to develop SAR around the chemical motif and determine whether enhanced phenotypic activity could be achieved through structural refinement and modification of the chemotype, aiming to promote improved binding and potency at the *PflspD* enzyme. Key objectives were to enhance the enzymatic and whole cell efficacy of the 1*R*,3*S* MMV-008138 isomer as well as improve the metabolic profile of this current lead inhibitor.

It was established from our molecular modelling studies that 1*R*,3*S*-MMV-008138 isomer binds tightly within the *PflspD* enzyme active site (**Section 5.2**; **Figure 5.8** is representative) therefore highlighting that only small structural refinements to the chemotype may be tolerated. Indeed, significant alteration to chemical features and misplaced steric bulk may prevent resulting MMV-008138 derivatives efficiently accessing and inhibiting the *PflspD* active site. The preliminary SAR map (**Figure 5.15**) depicts the SAR requirements that were known at this time, and the subsequent questions and regions of molecular development that were to be explored through chemical modifications to 1*R*,3*S*-MMV-008138 and the tetrahydro- β -carboline structural framework.

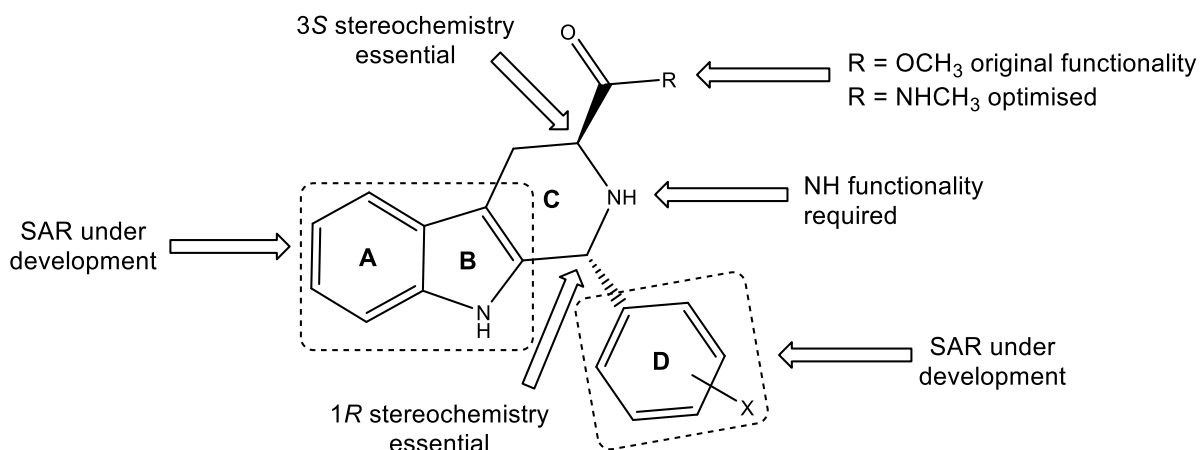


Figure 5.15 Preliminary SAR map of the tetrahydro- β -carboline chemotype.

As previously discussed (**Section 5.1.2, Table 5.2**) the requirement for $1R,3S$ stereochemistry across the C ring of the tetrahydro- β -carboline chemotype (**Figure 5.15**) has been shown by others to be essential for inhibitory activity against the *Pf*lspD target enzyme and parasite growth.^[9]

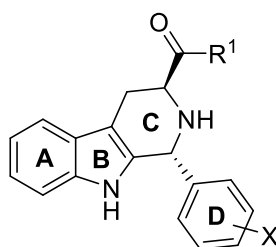
5.4.1.1 Modifications to the R Group at C-3

Work by Yao *et al.* evaluating the phenotypic activity of MMV-008138 compound analogues against parasite growth, using the *P. falciparum* Dd2 parasite strain, has highlighted some key structural requirements and constraints relating to the R functionality of the carboxylate group at the C-3 position of the C ring. Of note, the *P. falciparum* Dd2 parasite strain is both pyrimethamine-resistant and mefloquine-resistant, and shows intermediate resistance to chloroquine.^[46] To determine the precise influence of modifications in the C-3 substituent, Yao *et al.* made a number of R group variations, keeping all other structural features of the $1R,3S$ MMV-008138 isomer constant, including 2',4'-dichloro substitution in the D ring (**Table 5.4**).^[46]

The presence of a carboxylic acid group is often considered a liability in drug development; therefore, this functionality at C-3 was selected for modification. The carboxylic acid functionality can be an important contributor to a pharmacophore and is indeed present in a large number of drugs that have been successfully marketed world-wide, including nonsteroidal anti-inflammatory drugs (NSAIDs) and antibiotics as key examples. However, the presence of this functionality commonly leads to compound liabilities and idiosyncrasies with respect to drug bioactivation.^[5,47,48] Acidic compounds and groups tend to be associated with poor permeability as they cannot readily cross negatively charged lipid membranes, due to their frequent existence in a deprotonated state at physiological pH.^[47,49] In addition, acid-containing compounds often display high levels of protein binding in a cell^[50] and are particularly susceptible to glucuronide-adduct formation, mediated by glucuronidation in Phase II

metabolism;^[51,52] glucuronidation is a second-pass metabolic pathway that can generate undesirable side effects.^[47]

Since carboxylic acid groups can compromise the metabolism profile of drugs, Yao *et al.* replaced this functionality to promote metabolic stability and increase compound half-life ($t_{1/2}$), whilst aiming to retain activity against *P. falciparum* growth. Replacing the C-3 carboxylic acid of 1*R*,3*S*-MMV-008138 with a methyl ester, producing **5**, was found only to achieve weak inhibition of parasite growth (**Table 5.4**). A methyl ester functionality therefore does not mirror the binding capacity of the carboxylic acid, although Yao *et al.* concluded that **5** might serve well as prodrug. This result was supported by further work examining a number of other ester functionalities at the C-3 position; all of which were found to be inactive.^[46]



4 - 6

Compound number	R ¹	X	<i>P. falciparum</i> Dd2 strain IC ₅₀ (nM)
4	OH	2',4'-Cl ₂	250 ± 70
5	OCH ₃	2',4'-Cl ₂	6800 ± 1400
6	NHCH ₃	2',4'-Cl ₂	190 ± 30

Table 5.4 Phenotypic whole cell activity of compounds **4-6** against *P. falciparum* strain Dd2, demonstrating the effect of 3-C substitution on *P. falciparum* growth inhibition; data collected and reported by Yao *et al.*^[46]

In contrast, the methylamide derivative **6** was shown to be slightly more potent against *P. falciparum* Dd2 growth than **4**, consequently highlighting that small functional group modifications at the C-3 (R) position are tolerated.^[46] As a result, compound **6** was re-synthesised in our lab and tested using the *PflspD* enzymatic assay (**Chapter 2, Section 2.2.3**) to determine its activity against the *PflspD* target enzyme and provide a direct comparison to **4** (1*R*,3*S*-MMV-008138), which has also been re-synthesised in our lab (**Table 5.5**).

Compound number	R ¹	X	<i>Pf</i> lspD IC ₅₀ (nM)	Whole cell 3D7 EC ₅₀ (nM)
4	OCH ₃	2',4'-Cl ₂	25.3 ± 5.6	349 ± 30
6	NHCH ₃	2',4'-Cl ₂	21.6 ± 2.7	373 ± 85.5

Table 5.5 Inhibitory activity of **4** and **6** against the *Pf*lspD enzyme and *P. falciparum* growth in culture: 3D7 parasite strain. Mean data and SEM given, representative of $\geq n = 3$.

Encouragingly, our results are highly comparable to those outlined by Yao *et al.* as **6** was shown to be a potent inhibitor of the *Pf*lspD enzyme, demonstrating slightly increased potency against the target, compared with **4**. This was also mirrored by highly comparable activity of **4** and **6** against *P. falciparum* growth with EC₅₀ values in the mid-nanomolar region for both analogues (**Table 5.5**). Whilst a slight decrease in phenotypic activity was observed in our study, compared to the work by Yao *et al.*, this can perhaps be rationalised given that two different strains of *P. falciparum* parasite culture were used in the phenotypic whole cell assays conducted by the two groups.

The outcome of this follow-up study gave us confidence to adopt this R group modification, exchanging the carboxylic acid functionality at C-3 position (represented by **4**) for the methyl amide (represented by **6**): this adaptation was implemented and applied to the synthesis of all 1*R*,3*S*-MMV-008138 derivatives from this point. An additional benefit to the inclusion of the methyl amide functionality was a notable improvement in the synthetic methodology required to generate the resulting target compounds. Since carboxylic acid-containing derivatives of **4** required ester hydrolysis to generate target compounds, which was found to be problematic,^[53] the synthesis, purification and crystallisation of alternative methyl amide derivatives of **6** was notably more straightforward, since no hydrolysis step was required.

The ability to more easily crystallise target analogues is also a significant advantage as it facilitates the use of crystallography. Such studies not only informs knowledge of inhibitor-protein interactions, supporting mechanism of action evaluations, but also, in the case of MMV-008138 derivatives, enables the absolute stereochemistry of synthetic analogues to be determined. Since accurate isolation and characterisation of the required 1*R*,3*S* isomers is essential with this chemotype, the ability to crystallise target compounds for this purpose is a notable advantage.

Considering further evaluation of the R group, Yao *et al.* explored alternative amide functionalities to a methyl group at the R position of the MMV-008138 motif (**Figure 5.15**). These additional studies, featuring amides with larger alkyl groups such as *i*Pr and Bu, found the resulting compounds to be less potent than the methyl amide derivative **6**.^[46] It can therefore be rationalised that a narrow SAR around the R¹ group and C-3 substituent (**Figure 5.15**) reflects the nature of a very tight COOH binding

pocket in the *Pf*lspD active site, as previously highlighted by molecular modelling studies (**Figure 5.8**). Consequently, this may explain why groups larger than a methyl amide (**6**) are not tolerated. As a result, further modifications to R¹ were not explored further in our own SAR studies.

5.4.1.2 Modifications to the D Ring

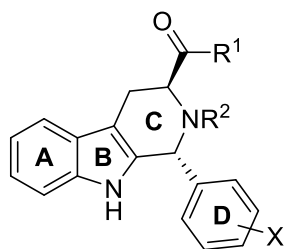
To establish more structural determinants of the *P. falciparum* inhibitory growth activity of **4**, Yao *et al.* generated a number of compounds to explore the effect of varying D ring substituents.^[46] The majority of compounds generated involving D ring substitutions which were found to be inactive phenotypically. The only example of 3',4'-disubstitution explored in the D ring did not inhibit parasite growth with a resulting IC₅₀ value > 20 μM; cases of mono-chloro substitution, at the 2'- and 4'-positions, demonstrated poor activity against the whole cell with inhibitory activity in the single digit micromolar region. An entirely un-substituted D ring was also shown to produce an inactive derivative with an IC₅₀ value of > 10 μM against parasite growth.^[46]

These results demonstrate that the steric requirements for D ring substituents are also very restricted since the majority of modifications resulted in compounds that were incapable of inhibiting *P. falciparum* parasite growth.^[46] This mirrors our expectations, established as a result of docking studies of 1*R*,3*S*-MMV-008138 in the *Pf*lspD homology model. Molecular modelling highlighted that 1*R*,3*S*-MMV-008138 occupies a tight binding pocket within the *Pf*lspD active site (**Figure 5.8**), indicating that only small structural refinements are likely to be possible around particular regions of the tetrahydro-β-carboline chemotype. Indeed, the structural explorations made by Yao *et al.* seem to confirm that substitution at the 2'- and 4'-positions of the D ring complement the shape of the rather tight *Pf*lspD binding pocket which 1*R*,3*S*-MMV-008138 is shown to occupy (**Figure 5.8**).^[15,46] In addition, Yao *et al.* have suggested that the presence of a 2'-substituent may induce constraints on the D ring, causing it to lie perpendicular to the C ring which may promote compound binding and shape fit within the *Pf*lspD active site.^[46]

5.4.1.3 Modifications to the 2° Amine in the C Ring

Early synthetic explorations within our group have revealed that the 2° amine functionality in the C ring of the tetrahydro-β-carboline core cannot be converted into a 3° amine if *Pf*lspD and parasite growth inhibition are to be maintained. Structural modifications to the 2° amine, replacing the NH functionality with larger R² groups, **7** and **8** respectively, highlight that additional steric bulk at this position is not tolerated since both **7** and **8** demonstrate a loss of activity against the *Pf*lspD enzyme and 3D7 parasite growth. Indeed, this small study indicates that increasing steric bulk at the C ring 2°

amine correlates with an increasing loss of inhibitory activity against both the *Pf*lspD enzyme and *Plasmodium* parasite growth.



7 - 8

Compound number	R ¹	R ²	X	<i>Pf</i> lspD IC ₅₀ (μM)	Whole cell 3D7 EC ₅₀ (μM)
7	NHCH ₃	CH ₃	2',4'-Cl ₂	> 2	8.07 ± 0.115
8	OH	Bn	2'-Cl,4'-CF ₃	> 25	8.36 ± 0.439

Table 5.6 Enzymatic and phenotypic activity of **7** and **8** against the *Pf*lspD enzyme and 3D7 *P. falciparum* growth in culture.

5.5 Further Modifications to the D Ring

5.5.1 Design Rationale and Synthesis

Since D ring modifications explored by Yao *et al.* focused mainly on variations around a di-substituted D ring motif, examination of tri-substituted functionalisation within the D ring was now considered. Molecular modelling suggests that the D ring and its alignment within the *Pf*lspD binding site (**Figure 5.8**) is less spatially restricted in the protein pocket that it occupies compared to the very tight binding pocket occupied by the C-3 group. Consequently, there may be potential for further exploitation and structural development within the D ring as small additional substituents may be tolerated. Yao *et al.* highlighted that steric requirements at this site are very specific and that therefore, any modifications must be subtle and not introduce significant steric bulk which may hinder compound binding.

Consequently, it was decided to introduce an additional substituent at the 6-position of the D ring, generating a 2',4',6'-trisubstitution pattern (**Figure 5.16**), which was also mirrored by a parallel study in our group considering 1',2',5'-trisubstitution at the D ring using the same chemical functionalisation. In the two parallel studies, di-chloro substitution at the 2'- and 4'- D ring positions was maintained, along with the methyl amide functionality at C-3, simply varying the substituent at the 6'- (and comparably 5'-) position of the D ring. Work conducted by others, as well as in our group,^[21,46,54] indicates that the presence of polar functionalities in the D ring tend to assist and promote the inhibitory activity of resulting analogues against the *Pf*lspD enzyme and *Plasmodium*

parasite growth. As a result, a small range of polar substituents were selected to functionalise the 6'-position of the D ring (**Figure 5.16**).

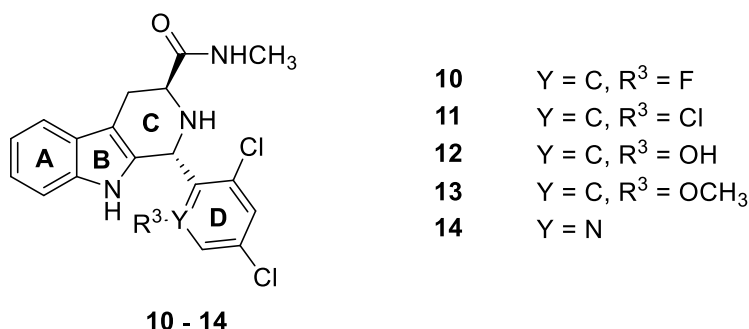


Figure 5.16 Chemical structure and substitution pattern of 1*R*,3*S*-MMV-008138 derivatives **10-14**.

Considering the reasonably tight binding site occupied by the D ring (**Figure 5.8**), it is clear that only the introduction of relatively small groups was likely to be tolerated. However, this subtle functionalisation had the potential to facilitate and capture additional hydrogen bonding interactions around the aromatic phenyl ring that could push compound activity into the single digit nanomolar region.

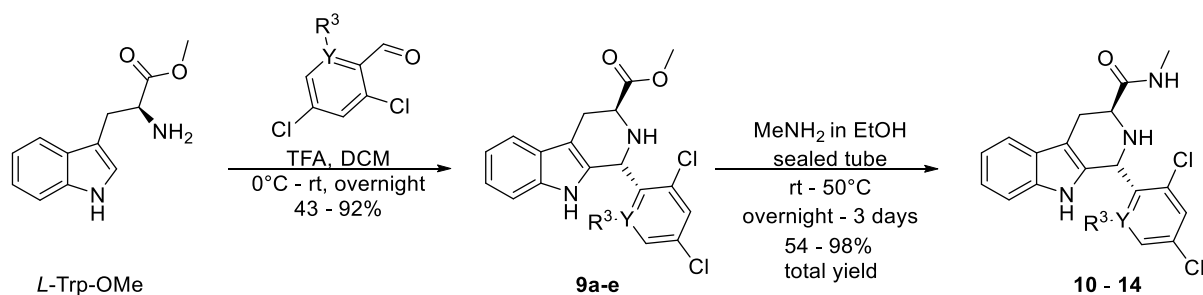
With this in mind 6'-fluoro substitution (**10**) was first considered since fluorine is a good isostere of hydrogen^[55], most notably due to its small size, making it more likely to be tolerated within the tight *Pf*lspD binding pocket. The presence of fluorine may facilitate additional hydrophobic and hydrogen bond acceptor contacts between compound **10** and the *Pf*lspD protein, potentially increasing the strength of compound binding, as was the rationale with this inhibitor series. In addition, the deployment of fluorine can also be used to improve compound stability through its ability to modulate metabolic processes. The high strength of the C-F bond and the powerful electron withdrawing properties of fluorine make the C-F bond almost inert under most biological conditions and can therefore slow down metabolism at the site at which it is introduced.^[55]

Introduction of chlorine at the 6'-position was also considered due to its analogous hydrogen bonding capacity as a halogen. Compound **11** therefore also has the potential to promote the strength of compound binding at *Pf*lspD through additional hydrogen bonding interactions with active site protein residues. However, the increased atomic size of chlorine, compared to fluorine, could hinder efficient binding of the resulting analogue due to the limited space of the *Pf*lspD binding pocket. This substitution therefore enables the tolerance to steric bulk at the 6'-position to be determined. In direct contrast to the hydrogen bond accepting capabilities of halogens, synthesis of the 6'-hydroxy derivative **12** allowed the effects of a hydrogen bond donating group at the same position to be assessed.

Compound **13** involved introduction of a methoxy group at the 6'-position of the D ring allowing further assessment of the tolerance to steric bulk at this position. In addition, **13** also evaluates the ability of the methoxy group to lock the conformation of the D ring with respect to the tetrahydro- β -carboline motif. It is plausible that hydrogen bonding between a methoxy group at the 6' position and the indole nitrogen of the tetrahydro- β -carboline motif could lock the conformation of the molecule, preventing rotation or ring flipping of the D ring within the *PflspD* active site. Such an effect may exert influence on the binding affinity of **13** and the resulting inhibitory activity of the compound. In addition, evaluation of 1*R*,3*S*-MMV-008138 docking poses at *PflspD* (**Figure 5.8**) suggests that the presence of a 6'-methoxy group could facilitate additional hydrogen bond contacts to the Arg-208 *PflspD* protein residue, increasing the number of non-covalent protein-inhibitor interactions in the binding pocket and promoting the strength of compound binding.

In contrast to the previously described analogues (**10-13**), the final compound of this series, **14**, differs slightly in that the carbon atom at the 6'-position of the D ring is replaced with a nitrogen atom, generating a pyridinyl analogue of the 1*R*,3*S*-MMV-008138 compound. Nitrogen atoms are spatially smaller than fluorine, therefore occupying a smaller area of space and contributing a reduced amount of steric bulk. Consequently, compound **14** has the potential to demonstrate an improved spatial and steric fit at the *PflspD* binding site compared to analogues **10-13**. Moreover, the introduction of a nitrogen atom into the aromatic D ring removes outward projections from the ring at the 6'-position, compared to the functionalization of **10-13**, further reducing steric clashes with the active site protein residues. An additional benefit to a pyridinyl D ring is the hydrogen bonding capacity of nitrogen, due to its available lone pair, providing a hydrogen bond acceptor site in the compound. Finally, the polarity of nitrogen also promotes compound solubility and reduces lipophilicity, as highlighted by the order of magnitude drop in calculated *LogD* compared to other series analogues (**Table 5.7**), therefore enhancing the pharmacokinetic profile of compound **14**.

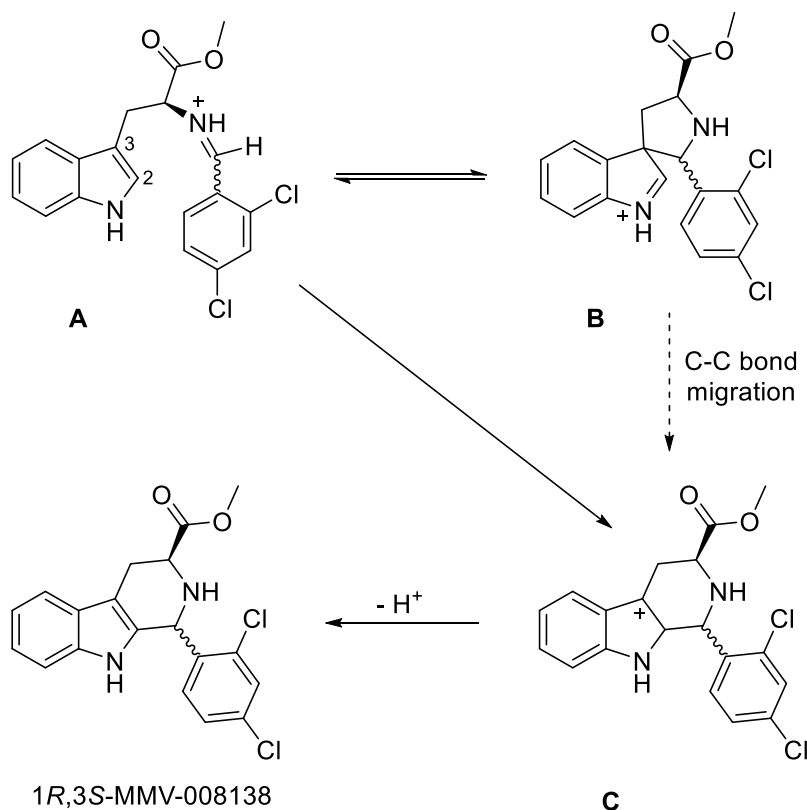
Generation of analogues **10-14** was achieved using a two-step synthesis for each compound (**Scheme 5.2**). The first step of the synthesis involved a Pictet-Spengler reaction^[56,57] between various tri-substituted benzaldehydes, the component providing D-ring functionalisation, and the *L*-isomer of tryptophan methyl ester (*L*-Trp-OMe) which was purchased as the corresponding hydrochloride salt and neutralised before use in the synthesis. The second and final synthetic step involved conversion of the C-3 methyl ester into the corresponding methyl amide, previously discussed in **Section 5.4.1.1**, *via* a substitution reaction with methyl amine (**Scheme 5.2**).



Scheme 5.2 Synthetic strategy for the generation of 1*R*,3*S*-MMV-008138 derivatives **10-14**.

The Pictet-Spengler reaction is an acid-catalysed transformation used to generate the tetrahydro- β -carboline chemotype from carbonyl compounds, here aromatic benzaldehydes, and tryptamine derivatives.^[58] When the carbonyl components used within this procedure are aldehydes, but not formaldehyde, the reaction is asymmetric. Reviews of the asymmetric methodology have suggested that tryptophan esters are more reactive in the Pictet-Spengler reaction than tryptophan derivatives,^[59] providing sufficient justification for the use of *L*-Trp-OMe (**Scheme 5.2**) as the tryptophan reagent in our syntheses.

The Pictet-Spengler reaction is characterised by formation of an iminium ion, mediated by an acid-catalysed reaction between the selected tryptamine and carbonyl components. Intramolecular attack of the resulting iminium ion **A** (**Scheme 5.3**) by electrons from within the pyrrole ring causes ring closure and generation of the specified tetrahydro- β -carboline derivative.^[60] There has been much debate regarding the mechanism by which ring closure occurs in the Pictet-Spengler reaction since ring closure is facilitated by attack of electrons from the pyrrole ring onto the sp^2 carbon atom of iminium ion **A**. It is therefore plausible that attack could occur from either the 2- or 3- position of pyrrole, assisted by the lone pair of the 2° amine ring nitrogen, facilitating generation of intermediates: **B** or **C** (**Scheme 5.3**).^[60,61]



Scheme 5.3 Possible ring closure mechanisms of the Pictet-Spengler reaction generating the tetrahydro-β-carboline chemotype; representative example provided using 1R,3S-MMV-008138.^[60]

Generation of *spiro*-indolenine intermediate **B** is suggested to occur following attack of pyrrole from the 3'-position onto the sp² carbon of intermediate **A** and has been proven to exist by isotopic labelling experiments conducted by Bailey *et al.*^[61] Intermediate **B** is able to rearrange *via* C-C bond migration to intermediate **C**, the tetrahydro-β-carboline structure, which can also form directly as a result of attack of pyrrole from the 2'-position onto the sp² carbon of intermediate **A** (**Scheme 5.3**). However, research by others has indicated that rearrangement of **B** to **C** is energetically unfavourable and that direct attack of pyrrole from the 2'-position (**Scheme 5.3**) is more likely to represent the mechanistic rearrangement, generating intermediate **C** directly in the Pictet-Spengler condensation.^[60,62]

Since it is sometimes the case that only one enantiomer of a chiral compound has the ability to produce a desired biological effect, when applied as a therapeutic agent, the development of an enantioselective Pictet-Spengler synthesis has long been of interest within synthetic and medicinal chemistry.^[60] A number of approaches aiming to develop enantioselective methodologies have used enantiopure tryptophan esters^[63] which we mirrored in our synthetic approach by selecting the enantiomerically pure *L*-Trp-OMe as our tryptophan starting reagent (**Scheme 5.2**). However, this does not make the Pictet-Spengler synthesis enantioselective as a mixture of the *cis*- (1*S*,3*S*) and *trans*- (1*R*,3*S*) diastereoisomers are still produced. In other words, the stereoselectivity of the method comes

from selecting the major (or required) diastereoisomer in the starting material (*L*-Trp-OMe). Formation of the *cis*-isomer tends to predominate in the asymmetric Pictet-Spengler reaction, which is slightly problematic for our work since it has already been established that the *1R,3S* (*trans*) isomer of tetrahydro- β -carboline derivatives is exclusively required to achieve inhibitory activity against *PflspD* and *Plasmodium* parasite growth.^[9,15]

Nonetheless, we found that isolation of the *cis*- and *trans*- isomers generated within the Pictet-Spengler reaction can be achieved with relative ease using flash column chromatography. The ease of separation and indeed the stereoselectivity of each synthesis seems to be dependent on the functionalisation and substitution pattern of the specific reagents used. Both synthetic yield and stereoselectivity were seen to vary considerably using different benzaldehydes to generate analogues **10-14**. However, we have found it possible to separate the resulting mixture of diastereoisomers following either step of the reaction scheme (**Scheme 5.2**). It was therefore possible to select the optimal point of isolation for the required *trans* isomer, as determined by the extent of polar separation between the *cis* and *trans* isomers when present as either the methyl ester intermediates **9a-e** or methyl amide target compounds **10-14** (**Scheme 5.2**).

Adding further complication to the isolation and characterisation of these chiral target compounds, varying the benzaldehyde component (**Scheme 5.2**) not only altered synthetic yields and stereoselectivity, but also affected the polarity of the resulting *cis* and *trans* isomers with respect to each other. It was therefore impossible to tell by polarity (monitored by tlc) whether an isolated isomer corresponded to either the *cis* or the *trans* product in each synthesis. As a result, both isomers of each analogue require isolation and characterisation to determine the identity and stereochemistry of each material.

NOE spectroscopy (NOESY) NMR experiments were employed to determine the stereochemistry of the various materials isolated. NOESY is a homonuclear (¹H) 2D technique that detects “through-space” coupling between atoms of the same nuclei, here ¹H atoms, and can therefore be used as a method of structural elucidation. In this instance, NOESY was used to detect interactions between the hydrogen atoms at the C-1 and C-3 positions of the tetrahydro- β -carboline motif (**Figure 5.15**) in order to determine the stereochemistry of the isolated isomer.^[64] The rationale was such that, in the case of the *cis* (*1S,3S*) isomer, the hydrogen atoms at the C-1 and C-3 positions would occupy the same face of the tetrahydro- β -carboline molecule (**Figure 5.17**) and therefore be able to “see each other” and interact “through-space”, producing a correlating signal in the 2D NOE spectrum.

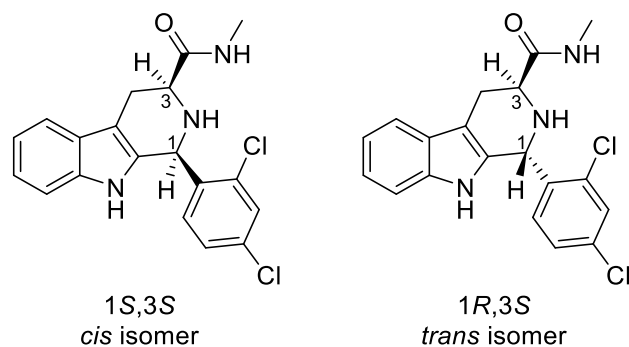


Figure 5.17 Absolute stereochemistry of the *cis* and *trans* isomers of the MMV-008138 compound.

Conversely, in the case of the *trans* (1*R*,3*S*) isomer, the hydrogen atoms at the C-1 and C-3 positions occupy opposite faces of the tetrahydro- β -carboline motif (**Figure 5.17**) and so would not be able to interact *via* “through-space” coupling due to increased obstruction and separation between the two atoms preventing their interaction. Therefore, the absence of an interaction between the C-1 and C-3 hydrogens in the 2D NOE spectra represents a positive result, indicating isolation of the *trans* (1*R*,3*S*) isomer.

In this study, 2D NOE spectroscopy represents an acceptable form of analysis for the initial characterisation of compound stereochemistry since work with *L*-Trp-OMe (**Scheme 5.2**) within our group, as well as studies conducted by others,^[65] suggests that this material is not prone to racemisation. We were therefore confident that the undesirable scenario of generating the four MMV-008138 diastereoisomers (**Figure 5.2**) from the Pictet-Spengler reaction was a low risk outcome. Rather, we were only likely to generate the 1*S*,3*S* and 1*R*,3*S* isomers (**Figure 5.17**) if *L*-Trp-OMe remained stable to racemisation, as it is believed to. So far, we have found this to be the case. However, as research with this chemotype progresses, further structural and stereochemical elucidation, by means of both crystallography and chiral HPLC, should be undertaken to more definitively confirm the absolute stereochemistry of 1*R*,3*S*-MMV-008138 derived compounds.

5.5.2 Enzymatic *Pf*lspD and Whole Cell Activity Data

Following the described synthesis of MMV-008138 derivatives **10-14** (**Scheme 5.2**) and the successful isolation and characterisation of each required *trans* (1*R*,3*S*) isomer; all target compounds were tested in the *Pf*lspD enzymatic assay (**Chapter 2, Section 2.2.3**) and *P. falciparum* whole cell growth assay (**Chapter 2, Section 2.3.5**) to determine the extent of their inhibitory activity against the *Pf*lspD enzyme and *P. falciparum* parasite growth. The resulting data is given below in **Table 5.7**.

Compound number	Y	R ³	<i>PflspD</i> IC ₅₀ (μM)	Whole cell 3D7 EC ₅₀ (μM)	MW (g mol ⁻¹)	<i>ClogD</i>	<i>CaqSol</i>
10	C	F	2.22	1.00	391.07	3.86	13.64
11	C	Cl	> 5	-	407.04	3.96	5.98
12	C	OH	> 5	-	389.07	3.64	17.90
13	C	OCH ₃	> 5	-	403.09	3.76	13.99
14	N	-	> 2	2.68	374.07	2.82	77.11

Table 5.7 Inhibitory activity of compounds **10-14** against the *PflspD* enzyme and *P. falciparum* growth in culture (strain 3D7); MW of compounds and calculated *ClogD* and *CaqSol* values given.

Unfortunately, evaluation of compounds **10-14** in the *PflspD* enzyme assay highlights that 2',4',6'-trisubstitution in the D ring of the MMV-008138 chemotype is not tolerated (**Table 5.7**). In comparison to the initial 1*R*,3*S*-MMV-008138 hit **4** (**Table 5.5**), consistent loss of activity (greater than 150 fold) against the *PflspD* enzyme is observed across the of MMV-008138 derivatives **10-14**.

These results further reflect the tight *PflspD* binding pocket that is occupied by 1*R*,3*S*-MMV-008138 derived compounds, again demonstrating that there is very little tolerance to structural variation and steric bulk around the tetrahydro-β-carboline motif, therefore supporting the results demonstrated by Yao *et al.*^[46] For compounds **11-13**, whole cell data, determining inhibitory activity against *P. falciparum* parasite growth, was not obtained since the measured activities of these compounds against the *PflspD* enzyme fell outside the specified activity threshold of < 5 μM (**Chapter 2, Section 2.3.5**) and therefore are not classified as active against the target enzyme. Interesting, these results show that **10** is the most tolerated analogue in the series, highlighting a clear advantage to reduced (or minimal) steric bulk at the 6'-position and corresponding pocket in the *PflspD* active site.

5.5.3 Further SAR Explorations

Additional work in the group, exploring further modifications to the D ring, continues to confirm that steric requirements around this group are very precise and only subtle variations are tolerated without causing a loss of inhibitory activity against *PflspD* or *Plasmodium* parasite growth. Indeed, the majority of compounds generated around the 1*R*,3*S*-MMV-008138 chemotype display suboptimal activity against the *PflspD* enzyme compared to the initial 1*R*,3*S*-MMV-008138 hit **4** (**Table 5.5**).^[53] This is seen in an analogous study within our group considering 1',2',5'-trisubstitution around the D ring, using the same chemical functionalities at the 5'-position as were introduced initially at the 6'-position (**Figure 5.16**). Disappointingly, this compound series was also inactive against *PflspD*.

Overall, the majority of modifications made on the previously unsubstituted face of the D ring (specifically the 5'- and 6'- positions) have been unsuccessful, generating compounds where inhibitory activity is completely abolished or only moderate against the *Pf*lspD enzyme and parasite growth. It can therefore be concluded that binding pocket of *Pf*lspD that is occupied by the D ring (**Figure 5.8**) is too tight to tolerate substitution at the 5'- and 6'- positions of the ring. However, in slight contrast to this assessment, compound **15** (**Figure 5.18**), the 6'-bromo variant of inhibitor **6** (**Table 5.5**), displays potent activity against the *Pf*lspD enzyme with an IC_{50} value of 160 ± 24.2 nM ($n = 3$ replicates). This is an interesting result as, whilst the 5'- and 6'-positions of the D ring remain un-substituted, bromine has a much larger atomic radius than chlorine [atomic radius of Br is 1.12 Å, compared to 0.97 Å and 0.57 Å for chlorine and fluorine respectively]^[66] therefore introducing increased steric bulk at the 4'-position compared to 4'-chloro substitution, but that is shown to be tolerated and active against *Pf*lspD.

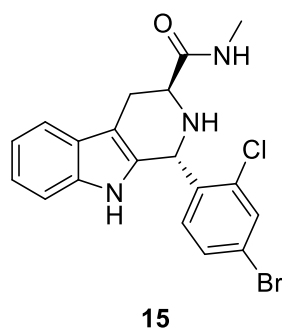


Figure 5.18 Chemical structure of compound **15**; currently the most potent tetrahydro- β -carboline-derived inhibitor against the *Pf*lspD enzyme.

In addition, not only is compound **15** more than twice as potent against *Pf*lspD than the corresponding 2',4'-dichloro analogue **6** (**Table 5.5**), but current biological analysis also suggests that **15** is capable of inhibiting *Plasmodium* parasite growth with a measured parasite EC_{50} value of 0.248 μ M. This therefore seems to suggest that MMV-008138 analogue activity is not solely an issue of sterics, at least at the *para*-position of the D ring, but that SAR around this ring could actually be determined to some extent by electronics.

5.6 Conclusions and Future Work

Having identified potential off-target reactivity with the BITZ chemotype (see **Chapter 3**) where additional off-target contributions to those against the *Pf*lspD enzyme may contribute to inhibition of *P. falciparum* parasite growth, an alternative chemical chemotype, active against *Pf*lspD, has also been explored. Robust biological data from a range of experiments confirms a proposed mechanism of *Pf*lspD enzyme inhibition by BITZ compounds as occurring *via* a covalent modification strategy (see **Chapter 4**). However, we are aware that the covalent modification of enzymes and proteins can be a risky strategy within drug design which has encouraged our consideration of an alternative chemical chemotype that inhibits the *Pf*lspD enzyme by an alternative, non-covalent mechanism of action.

As a result, our group is now involved in research focused around MMV-008138 derived compounds, based on the tetrahydro- β -carboline chemotype (**Figure 5.1**) as a potent and selective inhibitor of the *Pf*lspD enzyme. This work was initially pioneered by our collaborators (the Odom Molecular and Cellular Biology lab at Washington University in St Louis)^[15] and others.^[9,46] The MMV-008138 compound was first recognised in phenotypic screen carried out by GSK, showing it to be a potent antimalarial compound that was capable of inhibiting of *P. falciparum* growth in culture. Since its identification, extensive biological investigations have shown the MEP pathway *Pf*lspD enzyme to be the protein target of MMV-008138. Enzymatic data has also revealed that only the 1*R*,3*S*-MMV-008138 diastereoisomer of MMV-008138 is active against *Pf*lspD, giving a high degree of specificity and selectivity to this compound.

Assessment of species-selectivity and the potential antimicrobial activity spectrum of the 1*R*,3*S*-MMV-008138 isomer produced highly comparable results to those observed with the BITZ inhibitor chemotype. Indeed, the 1*R*,3*S*-MMV-008138 isomer potently inhibits *P. falciparum* and *P. vivax* homologues of the lspD enzyme but shows no inhibition against *E. coli* and *Mycobacterium tuberculosis* lspD, highlighting the species-selectivity of the MMV-008138 scaffold and its therapeutic scope as a broad-spectrum antimalarial agent. Metabolic profiling of MEP pathway metabolites in *P. falciparum* cells has demonstrated that 1*R*,3*S*-MMV-008138 is capable of inhibiting the *Plasmodium* MEP pathway at levels which affect asexual parasite growth. In addition, IPP rescue experiments have further established that the inhibition of parasite growth, shown by 1*R*,3*S*-MMV-008138, is specific to MEP pathway inhibition since the antimalarial effects of this compound are rescued by supplementation with IPP.

Since we are interested in alternative methods of *Pf*lspD inhibition to that demonstrated by the BITZ chemotype, molecular modelling studies and kinetic analysis of 1*R*,3*S*-MMV-008138 have rationalised

that the compound inhibits *Pf*lspD *via* a non-covalent mechanism of action, competing with the lspD enzyme substrate, CTP. Molecular modelling studies have also revealed that 1*R*,3*S*-MMV-008138 assumes a comparable binding alignment to that of the natural enzyme product, CDP-ME, which draws a direct comparison to the previously determined binding alignment of the BITZ chemotype (see **Chapter 4**). Therefore, it is now known that both the 1*R*,3*S*-MMV-008138 compound and BITZ derived compounds bind to the CTP binding pocket of *Pf*lspD with a degree of pose overlap. However, it is also clear that both the tetrahydro- β -carboline and BITZ chemotype occupy some distinct space within the CTP binding pocket, showing varying proximity to different protein residues in the *Pf*lspD active site.

The increasing number of comparable features between the tetrahydro- β -carboline and BITZ chemotypes prompted us to ask the question: how would these two chemical motifs behave if co-administered, and what would be the resulting effects on phenotypic activity? However, extensive competition experiments, generating isobolograms which combined 1*R*,3*S*-MMV-008138 with several distinct BITZ inhibitors, showed that these two chemical motifs behave antagonistically when co-administered and do not promote phenotypic antimalarial activity.

A number of exploratory SAR investigations have been conducted around the 1*R*,3*S*-MMV-008138 compound and tetrahydro- β -carboline chemotype. Whilst these investigations have been extensive, the measured activities of resulting compounds consistently indicate that the SAR around this compound is relatively limited, with little room for significant structural variation or additional functionality. Indeed, this notion is supported by molecular modelling studies and can be rationalised through the spatial demands of the *Pf*lspD CTP binding site in which 1*R*,3*S*-MMV-008138 adopts a binding pose that spatially, is very tight-fitting.

It was already known that the 1*R*,3*S* stereochemical relationship across the C ring is essential to observe activity against *Pf*lspD and *Plasmodium* parasite growth. It has also been shown that structural modifications to the 2° amine in the C ring are not tolerated. In addition, it is now evident that inclusion of a methyl-amide functionality, replacing the carboxylic acid group at the C-3 position of the C ring, promotes enzymatic and phenotypic activity. Most recently, SAR development have focused on modifications to the A and D rings of the 1*R*,3*S*-MMV-008138 motif, to determine if small structural variations in these regions are able to promote protein-ligand contacts within the *Pf*lspD active site and therefore promote inhibitor activity.

Considering the D ring, recent 1*R*,3*S*-MMV-008138 analogues have demonstrated that 2',4',6'-trisubstitution, varying functionalities at the 6'-position but maintaining 2',4'-dichloro substitution, is not tolerated since a loss of activity is seen against both *Pf*lspD and parasite growth. The lack of

enzymatic activity across these analogues, subsequently translating into loss of phenotypic activity, is likely due to limited free space within the *Pf*lspD binding pocket which the D ring occupies. Introducing functionalisation at the 6'-position of the D ring therefore prevents complementary binding within the *Pf*lspD active site, compromising the inhibitory capabilities of resulting analogues. A comparable effect is also observed introducing 2',4',5'-trisubstitution to the D ring of 1*R*,3*S*-MMV-008138.

From the broad SAR investigations conducted in the group, a close structural analogue of 1*R*,3*S*-MMV-008138 has been identified as one of the most potent tetrahydro- β -carboline analogues against *Pf*lspD to date. Compound **15** (Figure 5.18) has a 2'-chloro-4'-bromo substitution pattern in the D ring and a methyl-amide functionality at the C-3 position of the C ring. Compound **15** displays potent activity against the *Pf*lspD enzyme with an IC₅₀ value of 160 nM and initial whole cell data that suggests enhanced inhibitory activity against *Plasmodium* parasite growth, compared to the corresponding 2',4'-dichloro analogue **6** and the original 1*R*,3*S*-MMV-008138 hit compound (Table 5.5).

SAR development around 1*R*,3*S*-MMV-008138 and the tetrahydro- β -carboline chemotype is ongoing, with the aim of progressing towards an optimised lead structure that is suitable for clinical development as an antimalarial agent, targeting the *Pf*lspD enzyme. To assist SAR development, molecular modelling using the *Pf*lspD homology model to dock proposed 1*R*,3*S*-MMV-008138 analogues into the *Pf*lspD active site will be used to inform compound design. Further molecular modelling will therefore guide SAR development by predicting structural analogues likely to be tolerated at the *Pf*lspD active site, based on docking observations and identified binding poses. More extensive use of molecular modelling may better inform structural and chemical modifications by use of the molecular feedback loop. Indeed, docking inactive 1*R*,3*S*-MMV-008138 analogues **10-14** could be highly informative and may reveal specific structural clashes that prevent complementary binding of these compounds at the *Pf*lspD active site.

Continuing research will also focus on improving the metabolism and pharmacokinetic profiles of 1*R*,3*S*-MMV-008138 analogues to enable movement towards a fully optimised lead compound. In particular, structural modifications to the A ring of the tetrahydro- β -carboline motif, such as fluorine substitution at the 6'- and 7'-positions or alternatively, conversion of the phenyl A ring to a pyridinyl ring, will be undertaken.

5.7 Experimental

5.7.1 Computational Methods

Molecular Modelling

A homology model of *Pf*lspD was constructed using the PHYRE online homology modelling program.^[67] *Pf*lspD primary sequence Q8I273 was obtained from UNIPROT (<http://www.uniprot.org/>, accessed 10/12/2014). A number of protein alignments and homology models were constructed by PHYRE, and the model with 98.82% confidence was selected, which was based on an *E. coli* lspD structure (PDB accession code 1I52).^[68] 1I52 is a 1.50 Å resolution crystal structure of *E. coli* lspD, complexed with CDP-ME in the active site. The structure of the model was validated using the WHATIF web interface.^[69] 1*R*,3*S*-MMV008138 and selected BITZ inhibitor **1** were modelled *in silico* using the homology model described above in order to visualize the interactions between each analogue and the active site. Using GOLD, protons were added and docking was performed with default parameters, except that GoldScore was used and 50 docking poses were obtained for comparison and analysis.^[23]

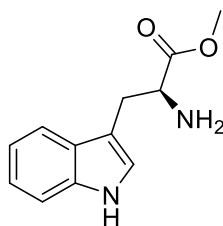
5.7.2 Biological methods

1*R*,3*S*-MMV008138 and BITZ Isobolograms

Asynchronous cultures of *P. falciparum* strain 3D7 were diluted to 0.5% parasitemia and cultured over a range of concentrations of 1*R*,3*S*-MMV008138 and/or **1**, **2** and **3** in 100 µL culture volumes. Stock solutions of **1**, **2**, **3** and 1*R*,3*S*-MMV008138 were prepared at concentrations such that the EC₅₀ values for these compounds alone would fall around the midpoint of a 10-point 2-fold dilution series. As previously described,^[30] drug response curves were then performed at **1**, **2**, **3**/1*R*,3*S*-MMV008138 ratios of 5:0, 4:1, 3:2, 2:3, 1:4, and 0:5. After 72 h, parasite growth was quantified using PicoGreen dye (Invitrogen) to measure the DNA content as previously described.^[18] EC₅₀ values were calculated, treating each **1**, **2**, **3**/1*R*,3*S*-MMV008138 combination as if it were a single unique drug, by nonlinear regression analysis using GraphPad Prism software. Following these calculations, EC₅₀ values were prorated between compounds according to **1**, **2**, **3**/1*R*,3*S*-MMV008138 ratios and plotted as an isobologram. Each data point represents the average of three independent experimental replicates.

5.7.3 Organic Synthesis

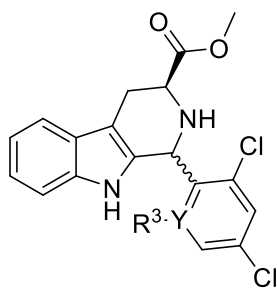
Preparation of *L*-tryptophan methyl ester



L-tryptophan methyl ester hydrochloride (3.0 g, 11.8 mmol) was stirred in 1:1 EtOAc:NaHCO₃ (150 ml), extracted into EtOAc (3 x 50 ml), washed with brine (100 ml), dried over MgSO₄ and concentrated under reduced pressure to give ***L*-tryptophan methyl ester** as an off-white crystalline solid in 90.6% yield. ¹H NMR (500 MHz, CDCl₃) δ 7.77 (d, *J* = 7.9 Hz, 1H), 7.57 (d, *J* = 8.1 Hz, 1H), 7.54 (s, 1H), 7.37 (t, *J* = 7.2 Hz, 1H), 7.29 (t, *J* = 7.5 Hz, 1H), 4.02 (t, *J* = 5.1 Hz, 1H), 3.92 (s, 3H), 3.48 (dd, *J* = 14.5, 4.7 Hz, 1H), 3.28 (dd, *J* = 14.5, 7.6 Hz, 1H). ¹³C NMR (101 MHz, CDCl₃) δ 175.4, 136.4, 127.2, 123.4, 121.8, 119.2, 118.3, 111.4, 109.6, 54.4, 52.1, 30.3; **CI+HRMS** *m/z* 219.1133 [M+H]⁺ C₁₂H₁₄N₂O₂ requires 218.11.

Preparation of methyl (*S*)-1-phenyl-2,3,4,9-tetrahydro-1*H*-pyrido[3,4-*b*]indole-3-carboxylates **9a-e**

General Procedure (1)



9a	Y = C, R ³ = F
9b	Y = C, R ³ = Cl
9c	Y = C, R ³ = OH
9d	Y = C, R ³ = OCH ₃
9e	Y = N

***L*-tryptophan methyl ester** (2.29 mmol), as the free base, was combined with the required 2',4',6'-trisubstituted benzaldehyde (2.52 mmol, 1.1 eq) in anhydrous DCM (15 ml) under a N₂ atmosphere. The resulting solution was cooled to 0°C before the dropwise addition of TFA (1.0 eq) and gradually warming to room temperature. The solution was stirred at room temperature over 18 hours to 3 days. The solution was quenched with 10% NH₄OH (30 ml), extracted into DCM (3 x 30 ml), washed with brine (50 ml), dried over MgSO₄ and concentrated under reduced pressure. The crude products were purified by flash column chromatography.

Preparation of methyl (S)-1-(2,4-dichloro-6-fluorophenyl)-2,3,4,9-tetrahydro-1H-pyrido[3,4-b]indole-3-carboxylate 9a

The general procedure (1) was followed using 2,4-dichloro-6-fluorobenzaldehyde to give 9a, purified by flash column chromatography (1% EtOAc:DCM) to give a 1:4 (*trans*:*cis*) diastereoisomer mixture as a white-yellow fine, crystalline solid in 83.9% yield. **Rf** = 0.41 (2:98 EtOAc:DCM). ¹H NMR (500 MHz, DMSO) δ 10.64 (s, 1H, *cis* NH), 10.60 (s, 0.4H *trans* NH), 7.65 (s, 1H, *cis*), 7.63 (s, 0.25H, *trans*), 7.47 – 7.37 (m, 2.5H, *cis/trans*), 7.20 (dt, *J* = 7.9, 0.8 Hz, 1H, *cis*), 7.19 (dt, *J* = 7.9, 0.9 Hz, 0.25H, *trans*), 7.05 – 6.94 (m, 2.5H, *cis/trans*), 6.02 (s, 0.25H, *trans*), 5.79 (d, *J* = 5.7 Hz, 1H, *cis*), 3.98 (m, 1.25H, *cis/trans*), 3.73 (s, 3H, *cis* CH₃), 3.62 (s, 0.75H, *trans* CH₃), 3.11 – 3.02 (m, 1.25H, *cis/trans*), 2.78 (ddd, *J* = 21.6, 12.0, 6.5 Hz, 2H); ¹³C NMR (126 MHz, DMSO) δ 173.2, 162.3 (d, ¹*J*_{CF} = 239.8 Hz), 136.5, 136.4, 135.9 (d, ³*J*_{CF} = 6.4 Hz), 127.0 (d, ³*J*_{CF} = 6.5 Hz), 125.8 (d, ⁴*J*_{CF} = 3.5 Hz), 121.2, 120.8 (d, ²*J*_{CF} = 29.5 Hz), 118.9 (d, ²*J*_{CF} = 23.3 Hz), 118.1 (2C), 111.5, 111.4, 106.5, 56.8, 52.3, 52.1, 25.7; **Elemental analysis** (%) found: C, 57.92; H, 3.87; N, 7.01%. C₁₉H₁₅ClF₂N₂O₂ requires C, 58.03; H, 3.84; N, 7.12%; **CI+HRMS** *m/z* 393.0579 [M+H]⁺ C₁₉H₁₅ClF₂N₂O₂ requires 392.05.

Preparation of methyl (S)-1-(2,4,6-trichlorophenyl)-2,3,4,9-tetrahydro-1H-pyrido[3,4-b]indole-3-carboxylate 9b

The general procedure (1) was followed using 2,4,6-trichlorobenzaldehyde to give 9b, purified by flash column chromatography to give a mixture of diastereoisomers as an off-white/cream solid in 42.7% yield. **Rf** = 0.32 (2:98 EtOAc:DCM). ¹H NMR (400 MHz, CDCl₃) δ 7.51(dd, *J* = 6.9, 1.6 Hz, 2H, *cis/trans*), 7.46 (d, *J* = 2.1 Hz, 2H *cis/trans*), 7.43 (br s, NH indole), 7.30 (d, *J* = 2.1 Hz, 2H *cis/trans*), 7.24 (dd, *J* = 6.8, 1.8 Hz, 2H *cis/trans*), 7.18 – 7.09 (m, 4H *cis/trans*), 6.44 (s, 1H, *trans*), 6.13 (s, 1H, *cis*), 4.22 (dd, *J* = 5.9, 2.7 Hz, 1H, *trans*), 4.02 (dd, *J* = 11.2, 4.3 Hz, 1H, *cis*), 3.82 (s, 3H, CH₃, *cis*), 3.71 (s, 3H, CH₃, *trans*), 3.38 (dt, *J* = 15.4, 1.9 Hz, 1H, *trans*), 3.25 (ddd, *J* = 15.5, 6.0, 2.3 Hz, 2H, *cis/trans*), 2.94 (ddd, *J* = 15.1, 11.2, 2.7 Hz, 1H, *cis*), 2.28 (br s, NH); ¹³C NMR (101 MHz, CDCl₃) δ 173.2, 137.4, 136.8, 135.9, 135.2, 133.1, 132.2, 130.4, 128.6, 127.0, 122.0, 119.9, 118.1, 111.0, 109.1, 57.2, 54.0, 52.4, 25.8; **ES+HRMS** *m/z* 409.0269 [M+H]⁺ C₁₉H₁₅Cl₃N₂O₂ requires 408.02.

Preparation of methyl (S)-1-(2,4-dichloro-6-hydroxyphenyl)-2,3,4,9-tetrahydro-1H-pyrido[3,4-b]indole-3-carboxylate 9c

The general procedure (1) was followed using 2,4-dichloro-6-hydroxybenzaldehyde to give 9c purified, and with diastereoisomers separated, by flash column chromatography in a 1.3:1 ratio of *cis*: *trans* isomers, as a white solid and yellow viscous oil respectively, with a combined 84.2% yield. **Rf** of *cis* isomer = 0.54 (2:98 EtOAc:DCM); **Rf** of *trans* isomer = 0.25 (2:98 EtOAc:DCM). **1S,3S (cis isomer)** ¹H NMR (400 MHz, CDCl₃) δ 11.72 (br s, 1H, NH), 7.61 (br s, 1H, OH), 7.50 (d, *J* = 7.5 Hz, 1H), 7.25 (dd, *J* =

7.4 Hz, 1H), 7.18 - 7.08 (m, 2H), 7.00 (d, $J = 2.1$ Hz, 1H), 6.73 (d, $J = 2.1$ Hz, 1H), 6.04 (s, 1H), 3.94 (dd, $J = 11.3, 4.1$ Hz, 1H), 3.88 (s, 3H), 3.33 (ddd, $J = 15.5, 4.1, 1.7$ Hz, 1H), 3.06 (ddd, $J = 15.4, 11.3, 2.6$ Hz, 1H); $^{13}\text{C NMR}$ (101 MHz, CDCl_3) δ 171.6, 159.9, 136.3, 135.4, 132.8, 130.3, 126.5, 122.6, 120.3, 120.0, 119.9, 118.3, 117.3, 111.2, 108.3, 56.2, 54.3, 52.8, 24.6. **1R,3S (trans isomer)** $^1\text{H NMR}$ (400 MHz, CDCl_3) δ 14.57 (br s, 1H, NH), 8.23 (s, 1H, NH), 8.08 (br s, 1H, OH), 7.60 (d, $J = 7.7$ Hz, 1H), 7.35 (d, $J = 8.1$ Hz, 1H), 7.20 (dt, $J = 7.2, 1.0$ Hz, 1H), 7.12 (dt, $J = 7.94, 1.0$ Hz, 1H), 6.94 (d, $J = 2.3$ Hz, 1H), 6.87 (d, $J = 1.9$ Hz, 1H), 6.78 (d, $J = 2.0$ Hz, 1H), 4.33 (dd, $J = 9.1, 4.4$ Hz, 1H), 3.79 (s, 3H), 3.58 (dd, $J = 14.5, 4.4$ Hz, 1H), 3.24 (dd, $J = 14.5, 9.1$ Hz, 1H); $^{13}\text{C NMR}$ (101 MHz, CDCl_3) δ 171.3, 164.3, 163.4, 138.7, 136.3, 136.2, 126.9, 123.6, 122.4, 119.8, 119.5, 118.5, 117.1, 113.8, 111.4, 110.2, 70.7, 52.7, 30.1; **ES+HRMS** m/z 391.0614 $[\text{M}+\text{H}]^+$ $\text{C}_{19}\text{H}_{16}\text{Cl}_2\text{N}_2\text{O}_3$ requires 390.05.

Preparation of methyl (*S*)-1-(2,4-dichloro-6-methoxyphenyl)-2,3,4,9-tetrahydro-1*H*-pyrido[3,4-*b*]indole-3-carboxylate **9d**

The general procedure (**1**) was followed using 2,4-dichloro-6-methoxybenzaldehyde to give **9d** purified by flash column chromatography (2% EtOAc:DCM) as a white solid, a mixture of diastereoisomers in 92.0% yield. **Rf** = 0.26 (2:98 EtOAc:DCM). *cis* rotamers $^1\text{H NMR}$ (400 MHz, DMSO) δ 10.47 (s, 1H, NH, R1), 10.42 (s, 1H, NH, R2), 7.40 (d, $J = 7.6$ Hz, 1H), 7.35 (d, $J = 2.0$ Hz, 1H, R2), 7.27 (d, $J = 2.0$ Hz, 1H, R1), 7.20 (d, $J = 7.5$ Hz, 1H), 7.16 (d, $J = 1.9$ Hz, 1H, R2), 7.12 (d, $J = 2.0$ Hz, 1H, R1), 7.02 – 6.92 (m, 2H), 5.96 (d, $J = 8.8$ Hz, 1H, R1), 5.75 (d, $J = 10.7$ Hz, 1H, R2), 3.93 (m, 1H), 3.72 (s, 3H), 3.06 (m, 1H), 2.73 (m, 1H); $^{13}\text{C NMR}$ (101 MHz, DMSO) δ 174.0, 173.5, 160.4, 160.0, 136.4, 136.2, 135.7, 135.6, 135.0, 134.5, 134.4, 134.3, 127.3, 127.1, 125.7, 125.3, 122.7, 121.8, 120.9, 118.8, 117.8, 112.7, 111.6, 111.6, 111.5, 107.1, 106.0, 57.4, 57.3, 57.0, 56.9, 53.2, 52.3, 52.2, 48.8, 26.2, 25.9. *Trans* isomer (lacking single CH_3 peak) $^1\text{H NMR}$ (500 MHz, CDCl_3) δ 7.52 (m, 2H), 7.21 (d, $J = 5.0$ Hz, 1H, NH), 7.11 (m, 2H), 7.07 (s, 1H), 6.80 (s, 1H), 6.22 (s, 1H), 4.23 (t, $J = 4.2$ Hz, 1H), 3.72 (s, 3H), 3.60 (br s, 3H), 3.25 (m, 2H), 1.27 (s, 1H, NH); $^{13}\text{C NMR}$ (101 MHz, CDCl_3) δ 174.1, 159.9, 136.3, 135.7, 135.0, 127.3, 125.6, 121.4, 119.3, 118.0, 110.8, 56.5, 54.6, 52.2, 48.0, 24.3; **Elemental analysis** (%) found: C, 59.11; H, 4.50; N, 6.79%. $\text{C}_{20}\text{H}_{18}\text{Cl}_2\text{N}_2\text{O}_2$ requires C, 59.27; H, 4.48; N, 6.91%; **ES+HRMS** m/z 405.0764 $[\text{M}+\text{H}]^+$ $\text{C}_{20}\text{H}_{18}\text{Cl}_2\text{N}_2\text{O}_2$ requires 404.07.

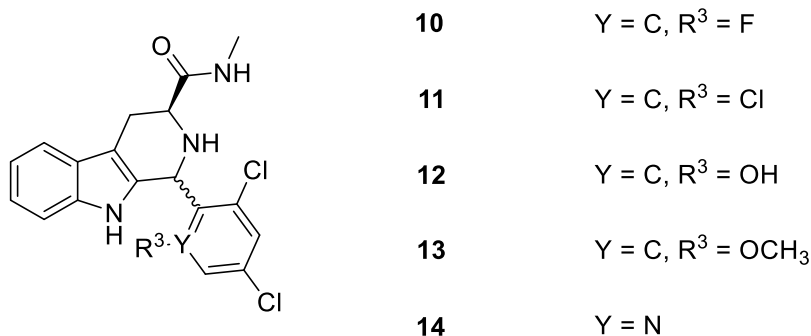
Preparation of methyl (*S*)-1-(3,5-dichloropyridin-2-yl)-2,3,4,9-tetrahydro-1*H*-pyrido[3,4-*b*]indole-3-carboxylate **9e**

The general procedure (**1**) was followed using 3,5-dichloropicolinaldehyde to give **9e** purified by flash column chromatography, giving a 1:2 ratio of mixed diastereoisomers as a cream-orange clumpy solid in 83.0% yield. **Rf** = 0.28 (5:95 EtOAc:DCM). $^1\text{H NMR}$ (400 MHz, CDCl_3) δ 8.45 (d, $J = 2.1$ Hz, 1H, *cis*), 8.38 (d, $J = 2.1$ Hz, 1H, *trans*), 7.84 (d, $J = 2.2$ Hz, 1H, *cis*), 7.80 (br s, *trans* NH indole), 7.78 (d, $J = 2.1$ Hz,

1H, *trans*), 7.65 (br s, *cis* NH indole), 7.53 (d, $J = 8.0$ Hz, 1H, *trans*), 7.50 (d, $J = 7.6$ Hz, 1H, *cis*), 7.24 (d, $J = 7.6$ Hz, 2H), 7.13 (m, 4H, *cis/trans*), 5.99 (s, 1H, *trans*), 5.92 (s, 1H, *cis*), 4.49 (dd, $J = 7.6, 5.2$ Hz, 1H, *trans*), 4.03 (d, $J = 6.0$ Hz, 1H, *cis*), 3.84 (s, 3H, *cis* CH₃), 3.77 (s, 3H, CH₃, *trans*), 3.32 – 3.18 (m, 2H, *cis/trans*), 3.10 (br s, *cis/trans* NH), 3.09 – 2.93 (m, 2H, *cis/trans*), 1.61 (br s, *cis/trans* NH); ¹³C NMR (101 MHz, CDCl₃) δ 173.4, 154.0, 147.1, 137.1, 136.1, 132.5, 131.6, 130.4, 126.9, 122.4, 119.9, 118.3, 111.0, 109.5, 56.3, 54.3, 52.3, 26.0 (peaks more intense: likely *cis* isomer); ¹³C NMR (101 MHz, CDCl₃) δ 174.0, 156.1, 146.8, 137.0, 136.2, 131.5, 131.2, 130.2, 126.9, 122.3, 119.6, 118.4, 110.9, 109.2, 53.0, 52.2, 51.6, 25.1 (peak intensity reduced: likely *trans* isomer); ES+HRMS m/z 376.0614 [M+H]⁺ C₁₈H₁₅Cl₂N₃O₂ requires 375.05.

Preparation of (1*R*,3*S*)-1-(2,4,6-trisubstituted-phenyl)-*N*-methyl-2,3,4,9-tetrahydro-1*H*-pyrido[3,4-*b*]indole-3-carboxamides 10-14

General Procedure (2)



The appropriate compound **9a-e** was transferred to a sealed tube and dissolved in methylamine solution, 33 wt. % in absolute EtOH (130.0 eq). The resulting solution was allowed to stir for 16hrs-3days at room temperature under an atmospheric atmosphere. Excess methylamine was removed under reduced pressure and the crude products were purified and diastereoisomers separated by flash column chromatography.

Preparation of (1*R*,3*S*)-1-(2,4-dichloro-6-fluorophenyl)-*N*-methyl-2,3,4,9-tetrahydro-1*H*-pyrido[3,4-*b*]indole-3-carboxamide **10**

The general procedure (2) was followed using **9a** overnight to give **10** as an off-white/yellow solid in 98.1% total yield, isolating 0.0504 g (15.5% yield) of the *trans* diastereoisomer. **Rf** of *trans* isomer = 0.30 (40:60 EtOAc:DCM); **Rf** of *cis* isomer = 0.49 (40:60 EtOAc:DCM). ¹H NMR (500 MHz, DMSO) δ 10.64 (s, 1H, NH), 7.87 (q, $J = 4.7$ Hz, 1H), 7.58 (s, 1H, NH), 7.42 (m, 2H), 7.21 (dt, $J = 7.1, 0.8$ Hz, 1H), 7.02 (td, $J = 7.01, 1.2$ Hz, 1H), 6.96 (td, $J = 7.9, 1.1$ Hz, 1H), 5.78 (d, $J = 5.6$ Hz, 1H), 3.67 (d, $J = 5.3$ Hz, 1H, NH), 3.21 (t, $J = 7.4$ Hz, 1H, NH), 2.95 (dd, $J = 15.2, 5.1$ Hz, 1H), 2.84 (dd, $J = 15.2, 7.5$ Hz, 1H), 2.62 (d, $J = 4.6$ Hz, 3H); ¹³C NMR (126 MHz, DMSO) δ 173.5, 161.9 (d, ¹ $J_{CF} = 253.6$ Hz), 136.4, 136.4 (d, ³ J_{CF}

= 8.1 Hz), 133.7 (d, $^3J_{CF}$ = 13.1 Hz), 133.3 (d, $^4J_{CF}$ = 2.0 Hz), 127.71 (d, $^2J_{CF}$ = 15.3 Hz), 127.19, 126.1 (d, $^4J_{CF}$ = 2.6 Hz), 121.1, 118.7, 118.0, 116.6 (d, $^2J_{CF}$ = 27.2 Hz), 111.4, 107.4, 54.0, 26.0, 25.0; **Elemental analysis** (%) found: C, 58.02; H, 4.12; N, 10.74%. $C_{19}H_{16}Cl_2FN_3O$ requires C, 58.18; H, 4.11; N, 10.71%; **ES+HRMS** m/z 414.0547 $[M+Na]^+$ $C_{19}H_{16}Cl_2FN_3O$ requires 391.07.

Preparation of **(1R,3S)-N-methyl-1-(2,4,6-trichlorophenyl)-2,3,4,9-tetrahydro-1H-pyrido[3,4-b]indole-3-carboxamide 11**

The general procedure **(2)** was followed using **9b** overnight to give **11** as an off-white solid in 91.0% total yield, isolating 0.0360 g (13.6% yield) of the *trans* diastereoisomer. **Rf** of *cis* isomer = 0.19 (10:80 EtOAc:DCM); **Rf** of *trans* isomer = 0.28 (10:80 EtOAc:DCM). 1H NMR (500 MHz, DMSO) δ 10.51 (s, 1H, indole NH), 7.86 (q, J = 4.8 Hz, 1H, amide NH), 7.79 (d, $^4J_{HH}$ = 1.9 Hz, 1H), 7.54 (d, $^4J_{HH}$ = 1.8 Hz, 1H), 7.40 (d, J = 7.7 Hz, 1H), 7.18 (dd, J = 7.8, 0.9 Hz, 1H), 6.99 (dt, J = 7.1, 1.2 Hz, 1H, NH), 6.94 (dt, J = 7.1, 1.2 Hz, 1H), 6.05 (d, $^3J_{HH}$ = 6.0 Hz, 1H), 3.89 (dd, J = 4.9, 5.6 Hz, 1H), 3.17 (t, J = 6.1 Hz, 1H), 3.08 (ddd, J = 15.1, 4.3, 1.7 Hz, 1H), 2.92 (ddd, J = 15.1, 5.6, 1.7 Hz, 1H), 2.62 (d, J = 4.6 Hz, 3H); ^{13}C NMR (101 MHz, $CDCl_3$) δ 172.6, 135.9, 135.0, 133.6, 131.1, 130.3 (2C), 128.7 (2C), 127.2, 121.7, 119.4, 118.3, 110.8, 108.2, 54.9, 50.2, 26.1, 21.8; **Elemental analysis** (%) found: C, 55.42; H, 4.04; N, 9.90%. $C_{19}H_{16}Cl_3N_3O$ requires C, 55.84; H, 3.95; N, 10.28%; **ES+HRMS** m/z 408.0431 $[M+H]^+$ $C_{19}H_{16}Cl_3N_3O$ requires 407.04.

Preparation of **(1R,3S)-1-(2,4-dichloro-6-hydroxyphenyl)-N-methyl-2,3,4,9-tetrahydro-1H-pyrido[3,4-b]indole-3-carboxamide 12**

The general procedure **(2)** was followed using **9c** (pure *trans* diastereoisomer) and 140.0 eq methylamine solution, 33 wt. % in absolute EtOH overnight to give **12** as a yellow solid in 54.2% yield. **Rf** = 0.33 (10:80 EtOAc:DCM). 1H NMR (500 MHz, $CDCl_3$) δ 12.14 (br s, 1H, indole NH), 8.17 (br s, 1H, OH), 7.59 (d, J = 8.0 Hz, 1H), 7.37 (dt, J = 8.1, 0.9 Hz, 1H), 7.21 (td, J = 8.1, 1.0 Hz, 1H), 7.12 (td, J = 8.0, 1.0 Hz, 1H), 7.09 (d, J = 2.2 Hz, 1H, amide NH), 6.89 (d, J = 2.1 Hz, 1H), 6.76 (d, J = 2.1 Hz, 1H), 5.96 (d, J = 1.9 Hz, 1H), 3.98 (dt, J = 7.7, 2.3 Hz, 1H), 3.60 (ddd, J = 14.8, 3.3, 0.9 Hz, 1H), 2.96 (dd, J = 15.0, 4.9 Hz, 1H), 2.71 (s, 3H), 1.26 (s, 1H, 2° amine); ^{13}C NMR (101 MHz, $CDCl_3$) δ 170.7, 161.0, 136.8, 136.4, 135.3, 126.9, 123.1, 122.4, 120.4, 119.8, 118.5, 117.5, 114.3, 111.4, 111.1, 71.1, 58.7, 28.1, 26.6; **Elemental analysis** (%) found: C, 58.55; H, 4.784; N, 9.70%. $C_{19}H_{17}Cl_2N_3O_2$ requires C, 58.48; H, 4.39; N, 10.77%; **ES+HRMS** m/z 390.0767 $[M+H]^+$ $C_{19}H_{17}Cl_2N_3O_2$ requires 389.07.

Preparation of **(1R,3S)-1-(2,4-dichloro-6-methoxyphenyl)-N-methyl-2,3,4,9-tetrahydro-1H-pyrido[3,4-b]indole-3-carboxamide 13**

The general procedure **(2)** was followed using **9d** and 160eq methylamine solution, 33 wt. % in absolute EtOH over 3 days to give **13** as an off-white solid in 61.7% yield. **Rf** = 0.23 (2:98 EtOAc:DCM). 1H NMR (500 MHz, DMSO) δ 10.37 (s, 1H, NH), 7.84 (q, J = 4.8 Hz, 1H), 7.40 (d, J = 7.5 Hz, 1H), 7.17 (d,

$J = 7.6$ Hz, 1H), 7.15 (d, $J = 4.6$ Hz, 1H), 6.95 (dtd, $J = 15.9, 7.1, 1.2$ Hz, 2H), 5.81 (s, 1H), 3.89 (unresolved dd, $J = 5.3$ Hz, 1H), 3.04 (ddd, $J = 15.0, 5.0, 1.6$ Hz, 1H), 2.91 (ddd, $J = 15.0, 5.6, 1.5$ Hz, 1H), 2.64 (d, $J = 4.7$ Hz, 3H), 1.25 (s, 1H, NH); $^{13}\text{C NMR}$ (101 MHz, CDCl_3) δ 172.6, 159.8, 136.1, 135.7, 135.3, 132.8, 127.6, 124.6, 122.5, 122.5, 121.4, 119.3, 118.3, 111.5, 110.6, 65.9, 56.5, 55.1, 29.7, 26.2; **Elemental analysis** (%) found: C, 60.10; H, 5.18; N, 9.82%. $\text{C}_{20}\text{H}_{19}\text{Cl}_2\text{N}_2\text{O}_2$ requires C, 59.42; H, 4.74; N, 10.39%; **ES+HRMS** m/z 404.0922 $[\text{M}+\text{H}]^+$ $\text{C}_{20}\text{H}_{19}\text{Cl}_2\text{N}_2\text{O}_2$ requires 403.09.

Preparation of **(1S,3S)-1-(3,5-dichloropyridin-2-yl)-N-methyl-2,3,4,9-tetrahydro-1H-pyrido[3,4-b]indole-3-carboxamide 14**

The general procedure (**2**) was followed using **9e** and 200.0 eq methylamine solution, 33 wt. % in absolute EtOH over 3 days to give **14** as an off-white solid in 55.9% total yield, isolating 0.0733 g (14.4% yield) of the *trans* diastereoisomer. $R_f = 0.32$ (2:98 EtOAc:DCM). $^1\text{H NMR}$ (500 MHz, DMSO) δ 10.53 (s, 1H, indole NH), 8.43 (d, $J = 2.2$ Hz, 1H), 8.29 (d, $J = 2.2$ Hz, 1H), 7.74 (q, $J = 4.5$ Hz, 1H, amide NH), 7.43 (d, $J = 7.7$ Hz, 1H), 7.21 (d, $J = 8.0$ Hz, 1H), 7.02 (dt, $J = 7.9, 1.0$ Hz, 1H), 6.96 (dt, $J = 7.8, 0.8$ Hz, 1H), 5.71 (d, $J = 5.8$ Hz, 1H), 3.66 (td, $J = 10.0, 4.4$ Hz, 1H), 2.95 (dd, $J = 15.2, 4.5$ Hz, 1H), 2.67 (dd, $J = 14.2, 10.0$ Hz, 10H), 2.59 (d, $J = 4.6$ Hz, 3H); $^{13}\text{C NMR}$ (126 MHz, DMSO) δ 173.0, 156.9, 145.3, 136.9, 136.1, 133.0, 130.9, 130.0, 126.7, 120.7, 118.2, 117.5, 110.9, 108.6, 52.0, 51.3, 25.4, 25.2; **Elemental analysis** (%) found: C, 58.01; H, 4.46; N, 14.56%. $\text{C}_{18}\text{H}_{16}\text{Cl}_2\text{N}_4\text{O}$ requires C, 57.61; H, 4.30; N, 14.93%; **ES+HRMS** m/z 375.0767 $[\text{M}+\text{H}]^+$ $\text{C}_{18}\text{H}_{16}\text{Cl}_2\text{N}_4\text{O}$ requires 374.07.

Overlay of $^1\text{H NMR}$ Spectra

Overlaid $^1\text{H NMR}$ spectra of the *cis* and *trans* isomers of compound **11** can be found in **Appendix 3**. The overlaid spectra highlight the observed change in chemical shift of the H-1 proton for corresponding *cis* and *trans* isomers of tetrahydro- β -carboline derivatives.

2D Nuclear Overhauser effect spectroscopy (NOESY) NMR

2D NOESY NMR experiments were recorded on Bruker Avance III HD 500 MHz spectrometer at ambient temperature. Standard parameters were used for each 2D NMR experiment; altering only the mixing time and number of scans (NS) specified. A mixing time of 1.0 second was used in order to verify an NOE build-up and identify through-space correlations; NS = 16 for each experiment. Gradient-enhanced 2D NOESY sequence (noesygpph) was used, and standard 2D processing was applied. Some non-through space couplings were also seen but these were discounted as they were not NOESY based. Representative NOE spectra for compound **11** can be found in **Appendix 4**. Positive enhancement observed between chemical shift values of H-1 and H-3 confirms presence of a tetrahydro- β -carboline *cis* isomer. Conversely, presence of the *trans* isomer is confirmed by lack of

positive enhancement between assigned chemical shift values for H-1 and H-3 protons within derived tetrahydro- β -carboline structures.

5.8 References

- [1] D. S. Johnson, E. Weerapana, B. F. Cravatt, *Future Med. Chem.* **2010**, *2*, 949–964.
- [2] J. Singh, R. C. Petter, T. a Baillie, A. Whitty, *Nat. Rev. Drug Discov.* **2011**, *10*, 307–317.
- [3] S. Aprile, E. Del Grosso, G. Grosa, *Xenobiotica* **2011**, *41*, 212–225.
- [4] Y. Hu, D. Gupta-Ostermann, J. Bajorath, *Comput Struct Biotechnol J* **2014**, *9*, e201401003.
- [5] B. K. Park, A. Boobis, S. Clarke, C. E. P. Goldring, D. Jones, J. G. Kenna, C. Lambert, H. G. Laverty, D. J. Naisbitt, S. Nelson, et al., *Nat. Rev. Drug Discov.* **2011**, *10*, 292–306.
- [6] F.-J. Gamo, L. M. Sanz, J. Vidal, C. de Cozar, E. Alvarez, J.-L. Lavandera, D. E. Vanderwall, D. V. S. Green, V. Kumar, S. Hasan, et al., *Nature* **2010**, *465*, 305–310.
- [7] T. Spangenberg, J. N. Burrows, P. Kowalczyk, S. McDonald, T. N. C. Wells, P. Willis, *PLoS One* **2013**, *8*, DOI 10.1371/journal.pone.0062906.
- [8] J. D. Bowman, E. F. Merino, C. F. Brooks, B. Striepen, P. R. Carlier, M. B. Cassera, *Antimicrob. Agents Chemother.* **2014**, *58*, 811–819.
- [9] W. Wu, Z. Herrera, D. Ebert, K. Baska, S. H. Cho, J. L. DeRisi, E. Yeh, *Antimicrob. Agents Chemother.* **2015**, *59*, 356–364.
- [10] F. Lovering, J. Bikker, C. Humblet, *J. Med. Chem.* **2009**, *52*, 6752–6756.
- [11] M. M. Hann, *Medchemcomm* **2011**, *2*, 349–355.
- [12] M. E. Bunnage, J. P. Mathias, A. Wood, D. Miller, S. D. A. Street, *Bioorganic Med. Chem. Lett.* **2008**, *18*, 6033–6036.
- [13] I. Hale, P. M. O’Neill, N. G. Berry, A. Odom, R. Sharma, *Medchemcomm* **2012**, *3*, 418–433.
- [14] W. N. Hunter, *J. Biol. Chem.* **2007**, *282*, 21573–21577.
- [15] L. S. Imlay, C. M. Armstrong, M. C. Masters, T. Li, K. E. Price, R. L. Edwards, K. M. Mann, L. X. Li, C. L. Stallings, N. G. Berry, et al., *ACS Infect. Dis.* **2015**, *1*, 157–167.
- [16] A. R. Odom, *PLoS Pathog.* **2011**, *7*, 1–4.
- [17] K. E. Price, C. M. Armstrong, L. S. Imlay, D. M. Hodge, C. Pidathala, N. J. Roberts, J. Park, M. Mikati, R. Sharma, A. S. Lawrenson, et al., *Sci. Rep.* **2016**, *6*, 36777.
- [18] B. Zhang, K. M. Watts, D. Hodge, L. M. Kemp, D. A. Hunstad, L. M. Hicks, A. R. Odom, *Biochemistry* **2011**, *50*, 3570–3577.
- [19] T. Masini, B. S. Kroezen, A. K. H. Hirsch, *Drug Discov. Today* **2013**, *18*, 1256–1262.
- [20] J.-Y. van der Meer, A. K. H. Hirsch, *Nat. Prod. Rep.* **2012**, *29*, 721.
- [21] N. G. Berry, *Personal Communication*, **2012**.
- [22] J. C. Cole, J. W. M. Nissink, R. Taylor, *Drug Discov. Ser.* **2005**, *1*, 379–415.
- [23] M. L. Verdonk, J. C. Cole, M. J. Hartshorn, C. W. Murray, R. D. Taylor, *Proteins Struct. Funct. Genet.* **2003**, *52*, 609–623.

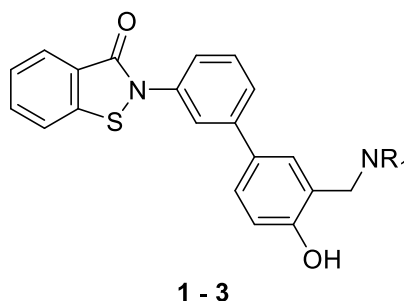
- [24] M. C. Witschel, H. W. Hoeffken, M. Seet, L. Parra, T. Mietzner, F. Thater, R. Niggeweg, F. Roehl, B. Illarionov, F. Rohdich, et al., *Angew. Chemie, Int. Ed.* **2011**, *50*, 7931–7935, S7931/1–S7931/29.
- [25] A. Kunfermann, M. Witschel, B. Illarionov, R. Martin, M. Rottmann, H. W. Hoeffken, M. Seet, W. Eisenreich, H.-J. Knoelker, M. Fischer, et al., *Angew. Chemie, Int. Ed.* **2014**, *53*, 2235–2239.
- [26] S. B. Richard, M. E. Bowman, W. Kwiatkowski, I. Kang, C. Chow, A. M. Lillo, D. E. Cane, J. P. Noel, *Nat. Struct. Biol.* **2001**, *8*, 641–648.
- [27] L. Schrödinger, *The {PyMOL} Molecular Graphics System, Version 1.3*, **2010**.
- [28] J. W. Liebeschuetz, J. C. Cole, O. Korb, *J. Comput. Aided. Mol. Des.* **2012**, *26*, 737–748.
- [29] A. M. Dondorp, S. Yeung, L. White, C. Nguon, N. P. J. Day, D. Socheat, L. von Seidlein, *Nat. Rev. Microbiol.* **2010**, *8*, 272–280.
- [30] Q. L. Fivelman, I. S. Adagu, D. C. Warhurst, *Antimicrob. Agents Chemother.* **2004**, *48*, 4097–4102.
- [31] N. J. White, *J. Clin. Invest.* **2004**, *113*, 1084–1092.
- [32] J. K. Baird, *N. Engl. J. Med.* **2005**, *352*, 1565–1577.
- [33] C. T. Keith, A. a Borisy, B. R. Stockwell, *Nat. Rev. Drug Discov.* **2005**, *4*, 71–78.
- [34] J. Foucquier, M. Guedj, *Pharmacol. Res. Perspect.* **2015**, *3*, e00149.
- [35] G. R. Zimmermann, J. Leh??r, C. T. Keith, *Drug Discov. Today* **2007**, *12*, 34–42.
- [36] R. W. Humphrey, L. M. Brockway-Lunardi, D. T. Bonk, K. M. Dohoney, J. H. Doroshow, S. J. Meech, M. J. Ratain, S. L. Topalian, D. M. Pardoll, *J. Natl. Cancer Inst.* **2011**, *103*, 1222–1226.
- [37] G. Glass, *Nat. Rev. Drug Discov.* **2004**, *3*, 731–732.
- [38] L. Oversteegen, M. Shah, H. Rovini, *Nat. Rev. Drug Discov.* **2007**, *6*, 951–952.
- [39] T. N. C. Wells, R. H. van Huijsduijnen, W. C. Van Voorhis, *Nat. Rev. Drug Discov.* **2015**, *14*, 424–442.
- [40] R. J. Tallarida, *J. Pharmacol. Exp. Ther.* **2012**, *342*, 2–8.
- [41] R. J. Tallarida, *Genes Cancer* **2011**, *2*, 1003–8.
- [42] R. J. Tallarida, *Pharmacol. Ther.* **2007**, *113*, 197–209.
- [43] I. Rodea-Palomares, M. González-Pleiter, K. Martín-Betancor, R. Rosal, F. Fernández-Piñas, *Toxics* **2015**, *3*, 342–369.
- [44] J. Wiesner, D. Henschker, D. B. D. B. Hutchinson, E. Beck, H. Jomaa, *Antimicrob. Agents Chemother.* **2002**, *46*, 2889–2894.
- [45] H. L. Sham, D. J. Kempf, A. Molla, K. C. Marsh, G. N. Kumar, C. M. Chen, W. Kati, K. Stewart, R. Lal, A. Hsu, et al., *Antimicrob Agents Chemother* **1998**, *42*, 3218–3224.
- [46] Z. K. Yao, P. M. Krai, E. F. Merino, M. E. Simpson, C. Slebodnick, M. B. Cassera, P. R. Carlier, *Bioorganic Med. Chem. Lett.* **2015**, *25*, 1515–1519.

- [47] A. Böcker, P. R. Bonneau, O. Hucke, A. Jakalian, P. J. Edwards, *ChemMedChem* **2010**, *5*, 2102–2113.
- [48] C. Ballatore, D. M. Huryn, A. B. Smith, *ChemMedChem* **2013**, *8*, 385–395.
- [49] G. Camenisch, J. Alsenz, H. Van De Waterbeemd, G. Folkers, *Eur. J. Pharm. Sci.* **1998**, *6*, 313–319.
- [50] J. Ghuman, P. A. Zunszain, I. Petitpas, A. A. Bhattacharya, M. Otagiri, S. Curry, *J. Mol. Biol.* **2005**, *353*, 38–52.
- [51] A. V Stachulski, X. Meng, *Nat. Prod. Rep.* **2013**, *30*, 806–48.
- [52] C. Skonberg, J. Olsen, K. G. Madsen, S. H. Hansen, M. P. Grillo, *Expert Opin. Drug Metab. Toxicol.* **2008**, *4*, 425–438.
- [53] M. Pye, *Personal Communication*, **2015**.
- [54] A. R. Odom, *Personal Communication*, **2012**.
- [55] N. A. Meanwell, *J. Med. Chem.* **2011**, *54*, 2529–2591.
- [56] A. Pictet, T. Spengler, *Gerichte der Dtsch. Chem. Gesellschaft* **1911**, *44*, 2030–2036.
- [57] G. Tatsui, *Yakugaku Zasshi* **1928**, *48*, 453–459.
- [58] J. Seayad, A. M. Seayad, B. List, *J. Am. Chem. Soc.* **2006**, *128*, 1086–1087.
- [59] M. Chrzanowska, M. D. Rozwadowska, *Chem. Rev. (Washington, DC, United States)* **2004**, *104*, 3341–3370.
- [60] C. Gremmen, B. Willemse, M. Wanner, G. Koomen, *Org. Lett.* **2000**, *2*, 1955–1958.
- [61] P. D. Bailey, *J. Chem. Res.* **1987**, 202.
- [62] P. Kowalski, A. J. Bojarski, J. L. Mokrosz, *Tetrahedron* **1995**, *51*.
- [63] E. D. Cox, J. M. Cook, *J. Org. Chem.* **1995**, *60*.
- [64] F. A. L. Anet, A. J. R. Bourn, P. Carter, S. Winstein, *J. Am. Chem. Soc.* **1965**, *87*, 5250–5251.
- [65] J. Arima, H. Usuki, T. Hatanaka, N. Mori, *Appl. Environ. Microbiol.* **2011**, *77*, 8209–8218.
- [66] K. Barbalace, “Periodic Table of Elements,” can be found under <http://environmentalchemistry.com/yogi/periodic/atomicradius.html>, **2016**.
- [67] L. A. Kelley, M. J. E. Sternberg, *Nat. Protoc.* **2009**, *4*, 363–371.
- [68] R. Baer, *Nat. Struct. Biol.* **2001**, *8*, 822–824.
- [69] G. Vriend, *J. Mol. Graph.* **1990**, *8*, 29,52-56.

Chapter 6
Considering Off-Target Interactions
of the BITZ Chemotype:
A Chemical Biology Approach

6.1 Potential Off-Target BITZ Chemotype Reactivity

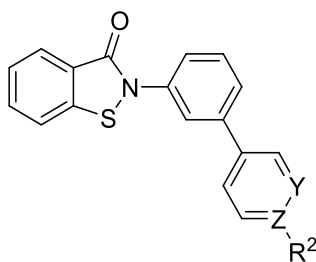
As previously alluded to (see **Chapter 3**), it is possible that the 1,2-benzo[*d*]isothiazol-3(2*H*)-one (BITZ) chemotype and derived inhibitors may be capable of exerting inhibitory effects at off-target proteins, in addition to the *Pf*lspD enzyme, which may contribute to observed inhibition of *Plasmodium* parasite growth. In particular, an indication of off-target reactivity was highlighted by the alkyl-amino biphenyl BITZ compound series **1-3** and the biphenyl-pyridinyl BITZ compound series **4-10** (**Table 6.1** and **6.2** respectively) since both inhibitor series displayed a marked increase in potency against *P. falciparum* parasite growth, compared to that observed against the *Pf*lspD enzyme (see **Chapter 3**). The inhibitory activity of compounds in the alkyl-amino biphenyl BITZ compound series **1-3** is ~ four to five times more potent against *Plasmodium* parasite growth than against the *Pf*lspD enzyme (**Table 6.1**).



Compound number	NR ₁	<i>Pf</i> lspD IC ₅₀ (μM)	Whole cell 3D7 EC ₅₀ (μM)
1	Morpholine	0.501	0.736
2	Diethylamine	2.33	0.438
3	Pyrrolidine	0.507	0.133 ± 0.016

Table 6.1 Inhibitory activity of alkyl-amino biphenyl BITZ analogues **1-3** against the *Pf*lspD enzyme and *P. falciparum* growth in culture (strain 3D7).

This observation is strongly echoed by the biphenyl pyridinyl BITZ analogue series. Indeed, BITZ compounds **4-10** demonstrate a complete loss of inhibitory activity against *Pf*lspD but show activity in the low micromolar region against *Plasmodium* parasite growth (**Table 6.2**). This clear distinction between enzymatic and phenotypic antimalarial activity therefore indicates that BITZ derived compounds may be capable of exerting off-target inhibitory effects which are not specific to the *Pf*lspD enzyme but that contribute to *P. falciparum* parasite growth inhibition.



4 - 7

Compound number	Y	Z	R ²	<i>Pf</i> ispD IC ₅₀ (μM)	Whole cell 3D7 EC ₅₀ (μM)
4	C	N	-	5.94	3.65
5	N	C	OCH ₃	58.5	1.67
6	N	C	Cl	> 100	2.34
7	N	C	CF ₃	> 100	1.91

Table 6.2 Inhibitory activity of biphenyl pyridinyl BITZ analogues **4-7** against the *Pf*ispD enzyme and *P. falciparum* growth in culture (strain 3D7).

If this assumption is correct, further knowledge regarding an additional molecular target would be highly beneficial for ongoing and informed antimalarial design. It was therefore appropriate to ask the question: are there any additional protein targets within *P. falciparum* parasites that the BITZ chemotype and derived compounds are capable of targeting and inhibiting?

Consequently, a chemical-biology approach was employed aiming to identify the localisation and identity of any additional molecular target within malarial-causing *P. falciparum* parasites that the BITZ chemotype may be able to interact with. In order to facilitate this study, a small range of tagged-chemical probes were designed and synthesised which were used to monitor the behaviour of BITZ derived compounds in the cell.

6.2 Biological Probes

It is not uncommon that potential clinical compounds are unsuccessful due to a lack of specificity (prominent off-target effects) and a limited understanding of their role or behaviour at a suggested protein target. It is therefore important to have knowledge of the overall behaviour of a compound, looking beyond target-directed design and *in vitro* optimisation.^[1] A broad range of technologies are available to assess and enhance the understanding of drug and chemotype selectivity within cells and animal models including chemical probes, proteomics and screening tools. In particular, activity-based probes (ABPs) are widely used to more fully understand the biological roles of chemical agents, measuring both off-target effects and on-target inhibition within *in vitro* and *in vivo* studies.^[1]

Chemical probes can be described as small, often synthetic molecules that are used to establish the relationship between a molecular target and a drug, or to explore the role of a protein or a chemical agent in the broader biological context of cells and organisms.^[2] A chemical probe is therefore a selective small-molecule that is able to modulate a protein's function and can itself be monitored within the cell. Such a tool enables specific biological questions to be addressed regarding the behaviour of drugs and the cellular function of proteins in biochemical, cell-based and animal studies.^[3]

6.2.1 Using Biological Probes to Address Research Questions

Chemical probes are used widely in modern research programs since they facilitate the study of specific binding events between chemical agents and specified cellular components in organisms and cells. Recent work by Wang *et al.*^[4] highlights the use of a fluorescent mD1 probe to study the specific binding of the mD1 protein to an inhibitor and its target HIV protein for the development of HIV detection methods. The designed fluorescent mD1 probe (or protein sensor) contained a Förster resonance energy transfer (FRET pair) that can directly detect the gp120 protein of the HIV virus, potentially enabling earlier detection of HIV infection.^[4]

The use of ABPs have also been successfully applied within a number of drug discovery projects focused on the development of protease inhibitors. Proteases are well-established drug targets within pharmaceutical development due to their regulatory roles in many human pathologies, including degenerative, inflammatory and infectious diseases. However, the development of protease inhibitors as drugs remains a challenge since achieving target specificity represents a significant hurdle, despite major advances in many biochemical technologies. The use of ABPs has enabled the enhanced assessment of drug selectivity within this area, as well as improved understandings of the biological role of proteases.^[1,5] Indeed, Xiao *et al.* developed ABPs to label and inhibit engineered caspases, which are cysteine proteases with essential roles in apoptosis and inflammation. The engineered labelling of these proteins enabled the study of caspase function within a timeframe suitable for monitoring the events of apoptosis.^[5]

In a contrasting area of research, development of BET bromodomain inhibitors provides an appropriate demonstration of the power of chemical probes in opening up new areas of biology and developing biochemical and molecular understanding.^[6] BET proteins govern the assembly of histone complexes which regulate inflammatory gene expression and therefore represent a point of potential intervention in inflammatory gene expression.^[7] The use of chemical probes in this field was initiated

by the development of small molecule BET inhibitor probes that were structurally related to previously identified small molecule inhibitors of the BET family of bromodomains (**Figure 6.1**).^[7,8]

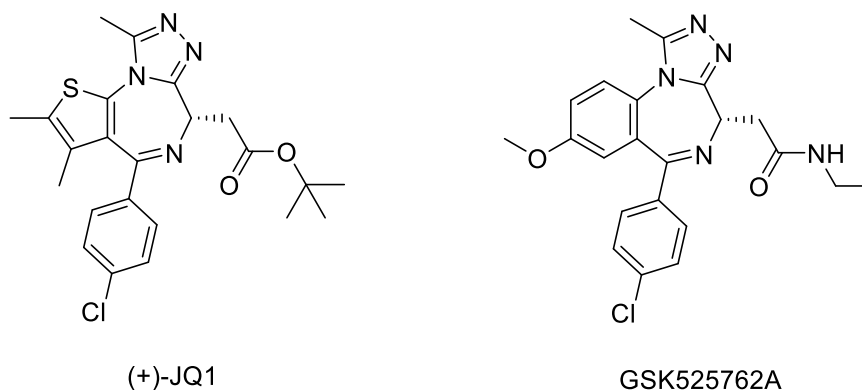


Figure 6.1 Chemical structures of (+)-JQ1^[8] and GSK525762A^[7]; structurally related small molecule BET inhibitor probes which highlighted key protein-protein interactions between BET bromodomains and histone *N*-acetyl lysine residues, highlighting the therapeutic potential of BET inhibition in tumour cell proliferation therapy.

These structurally similar probes were shown to inhibit protein-protein interactions (PPIs) between BET bromodomains and *N*-acetyl lysine residues on histones; subsequently regulating gene expression and suppressing transcription of pro-inflammatory genes involved in the propagation of inflammation and tumour cell proliferation. Facilitated and assisted by the use of chemical probes, these discoveries broadened the therapeutic potential of BET inhibition and ultimately led to the initiation of more BET inhibitor drug discovery programs.^[6]

It is therefore clear that biological probes can be highly diverse and designed with specific purpose to tackle individual research questions within a wide range of clinical and biochemical settings.

In order to address our own research question, a small series of chemical probes were designed and synthesised to monitor the localisation of BITZ derived inhibitors within *Plasmodium* parasites, with the aim of determining any additional proteins to which the BITZ chemical chemotype may be capable to bind. Two distinct chemical probes were used to evaluate whether the BITZ chemotype is indeed capable of binding to additional molecular proteins within the *Plasmodium* parasite and where these protein targets may localise. Consequently, these studies aimed to determine whether enhanced inhibitory activity of BITZ compounds against *Plasmodium* parasite growth, compared to the isolated *Pf*lspD enzyme, is the result of interaction with additional cellular targets within the parasite in addition to the known and confirmed activity against the *Pf*lspD enzyme.

A fluorescent-labelled BITZ inhibitor was designed as an initial tool to evaluate localisation of the BITZ chemotype with *Plasmodium* parasites. In addition, a biotin-tagged probe was generated to facilitate

pull-down assays, using streptavidin-agarose beads, for the purpose of determining the parasite proteins to which the BITZ chemotype can bind.

6.3 Identification of Suitable Chemical Motifs to Generate BITZ and Control Probes

It was proposed that the use of a simple BITZ derivative as the core recognition structure for our fluorescent-labelled and biotin-tagged chemical probes would be appropriate for these studies. Chemical- or activity-probes are generally small-molecule reporters that are designed to be selective for a specified biological target, providing a representative assessment of a particular chemical motif and its behaviour within living cells and organisms.^[1] Generally, chemical probes consist of three distinct parts: a chemical warhead (the drug motif), a spacer region and a specified tag (i.e. a fluorophore or biotin tag).^[1]

With a chemical probe construct such as this, designed probes can also behave as inhibitors of a target enzyme, allowing them to function as suitable mimetics of the chemical chemotype in question, enabling activity, localisation and distribution studies to be conducted within organisms and cells. It was decided that compound **8** (Figure 6.2) would be used as the chemical warhead of BITZ probe molecule **10** (Figure 6.2) with added functionalities to incorporate the required spacer region and appropriate tag molecule, as required for the described probe construct.^[1]

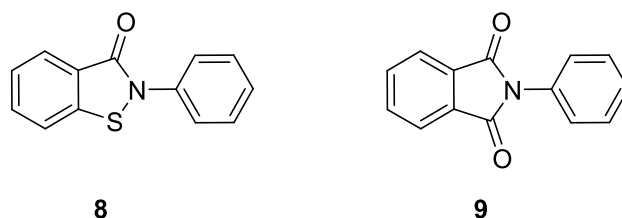


Figure 6.2 Chemical structures of simple BITZ derivative **8** and related isostere 2-phenylisoindoline-1,3-dione, **9**.

As described in **Chapter 2**, **8** is a simple BITZ core derivative with an un-substituted *N*-phenyl ring that functions as a basic side chain and is therefore a very simplified derivative of the original **DT2009-0168020** HTS hit (**Chapter 2**, **Figure 2.8**). Following *PflspD* enzymatic and 3D7 whole cell growth assays, we have shown **8** to be an active inhibitor against the *PflspD* enzyme and *Plasmodium* parasite growth (**Table 6.3**). **8** has consequently been used as a robust reference point for SAR development around the BITZ chemotype (**Chapter 2**, **Section 2.4**) and therefore represents a suitable starting point for the design of inhibitory chemical probes that function as an accurate representative of the BITZ chemotype and derived inhibitors.

Compound number	<i>Pf</i> lspD Inhibition IC ₅₀ (μM)	3D7 Whole Cell Growth Inhibition IC ₅₀ (μM)
8	0.599	5.49
9	> 100	-

Table 6.2 Inhibitory activity of **8** and **9** against *Pf*lspD and *P. falciparum* 3D7 growth in culture.

It was also necessary to generate a control probe which could be used in inhibitor localisation studies and pull-down assays that would be inactive against both the *Pf*lspD enzyme and *Plasmodium* parasite growth. A suitable control motif must be deficient in the ability to inhibit *Pf*lspD and parasite growth and therefore provide a distinction between reactive and non-reactive probes. An appropriate chemical motif for the control probe must therefore lack the 'active' electrophilic sulfur atom and N-S heteroatom bond of the BITZ thiazolone ring. As a result, the related BITZ isostere, 2-phenylisoindoline-1,3-dione (**9**, **Figure 6.2**) was selected as the warhead for the control probe **11** (**Figure 6.3**) as this motif has been shown to be inactive against the *Pf*lspD enzyme (**Table 6.3**) in previous chemotype validation studies (see **Chapter 2, Section 2.4**). Having identified compounds **4** and **5** (**Figure 6.1**) as the warheads for the reactive and non-reactive chemical probe species, these motifs were used for the development of novel BITZ probes and isoindoline-1,3-dione derived control probes respectively.

6.4 Localisation Studies

6.4.1 Fluorescent Molecular Probes

A fluorescent 7-nitrobenza-2-oxa-1,3-diazole (NDB) tagged BITZ probe, and corresponding NBD-tagged control probe were designed and synthesised to facilitate the use of laser scanning confocal microscopy in order to observe the localisation of the BITZ motif and derived inhibitors within the *Plasmodium* parasite.

Fluorescence is highly exploited in the employment of chemical probes and biosensors. To date, a huge variety of fluorescent probes have been designed to enable the recognition and evaluation of a diverse range of molecules and their biochemical effects within biological systems.^[9] Many analytical methods are available for gathering information about the interaction of chemical agents with living cells including absorption and fluorescence spectroscopy, electrochemical methods, fluorescent microscopy, and isotope-based methods. Fluorescent microscopy is a particularly valuable fluorescence imaging technique since it is both straightforward and easily initiated, and now supported by advanced optical and microscopy equipment, with better access to specialised confocal

laser scanning microscopy instruments which can provide enhanced cellular images.^[9] The operational simplicity of fluorescent sensors and probes, alongside their sensitivity and suitability for bio-imaging within living systems, has led to wide spread use and development of this detection technique.^[10]

Various types of fluorescent probe are widely used by analytical scientists, organic chemists, and medical scientists across a vast number of research programs to provide insight into the behaviours of chemical agents within cells and organisms. Fluorescent probes can determine the function of specific proteins and the structural and biological responses of a cell to molecular modifiers. Successful applications of fluorescent probes have been demonstrated by many researchers and are well reviewed in literature.^[4,5,9,11–13,13–24] Whatever the function or application of a fluorescent probe, several requirements need to be accounted for when designing such a molecular probe. A fluorescent molecule should contain: a fluorophore capable of displaying an efficient level of emission which can be observed by the detection instrument, show minimal interference with auto fluorescence from the biological sample, and contain specific functional groups that allows the recognition and interaction of the probe with the appropriate molecular features of the cell or organism under study.^[9]

Fluorophores emit electromagnetic radiation when luminescing at an appropriate excitation wavelength (λ_{ex}). The absorption of a photon of light at λ_{ex} excites the fluorophore from its ground state to an accessible excited electronic state; subsequent relaxation (or radiative deactivation) of the excited fluorophore back to the original ground state results in fluorescence.^[17,25] The fluorescence quantum yield (ϕ_F) of any given fluorophore gives the ratio of photons absorbed to photons emitted *via* fluorescence.^[26]

Considering the requirements outlined above, the NBD fluorophore (highlighted in green, **Figure 6.3**) was selected and incorporated into the NBD-tagged BITZ probe **10** and corresponding NBD-tagged control probe **11** (**Figure 6.3**). **10** and **11** were specifically designed as a fluorescent-labelled inhibitor and a fluorescent-labelled non-inhibitor of the *PflspD* enzyme respectively, to facilitate imaging of the BITZ motif at the cellular level. The chemical warhead of probes **10** and **11** are highlighted in red with the spacer region of each probe highlighted in blue (**Figure 6.3**).

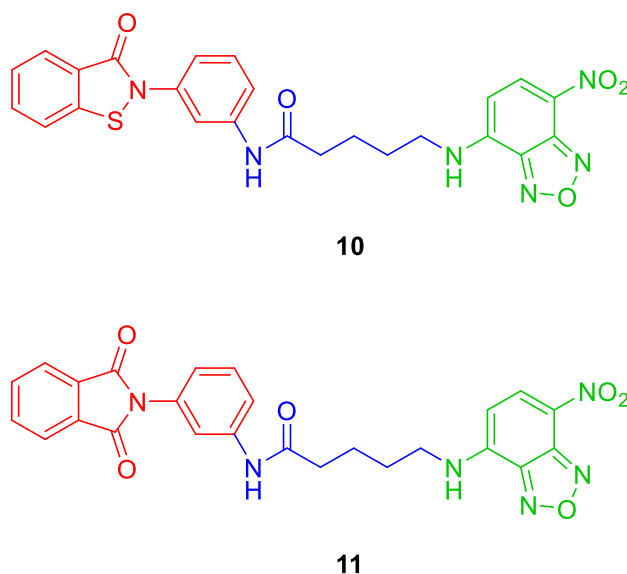


Figure 6.3 Chemical structures of the NBD-tagged BITZ probe **10** and NBD-tagged control probe **11**; chemical warheads are highlighted in red, the spacer regions in blue and NBD fluorophore in green.

4-chloro-7-nitrobenza-2-oxa-1,3-diazole (NDB-Cl) (**Figure 6.4**) is a commercially available, amine-reactive chemical compound where NBD-amine adducts display a fluorescent excitation/emission spectrum of $\lambda_{\text{ex}}/\lambda_{\text{em}} = 464/512$ nm respectively, in aqueous solutions. NDB-Cl is widely used in the labelling of peptides, proteins, drugs and other biomolecules for a broad range of applications.^[17,27] NDB-Cl itself is non-fluorescent but forms highly fluorescent compounds on reaction with amine groups in synthetic amines, amino acids, peptides and proteins; NDB-Cl also reacts with thiol groups to form fluorescent adducts.^[28]

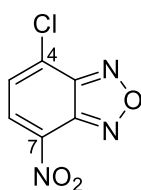


Figure 6.4 Chemical structure of 4-chloro-7-nitrobenza-2-oxa-1,3-diazole (NDB-Cl).

Literature data has illustrated that the nature of substituents attached to the NBD platform have significant influence on the fluorescence quantum yield of the NBD fluorophore. NBD-derivatives with electron withdrawing groups at both the 4- and 7-positions are generally not emissive,^[17] as is the case with the non-fluorescent reagent NBD-Cl (**Figure 6.4**). The transformation of one of these two functionalities into an electron donating group, as is achieved through substitution with an amine, subsequently enabling radiative deactivation of the excited fluorophore and consequently fluorescence emission from the NBD-derivative.^[17] The strong electron withdrawing nitro-group

makes the *para* C-Cl bond highly reactive towards nucleophilic substitution and therefore able to react readily with a wide range of amines, forming fluorescent NBD-derivatives.^[10]

Altogether, the established chemistry of the 2-nitrobenzyl group, alongside the synthetic accessibility of NBD derivatives, the ability to excite the NBD fluorophore with visible photons and the high fluorescence quantum yield of NBD derivatives, all contributed to the selection of the NBD fluorophoric group for the generation of our fluorescent-labelled probes.^[17,27]

6.4.2 Synthesis of the NBD-Tagged BITZ Probe and NBD-Tagged Control Probe

The generation of NBD-tagged BITZ probe **10** required a linear five-step synthesis involving several coupling and de-protection reactions (**Scheme 6.1**). The synthetic strategy was initiated by a simultaneous amide coupling and ring closure between *N*-Boc-*m*-phenylenediamine and the stable and isolatable acid chloride, 2-(chlorothio)-benzoyl chloride **X** (**Figure 6.5**, previously described in **Chapter 2, Section 2.3.3**).^[29,30]

Following coupling of **X** with the mono-Boc protected diamine, the Boc-group of **10a** was removed mediated under acidic conditions by TFA,^[31] to provide the free amine **10b**. **10b** was subsequently coupled with a second mono-Boc protected reagent, Boc-5-Ava-OH, using a standard amide-coupling reaction^[32,33] to give **10c**. The Boc-group of **6c** was also removed under acidic conditions using TFA to generate **10d**.^[34] Boc-5-Ava-OH was incorporated into the outlined syntheses (**Scheme 6.1** and **6.2**) to facilitate the introduction of the required spacer region (highlighted in blue, **Figure 6.3**) within both the NBD-tagged BITZ probe **10** and NBD-tagged control probe **11**.

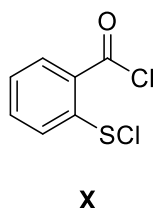
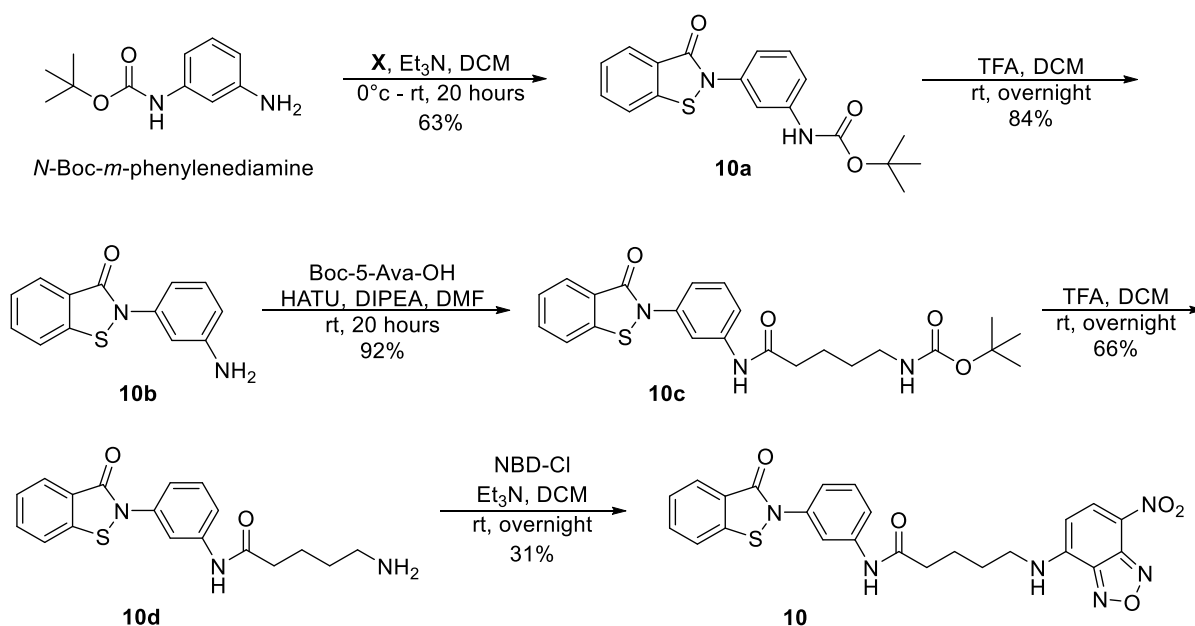


Figure 6.5 Chemical structure of the stable and isolatable acid chloride 2-(chlorothio)-benzoyl chloride **X**.

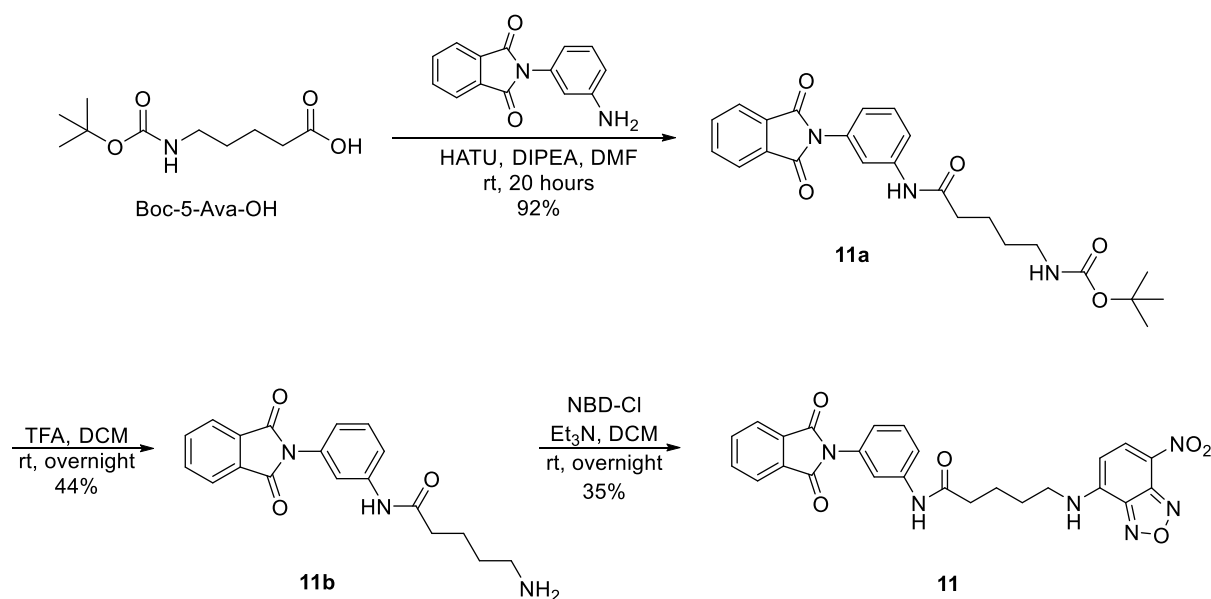
The final step of the illustrated synthesis (**Scheme 6.1**) involved a nucleophilic substitution reaction between **10d** and NBD-Cl to incorporate the NBD fluorophore and generate the fluorescent NBD-amine probe **10**. A similar approach was previously demonstrated by Ellis *et al.* where a comparable synthetic approach and research strategy was employed to determine the parasitic accumulation sites of tetraoxane antimalarial agents using fluorescent microscopy to visualise NBD-tagged tetraoxane derivatives.^[21]



Scheme 6.1 Synthetic strategy for generation of NBD-tagged BITZ probe **10**.

All reactions within the described synthetic route (**Scheme 6.1**) preceded in moderate to high yields, with the exception of the final coupling between **10d** and NBD-Cl to generate **10**. For the generation of the control probe **11**, a shorter three-step synthesis (**Scheme 6.2**) was feasible due to the commercial availability of 2-(3-aminophenyl)-2,3-dihydro-1*H*-isoindole-1,3-dione, which is the *meta*-amine derivative of 2-phenylisoindoline-1,3-dione, **12** (**Figure 6.2**), the structural warhead of **11**.

The first of the three-step synthesis involved amide-coupling of 2-(3-aminophenyl)-2,3-dihydro-1*H*-isoindole-1,3-dione and the mono-Boc protected species, Boc-5-Ava-OH, generating **11a** in an analogous amide-coupling reaction to that describe in the synthesis of **10**.^[32,33] Using HATU as the coupling reagent, this amide-coupling reaction again performed well and proceeded in high yield. TFA-mediated Boc-deprotection of **11a**^[31] subsequently generated the free amine **11b** which was able to undergo nucleophilic substitution with NBD-Cl to incorporate the specified fluorescent NBD functionality and afford the designed control probe **11**.



Scheme 6.2 Synthetic strategy for generation of NBD-tagged control compound **11**.

Across both outlined synthetic strategies (**Scheme 6.1** and **6.2**), the incorporated Boc-deprotection reactions, mediated by TFA,^[31] showed varying efficiency where poor reaction yields appear to correlate with increasing reagent complexity, potentially impeding reaction efficiency. HATU-mediated amide-coupling reactions were efficient and high yielding for both syntheses. Nucleophilic substitution of NBD-Cl with **10d** and **11b**, as outlined by Niu *et al.*^[10] was successful and generated the target compounds in both instances. However, the aromatic nucleophilic substitution was consistently low yielding in the synthesis of both **10** and **11** which was a contrast to the results demonstrated by Niu *et al.*^[10]

6.4.3 Inhibitory Activity of the NBD-Tagged BITZ Probe and NBD-Tagged Control Probe Against *PflspD*

Having generated both the NBD-tagged BITZ probe **10** and the NBD-tagged control probe **11**, it was necessary to determine the extent of their inhibitory activity against the *PflspD* enzyme. If selection of the 2-phenylisoindoline-1,3-dione motif (**9**, **Figure 6.2**) was appropriate for the chemical warhead of the control probe **11** (**Figure 6.3**), a lack of inhibitory activity against *PflspD* on exposure to **11** should be seen. In direct contrast, there was a strong requirement for the NBD-tagged BITZ probe **10** to exhibit inhibitory activity against the *PflspD* enzyme. Ideally, a comparable or enhanced IC₅₀ value to that displayed by (**8**, **Table 6.2**) would be seen therefore enabling **10** to function as an accurate BITZ inhibitor mimetic, providing a representative picture of BITZ chemotype behaviour within the parasite.

Evaluation of **10** and **11** in the *PflspD* enzymatic assay^[35] (previously discussed in **Chapter 2, Section 2.2.3**) highlighted that we were correct in our assessment and selection of the required chemical warheads for the BITZ probe (**10**) and control probe (**11**). The NBD-tagged BITZ probe **10** was found to have an IC₅₀ value of 0.335 μM against the *PflspD* enzyme and is therefore almost twice as potent against the enzyme as the simple BITZ derivative **8**. Whereas **11** was shown to be inactive against *PflspD*, with an IC₅₀ value of > 40 μM (**Table 6.4**).

Compound number	<i>PflspD</i> Inhibition IC ₅₀ (μM)	SEM value (n = 3)
10	0.335	0.073
11	> 40	-

Table 6.4 Inhibitory activity of NBD-BITZ probe **10** and control probe **11** against the *PflspD* enzyme; mean IC₅₀ and SEM values given which are representative of n = 3 replicates.

The lack of activity displayed by **11** confirms that the 2-phenylisoindoline-1,3-dione derived headgroup is a suitable chemical control, again demonstrating that loss or replacement of the sulfur heteroatom in the thiazolone ring (B ring) of BITZ abolishes *PflspD* inhibitory activity. It is also evident that the extent of *PflspD* activity loss, comparing **10** and **11**, is of a similar magnitude to that observed between **8** and **9**; where greater than a 100-fold potency loss was observed in each case on alteration of the BITZ headgroup. Overall, the measured *PflspD* enzymatic activity data illustrates that **10** and **11** can be used effectively as fluorescent probes to assess the behaviour and localization of BITZ derived inhibitors in *Plasmodium* parasites, monitoring the cellular accumulation of these compounds by fluorescent microscopy.

6.4.4 Inhibitory Activity of the NBD-Tagged BITZ Probe and NBD-Tagged Control Probe Against 3D7 *P. falciparum* Parasite Growth

Since use of the NBD-tagged BITZ probe in fluorescent microscopy aims to assess localization of the BITZ chemical motif within *Plasmodium* parasites by observation of the whole cell, it was also appropriate to determine the inhibitory activity of **10** and **11** against *P. falciparum* growth in culture. As previously described (see **Chapter 2, Section 2.3.5**), a DNA-based microfluorometric assay measuring the extent of *P. falciparum* growth in culture, after treatment with various chemical agents, is used to determine the ability of a compound to inhibit parasite growth. This assay is facilitated by the detection of parasite DNA intercalation with PicoGreen®, an ultrasensitive fluorescent nucleic acid dye.^[36]

Having generated the fluorescent BITZ probe and control probe, **10** and **11**, incorporating the NBD fluorophore to achieve compound fluorescence, the described whole cell *P. falciparum* growth assay using PicoGreen® as the nucleic acid detection dye, was no longer appropriate to assess levels of parasite growth inhibition. This is a result of overlap between the excitation (λ_{ex}) and emission (λ_{em}) wavelengths of the NBD-amine fluorophore present in **10** and **11** and PicoGreen® (**Table 6.5**).

Fluorophore	Excitation/Emission Wavelengths (nm)
NBD-amine	464/512
PicoGreen®	485/520
Hoechst 33258	352/455
Acridine Orange	460/530

Table 6.5 Excitation (λ_{ex}) and emission (λ_{em}) wavelengths (in nm) of various fluorophores.

The overlapping excitation (λ_{ex}) and emission (λ_{em}) spectra of the NBD-amine and PicoGreen® fluorophores prevents the use of the *P. falciparum* growth assay as previously employed.^[37,38] Interference between the two fluorophores would distort measurement of the PicoGreen® nucleic acid detection dye, therefore misrepresenting the magnitude of *P. falciparum* growth inhibition. Consequently, an alternative nucleic acid dye was required, displaying a $\lambda_{ex}/\lambda_{em}$ spectrum distinct from the NBD-amine fluorophore to enable the activity of **10** and **11** against *P. falciparum* parasite growth in culture to be determined.

Hoechst 33258 was identified as a suitable nucleic acid dye to replace PicoGreen® in our *P. falciparum* growth assay since the $\lambda_{ex}/\lambda_{em}$ spectra of NBD-amine and Hoechst 33258 are appropriately distinct (**Table 6.5**). In order to assess the efficiency of Hoechst 33258 as a nucleic acid detection dye within the *P. falciparum* growth assay, a test assay was conducted using untreated *P. falciparum* culture and a two-fold parasitaemia (Pt) dilution series. The parasite DNA content of untreated cultures in two parallel assays was measured independently with both Hoechst 33258 and PicoGreen® to provide a measure of assay efficiency and read-ability using each dye (**Figure 6.6**).

The linear relationship observed between the detected levels of Hoechst 33258 fluorescence and the parasitaemia of *P. falciparum* culture, illustrates that Hoechst 33258 is a suitable replacement for PicoGreen® as a nucleic acid dye within the *P. falciparum* growth assay. This result therefore enabled measurement of the inhibitory *P. falciparum* parasite growth activity of **10** and **11** using the standard *P. falciparum* parasite growth assay.

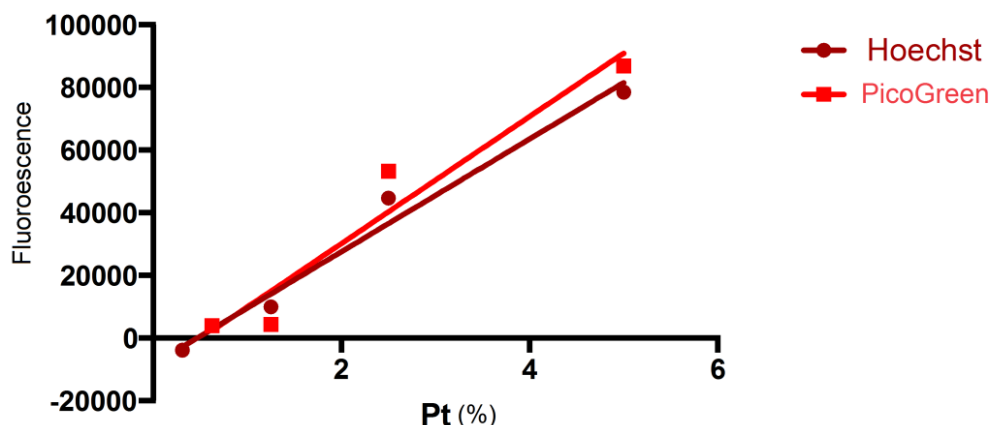


Figure 6.5 Comparison of the detected fluorescence from *P. falciparum* infected cultures determined using microfluorimetrics, measured separately using Hoechst 33258 and PicoGreen® as nucleic acid dyes. Asynchronous *P. falciparum* infected culture was used in the assay which was set up using a two-fold series dilution of parasitaemia.

Further analysis of the collected data highlighted that both high and comparable R^2 values were determined with the use of each nuclear dye (PicoGreen® $R^2 = 0.9385$; Hoechst 33258 $R^2 = 0.9773$). R-squared (R^2), the coefficient of determination (ranging from 0 and 1), defines the proportion of variance in a dependent variable that is predictable from an independent variable. The resulting value of R^2 therefore indicates the extent to which the dependent variable can be predicted by the independent variable, consequently providing a measure of accuracy.^[39,40] R^2 values close to a value of one indicate that a model can explain the majority of variability seen in measured data and therefore gives confidence in the parameters or protocol being measured.^[39] Hence R^2 analysis of the DNA-based microfluorometric assay (**Figure 6.6**) gives confidence in the use of Hoechst 33258 as a nucleic acid dye to provide an accurate measurement of the inhibitory activity of **10** and **11** against *P. falciparum* parasite growth.

Despite this encouraging assessment, application of the adapted whole cell assay using Hoechst 33258 did not produce interpretable results. It is possible that reduced sensitivity of Hoechst 33258, as a DNA intercalator, compared to PicoGreen® is responsible for the lack of interpretable results in the adapted assay protocol.^[36] As such, further work is needed to identify a suitable fluorescent nucleic acid dye, or an alternative assay procedure, to enable the inhibitory activity of fluorescent probes **10** and **11** to be determined against *P. falciparum* parasite growth.

6.4.5 Localisation Studies using Fluorescent Microscopy

To identify the cellular localisation of the inhibitory *PflspD* BITZ motif, a series of incubation and localization experiments were performed to enable the fluorescent imaging of BITZ probe **10** in 3D7 culture. These studies were also mirrored by analogous control experiments using the non-BITZ control probe **11**, shown to be inactive against the *PflspD* enzyme (**Table 6.4**).

To initiate this body of work, protocol modifications were conducted to determine optimal conditions for incubation of 3D7 *P. falciparum* cultures with fluorescent probes **10** and **11**, prior to visualisation of the treated cultures by fluorescent microscopy. It was found that an overnight incubation period of ~ 20 - 22 hours, maintaining 500 μ L of parasite culture at 37 °C in an atmosphere of 5% O₂; 5% CO₂ and 90% N₂, with a 1:1000 dilution factor of **10** and **11**, to be most optimal. Asynchronous parasite cultures were used to enable visualisation of *Plasmodium* parasites at all stages of the parasite life cycle. A high level of parasitaemia was maintained within cultures to ease the identification of parasite infected cells and therefore enable cellular images to be easily captured during fluorescent, live-imaging microscopy.

Fluorescent microscopy was carried out using Olympus BH8 and Olympus Fluoview FV1000 confocal microscopes to visualise the fluorescent NBD-tagged BITZ probe **10** and the fluorescent NBD-tagged control probe **11** within *P. falciparum* infected cultures. Hoechst 33258 nucleic acid dye was also added to the treated cultures to enable the identification of parasite nuclei by blue ultraviolet (UV) light and therefore inform the assessment of BITZ compound localisation with respect to parasite nuclei.

Imaging of treated parasite cultures (**Figures 6.6 - 6.9**) immediately revealed that both the fluorescent BITZ probe **10** and control probe **11** are able to penetrate the cell and continue to emit green fluorescence at an easily detectable level. An extensive range of images were obtained using live microscopy imaging, facilitated with the Olympus Fluoview FV1000 confocal microscope; a selection of representative images are presented in **Figures 6.6 - 6.9**. **Figures 6.6** and **6.7** depict 3D7 *P. falciparum* parasite cultures that were treated with fluorescent BITZ probe **10**; whereas **Figures 6.8** and **6.9** exemplify selected parasite cultures that were treated with the fluorescent control probe **11**.

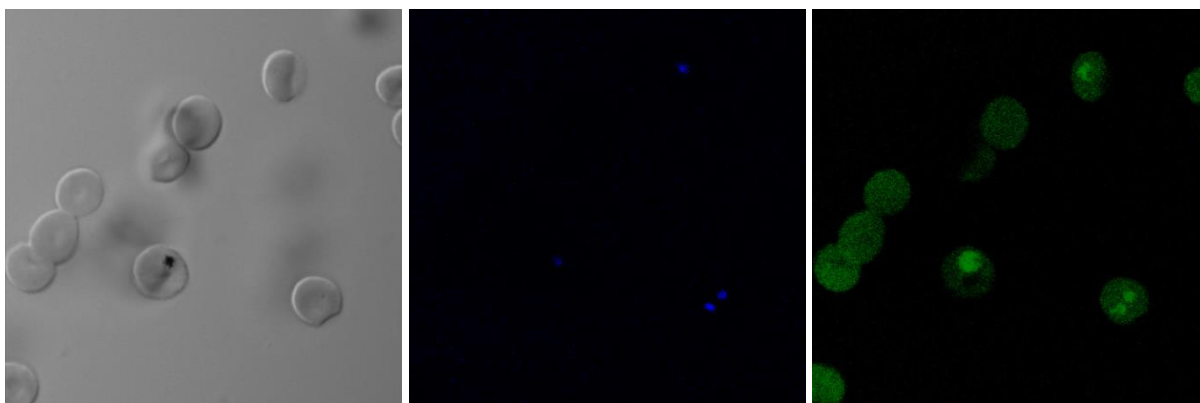


Figure 6.6 Representative images of BITZ probe **10** after incubation with 3D7 *P. falciparum* cultures; images of infected cells were taken using white light, blue UV light and green UV light providing a phase image, visualisation of parasite nuclei and the fluorescent BITZ probe respectively.

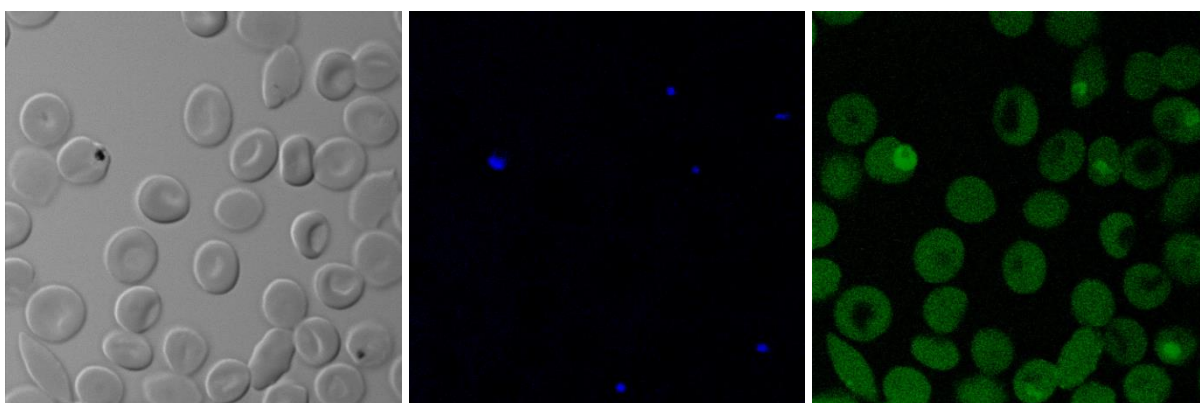


Figure 6.7 Representative images of BITZ probe **10** after incubation with 3D7 *P. falciparum* cultures; images of infected cells were taken using white light, blue UV light and green UV light providing a phase image, visualisation of parasite nuclei and the fluorescent BITZ probe respectively.

The microscopy images taken using natural (or white) light provide phase contrast and were used to initially identify and focus on a parasite infected cells of interest for further fluorescent imaging. A short exposure time of 1/200 of a second was required to capture phase images. Blue UV light was used to view the nuclear Hoechst 33258 dye which enables cells to be seen under UV light and consequently parasite nuclei to be identified; a slightly longer exposure time of 1/10 of a second enabled these images to be obtained. The GFP (green fluorescent protein) images were obtained using green UV light and depict the NBD-tagged probe compounds following incubation with the parasite cultures. An exposure time of 2 seconds was required for these images.

These described localisation studies, facilitated by fluorescent microscopy, are only in preliminary stages but some initial conclusions have been drawn. As illustrated in **Figures 6.6** and **6.7**, a clear distinction in cellular localisation is observed between the Hoechst nuclear dye and our fluorescent BITZ probe **10**, highlighting that the BITZ chemotype and derived compounds are excluded from the parasite nucleus. It can also be seen that green fluorescence distribution is cytoplasmic, with reasonably uniform distribution across the cell. In addition, green fluorescence appears also to be

excluded from the parasite food vacuole, although further microscopy studies should be conducted to validate this.

Whilst it may not be apparent from the representative images provided here, more extensive and ongoing microscopy work has highlighted that the accumulation of fluorescent BITZ probe **10** appears to be parasite selective. In other words, penetration of the fluorescent NBD-tagged probes **10** and **11** was not observed in red blood cells (RBCs) that were not infected with *Plasmodium* parasites.

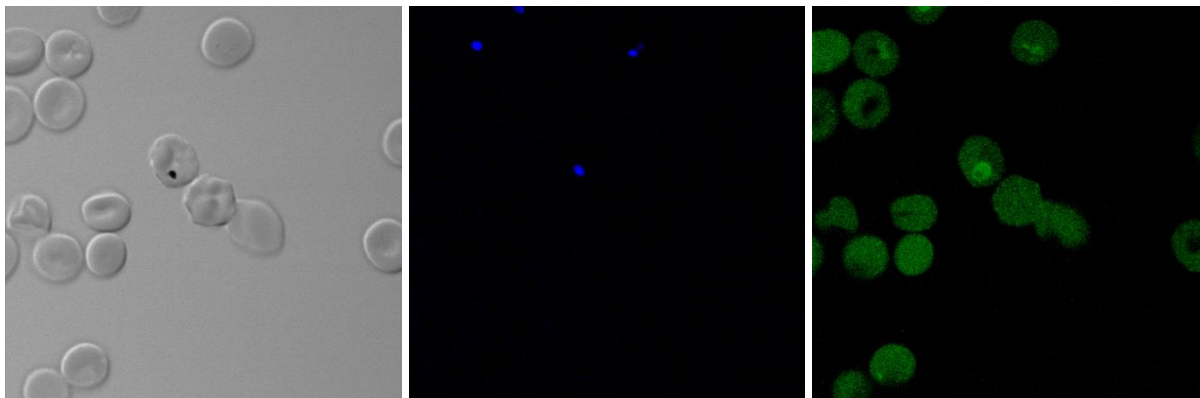


Figure 6.8 Representative images of BITZ probe **11** after incubation with 3D7 *P. falciparum* cultures; images of infected cells were taken using white light, blue UV light and green UV light providing a phase image, visualisation of parasite nuclei and the fluorescent BITZ probe respectively.

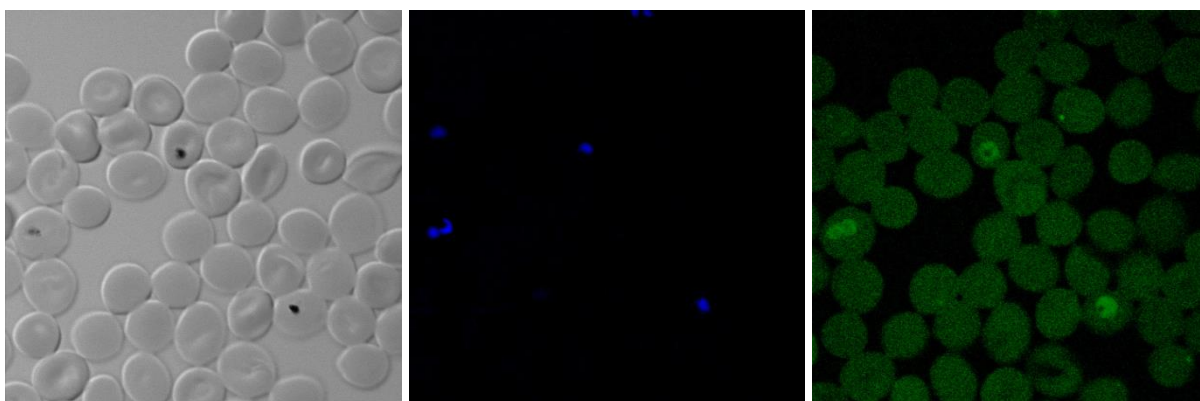


Figure 6.9 Representative images of BITZ probe **11** after incubation with 3D7 *P. falciparum* cultures; images of infected cells were taken using white light, blue UV light and green UV light providing a phase image, visualisation of parasite nuclei and the fluorescent BITZ probe respectively.

Figures 6.8 and **6.9** provide representative images of the microscopic observations following the treatment of 3D7 *P. falciparum* cultures with the fluorescent control probe **11**. Interestingly, no distinct contrast in fluorescence patterns are observed by comparison of these images (**Figures 6.8** and **6.9**) to those obtained after treatment of 3D7 *P. falciparum* cultures with fluorescent BITZ probe **10** (**Figures 6.6** and **6.7**). **Figures 6.8** and **6.9** highlight that green fluorescence distribution remains cytoplasmic with probe compound **11** and is excluded from both the parasite nucleus and food vacuole. This observation is perhaps somewhat unexpected since it has already been shown that control probe **11** is inactive against the *Pf*ispD enzyme (**Table 6.4**). As a result of this, we may have

expected to see a difference in cellular distribution compared to BITZ probe **10**, which is known to actively inhibit *Pf*lspD (**Table 6.4**).

It is therefore clear that additional fluorescent microscopy is required to further evaluate BITZ treated *Plasmodium* parasite cultures and determine a more precise localisation pattern of the BITZ chemotype. In turn, it may then be possible to highlight any contrasting patterns of distribution that may be observed with chemical motifs that do not inhibit the *Pf*lspD enzyme. Additional microscopy studies should also be considered to shed further light on the behaviour of these chemical probes within *Plasmodium* parasite and RBCs. Indeed, the use of an apicoplast marker could be introduced to more explicitly highlight the organelle within the parasite, providing a clearer indication of BITZ localisation with respect to this cellular component. The apicoplast is a plastid organelle that is a unique feature of Apicomplexan species and houses the MEP biosynthetic pathway and constituent enzymes.^[41] Therefore, analysis of BITZ probe localisation in *Plasmodium* infected RBCs, with an added awareness of this crucial and highly relevant parasite organelle, may enable more informed fluorescent microscopy studies from here-on in.

Furthermore, an assessment of cellular morphology, facilitated by GIEMSA staining of cultures in a non-fluorescent microscopy setting, could highlight and physiological differences that may be apparent between BITZ-treated and untreated cells. Consequently, such a study has the potential to highlight any effects on cell that may be induced by treatment with BITZ compounds in terms of cellular health and viability.

6.5 Protein Binding Assays

6.5.1 Streptavidin Affinity Pull-down Assays

An alternative biochemical method, suitable for determining the parasite proteins to which the BITZ chemotype can bind, is a peptide pull-down assay. Pull-down assays are used to identify the natural binding partners of captured proteins or chemical agents and can also confirm the presence of a protein species or an enriched protein within a biological or cellular system. Therefore, pull-down experiments can be used to determine the interactions that occur between a biochemical probe and un-identified proteins, as well as confirm suspected interactions between a probe protein and a known protein.^[42]

Pull-down assays represent an *in vitro* method of affinity purification where a 'bait molecule' is used to tag and capture proteins, quickly isolating the proteins which are able to bind to the 'bait molecule' (or tag) and allowing their identification.^[43] The 'bait molecule' must therefore contain a functional or chemical recognition element (or 'warhead': represented by a red triangle, **Figure 6.10**) that is able to

capture certain proteins within cell lysate. The 'bait molecule' must also contain a separate reactive 'tag' (represented by a green star, **Figure 6.10**) that is able to bind to a specific affinity ligand, enabling capture of the probe and consequently identification of the proteins which are bound to the chemical recognition element of the probe.

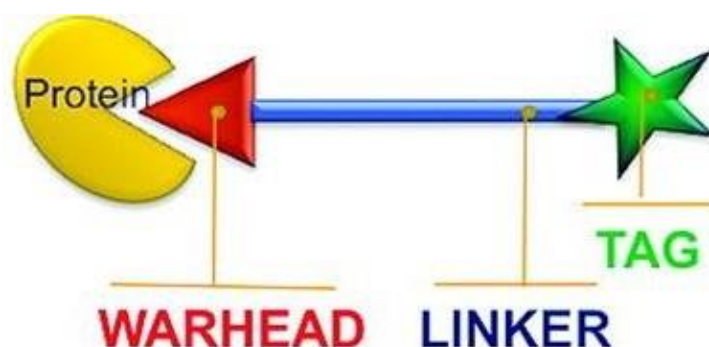


Figure 6.10 Illustration of the general components and construct of a chemical probe for use in protein binding, pull-down assays: image reproduced from ^[44].

A number of reactive 'tags' are commonly used within these labelling experiments where each 'tag' has a specific affinity ligand to which it is able to bind; a number of tag-affinity ligand pairs are summarised in **Table 6.6** below.^[43]

Tag Molecule	Affinity Ligand
Glutathione S-transferase (GST)	Glutathione
Poly-histidine	Nickle or Cobalt chelate complexes
Biotin	Streptavidin

Table 6.6 Commonly used protein-reactive 'tags' and their associated affinity binding ligands.^[43]

The binding of a reactive 'tag' to its immobilised affinity ligand generates a secondary affinity support, enabling proteins that have become attached to the chemical recognition element ('warhead') of the probe following exposure to a protein source (i.e. cell lysate), to be identified. Following incubation with nuclear extract, the secondary affinity support is extensively washed, allowing the separation of bound and un-bound proteins; bound proteins are then released and eluted from the support to enable their purification and identification. The method of protein release and elution is generally specific to the affinity ligand used, and can be modified as appropriate.^[43,45] In addition to its simplicity, another advantage to a peptide pull-down assay is the unbiased nature of the approach, which allows the identification of binding partners, even if they had not been considered likely binding

candidates.^[45–47] As a result, this methodology is appropriate for addressing research questions considering off-target effects of molecular and chemical agents.

A commonly used peptide pull-down experiment is the streptavidin-agarose pull-down assay as it is easy to perform and does not require the use of radiolabelled probes.^[48] Employment of the biotin-streptavidin tag-affinity ligand pair (**Table 6.6**) facilitates this assay, which involves the incubation of nuclear extract from a specific cell with biotinylated molecular probes and streptavidin-agarose beads. These beads capture and immobilise any proteins within the nuclear extract that are able to bind to the chemical recognition element (biotin) of the molecular probes. The cellular proteins bound to the resulting biotin-streptavidin complex can then be dissociated from the support and identified using a number of methods, such as Western blotting and LC-MS/MS.^[48] A streptavidin-agarose pull-down assay can therefore quantitatively analyse an array of proteins to which a probe molecule is found to bind.^[48] Biotinylated probes are compounds or proteins that have been labelled with biotin (**Figure 6.11**) and also contain a specific chemical recognition element (or ‘warhead’, see **Figure 6.10**), the cellular reactivity of which is likely under investigation.

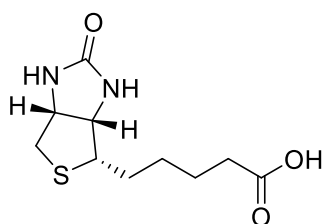


Figure 6.11 Chemical structure of biotin.

The model pull-down technique is an invaluable tool for enabling the enhanced study of cellular pathways, the PPIs (protein-protein interactions) that occur within them and how small molecular or chemical agents may interact with components in a defined biological pathway. It is perhaps most common for pull-down assays to be used in the confirmation or detection of PPIs within a cell or biological system, where a ‘bait protein’ is tagged and captured using a specific affinity ligand, enabling the identification of cellular proteins which interact with the bait protein.^[43] Within the context of our research, the use of a streptavidin pull-down assay will involve tagging a chemical probe as a ‘bait molecule’ to both confirm and detect the proteins to which the BITZ chemical motif is able to bind within *Plasmodium* parasites.

Consequently, the aim of our own streptavidin pull-down assay is to incubate *Plasmodium* parasite nuclear extract with a biotinylated BITZ probe in the presence of streptavidin-conjugated agarose beads. Proteins in the parasite nuclear extract, with which the BITZ chemotype can interact, will bind to the BITZ motif that is incorporated as the ‘warhead’ of our biotinylated chemical probes (**Figure**

6.12). Following BITZ-protein binding events, the entire complex can bind to the streptavidin-agarose beads *via* interaction of the biotin tag. Having immobilised the biotinylated probe on streptavidin-agarose beads, the proteins bound to the BITZ motif can then be identified and analysed.^[48] The streptavidin-agarose pull-down has been shown to be a suitable tool for the analysis of PPIs and protein-chemical interactions in a number of diverse research projects ^[1,6,44,45,48–56] and therefore represents an appropriate assay for our own research, enabling the question of promiscuous binding of the BITZ motif to be addressed.

The biochemical streptavidin pull-down method was therefore employed to facilitate the unbiased identification of proteins to which the BITZ chemotype and derived inhibitors can bind in *Plasmodium* parasites.

6.5.2 Design of Biotinylated BITZ and Control Probes

It was necessary to generate a biotinylated BITZ probe compound, accompanied by an appropriate control probe, to enable application of the described streptavidin pull-down technique. The ‘bait molecules’, as discussed, are represented by the designed biotinylated chemical probes **12** and **13** (Figure 6.12). In order to generate a biotinylated BITZ probe and control probe, a similar design strategy, mirroring the rationale employed for generation of the fluorescent NBD-tagged BITZ probe and control probe, **10** and **11** (Section 6.3 and 6.4) was used. The simple BITZ derivative **8** and related 2-phenylisoindoline-1,3-dione isostere, **9** (Figure 6.2), were again selected as warheads for the active and non-active biotin-tagged BITZ probe and biotin control probe respectively.

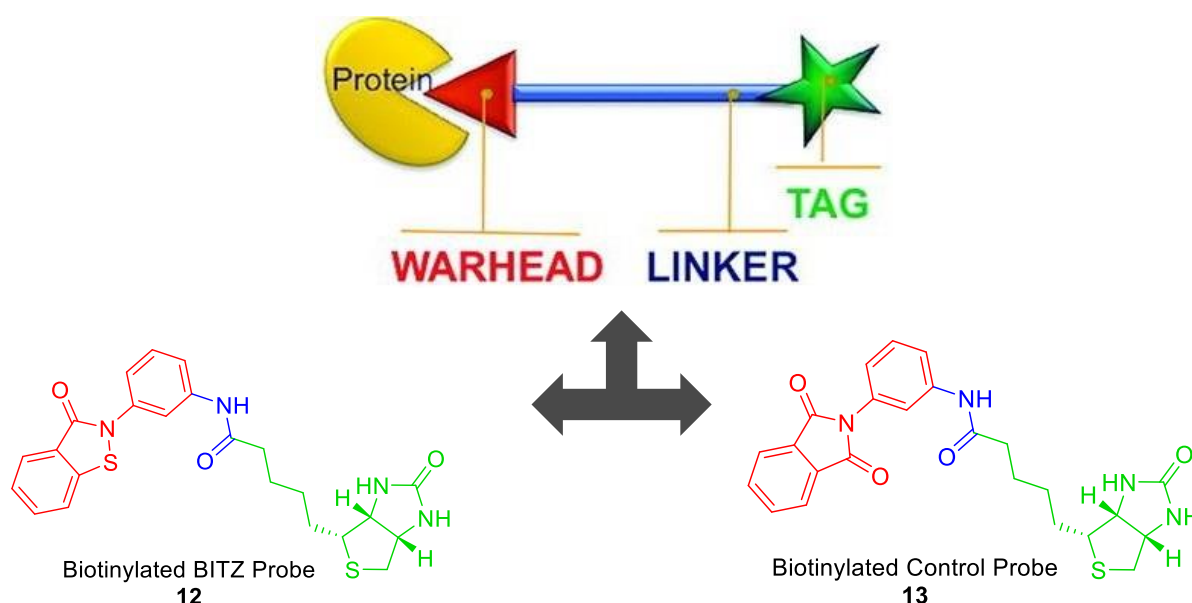
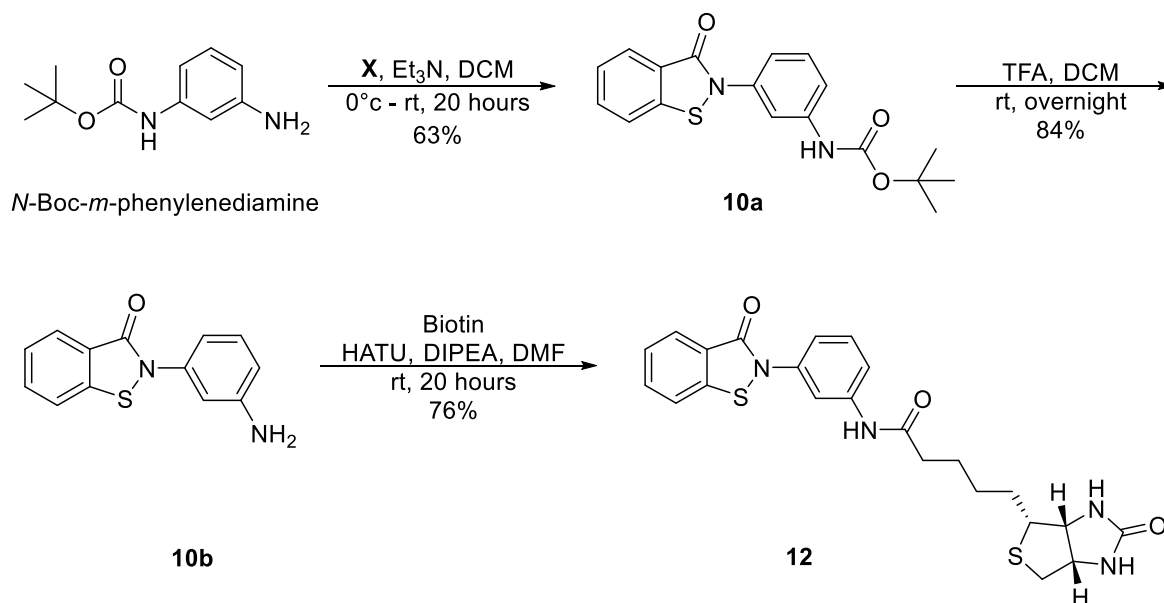


Figure 6.12 Biotin probe motif and resulting structures of the biotinylated BITZ probe **12** and biotinylated control probe **13**; image reproduced from ^[44].

Work by others has found that carbamate-biotin and amide-biotin connections are amongst the most stable linkages that can be used in the biotinylation of chemical compounds.^[44,56] Since an amide-biotin linkage is easily generated between our selected chemical warheads and the carboxylic acid side chain of biotin (**Figure 6.12**), this linkage was incorporated into both the biotinylated BITZ probe **12** and biotinylated control probe **13**, reflecting a design strategy that has been successfully demonstrated in previous work by others.^[44]

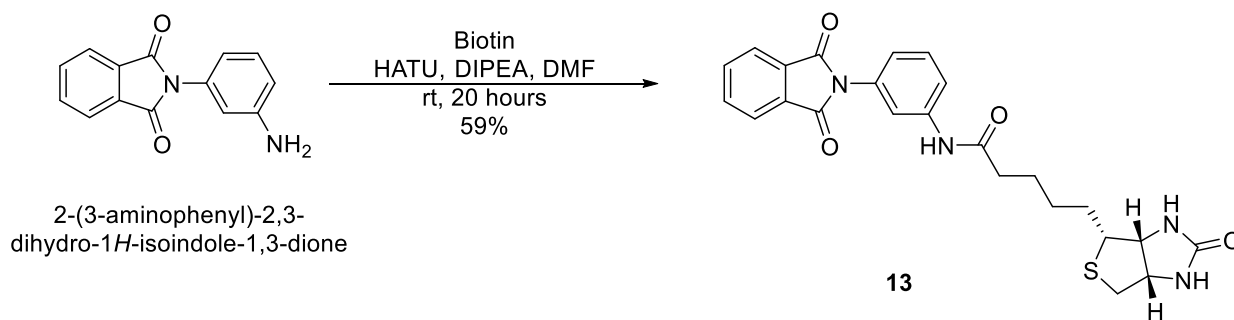
6.5.3 Synthesis of the Biotinylated BITZ Probe and Control Probe

The generation of biotinylated BITZ probe **12** was achieved using a three-step synthesis, in which all reactions proceeded in moderate to high yields (**Scheme 6.3**). Analogous to the synthesis of NBD-tagged BITZ probe **10** (**Figure 6.3**), the first two synthetic steps involved an amide coupling and ring closure between the mono-Boc protected diamine, *N*-Boc-*m*-phenylenediamine, and the stable and isolatable acid **X** (**Figure 6.5**) to give **10a**.^[29,30] This was followed by removal of the Boc-protecting group, mediated by TFA,^[31] to generate the free amine **10b**.



Scheme 6.3 Synthetic strategy for generation of biotinylated BITZ probe **12**.

The final step of the synthesis required the use of an amide-coupling reaction^[32,33] in which **10b** was coupled to biotin to generate the target biotinylated BITZ probe **12**. Due to the commercial availability of 2-(3-aminophenyl)-2,3-dihydro-1*H*-isoindole-1,3-dione, which comprises the structural warhead of **13**, this biotinylated control probe was generated in a single synthetic step using the same synthetic procedure (**Scheme 6.4**).



Scheme 6.4 Synthetic strategy for generation of biotinylated control probe **13**.

The depicted single-step amide-coupling^[32,33] between 2-(3-aminophenyl)-2,3-dihydro-1*H*-isoindole-1,3-dione and biotin proceeded in moderate yield. It was noted that the amide-coupling reactions carried out with biotin (see **Schemes 6.3** and **6.4**) generally performed less well than amide-coupling reactions with the Boc-5-Ava-OH reagent as the carboxylic acid coupling partner, in similar reactions for the synthesis of **10** and **11** (**Schemes 6.1** and **6.2**).

6.5.4 Inhibitory Activity of the Biotin-Tagged BITZ Probe and Biotin-Tagged Control Probe Against *PflspD*

Having generated the biotinylated BITZ probe **12** and corresponding control probe **13**, the inhibitory activity of these two compounds was determined against the *PflspD* enzyme using the discussed *PflspD* enzymatic assay^[35] (see **Chapter 2, Section 2.2.3**). The biotinylated BITZ probe **12** was found to have an IC₅₀ value of 0.632 μM against the *PflspD* enzyme (**Table 6.7**) and therefore demonstrates comparable activity to that of the simple BITZ derivative **8** (**Table 6.3**). In contrast, the biotinylated control probe **13** was found to be inactive against *PflspD*, with an IC₅₀ value of > 40 μM (**Table 6.7**).

Compound number	<i>PflspD</i> Inhibition IC ₅₀ (μM)	SEM value (n = 3)
12	0.632	0.028
13	> 40	-

Table 6.6 Inhibitory activity of biotinylated BITZ probe **12** and control probe **13** against the *PflspD* enzyme; mean IC₅₀ and SEM values given which are representative of n = 3 replicates.

The determined activities of **12** and **13** (**Table 6.7**) are highly analogous to the *PflspD* inhibitory activities of the fluorescent NBD-tagged probes **10** and **11** (**Table 6.4**). The BITZ-derived chemical probes **10** and **12** demonstrate potent and comparable activity, in the low micromolar region, against the *PflspD* enzyme. Whereas, the non-BITZ control probes **11** and **13**, using the 2-phenylisoindoline-1,3-dione motif **9** (**Figure 6.2**) as the chemical ‘warhead’ were both found to be inactive against the

PflspD enzyme, with measured IC_{50} values consistently $> 40 \mu\text{M}$. This therefore validates the use of the 2-phenylisoindoline-1,3-dione motif, **9** (Figure 6.2), as an inactive chemical motif against the *PflspD* enzyme and an appropriate headgroup for the biotinylated control probe **13**. Consequently, these results show that the biotinylated probes **12** and **13** are suitable for use in the previously described streptavidin affinity pull-down assays (Section 6.5.1) to determine the *Plasmodium* parasite proteins to which the BITZ chemotype, and therefore derived inhibitors, are able to bind and potentially inhibit.

6.5.5 Inhibitory Activity of the Biotin-Tagged BITZ Probe and Biotin-tagged Control Probe Against 3D7 *P. falciparum* Parasite Growth

The antimalarial activity of the biotinylated BITZ probe **12** and the biotinylated 2-phenylisoindoline-1,3-dione control probe **13** must also to be evaluated against 3D7 *P. falciparum* parasite growth. Demonstration of significant phenotypic antimalarial activity by **12** and a contrasting lack of antimalarial activity by **13** would confirm these two compounds ideal antimalarial probes with which to conduct the described streptavidin affinity pull-down experiments. Unfortunately, very poor solubility of **12** and **13** has meant that, as yet, it has not been possible to determine the inhibitory activity of either of these biotinylated probes against 3D7 *P. falciparum* parasite growth. As a result, the discussed streptavidin affinity pull-down experiments are currently suspended until this data can be obtained.

6.6 Conclusions and Future Work

A small series of chemical probes have been designed and synthesised to address the question of BITZ chemotype localisation with *Plasmodium* parasite infected cells and potential off-target reactivity of the BITZ chemotype and derived *Pf*lspD inhibitors.

In addition to fluorescent NBD-tagged and biotin-tagged probes generated directly around the BITZ chemotype, the related but distinct 2-phenylisoindoline-1,3-dione chemotype and BITZ isostere was employed as a suitable motif around which control compounds were generated for each probe. Use of the *P. falciparum* lspD enzymatic assay has highlighted a strong activity distinction between the BITZ probes and control probes, consistent in both the fluorescent and biotinylated probe series. The control probes (**11** and **13**) display ~ 100-fold loss of inhibitory activity against the *Pf*lspD enzyme compared to the corresponding BITZ derived probes (**10** and **12**).

The fluorescent NBD-tagged BITZ probe was generated to facilitate localisation studies of the BITZ chemotype by means of fluorescent microscopy. Incubation of the BITZ probe with 3D7 *P. falciparum* cultures and visualisation of the resulting cultures using the Olympus Fluoview FV1000 confocal microscope has shown that the designed BITZ probe is able to penetrate host RBCs and emit detectable fluorescence from within the cell. The resulting fluorescence pattern shows that distribution of the BITZ probe is broadly cytoplasmic, where the compound is excluded from both the parasite nucleus and food vacuole. Since comparable patterns of fluorescence are also observed with the corresponding non-BITZ (and *Pf*lspD inactive) control compound, further investigations must be conducted to further evaluate BITZ treated *Plasmodium* cultures and determine more precise localisation patterns of the BITZ chemotype and how they may be distinct from the distribution of non-*Pf*lspD inhibitors within the cell. Addition of an apicoplast marker as a supplementary visualisation tool represents an initial approach that could be taken. Additional studies will also be conducted to assess cellular morphology and the physiological effects of BITZ compound treatment on both parasite-infected and non-infected RBCs.

A biotinylated probe of the BITZ chemotype, and a non-BITZ biotinylated control probe, have been prepared to facilitate a controlled streptavidin pull-down strategy to provide a direct assessment of the proteins to which BITZ is able to bind within a solution of *P. falciparum* parasite lysate. Elution of proteins bound to the BITZ probe and subsequent analysis by LC-MS/MS would identify the parasite proteins bound to the BITZ chemotype in an unbiased BITZ-protein binding assessment. Disappointingly, a lack of compound solubility in the resulting biotinylated probes has prevented use

of the *P. falciparum* parasite growth assay and, as a result, a measure of inhibitory activity against *Plasmodium* parasite growth has not yet been obtained for these compounds.

Since this phenotypic activity data is required before protein pull-down assays can be initiated, attentions must first focus on improving the solubility of biotinylated BITZ probes, enabling the *P. falciparum* parasite growth assay to be conducted. An initial approach should consider modifying chemical components of the probe structures to promote the solubility of resulting compounds. Since the chemical recognition element (the BITZ chemotype) and 'tag' component (biotin) cannot be modified, variation of the linker group within the probe motif, should be addressed. Previously, amide-biotin linkages were incorporated into designed biotinylated probes since this linkage was easily generated between the BITZ warhead and the carboxylic acid side chain of biotin. Since work by others has identified that a carbamate-biotin group also represents a stable linkage,^[44,56] this functionality should be incorporated as an alternative group to the amide-biotin linker with the purpose of improving the solubility of the resulting probe structure. Following this, more structurally divergent biotinylated BITZ probes should also be explored in order to generate the required chemical probes with appropriate pharmacokinetic properties. This will enable the inhibitory activity of the required BITZ probes to be assessed within the *P. falciparum* parasite growth assay, ultimately allowing the streptavidin pull-down assays to be conducted to determine the extent of BITZ chemotype off-target binding with *Plasmodium* parasite proteins.

6.7 Experimental

For general chemical and biological methodologies see **Chapter 2, Section 2.7.1**.

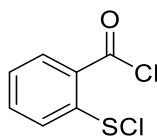
6.7.1 Biological Methods

Fluorescent microscopy

For fluorescent microscopy, cells at ~ 10% parasitaemia were fixed in 4% paraformaldehyde in PBS and stored in fixative at 4 °C as required. 200 μ L aliquots of cells were incubated with the following dilutions: 1:1000 of **10** and 1:1000 of **11** for the detection of GFP. Hoechst 33258 (Life Technologies) was used as a nuclear counterstain. Images were obtained using the Olympus Fluoview FV1000 confocal microscope. For imaging of live cells, cells were stained with 10 mg mL⁻¹ Hoechst 33258 for 10 minutes and mounted under coverslips on polysine adhesion slides using ProLong Gold mounting media. Cells were visualised on an Olympus BH8 microscope at room temperature for no longer than 15 minutes. For all microscopy, minimal adjustments in brightness and contrast were applied equally to images.

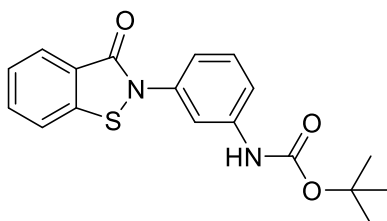
6.7.2 Organic Synthesis

Preparation of 2-(chlorothio)-benzoyl chloride **X**



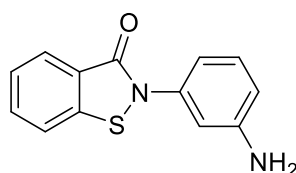
Thionyl chloride (22.8 mmol, 7 eq) and *N,N*-dimethylformamide (3 drops) were added to a solution of 2,2'-dithiobenzoic acid (3.26 mmol) in anhydrous dichloroethane (25 ml) under a N₂ atmosphere at room temperature. The stirring solution was heated to reflux at 80°C for 1.5 hours. Sulfuryl chloride (4.24 mmol, 1.3 eq) was added to the cooled solution at 25°C before heating the solution to 50°C for 45 minutes. Solvent, excess thionyl chloride and excess sulfuryl chloride were removed under reduced pressure to generate **X**, a yellow-green solid as pure product in quantitative yield. *R*_f = 0.79 (50:50 EtOAc:hexane). ¹H NMR (400 MHz, CDCl₃) δ 8.34 (dd, *J* = 8.0, 1.2 Hz, 1H), 7.93 (dd, *J* = 8.2, 0.4 Hz, 1H), 7.77 (dt, *J* = 8.5, 1.3 Hz, 1H), 7.42 (dt, *J* = 8.0, 0.8 Hz, 1H); ¹³C NMR (101 MHz, CDCl₃) δ 169.5, 146.1, 135.8, 134.7, 127.4, 125.8, 124.4.

Preparation of **tert-butyl (3-(3-oxobenzo[d]isothiazol-2(3H)-yl)phenyl)carbamate 10a**



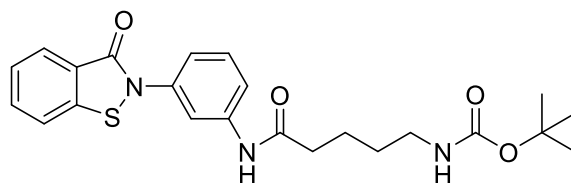
To a solution of *N*-Boc-*m*-phenylenediamine (1.16 g, 5.57 mmol) in DCM (20 ml), 2-(chlorothio)benzoyl chloride (**X**) (1.50 g, 7.24 mmol, 1.2 eq) was added at 0°C under a N₂ atmosphere. Triethylamine (2.56 ml, 18.4 mmol, 3.3 eq) was added to the solution which was allowed to warm to room temperature and stirred overnight. The solution was quenched with NaHCO₃ (30 ml), the organic layer was extracted into DCM (3 x 40 ml), washed with brine (40 ml) and dried over MgSO₄ before concentrating under reduced pressure. The crude product was purified by flash column chromatography and by trituration with Et₂O to give **10a** as an off white-cream solid in 63.0% yield. **Rf** = 0.37 (3:7 EtOAc:hexane and 1% triethylamine). ¹H NMR (400 MHz, CDCl₃) δ 8.10 (d, *J* = 7.9 Hz, 1H), 7.87 (s, 1H), 7.66 (dt, *J* = 8.2, 1.1 Hz, 1H), 7.57 (d, *J* = 8.1 Hz, 1H), 7.44 (dt, *J* = 7.9, 0.8 Hz, 1H), 7.42 – 7.28 (m, 3H), 6.67 (br s, 1H, NH) 1.52 (s, 9H); ¹³C NMR (101 MHz, CDCl₃) δ 164.1, 152.5, 139.9, 139.5, 137.8, 132.4, 129.8, 127.2, 125.8, 124.9, 120.1, 118.71, 116.8, 114.41, 80.9, 28.3; **ES+HRMS** *m/z* 365.0929 [M+Na]⁺ C₁₈H₁₈N₂O₃S requires 342.10.

Preparation of **2-(3-aminophenyl)benzo[d]isothiazol-3(2H)-one 10b**



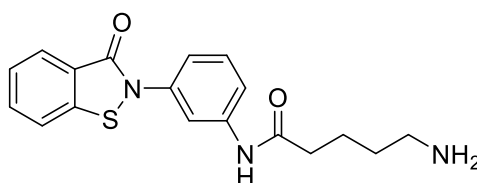
To a solution of **10a** (3.49 mmol) in DCM (20 ml) under a N₂ atmosphere, trifluoroacetic acid (TFA) (4.0 ml, 52.4 mmol, 15.0 eq) was added and allowed to stir at room temperature overnight. After this time, DCM and excess TFA were removed under reduced pressure. The crude material was re-dissolved in DCM, quenched with NaHCO₃ and the organic layer extracted into DCM (3 x 40 ml), washed with brine (40 ml), dried with MgSO₄ and concentrated *in vacuo* to give the pure product **10b** as a yellow-orange solid in a 84.4% yield. **Rf** = 0.31 (65:35 EtOAc:hexane and 1% triethylamine). ¹H NMR (400 MHz, CDCl₃) δ 8.09 (d, *J* = 7.9 Hz, 1H), 7.65 (t, *J* = 7.5 Hz, 1H), 7.57 (d, *J* = 8.0 Hz, 1H), 7.43 (t, *J* = 7.5 Hz, 1H), 7.22 (t, *J* = 8.0 Hz, 1H), 7.16 (t, *J* = 1.9 Hz, 1H), 7.01 (dd, *J* = 8.0, 1.2 Hz, 1H), 6.63 (dd, *J* = 8.0, 1.9 Hz, 1H), 3.52 (br s, 2H, NH₂); ¹³C NMR (101 MHz, CDCl₃) δ 164.1, 147.4, 139.9, 138.2, 132.3, 130.2, 127.4, 125.2, 125.1, 120.0, 114.2, 113.8, 111.1; **CI+HRMS** *m/z* 243.0597 [M+H]⁺ C₁₃H₁₀N₂OS requires 242.05.

Preparation of **tert-butyl (5-oxo-5-((3-(3-oxobenzo[d]isothiazol-2(3H)-yl)phenyl)amino) pentyl)carbamate 10c**



Boc-5-Ava-OH (0.404 g, 1.86 mmol) and HATU (1.059 g, 2.79 mmol, 1.5 eq) were dissolved in DMF (10 ml) and allowed to stir at room temperature for 20 minutes. **10b** (0.45 g, 1.86 mmol, 1.0 eq), dissolved in DMF (5 ml), was added after this time, followed by DIPEA (0.96 ml, 5.57 mmol, 3.0 eq) and the solution was stirred at room temperature for a further 20 hours, after which time the reaction was complete. Ninhydrin solution required to visualise Boc-5-Ava-OH. The solution was quenched with NaHCO₃ (40 ml) and the organic layer extracted into EtOAc (3 x 40 ml), then washed with H₂O (2 x 40 ml) and brine (40 ml), dried over MgSO₄, filtered through a pad of ceolite and concentrated *in vacuo*. The crude product was purified by trituration with Et₂O and EtOAc to give **10c** as an off-white solid in a 92.4% yield. **Rf** = 0.23 (50:50 EtOAc:hexane and 1% triethylamine). ¹H NMR (400 MHz, DMSO) δ 10.13 (s, 1H, NH), 8.09 (s, 1H), 8.06 (d, J = 8.1 Hz, 1H), 7.95 (d, J = 7.8 Hz, 1H), 7.76 (dd, J = 7.2, 0.9 Hz, 1H), 7.55 – 7.47 (m, 2H), 7.43 (d, J = 5.2 Hz, 2H), 6.83 (t, J = 5.4 Hz, 1H, NH), 2.93 (unresolved dt, J = 7.8, 6.2 Hz, 2H), 2.33 (t, J = 7.3 Hz, 2H), 1.63 – 1.51 (m, 2H), 1.46 – 1.37 (m, 2H), 1.36 (s, 9H); ¹³C NMR (101 MHz, DMSO) δ 172.0, 163.7, 156.1, 140.7, 140.5, 137.9, 133.1, 130.1, 126.6, 126.5, 124.9, 122.5, 119.1, 117.6, 115.0, 77.8, 36.5, 29.6, 28.7 (3C), 28.7, 22.9; **ES+HRMS** m/z 464.1622 [M+Na]⁺ C₂₃H₂₇N₃O₄S requires 441.17.

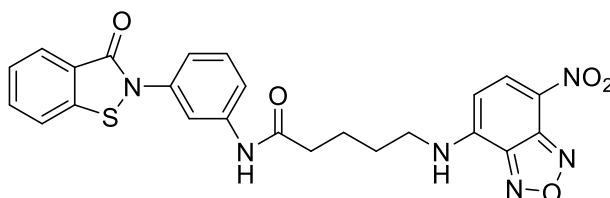
Preparation of **5-amino-N-(3-(3-oxobenzo[d]isothiazol-2(3H)-yl)phenyl) pentanamide 10d**



To a solution of **6c** (0.523 g, 1.19 mmol) in DCM (20 ml) under a N₂ atmosphere, trifluoroacetic acid (TFA) (2.74 ml, 35.5 mmol, 15.0 eq) was added and allowed to stir at room temperature overnight. After this time, DCM and excess TFA were removed under reduced pressure. The crude material was re-dissolved in DCM, quenched with NaHCO₃ (40 ml) and the organic layer extracted into DCM (3 x 40 ml), washed with brine (40 ml), dried with MgSO₄ and concentrated *in vacuo* to give **10d** as an orange-brown viscous oil in a 66.1% yield. **Rf** = 0.00 (5:95 MeOH:EtOAc). ¹H NMR (400 MHz, DMSO) δ 10.15 (s, 1H, amide NH), 8.10 (s, 1H), 8.06 (d, J = 8.1 Hz, 1H), 7.95 (d, J = 7.8 Hz, 1H), 7.76 (t, J = 7.5 Hz, 1H),

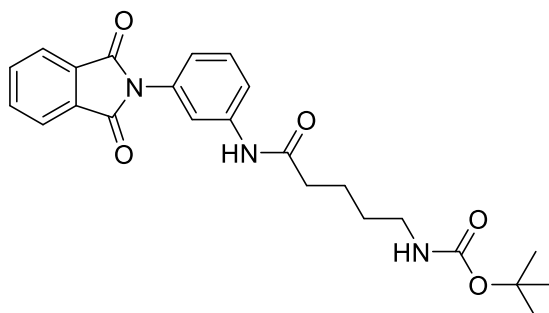
7.51 (t, $J = 7.6$ Hz, 2H), 7.42 (d, $J = 4.5$ Hz, 2H), 2.95 (s, NH₂), 2.55 (t, $J = 6.7$ Hz, 2H), 2.32 (t, $J = 7.2$ Hz, 2H), 1.61 (tt, $J = 7.3, 7.3$ Hz, 2H), 1.38 (tt, $J = 7.2, 6.8$ Hz, 2H); ¹³C NMR (101 MHz, DMSO) δ 172.2, 163.7, 140.8, 140.5, 137.9, 133.1, 130.1, 126.6, 126.5, 124.9, 122.5, 119.1, 117.7, 115.0, 41.8, 36.8, 33.2, 23.0; **ES+HRMS** m/z 342.1270 [M+H]⁺ C₁₈H₁₉N₃O₂S requires 341.12.

Preparation of 5-((7-nitrobenzo[*c*][1,2,5]oxadiazol-4-yl)amino)-*N*-(3-(3-oxobenzod-*d*-isothiazol-2(3*H*)-yl)phenyl)pentanamide **10**



To a solution of **6d** (0.120 g, 0.351 mmol) in anhydrous ethanol (12 ml) under a N₂ atmosphere, 4-chloro-7-nitrobenzofurazan (NBD-chloride) (0.077 g, 0.387 mmol, 1.1 eq) was added and allowed to stir at room temperature overnight. Additional anhydrous ethanol (5 ml) was added and the solution heated to 50°C for 4 hours under a restored N₂ atmosphere. The solution was then cooled to room temperature and stirred overnight. Ethanol was removed under reduced pressure and the crude product purified by column chromatography to give **10** a red-brown solid in a 30.6% yield. **R_f** = 0.38 (7:3 EtOAc:hexane). ¹H NMR (400 MHz, DMSO) δ 10.16 (s, 1H, amide NH), 9.57 (s, 1H, amide NH), 8.50 (d, $J = 8.6$ Hz, 1H), 8.10 (s, 1H), 8.06 (d, $J = 8.1$ Hz, 1H), 7.95 (d, $J = 7.8$ Hz, 1H), 7.77 (t, $J = 7.8$ Hz, 1H), 7.51 (t, $J = 7.2$ Hz, 2H), 7.46 – 7.39 (m, 2H), 6.43 (d, $J = 8.9$ Hz, 1H), 3.52 (s, 2H), 2.41 (s, 2H), 1.74 (s, 4H); ¹³C NMR (101 MHz, DMSO) δ 171.7, 163.7, 145.7, 140.6, 140.5, 138.4, 137.9, 133.1, 130.1, 126.6 (2C), 126.5 (2C), 124.9, 122.4 (2C), 119.1, 117.7, 115.0, 99.6, 43.6, 36.4, 27.7, 23.0; **Elemental analysis** (%) found: C, 57.46; H, 4.29; N, 15.73; S, 6.01%. C₂₄H₂₀N₆O₅S requires C, 57.14; H, 4.00; N, 16.66; S, 6.36%; **ES+HRMS** m/z 527.1115 [M+Na]⁺ C₂₄H₂₀N₆O₅S requires 504.12.

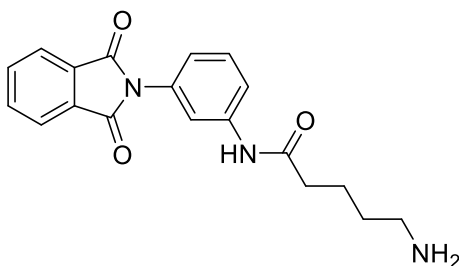
Preparation of *tert*-butyl (5-((3-(1,3-dioxoisindolin-2-yl)phenyl)amino)-5-oxopentyl) carbamate **11a**



Boc-5-Ava-OH (0.40 g, 1.84 mmol) and HATU (1.1 g, 2.76 mmol, 1.5 eq) were dissolved in DMF (10 ml) and allowed to stir at room temperature for 20 minutes. 2-(3-aminophenyl)-2,3-dihydro-1*H*-isindole-

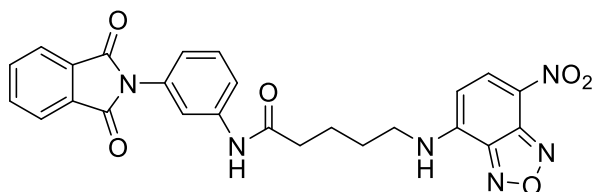
1,3-dione (0.48 g, 2.03 mmol, 1.1 eq), dissolved in DMF (5 ml), was added after this time, followed by DIPEA (0.95 ml, 5.52 mmol, 3.0 eq) and the solution was stirred at room temperature for a further 20 hours, after which time the reaction was complete. Ninhydrin solution required to visualise Boc-5-Ava-OH. The solution was quenched with NaHCO₃ (40 ml) and the organic layer extracted into EtOAc (3 x 40 ml), then washed with H₂O (2 x 40 ml) and brine (40 ml), dried over MgSO₄ and concentrated *in vacuo*. The crude product was purified by trituration with Et₂O and EtOAc to give **11a** as a light brown solid in a 91.7% yield. **Rf** = 0.28 (6:4 EtOAc:hexane and 1% triethylamine). ¹H NMR (400 MHz, MeOD) δ 7.99 – 7.83 (m, 4H), 7.72 (t, J = 1.9 Hz, 1H), 7.63 (t, J = 8.2, 1.1 Hz, 1H), 7.44 (t, J = 8.1 Hz, 1H), 7.17 (dd, J = 7.9, 0.9 Hz, 1H), 3.07 (t, J = 6.9 Hz, 2H), 2.41 (t, J = 7.3 Hz, 2H), 1.77 – 1.66 (m, 2H), 1.60 – 1.49 (m, 2H), 1.43 (s, 9H); ¹³C NMR (101 MHz, MeOD) δ 173.1, 167.3 (2C), 157.2, 139.3, 134.4 (2C), 131.7, 129.7, 127.4, 123.2 (2C), 122.1, 119.1, 118.2, 116.01, 78.5, 39.55 36.1, 29.1, 27.4 (3C), 22.6; **ES+HRMS** m/z 460.1843 [M+Na]⁺ C₂₄H₂₇N₃O₅ requires 437.20.

Preparation of 5-amino-N-(3-(1,3-dioxoisindolin-2-yl)phenyl)pentanamide **11b**



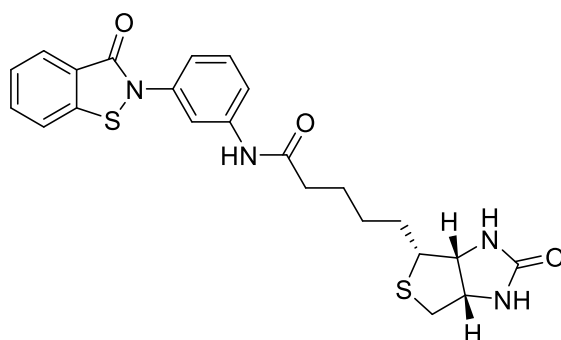
To a solution of **11a** (0.732 g, 1.67 mmol) in DCM (20 ml) under a N₂ atmosphere, trifluoroacetic acid (TFA) (1.9 ml, 25.1 mmol, 15.0 eq) was added and allowed to stir at room temperature overnight. After this time, DCM and excess TFA were removed under reduced pressure. The crude material was re-dissolved in EtOAc, quenched with NaHCO₃ and the organic layer extracted into EtOAc (3 x 40 ml), washed with brine (40 ml), dried with MgSO₄ and concentrated *in vacuo*. The crude product was purified by washing with MeOH to give **11b** as a grey-brown solid in a 44.2% yield. **Rf** = 0.00 (EtOAc and 1% triethylamine). ¹H NMR (400 MHz, DMSO) δ 10.31 (s, 1H, NH), 8.01 – 7.90 (m, 4H), 7.88 (br s, 2H, NH₂), 7.76 (s, 1H), 7.66 (d, J = 8.2 Hz, 1H), 7.45 (t, J = 8.0 Hz, 1H), 7.12 (d, J = 7.9 Hz, 1H), 2.80 (t, J = 7.2 Hz, 2H), 2.39 (t, J = 6.8 Hz, 2H), 1.63 (m 4H); ¹³C NMR (101 MHz, DMSO) δ 171.6, 167.4, 140.3, 135.2 (2C), 132.6, 132.0 (2C), 129.5, 123.9 (2C), 122.5, 119.1, 118.4, 39.0, 36.1, 27.0, 22.5; **ES+HRMS** m/z 338.1508 [M+H]⁺ C₁₉H₁₉N₃O₃ requires 337.14.

Preparation of **N-(3-(1,3-dioxisoindolin-2-yl)phenyl)-5-((7-nitrobenzo[c][1,2,5]-oxadiazol-4-yl) amino)pentanamide 11**



To a solution of **11b** (0.235 g, 0.698 mmol) in anhydrous DCM (12 ml) under a N₂ atmosphere, 4-chloro-7-nitrobenzo-2-oxa-1,3-diazole (NBD-Cl) (0.116 g, 0.581 mmol, 1.0 eq) was added. The solution was evacuated and purged with N₂ before the addition of triethylamine (0.08 ml, 0.581 mmol, 1.0 eq) and was allowed to stir at room temperature overnight. The crude solution was diluted with DCM, washed with brine (3 x 30 ml) and the organic layer dried with MgSO₄ and concentrated *in vacuo*. The crude product was purified by column chromatography to give **11** a red-brown solid in a 35.4% yield. **Rf** = 0.63 (5:95 MeOH:EtOAc and 1% triethylamine). ¹H NMR (400 MHz, DMSO) δ 10.13 (s, 1H, amide NH), 9.60 (s, 1H, NH), 8.49 (d, J = 8.9 Hz, 1H), 8.03 – 7.86 (m, 4H), 7.72 (s, 1H), 7.61 (d, J = 8.1 Hz, 1H), 7.43 (t, J = 8.0 Hz, 1H), 7.11 (d, J = 7.8 Hz, 1H), 6.43 (d, J = 9.0 Hz, 1H), 3.51 (unresolved t, 2H), 2.40 (t, J = 6.2 Hz, 2H), 1.72 (m, 4H); ¹³C NMR (126 MHz, DMSO) δ 171.7, 167.4, 145.7, 145.0, 144.7, 140.2, 138.4 (2C), 135.2, 132.6, 132.0 (2C), 129.5, 123.9 (2C), 122.5, 121.0, 119.1, 118.4, 99.6, 58.4, 43.6, 36.4, 27.7, 23.0; **Elemental analysis** (%) found: C, 60.03; H, 4.32; N, 15.85%; C₂₅H₂₀N₆O₆ requires C, 60.00; H, 4.03; N, 16.79%; **ES+HRMS** m/z 523.1348 [M+Na]⁺ C₂₅H₂₀N₆O₆ requires 500.14; **HPLC** (purity analysis %) found: 94.67%; RT: 14.12 min/ 40 min (66.5/33.5, 0.3 ml/min IPA:HEXANE, Signal = 254 nm, SYNCHROSILICA).

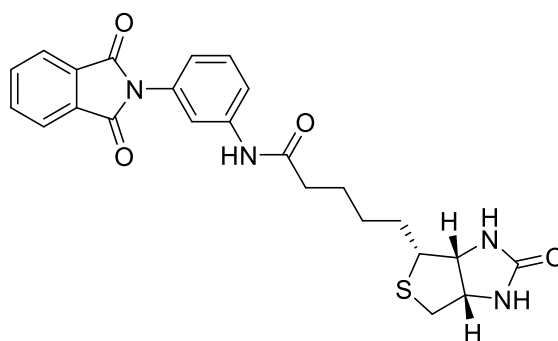
Preparation of **N-(3-(3-oxobenzothiazol-2(3H)-yl)phenyl)-5-((3aS,4S,6aR)-2-oxohexahydro-1H-thieno[3,4-d]imidazol-4-yl)pentanamide 12**



Biotin (0.231 g, 0.944 mmol) and HATU (0.538 g, 1.42 mmol, 1.5 eq) were dissolved in DMF (10 ml) and allowed to stir at room temperature for 20 minutes. **10b** (0.252 g, 1.04 mmol, 1.1 eq), dissolved in DMF (5 ml), was added after this time, followed by DIPEA (0.49 ml, 2.83 mmol, 3.0 eq) and the solution was stirred at room temperature for a further 20 hours, after which time the reaction was

complete. The solution was quenched with NaHCO_3 (40ml) and the organic layer extracted into DCM (3 x 40 ml), then washed with H_2O (2 x 40 ml) and brine (40 ml), dried over MgSO_4 and concentrated *in vacuo*. The crude product was purified by trituration with Et_2O and EtOAc to give **12** as an off-white solid in a 76.3% yield. $R_f = 0.08$ (5:95 MeOH:EtOAc and 1% triethylamine). $^1\text{H NMR}$ (400 MHz, DMSO) δ 10.14 (s, 1H, amide NH), 8.09 (s, 1H), 8.06 (d, $J = 8.2$ Hz, 1H), 7.95 (d, $J = 7.8$ Hz, 1H), 7.76 (t, $J = 7.5$ Hz, 1H), 7.51 (m, 2H), 7.44 (d, $J = 4.8$ Hz, 2H), 6.45 (s, 6H, NH), 6.37 (s, 6H, NH), 4.30 (t, $J = 6.8$ Hz, 1H), 4.14 (t, $J = 6.4$ Hz, 1H), 3.13 (dd, $J = 11.1, 7.5$ Hz, 1H), 2.82 (dd, $J = 12.4, 5.0$ Hz, 1H), 2.58 (d, $J = 12.4$ Hz, 1H), 2.34 (t, $J = 7.2$ Hz, 2H), 1.72 – 1.29 (m, 6H); $^{13}\text{C NMR}$ (101 MHz, DMSO) δ 172.0, 163.7, 163.2, 140.7, 140.5, 137.9, 133.1, 130.1, 126.6, 126.5, 124.9, 122.4, 119.1, 117.7, 115.0, 61.5, 59.7, 55.9, 40.3, 36.7, 28.7, 28.6, 25.5; **Elemental analysis** (%) found: C, 57.30; H, 5.16; N, 11.71; S, 13.34%. $\text{C}_{23}\text{H}_{24}\text{N}_4\text{O}_3\text{S}_2$ requires C, 58.95; H, 5.16; N, 11.96; S, 13.96%; **ES+HRMS** m/z 491.1190 $[\text{M}+\text{Na}]^+$ $\text{C}_{23}\text{H}_{24}\text{N}_4\text{O}_3\text{S}_2$ requires 468.13.

Preparation of ***N*-(3-(1,3-dioxoisindolin-2-yl)phenyl)-5-((3*a*S,4*S*,6*a*R)-2-oxohexahydro-1*H*-thieno[3,4-*d*]imidazol-4-yl)pentanamide 13**



Biotin (0.202 g, 0.819 mmol) and HATU (0.467 g, 1.23 mmol, 1.5 eq) were dissolved in DMF (7 ml) and allowed to stir at room temperature for 20 minutes. 2-(3-aminophenyl)-2,3-dihydro-1*H*-isoindole-1,3-dione (0.215 g, 0.901 mmol, 1.1 eq), dissolved in DMF (5 ml), was added after this time, followed by DIPEA (0.42 ml, 2.46 mmol, 3.0 eq) and the solution was stirred at room temperature for a further 20 hours, after which time the reaction was complete. The solution was quenched with NaHCO_3 (40 ml) and the organic layer extracted into EtOAc (3 x 40 ml), then washed with H_2O (2 x 40 ml) and brine (40 ml), dried over MgSO_4 and concentrated *in vacuo*. The crude product was purified by trituration with EtOAc and MeOH to give **13** as a yellow-cream solid in a 58.7% yield. $R_f = 0.13$ (5:95 MeOH:EtOAc and 1% triethylamine). $^1\text{H NMR}$ (400 MHz, DMSO) δ 10.11 (s, 1H), 8.04 – 7.86 (m, 4H), 7.74 (s, 1H), 7.63 (d, $J = 8.2$ Hz, 1H), 7.44 (t, $J = 8.0$ Hz, 1H), 7.12 (d, $J = 7.9$ Hz, 1H), 6.46 (s, 1H, NH), 6.38 (s, 1H, NH), 4.31 (t, $J = 7.3$ Hz, 1H), 4.14 (t, $J = 5.9$ Hz, 1H), 3.17 – 3.08 (m, 1H), 2.83 (dd, $J = 12.4, 5.0$ Hz, 1H), 2.58 (d, $J = 12.4$ Hz, 1H), 2.34 (t, $J = 7.3$ Hz, 2H), 1.72 – 1.31 (m, 6H); $^{13}\text{C NMR}$ (101 MHz, DMSO) δ 171.9, 167.4 (2C), 163.2, 140.3, 135.2 (2C), 132.6, 132.00 (2C), 129.5, 123.9 (2C), 122.4, 119.1, 118.4, 61.5, 59.7,

55.9, 49.1, 36.7, 28.7, 28.6, 25.6; **Elemental analysis** (%) found: C, 60.66; H, 5.31; N, 11.77; S, 6.73%.
 $C_{24}H_{24}N_4O_4S$ requires C, 62.05; H, 5.21; N, 12.06; S, 6.90%; **ES+MS** m/z 487.1417 $[M+Na]^+$ $C_{24}H_{24}N_4O_4S$
requires 464.15.

6.8 References

- [1] E. Deu, M. Verdoes, M. Bogyo, *Nat. Struct. Mol. Biol.* **2012**, *19*, 9–16.
- [2] S. V Frye, *Nat. Chem. Biol.* **2010**, *6*, 159–161.
- [3] C. H. Arrowsmith, J. E. Audia, C. Austin, J. Baell, J. Bennett, J. Blagg, C. Bountra, P. E. Brennan, P. J. Brown, M. E. Bunnage, et al., *Nat. Chem. Biol.* **2015**, *11*, 536–541.
- [4] Z. Wang, P. Talukder, S. M. Hecht, S. Chen, *Bioorganic Med. Chem. Lett.* **2015**, *25*, 1182–1185.
- [5] J. Xiao, P. Broz, A. W. Puri, E. Deu, M. Morell, D. M. Monack, M. Bogyo, *J. Am. Chem. Soc.* **2013**, *135*, 9130–9138.
- [6] M. E. Bunnage, E. L. P. Chekler, L. H. Jones, *Nat. Chem. Biol.* **2013**, *9*, 195–199.
- [7] E. Nicodeme, K. L. Jeffrey, U. Schaefer, S. Beinke, S. Dewell, C. Chung, R. Chandwani, I. Marazzi, P. Wilson, H. Coste, et al., *Nature* **2010**, *468*, 1119–1123.
- [8] P. Filippakopoulos, J. Qi, S. Picaud, Y. Shen, W. B. Smith, O. Fedorov, E. M. Morse, T. Keates, T. T. Hickman, I. Felletar, et al., *Nature* **2010**, *468*, 1067–1073.
- [9] Y. Suzuki, K. Yokoyama, *Biosensors* **2015**, *5*, 337–363.
- [10] L.-Y. Niu, H.-R. Zheng, Y.-Z. Chen, L.-Z. Wu, C.-H. Tung, Q.-Z. Yang, *Analyt* **2014**, 1389–1395.
- [11] D. C. J. Waalboer, J. A. Muns, N. J. Sijbrandi, R. B. M. Schasfoort, R. Haselberg, G. W. Somsen, H. J. Houthoff, G. A. M. S. Van Dongen, *ChemMedChem* **2015**, *10*, 797–803.
- [12] R. Liang, G. J. Broussard, L. Tian, *ACS Chem. Neurosci.* **2015**, *6*, 84–93.
- [13] J. H. Lee, J. H. Lee, S. H. Jung, T. K. Hyun, M. Feng, J. Kim, J. Lee, H. Lee, J. S. Kim, C. Kang, et al., *Chem. Commun.* **2015**, *51*, 7463–7465.
- [14] E. Yamaguchi, C. Wang, A. Fukazawa, M. Taki, Y. Sato, T. Sasaki, M. Ueda, N. Sasaki, T. Higashiyama, S. Yamaguchi, *Angew. Chemie - Int. Ed.* **2015**, *54*, 4539–4543.
- [15] Z. Lin, Y. Guo, Y. Gao, S. Wang, X. Wang, Z. Xie, H. Niu, W. Chang, L. Liu, H. Yuan, et al., *J. Med. Chem.* **2015**, *58*, 3944–3956.
- [16] N. G. R. D. Elshan, T. Jayasundera, C. S. Weber, R. M. Lynch, E. A. Mash, *Bioorganic Med. Chem.* **2015**, *23*, 1841–1848.
- [17] S. Shaban Ragab, A. Subramani Swaminathan, J. Garcia-Amoró, B. Captain, F. M. Raymo, *New J. Chem* **2015**, *39*, 1570–1573.
- [18] O. Planas, T. Gallavardin, S. Nonell, *Chem. Commun.* **2015**, *51*, 5586–5589.
- [19] C. Zhang, L. Wei, C. Wei, J. Zhang, R. Wang, Z. Xi, L. Yi, *Chem. Commun. (Camb)*. **2015**, *51*, 7505–8.
- [20] H. M. Ismail, P. M. O'Neill, D. W. Hong, R. D. Finn, C. J. Henderson, A. T. Wright, B. F. Cravatt, J. Hemingway, M. J. I. Paine, *Proc. Natl. Acad. Sci. U. S. A.* **2013**, *110*, 19766–71.
- [21] G. L. Ellis, R. Amewu, S. Sabbani, P. A. Stocks, A. Shone, D. Stanford, P. Gibbons, J. Davies, L. Vivas, S. Charnaud, et al., *J. Med. Chem.* **2008**, *51*, 2170–2177.

- [22] F. J. Williams, D. Fiedler, *ACS Chem. Biol.* **2015**, *10*, 1958–1963.
- [23] S. C. Burdette, G. K. Walkup, B. Spingler, R. Y. Tsien, S. J. Lippard, *J. Am. Chem. Soc.* **2001**, *123*, 7831–7841.
- [24] D. W. Domaille, E. L. Que, C. J. Chang, *Nat. Chem. Biol.* **2008**, *4*, 168–175.
- [25] J. R. Lakowicz, *Principles of Fluorescence Spectroscopy*, Springer, **2006**.
- [26] A. T. R. Williams, S. A. Winfield, J. N. Miller, *Analyst* **1983**, *108*, 1067–1071.
- [27] A. Chattopadhyay, *Chem. Phys. Lipids* **1990**, *53*, 1–15.
- [28] “FluoProbes - NBD Product Information,” can be found under <http://www.interchim.fr/ft/4/46540A.pdf>, **2015**.
- [29] M. Pietka-Ottlik, P. Potaczek, E. Piasecki, J. Mlochowski, *Molecules* **2010**, *15*, 8214–8228.
- [30] S. Aprile, E. Del Grosso, G. Grosa, *Xenobiotica* **2011**, *41*, 212–225.
- [31] S. Hartwig, M. M. Nguyen, S. Hecht, *Polym. Chem.* **2010**, *1*, 69–71.
- [32] L. Carpino, *J. Am. Chem. Soc.* **1993**, *115*, 4397–4398.
- [33] C. A. G. N. Montalbetti, V. Falque, *Tetrahedron* **2005**, *61*, 10827–10852.
- [34] A. Wahhab, D. Smil, A. Ajamian, M. Allan, Y. Chantigny, E. Therrien, N. Nguyen, S. Manku, S. Leit, J. Rahil, et al., *Bioorganic Med. Chem. Lett.* **2009**, *19*, 336–340.
- [35] A. R. Odom, *Personal Communication*, **2012**.
- [36] Y. Corbett, L. Herrera, J. Gonzalez, L. Cubilla, T. L. Capson, P. D. Coley, T. A. Kursar, L. I. Romero, E. Ortega-Barria, *Am. J. Trop. Med. Hyg.* **2004**, *70*, 119–124.
- [37] H. Corbett Y Capson , Coley PD, Kursar, Romero LI, Ortega-Barria E, **2002**, *67*, 209–210.
- [38] B. Zhang, K. M. Watts, D. Hodge, L. M. Kemp, D. A. Hunstad, L. M. Hicks, A. R. Odom, *Biochemistry* **2011**, *50*, 3570–3577.
- [39] N. J. D. Nagelkerke, *Biometrika* **1991**, *78*, 691–692.
- [40] A. C. Cameron, A. G. F. Windmeijer, *J. Econom.* **1997**, *77*, 329–342.
- [41] J.-Y. van der Meer, A. K. H. Hirsch, *Nat. Prod. Rep.* **2012**, *29*, 721.
- [42] J. Sambrook, D. W. Russell, *Detection of Protein-Protein Interactions Using the GST Fusion Protein Pulldown Technique*, **2006**.
- [43] ThermoFisher, “Pull-Down Assays,” can be found under <https://www.thermofisher.com/uk/en/home/life-science/protein-biology/protein-biology-learning-center/protein-biology-resource-library/pierce-protein-methods/pull-down-assays.html>, **2016**.
- [44] V. Barton, S. A. Ward, J. Chadwick, A. Hill, P. M. O’Neill, *J. Med. Chem.* **2010**, *53*, 4555–4559.
- [45] J. Wysocka, *Methods* **2006**, *40*, 339–343.
- [46] J. Wysocka, T. Swigut, T. A. Milne, Y. Dou, X. Zhang, A. L. Burlingame, R. G. Roeder, A. H.

- Brivanlou, C. D. Allis, *Cell* **2005**, *121*, 859–872.
- [47] J. Wysocka, T. Swigut, H. Xiao, T. A. Milne, S. Y. Kwon, J. Landry, M. Kauer, A. J. Tackett, B. T. Chait, P. Badenhorst, et al., *Nature* **2006**, *442*, 86–90.
- [48] K. K. Wu, *Methods Mol. Biol.* **2006**, *338*, 281–90.
- [49] E. A. Bayer, M. Wilchek, *Methods Biochem. Anal.* **1980**, *26*, 1–45.
- [50] W.-G. Deng, Y. Zhu, A. Montero, K. K. Wu, *Anal. Biochem.* **2003**, *323*, 12–18.
- [51] M. Wilchek, E. A. Bayer, *Trends Biochem. Sci.* **1989**, *14*, 408–412.
- [52] R. A. Copeland, *Evaluation of Enzyme Inhibitors in Drug Discovery*, **2013**.
- [53] S. D. Furdas, I. Hoffmann, D. Robaa, B. Herquel, W. Malinka, P. Swia, A. Akhtar, W. Sippl, M. Jung, **2014**, 1856–1862.
- [54] H. M. Ismail, V. Barton, M. Phanchana, S. Charoensutthivarakul, M. H. L. Wong, J. Hemingway, G. A. Biagini, P. M. O’Neill, S. A. Ward, *Proc. Natl. Acad. Sci. U. S. A.* **2016**, *113*, 2080–5.
- [55] I. D. Kuntz, K. Chen, K. a Sharp, P. a Kollman, *Proc. Natl. Acad. Sci. U. S. A.* **1999**, *96*, 9997–10002.
- [56] N. Murakami, M. Kawanishi, S. Itagaki, T. Horii, M. Kobayashi, *Bioorganic Med. Chem. Lett.* **2004**, *14*, 3513–3516.

Chapter 7

Final Conclusions and Perspectives

7.1 Final Conclusions and Perspectives

Malaria is a life-threatening, vector-borne disease which causes over 200 million cases per year and is responsible for nearly half a million deaths. Despite significant scientific progress over the last two decades, achieving a 30% decrease in the global incidence of malaria between 2000 and 2013, malaria remains a major global health problem, putting almost half the world's population at risk of contracting the disease. Consequently, the development of new and effective antimalarial chemotherapeutics is a fundamental priority but represents a significant challenge within drug discovery. It is the ability of the *Plasmodium* parasite to develop drug resistance which significantly hinders the fight against malaria, where the present acceleration of *Plasmodium* resistance is seriously threatening advances made in malaria treatment and prevention. With 95 countries registering malaria transmission in 2015, the development of new antimalarial drugs and battle to overcome *Plasmodium* parasite resistance has never been more crucial.

Amidst significant research efforts pursuing the identification of novel drugs and novel drug targets to expand the antimalarial drug pipeline, considerable interest has developed around the chemical manipulation of isoprenoid biosynthesis. Isoprenoids are a diverse class of natural products which play vital roles in many cellular functions and are essential for *Plasmodium* parasite survival. *Plasmodium* parasites use the non-mevalonate (MEP) pathway to generate isoprenoid precursors, delivering a key biological selectivity to humans and other mammals which use the mevalonate (MVA) pathway for this purpose. Research by others into fosmidomycin, a potent and well-characterised MEP pathway inhibitor, have validated the pathway as a viable target for antimalarial drug discovery. These results provoked our interest in the third enzyme of the MEP pathway, IspD, a novel and underexplored biological target with which to advance antimalarial drug development.

Virtual screening and chemoinformatics studies facilitated the generation of a focused ligand library of 5000 compounds that was assessed in a HTS to identify novel inhibitors of the *Pf*IspD target enzyme. The HTS identified 54 novel compound structures that demonstrate inhibitory activity against *Pf*IspD. From the structures identified, the 1,2-benzo[*d*]isothiazol-3(2*H*)-one (BITZ) chemotype was selected as the hit chemotype for *Pf*IspD inhibitor design and SAR development. A number of synthetic strategies have been identified which facilitate the efficient generation of the BITZ chemotype and derived inhibitors. These strategies have been employed throughout the generation of all BITZ compounds discussed and were used to initiate preliminary SAR work which confirmed the specific chemical construct of the BITZ headgroup essential to achieve inhibition of the *Pf*IspD enzyme.

Following the transition into hit-to-lead optimisation, extensive SAR investigations around the BITZ chemotype have generated a broad and diverse range of BITZ compounds which include three of the most potent BITZ derived *PflspD* inhibitors to date. Indeed, the most potent BITZ inhibitor demonstrates an impressive IC_{50} value of 73 nM against *PflspD*, which is six-times more potent than the HTS hit. In addition, potent *PflspD* inhibition translates into efficacious phenotypic activity, with several BITZ compounds displaying EC_{50} values as low as 206 nM against *P. falciparum* parasite growth. Subsequent BITZ compound evaluation demonstrates good correlation between *PflspD* enzyme inhibition and inhibition of *Plasmodium* parasite growth, indicating that inhibition of the MEP pathway, *via* the *PflspD* target, is able to cause parasite death. This is also supported by metabolic profiling of MEP pathway intermediates which highlights that anti-parasitic activity is the result of MEP pathway inhibition which is sufficient to disrupt *de novo* production of isoprenoid precursors. These results, further backed up by the work of others, enables one of our key research questions to be answered, as we have demonstrated that arrest of the MEP pathway *via PflspD* inhibition is able to cause *Plasmodium* parasite death through the disruption of isoprenoid precursor generation.

In addition, biological studies have shown BITZ compounds to offer potential as a broad spectrum antimalarial agents with several BITZ analogues demonstrating low micromolar to nanomolar activity against *PvlspD*, therefore meeting a key developmental requirement of antimalarial drug design. Biological evaluations have also established that BITZ derived compounds express inhibitory activity against *P. falciparum* parasite strains which show drug resistance to existing antimalarial therapies. This is of significant importance given the current wide spread and accelerating *P. falciparum* species drug resistance which means existing drug-resistant parasites must be sensitive to novel antimalarial therapies if new drugs and research efforts are to succeed.

In order to determine the mechanism of action by which the BITZ chemotype inhibits *PflspD*, a combination of molecular modelling studies and biological assays have been conducted. Since a *PflspD* crystal structure is unavailable, *EclspD* was used to identify a suitable modelling protocol with which to dock small molecules at the *lspD* active site, that was then applied to a *PflspD* homology model. Molecular modelling studies investigated the orientation of BITZ compounds at the *PflspD* active site; where the examination of docking poses revealed a consistent molecular alignment. As a result, a mechanism of enzyme inhibition has been proposed which is initiated by non-covalent active site recognition but ultimately relies on the formation of a covalent *PflspD*-BITZ adduct, rendering the enzyme inactive. More specifically, the proposed mechanism involves formation of a disulfide protein-inhibitor adduct between the *PflspD* active site Cys-202 residue and the electrophilic sulfur atom of the BITZ inhibitor core, facilitated by their proximal alignment in the *PflspD* binding site.

A range of biological methodologies, including site directed mutagenesis (SDM), enzyme activity assays and crystallographic evaluation, confirm and support the proposed mechanism of enzyme inhibition. SDM has been used to verify the specific requirement for the Cys-202 active site residue in facilitating *Pf*lspD enzyme inhibition. The wildtype *Ecl*spD enzyme, against which BITZ compounds are ineffective, has been rendered sensitive to the effects of BITZ inhibitors through introduction of the active site Cys-202 residue and generation of the *Ecl*spD-A14C mutant enzyme. This result therefore supports the role of the Cys-202 protein residue in *Pf*lspD active site inhibition. In addition, generation of the *Pf*lspD-C202A mutant enzyme, replacing Cys-202 with Ala, causes a six-fold decrease in enzyme sensitivity when treated with BITZ compounds compared to wildtype *Pf*lspD. This observation highlights that covalent enzyme inhibition is no longer able to occur at *Pf*lspD-C202A, but that weak inhibitory effects are retained and likely signify non-covalent recognition contributions of BITZ compounds at the enzyme.

Several lines of evidence now suggest that some BITZ derived compounds may be capable of eliciting off-target inhibitory effects that may contribute to observed inhibition of *Plasmodium* parasite growth. A loss of *Pf*lspD enzymatic activity is observed within several BITZ compound series but where a notable level of anti-parasitic activity is maintained and in some instances markedly enhanced. Such an activity trend is indicative of off-target interactions that are capable of inhibiting *Plasmodium* parasite growth, despite a lack of activity against the *Pf*lspD enzyme. This observation is supported by the negative result of IPP rescue experiments, indicating that parasite growth inhibition by BITZ compounds does not solely result from activity against the *lspD* enzyme. Recent research has therefore focused on the question of potential off-target reactivity of the BITZ chemotype, as well as an alternative chemical chemotype which has been shown to be a potent inhibitor of the *Pf*lspD enzyme.

A small series of chemical probes have been designed to address the question of BITZ chemotype localisation with *Plasmodium* infected cells as well as the potential off-target reactivity of BITZ. NBD-tagged and biotin-tagged BITZ probes were generated, along with suitable non-*Pf*lspD active control probes, for the purpose of fluorescent microscopy and streptavidin pull-down assays. Fluorescent microscopy showed distribution of the NBD-tagged BITZ probe to be broadly cytoplasmic and excluded from both the parasite nucleus and food vacuole. Further microscopy is needed to determine more precise BITZ localisation patterns and how these may be distinct from the distribution of non-*Pf*lspD inhibitors within *Plasmodium* culture. A biotinylated BITZ probe was designed to facilitate a streptavidin pull-down experiment to determine the proteins to which the BITZ chemotype is able to bind in a solution of *P. falciparum* parasite lysate. As yet, assessment of off-target BITZ reactivity by

this means has not been feasible; research must first focus on the design of an alternative biotinylated BITZ probe to enable inhibitory activity against *Plasmodium* parasite growth to be confirmed.

Robust biological data has confirmed the proposed mechanism of *PflspD* inhibition by BITZ compounds as occurring *via* covalent modification. However, the covalent modification of enzymes and proteins can be a risky strategy within drug design. This has therefore driven our consideration of a distinct chemical chemotype shown to inhibit the *PflspD* enzyme by an alternative, non-covalent mechanism of action. MMV-008138, a tetrahydro- β -carboline derivative, was recognised in phenotypic screen showing it to be a potent inhibitor of *P. falciparum* growth in culture. Further work has highlighted that only the 1*R*,3*S*-MMV-008138 diastereoisomer is active against *PflspD*, providing a high degree of specificity and selectivity to this compound.

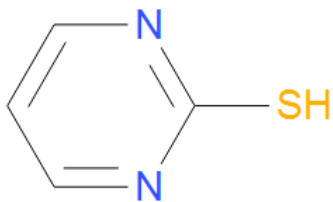
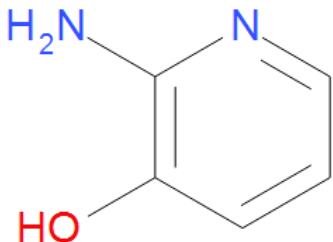
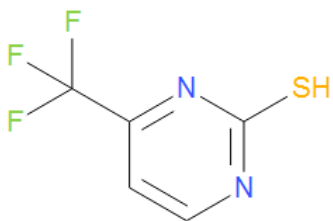
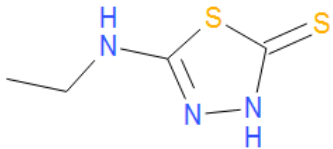
Metabolic profiling of MMV-008138 and assessments of species-selectivity have revealed comparable results to those of the BITZ chemotype, highlighting therapeutic scope of MMV-008138 as a broad-spectrum antimalarial agent as well as its ability to inhibit the MEP pathway at levels which affect asexual parasite growth. In addition, positive IPP rescue experiments show that the inhibition of *Plasmodium* parasite growth is specific to MEP pathway inhibition. The comparable features identified between the tetrahydro- β -carboline and BITZ chemotypes inspired a series of competition experiments, generating isobolograms which combined 1*R*,3*S*-MMV-008138 with several BITZ inhibitors. However, the resulting data highlighted that the two chemical motifs behave antagonistically when co-administered, producing a lessened phenotypic effect.

SAR development around 1*R*,3*S*-MMV-008138 is currently quite limited, with little room for significant structural variation or additional functionality. This can be rationalised through the spatial demands of the *PflspD* binding site, in which 1*R*,3*S*-MMV-008138 adopts a spatially tight-fitting binding pose, as demonstrated by molecular modelling. More recent SAR development have focused on modifications to the A and D rings of 1*R*,3*S*-MMV-008138 and again highlight that structural modifications must be both precise and discrete to maintain complementary binding and activity against *PflspD*. In analogues where this is achieved, the resulting activity against both *PflspD* and *Plasmodium* parasite growth is of nanomolar potency. Further work must address the metabolism and stability profiles of 1*R*,3*S*-MMV-008138 derivatives to enable movement towards an optimised lead structure. As such, development of 1*R*,3*S*-MMV-008138 analogues remains ongoing, with the aim of progressing towards a lead compound that is suitable for clinical development as an antimalarial agent, targeting the *PflspD* enzyme.

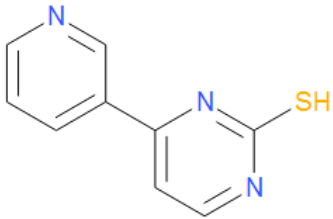
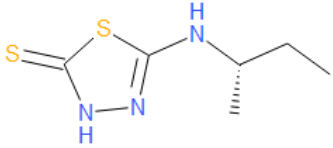
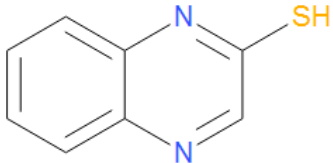
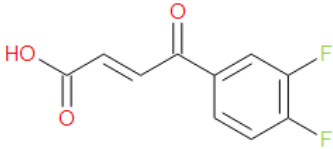
Appendix

Appendix

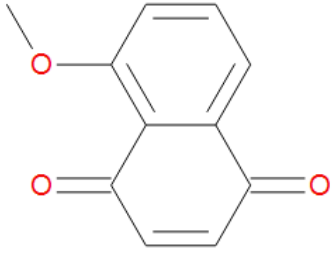
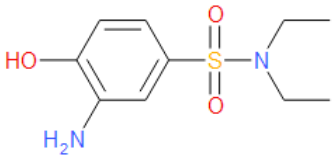
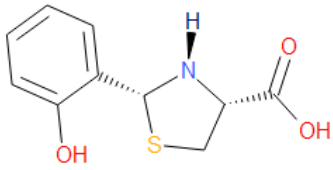
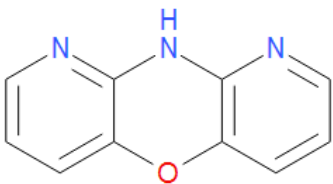
Appendix 1. HTS Output: 54 Hit Compounds Identified as Active Inhibitors of the *Pf*ispD enzyme.

Molecule	Name	Average_y50_ic50	Average_PoI_IC50
	DT2009-0227269	7.03202603259607	
	DT2008-0020810	17.5000659484204	17.0610853174343
	DT2000-0116845	0.733630434301403	1.1870997360023
	DT2009-0247407	15.3490211697382	

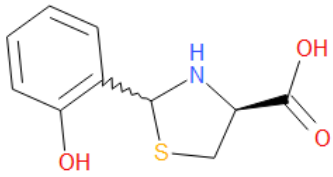
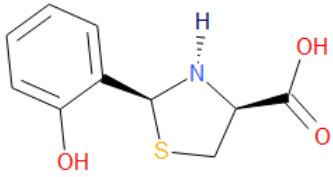
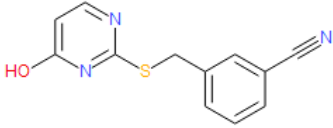
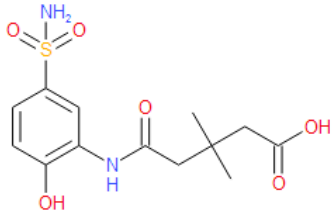
Appendix

Molecule	Name	Average_y50_ic50	Average_PoI_IC50
	DT2000-0126493	0.480308558816649	0.71084295103192
	DT2009-0247548	14.5169215066037	
	DTSM98-0101027	15.7667806712807	
	DT2009-0206069	4.507725002528555	

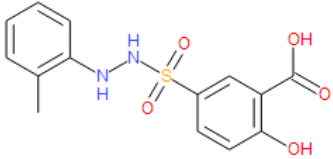
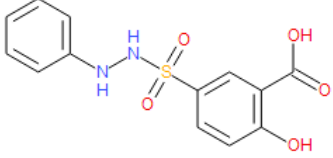
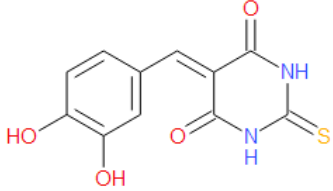
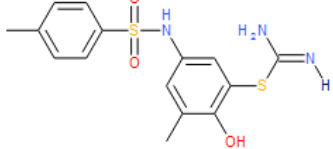
Appendix

Molecule	Name	Average_y50_ic50	Average_PoI_IC50
	DT2000-0136827	10.255928237383886	
	DT2009-0164115	2.402172803479325	2.24848250381503
	DT2008-0000035	7.148572525926485	10.43170707606461
	DT2000-0135075	16.685826501255647	

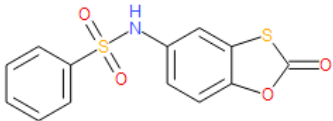
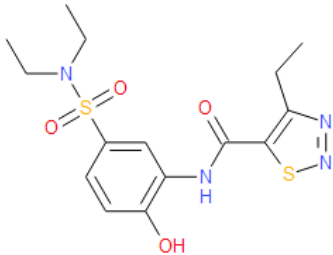
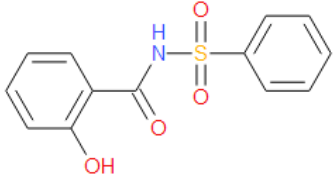
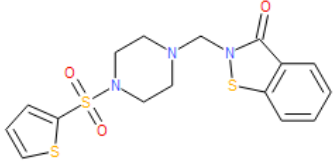
Appendix

Molecule	Name	Average_y50_ic50	Average_PoI_IC50
<p style="text-align: center;">AND Enantiomer</p> 	DT2000-0128723	14.5774880632643	
	DT2000-0136049	18.3298454094685	
	DT2000-0119883	15.55286251864185	
	DT2009-0090905	1.2463692134564235	0.8865782587574005

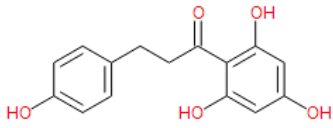
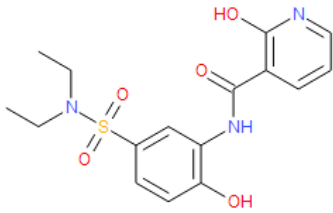
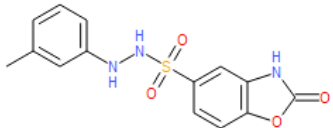
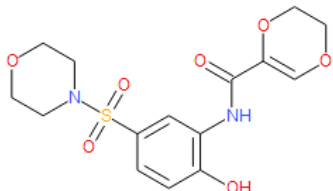
Appendix

Molecule	Name	Average_y50_ic50	Average_PoI_IC50
	DT2009-0197587	1.2592941297286049	1.1479302338350101
	DT2009-0238296	3.04214041177281	3.0823472876018547
	DT2000-0109708	19.08394762430325	
	DT2009-0169780	0.9476163182017314	1.67971337199364

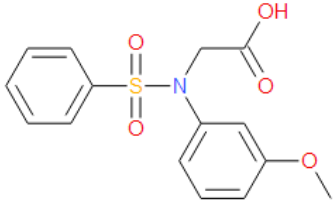
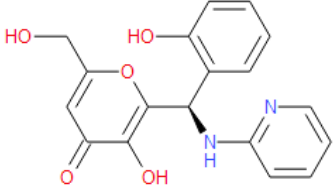
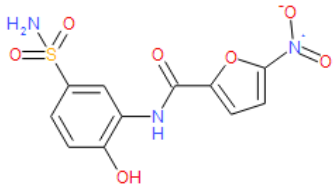
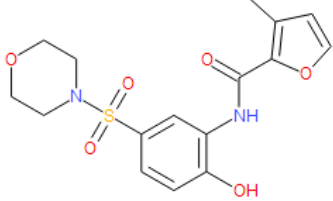
Appendix

Molecule	Name	Average_y50_ic50	Average_PoI_IC50
	DT2006-0006337	12.091974704704425	
	DT2009-0097223	0.7747256497462689	0.624068175828197
	DT2006-0007319	23.1591405789121	17.5093288672365
	DT2009-0032351	0.9272268354869505	1.2208938217988652

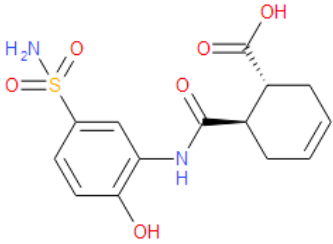
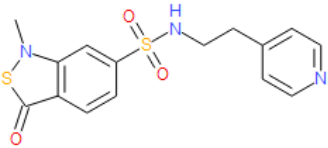
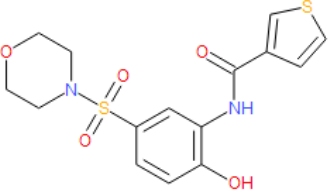
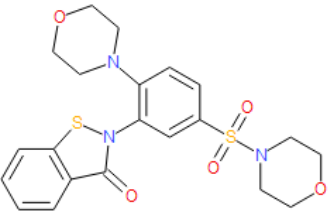
Appendix

Molecule	Name	Average_y50_ic50	Average_PoI_IC50
	DT2000-0136025	20.15547970783745	14.384541220867
	DT2009-0102048	1.6423453663692884	0.7692260744865165
	DT2009-0328226	9.84792600245126	
	DT2009-0132865	2.162365782392854	1.2926906729520065

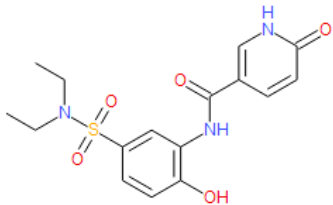
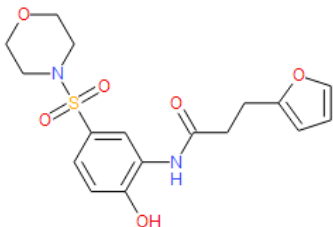
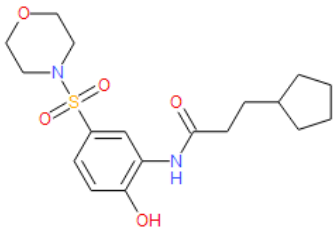
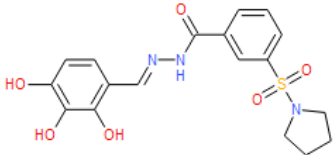
Appendix

Molecule	Name	Average_y50_ic50	Average_PoI_IC50
	DT2008-0070573	13.273253266229315	
	DT2009-0048657	2.932437993284895	3.4329125803617897
	DT2009-0203409	18.827306899591424	
	DT2009-0081611	4.820871557110305	3.471695102325325

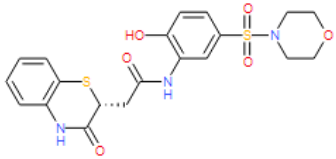
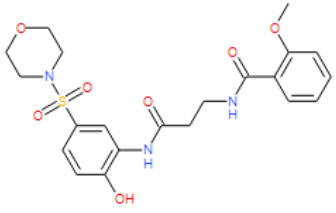
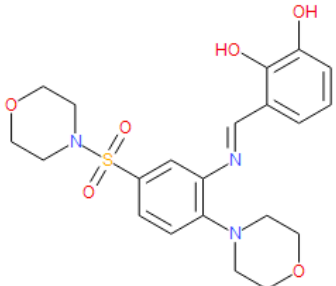
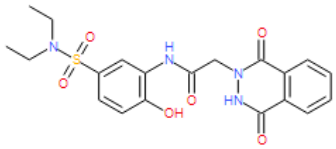
Appendix

Molecule	Name	Average_y50_ic50	Average_PoI_IC50
	DT2009-0017415	13.8935181844736	
	DT2000-0102643	15.37869421239187	
	DT2009-0131944	12.506689922684764	
	DT2009-0168020	0.4842657743919	0.500882689726589

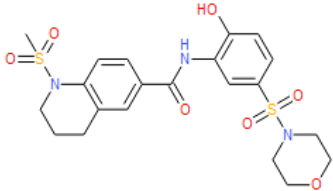
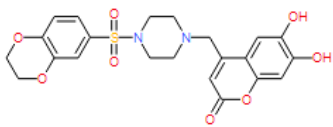
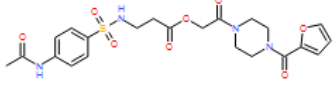
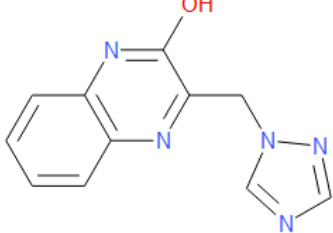
Appendix

Molecule	Name	Average_y50_ic50	Average_PoI_IC50
	DT2009-0035277	10.72710567375365	
	DT2009-0094990	10.045378741228475	
	DT2009-0089063	19.654450705390452	
	DT2009-0268251	11.487416956560232	13.565005495251876

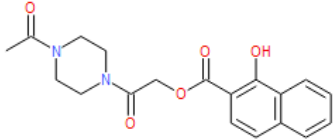
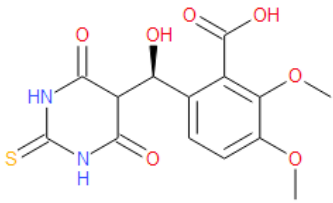
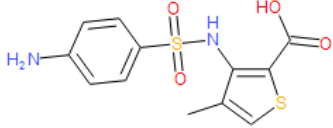
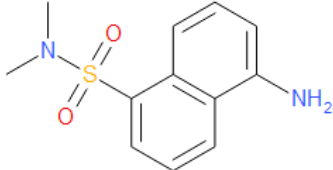
Appendix

Molecule	Name	Average_y50_ic50	Average_PoI_IC50
	DT2009-0322309	9.352295896201401	16.68178704885093
	DT2009-0321049	7.58759454619746	6.881541913527065
	DT2009-0201963	18.7442736172293	11.16984375981911
	DT2009-0345820	19.452120590570942	

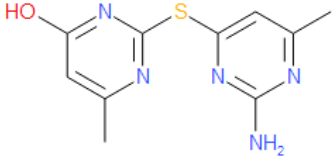
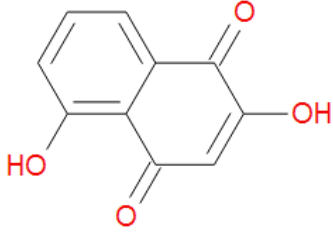
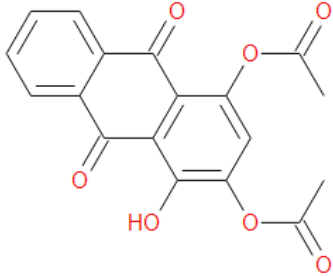
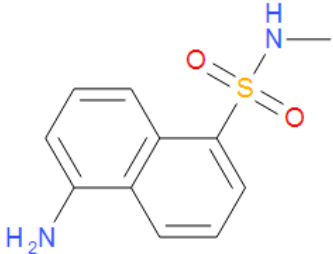
Appendix

Molecule	Name	Average_y50_ic50	Average_PoI_IC50
	DT2009-0333123	12.847395523417969	
	DT2009-0207866	16.9858512508433	9.956640068396245
	DT2009-0352427	18.9949477301429	4.655280586935145
	DTSM98-0111022		9.55619986553237

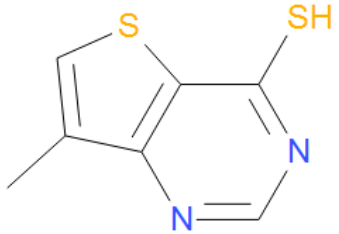
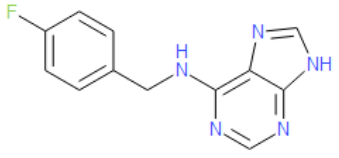
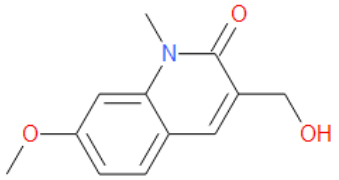
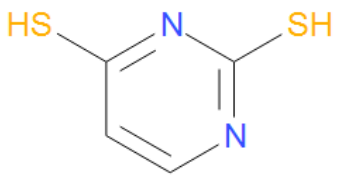
Appendix

Molecule	Name	Average_y50_ic50	Average_PoI_IC50
	DT2009-0066593		15.542269418861201
	DT2008-0070374		10.602889201919416
	DT2000-0115791		13.26200091185505
	DT2000-0127491		7.54852907132642

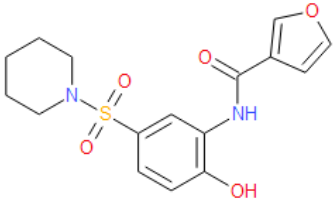
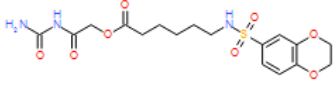
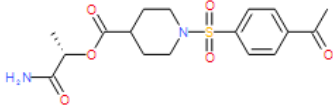
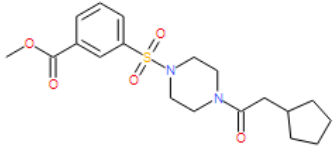
Appendix

Molecule	Name	Average_y50_ic50	Average_PoI_IC50
	DT2000-0130880		4.40303147445304
	DT2000-0119432		9.43310528764642
	DT2000-0136800		3.448266055033215
	DT2000-0127480		10.20248397263947

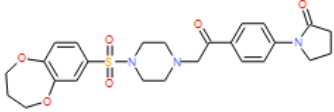
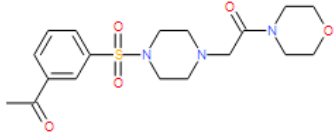
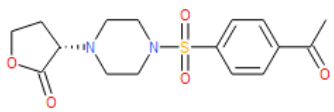
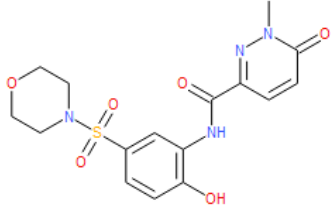
Appendix

Molecule	Name	Average_y50_ic50	Average_PoI_IC50
 <p>The structure shows a benzothiazole ring system. A methyl group is attached to the benzene ring at the 5-position. A thiol group (-SH) is attached to the benzothiazole ring at the 2-position.</p>	DT2000-0115966		5.0187933127403745
 <p>The structure shows a benzimidazole ring system. A 4-fluorophenylmethyl group (-CH₂-C₆H₄-F) is attached to the benzimidazole ring at the 2-position.</p>	DT2009-0153632		14.8867515210919
 <p>The structure shows a pyridinone ring system. A methoxy group (-OCH₃) is attached to the benzene ring at the 6-position. A hydroxymethyl group (-CH₂OH) is attached to the pyridinone ring at the 4-position.</p>	DT2008-0034171		7.523054206758156
 <p>The structure shows a pyrimidine ring system. Two thiol groups (-SH) are attached to the pyrimidine ring at the 2 and 6 positions.</p>	DT2009-0353343		9.513821388099789

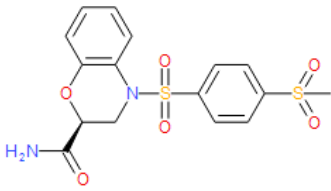
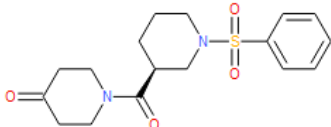
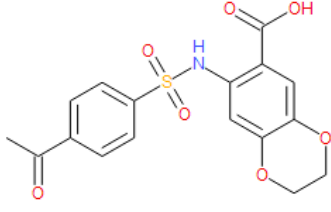
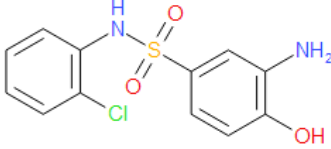
Appendix

Molecule	Name	Average_y50_ic50	Average_PoI_IC50
	DT2009-0052222		14.6449455764165
	DT2009-0162688		16.0660570696822
	DT2009-0015505		11.57554359867045
	DT2009-0020948		12.79319533611198

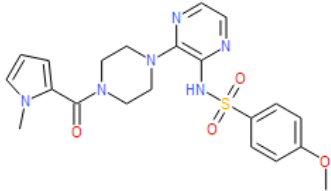
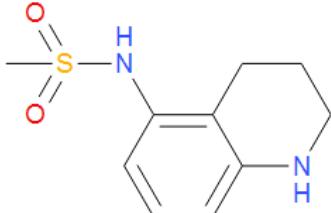
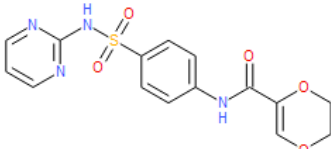
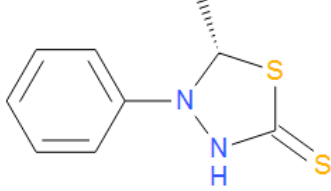
Appendix

Molecule	Name	Average_y50_ic50	Average_PoI_IC50
	DT2009-0293768		19.60292487126805
	DT2009-0175118		13.31359962380203
	DT2009-0079986		11.289801800925005
	DT2009-0013155		13.7052614908778

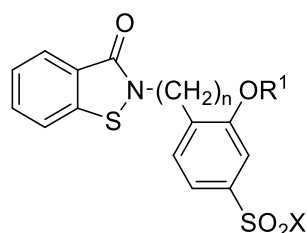
Appendix

Molecule	Name	Average_y50_ic50	Average_PoI_IC50
	DT2009-0095909		17.747081194354724
	DT2008-0026962		12.84379556735405
	DT2009-0089318		7.5644147154055155
	DT2009-0168225		14.08858741481878

Appendix

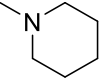
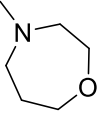
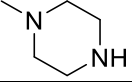
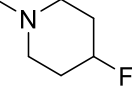
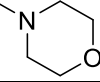
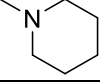
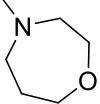
Molecule	Name	Average_y50_ic50	Average_PoI_IC50
	233_6904_6951		7.693365227297585
	DT2011-0006386		19.5928124455411
	DT2009-0098750		5.893072655236595
	DT2009-0220609		0.796819877667287

Appendix 2. Summary of preliminary SAR studies around close structural analogues of the DT2009-0168020 hit.^[1]



Compound name	n	R ¹	X	PfispD Inhibition IC ₅₀ (μM)	Whole Cell Growth (3D7) Inhibition IC ₅₀ (μM)
MM1-28b	0	H		13.200	10.056
MM1-26	0	H		0.710	7.588
MM1-31b	0	H		5.400	9.208
MM1-32b	0	H		1.900	14.635
MM1-17b	0	CH ₃		1.500	10.202
MM1-24 (12)	0	CH ₃		1.100	0.974
MM1-9T3	0	CH ₃		0.866	6.110
MM1-15	0	CH ₃		1.954	2.470
MM1-6T2	0	CH ₃		1.011	8.610
MM1-8T3	0	CH ₃		0.809	14.300
MM1-14	0	CH ₃		0.542	9.100
MM2-29T	1	H		4.613	4.950
MM2-28T	1	H		1.149	16.750
MM2-18	1	H		> 100	46.169

Appendix

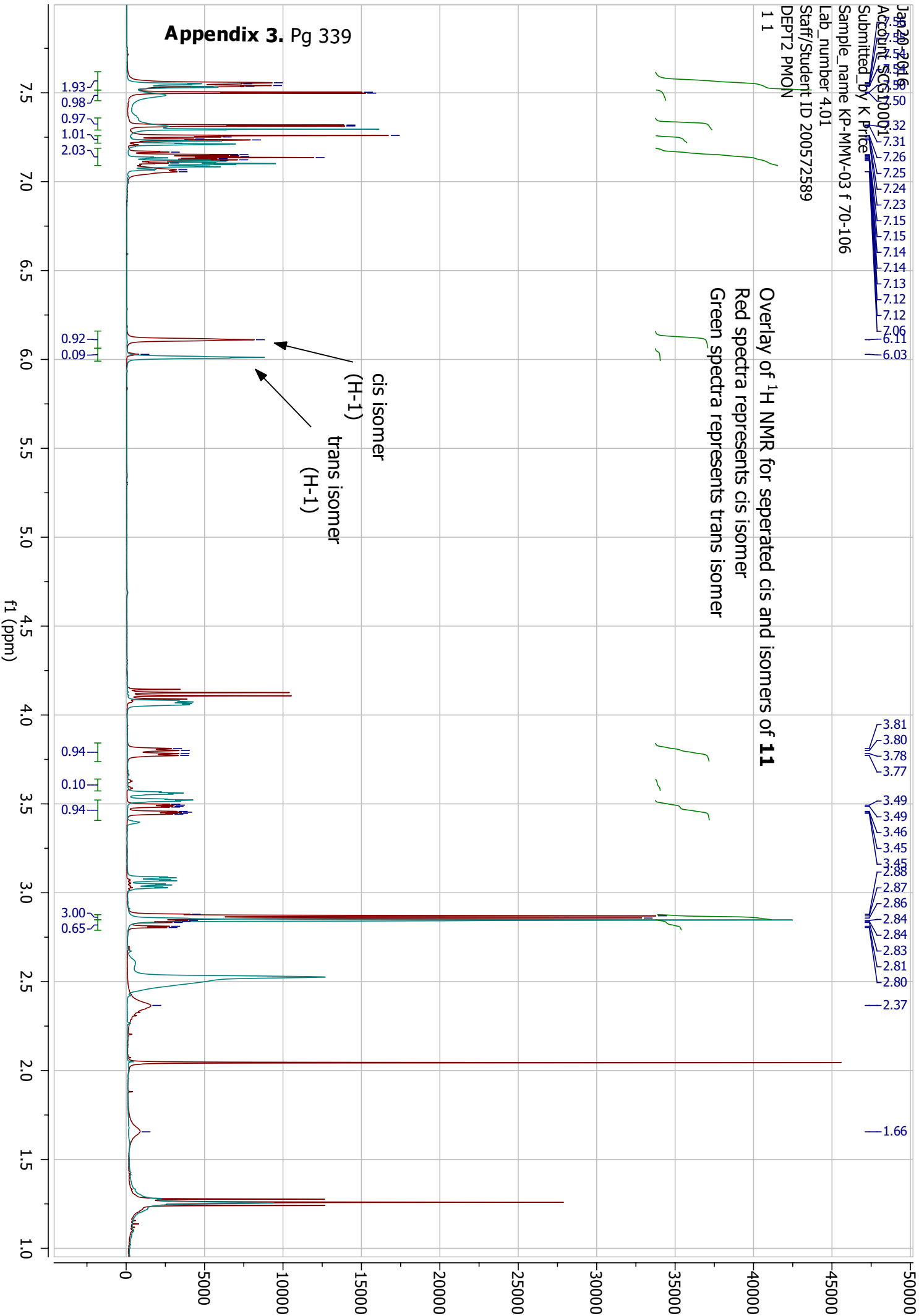
MM2-27T	1	H		0.493	17.870
MM2-25T	1	H		5.602	19.020
MM2-17	1	CH ₃		15.80	3.900
MM2-13	1	CH ₃		1.550	26.720
MM2-9	1	CH ₃		1.100	33.030
MM2-12	1	CH ₃		0.560	21.340
MM2-10	1	CH ₃		2.870	32.700

- [1] Maria Mondini, Novel Antimalarial Compounds Targeting the Non-Mevalonate Pathway: Design and Synthesis Optimization, **2014**.

Jan 20 2018 15:50
Account SC610001
Submitted by K Price
Sample_name KP-MMV-03 f 70-106
Lab_number 4.01
Staff/Student ID 200572589
DEPT2 PMON
1 1

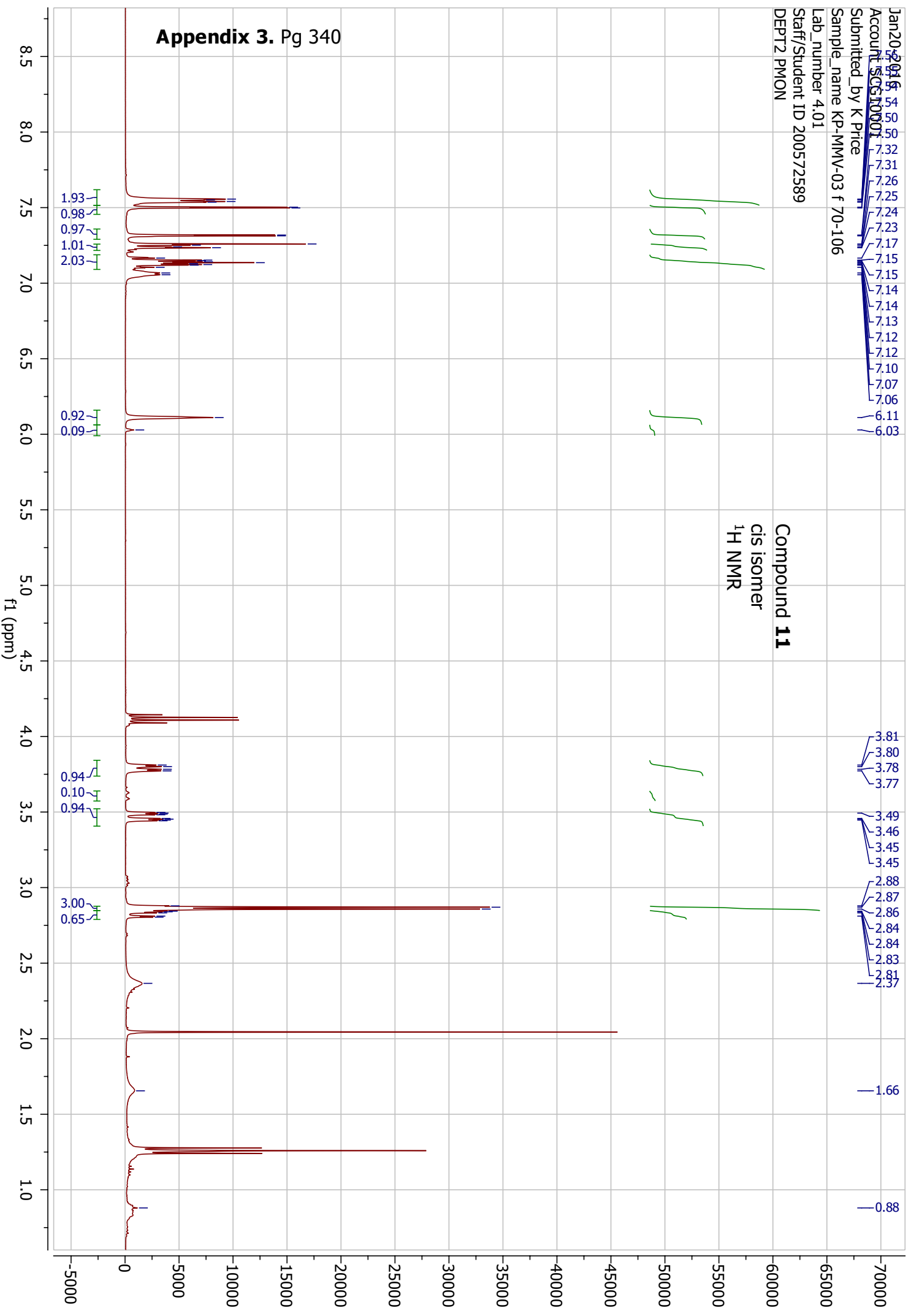
Overlay of ¹H NMR for separated cis and isomers of **11**

Red spectra represents cis isomer
Green spectra represents trans isomer



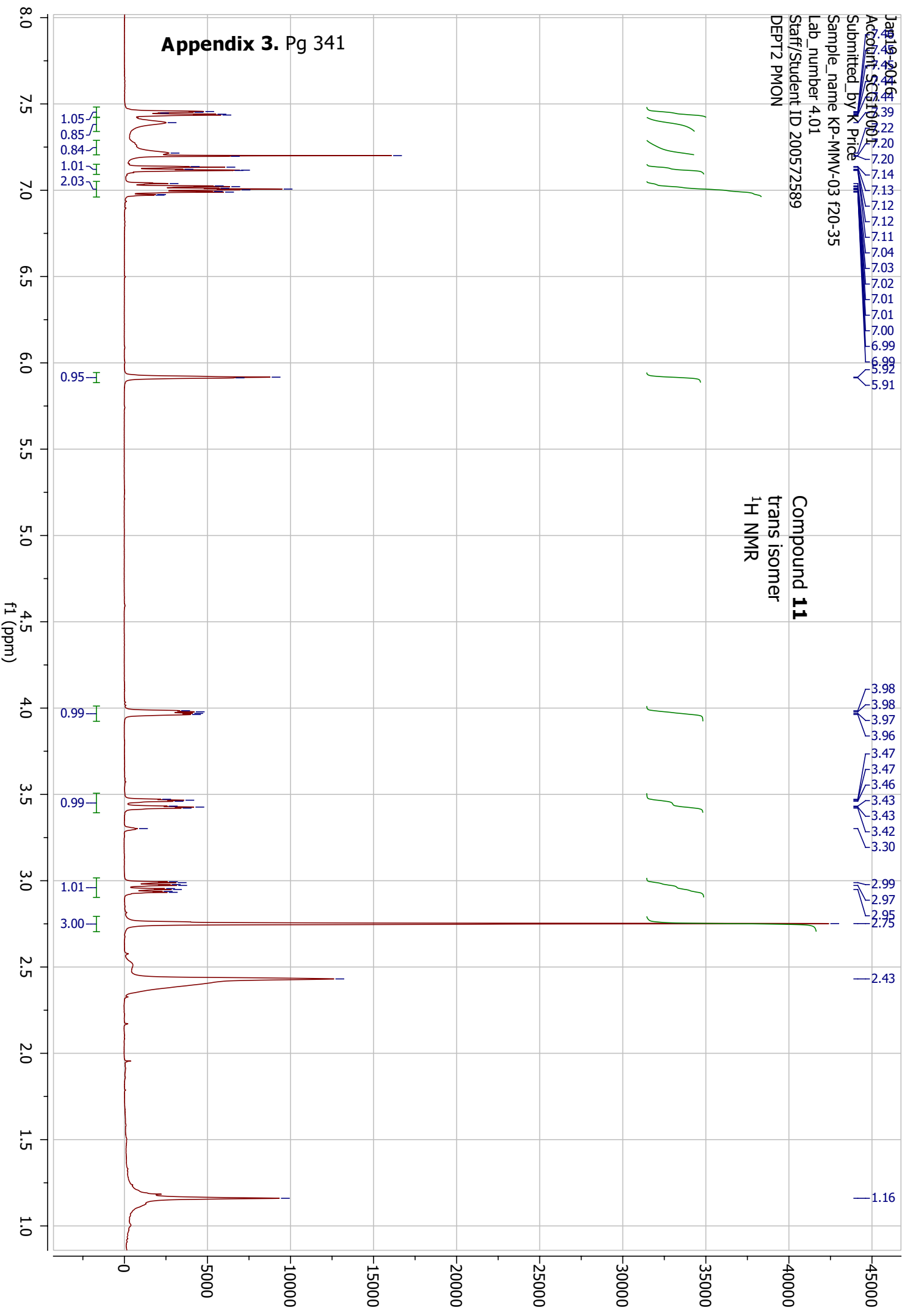
Jan20-2015
Account: SCS10001
Submitted by K Price
Sample_name KP-MMV-03 f 70-106
Lab_number 4.01
Staff/Student ID 200572589
DEPT2 PMON

Compound **11**
cis isomer
¹H NMR

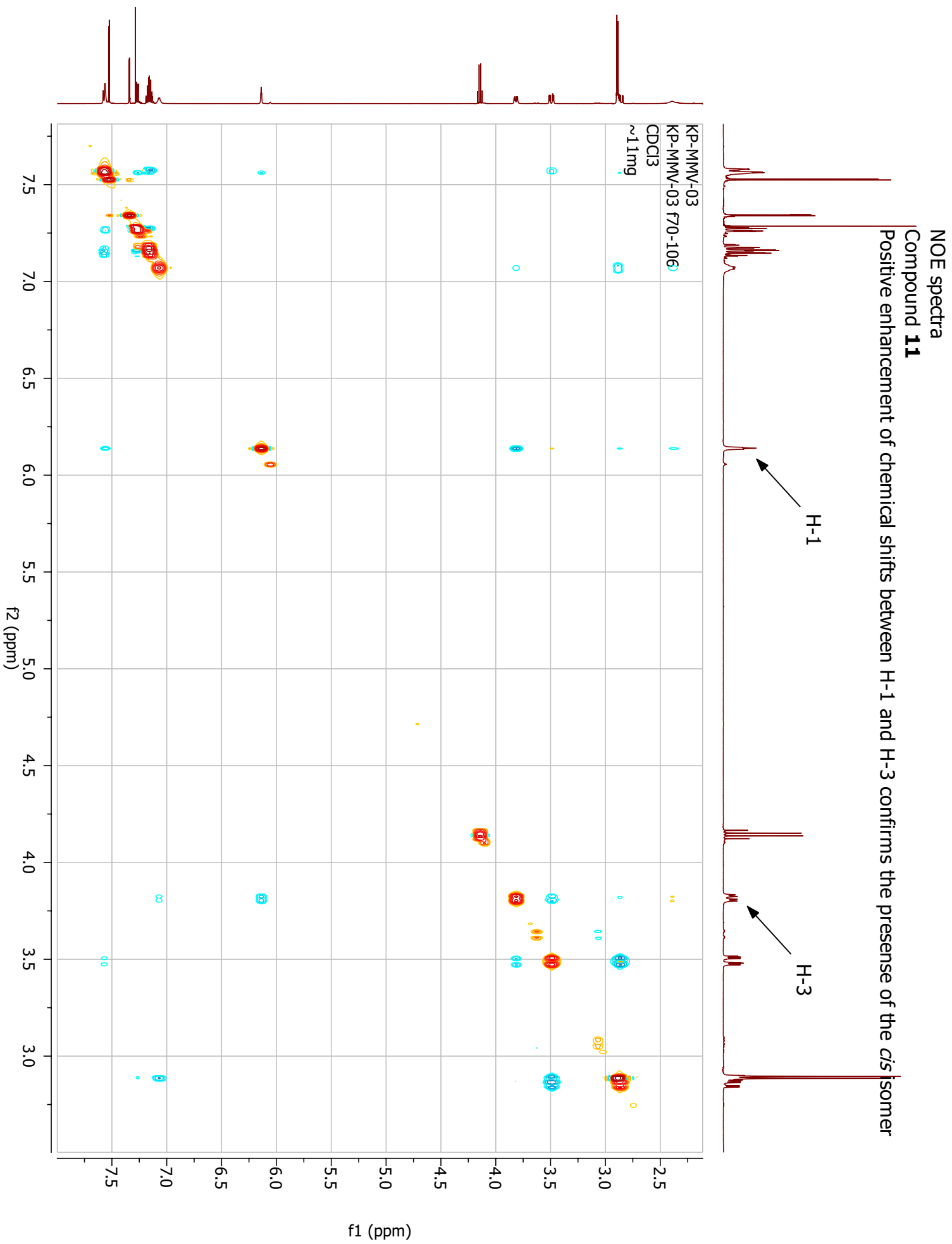


Jan 19, 2014 4:39
Account SC510001
Submitted by R Price
Sample_name KP-MMV-03 f20-35
Lab_number 4.01
Staff/Student ID 200572589
DEPT 2 PMON

Compound **11**
trans isomer
¹H NMR



Appendix 3. Pg 341



NOE spectra
Compound **11**

No observation of positive enhancement between the chemical shifts of H-1 and H-3 confirms presence of the *trans* isomer

